SRS-TR146
6 MARCH 1967

CR 73140

MULTIPLE SATELLITE SYSTEMS STUDY Final Report

NAS2-3926

Submitted to:
National Aeronautics and Space Administration
Ames Research Center
Moffett Field, California

Technical Report SRS-TR146

6 March 1967

MULTIPLE SATELLITE SYSTEMS STUDY
FINAL REPORT

Submitted to

National Aeronautics and Space Administration
Ames Research Center
Moffett Field, California

NAS2-3926

PHILCO-FORD CORPORATION
Space & Re-entry Systems Division
Palo Alto, California

ABSTRACT

PHILCO-FORD SRS-TR146 UNCLASSIFIED
MULTIPLE SATELLITE
SYSTEMS STUDY FINAL REPORT 449 Pages
6 March 1967 Contract NAS2-3926

A feasibility study has been performed for a multiple launch of four scientific satellites into highly elliptical earth orbit, to make simultaneous field and particle measurements in the region of the interaction between the solar wind and the magnetosphere. This report covers parametric mission analyses which examine methods of deploying the four satellites into the desired orbital array, the specification of the important resultant system requirements, and the development of a configuration concept which will meet the requirements. The basic conclusions are that the mission is indeed feasible, and that the most promising configuration concept is one in which four satellites are deployed simultaneously, near apogee, with radial velocities obtained from the centrifugal forces of a spinning payload cluster.

TABLE OF CONTENTS

TABLE OF CONTENTS (Continued)

TABLE OF CONTENTS (Continued)

TABLE OF CONTENTS (Continued)

LIST OF ILLUSTRATIONS

LIST OF ILLUSTRATIONS (Continued)

LIST OF ILLUSTRATIONS (Continued)

LIST OF ILLUSTRATIONS (Continued)

LIST OF ILLUSTRATIONS (Continued)

LIST OF ILLUSTRATIONS (Continued)

LIST OF TABLES

LIST OF TABLES (Continued)

SECTION 1

INTRODUCTION

This report conveys the results of a study which has been performed by Philco-Ford under contract to NASA Ames Research Center, for the purpose of examining the feasibility of a multiple launch of satellites to accomplish a specified scientific mission. The mission objectives and requirements were defined in the NASA/ARC Specification A-11967 Rev. B. The task of the study then was to perform the parametric analyses necessary to define the system requirements, to develop deployment strategies which would optimize the experiment value, to derive corresponding spacecraft requirements and to develop a configuration concept which would meet the requirements. A basic objective was to identify any problem areas which would require resolution before proceeding to a design study phase of the program. The preliminary design was to be carried to the extent necessary to establish the major features and feasibility of approach of the deployment method and of each satellite subsystem.

SECTION 2

MISSION OBJECTIVES

2.1 SCIENTIFIC MEASUREMENTS

The purpose of the proposed mission is to make measurements that better define the physical characteristics of the region of the interaction between the solar wind and the earth's magnetosphere. The region of interest encompasses the entire progression from the interplanetary plasma (freely expanding solar wind), to the shock wave, boundary layer (magnetosheath), and the magnetosphere itself. Of particular interest are:

- Separation of temporal and spatial variations (relatively long-term structural features)
- Detailed definition of the disturbances responsible for temporal variations.

To accomplish this requires the making of simultaneous measurements over a spatial matrix which, over a period of time, maps the region of interest. The shape and size of this matrix (array of satellites) is defined only as being three dimensional, and being characterized by initial separation distances of approximately 500 to 1000 kilometers, with separations at the end of mission life increasing (due to drifts) to no more than 15,000 kilometers. Each satellite measures magnetic field strength, using a boom-mounted magnetometer, and makes energetic particle counts, using a plasma probe. To correlate the data from the four satellites, a time reference is added to each measurement.

2.2 ORBIT REQUIREMENTS

Size and Shape. The orbit is highly elliptical to allow the satellite to pass through the region of interest, which lies, approximately, between 10 and 14 earth radii.

The nominal apogee is 20 earth radii. Perigee, established by direct injection, is only high enough to preclude unacceptable drag effects; the actual value of perigee, which depends on the launch window, is approximately 140-160 nautical miles.

Orbit Plane. From the experimenter's standpoint, a minimal dihedral angle between the plane of the orbit and the ecliptic plane is desirable, consistent with other launch date and azimuth constraints.

Line of Apsides. Initially, the line of apsides should be so oriented with respect to the sun that most of the early part of the mission is spent with the apogee region toward the sun. This implies an orbit with its major axis pointed at a certain angle "behind" the sun, so that the earth's orbital motion causes the apparent sun vector to sweep the apogee region at approximately one degree per day. Thus, the contemplated angle (15 to 20 degrees) gives 15 to 20 days between launch and the point when the sun vector projection passes through apogee.

2.3 SPACECRAFT REQUIREMENTS

Orientation. The satellite is spin-stabilized, with the spin axis approximately normal to the ecliptic plane. The scientific instruments dictate a spin rate of 50 to 70 rpm.

Magnetic Cleanliness. The magnetic field produced by the satellite does not exceed 0.5 gamma at the magnetometer sensor.

Lifetime and Reliability. The nominal orbit life is a minimum of six months. However, since the most important part of the mission occurs in the first three months, the primary design consideration is to achieve a high reliability for the three month's operation, rather than to extend the mission life. As a design goal, the reliability of the four-satellite system for a period of three months is 0.70.

SECTION 3

SUMMARY AND CONCLUSIONS

3.1 STUDY APPROACH

The approach that has been taken in the feasibility study is as follows: The mission objectives were exercised to determine what sort of satellite arrays would be desirable. Then the question was addressed, what are the essential features of the deployment schemes which are required to establish these arrays? The parametric studies of these deployment schemes constituted the major part of the mission analysis work, and then resulted in the specification of certain important system requirements, particularly values for velocity increments and allowable execution errors. These requirements which derive from the deployment scheme together with other mission-related spacecraft requirements, formed the basis for the configuration studies which were done. The basic alternative configuration concepts then were identified. There were two of these, and parallel preliminary design efforts were carried out on both. Subsystem requirements and mechanization were developed for each satellite configuration and for the carrier modules which are associated with each configuration concept. Involved in this was a considerable amount of tradeoff analysis within subsystems, particularly in the areas of communications and attitude control. At the end of the parallel design studies, a detailed comparison was made between the two configuration concepts, and a single preferred configuration selected. In parallel with this, additional mission analysis tasks were proceeding to optimize launch date, and position in orbit of the deployment maneuvers.

3.2 MISSION ANALYSIS

The mission analysis tasks have been divided into three main categories: reference orbit studies, separation studies, and orbit determination predictions. In the reference orbit category, studies were made to establish the relationships between

launch date, ecliptic inclination of the orbit plane, line of apsides location relative to the sun, and perigee height variations. Definition of the perigee variation due to lunar and solar gravitational forces was necessary in order to select a launch date for which the relative positions of the earth, the sun, and the moon are such that subsequent decay in perigee height does not result in an unacceptable level of aerodynamic drag. This requirement results in a tradeoff between the initial orbit relation to the sun (determined by time of day of launch) and initial perigee (injection altitude, which has a strong effect on launch vehicle payload capability). In addition, it is desirable to minimize the inclination of the orbit plane with respect to the ecliptic, which also varies with launch date. An optimization of all of these parameters resulted in choosing an initial orientation of the line of apsides about fifteen degrees from the sun's position, so that the apparent sun vector sweeps through apogee about fifteen days after launch. Three launch windows of a few days' duration each were selected in late January, mid-February, and late February. These choices result in an initial perigee altitude requirement of about 150 n. mi. A drag analysis and an occulation time analysis were then done on this reference orbit; the results of these simulations are given in the report.

A principal task of the separation studies was the generation of parametric satellite array configurations as a function of position in orbit. The parameters which were varied are the true anomaly, the velocity increment magnitude, and velocity increment direction of the separation events. To obtain maximum separation distances in the regions of scientific interest, the analysis showed that the best place to make the separation maneuvers is in the region of apogee. If that is done, separations on the order of 500 km can be obtained with total relative velocity increments of about 10 meters/sec between satellites.

Two methods of separation were extensively investigated. The first of these, called the radial case, makes use of centrifugal forces to supply the separation velocity increments. The four satellites are clustered radially, in a single plane. The launch vehicle imparts a spin to the entire payload at injection, which is near the perigee point of the orbit with the spin axis colinear with the orbital velocity vector. The payload coasts, spin-stabilized, to apogee, where the spin axis again is along the velocity vector. At that point, the four satellites are released simultaneously,

so that they acquire separation velocities in four quadrants, all in a plane perpendicular to the orbital velocity. Subsequent to separation, the invidiaul satellites extend booms for spin stability, erect their spin axes normal to the ecliptic, and spin up to the desired orbital spin rate.

The other deployment method is called the stacked case. The four satellites are stacked longitudinally and employ a carrier module which has attitude and orbit control capability. Following separation from the launch vehicle, the entire payload, which is spinning and has booms extended for stability, is erected so that its spin axis is normal to the orbit plane. At any desired point in the orbit, the two outer satellites are separated, and an axial solid rocket on each satellite is used to impart a velocity increment normal to the orbit plane. The reaction control system of the carrier module is then used to give the remaining two satellites a velocity increment in the orbit plane and normal to the velocity vector. These satellites are then separated as the first two were normal to the orbit plane.

In both of the above concepts, all of the velocity increments are nominally perpendicular to the orbital velocity vector. This is because any component of the increment which is additive (or opposite) to the orbit velocity causes changes in period, and thus secular drift rates between satellites. The principal constraint on execution errors is the need to limit these drift rates; the experiment requires that two satellites be separated by no more than 15,000 km at the end of the six month mission life. Analyses of the propagation of direction errors in the two cases have resulted in the conclusion that a nominal 5 degree pointing accuracy will result in drift rates which will not violate this condition.

It should be noted that both of the concpets, as described herein, result in arrays which, in the absence of errors, remain planar throughout their life. In the stacked configuration concept, however, certain combinations of direction errors result in a degree of three-dimensionality. It is recommended that further studies be made of the statistics of these separation errors and the corresponding effects on array configuration, particularly on the three-dimensional features of the resulting arrays. There are also many methods of establishing intentionally a tetrahedral array with the stacked configuration, but these involve the addition of in-plane velocity increment

capability to individual satellites. In the radial case, this can be done with the existing capability by imparting velocity increments normal to the separation plane to two of the four satellites, prior to erecting their spin axes. The only effect on satellite requirements is a very small additional full requirement, and a pointing accuracy of about 3 degrees, which can be met by the proposed attitude control concept.

The final mission analysis task was the tracking analysis, and the establishment of orbit determination capabilities. The results were that angle tracking of the payload prior to satellite separation is adequate to determine the actual orbit apogee with the precision required for proper sequencing of the separation maneuvers. For the determination of the relative positions of the individual satellites to the desired accuracy, the study showed that determining the position of each individual satellite by RF tracking and then combining the data would be a feasible method. The Goddard range-and-range-rate system (S-band) will be used to accomplish this tracking to the desired accuracy. Simulations have been made of both tracking modes using six appropriate ground stations of the STADAN network, and the results are presented in terms of velocity and position prediction errors, as a function of accumulated tracking time.

3.3 CONFIGURATION STUDIES

The configuration studies which have been done consisted primarily of parallel efforts for the preliminary design of a configuration to implement each of the two separation methods, stacked and radial. Each configuration evolved through a series of iterations of overall satellite shape and general arrangement, and various methods of equipment packaging. Packaging of satellites during ascent and the preliminary design of appropriate mounting and release mechanisms received particular attention. In the stacked case, a major objective was to make the inertia ratios of the entire spinning payload as nearly as possible dynamically stable; however, it was found that in any arrangement it is necessary to deploy the satellite booms to achieve stability. In the radial case, the clustered payload is inherently stable without boom deployment. Extensive work was done on the design of deployable booms and of trusswork adapter structures.

The two configurations which resulted from this work are described in detail in the report. The satellite in each case is essentially a cylinder covered with solar cells, with three single-hinged radial booms. The radial satellite, which is longer and of smaller diameter, also has an axial mast which supports a biconical antenna, and has a band around the center from which sensor viewing angles are provided. In the stacked configuration; the basic cylinder is essentially a skirt, with the equipment platform protruding above it to provide field of view for the sensors and for a strip-array antenna around its circumference. The carrier module for the stacked case is a trusswork structure which contains the attitude and reaction control equipment, and is located between the two pairs of satellites. In the radial case, there is a small structure in the center of the cluster which serves to hold the four satellites together and then to release them simultaneously on command; it has no maneuvering capability. Comprehensive weight estimates were developed for each configuration. The results, including an assumed 12-pound science load to each satellite, were 266 pounds total payload for the radial case and 302 pounds for the stacked case.

Subsystem tradeoff analyses were done and subsystem functional designs were developed for each configuration. For the telecommunications subsystem, there is no difference between the two configurations, except for requirements during the ascent and deployment sequence. The orbital system serves to record ten hours of scientific data per orbit, and then to play it back and transmit it to a ground station on command. Telemetry of a small amount of engineering status information also is provided. Studies of the relation between satellite separations and ground antenna coverage capabilities revealed that readout of the four satellites must be sequential rather than simultaneous. This, together with an assumed single ground station coverage allocation of three hours per orbit resulted in specification of a nominal readout time of 30 minutes per satellite. A solid-state S-band transponder is used for data transmission, PCM command reception, and range-and-range-rate tracking. For a two-watt output transmitter, which can be operated by the solar power system without any battery capacity, a total capacity of 1.3×10^7 bits per orbit and a corresponding experiment information rate of 360 bps are obtained. It is intended to use the Goddard designed six pound tape recorder, which has a storage capacity of about 4×10^7 bits. To fully utilize this capacity, a six-

watt output transmitter would be used and a small rechargeable battery would supplement the solar array power in this high-rate mode for 30 minutes per orbit. This will provide capability for experiment data rates of about 1100 bps.

The altitude control studies addressed the major areas of defining the initial orientation and control requirements, developing orientation sequences and operational modes for the two configuration concepts, and specifying subsystem functional design and equipment requirements to accomplish these procedures. First, the orbital disturbance torque environment was evaluated, and it was determined that, for orbital spin axis alignment accuracy requirements on the order of five degrees, an initial orientation will be sufficient, i. e., no updating of attitude throughout the life of the mission is required. Therefore in the stacked configuration, where initial orientation of the entire payload is accomplished prior to satellite separation by the carrier module, the satellites will contain no attitude control subsystem. In the radial case, initial orientation is done by individual satellite, and therefore this capability will be available throughout the mission, should it be desired. For the stacked case, a comparative study was made of a self-contained system for orientation during the first half orbit vs a ground-commanded system which requires delaying satellite separation until the second apogee, with the result that the ground-commanded system is recommended. The orientation of the radial satellites also is by ground command. Preliminary subsystem designs were developed for each configuration. In the stacked case, this involved a single system on the carrier, consisting of infrared earth horizon sensors and narrow angle sun sensors for reference and pulse synchronization, and a monopropellant hydrazine system for reaction control. In the radial case, there is a system on each satellite; a simpler albedo sensor can be used in place of IR sensors. Essentially the same sun-sensor network is needed, and a simpler and much smaller ammonia vapor reaction control system is used, mounted on one of the booms. Error analyses of the operation of these systems showed that the pointing accuracy requirements of about three degrees could be met.

A satellite electrical power subsystem preliminary design also was done. The design is conventional for a solar array-powered, regulated direct current bus, including a small secondary battery. With the current solar array configurations,

total conditioned load power available at the end of six months is 22.8 watts in both cases. The radial configuration has solar array growth potential to about 30 watts, while the stacked configuration is now near its limit, and could provide 25 watts maximum.

3.4 SYSTEM STUDIES

Certain tradeoff studies of an overall nature were necessary in order to define the system configuration. The first of these was the selection of the preferred launch vehicle from the Thor-Delta family. This selection was made on the basis of payload capability, injection accuracy, projected vehicle availability, and comparative costs. The principal contenders were the DSV-3E and DSV-3J vehicles; based on a comfortable payload margin and growth potential at a modest incremental cost, the DSV-3J was selected. Also, a cursory examination was made of the applicability of the Burner II upper stage to this mission. This assumes the use of the DSV-3L (long-tank Thor) booster (or an Atlas booster). The conclusion was that this is feasible, and should be further evaluated as an alternative approach.

Studies were made to establish detailed sequences of operations required during ascent and coast and during the extended orbital operations, and identify the resultant equipment requirements on the satellites and on the carrier modules. It was found that for both configurations, it is not feasible to use the satellite orbital S-band antennas prior to satellite separation. Therefore, a separate VHF beacon and command receiver were included in the carrier module in each case, to allow tracking, command control, and, in the case of the stacked configuration, some telemetry transmission during the coast phase. Orbital operations were broken into four modes, and power requirement summaries made for each mode. These are record, playback, standby, and a real time transmission at reduced data rate for backup mode. Selection of bit rate during the playback mode determines the need for battery capacity to support orbit operations. Inclusion of a secondary battery of under two pounds allows for operation of the data link in a high-rate, 6 watt output mode, as well as standby operation during eclipse periods of up to one hour. For longer eclipse periods which, depending on launch date, might occur during the later months of the mission, the satellite will have the capability to turn itself

completely off after one hour, and to be reactivated when it emerges into the sunlight.

A study was made of possible spin axis orientations. In the stacked configuration, the spin axis is constrained by the separation method to be normal to the orbit plane. In the radial configuration, analysis showed that the increase in the antenna beamwidth requirement to maintain earth coverage due to aligning normal to the ecliptic plane is acceptable, and therefore this experimentally desirable orientation is feasible.

Finally, a detailed comparison of the two alternative configuration concepts was made on the basis of salient features of design, reliability, operational considerations, and experiment suitability. The result of this comparison was that the radial configuration is the lighter, simpler, and more reliable of the two concepts, and offers at least equivalent mission value, and therefore should be the recommended concept.

3.5 CONCLUSIONS

The conclusions resulting from the study are as follows:

1. Accomplishment of the proposed mission is feasible, based on satellite technology either existing now or projected for the time period of interest, and using a standard launch vehicle of the Thor-Delta series.

2. The most promising system concept is one in which four identical satellites are clustered in a plane during ascent, and are simultaneously released near apogee, where the spin axis is colinear with the velocity vector, and deployed by centrifugal force.

3. Based on preliminary design of the radial configuration concept the following fundamental system parameters and spacecraft requirements have been established:

- Separation velocity increment magnitudes of approximately 10 meters/sec (between satellites) are required to obtain the desired initial separations in the region of interest on the order of 500 km.

- The radial deployment concept can provide the required velocity increments with centrifugal force alone, based on angular momentum capabilities of the standard Delta spin table.

- The radial deployment concept requires a spin axis pointing accuracy of the payload prior to satellite separation of about 3 degrees, which can be provided. An orbital pointing accuracy of about 5 degrees is adequate for the experiments, provided the actual attitude is accurately known. The attitude control system described in this report will satisfy these requirements.

- The reaction control system can be used to give two of the satellites an additional velocity increment, should it be desired to establish a particular three-dimensional array.

- A total capacity for experiment information of approximately 4×10^7 bits of data can be collected per satellite per orbit. An S-band data link using a solid-state transmitter of 6 watts output power will provide the necessary communications capability.

4. Based on the results of this feasibility study, it is recommended that further investigation be made of the following items:

   a. More detailed array analysis to establish the effect of separation errors and orbit perturbations on the initial formation of the array and the change in that formation with time.

   b. A more detailed investigation of secular orbit determination problems including all secondary orbit perturbation effects

of station location errors and measurement biases.

c. Additional system trade-off studies to define in more detail optimum separation and attitude control techniques for the various alternatives.

d. A more detailed examination of the operational problems and communications requirements for the coast phase prior to satellite separations.

e. A more extensive examination of the application of the Burner II stage to this mission, including a detailed definition of the required maneuver sequence and flight system modification requirements and a comprehensive cost analysis.

SECTION 4

ORBIT ANALYSIS

4.1 REFERENCE ORBIT

The launch analysis was performed to determine the best possible launch window for the Ames project. The mission calls for the injection of a multiple satellite package into a highly elliptical orbit, using a booster from the Thor-Delta series. The apogee radius for the orbit was set at twenty earth radii, with a perigee altitude of 318.76 km. The general information on the orbit, as well as the nominal injection conditions used to achieve this orbit, is presented below:

- Radius = 6696.959 km
- Latitude - 14.2 deb
- Longitude - 328.0 deg
- Inertial velocity - 10.63615 km/sec
- Inertial flight path angle = 2.199 deg
- Inertial azimuth = 114.984 deg
- Period - $1^{d}\ 23^{h}\ 48^{m}$

Figures 4.1-1 through 4.1-3 are concerned with this nominal orbit and the approximate times at which several of the critical events occur. Figure 4.1-1 is a plot of true anomaly and radial distance as a function of time and suggests the approximate shape of the orbit. Figure 4.1-2 presents in greater detail the orbit in the neighborhood of perigee. Figure 4.1-3 shows the subsatellite points on the first orbit about the earth. The period of the orbit is so close to two days that the vehicle will pass over nearly the same points for the first few weeks.

Several orbital requirements must be considered when choosing the launch window. One is that the inclination of the orbit plane with respect to the ecliptic plane should be minimized. The other is that the line of apsidies should lead the sun by an angle of up to 26 degrees. Figure 4.1-4 indicates that to put the inclination in the desired

* The injection conditions are based on a specific Pioneer trajectory, which is representative of the type of ascent which will be used for this mission. The perigee altitude of 172 nautical miles represents an upper bound; launch date optimization will result in the selection of a perigee altitude of about 150 nautical miles.

region, the launch date must be picked in late January or early February. These dates are independent of year since the inclination repeats itself from year to year.

Once the approximate time of launch is determined, it becomes a question of what effect the lunar-solar perturbation forces have on the perigee altitude. The 31 January, 1969 date was chosen as a possible launch date and the complete set of equations of motion were integrated for 16 orbits (about a month) to see how perigee altitude is affected by these forces. If the line of apsidies lies ahead of the sun by 26 degrees, the perigee altitude drops far below the minimum allowable altitude. However, it is noted that if injection had occured a little later in time (around four days), the perigee altitude would have been at the bottom of the ripple and would have started up instead of down, thus keeping the minimum perigee altitude above the 120 n. mi. limit.

It may also be noted from Figure 4.1-5 that the various curves of 0, 13, and 26 degrees seem to be of the same form, but shifted to the right for larger lead angles. If the orbit is integrated for a longer period of time, as was done with the results presented in Figure 4.1-6, it is noted that the perigee altitude curve is composed of two parts: an oscillation with a period of half a year due to the sun's apparent motion about the earth, and a short period oscillation due to the moon's motion. The period of the rapid oscillation is nearly 14 days.

An attempt was then made to separate the sun's effect from that of the moon. The sun's effect is best represented by the lines passing between the sun-moon oscillations in Figure 4.1-6. These curves are very similar and are shifted about two days to the right for each degree lead of the sun by the line of apsides. The best place to start on this curve is at the minimum point, which corresponds to pointing directly at the sun. However, to lead the sun by some angle, the corresponding perigee altitude loss must be accepted. If the moon's position is picked properly this loss will not be great. To lead the sun by much more than 26 degrees is not advisable. To assure this, the nominal launch window was chosen to be 13 degrees ahead of the sun. To show that the perigee altitude never drops below its first minimum, the equations were integrated for 256 days and the perigee altitude plotted in Figure 4.1-7.

The most important consideration is to inject the satellites when the moon is in its most favorable position. To determine this, the positions of the sun and the moon were plotted on polar paper with the probe at perigee. By comparing the points at the bottom of the lunar perturbation curve with their positions in Figure 4.1-8, it can be seen the best time to inject is when the moon lies ahead of the line of apsides by 0 to 45 degrees. This will always put the perigee altitude curve on the upswing portion of the lunar curve. Figure 4.1-9 shows three possible launch windows for 1969 and 1971 in which this condition is satisfied.

The above analysis did not include drag. The program was then run with drag included, and it was found that the perigee altitude was hardly affected by the drag. However, the drag did tend to decrease the energy on each pass and thus caused the apogee altitude to decrease. Figure 4.1-10 presents this effect in terms of the change in period as a function of orbit number. Again, the effect is very small.

Figure 4.1-11 is a plot of occultation time (the time the vehicle is occulted from the sun by the earth) as a function of time from injection into an orbit whose line of apsides leads the sun by 13 degrees and which has an inclination of 6.6 degrees with respect to the ecliptic plane. The date of injection was 31 January, 1971. The period of least occultation occurs when the right ascension of the sun is 180 degrees ahead of the right ascension of the probe at perigee and the maximum occurs when the sun is in the same position with respect to the right ascension of the probe at apogee. This injection inclination corresponds to maximum occultation times and any increase in inclination will tend to reduce the occultation times.

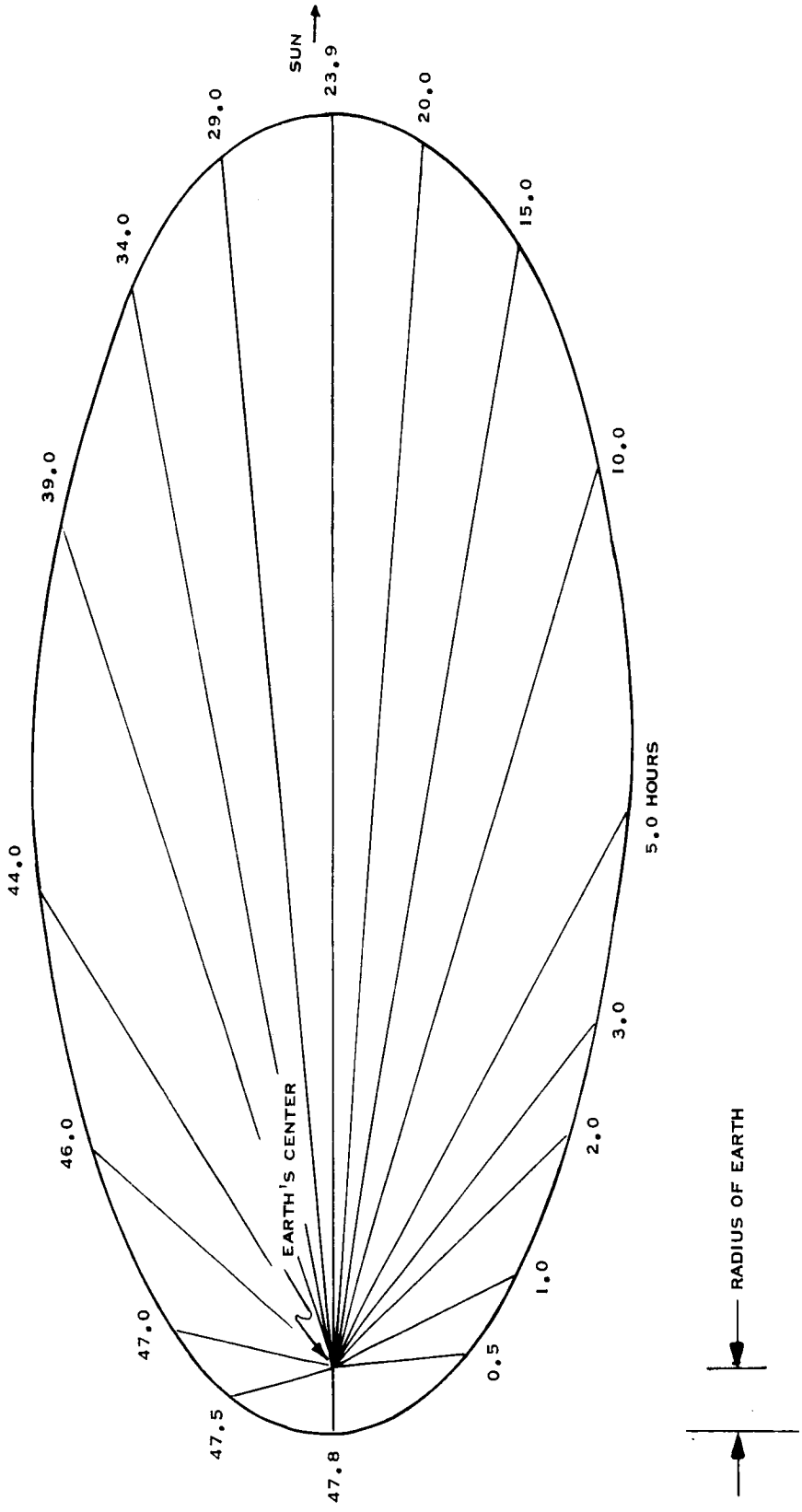

Figure 4.1-1 Shape of the Orbit

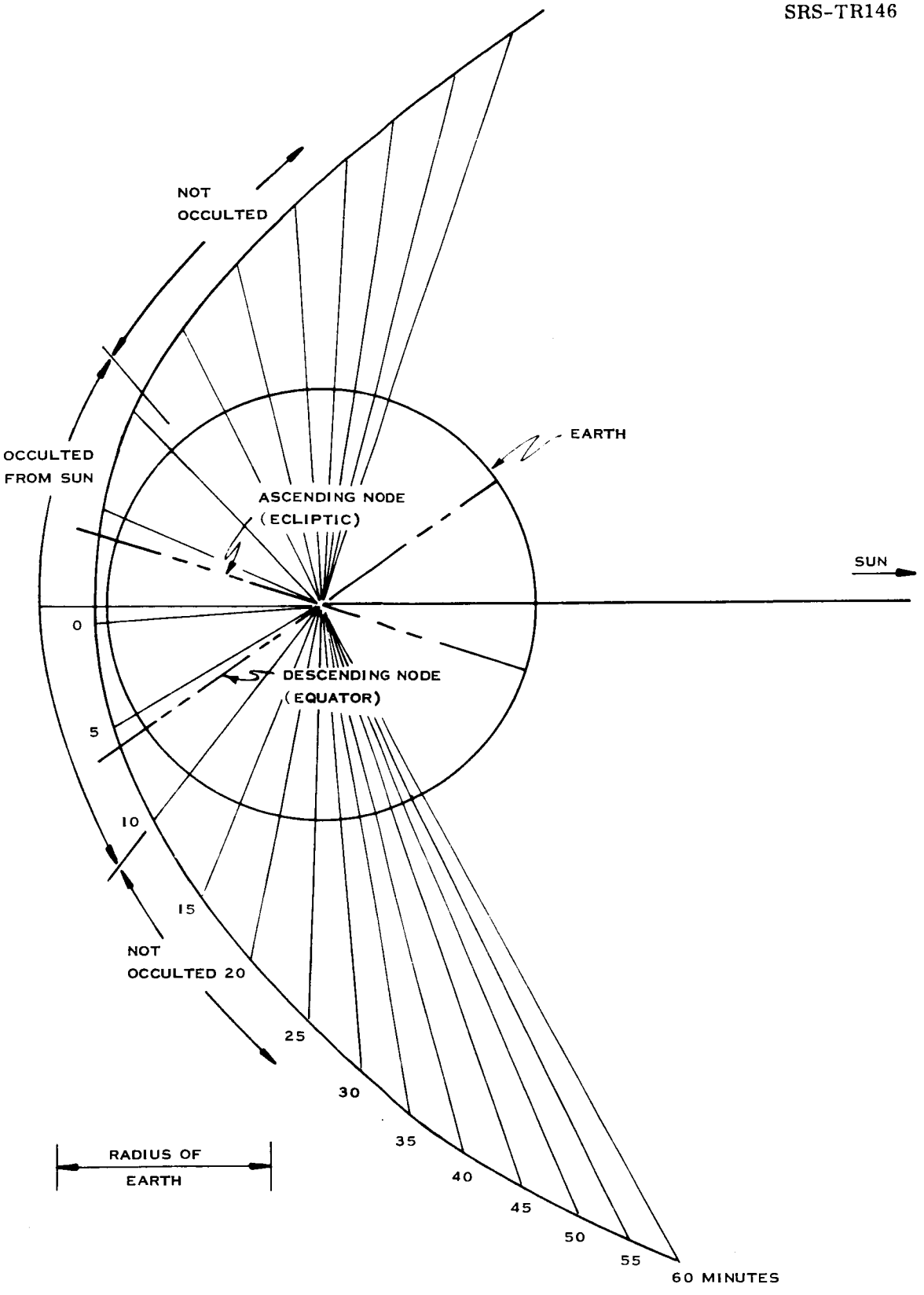

Figure 4.1-2 Orbit Characteristics Near Perigee

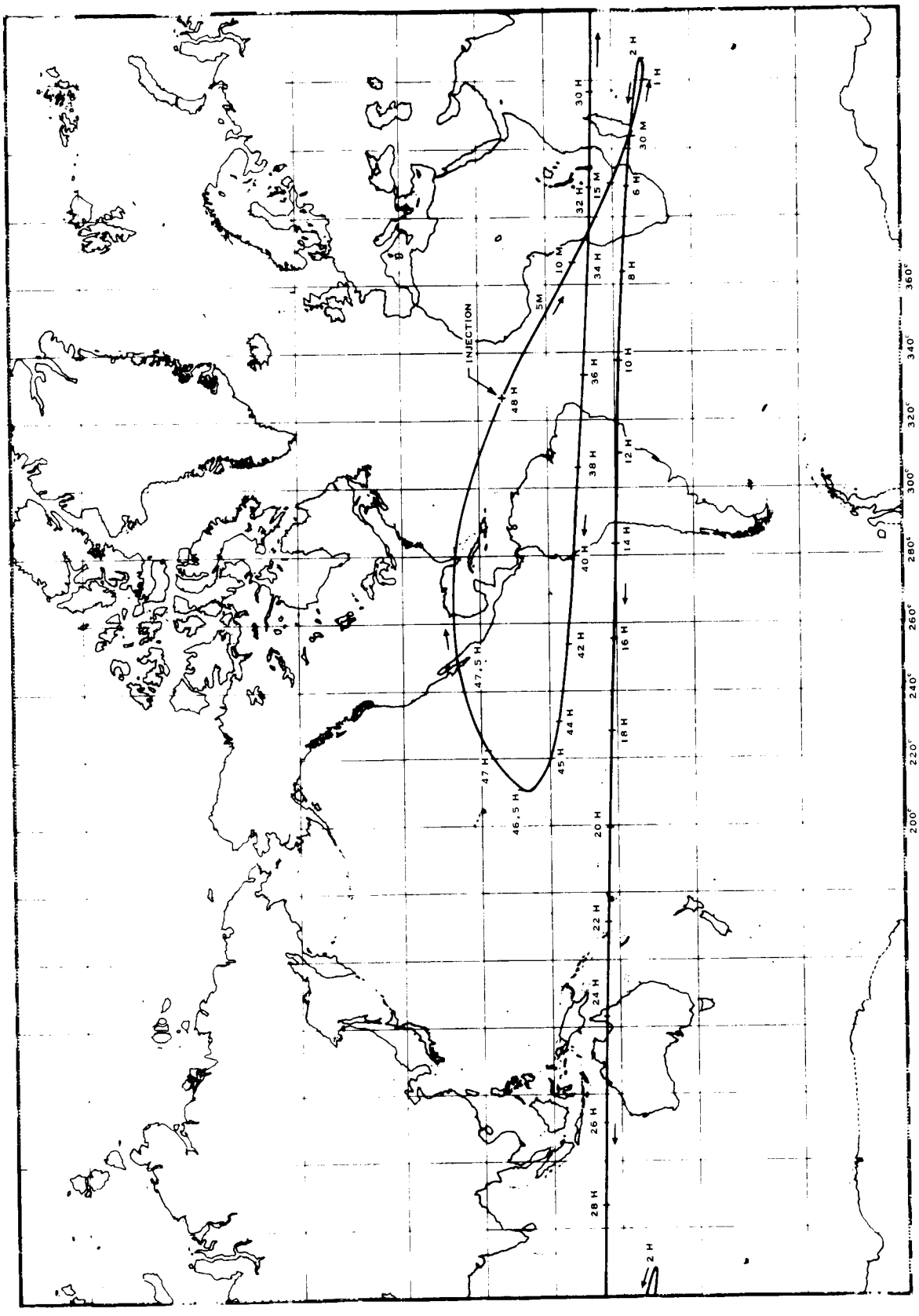

Figure 4.1-3 Subsatellite Points on First Orbit

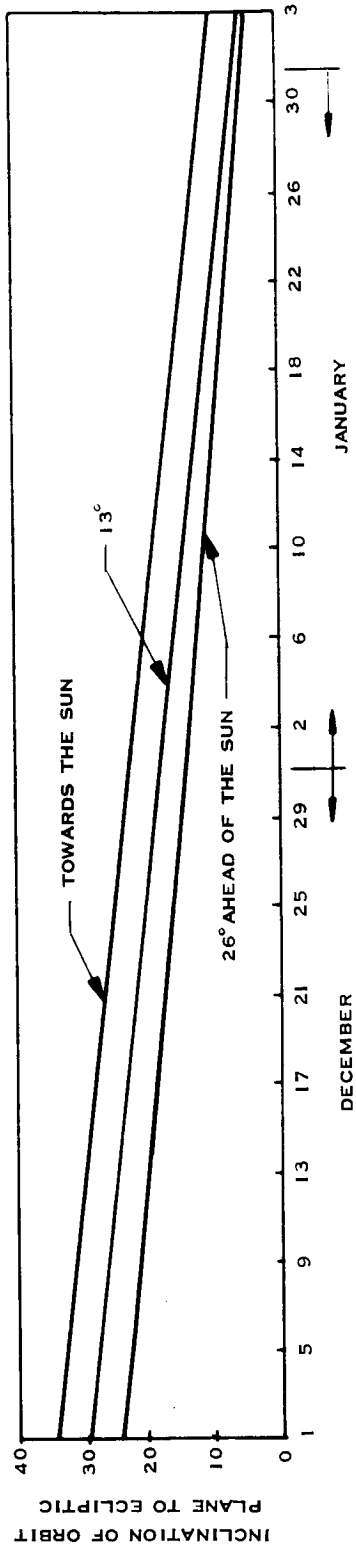

Figure 4.1-4 Inclination of Orbit Plane to Ecliptic v.s. Launch Date

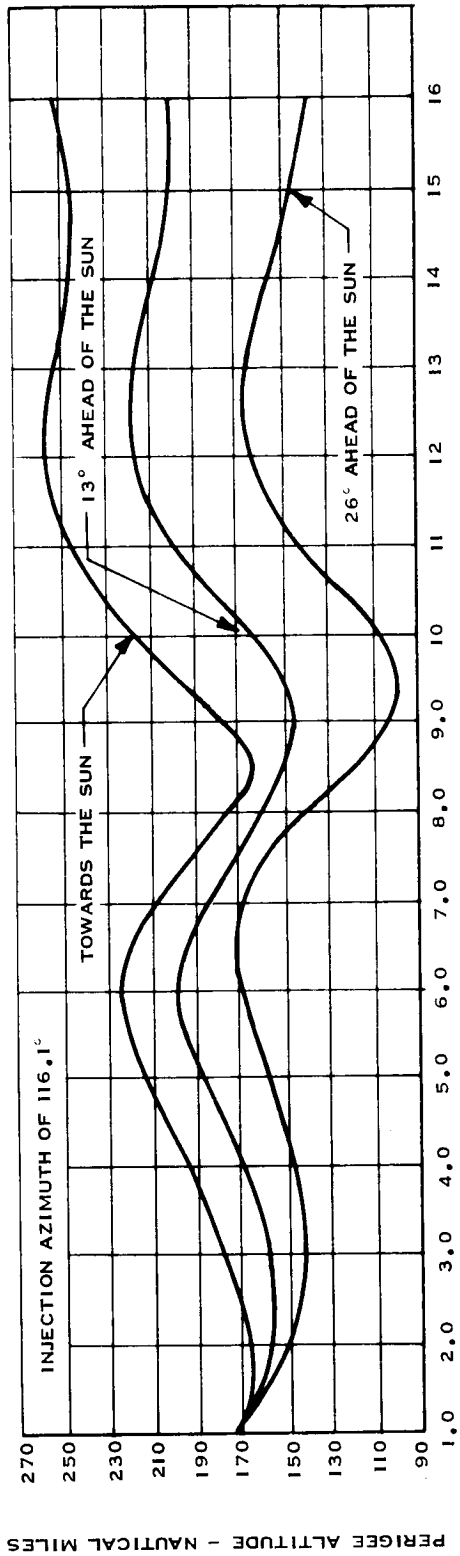

Figure 4.1-5 Perigee Altitude v.s. Orbit Number

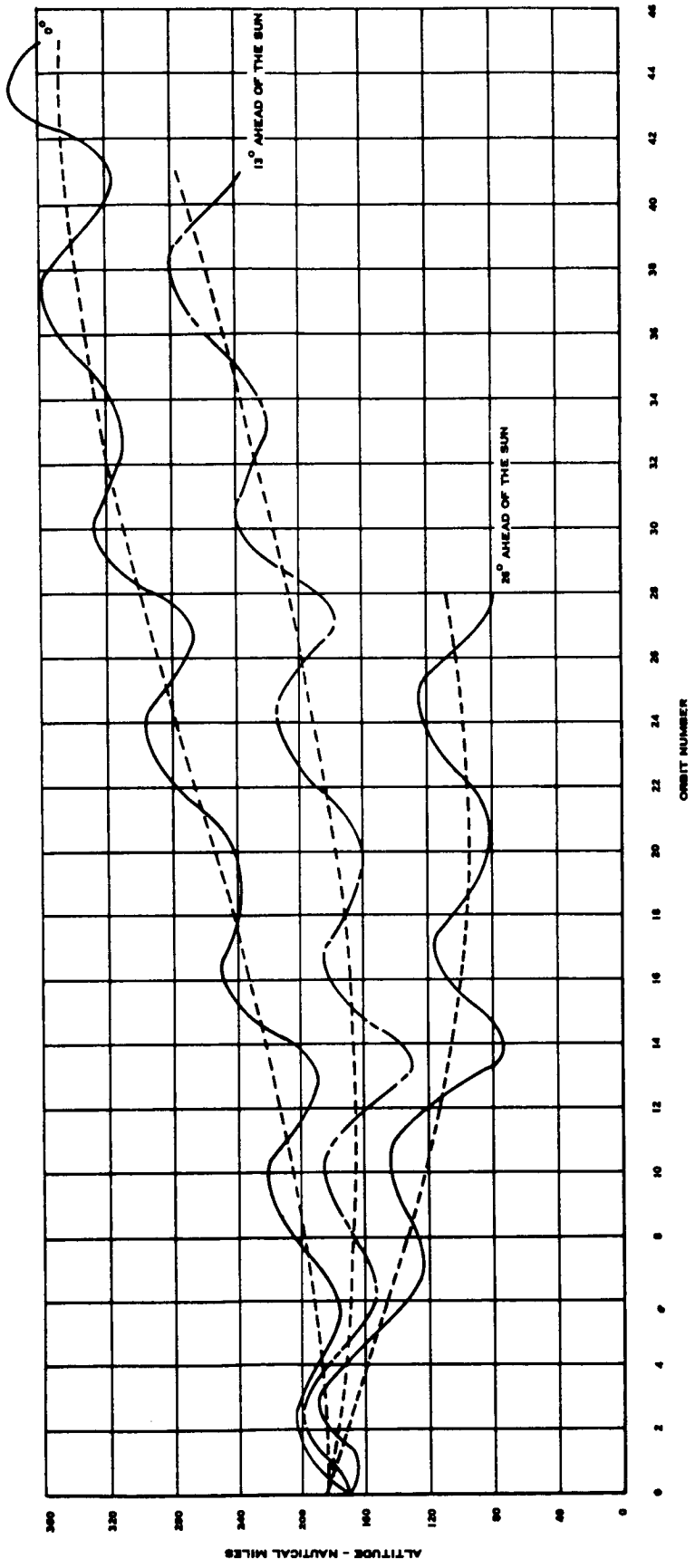

Figure 4.1-6 Perigee Altitude vs Orbit Number for 46 Orbits

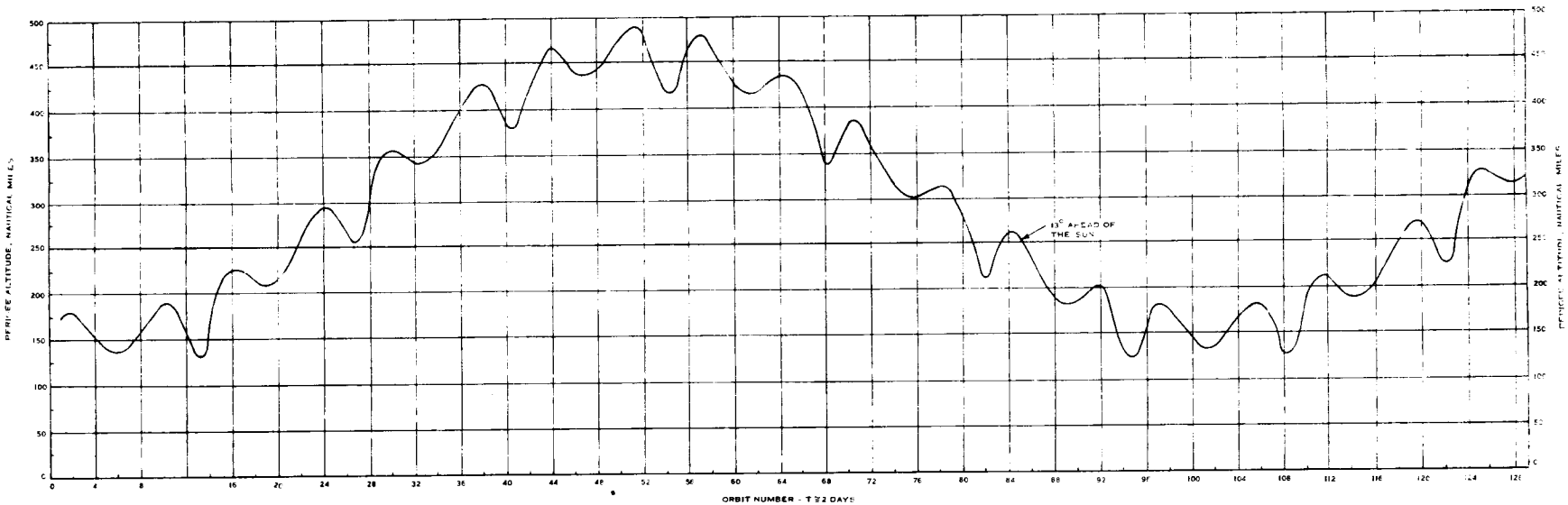

Figure 4.1-7 Perigee Altitude vs Orbit Number

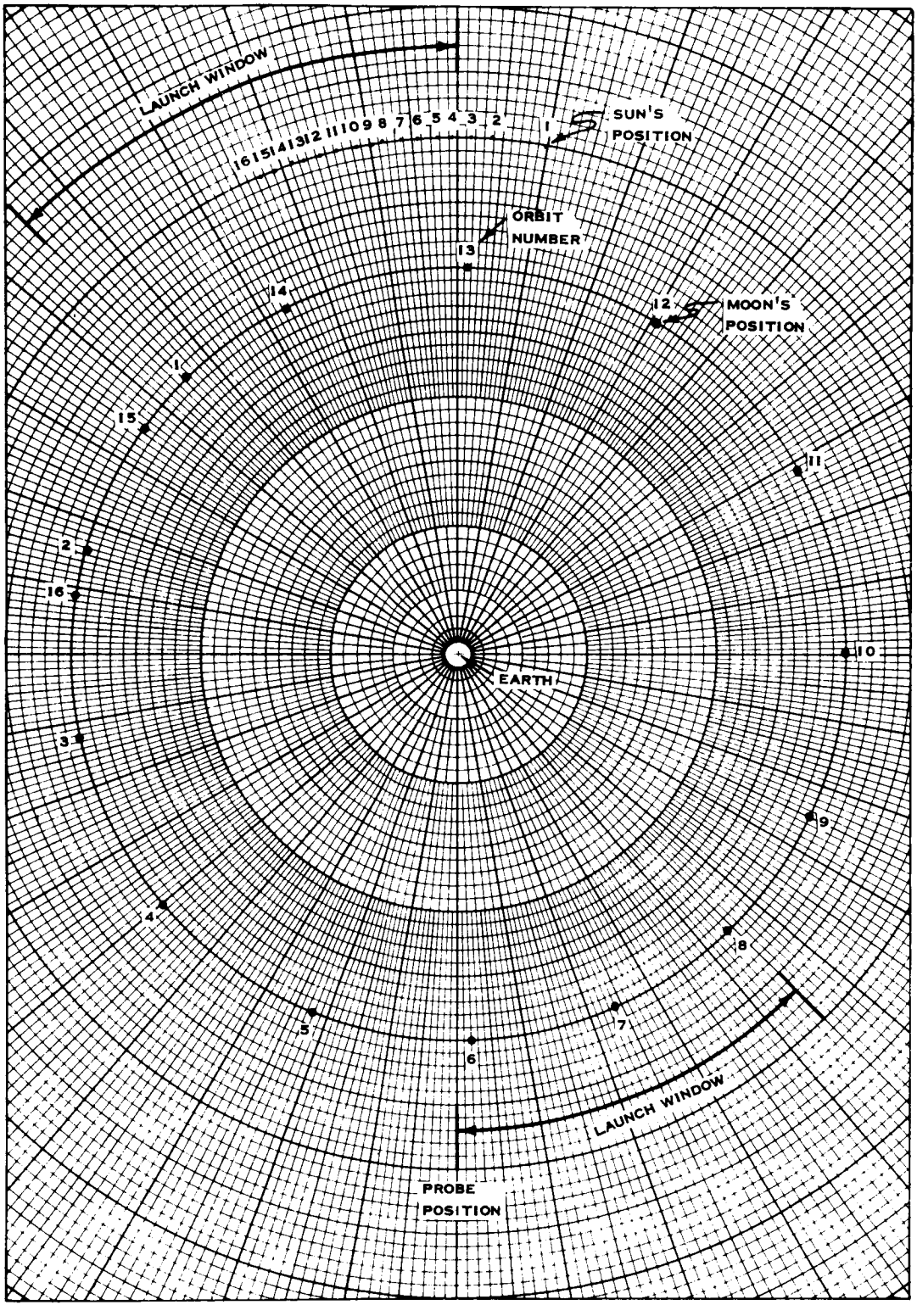

Figure 4.1-8 Lunar-Solar Positions with Respect to Probe at Perigee

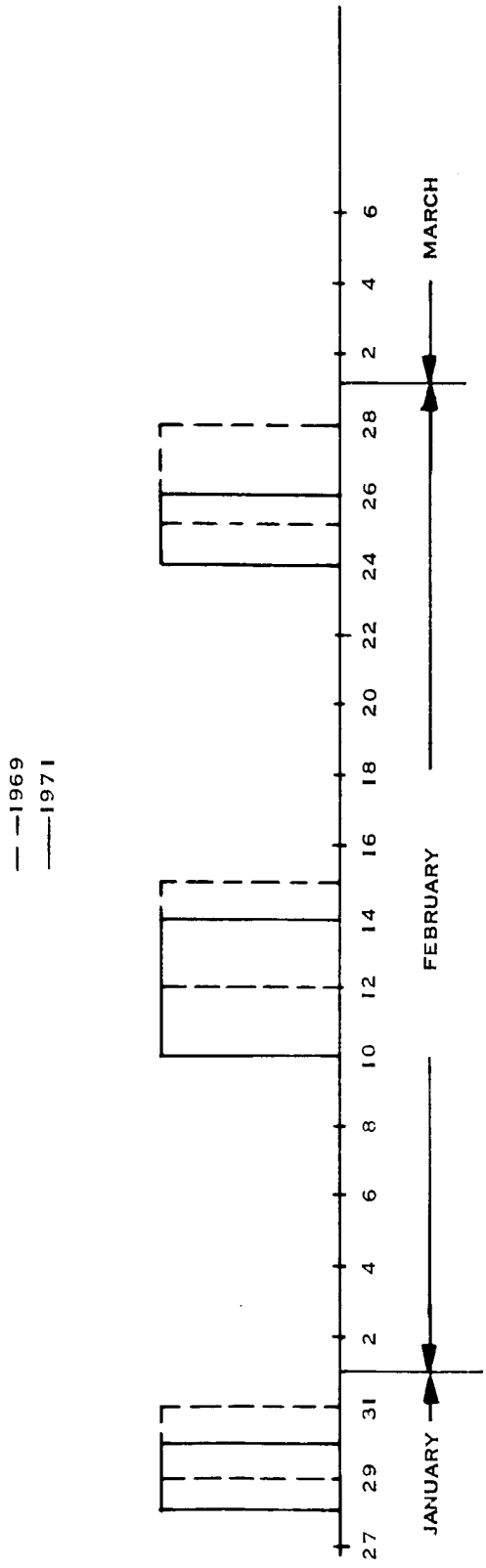

Figure 4.1-9 Possible Launch Windows for Launching in 1969 and 1971

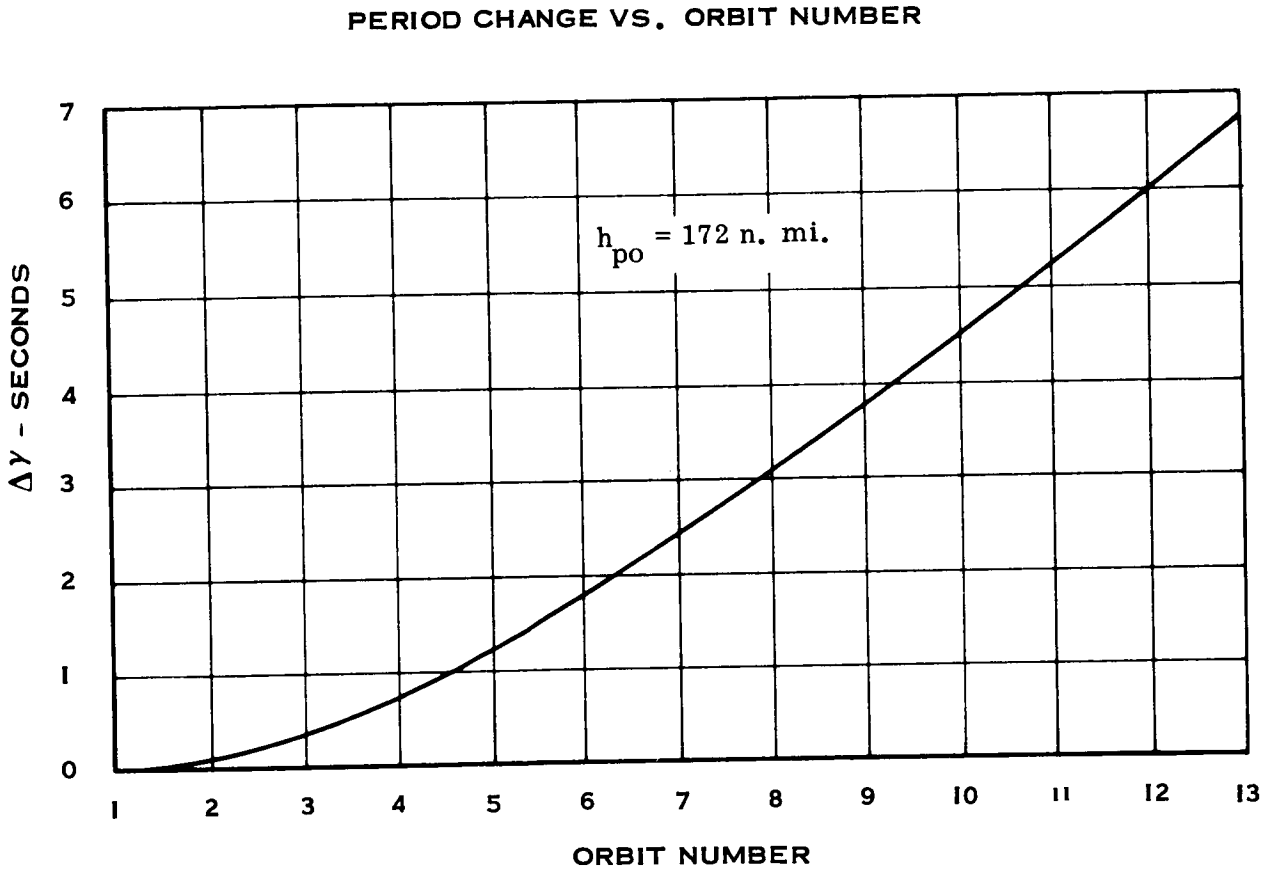

Figure 4.1-10 Period Change vs Orbit Number

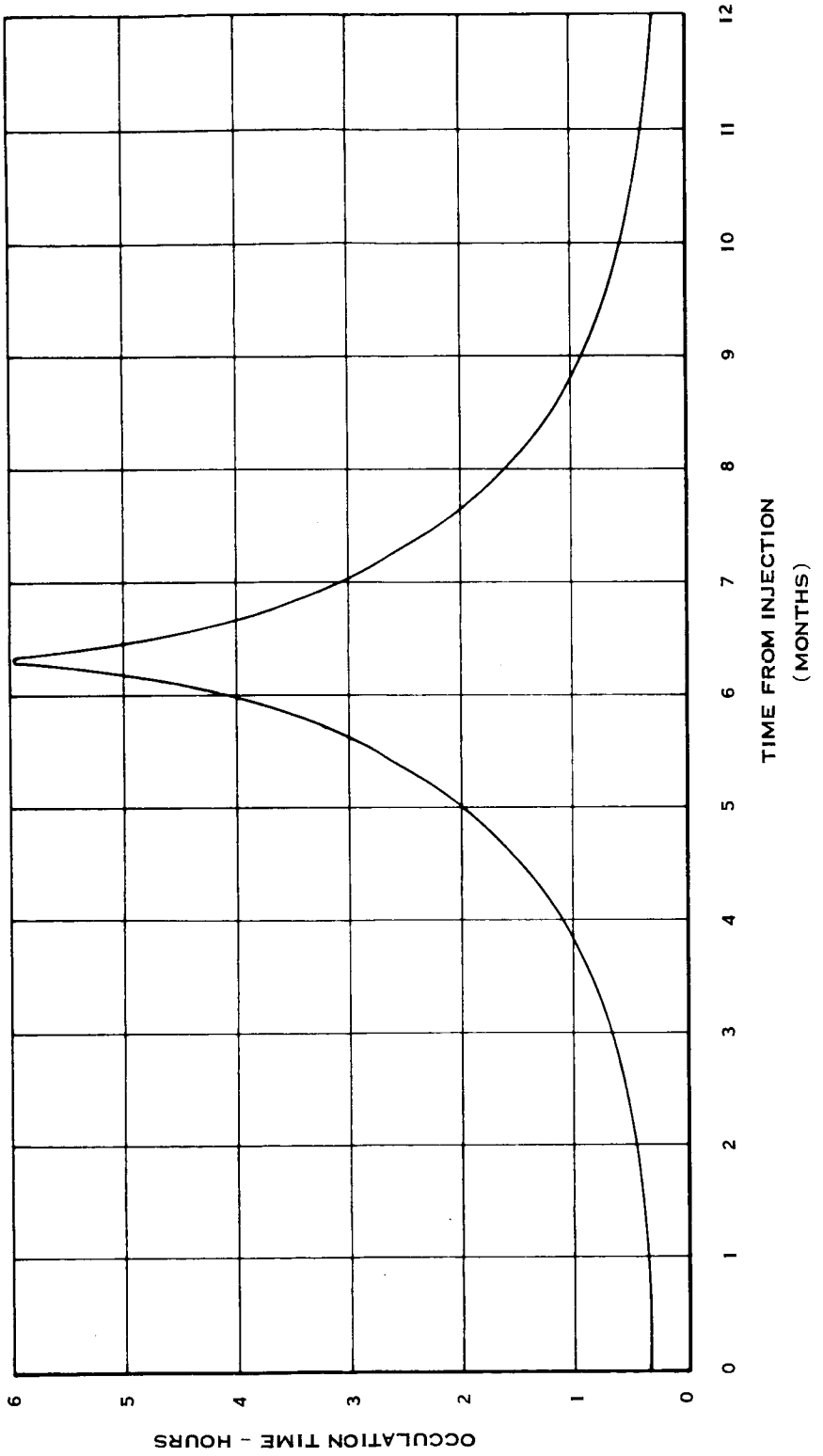

Figure 4.1-11 Occultation Time as a Function of Time from Injection

4.2 SATELLITE DEPLOYMENT

4.2.1 Introduction

The object is to deploy four satellites in an array to facilitate a study of the solar wind, the magnetosheath, and the magnetosphere. The satellites must be arranged so that time and space gradients can be computed from the observations. The region of principal interest is ten to sixteen earth radii from the center of earth. In this region a minimum separation of 500 km between satellites is required to obtain the desired data. Also, the distance between any two satellites must not exceed 15,000 km.

The satellites are deployed from a highly eccentric orbit with a perigee height of approximately 100 nm (185 km) and an apogee height of approximately 19 earth radii (120,000 km). The deployment is implemented by imparting a small relative velocity (ΔV) to the satellites at appropriate points along the orbit.

The first step in determining optimum deployment conditions was a parametric study of satellite separation. The parameters examined were the separation true anomaly, and the magnitude and direction of ΔV. The effect of these parameters on the subsequent motion of the satellites was studied in detail. The position of the satellite relative to the nominal orbit was determined as a function of the nominal true anomaly, as well as the change in the orbit parameters.

Some of the main results of the study are discussed briefly in the following. For a detailed discussion of these results, the reader is referred to the body of this report.

It was found that the effect of ΔV could be studied most effectively in terms of its components along (or opposed to) the velocity vector of the satellite; normal to the velocity vector and also normal to the orbit plane (up or down); and finally normal to the velocity vector but in the orbit plane. See Figure 4.2-1. A ΔV applied normal to the orbit has the effect of slightly rotating the orbit about the line from the satellite to the center of earth, that is, the perturbed satellite oscillates above and

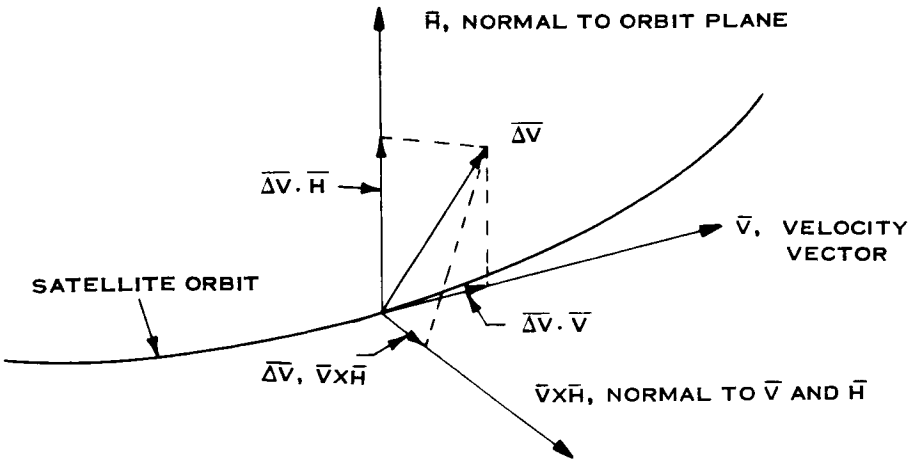

Figure 4.2-1 Velocity Increment, ΔV, Resolved Into Components

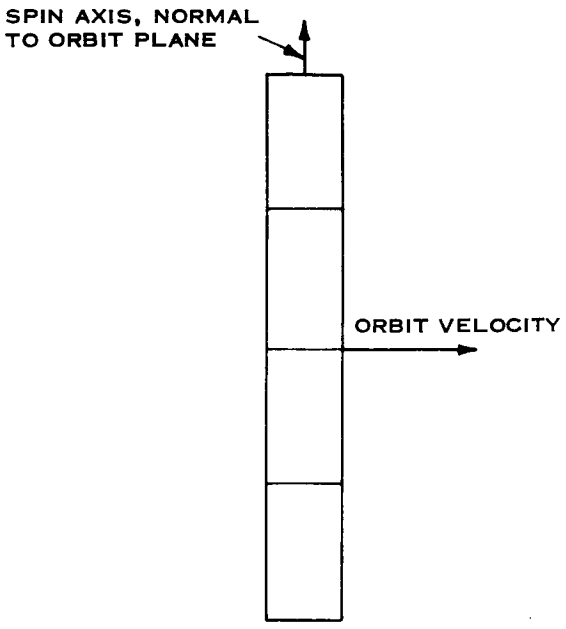

Figure 4.2-2 Stacked Array

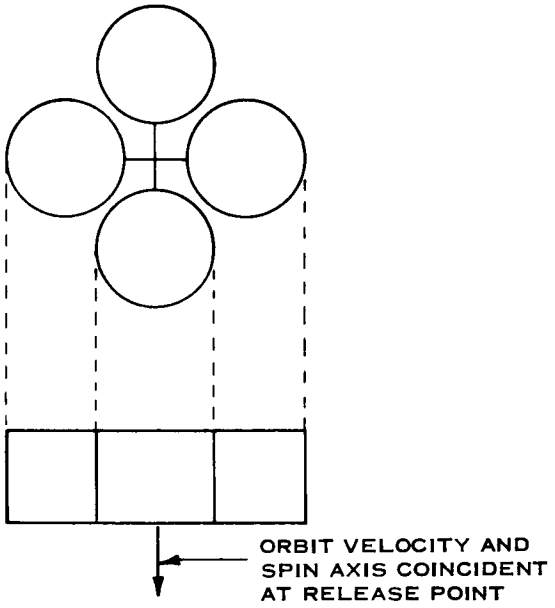

Figure 4.2-3 Radial Array

below the nominal position with the same period as the orbital period. A ΔV applied normal to the velocity vector and in the plane of the orbit may be directed either in (along $\bar{H}X\bar{V}$) or out (along $\bar{V}X\bar{H}$). In-plane maneuvers cause small changes in the shape and orientation of the orbit. The orbit may be rotated either clockwise or counter-clockwise depending upon whether the maneuver is "in" or "out" and also upon the true anomaly at which the maneuver is made. It was found that the most desirable separation points are in the neighborhood of apogee, 175 to 185 degrees true anomaly. In this region, in-plane "in" maneuvers cause the orbit to rotate clockwise about earth, and "out" maneuvers cause the orbit to rotate counter-clockwise. The magnitude of these rotations is small compared to other effects. The main significance of the rotation is the phase shift introduced, i. e., apogee occurs at a slightly different time, hence the satellite in the perturbed orbit tends to lead or lag the nominal position. The separation between satellites is due principally to this effect. Clockwise rotations cause the perturbed satellite to lead the nominal position, while counter-clockwise rotations cause the perturbed position to lag the nominal position.

A ΔV along (or opposed to) the velocity causes the orbit to increase (or decrease) in size and hence the orbital period increases (or decreases). If the orbital period of two satellites differs, their relative positions are not periodic, but change with every orbit. Thus, it is generally undesirable to have a component of ΔV along the velocity vector. It is this secular drift that tends to cause the satellites to drift apart and eventually exceed the operating range. To maintain a useable array for the lifetime of the experiment it has been assumed that the ΔV direction is ± 3 degrees of being normal to the velocity vector. This is a reasonable value to achieve, and results in dispersions at the end of life that are within the 15,000 km limit.

The magnitude of the velocity increment(s) was chosen to give an initial separation of 500 km when the satellites are at about twelve earth radii. The values may be readily scaled since the relation between ΔV and separation is linear, where ΔV is much smaller than V.

Two configurations are considered, both of which result in satisfactory arrays. One configuration, referred to as the "stacked" configuration consists of four satellites stacked one on top of another (Figure 4.2-2.) The other configuration, called the "radial" configuration, consists of four satellites symmetrically arranged in a plane normal to the spin axis of the carrier so that when released they have a ΔV normal to the velocity vector. (See Figure 4.2-3.)

The stacked array is deployed by a series of maneuvers executed at predetermined points on the orbit. These maneuvers result in a planar array with a satellite separation of 100 to 500 Km in the region of interest. Small errors in directing ΔV (3 degrees or less) do not greatly effect the initial orientation of the array. Errors in directing ΔV, however, are the prime source of array decay.

The radial array is deployed by simultaneously releasing all four satellites. This must be done at a time when the spin axis and the orbit velocity vector are within 3 degrees of each other to ensure that the ΔV components along V will be small. A non-planar array then can be obtained by giving two of the satellites an additional velocity impulse. The spin axis and the velocity vector are nominally aligned at perigee and apogee. Separation is at apogee since this is point that is most efficient and least sensitive to direction errors.

Both modes result in satisfactory arrays; however, the sequence of positioning events is simpler for the radial configuration. The resulting array in either case tends to become elongated and unsymmetrical over the lifetime of the mission if stationkeeping is not performed.

4.2.2 Theory

The analysis is based on elliptic orbits, therefore it will be useful to give several definitions and formulas which will be used in the derivations to follow.

Given the radius at apogee, r_a, and the radius at perigee, r_p, the semi-major axis, a, is given by

$$a = (r_a + r_p)/2 \tag{1}$$

Perigee is the point of closest approach to and apogee is the point of greatest excursion from the earth.

The eccentricity, ϵ, of the orbit is given by

$$\epsilon = 1 - {}^{r_p}/_{a} \tag{2}$$

The velocity, v, at a radius, r, from the central body center is given by

$$v^2 = \mu \left(\frac{2}{r} - \frac{1}{a} \right) \tag{3}$$

where μ is the gravitational constant associated with the central body. The semi-latus rectum, p, is given by

$$p = a(1 - \epsilon^2) \tag{4}$$

The period, τ, of the orbit is given by

$$\tau = 2\pi\sqrt{a^3/\mu} \tag{5}$$

The familiar equation of the ellipse in polar form is

$$r = \frac{p}{1 + \epsilon \cos \theta} \tag{6}$$

where the angle θ, called true anomaly, is measured from the radius of perigee.

To get θ as a function of time, it is convenient to introduce the eccentric anomaly, E. The eccentric anomaly is related to the true anomaly by the relation

$$\tan \frac{\theta}{2} = \sqrt{\frac{1 + \epsilon}{1 - \epsilon}} \tan \frac{E}{2} \tag{7}$$

and eccentric anomaly is related to the time since perigee passage, t, by the equation

$$E - \epsilon \sin E = nt \tag{8}$$

where $n = 2\pi/\tau$ is the mean motion. Equation (8), known as Kepler's equation, is transcendental, hence not solvable by algebraic means. With today's digital computers, however, numerical solutions are readily obtained by iterative means. Another important quantity to be defined is the path angle ϕ. It is the acute angle between the velocity vector and the normal to the radius vector. The path angle may be computed from the relation

$$\tan \phi = \frac{\epsilon \sin \theta}{1 + \epsilon \cos \theta} \tag{9}$$

It is convenient to establish a cartesian co-ordinate system and introduce vector notation. Let the first axis be a unit vector $\hat{R}_{ap}$ directed along the radius vector at apogee; let the second axis be a unit vector $\hat{V}_{ap}$ directed along the velocity vector at apogee; and let the third axis be a unit vector $\hat{H}_{ap}$ directed along the angular momentum vector and completing the right-handed orthogonal co-ordinate system.

See Figure 4.2-4. In this co-ordinate system, the radius vector $\bar{R}$ and the velocity vector $\bar{V}$ are given by

$$\bar{R} = -r \left(\cos \theta \hat{R}_{ap} + \sin \theta \hat{V}_{ap}\right) \tag{10}$$

$$\text{and} \quad \bar{V} = V \left[\sin (\theta - \phi) \hat{R}_{ap} - \cos (\theta - \phi) \hat{V}_{ap}\right]$$

Several formulas are given below showing the effect of varying the velocity. The formulas may be readily derived by differentiating the defining equations and making appropriate substitutions.

$$\delta a = \frac{2a^2}{\mu} (\bar{V} \cdot \bar{\delta V}) \tag{11}$$

$$\delta \tau = \frac{3a\tau}{\mu} (\bar{V} \cdot \bar{\delta V}) \tag{12}$$

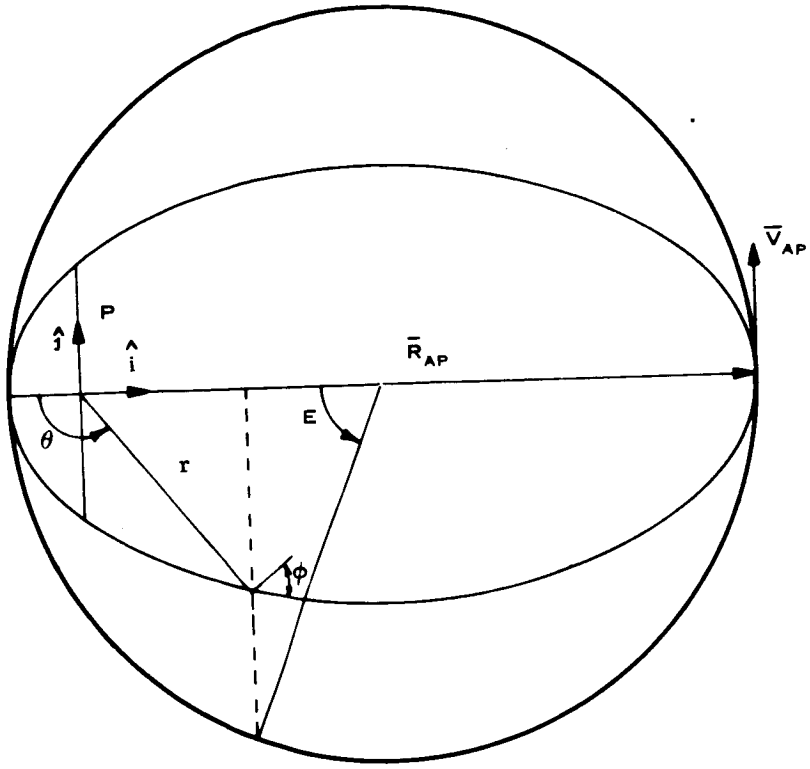

Figure 4.2-4 Geometry of Ellipse

$$\delta\tau = \frac{(r_p r_a - r^2)\ (\bar{V} \cdot \delta\bar{V}) + (\bar{R} \cdot \bar{V})\ (\bar{R} \cdot \delta\bar{V})}{\mu\ \epsilon\ a} \tag{13}$$

$$\delta p = \frac{2}{\mu}\ \left[r^2\ (\bar{V} \cdot \delta\bar{V}) - (\bar{R} \cdot \bar{V})\ (\bar{R} \cdot \delta\bar{V})\right] \tag{14}$$

$$\delta r_p = \frac{(r^2 - r_p^2)\ (\bar{V} \cdot \delta\bar{V}) - (\bar{R} \cdot \delta\bar{V})}{\mu\ \epsilon} \tag{15}$$

$$\delta r_a = \frac{(r_a^2 - r^2)\ (\bar{V} \cdot \delta\bar{V}) + (\bar{R} \cdot \bar{V})\ (\bar{R} \cdot \delta\bar{V})}{\mu\ \epsilon} \tag{16}$$

Upon examining equations (11) through (16), we see that if $\overline{\delta V}$ is normal to $\overline{V}$, $\overline{V} \cdot \overline{\delta V}$ becomes zero and a considerable simplification of the equations results. Specifically,

$$\delta a = \delta \tau = 0 \tag{17}$$

and

$$\delta r_a = -\delta r_p = a\delta\epsilon = \frac{-\delta p}{2\epsilon} = \frac{(\bar{R}\cdot\bar{V})(\bar{R}\cdot\overline{\delta V})}{\mu\epsilon} \tag{18}$$

Furthermore we note that if $\overline{\delta V}$ is normal to the orbit, and hence normal to both $\overline{V}$ and $\overline{R}$, then the parameters of equation (18) also become zero, i.e.,

$$\delta r_p = \delta r_p = \delta\epsilon = \delta p = 0 \tag{19}$$

To take advantage of these simplications, $\overline{\delta V}$ is considered to be made up of three components: one normal to the orbit; another along the velocity vector; and the third normal to the other two. Formally, these relations may be stated

$$\overline{\delta V} = \delta V \begin{bmatrix} \sin\psi \cos\eta \\ \cos\psi \cos\eta \\ \sin\psi \end{bmatrix} = \begin{bmatrix} \delta V_R \\ \delta V_v \\ \delta V_H \end{bmatrix} \tag{20}$$

where ψ is an angle measured in the plane of the orbit, from the velocity vector and positive toward $\overline{V} \times \overline{H}$; and η is the angle between the orbit plane and $\overline{\delta V}$.

Let us now consider separately the effects of the three components of $\overline{\delta V}$.

$\overline{\delta V}$ Normal to Orbit. Since δV_H is, by definition, normal both to $\overline{V}$ and $\overline{R}$, equations (17) and (19) hold; thus, the size and shape of the orbit are unchanged. The only effect of δV_H is to change the orbit orientation. This change is a rotation of the orbit about the line from the body center to the satellite. Since $\delta V_H \ll V$, the angle of the rotation, ρ, is given by

$$\rho = \tan \rho = \frac{\delta V_H}{V \cos \phi} \tag{21}$$

Let $\overline{\Delta R(t)}$ be the vector from the point on the nominal orbit to the point on the perturbed orbit at the time t. $\overline{\Delta R}$ can be expressed in components in the $\hat{R}_{ap} \hat{V}_{ap} \hat{H}_{ap}$ coordinate system. In particular the component normal to the orbit plane is given by

$$\Delta r_H = \overline{\Delta R} \cdot \hat{H}_{ap} \tag{22}$$

Now suppose that θ_s is the true anomaly at separation. Then (since ρ is quite small),

$$\Delta r_H \doteq \left|\overline{\Delta R}\right| = \rho R \sin (\theta - \theta_s) \tag{23}$$

Thus, we see that a δV applied normal to the orbit plane produces a displacement from the nominal that has essentially no in-plane component.

$\overline{\delta V}$ In-plane, Normal to $\overline{V}$. Let us now consider the effect of a δV_R in-plane and normal to $\overline{V}$. By the definition of δV_R, equations (17) and (18) are applicable. Since there are no out-of-plane components of velocity, it is clear that there can be not out-of-plane displacement, i.e., $\overline{\Delta R} \cdot \hat{H}_{ap} = 0$. Equation (18) is useful in computing the in-plane components of the separation; however, there are two more effects that must be considered.

The first is the rotation of the major axis about the central body center. Let θ_o be the time anomaly at some time, t_o. Then, rotations of the semi-major axis can be expressed as $\delta\theta_o$. It is found that, in general,

$$\delta\theta_o = \frac{r\cos\theta\,\delta\epsilon - \delta_p}{\epsilon\, r \sin\theta} \tag{24}$$

If $(\bar{V}\cdot\bar{\delta V}) = 0$, equation (18) becomes

$$\delta\theta_o = \left(\frac{\cos\theta}{ae} + \frac{2}{r}\right)\left[\left(\frac{(\bar{R}\cdot\bar{V})(\bar{R}\cdot\bar{\delta V})}{\mu e \sin\theta}\right)\right] \tag{25}$$

The polarity of the rotation changes when $\theta = \theta_p = \tan^{-1}\left[\frac{1-e^2}{2e}\right]$. Let $\bar{R}\cdot\bar{\delta V} > 0$, then the major axis rotates clockwise for $-\theta_p < \theta < \theta_p$ and counterclockwise for $\theta_p < \theta < 2\pi - \theta_p$.

In the special case of $\theta = \pi$, we get

$$\delta\theta_o = \sqrt{\frac{a}{\mu}\left(\frac{1}{\epsilon^2} - 1\right)}\,\delta V \tag{26}$$

The second quantity, phase difference δt, is more difficult to define. First, we note that even though two co-planar orbits have the same period, they are not, in general, at the same true anomaly simultaneously, even though they do pass through some point simultaneously. For two orbits of the same period (and hence of equal semi-major axes, a), the angular and linear velocity of the vehicle nearer the central body center is greater. For example, when two satellites are separated at some point by the application of an in-plane, inward $\bar{\delta V}$ that is normal to the velocity vector $\bar{V}$ of one of the satellites, the inner satellite gains on the outer satellite until the outer satellite becomes the inner satellite. At this point, the lagging satellite gains back all it had lost, and the satellites simultaneously reach the original separation point one period later.

The size of the phase difference depends on the amount the orbit is rotated, the degree the shape is changed, and the point on the orbit that is being considered. No closed form solution can be written for the phase difference δt since solution of Kepler's equation is involved. The solution in a number of specific instances was obtained, however, using a digital computer program. To convert the phase time difference to a position difference, it is necessary to multiply by the velocity at the point of interest. Thus, the separation due to phase difference is given by

$$\overline{\delta R}_t = \overline{V}\,\delta t \tag{27}$$

The components of the in-plane separation at the point where the orbit intersects the semi-minor axis, b, are given by

$$\begin{aligned} \delta r_R &= \overline{\delta R}\cdot\hat{R}_{ap} = \delta r_a + r\sin\theta\,\delta\theta_o + (\overline{V}\cdot\hat{R}_{ap})\,\delta t \\ \delta r_V &= \overline{\delta R}\cdot\hat{V}_{ap} = \delta b + r\cos\theta\,\delta\theta_o + (\overline{V}\cdot\hat{V}_{ap})\,\delta t \end{aligned} \tag{28}$$

Figure 4.2-5 illustrates the in-plane separation components with the relative magnitudes greatly exaggerated so that the effects can be seen.

$\overline{\delta V}$ Along $\overline{V}$. Equation (12) shows that the change in period, $\delta\tau$, is directly proportional to the component of $\overline{\delta V}$ along $\overline{V}$. The displacement due to period difference is cumulative, being given by

$$\overline{\Delta R}_\tau = n\overline{V}\,\delta\tau \tag{28A}$$

where n is the pass or orbit number. Thus, to minimize the rate of growth of $\overline{\Delta R}$, the component of $\overline{\delta V}$ along $\overline{V}$ must be minimized.

It should also be noted that $\delta\tau$ is directly proportional to V at the maneuver point. Thus, for a given component of δ V along V, $\delta\tau$ is minimum where V is minimum, i.e., apogee.

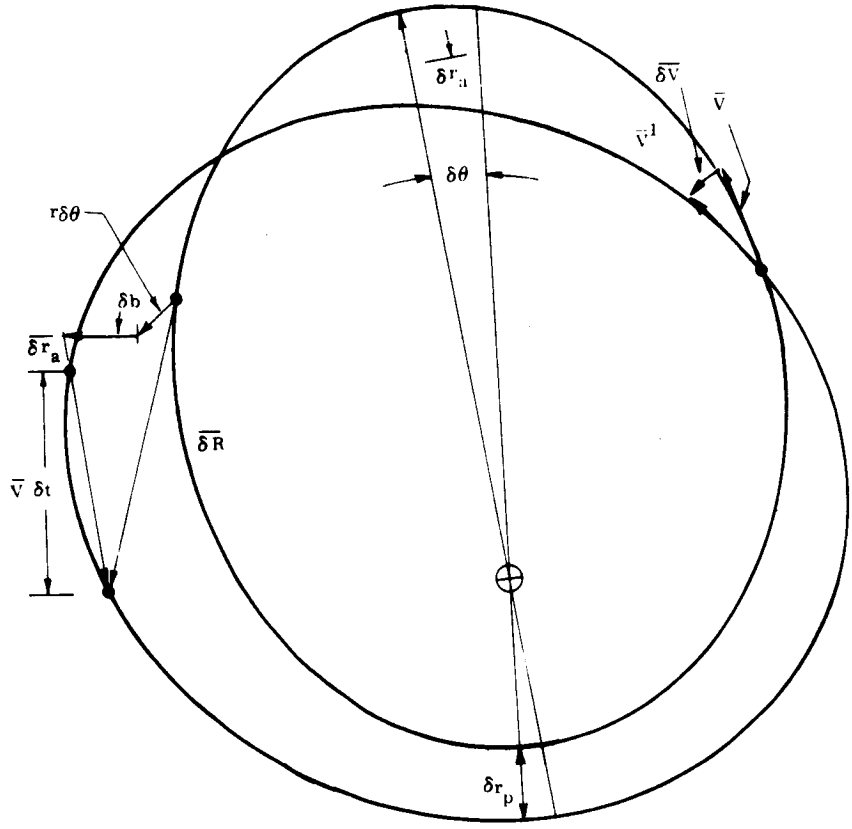

Figure 4.2.5 Components of In-Plane Separation

$\overline{\Delta V}$ of Finite Magnitude. All the equations derived above assume that the velocity variation $\overline{\delta V}$ is infinitesimal. In practice, a velocity increment $\overline{\Delta V}$, of finite magnitude, is applied. Thus, we have for example

$$\Delta\tau = \frac{3a\tau}{\mu}\left[\overline{V}\cdot\overline{\Delta V} + \frac{\Delta V^2}{2}\right] \tag{29}$$

instead of (12). In practice, this makes little difference since ΔV is at least two orders of magnitude less than V for the maneuvers considered. However, it does account for $\Delta\tau$ not being zero when $\overline{V}\cdot\overline{\Delta V} = 0$, for, in that case, we have

$$\Delta\tau = \frac{3a\tau}{2\mu}\ \Delta V^2 \tag{30}$$

Computer Simulation. The equations derived and discussed above are presented to give some insight into the factors involved in separating two satellites in orbit. The data to be discussed below were actually obtained from a digital computer simulation of the satellite separation problem. The computer program, called the satellite separation program (SSP), gives $\overline{\Delta R}$ and its components as well as the variation in orbit parameters for a specified separation true anomaly, θ_s, and $\overline{\Delta V}$. The program gives $\overline{\Delta R}$ for all points on the orbit where the range is a multiple of the earth's radius, e.g., $r = 12\ R_E$. Also the $\overline{\Delta R}$ are given for any pass desired.

Tables 4.2-1 and 4.2-2 give some typical in-plane separations broken down into components. Table 4.2-1 gives the separation of two satellites at 12 R_E (R_E = earth radius) on both the incoming and the outgoing leg of the orbit. The two satellites were initially separated at 176 degrees true anomaly with an in-plane velocity increment of 5 m/sec inward. Data for three cases are given: one where $\overline{\Delta V}$ is normal to $\overline{V}$; and two cases where $\overline{\Delta V}$ is ± 5 degrees from normal, but still in plane. Table 4.2-2 gives the same information for satellites separated at 180 degrees true anomaly. The tables also indicate the period differences $\Delta\tau$ for the corresponding cases. Period differences may be regarded as secular phase changes. It is primarily this factor that causes the satellite array to decay in time. The rate of decay may be estimated by multiplying the period differences by the orbit number, n, and the velocity, V, at the point of interest. Thus, at 12 R_E, where $V \approx 2$ km/sec, for $\Delta\tau = 20$ sec we see that after 90 orbits, $\Delta R \approx 90 \times 20 \times 2 \approx 4500$ km.

Pointing Errors in ΔV. Misdirection of the ΔV's results in different periods for the four satellites. Consequently, the shape of the array changes slowly, tending to become more spread out along the orbit. The extent of the array, ΔR_{max}, for a given orbit number, n, is given approximately by

$$\Delta R_{max} = \Delta R_o + NV\ \Delta\tau_{max} \tag{31}$$

TABLE 4.2-1

ΔR AT 12 R_E WHEN SEPARATED AT θ = 176°

ΔV = 5 m/sec, θ_{sep} = 176°	Separation Components at 12 R_E			
	$\overline{\Delta R} \cdot \overline{R}_{ap}$ (km)		$\overline{\Delta R} \cdot \overline{V}_{ap}$ (km)	
η = 0°, ψ = 90°	in	out	in	out
Rotation ($\Delta\theta$ = .025°)	15	-15	-25	-25
Translation (Δr_p = 65.3, Δa - 0.2)	-65	-65	—	—
Eccentricity (Δp = 117.8)	—	—	136	-126
Phase ($\Delta\tau \approx 1.1$)	-445	332	23	19
Total	-495	252	134	-142

ΔV = 5 m/sec, θ_{sep} = 176°	Separation Components at 12 R_E			
	$\overline{\Delta R} \cdot \overline{R}_{ap}$ (km)		$\overline{\Delta R} \cdot \overline{V}_{ap}$ (km)	
η = 0°, ψ = 95°	in	out	in	out
Rotation ($\Delta\theta$ = 0.030°)	20	20	-35	-35
Translation (Δr_p = 56.0, Δa = -6.3)	-59	-59	—	—
Eccentricity (Δp = 101.0)	—	—	115	-115
Phase ($\Delta\tau \approx 220$ $\Delta\tau$ = -25.3)	-491	395	24	24
Total	-530	316	109	-125

E = 0.091053

ΔV = 5 m/sec, θ_{sep} = 176°	Separation Components at 12 R_E			
	$\overline{\Delta R} \cdot \overline{R}_{ap}$ (km)		$\overline{\Delta R} \cdot \overline{V}_{ap}$ (km)	
η = 0°, ψ = 85°	in	out	in	out
Rotation ($\Delta\theta$ = .019°)	9.5	-9.5	-23.6	-23.6
Translation (Δr_p = 74.1, Δa = 6.8)	-67.3	-67.3	—	—
Eccentricity (Δp = 133.7)	—	—	-155.6	-155.6
Phase ($\Delta\tau \approx 180$ $\Delta\tau$ = 26.5)	-389.5	314.2	25.8	23.4
Total	-456.3	237.4	157.8	-155.8

TABLE 4.2-2

ΔR AT 12 R_E WHEN SEPARATED AT $\theta = 180°$

ΔV = 5 m/sec, θ_{sep} = 180°	Separation Components at 12 R_E			
	$\Delta\bar{R}\cdot\bar{R}_{ap}$ (km)		$\Delta\bar{R}\cdot\bar{V}_{ap}$ (km)	
$\eta = 0°, \psi = 90°$	in	out	in	out
Rotation ($\Delta\theta$ = 0.057°)	28.0 km	-28.0	-70.5	-70.5
Translation (Δr_p = 0, Δa = 0.2)	0.2	0.2	—	—
Eccentricity (Δp = 0)	—	—	0.1	0.1
Phase ($\Delta t \approx 240$, $\Delta\tau$ = 1.1	-478.0	476.7	33.2	33.8
Total	-449.8	448.9	-37.2	-36.8

ΔV = 5 m/sec, θ_{sep} = 180	Separation Components at 12 R_E			
	$\Delta\bar{R}\cdot\bar{R}_{ap}$ (km)		$\Delta\bar{R}\cdot\bar{V}_{ap}$ (km)	
$\eta = 0°, \psi = 95°$	in	out	in	out
Rotation ($\Delta\theta$ = 0.056°)	27.8	-27.8	-69.3	-69.3
Translation (Δr_p = - 10.9, Δa = -5.2)	5.7	5.7	—	—
Eccentricity (Δp = 19.7)	—	—	-23.9	23.9
Phase ($\Delta t \approx 240$, Δ = 19.9)	-484.4	466.5	33.1	31.9
Total	-450.9	444.4	-60.1	-13.5

ΔV = 5 m/sec, θ_{sep} = 180°	Separation Components at 12 R_E			
	$\Delta\bar{R}\cdot\bar{R}_{ap}$ (km)		$\Delta\bar{R}\cdot\bar{V}_{ap}$ (km)	
$\eta = 0°, \psi = 85°$	in	out	in	out
Rotation ($\Delta\theta$ = 0.056°)	27.8	-27.8	-69.3	-69.3
Translation (Δr_p = 10.9, Δa = 5.7)	-5.2	-5.2	—	—
Eccentricity (Δp = 19.7)	—	—	23.5	-23.5
Phase ($\Delta t \approx 240$, $\Delta\tau$ = 22.1)	-467.8	48.3	31.9	33.0
Total	-445.2	450.0	-13.9	-59.8

Where ΔR_o is the initial separation, V is the orbit velocity in the region of interest, and $\Delta\tau_{max}$ is the period difference between the slowest and the fastest satellite.

An estimate of the precision required in performing the ΔV maneuvers can be obtained by solving equation (31) for $\Delta\tau_{max}$ and substituting values for ΔR_{max}, n V and ΔR_o.

$$\Delta\tau_{max} = (\Delta R_{max} - \Delta R_o)/nV \tag{32}$$

The mission requires that $\Delta R_{max} \leq 15,000$ for a period of six months. Since the orbit period is very nearly two days, six months is equivalent to $n \doteq 90$ orbits. In the region of interest (in the neighborhood of 12 R_e), $V \doteq 2$ km/sec. ΔR_o differs for the radial and stacked arrays.

Stacked Array. For the stacked array $\Delta R_o = 1600$ km; hence

$$\Delta\tau_{max} = \frac{(15000 - 1600)\text{ km}}{90.2\text{ km/sec}} = 74.5\text{ sec}$$

The combined relative velocity for the stacked array deployment is 20 m/sec. Thus, if all the errors combined linearly (the worst possible case) the overall accuracy requirement may be computed from the formula

$$\alpha = \sin^{-1}\left[\frac{\mu\Delta\tau}{3a\tau V\Delta V}\right] \tag{33}$$

where V is the orbit velocity at the separation point.

Since a = 67061 km, τ = 172,828 sec, μ = 398,604 km^3/sec^2 and for the stacked array V = 1.084 km/sec at the separation points (170 degrees and 190 degrees true anomaly), we have

$$\alpha = \sin^{-1}(0.395) = 2.3\text{ degrees}$$

Radial Array. For the radial configuration, ΔR_o = 800 km; thus

$$\Delta\tau_{max} = \frac{(15000 - 800)\text{ km}}{90.2\text{ km/sec}} = 79\text{ sec}$$

For the radial deployment scheme to give an initial three-dimensional array, an additional factor must be taken into consideration. The deployment is completed by giving a 1.1 m/sec relative ΔV to two of the satellites in the direction of the orbit velocity. This introduces a built-in period difference of approximately 48 seconds. Thus, the allowable $\Delta\tau_{max}$ is reduced by that amount, i.e.,

$$\Delta\tau_{max} = 31\text{ sec}$$

For the radial configuration, the separation velocity is 12.3 m/sec (relative) and the orbit velocity at the point of separation (180 degrees true anomaly) is 0.553 km/sec. Using equation (33), we get

$$\alpha = \sin^{-1}(0.523) = 3\text{ degrees}$$

4.2.3 Study Results

4.2.3.1 Coordinates and Terminology. These results have been based on ideal elliptical orbits. Air drag and secular perturbations have been neglected.

Figure 4.2-6 shows various parameters describing an elliptical orbit. The true anomaly, θ, is an angle measured from perigee around the orbit in the direction of travel. Thus, apogee is at true anomaly 180 degrees. The velocity vector at any point on the orbit is along the line tangent to the ellipse at that point. The flight-path angle is measured from the perpendicular to the radius vector to the velocity vector. This angle is positive on the outgoing portion of the orbit and negative on the incoming portion. Notice that only at perigee and apogee does the flight-path angle equal zero. The magnitude of the radius vector is sometimes called range.

Positions on the orbit can be specified in many ways. In this report, position is usually specified in terms of true anomaly or range in multiples of earth radii (R_e). Specification of position by range is ambiguous because each value of range occurs on both outgoing and incoming parts of the orbit. It is convenient, however, because we are concerned with that portion of the entire orbit that lies between about 8 R_e and 16 R_e.

The orbit used in the study is described in Figures 4.2-7 thru 4.2-9. Figure 4.2-10 gives a more detailed look at the behavior of flight-path angle in the region of 150 to 180 degrees true anomaly. This curve also shows the time variation of flight-path angle; time is measured in seconds from perigee.

4.2.3.2 Satellite Separation Coordinate System. A discussion of multiple satellite separation requires a coordinate system in which the subsequent satellite array can be described.

The system chosen is a right-handed orthogonal system with the X-Y plane in the orbital plane. The X-axis is parallel with the line of apsides (major axis) pointing toward apogee; the Z-axis is perpendicular to the orbital plane, pointing upward; and the Y-axis is in the orbital plane, pointing in the direction that the orbital

velocity vector points when it is at apogee. Figure 4.2-11 shows this coordinate system at various locations around the orbit.

4.2.3.3 Separation Magnitude vs. True Anomaly of Separation. Figures 4.2-12 and 4.2-13 give an indication of the "efficiency" of a one meter-per-second separation velocity when performed at different true anomalies of separation around the orbit.

In Figure 4.2-12, the satellite is separated up along the H-direction, perpendicular to the orbital plane. It then proceeds in a new orbit, which is very nearly directly above the primary orbit. (The primary orbit is the orbit existing before any separations take place.) A convenient way to visualize the new orbit resulting from a maneuver (which is directly out-of-plane, either upward or downward), is the following: The new orbit, for our purposes, is the same size and shape as the primary orbit, but is rotated about the line passing through the point of separation and the center of the earth. Thus, if the satellite is separated upward, its distance above the primary orbit increases as the point of separation travels around the primary orbit. When it reaches a maximum at some true anomaly on the opposite side of the orbit, the distance of the satellite above the primary orbit decreases until the new orbit crosses the primary orbit. This occurs at a point 180 degrees around the orbit, in true anomaly, from the separation point. From this point, the satellite continues below the orbit until it again reaches a maximum, at which point it comes back up toward the primary orbit until it reaches the separation point, where the two orbits coincide. Figure 4.2-12 shows the absolute magnitude of this vertical separation of the satellite from the primary orbit at 12 R_e, outgoing and incoming. For example, if separation occurred at 170 degrees true anomaly, with separation velocity of one meter-per-second, the vertical separation between satellite and primary orbit would be 25 kilometers at 12 R_e, outgoing, and 64 kilometers at 12 R_e, incoming. For separation velocities up to about 15 meters per second, these curves can be scaled up linearly. For example, if the desired separation is 5 meters per second, the separation in kilometers from the curves would be five times the separations given, to within 0.005 percent.

Figure 42-13 gives similar data for in-plane separations. An in-plane inward separation is defined to be in the orbital plane, at 90 degrees to the velocity vector, and pointing toward the interior of the orbit. (In this case, "inward" means to the left of the orbital path.) An in-plane outward separation is exactly the opposite. The magnitudes given are the same for both inward and outward separations. As in Figure 4.2-12, the separation magnitudes can be scaled up for larger separation velocities.

Visualization of the effect of in-plane maneuvers is more difficult than for the out-of-plane maneuver because the differences between the new and primary orbits are more pronounced. A more detailed exposition of these differences will be found in Paragraph 4.2.2.

Separation magnitude, as used in Figure 4.2-12 and 4.2-13, is the magnitude of the vector from the primary orbit to the satellite for any subsequent position. The definition of this separation vector requires more explanation. Consider that the satellite is separated from a vehicle large enough that the vehicle continues unperturbed in the primary orbit. The separation vector is the vector from this large vehicle to the separated satellite at any subsequent time. When a later position is specified, such as 12 R_e, incoming, it is the position of the large vehicle. In reality, of course, we have no large vehicle, only a point. This point of separation travels around the orbit and the separation is measured from this point to the satellite.

The separation vector magnitude is expressed in terms of components in the R, V, H coordinate system.

For a pure out-of-plane separation, the R and V coordinates are negligible. Only the H-component has a value, and this is the component plotted in Figure 4.2-12.

For a pure in-plane separation, the H-component is zero after separation. The separation vector is in the R-V (orbital) plane. The separation given in Figure 4.2-13 is the resultant of the R and V components of the separation vector.

Figure 4.2-14 gives the R and V components which, when combined, give Figure 4.2-13. For example, if separation was at 170 degrees, the R and V components of the separation vector at 12 R_e incoming are -80 km and 53 km, respectively. Combining these via Pythagorus' rule yields 97 km as the resultant. Looking at Figure 4.2-13, we see that the separation magnitude at 12 R_e incoming for a separation at 170 degrees is, indeed, 97 km. Figure 4.2-14, too, can be linearly scaled if a different separation velocity is desired.

If it is desired that the separation between two satellites be some fixed number at some point in the orbit, both the true anomaly of separation and the velocity of separation must be adjusted. Figure 4.2-15 gives this information for a separation of 500 kilometers at 12 R_e, incoming and outgoing. For example, assume an in-plane separation between two satellites at 170 degrees true anomaly. When the point of separation moves around to 12 R_e incoming, (202 degrees true anomaly), the two satellites are separated by 500 kilometers if the relative separation velocity was 5.2 meters per second. If, for the same separation, a 500 kilometer separation is required at 12 R_e outgoing (158 degrees true anomaly), the separation velocity required is 17.5 meters per second. Notice that the curves go off-scale near 158 and 202 degrees true anomaly. Theoretically, the two satellites come back together at the point of separation. Since these curves require a separation of 500 kilometers at 12 R_e incoming and outgoing, separation <u>at</u> 12 R_e incoming and outgoing requires infinite separation velocity.

4.2.3.4 <u>Effect of Errors in Separation.</u> None of the curves presented so far involve errors in the direction of the separation velocity vector. All separations are perpendicular to the velocity vector. In this section, we consider separation velocities that have a component along or against the velocity vector.

An error of 5 degrees means that the separation velocity vector is tilted 5 degrees out of the plane perpendicular to the velocity vector. An error forward means that the separation velocity vector is tilted in the direction of the velocity vector. A backward error is one that is tilted in a direction opposite to the velocity vector. Since this definition applies to a vector pointing in any direction in the plane perpendicular to the velocity vector, it must be stated whether the separation is in-plane, out-of-plane, or in some intermediate direction.

Almost any separation maneuver affects the perigee distance of the orbit. The effect of a given maneuver on perigee varies with the true anomaly of separation. The in-plane maneuvers affect the perigee much more than the out-of-plane maneuvers.

Figure 4.2-16 shows the difference in perigee altitude between the primary orbit and the orbit subsequent to a maneuver, for various separation modes, without errors and with 5-degree errors. The perfect out-of-plane error, up or down, does not affect perigee height, regardless of true anomaly of separation. For example, suppose the separation is at 160 degrees true anomaly, with a separation velocity of one meter per second. If the separation is in-plane inward, with a 5-degree error forward, the perigee height increases by 15 kilometers, as read from curve number 5. If the same separation is out-of-plane upward, with a 5 degree error forward, the perigee height increases by 0.6 kilometer. The period of the orbit is also changed by a separation velocity error. If the periods of the orbits of two separated satellites are different by some amount, there will be a relative drift between them. If the drift is such that the satellites are moving apart, the distance between them increases by the same amount during each subsequent orbit. Thus, a period difference produces accumulative effects. This is different from the perigee height change, which occurs only once.

The change in period as a function of true anomaly of separation is given in Figure 4.2-17. Note that the period change is governed by the size of the component of separation velocity along the velocity vector, rather than the specific attitude of separation. In other words, an in-plane inward separation with 5-degree error forward gives the same period change as an out-of-plane upward separation with 5-degree error forward. For a perfect separation (that is, normal to the velocity vector), the period change is less than one-half second. Both Figures 4.2-16 and 4.2-17 can be scaled linearly.

Figure 4.2-18 is composed of data from Figures 4.2-15 and 4.2-16. In Figure 4.2-18, the error used ia 5 degrees forward for both in-plane and out-of-plane separations. The period changes in Figure 4.2-17 were scaled up accordingly to the velocities in Figure 4.2-15. Thus, if separation is in-plane at 170 degrees

true anomaly, and 500 kilometers is required at 12 R_e incoming, the resulting period change is 43 seconds.

4.2.3.5 Results of Specific Separation Modes. Two configurations are being considered for the four-satellite separation: the radial array and the stacked array. The remaining data show the satellite array after separation for different combinations of errors for the two arrays.

Radial Array. In the radial array, the four satellites are clustered about the spin axis of the vehicle. At the separation point, they are simultaneously released, after which they proceed radially outward, separated 90 degrees from each other. Unless further impulses are applied to individual satellites, the array resulting from the radial separation remains essentially planar over 90 orbits. Figure 4.2-19 shows the separation sequence.

Composite Separation Graph. Figure 4.2-20 describes the motion of the four satellites for the first orbit after separation at apogee. The separation velocity between each pair of satellites is 12.3 meters per second. The graphs are centered at the separation point, or roughly, the center of mass of the system of four satellites. The H. V. H coordinate system is used to plot the separations. The top part of the figure shows the motion in the R-V (orbital) plane. This separation was chosen so that, when released, the satellites A, B, C, and D move out along paths 45 degrees to the orbital plane. Because of this separation symmetry, the two satellites separated in an inward direction, A and B, remain lined up vertically. Thus, when looking down on the orbital plane, they appear as one. We can consider the curves in the top part of Figure 4.2-20 as the motion of two satellites sets. Figure 4.2-20 describes a perfect separation at apogee. The two sets separate at apogee and proceed in an opposite sense along the general direction of R. As they get farther from apogee, they acquire a separation in the V-direction. They continue around the orbit to perigee, where their R-separation is almost zero and their V-separation is maximum. The reason for this is easily seen when we remember that the V-axis is parallel with the velocity vector at apogee and perigee. If there were any significant R-separation at perigee, it would mean that the perigee heights were different. As the figure shows, the perigee heights are the same, but the two sets pass the perigee points one after the other. As they return to apogee on the outgoing leg of the orbit,

their separation decreases, until at apogee, they theoretically recombine. The lower half of the figure shows the same motion as seen from a different aspect. We are looking parallel with the line of apsides from the earth toward apogee. In this view, all four satellites could be seen. They separate at apogee, two proceeding upward and two proceeding downward. They reach their maximum out-of-plane separation (H-direction) at about $10R_e$. At this point they start back toward the orbital plane and their V-separation increases. Again, they are separated widely in the V-direction when they pass perigee. Figure 4.2-15 shows only the path followed by the two satellites that start out upward. The path for the remaining two satellites, which start out downward, is the mirror image about the V-axis of the curve shown.

Three Views of Arrays. A method of presenting the data in Figure 4.2-20 in more detail is to show three views of the entire array as seen at some point in the orbit. Figures 4.2-21 through 4.2-23 show the array for the separation shown in Figure 4.2-20 (perfect separation at apogee) at 12, 14, and 16 R_e incoming. Figure 4.2-21 shows the array as seen on the R-V plane, the orbital plane. The array is approximately planar for most separations. Non-planar arrays are presented at the end of this section. The 10 R_e array is included in Figure 4.2-21. Figure 4.2-22 shows the array as seen on the V-H plane. The V-H plane is the plane perpendicular to the line of apsides. We are looking at it in the direction of earth from apogee. Notice that the array grows as it progresses around the orbit from 16 R_e to 12 R_e. Figure 4.2-23 is a side view of the array, as seen looking at the "edge" of the orbital plane with the earth on the left and apogee on the right. For this particular perfect separation, the relative drift rates between the satellites of the array are small enough that the change in the array, as seen at a given point in the orbit, may be neglected over a period of 90 orbits. The three views that follow, however, show significant drift over 90 orbits, so they are presented as seen only at 12 R_e incoming, but for 0, 30, 60 and 90 orbits.

Figures 4.2-24 through 4.2-26 are the three views for a radial separation at apogee with a 5-degree error in the satellite spin-vector at release. A perfect separation at apogee for the radial case is defined as a separation that occurs

when the spin axis of the vehicle is aligned with the orbital velocity vector at apogee. The separation described by Figures 4.2-24 through 4.2-26 has the spin axis in the orbital plane, but pointing 5 degrees to the left of the velocity vector at apogee. Figure 4.2-26 clearly shows the growth of the array throughout the 90 orbits. Other separations five similar arrays.

Stacked Array. Figure 4.2-27 shows a separation sequence from the stacked array. The four satellites start out aligned (stacked) along the spin axis of the vehicle. The vehicle spin axis is initially perpendicular to the orbital plane. At some position in the orbit, the first out-of-plane separation is performed by separating the end satellites in opposite directions. As soon as possible after this separation, the two middle satellite are moved in-plane inward. After a short time, the two middle satellites are separated out-of-plane. The timing of these maneuvers is dependent on the orientation and size of array desired. The separation sequence described in Figures 4.2-28 through 4.2-36 is the following: First out-of-plane separation at 176 degrees true anomaly, in-plane inward separation at 176 degrees true anomaly, and second out-of-plane separation velocities are 10 meters per second relative to two satellites for out-of-plane separations and 5 meters per second for the in-plane motion of the two joined together, relative to the primary orbit.

This particular sequence for the stacked configuration will yield a planar array if done without errors. Some combinations of separation errors will give non-planar arrays. These cases are not discussed as the random errors cannot be depended on to give specific arrays. The data given in Figures 4.2-28 through 4.2-37 give data for a stacked array separation designed to give a planar array.

Three Views of the Arrays. Figures 4.2-28 through 4.2-30 show the three views of the perfect separations as described above. All maneuvers are at right angles to the velocity vector. Notice that, for the particular true anomalies of separation used for this case, the size of the array shrinks over the period of 90 orbits. These views are all looking at the array occurring at 12 R_e incoming.

Two error cases are considered for this separation. Figures 4.2-31 through 4.2-33 describe the case where the in-plane inward maneuver has an error of 5 degrees forward and the out-of-plane maneuvers have no error. Figures 4.2-34 through 4.2-36 describe exactly the same situation except that the in-plane inward separation has the 5-degree error backward, instead of forward. Both of these arrays expand during the mission, reaching a dimension of 5000 kilometers by 600 kilometers at the end of 90 orbits. The out-of-plane dimension does not change over this time. The main drift rate is along the R direction.

An interesting difference between these two error cases should be noted. When the in-plane error is backward, the array dimension along R increases monotonically out to 90 orbits, as shown in Figure 4.2-34.

When the in-plane error is forward, the array shrinks from its first orbit (Pass 0) to about the seventh, from the on, the array increases in size monotonically out to orbit 90. This is shown in Figure 4.2-31. The array "swaps ends" between the initial orbit and orbit 30; from then on, it increases smoothly. This behavior is reasonable when we look at the effects which forward and backward errors have on the subsequent orbits. A forward error increases the period of the orbit and a backward error decreases it. Therefore, a satellite separated with a forward error takes longer to complete an orbit, while one separated with a backward error completes an orbit faster. The satellite separated backward overtakes the satellite separated forward after a certain length of time, depending on the relative magnitudes involved. This is exactly what is happening in Figure 4.2-31. The pair of satellites (see Figure 4.2-27) are separated in-plane inward with a forward error. Thus, they are initially propelled ahead of the pair (1, 4). But, by being separated with a forward error, they are sent into a slower orbit, so they eventually fall behind and are passed by pair (1, 4). For this case, the pairs pass at about the seventh orbit.

Composite Separation Graph. Figure 4.2-37 is similar to Figure 4.2-20 except that it is for the stacked array instead of the radial array. Also, both out-of-plane maneuvers are performed at 180 degrees true anomaly, instead of at 176

degrees. Since the (1, 4) set of satellites remains on the primary orbit, when seen on the orbital plane, we can consider the pair (1, 4) as remaining at the origin of the plot, while the other pair revolves about it.

The angle which the array plane makes with the line of apsides (R axis) can be seen from the upper part of Figure 4.2-37 from the angular reference lines provided. For example, the angle made by the array plane when it is at 14 R_e inward is 20 degrees. As in Figure 4.2-20, the separation along V is a maximum at perigee, where the R-separation is zero.

The lower part of the figure shows the out-of-plane behavior of the pair that was separated in-plane. The pair we are holding at the origin would just oscilliate up and down the H-axis. The pair leaving apogee (20 R_e), upward and downward, achieve their maximum out-of-plane separation at about 11 R_e, when they move back down toward the orbital plane.

4.2.3.6 Summary of Planar Arrays. The various separations presented above are only a few of the infinite number of combinations of separation parameters. Most of the combinations yield results similar to those shown.

4.2.3.7 Non-Planar Arrays. Many combinations of errors yield arrays that are non-planar. For example, in the stacked array, if the first out-of-plane separation has a forward error, the second out-of-plane separation has a forward error, and the second out-of-plane separation has a backward error, the array will be an elongated tetrahedron.

Achieving a non-planar array with the radial array is easily accomplished. One method is to move two of the four satellites forward or backward out of the separation plane. Figures 4.2-24 through 4.2-40 shown the perfect separation for this case for the first orbit. Two diametrically opposite satellites are each given a 1.1 meter per second velocity forward out of the array plane at about 180 degrees true anomaly. To avoid difficulties in visualization, only orbits 0 and 90 are shown for this case. The arrays on orbit 90 are shown in Figures 4.2-41 through 4.2-43.

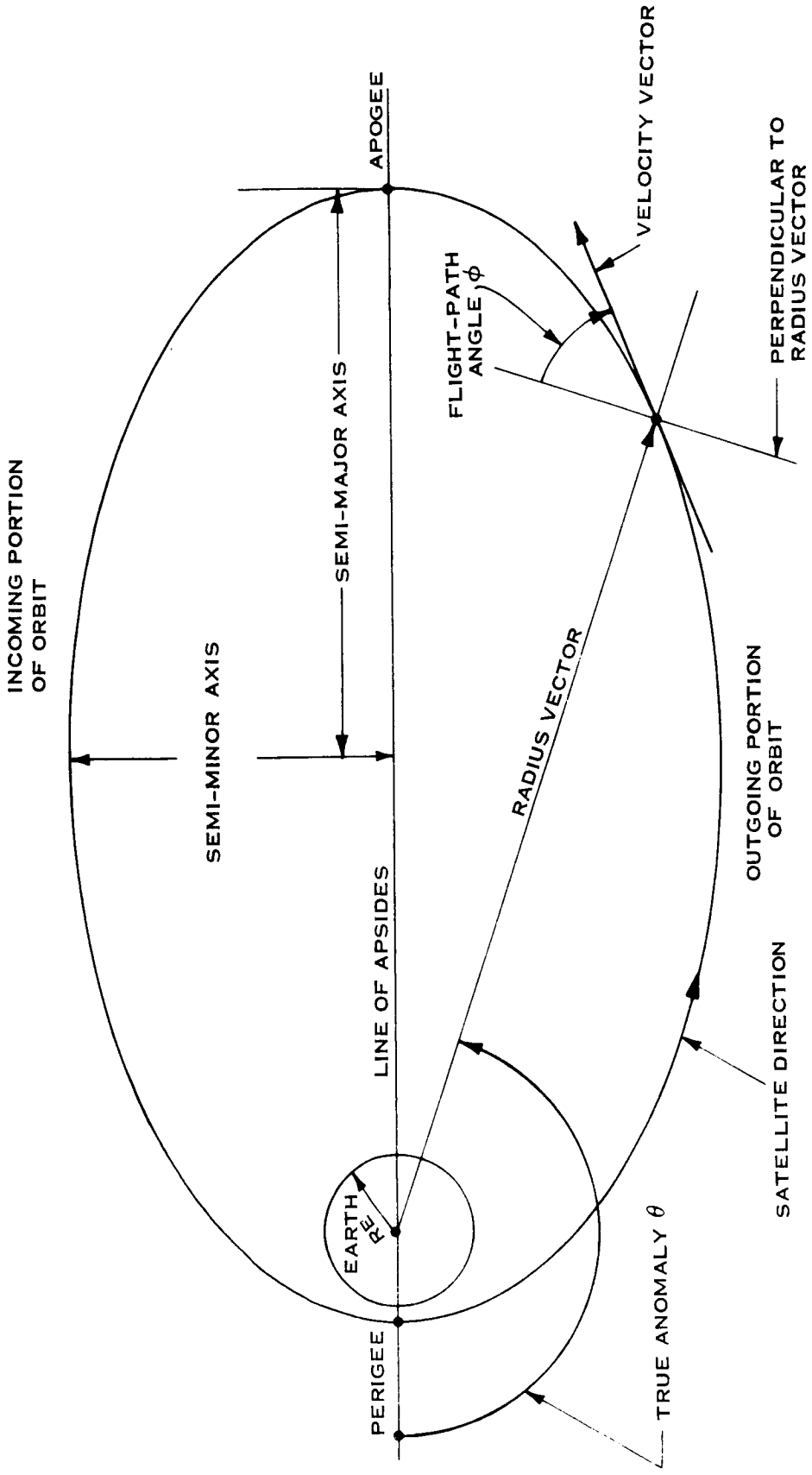

Figure 4.2-6 Various Parameters Describing an Elliptical Orbit

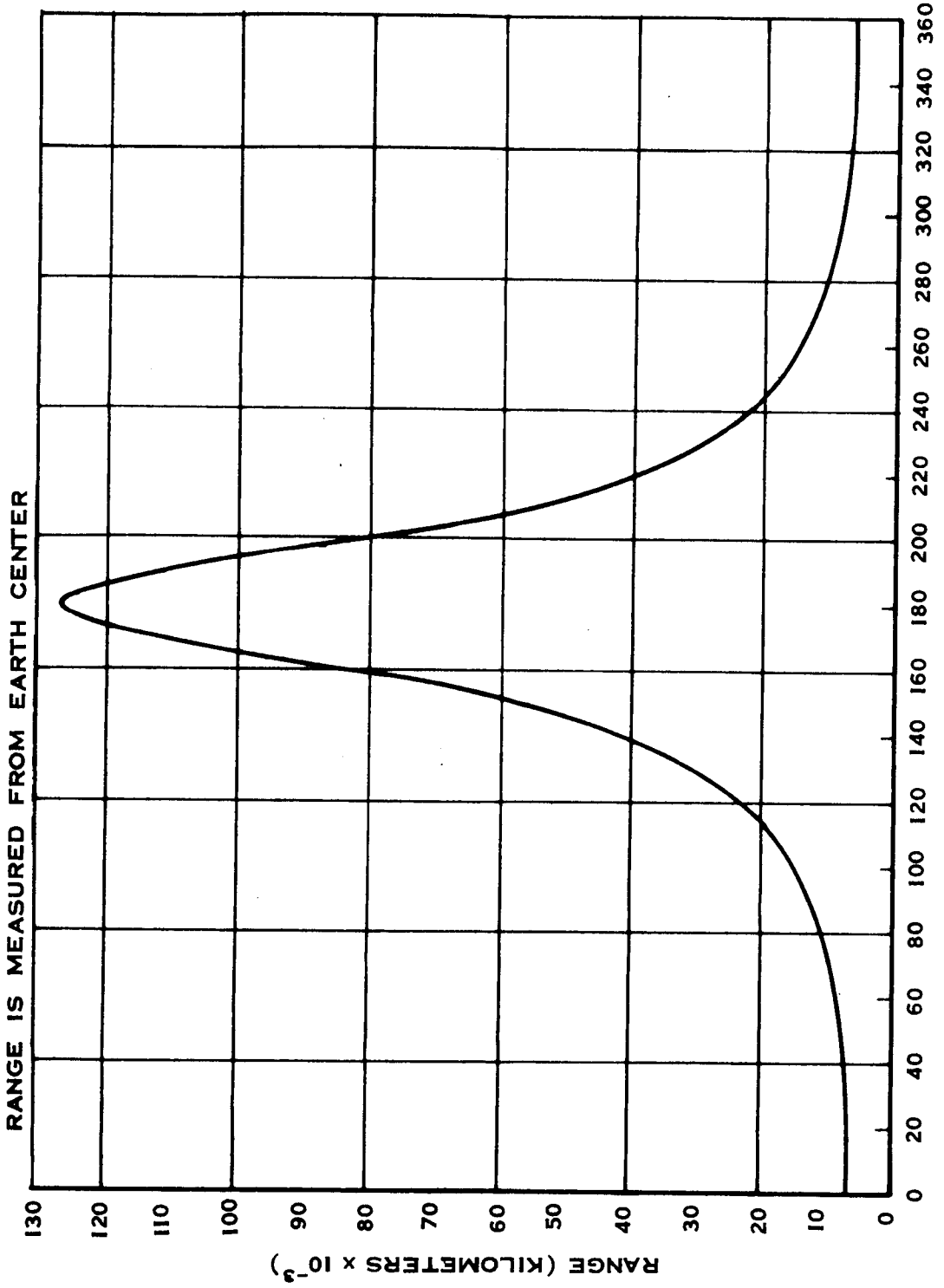

Figure 4.2-7 True Anomaly vs Range

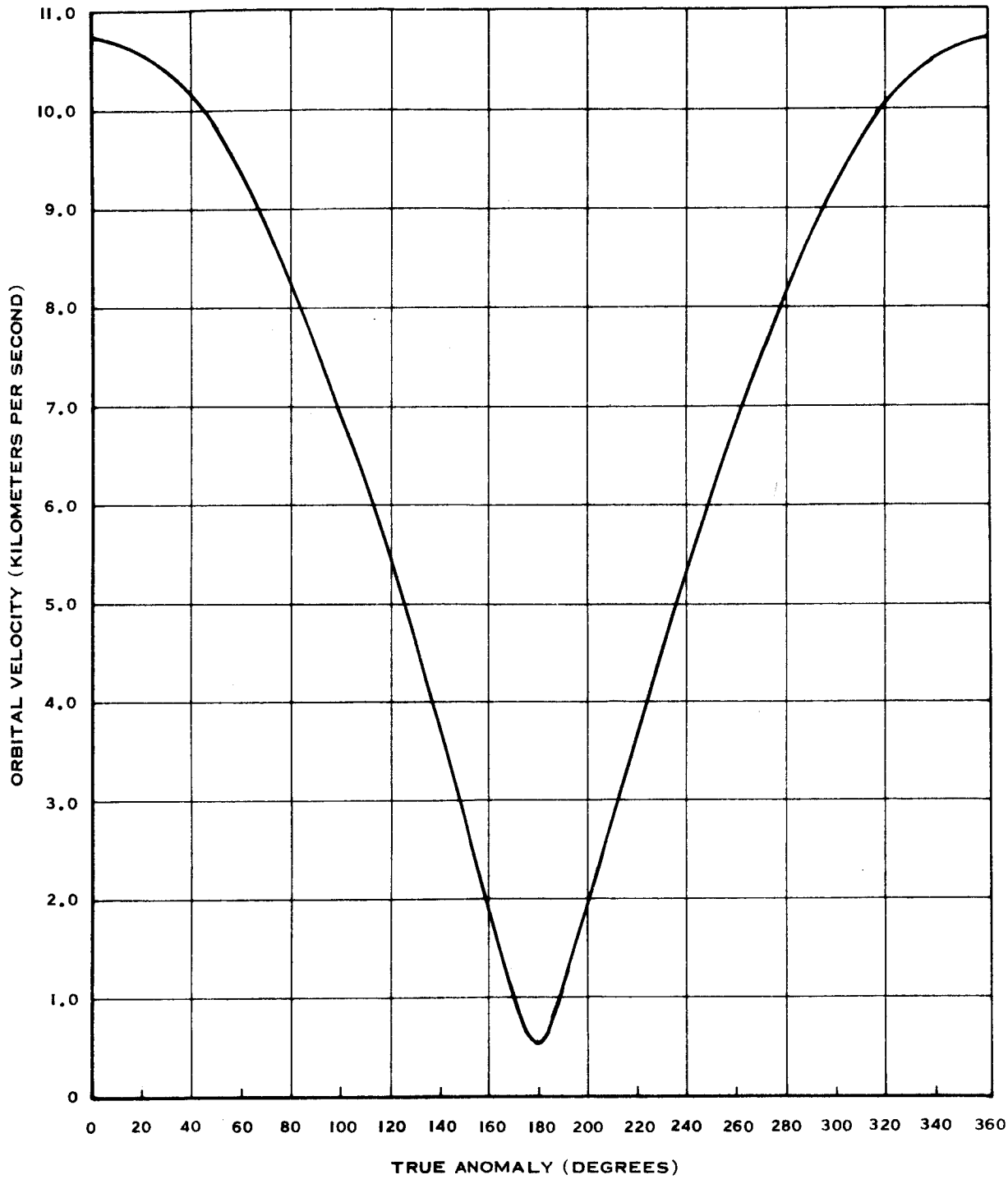

Figure 4.2-8 True Anomaly vs Orbital Velocity

$e = 0.903$

$$\tan = \frac{e \sin}{1 + e \cos}$$

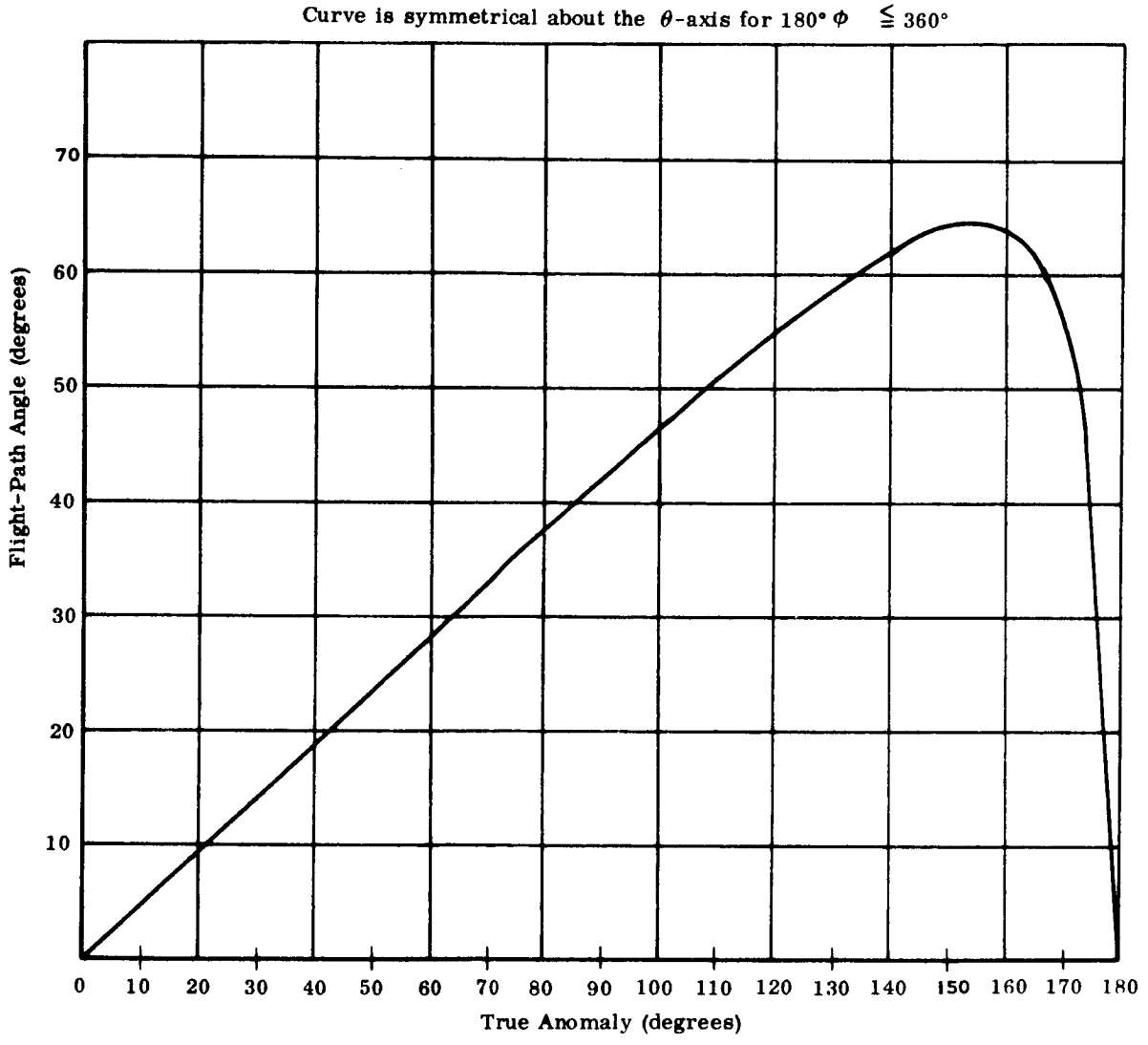

Figure 4.2-9 True Anomaly (θ) vs Flight-Path Angle (φ)

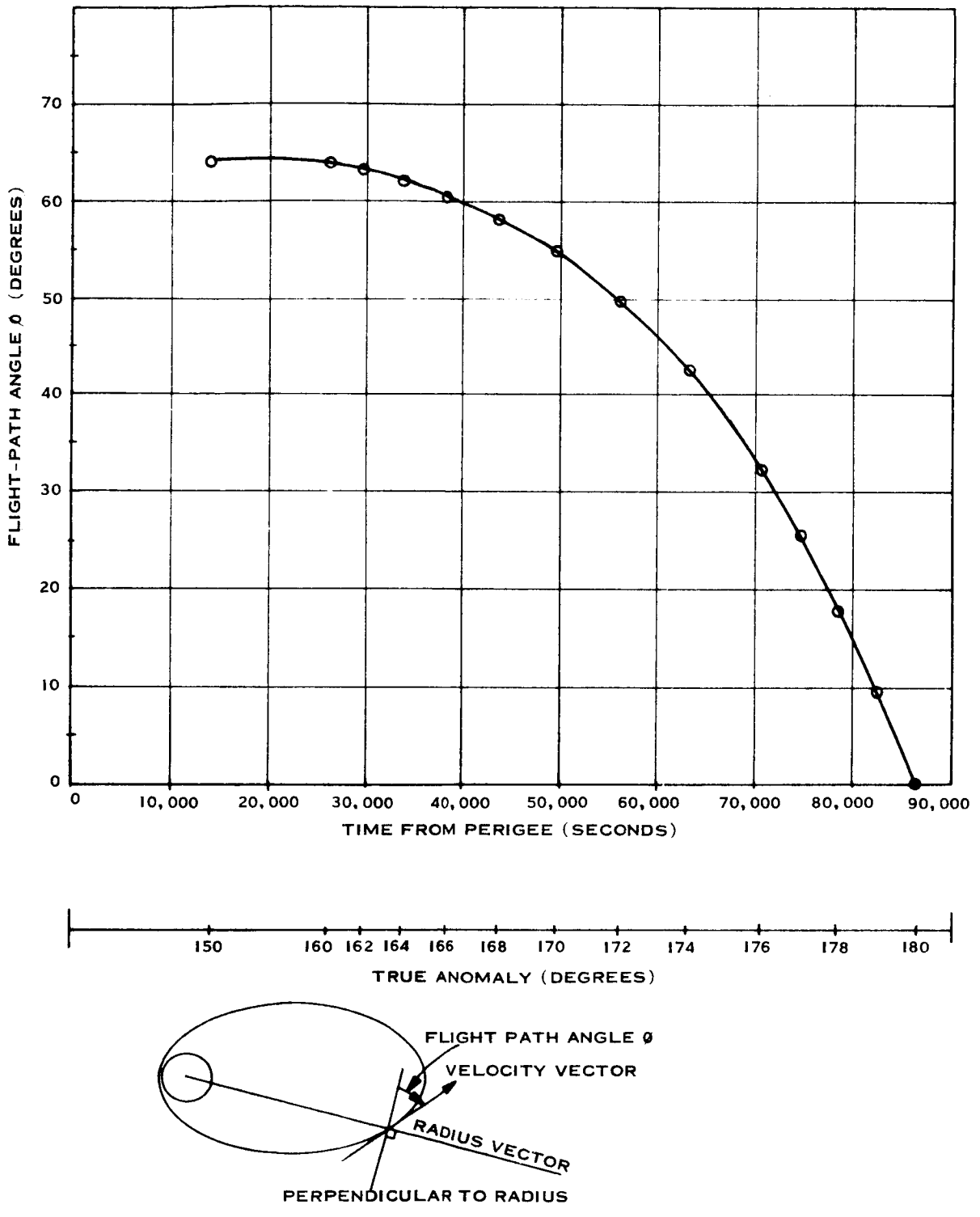

Figure 4.2-10 Flight Path Angle ϕ vs Time and True Anomaly

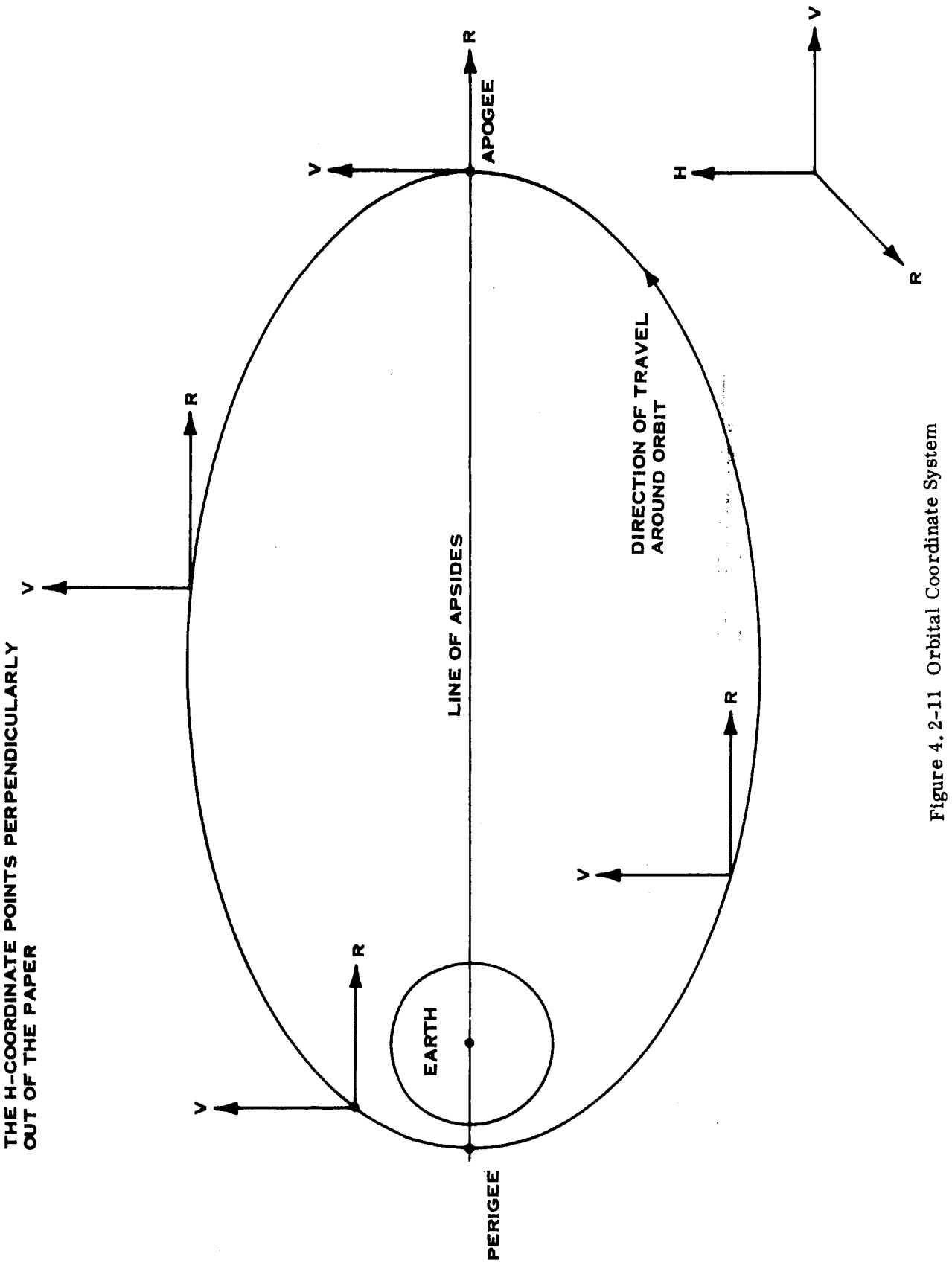

Figure 4.2-11 Orbital Coordinate System

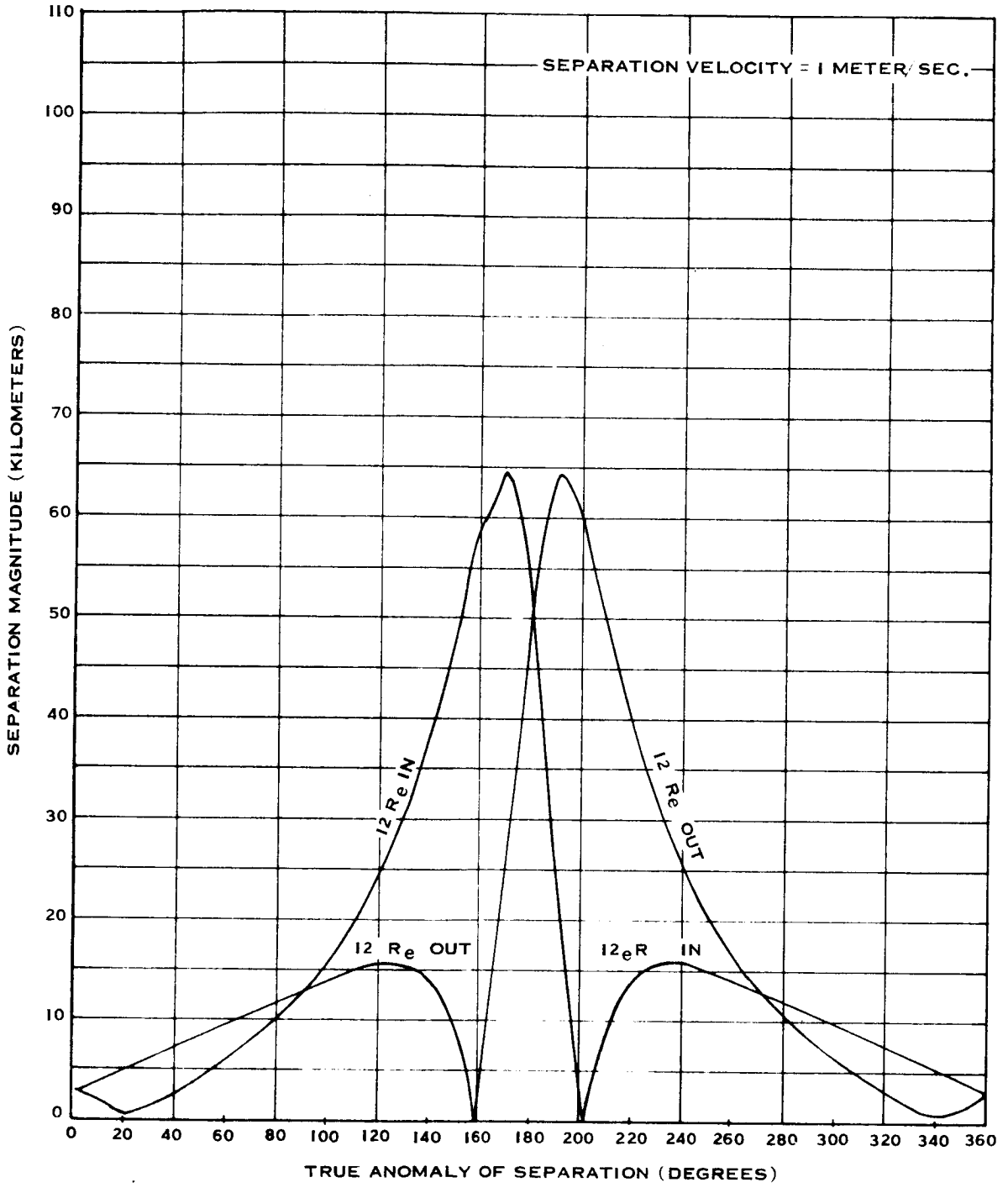

Figure 4.2-12 True Anomaly of Separation vs Absolute Separation Magnitude for Out-of-Plane Upwards Separation

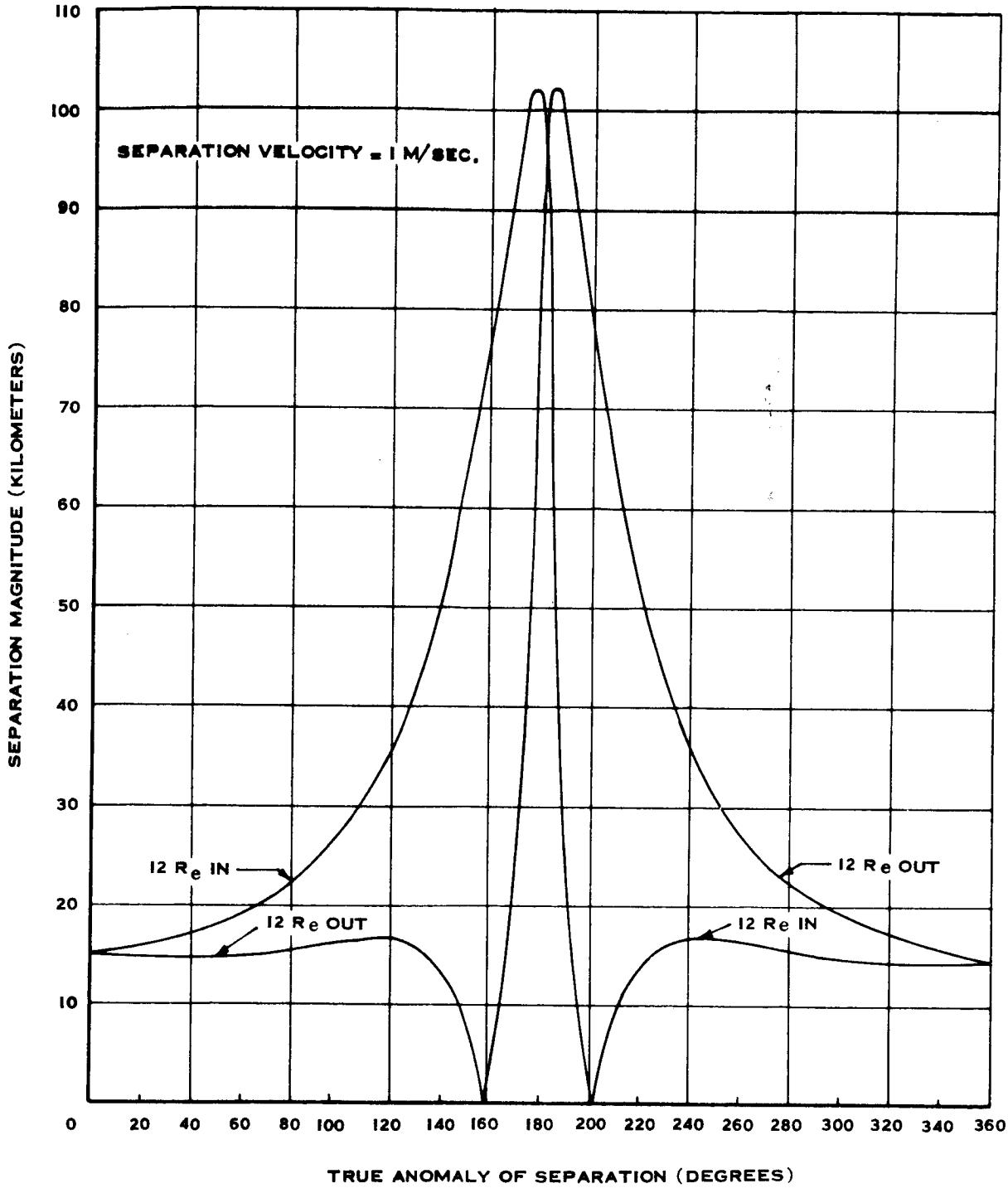

Figure 4.2-13 True Anomaly of Separation vs Absolute Separation Magnitude for In-Plane Inward Separation

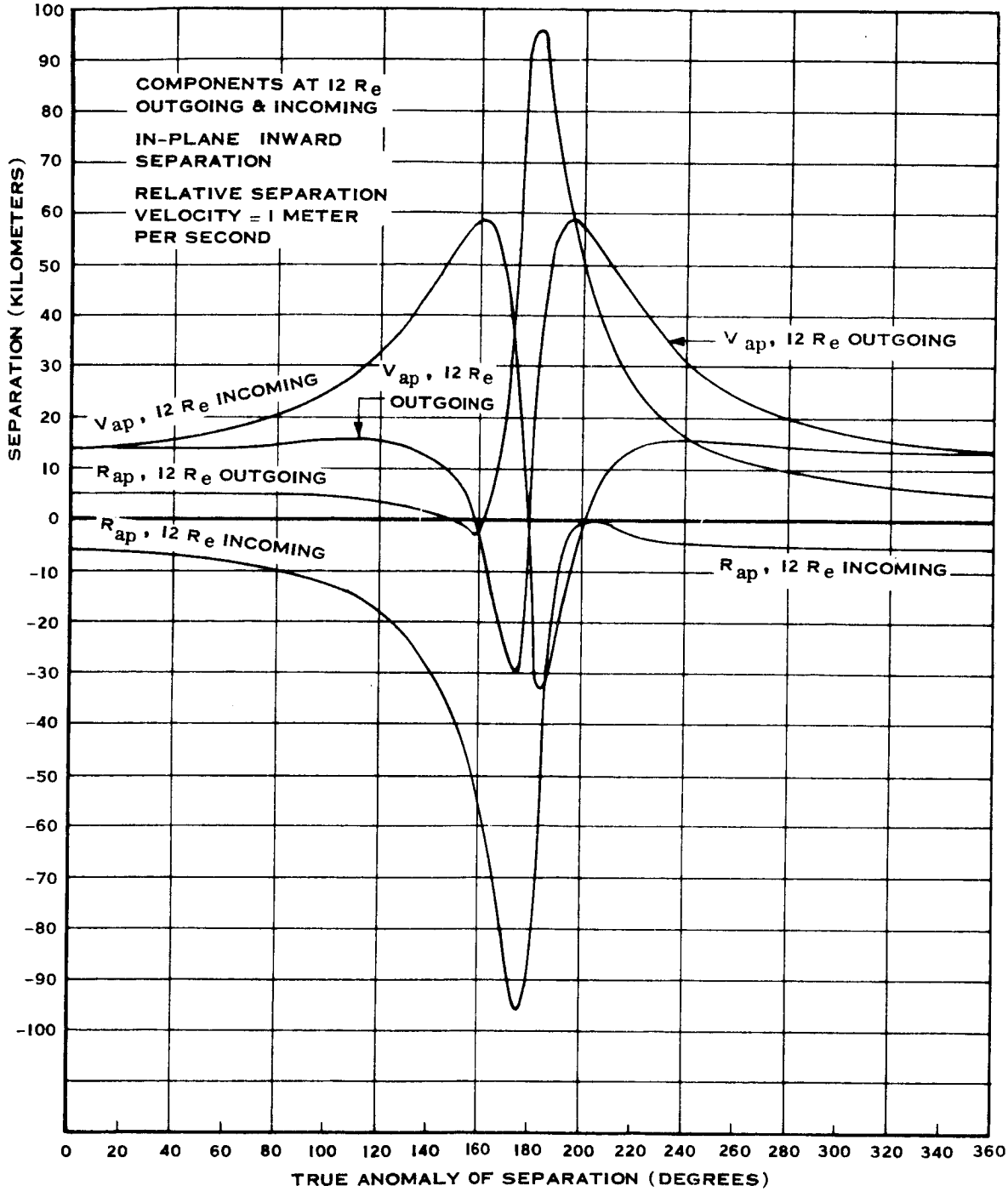

Figure 4.2-14 True Anomaly of Separation vs Magnitude of V_{ap} and R_{ap}

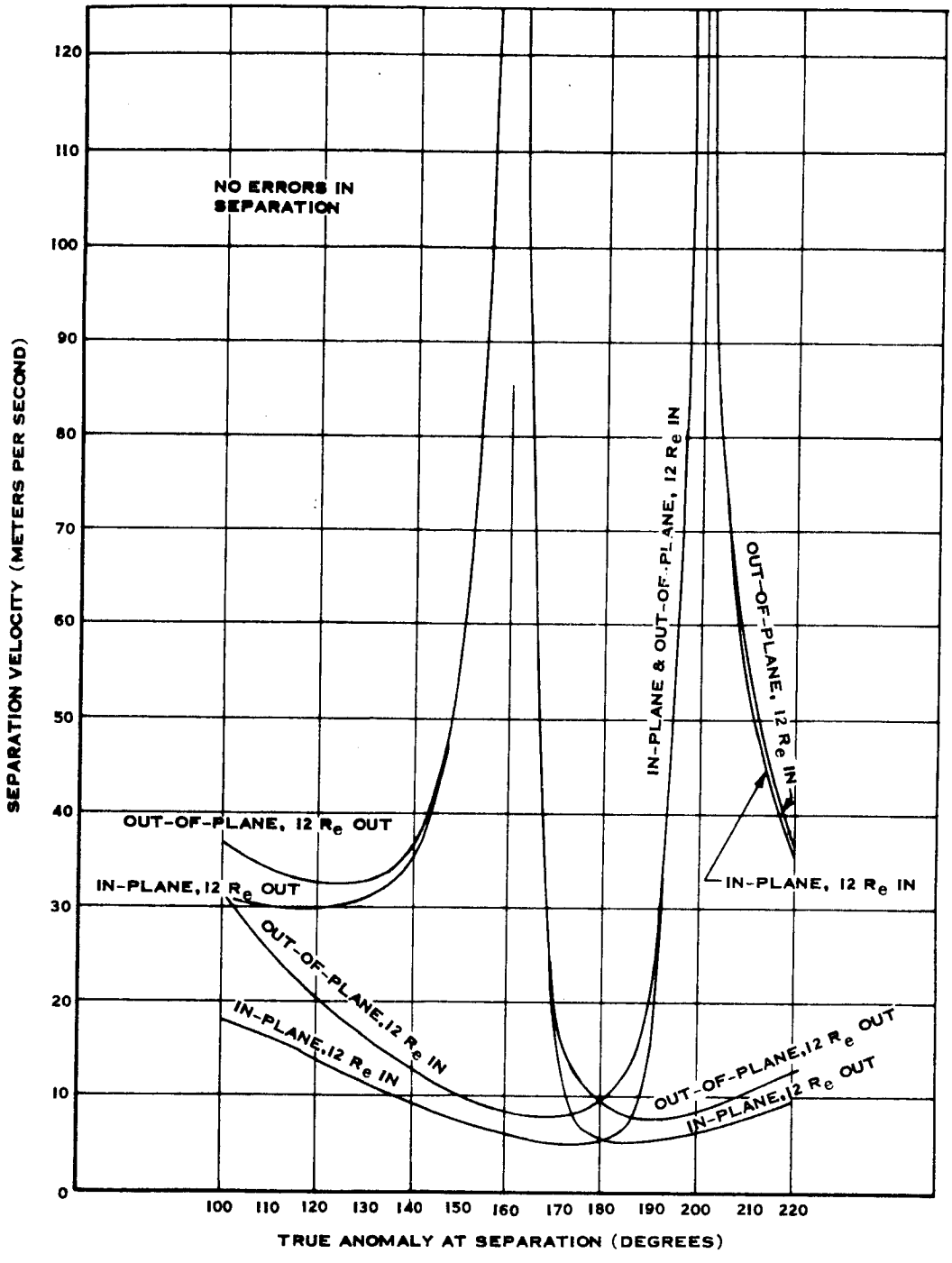

Figure 4.2-15 True Anomaly at Separation vs Separation Velocity Required to Give 500 km Separation at 12 R_e, Outgoing, and 12 R_e, Incoming

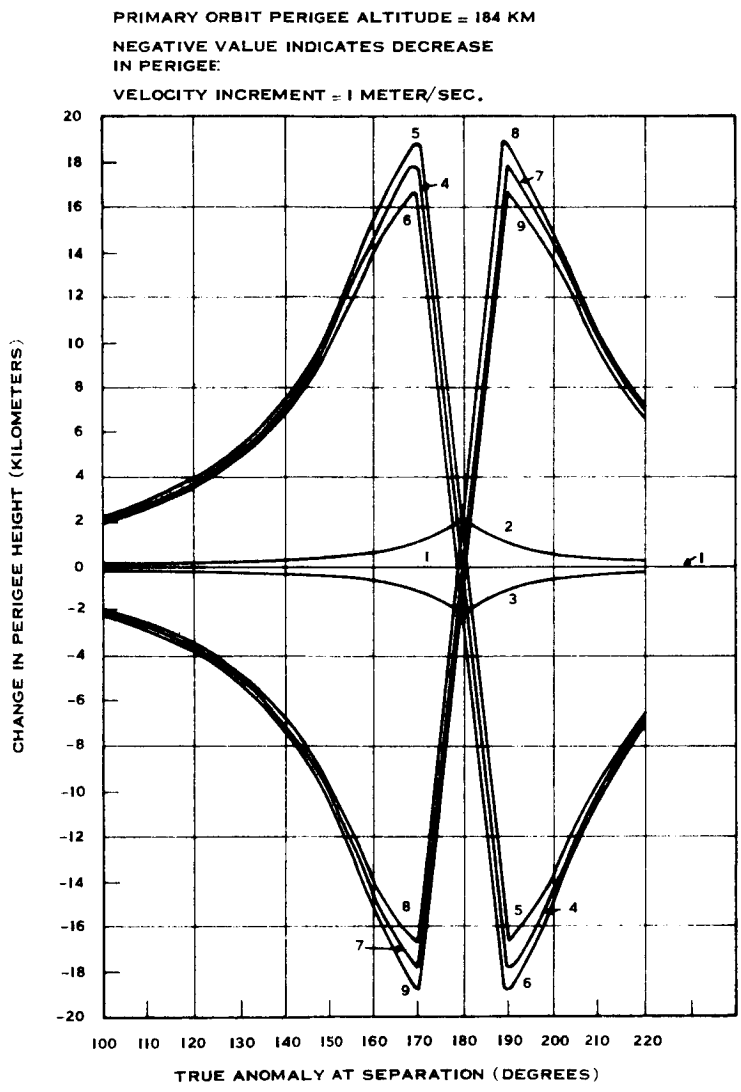

KEY:

CURVE NUMBER	ORIENTATION OF SEPARATION VELOCITY
1	OUT-OF-PLANE UP. NO ERROR
2	OUT-OF-PLANE UP. 5° ERROR FORWARD
3	OUT-OF-PLANE UP. 5° ERROR BACKWARD
4	IN-PLANE INWARD. NO ERROR
5	IN-PLANE INWARD. 5° ERROR FORWARD
6	IN-PLANE INWARD. 5° ERROR BACKWARD
7	IN-PLANE OUTWARD. NO ERROR
8	IN-PLANE OUTWARD. 5° ERROR FORWARD
9	IN-PLANE OUTWARD. 5° ERROR BACKWARD

Figure 4.2-16 True Anomaly at Separation vs Change in Perigee Height with Respect to Primary Orbit

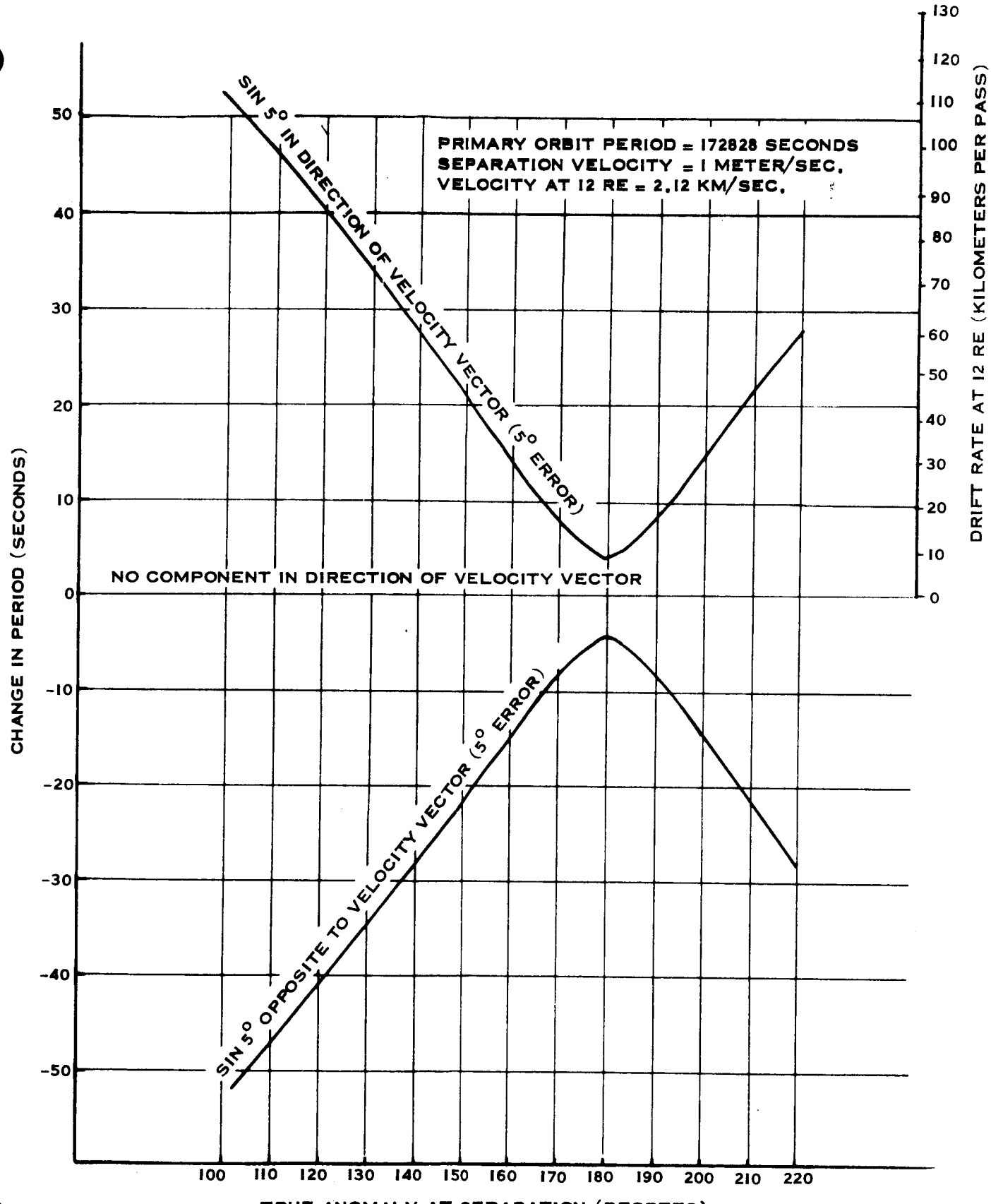

Figure 4.2-17 True Anomaly at Separation vs Change in Period

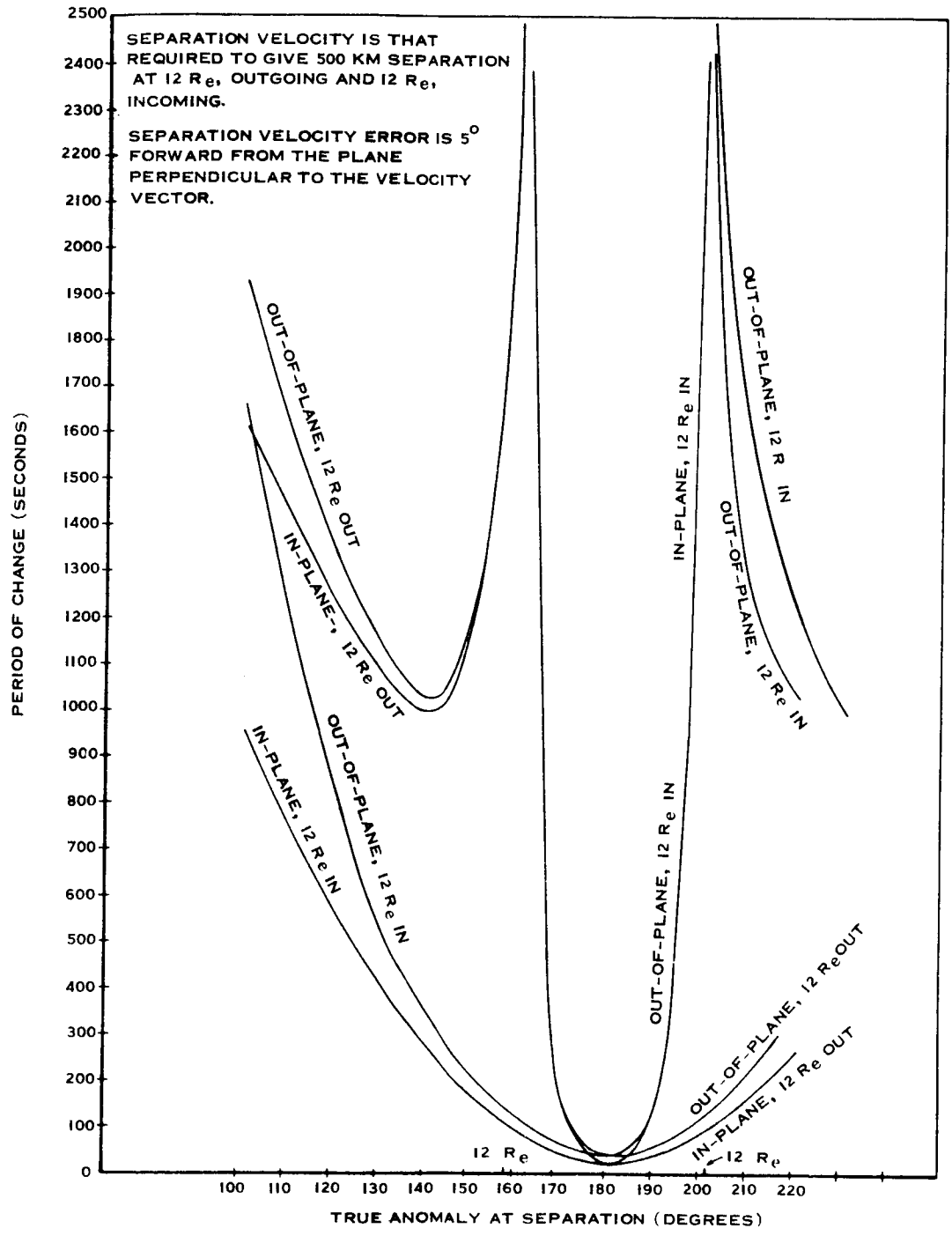

Figure 4.2-18 Period Change vs True Anomaly at Separation

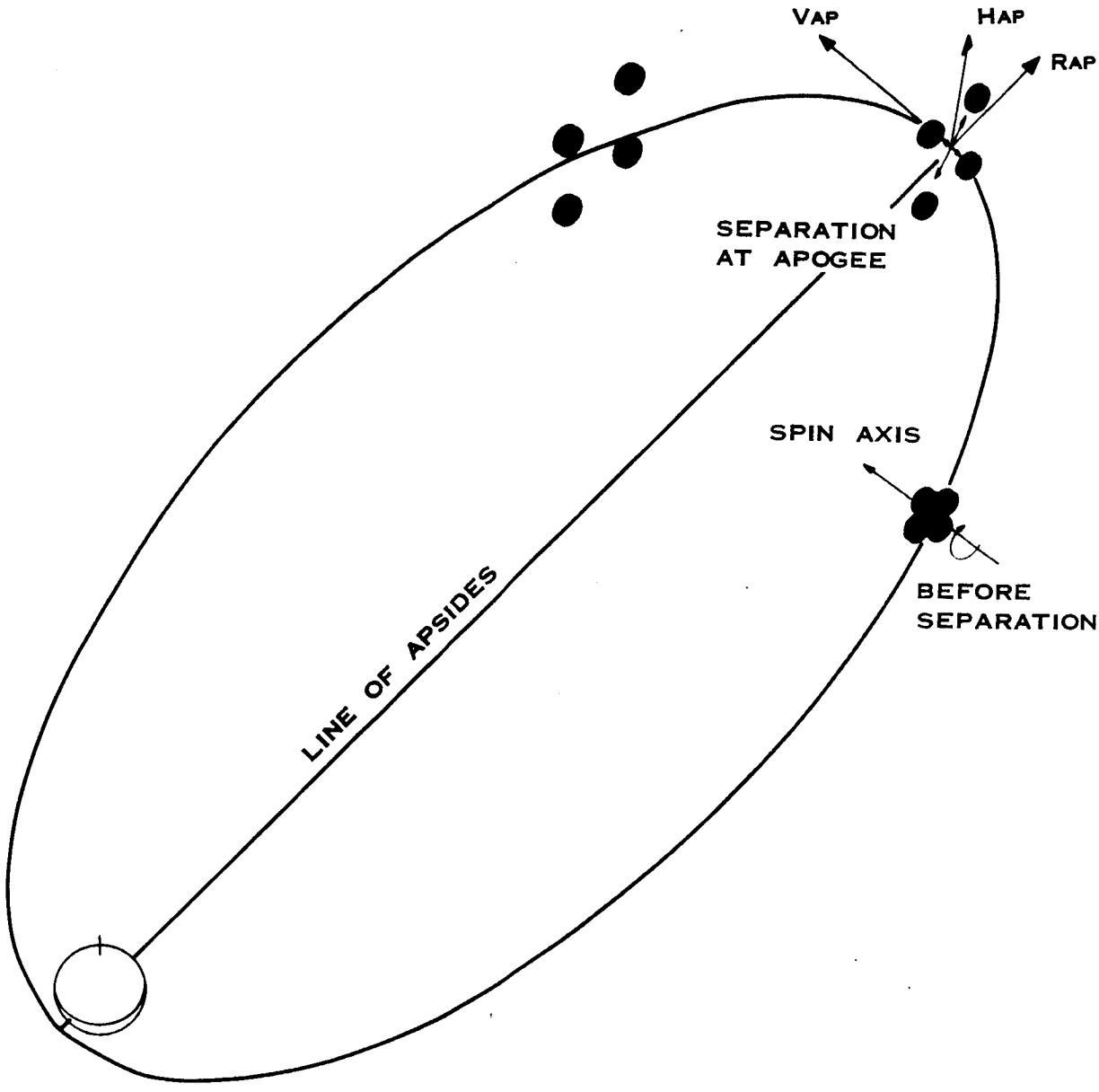

Figure 4.2-19 Radial Array

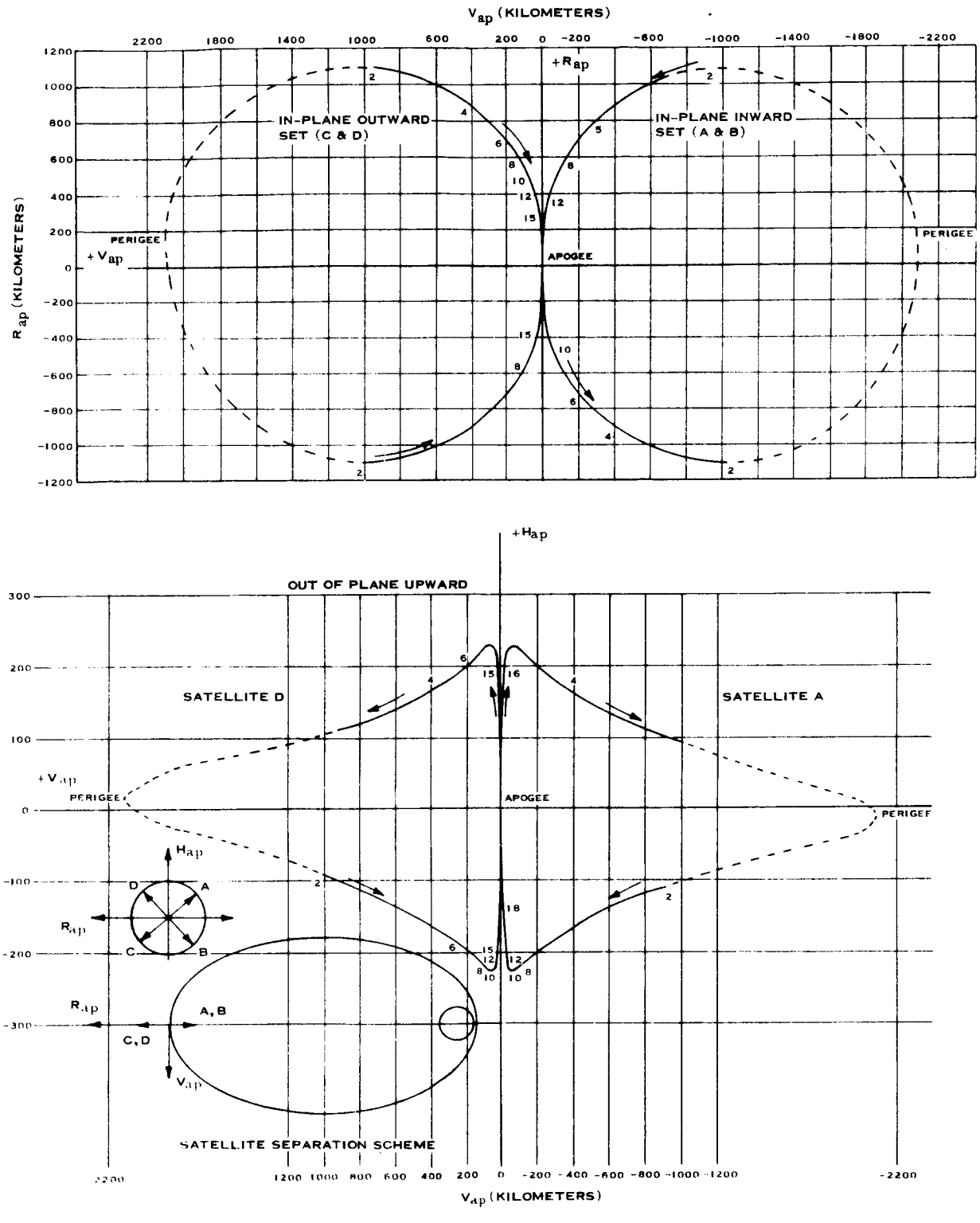

Figure 4.2-20 Radial Separation at Apogee (Separation velocity of each satellite with respect to primary orbit = 6.15 meters/sec)

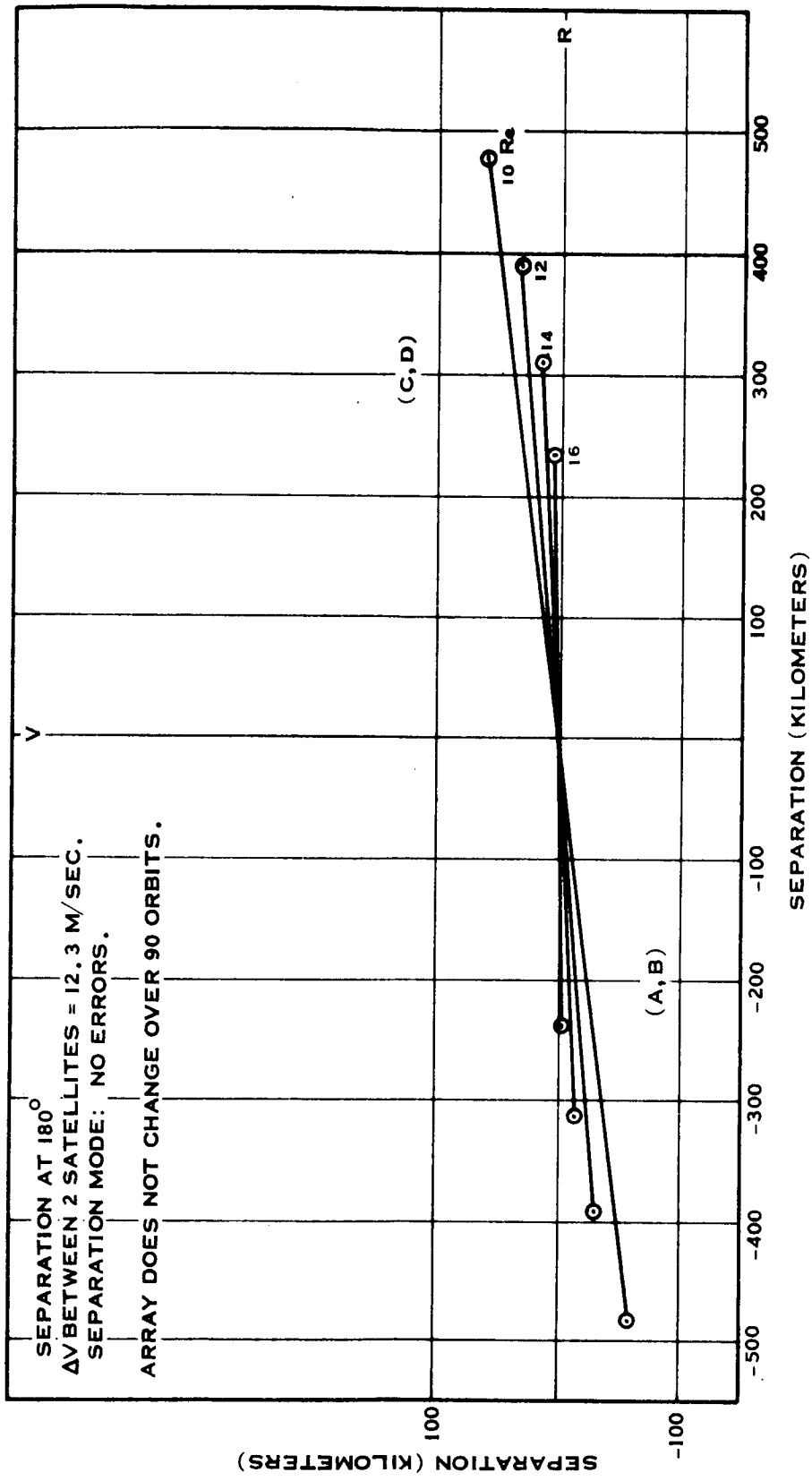

Figure 4.2-21 Radial Array Seen at 12 Re Incoming, 14 Re Incoming, and 16 Re Incoming

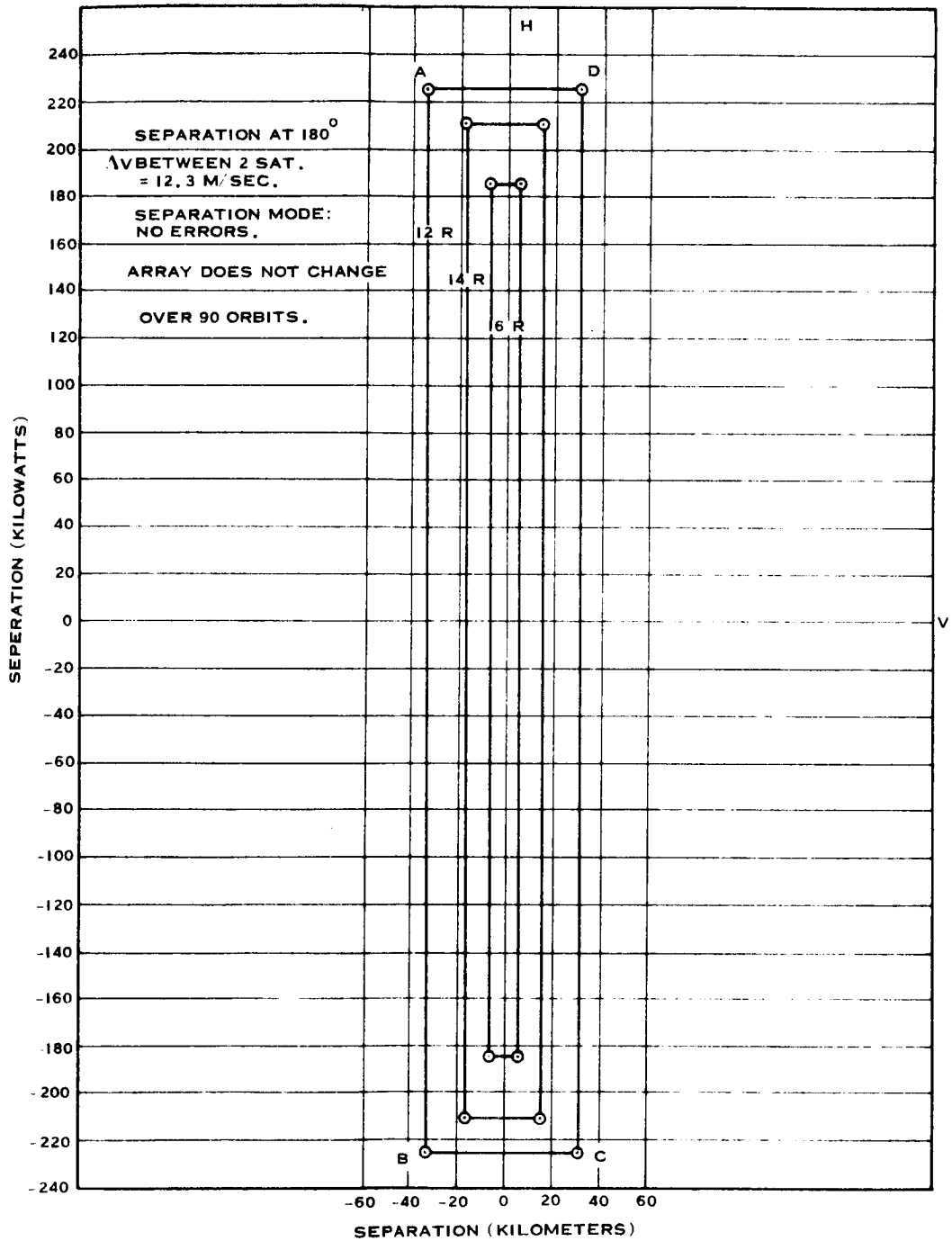

Figure 4.2-22 Radial Array Seen at 12, 14, & 16 Re Incoming

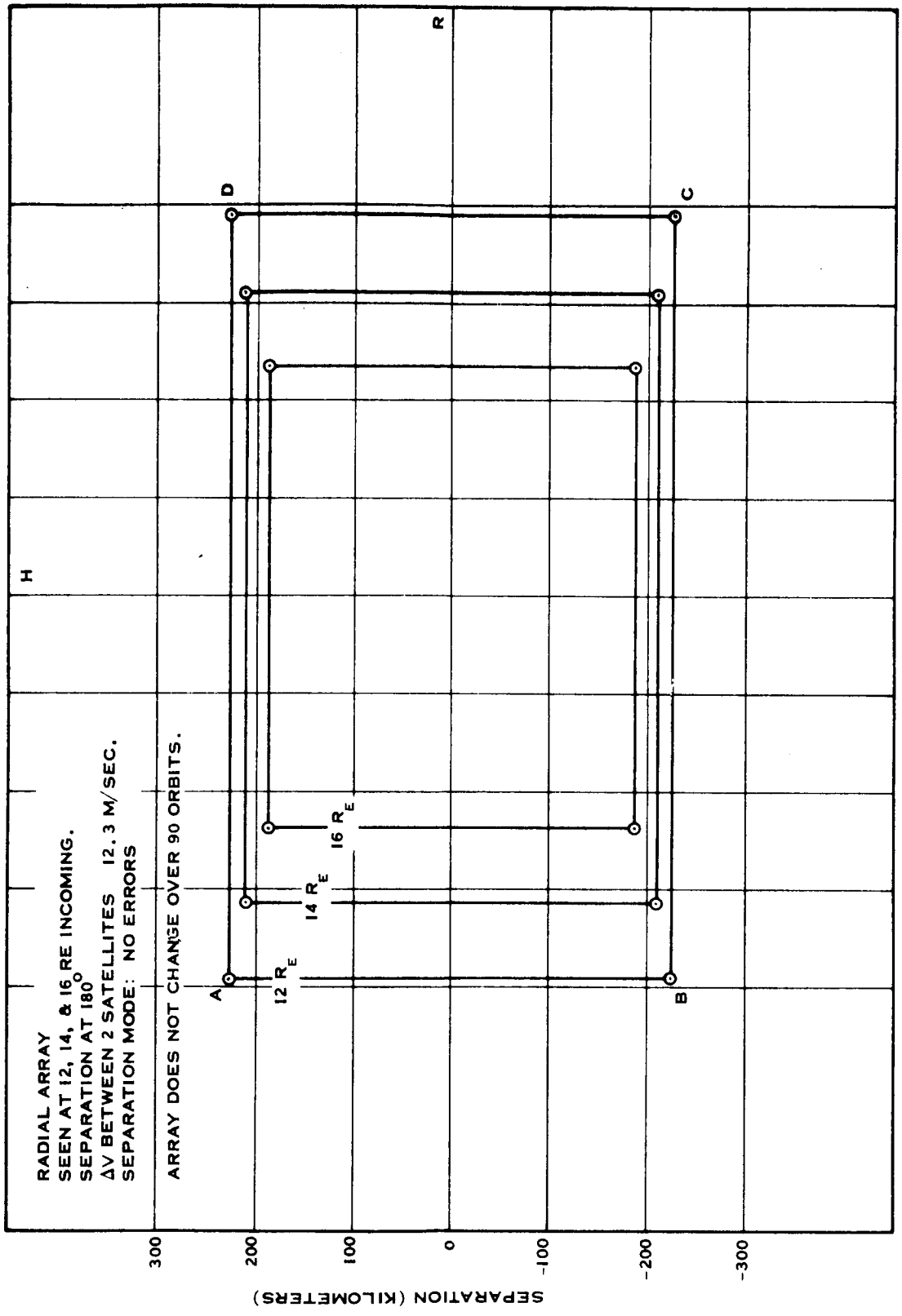

Figure 4.2-23 Radial Array Seen at 12, 14, & 16 Re Incoming

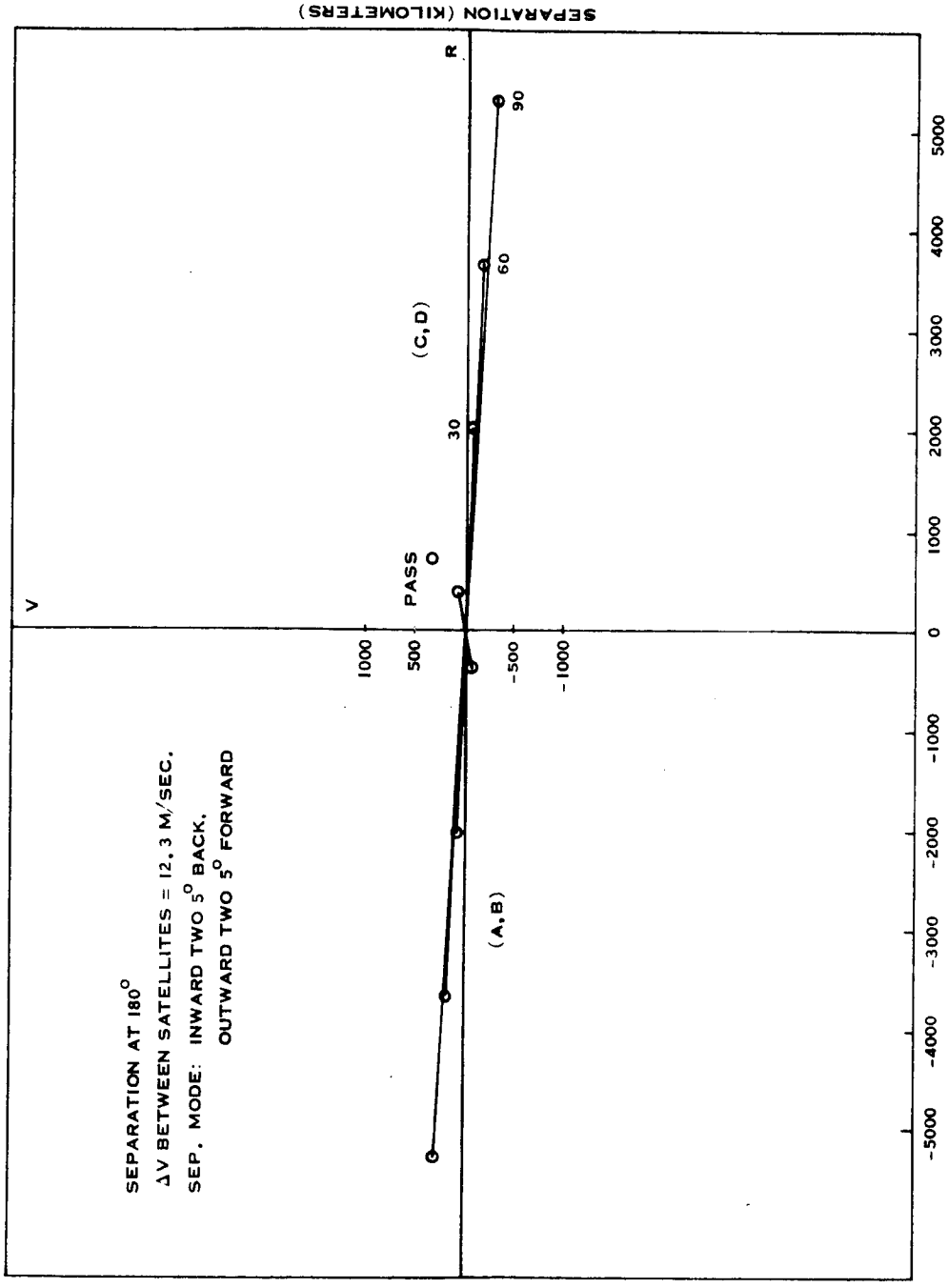

Figure 4.2-24 Radial Array Seen at 12 R_e Incoming

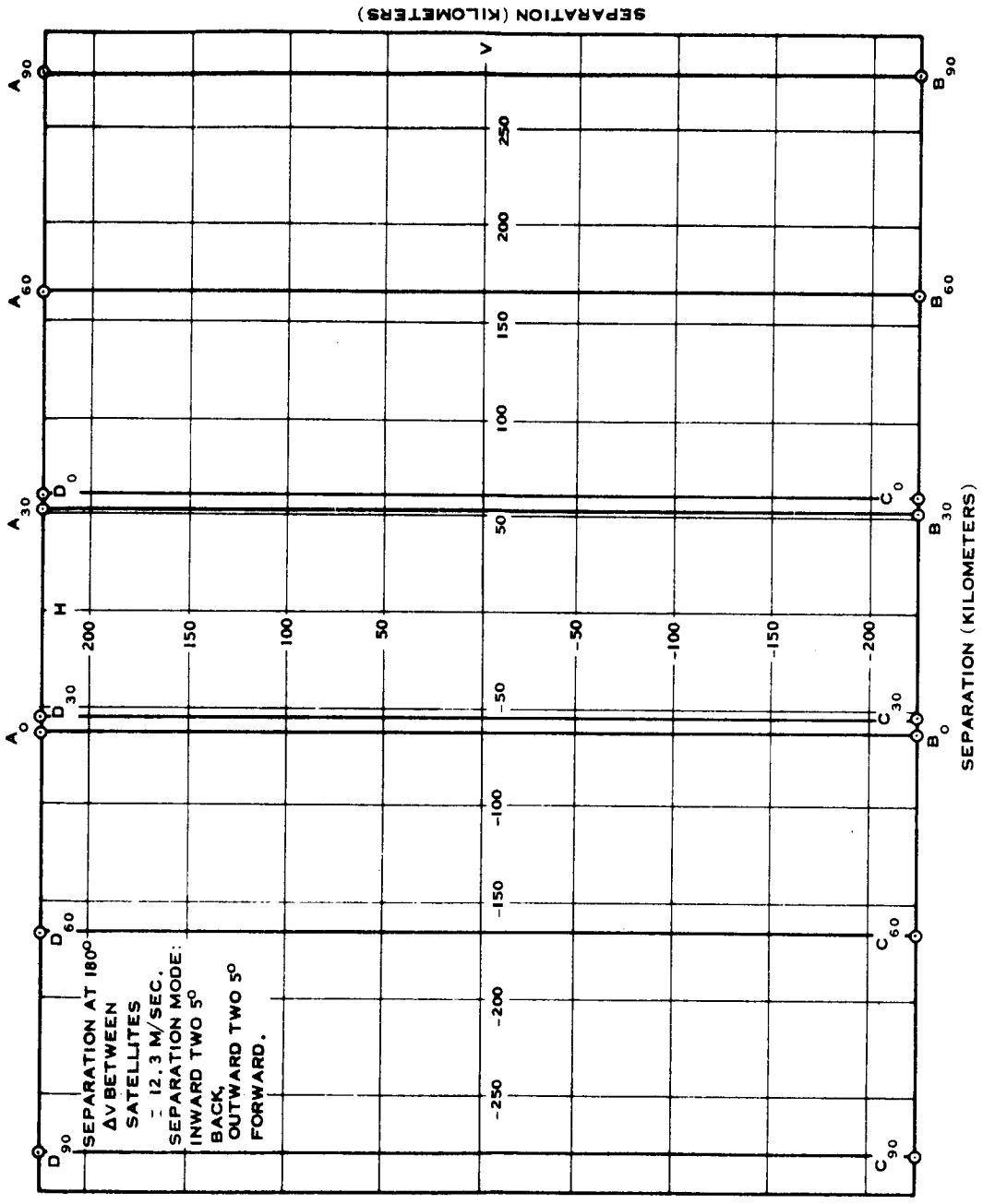

Figure 4.2-25 Radial Array Seen at 12 R_e Incoming

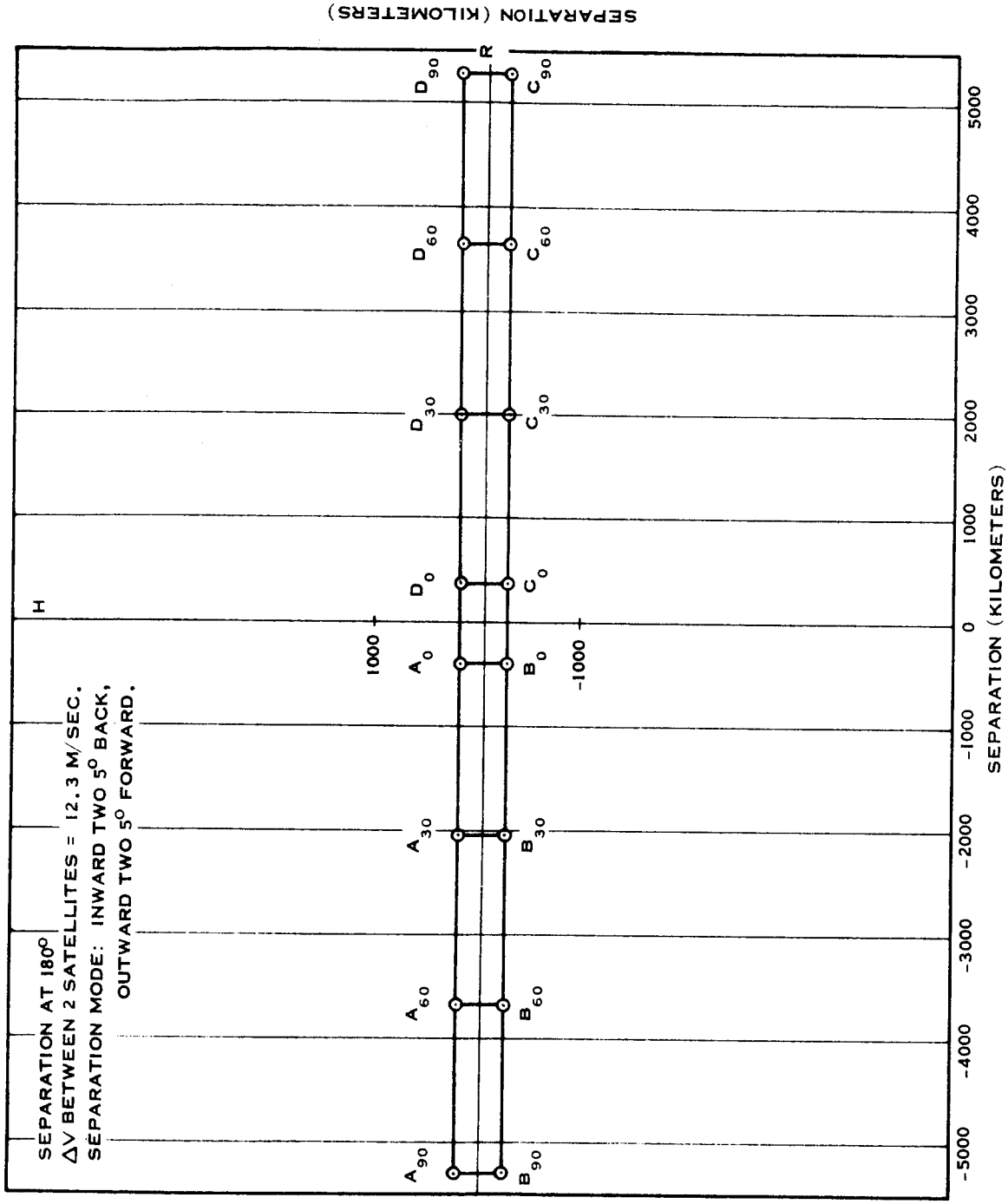

Figure 4.2-26 Radial Array Seen at $12R_e$ incoming.

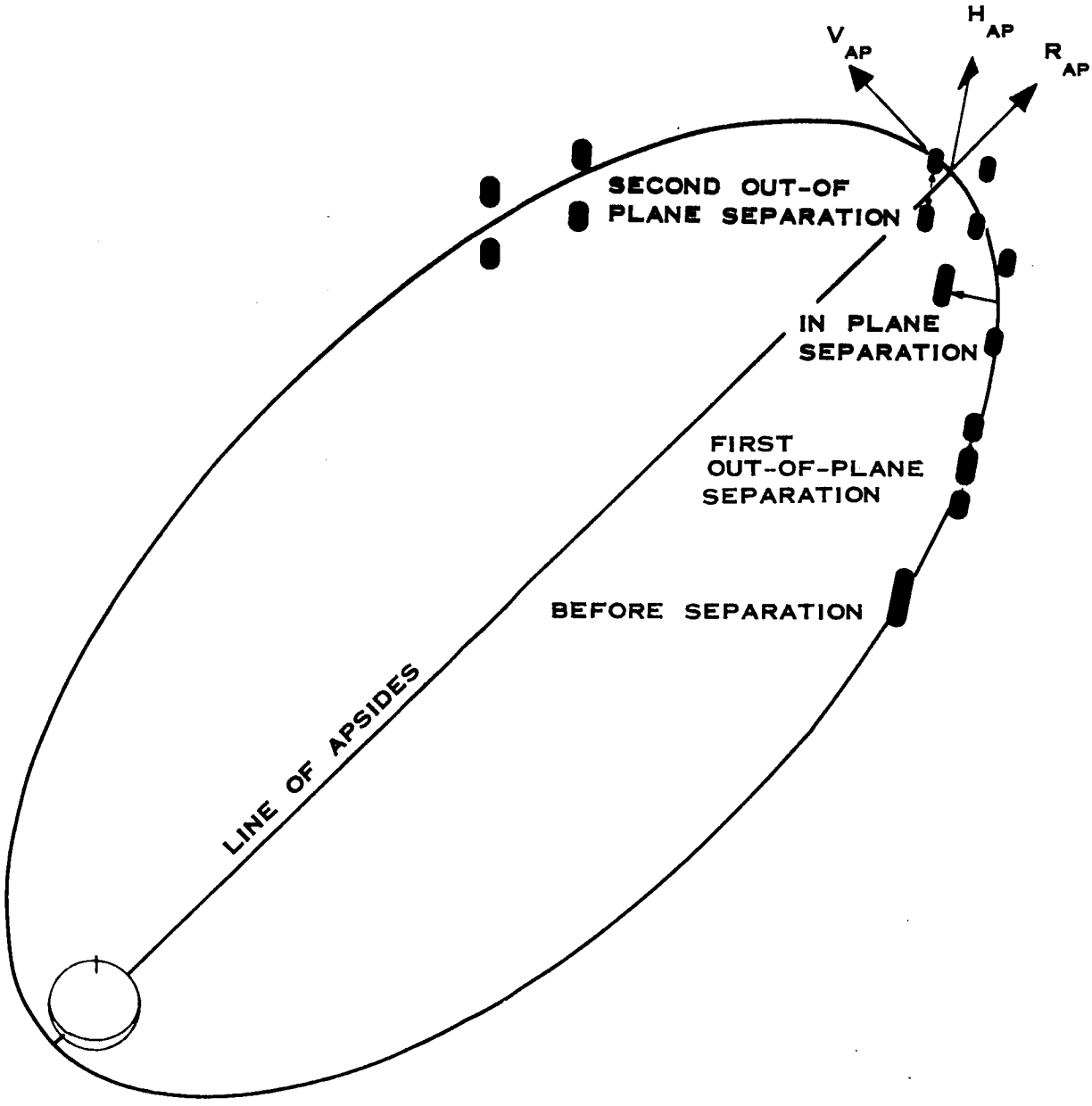

Figure 4.2-27 Stacked Array

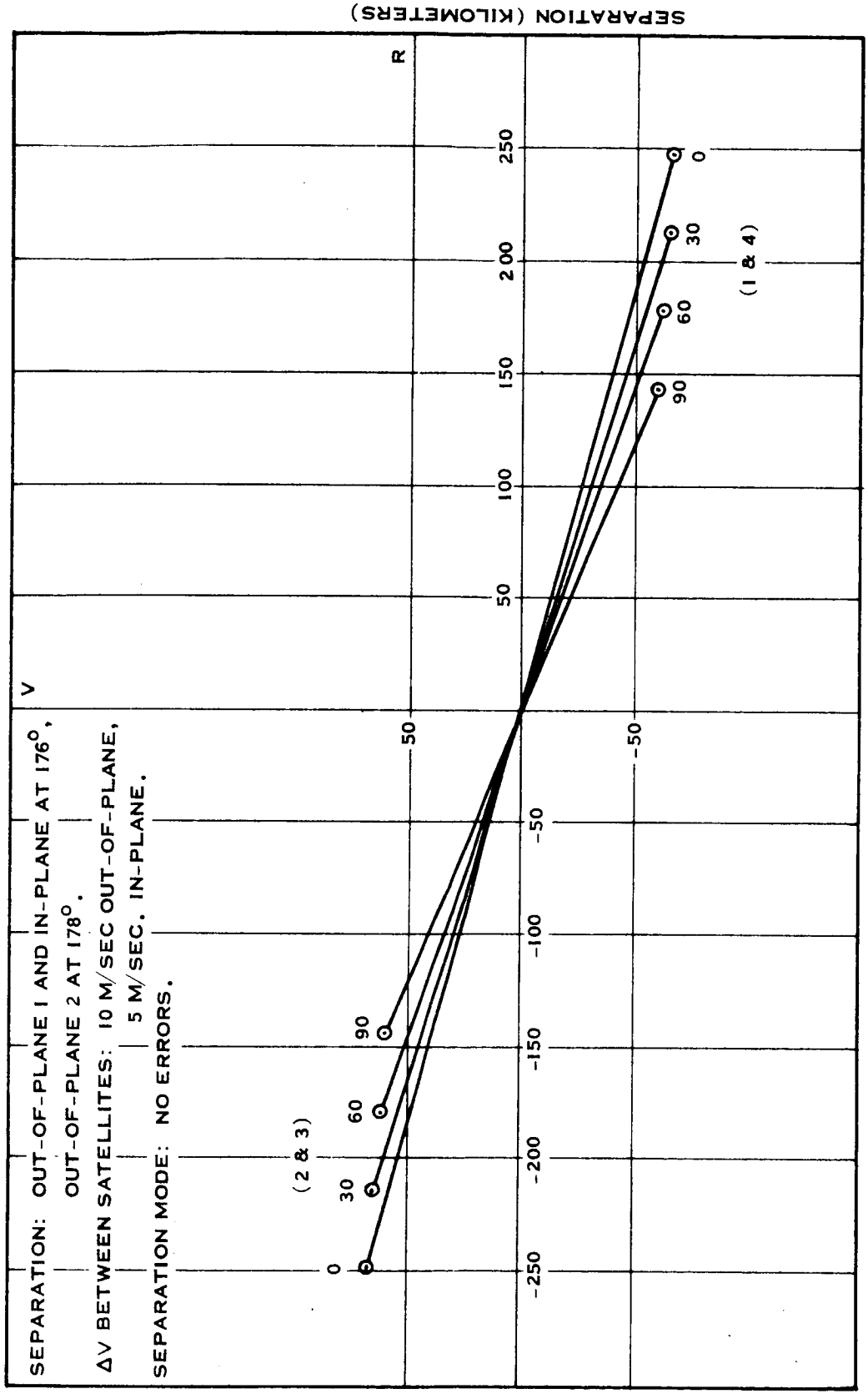

Figure 4.2-28 Stacked Array Seen at $12R_e$ incoming

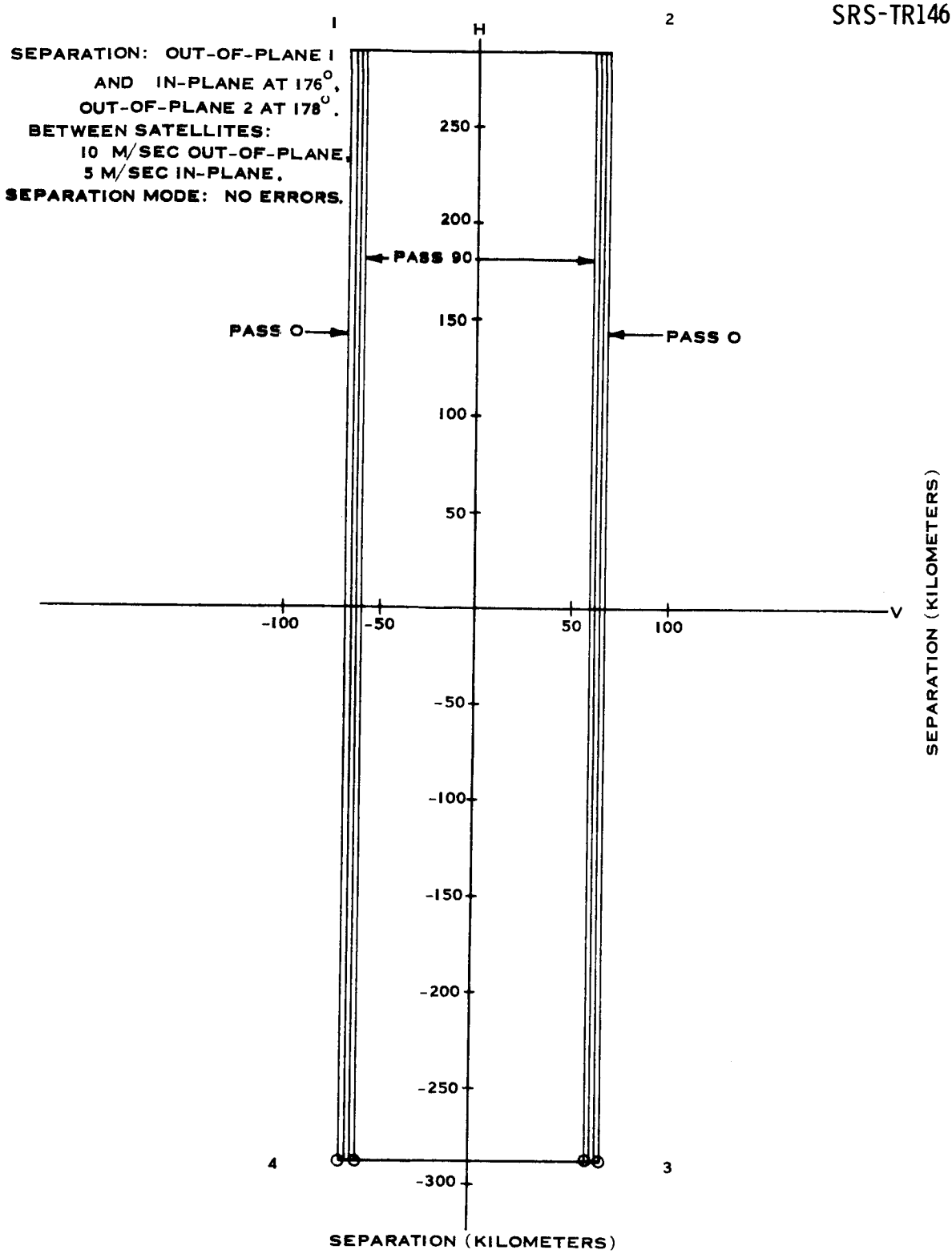

Figure 4.2-29 Stacked Array Seen at 12 R_e Incoming

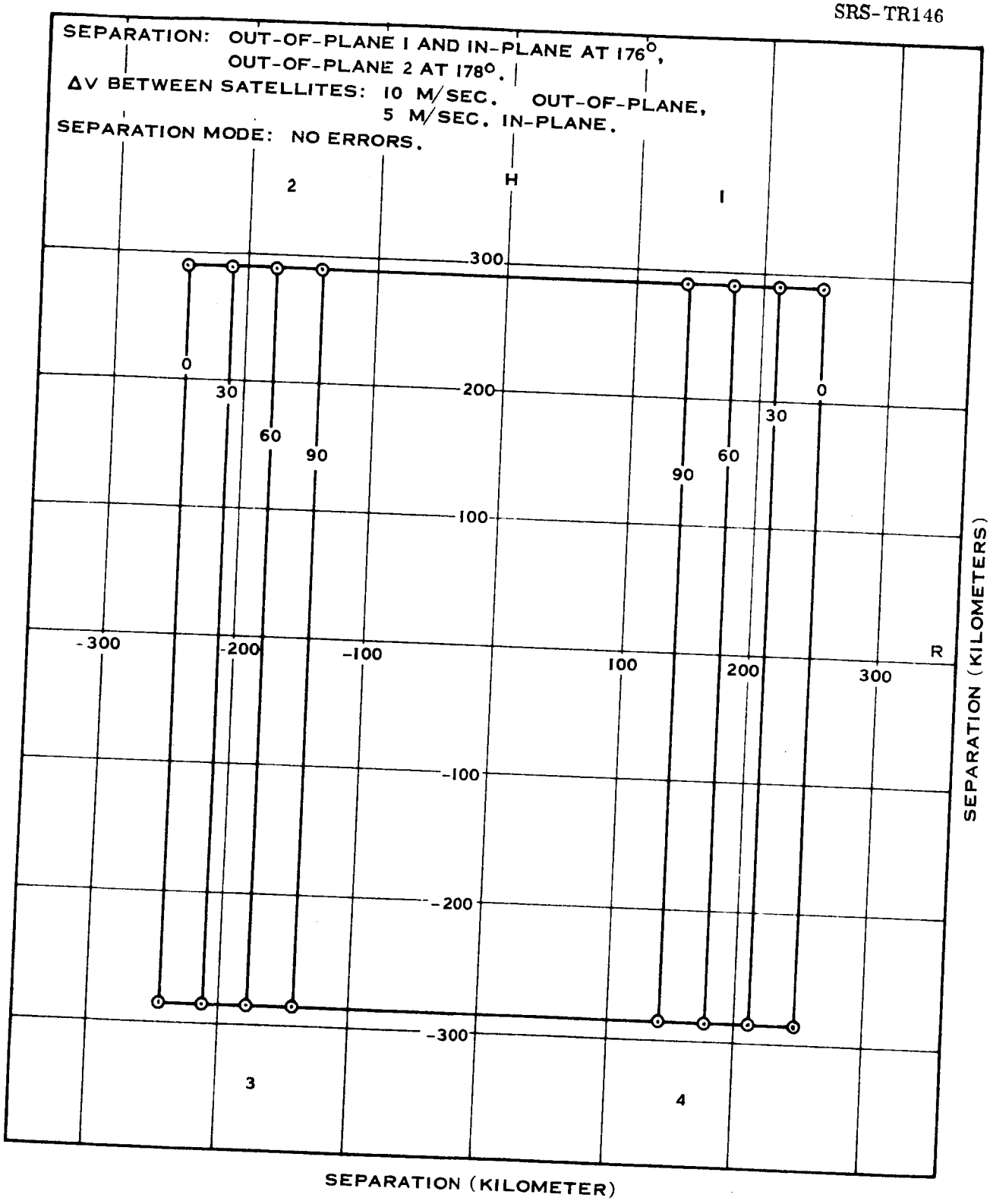

Figure 4.2-30 Stacked Array Seen at $12R_e$ incoming

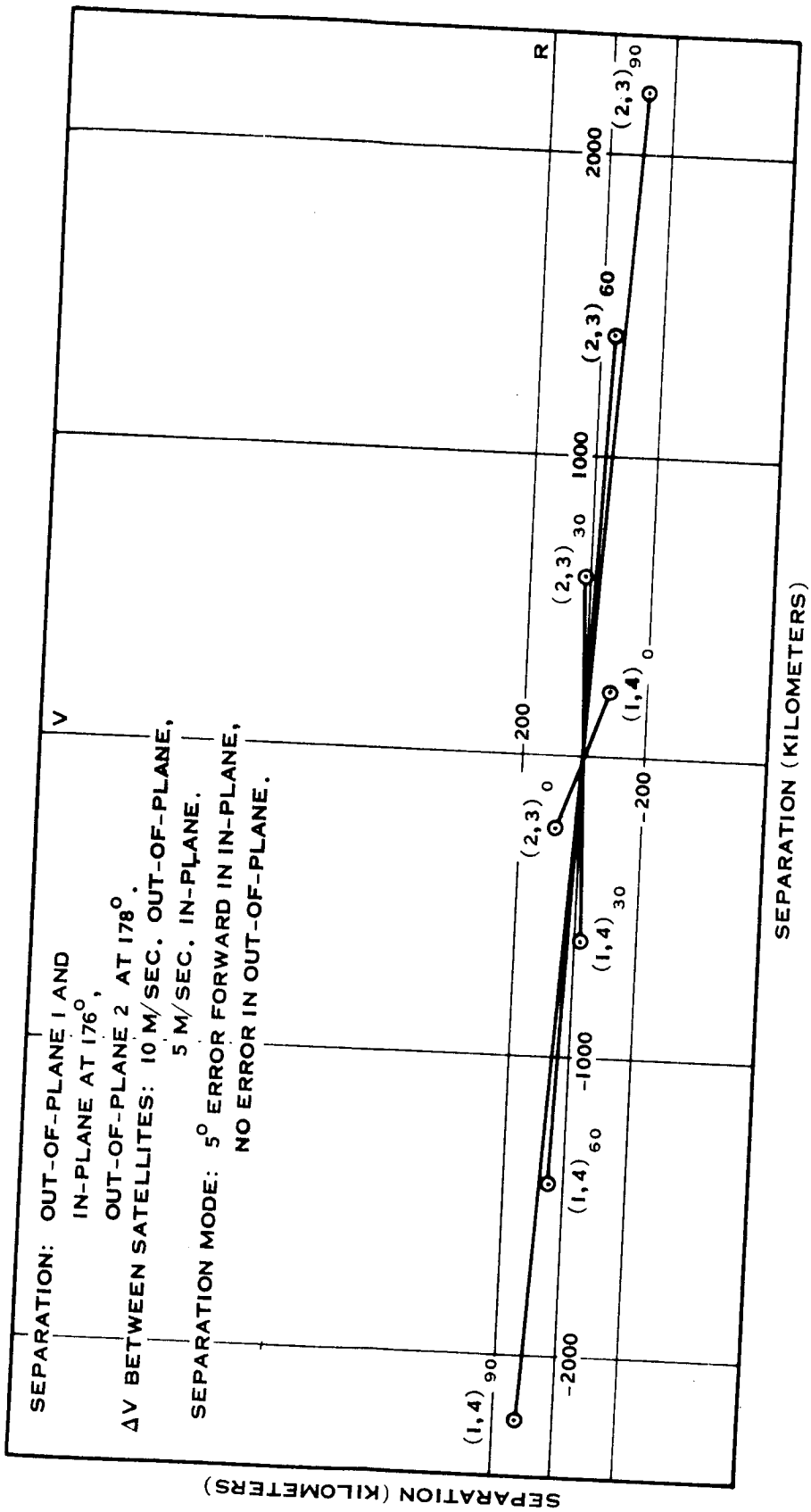

Figure 4.2-31 Stacked Array Seen at 12 R_e Incoming

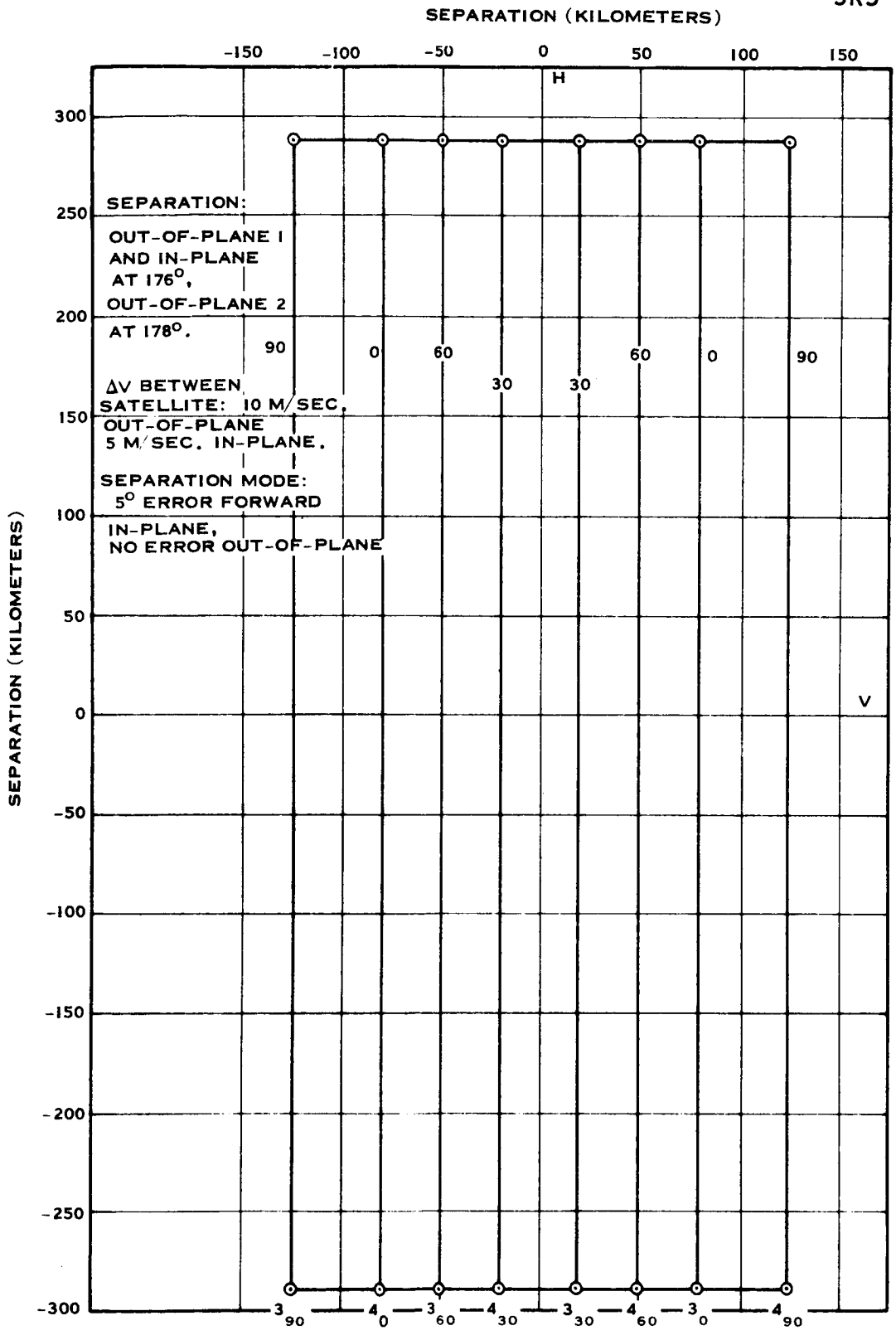

Figure 4.2-32 Stacked Array Seen at 12 Re in.

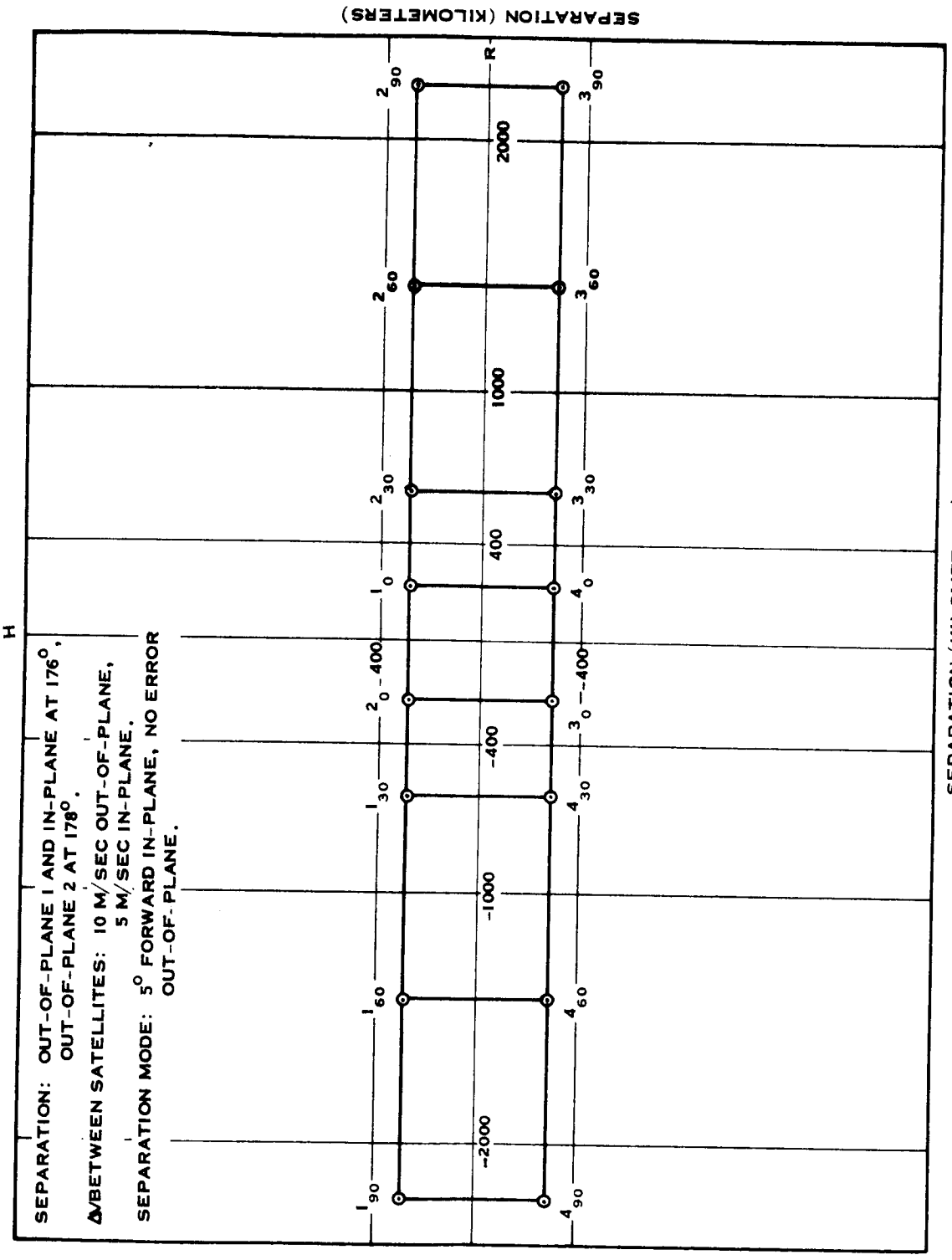

Figure 4.2-33 Stacked Array Seen at 12 R_e Incoming

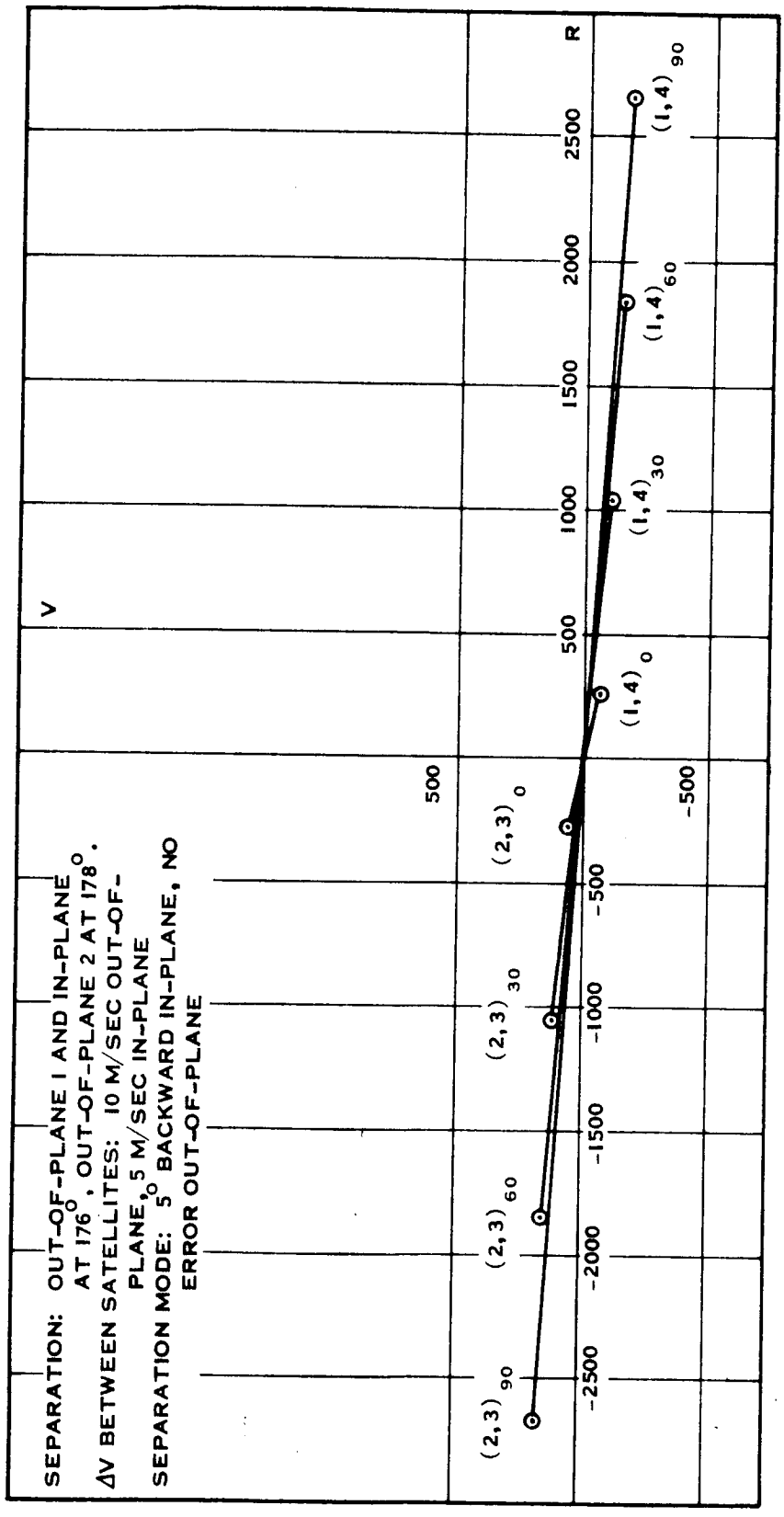

Figure 4.2-34 Stacked Array Seen at $12R_e$ incoming.

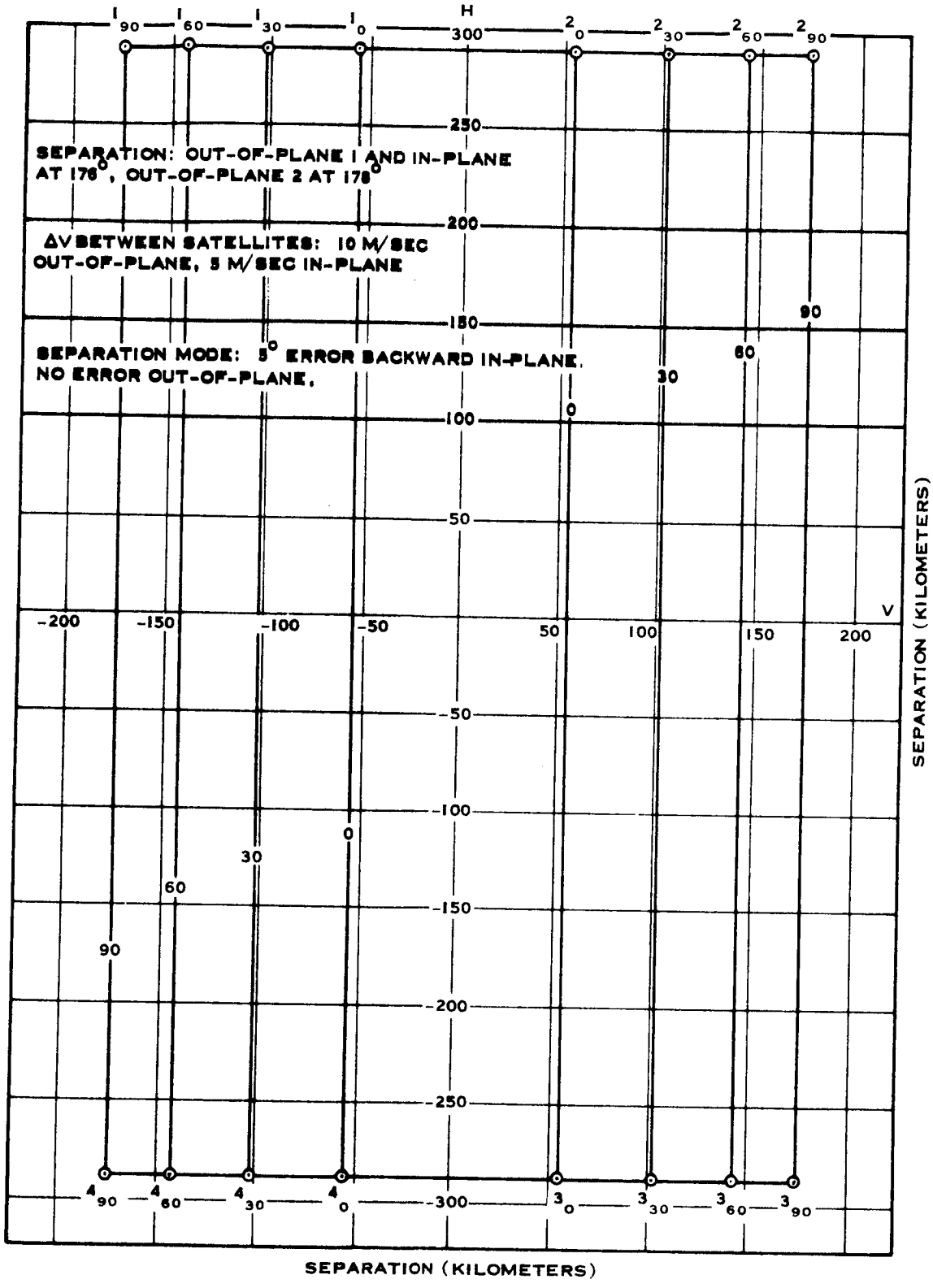

Figure 4.2-35 Stacked Array Seen at $12R_e$ incoming

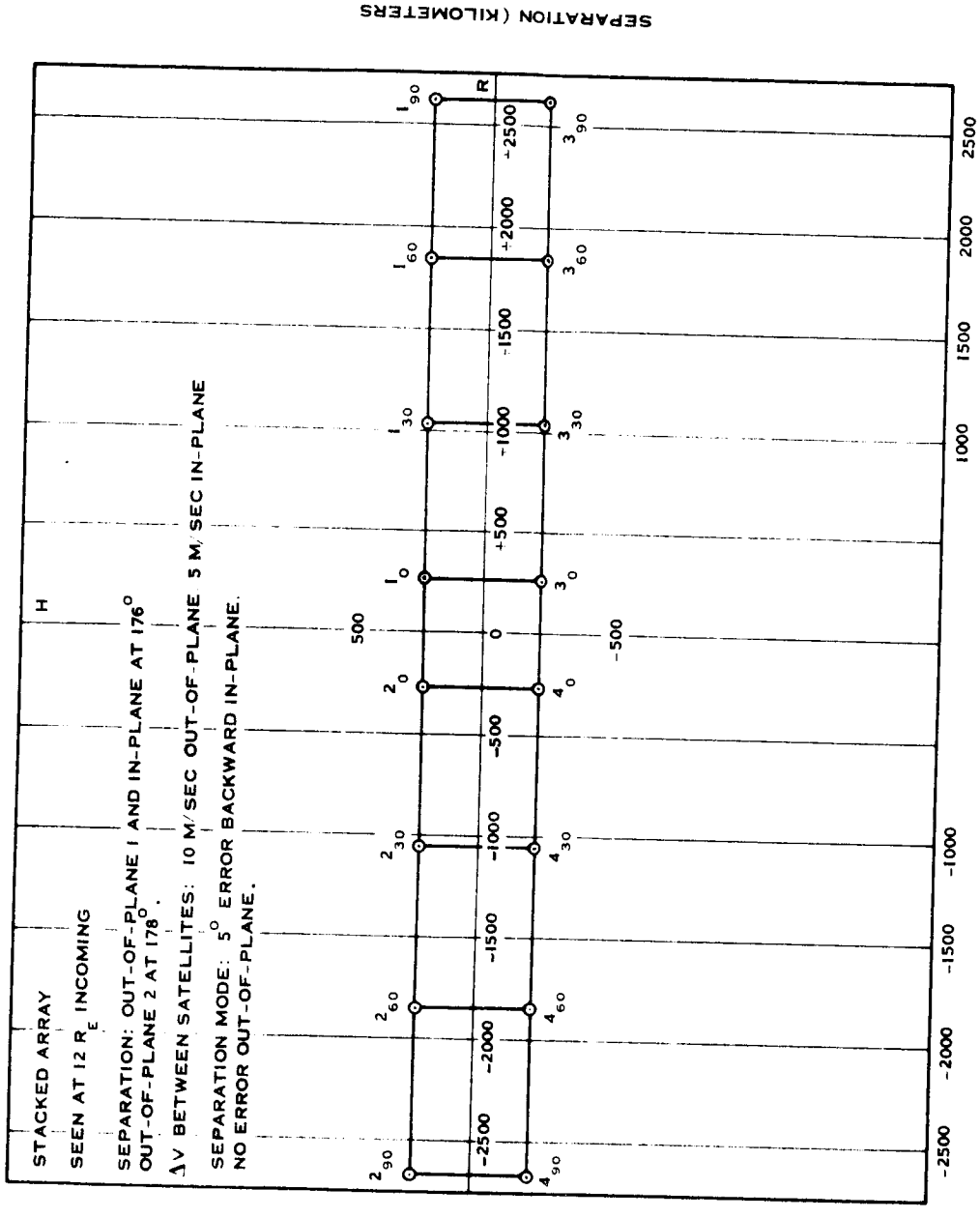

Figure 4.2-36 Stacked Array Seen at 12 R_e Incoming

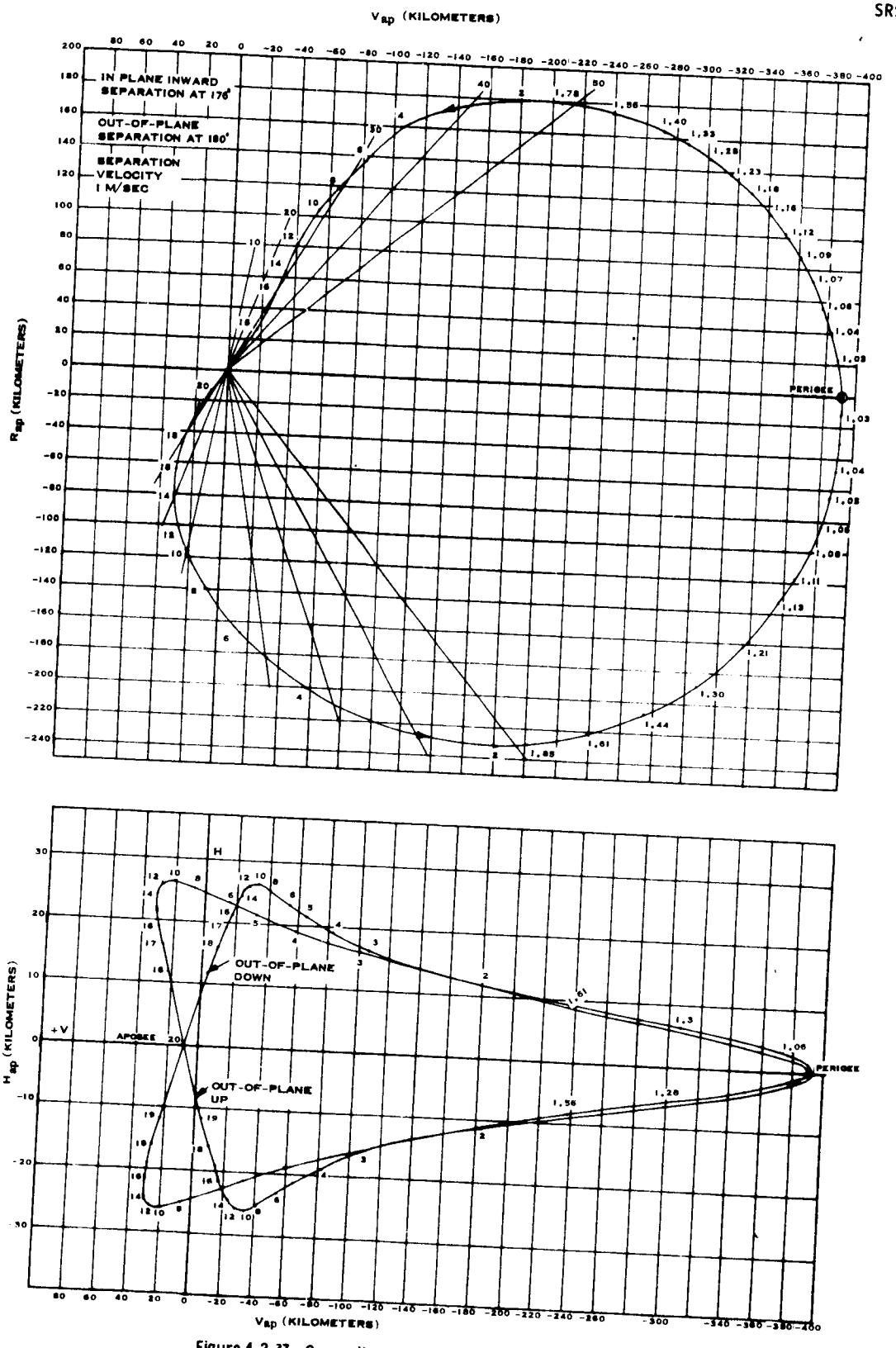

Figure 4.2-37 Composite Separation Graph, Stacked Array

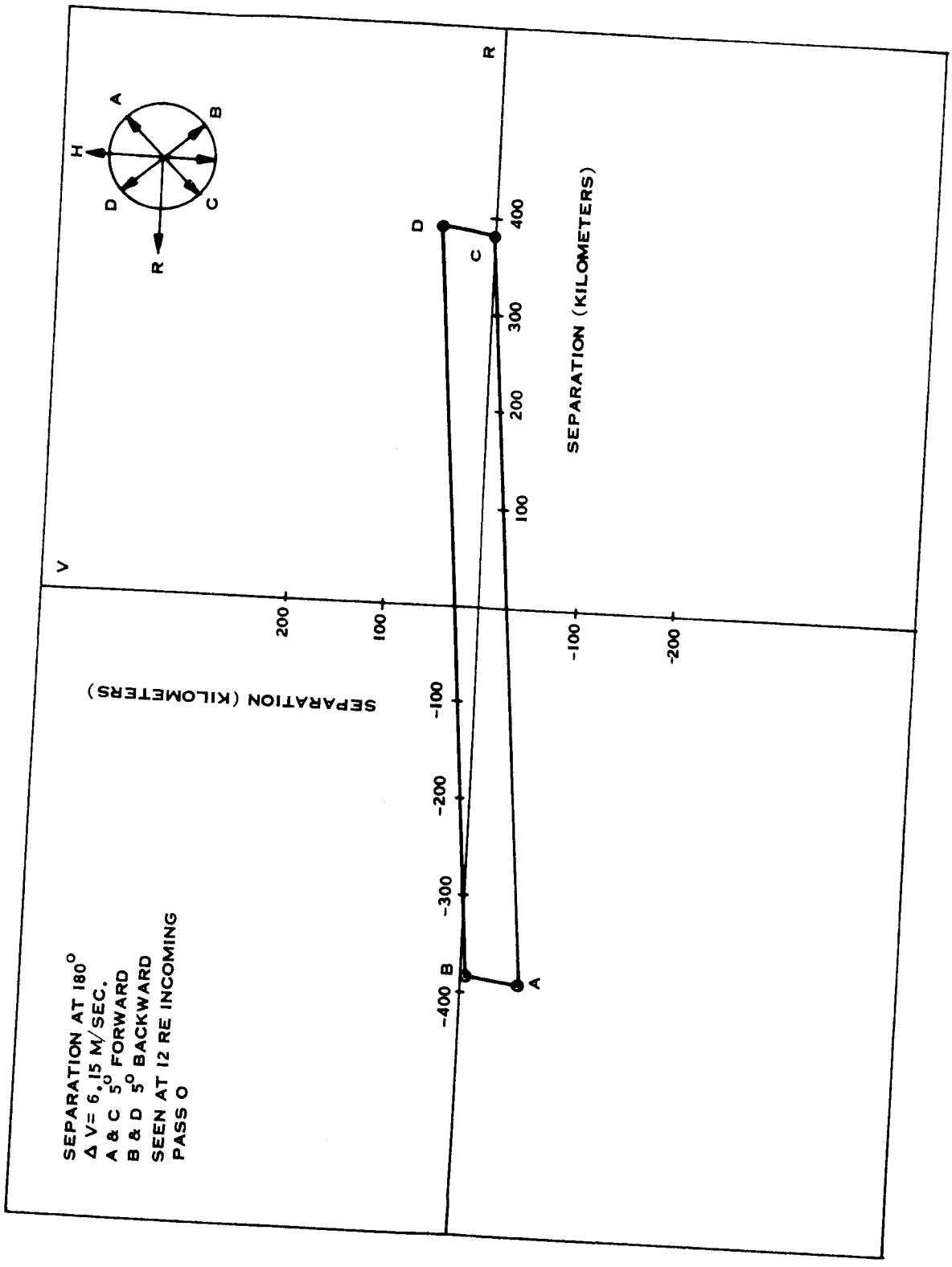

Figure 4.2-38 Non-Planar Radial Array

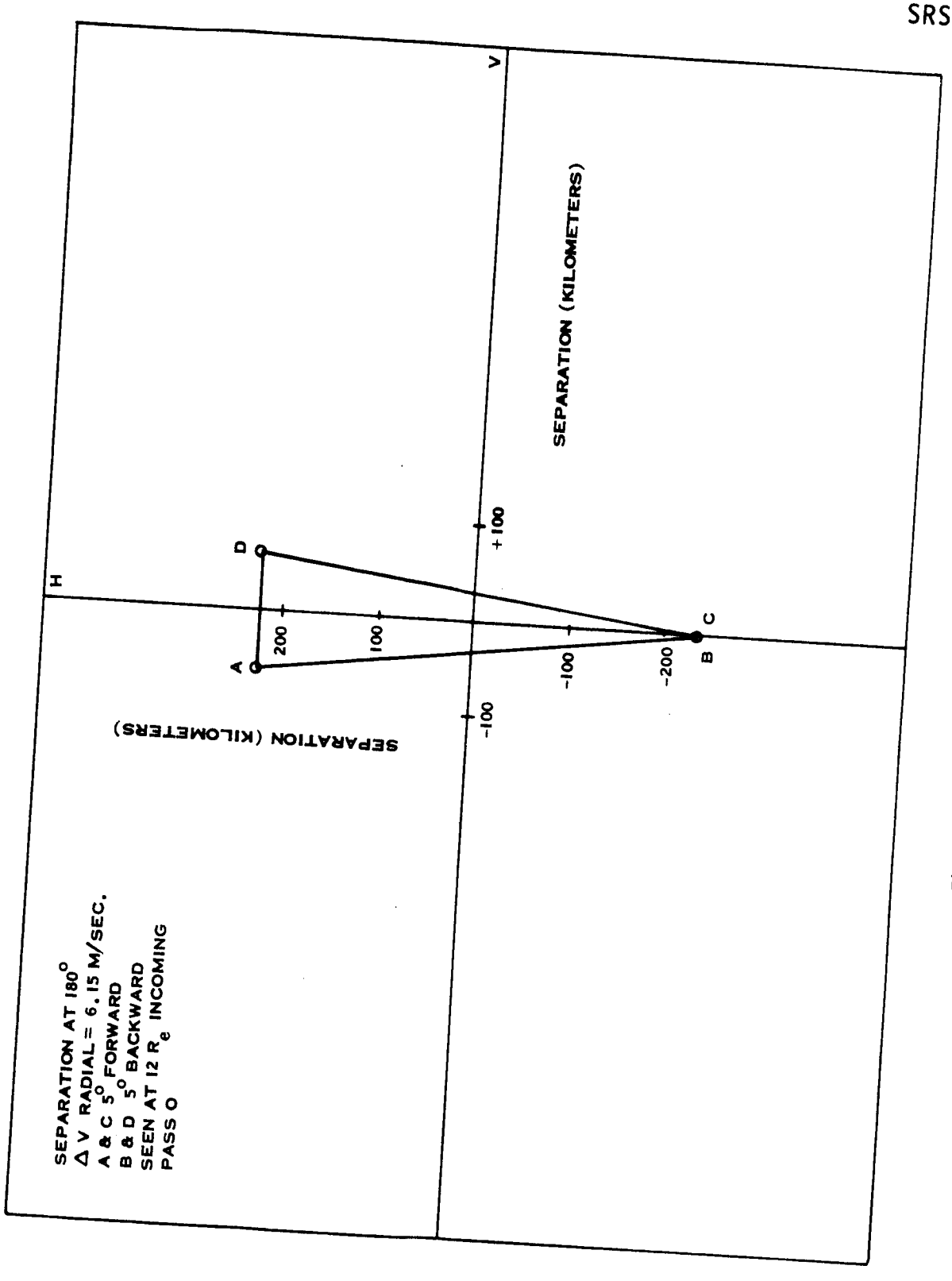

Figure 4.2-39 Non-Planar Radial Array

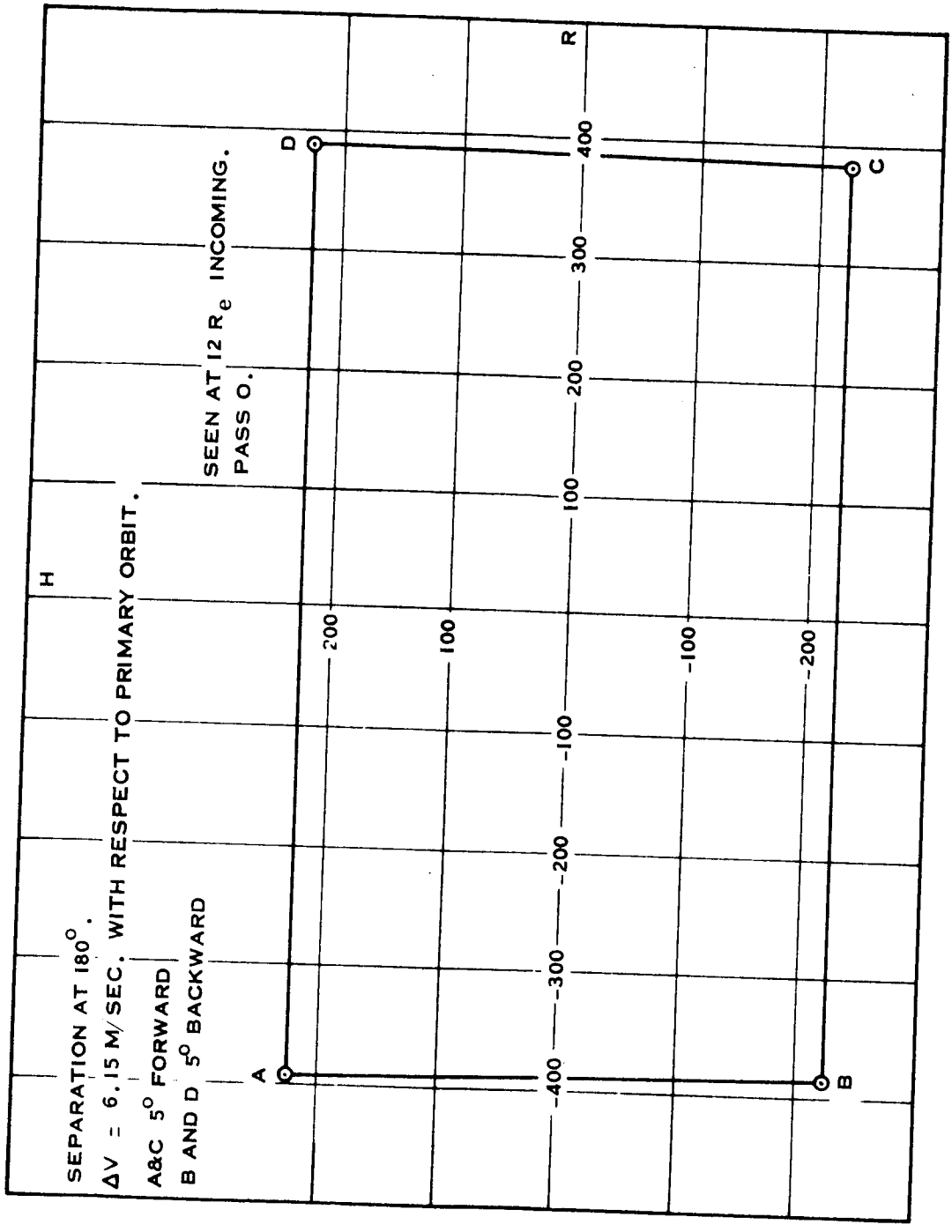

Figure 4.2-40 Non-Planar Radial Array

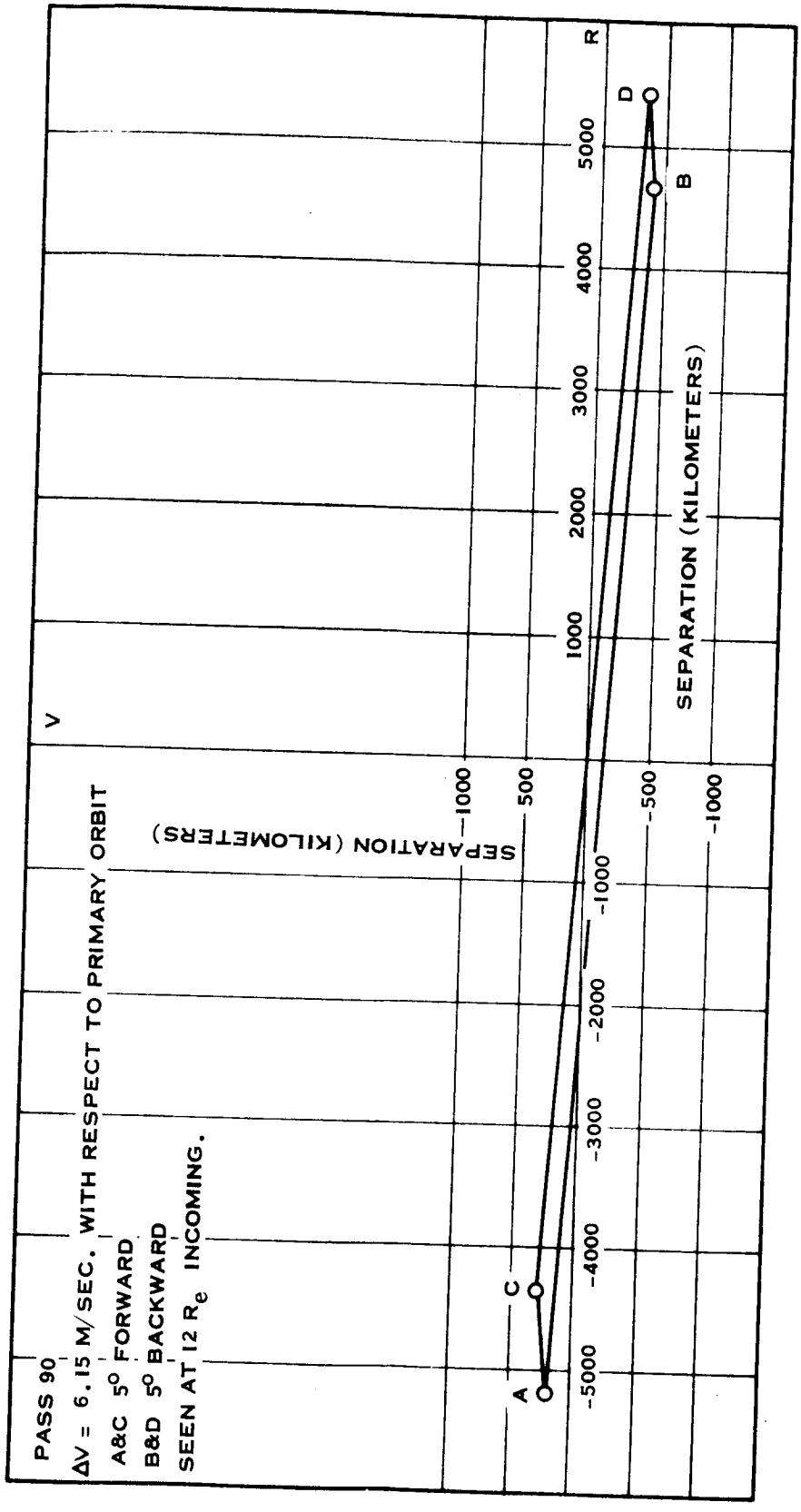

Figure 4.2-41 Non-Planar Radial Array

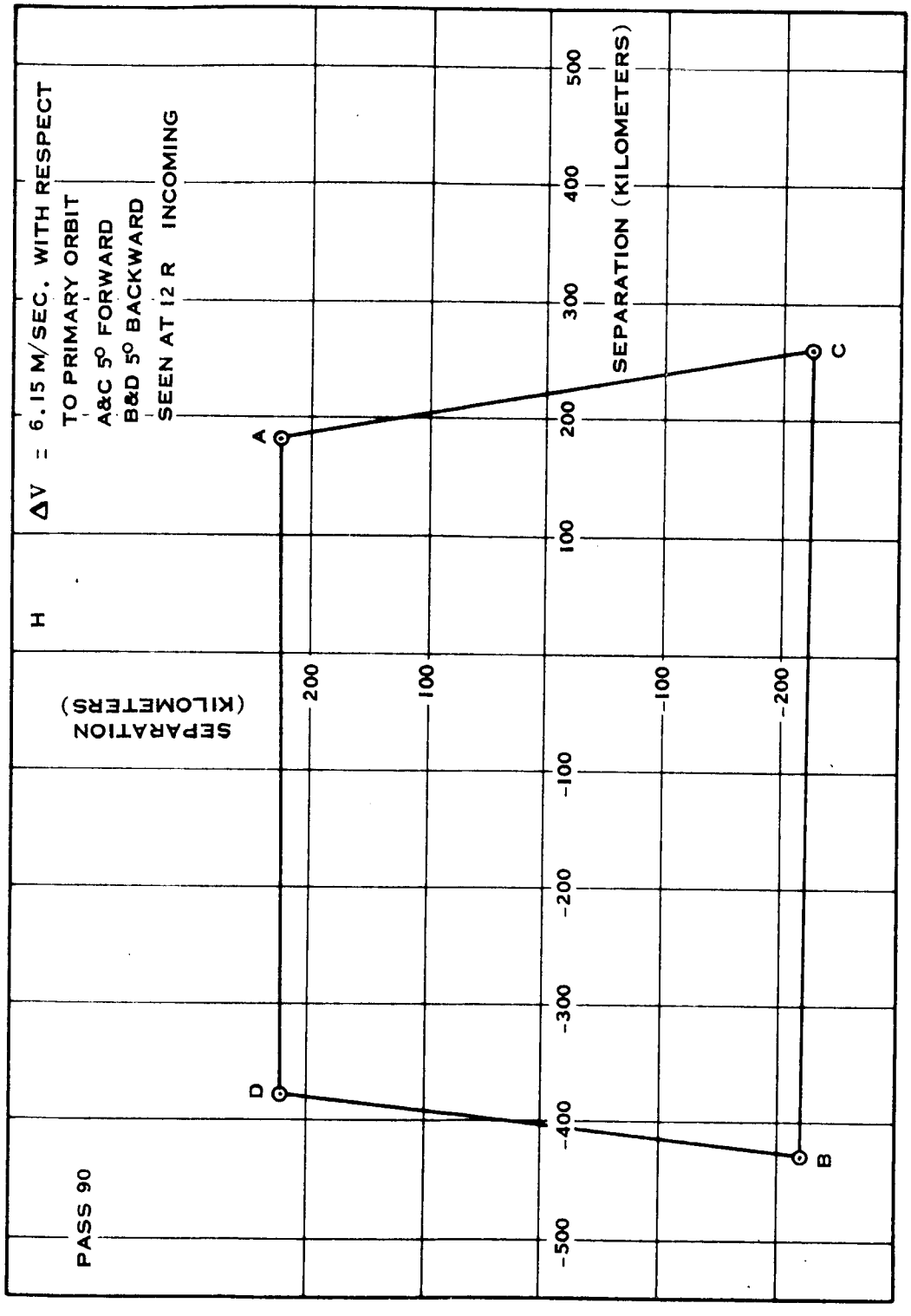

Figure 4.2-42 Non-Planar Radial Array

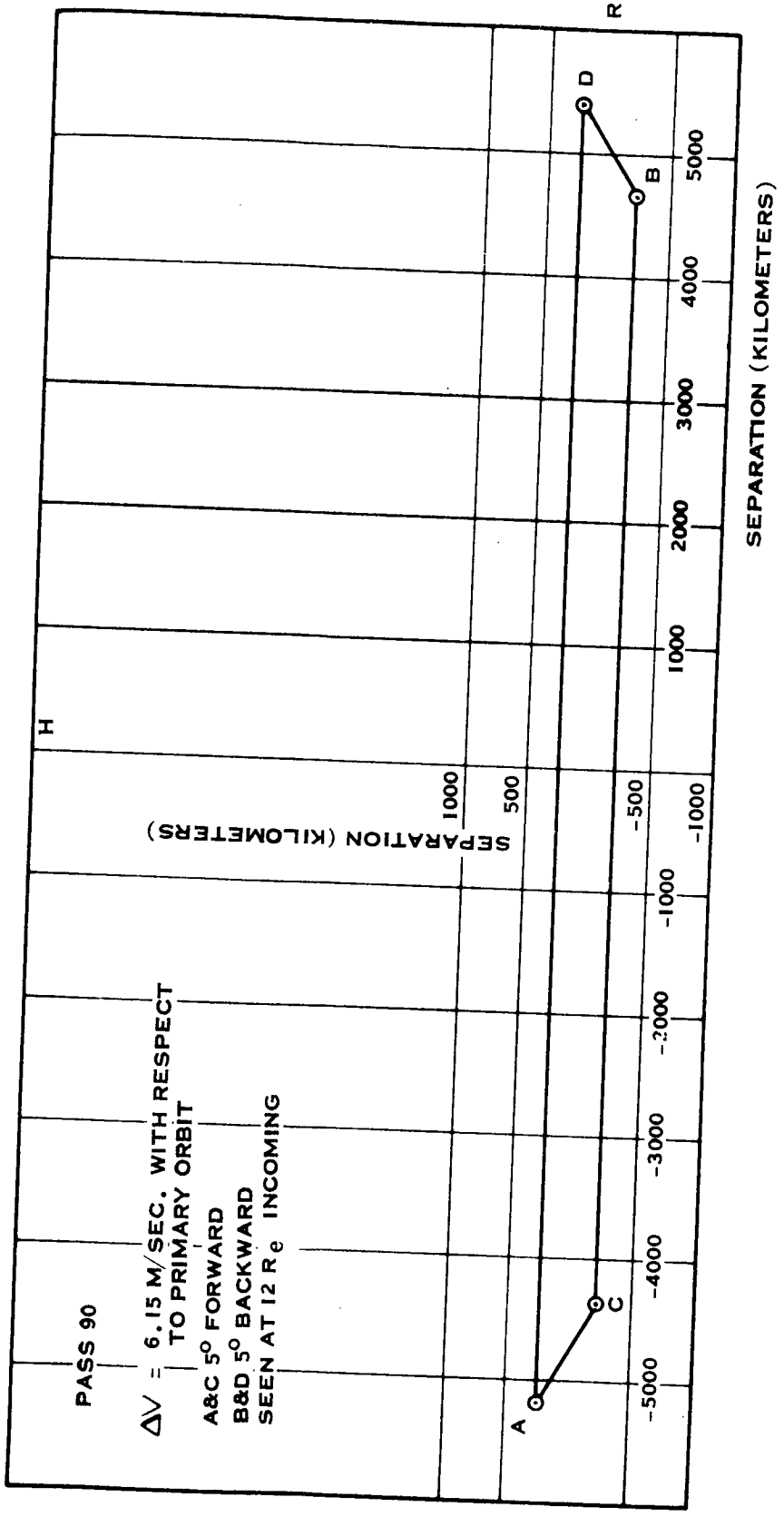

Figure 4.2-43 Non-Planar Radial Array

4.3 ORBIT DETERMINATION

The value of the scientific data being obtained from this mission is dependent on the accuracy to which the individual satellite positions can be determined as a function of time. Then, from the individual satellite positions, the relative positions of the satellites in their configuration can be established. An error analysis of the orbit determination process was performed using the Philco-Ford Mark II Error Analysis Program to establish the accuracy to which the positions could be estimated.

4.3.1 Tracking Network Simulation

The STADAN Tracking Network is used in the evaluation of the accuracy of the orbit determination process. Table 4.3-1 presents a description of the tracking stations that are used and the associated error data used in the analysis. Two modes of station operation are considered in the analysis: (1) using the tracking dishes to provide angle data and (2) the range and range rate measurements. The analysis of the angle tracking includes the effect of bias errors in both the angles being measured and the station locations. The tracking coverage provided by the network is shown at the bottom of Figure 4.3-1.

TABLE 4.3-1

ERROR DATA

Station	Range σ_R (Meters)	Range Rate σ_R (m/sec)	Angles $\sigma_\measuredangle$ (Deg)	Angle Bias $\sigma_\measuredangle$ (Deg)	Station Location Errors			Data Period (Sec)
					Lat (Ft)	Long (Ft)	Alt (Ft)	
Santiago	15	0.1	0.0167	0.022	300	300	50	60
Tananarive	15	0.1	0.0167	0.022	300	300	50	60
Carnarvon	15	0.1	0.0167	0.022	300	300	50	60
Rosman	15	0.1	0.0167	0.022	60	60	30	60
Fairbanks	15	0.1	0.0167	0.022	120	120	50	60

4.3.2 Results

The results of the error analysis are presented in Figures 4.3-1 through 4.3-4. Figure 4.3-1 presents the results obtained with angle tracking. The figure shows the rms error in estimate of position as a function of time. The curves show the influences of the angle measurements being taken when stations are in view and the propagation of the errors around the orbit. The solid line illustrates the position accuracy obtained when the bias errors are neglected in the orbit determination process. The dotted and dashed curves show the performance degradation when angle biases and station location errors are included in the estimation process. They show a relatively minor effect on the accuracy. The first apogee position error is approximately 10 kilometers. By the time of the second orbit, the position error is reduced to an average value of approximately 0.5 kilometer. Figure 4.3-2 shows the individual position uncertainties in $\hat{N}$, $\hat{V}$, $\hat{W}$ coordinates. These coordinates are vehicle centered and rotating such that: $\hat{V}$ is along the velocity vector, $\hat{W}$ is along the angular momentum, and $\hat{N}$ is equal to $(\hat{V} \times \hat{W})$. This figure illustrates the manner in which the position error ellipsoid changes as the vehicle traverses the orbit. After 2 days the figure shows that all three coordinates are known to better than 0.5 kilometer. Figures 4.3-3 and 4.3-4 show the same data for the range and range rate measurements. Figure 4.3-3 shows a position uncertainty of 30 meters at first apogee and less than 10 meters after the first orbit. Figure 4.3-4 shows the position uncertainty in the $\hat{N}$, $\hat{V}$, $\hat{W}$ coordinates. After 2 days the uncertainty in all three coordinates is below 10 meters.

The analysis described above pertains to the orbit determination of a single satellite. The process for computing relative satellite positions should be studied in a statistical sense, but this has not been done. If one assumes that each of the individual satellite orbit determination processes is independent of the others, then one could compute relative satellite positions by combining the position errors in an rss method. It is recommended that this particular computation be investigated in a follow-on effort.

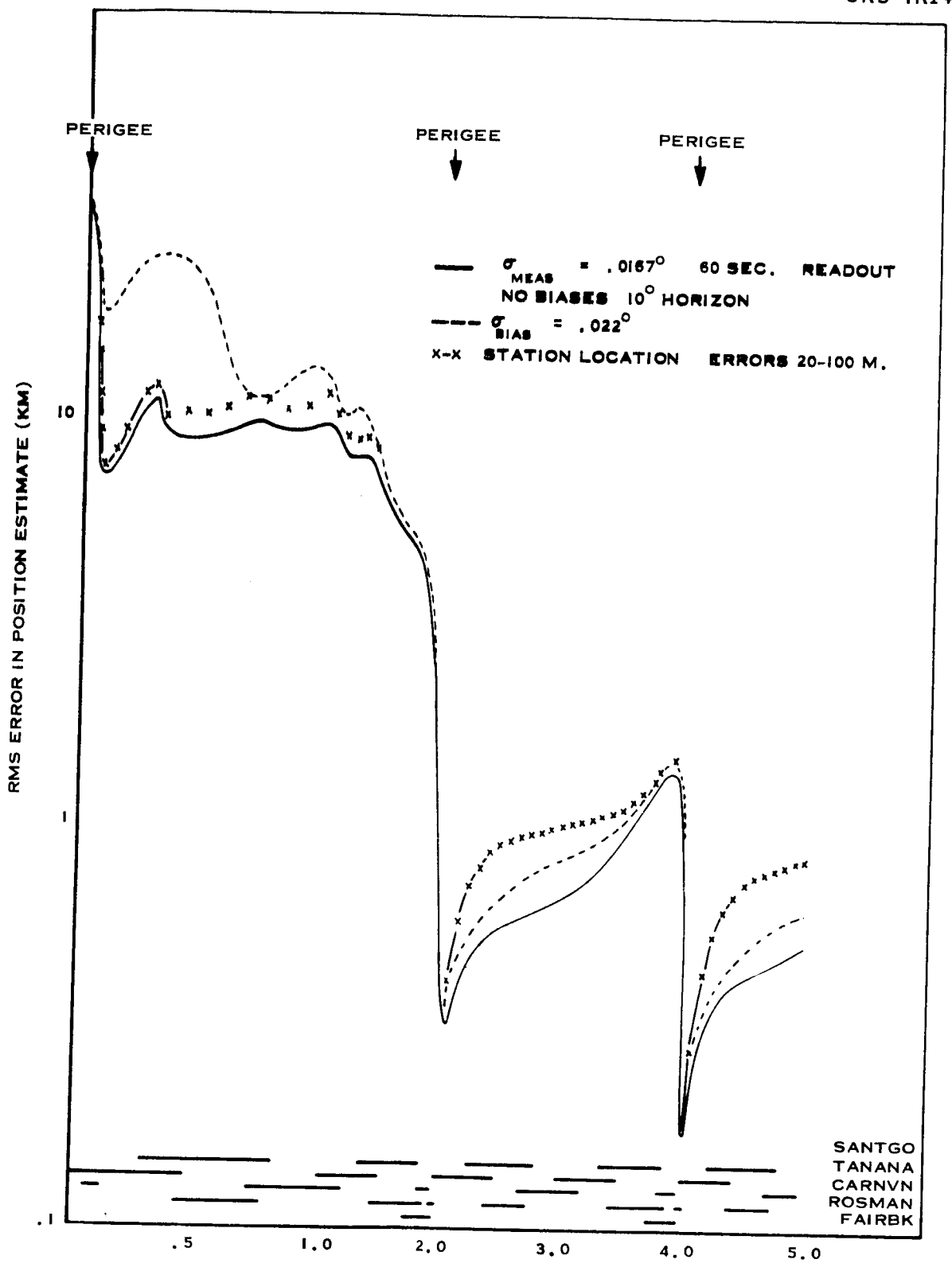

Figure 4.3-1 Angle Tracking Only

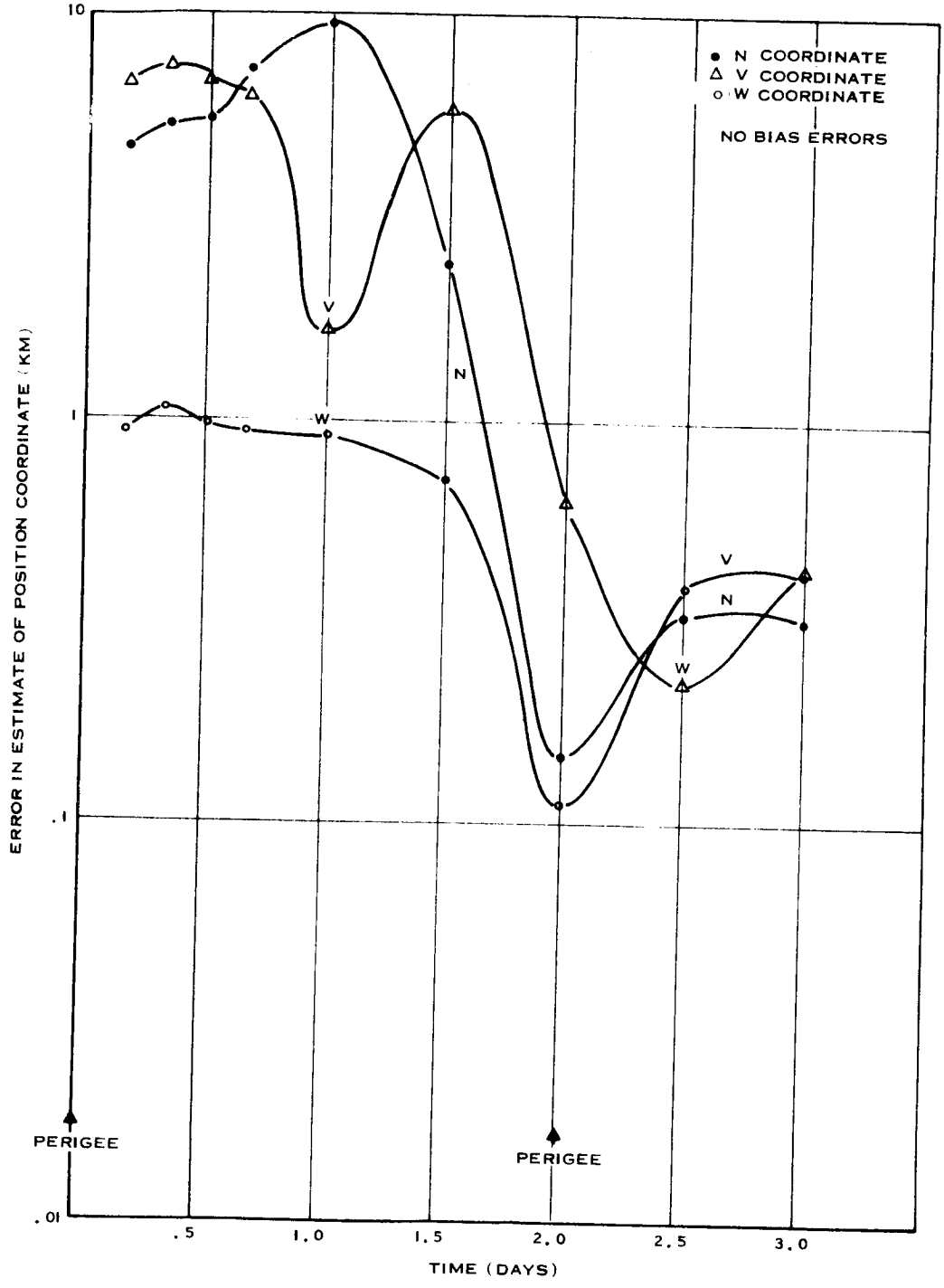

Figure 4.3-2 Angle Tracking Only

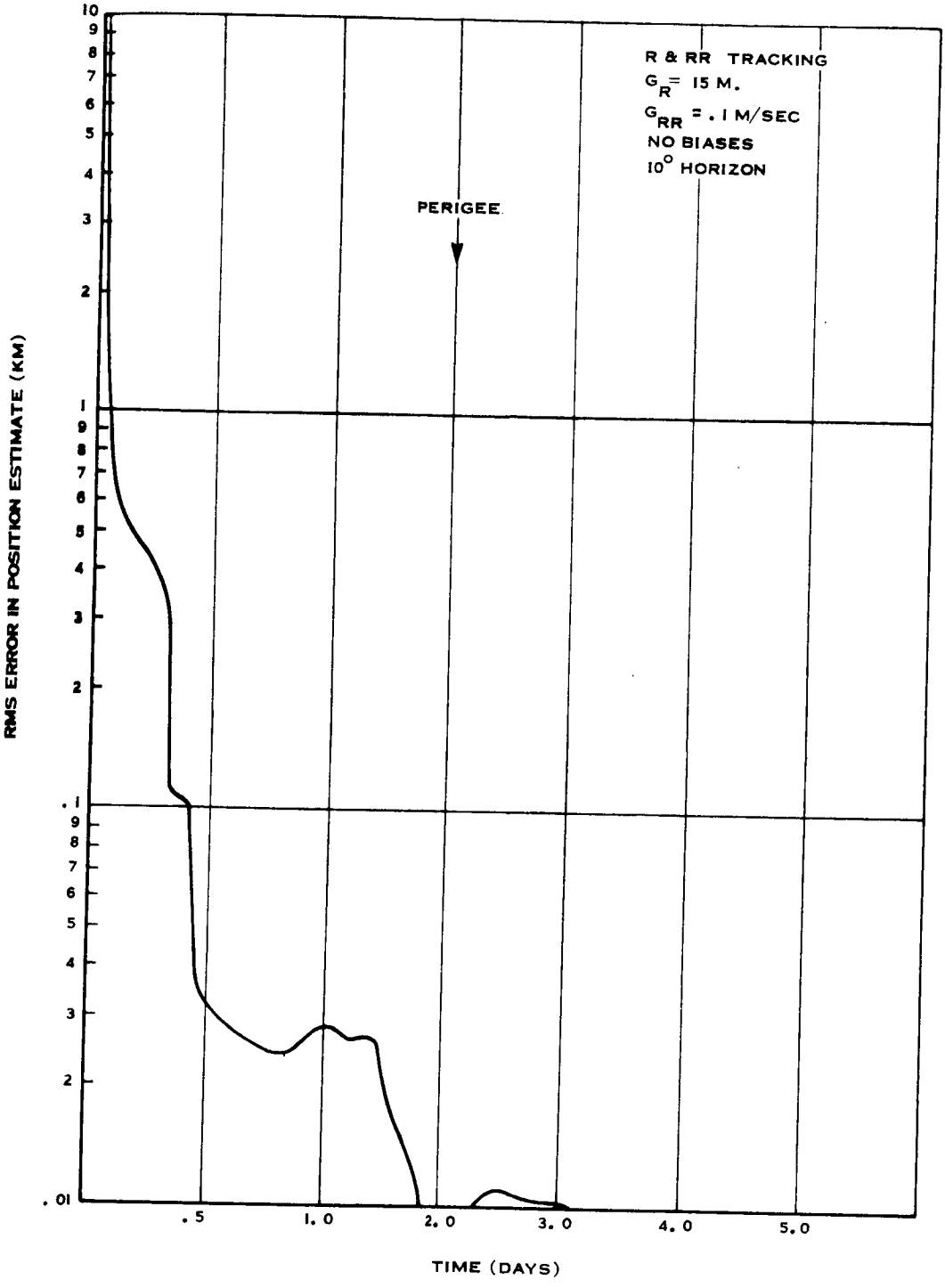

Figure 4.3-3 Range and Range-Rate Tracking

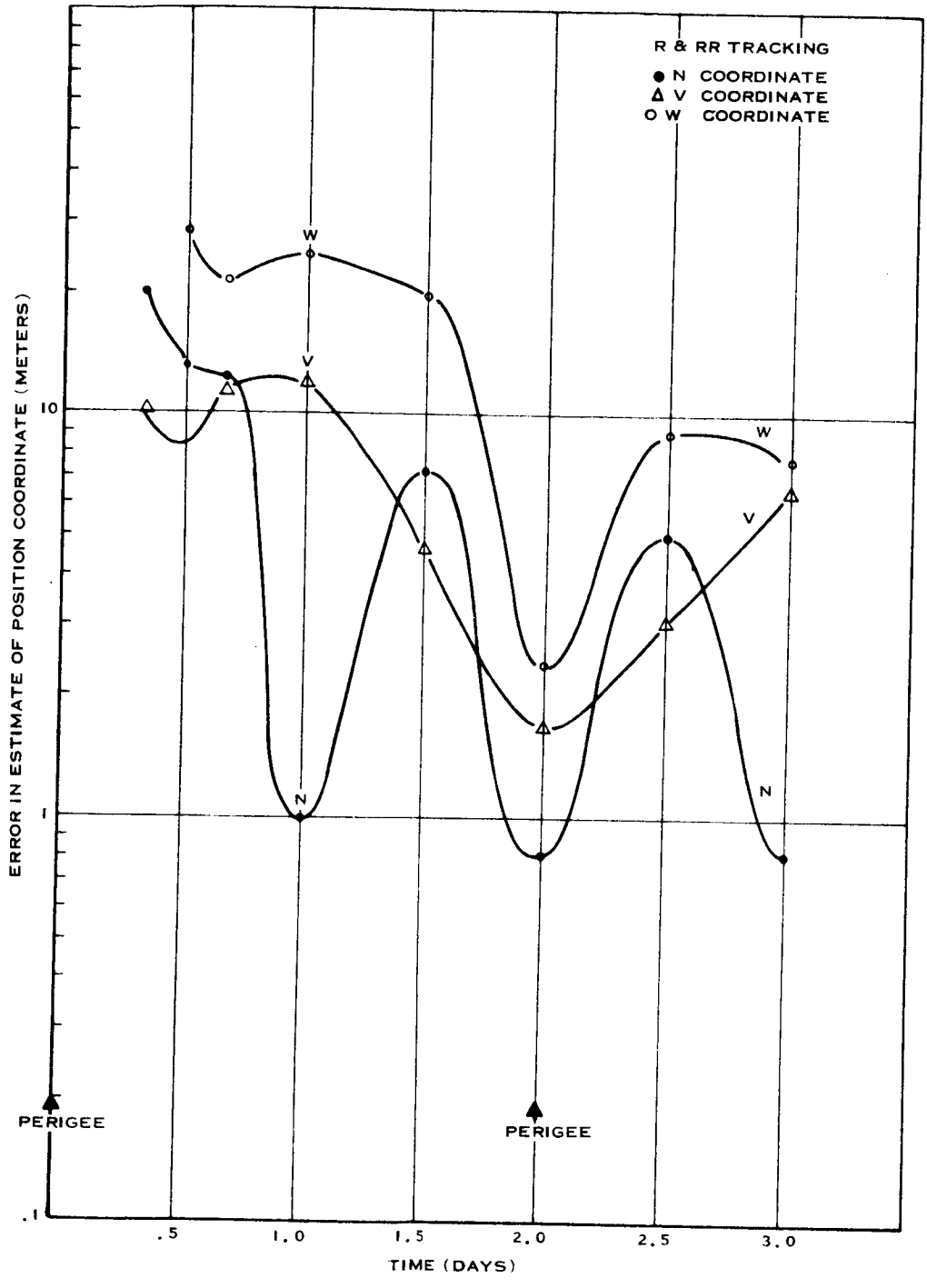

Figure 4.3-4 Range and Range-Rate Tracking

SECTION 5

SPACECRAFT DESIGN CONCEPTS

5.1 CONFIGURATION STUDIES

Preliminary configuration studies were conducted during the contract to examine a number of possible concepts and compare their relative merits. As a result of these studies, two configurations emerged as the most desirable.

This section of the report describes the results of the studies and discusses the features of the various concepts that were considered. All of the concepts involved the use of four identical satellites. In addition, the two configurations selected are described in somewhat more detail and a comparison between them is made.

5.1.1 Deployment Concepts

As indicated in the Ames Research Center Specification for the multiple satellite system, certain constraints exist which influence the system configuration. The constraints can be briefly summarized as follows:

a. The launch vehicle to be utilized shall be one of the Thor Delta series.
b. A standard Delta fairing shall be employed.
c. There shall be four satellites which shall be in identical pairs.
d. The scientific payload is not specified but will consist of at least a plasma probe and a boom mounted magnetometer sensor per spacecraft.
e. The satellites shall be spin stabilized with a final spin rate of 50-70 rpm.
f. The spacecraft shall be magnetically clean producing not more than .5 gamma at the magnetometer sensor.
g. Simplicity and reliability are of prime importance

The capabilities of the launch vehicles of the Delta series are discussed in greater detail in Paragraph 7.1 of this report; however, for the purpose of the configuration studies the DSV-3E vehicle has been assumed. Greater payload capability exists in the DSV-3J version, but the added load capacity is not expected to affect the system configuration significantly, except at the detail design level. In terms of available envelope within the standard fairing, a change from the 3E to 3J version would not affect the outcome of the configuration studies.

Figure 5.1-1 shows the payload envelope that was used in the study effort.

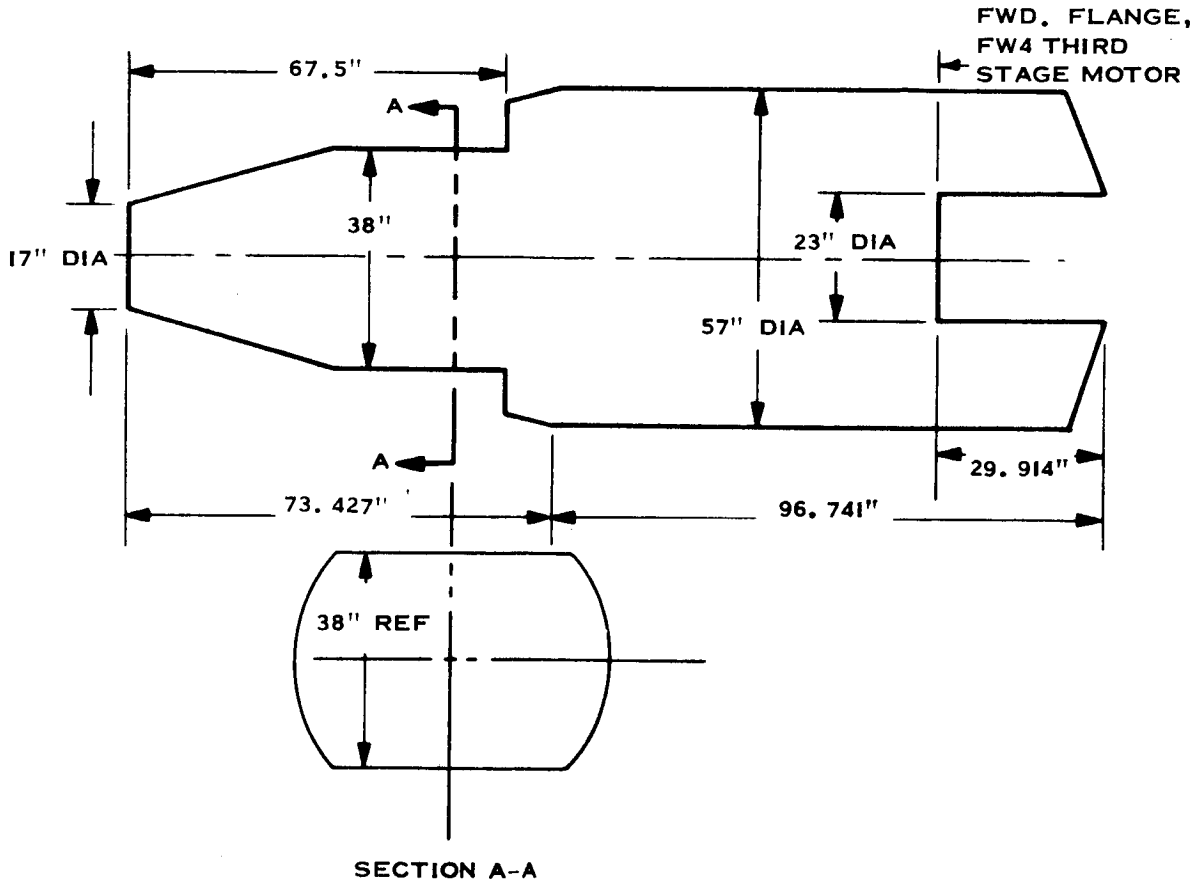

Figure 5.1-1 Payload Envelope

The study revealed that all satellites within the payload could be identical. Since this was considered a desirable feature, it was adopted as a criterion for all concepts studied.

It should be noted that preliminary consideration was given to using an array consisting of a "mother" satellite and several "outlying" satellites. In this configuration, data are gathered by the outlying satellites, transmitted to the mother satellite for integration and storage, and then relayed by a single data link to the ground. The concept offers some potential advantages in compact packaging and savings in total recorder weight. It would not, however, result in any appreciable savings in transmitter weight. The principal disadvantage, and it is an important one, is the additional equipment that would be required on the mother satellite to demodulate the digital information from the other satellites. This type of equipment ordinarily is found only at the ground station, and would represent a major additional complexity to the airborne system. Also, the concept sacrifices the redundancy feature of four totally independent satellites. Based on these considerations, the concept was discarded.

Because the scientific payload was not specified, it was assumed that this capability should be maximized within the constraints of the payload capacity and space available. The scientific payload weight and volume available within each spacecraft were considered of prime importance in selecting candidates for further study.

The magnetometer sensors must be boom-mounted to minimize the magnetic field disturbance at the sensor head. This requirement necessitates the utilization of a three-boom configuration to maintain spacecraft stability. Previous experience with magnetically clean spacecraft (the Pioneer, for example) suggests that a boom length of approximately 6 feet permits the 0.5 gamma requirement to be achieved.

Initial spin velocity of the payload is achieved by the third stage of the Delta vehicle prior to third stage burn and payload separation. This initial velocity is further modified to meet the spacecraft requirements.

Based on the constraints as described above, two fundamental concepts have been studied. The two categories are referred to as "stacked" and "radial" configurations and are described in principle below.

Stacked Deployment. This basic scheme consists of the four identical spacecraft arranged in line along the vehicle centerline. The structure of each spacecraft is constructed around a central cylinder and the central cylinders of the four spacecraft are joined together forming a continuous structure. The upper pair of satellites are separated from the lower pair by a carrier structure, which contains an attitude control and propulsion system. In the launch configuration, the three booms of each satellite are folded along the long cylinder formed by the assembled payload.

After spin-up by the third stage of the Delta and third stage burn, the payload is separated from the launch vehicle by a spring-actuated separation system. At an appropriate time, the payload is oriented normal to the orbit plane by the carrier attitude control system. The spring-actuated system simultaneously separates the upper and lower satellites along the spin axis of the payload. The remaining two satellites are then moved along a line normal to the velocity vector in the plane of the orbit. In this new position the remaining two satellites are separated from the carrier. Figure 5.1-2 shows the stacked arrangement in principle and illustrates the deployment concept.

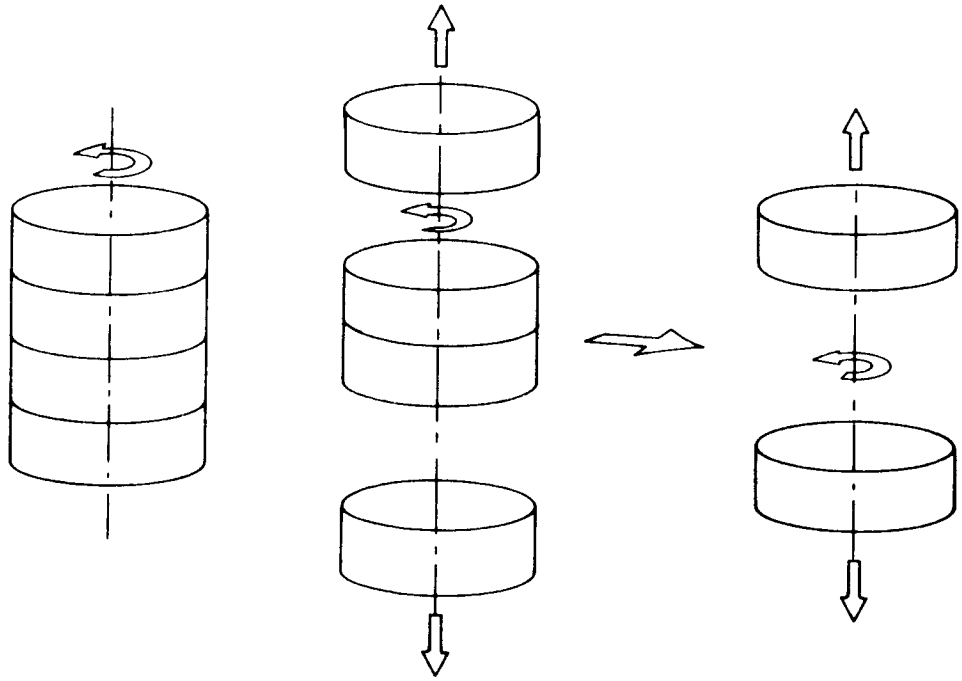

Figure 5.1-2 Principle of Deploying Stacked Payloads

In this arrangement, the spacecraft' s diameter is maximized within the available envelope, giving each spacecraft a small L/D ratio.

Radial Deployment. The initial spin velocity imparted by the Delta third stage is used to provide the deployment velocity and spin rate to the individual spacecraft. Four identical spacecraft are arranged in radial fashion within the 57-inch diameter of the fairing envelope.

In this arrangement, the spin axis of each is approximately 16.5 inches from the launch vehicle centerline (the initial payload spin axis). The carrier holds the four spacecraft together until the appropriate position in the orbit is reached. At this point, the satellites are simultaneously released. In doing so, velocity is imparted to each satellite. This velocity is a function of the initial spin rate and the distance of each satellite from the vehicle spin axis. Upon release, each satellite assumes a spin rate about its own principal axis, which is equal to the initial spin rate (principle of conservation of momentum). Figure 5.1-3 shows the principles of this deployment arrangement schematically.

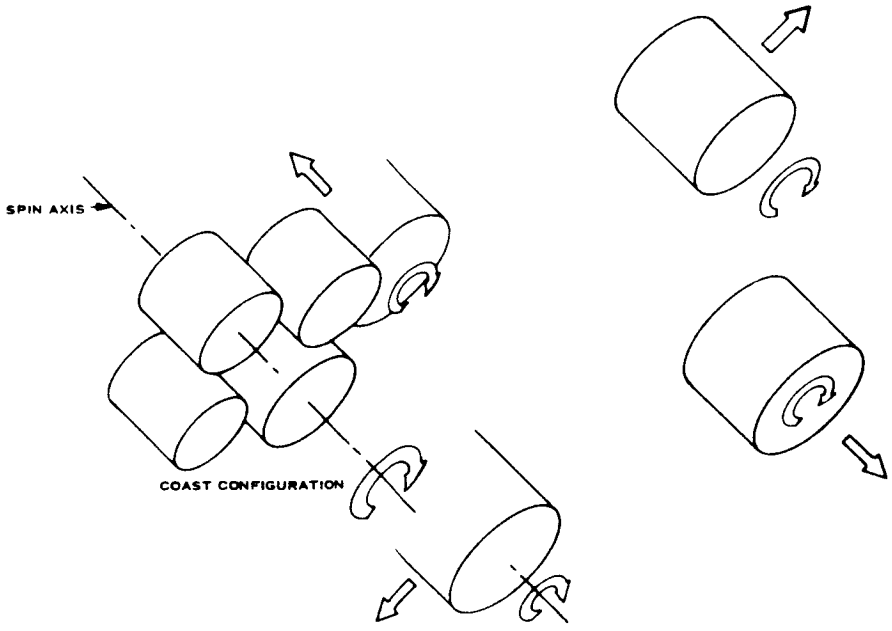

Figure 5.1-3 Principle of Deploying Radial Payloads

Configuration studies based on the two deployment principles described have been conducted and a preliminary design based on each is presented here. From the configuration, mechanization, and structural point of view, the radial design is preferable.

5.1.2 Spacecraft Requirements

Section 4 of this report described the mission analysis studies. Out of these studies further requirements have been identified which affect the spacecraft/payload configurations. These are briefly summarized as follows:

a. Separation of the payload from the third stage of the launch vehicle occurs at or near perigee.

b. Deployment of the satellites occurs at or near apogee. Prior to deployment, the payload coasts for a minimum of 24 hours. As a result, the assembled payload must be inherently stable in both the four-satellite and the two-satellite configurations, i.e., the payload spin axis inertia must be greater than any transverse axis inertia.

c. To achieve the desired satellite array during the mission lifetime, a minimum deployment velocity of 15 feet per second (5m/sec) is required. It is necessary for the spacecraft's separation system to achieve this velocity at deployment. It will be shown later that supplementary means must be provided in addition to separation springs in the case of the stacked configuration.

In addition, a tentative estimation of the spacecraft power requirements determined that a minimum of 20 watts is required. This, of course, ultimately depends on the final selection of the scientific payload and its power requirements. However, the 20-watt figure was used during the study as a basis for sizing the spacecraft solar arrays. Due to the tentative nature of this allocation, it was considered most desirable to provide the means for future growth.

Means of achieving the above requirements have been studied for both deployment arrangements and are discussed in the following sections.

Payload Separation. Separation of the payload from the Delta third stage occurs in both arrangements immediately following third stage burn out. Although the details of the separation system differ for the two configurations, both are achieved in a similar fashion. Both employ squib-actuated release devices; a small separation velocity is imparted to the payload by compression springs. The magnitude of the required separation velocity is not established but, since it is the relative motion between the payload and the burned out third stage motor which is of primary importance, it is considered a relatively simple matter to achieve adequate separation. The velocity imparted to the payload is accompanied by a corresponding reduction in velocity of the burned out third stage motor. This reduction in velocity is proportional to the ratio of the masses of the two separating bodies. Since the mass of the payload is approximately four times that of the third stage, the reduction in velocity of the latter is approximately four times that of the increase in velocity of the payload. A similar relationship also exists with respect to attitude errors induced at separation, that is, most of the error is experienced by the third stage motor.

Stability. As has already been mentioned, inherent stability of the payload is required following separation from the third stage motor and during coast for a period of at least twenty-four hours. Stability can be achieved by making the moment of inertia about the spin axis of the payload greater than the moment of inertia about any transverse axis so that the payload will continue to spin about the axis of greatest inertia. This requirement was the most difficult to achieve in the stacked configurations since the assembled payload is essentially a cylinder having a large L/D ratio of approximately 1.5. A cylinder of uniformly distributed mass requires a L/D ratio of 0.65 maximum to achieve a stable configuration about its centerline. It was therefore apparent that every effort would have to be expended to concentrate the bulk of the payload mass into as short a cylinder as possible. Of the several stacked configurations investigated, none were stable without first deploying all of the booms on each satellite. Even with these expedients, the spin-axis inertia was only 3 percent in excess of the inertia about the transverse axes. Having reached the required inertia ratio with the four satellite payload, no stability problems were encountered with the two-satellite configuration.

On the other hand, the four-satellite radial configuration is inherently stable having a high inertia ratio. In this arrangement boom deployment is not possible nor required. If two satellites were to be launched to 40 earth radii, the radial con figuration requires the addition of two ballast weights, which would replace the two satellites omitted from the payload. It will be shown later that this is well within the capability of the launch vehicle for an apogee of 40 earth radii.

Satellite Deployment, Stacked. Figure 5.1-2 has shown a schematic of the stacked configuration in which two satellites are ejected from the payload in opposite directions normal to the plane of the orbit. The required velocity of separation has also been specified as at least 15 feet/sec (30 ft/sec relative velocity between satellites). This velocity must be achieved with booms deployed; therefore, it is necessary to minimize the separation accelerations, that is, the stroke of the separation springs must be maximized.

Assuming that the booms withstand a 2g acceleration (this depends on the boom configuration, but it will be shown later that this acceleration is not unreasonable for the stacked payload configuration) and assuming a satellite weight of 70 lbs, accelerated with a linearly decreasing force, F, then

$$\int_0^x F\,dx = \frac{1}{2} MV^2 \qquad (1)$$

where $F = 70 \times 2 = 140$ lbs

$M = \frac{70}{32.2}$

V = velocity at separation

= 15 ft/sec

and x = the required spring stroke

$$\frac{140}{2}x = \frac{1}{2} \cdot \frac{70}{32.2} \cdot 15^2$$

$$x = \frac{70}{32.2} \cdot \frac{15^2}{140}$$

$$= \underline{3.5} \text{ feet}$$

That is, to achieve the required separation velocity and to hold the acceleration to a maximum of 2g, a spring stroke of at least 3.5 feet and a force of 140 lbs. would be required. Such a spring, or set of springs, would not be practical. Therefore, it is concluded that supplementary means of providing the velocity after separation will be required. This can be achieved by the addition of a small solid rocket motor to each satellite. Initial separation will then be achieved by conventional springs and separation accelerations minimized still further.

Assuming initial velocity from springs is 2 ft/sec from equation (1) with 0.5g maximum acceleration

$$\frac{35}{2}x = \frac{1}{2} \cdot \frac{70}{32.2} \cdot 2^2$$

$$x = \frac{70}{35} \cdot \frac{2^2}{32.2} \cdot 12$$

$$\text{required spring stroke} = \underline{3} \text{ in.}$$

The remaining 13 ft/sec can then be provided by the solid motor as follows:

$$\text{Required impulse} = \int_0^T F\,dt = MV$$

$$= \frac{70}{32.2} \cdot 13$$

$$= \underline{28.2} \text{ lb sec.}$$

Assuming a maximum of 0.5g acceleration, this can be accomplished by a solid rocket of 35 lb thrust and a burning time of $\frac{28.2}{35}$ secs (0.8 sec).

The solid motor required to provide the necessary impulse may be selected from many "off the shelf" sources. For example, Atlantic Research Company model MARC 15 has a maximum thrust of 38 lbs and a burning time of 0.75 second. Selection of a flight proven motor of approximately this size would not be difficult to provide the major portion of the required velocity. The contribution by the initial spring separation can be designed to match the solid motor selection.

Satellite Deployment, Radial. Deployment of the satellites from the radial configuration payload is achieved by simultaneous release of all four satellites from a central carrier structure. The deployment velocity is therefore a function of the radial distance to each satellite center of gravity and the initial spin rate. The distance from the payload spin axis to the satellite center of gravity is 16.5 inches. The initial spin rate is a function of the combined spin axis moment of inertia of the payload and the Thor Delta third stage motor. Figure 5.1-4 shows an envelope of spin rates available versus the spin axis inertias of the payload plus the third stage motor. From this information it can be seen that for a spin axis inertia of 27.0 slugs ft^2 (based on the final radial concept described later, plus third stage motor), a spin rate range of 90 to 142 rpm is possible. Choosing the maximum rate available of 142 rpm

$$\text{deployment velocity} = \frac{2\pi}{60} \; r \cdot n$$

where r = radius of satellite c.g. (ft)

and n = spin rate in rpm

$$\text{Velocity} = \frac{2\pi}{60} \cdot \frac{16.5}{12} \cdot 142$$

$$= \underline{20.4} \text{ ft/sec.}$$

The required velocities can obviously be readily achieved by this method.

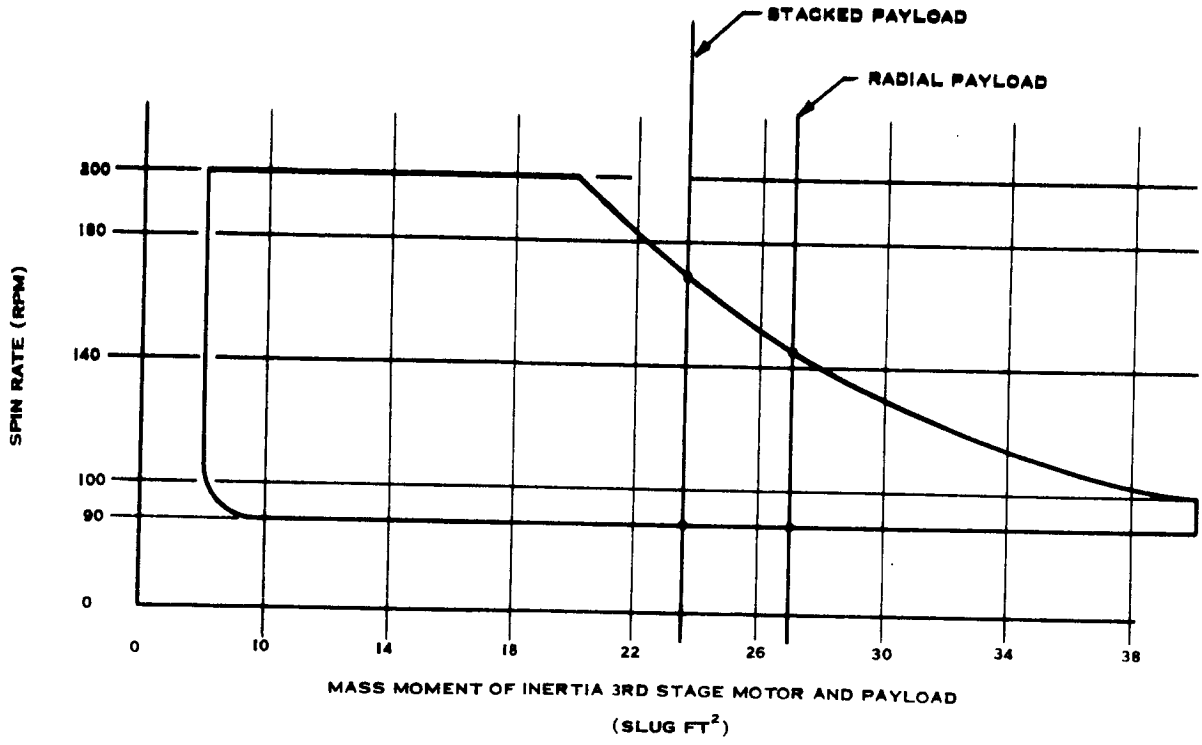

Figure 5.1-4 Envelope of Available Spin Rates - Delta Third Stage

Satellite Size and Shape. The final on-orbit attitude of the satellites is preferred to be with their spin axes normal to the plane of the ecliptic. The most suitable shape, therefore, is a cylinder having body mounted solar cells. All configurations studied, with one exception, were of a cylindrical shape whose projected area of

solar cells was approximately 3.5 square feet. The one exception to the cylindrical shape was a concept having three paddles with solar cells on both sides of the paddles. This configuration had sufficient projected solar cell area to provide approximately an amount of power equivalent to the rest of those considered.

5.1.3 Conceptual Designs

Several iterations of the stacked and radial concepts were investigated before the two final versions were reached. Each configuration was examined until sufficient evidence was obtained to eliminate it from further consideration. Since the concepts fell into the two general categories already described, there was a great deal of similarity between them. The concepts leading up to the two final designs are described in the next sections.

5.1.3.1 Stacked Concepts.

Concept No. 1. The first iteration of the stacked payload consists of the four identical satellites joined together by means of their central cylinders "in line" along the vehicle spin axis. Between the upper and lower pairs of satellites is the carrier structure, which is the same diameter as the satellite's central cylinders. This central structure supports the attitude control system used to erect the payload normal to the orbit plane after separation fron the third stage motor. The satellite's central cylinders and the carrier structure are joined together by means of V-band clamps, thus forming a continous cylindrical structure for the complete length of the payload. This continuous cylinder is the same diameter as a Standard Thor Delta adaptor structure, which is used between the payload and the third stage motor. Separation from the Delta adaptor is effected by means of springs and the squib-actuated V-band clamp provided with the adaptor. Separation of the individual satellites is by similar means, plus the small solid rocket motors in each satellite. Five V-band joints hold the payload and adaptor together.

The individual satellite structures are constructed around the central cylinders, utilizing a horizontal equipment plat form supported by an internal truss. The

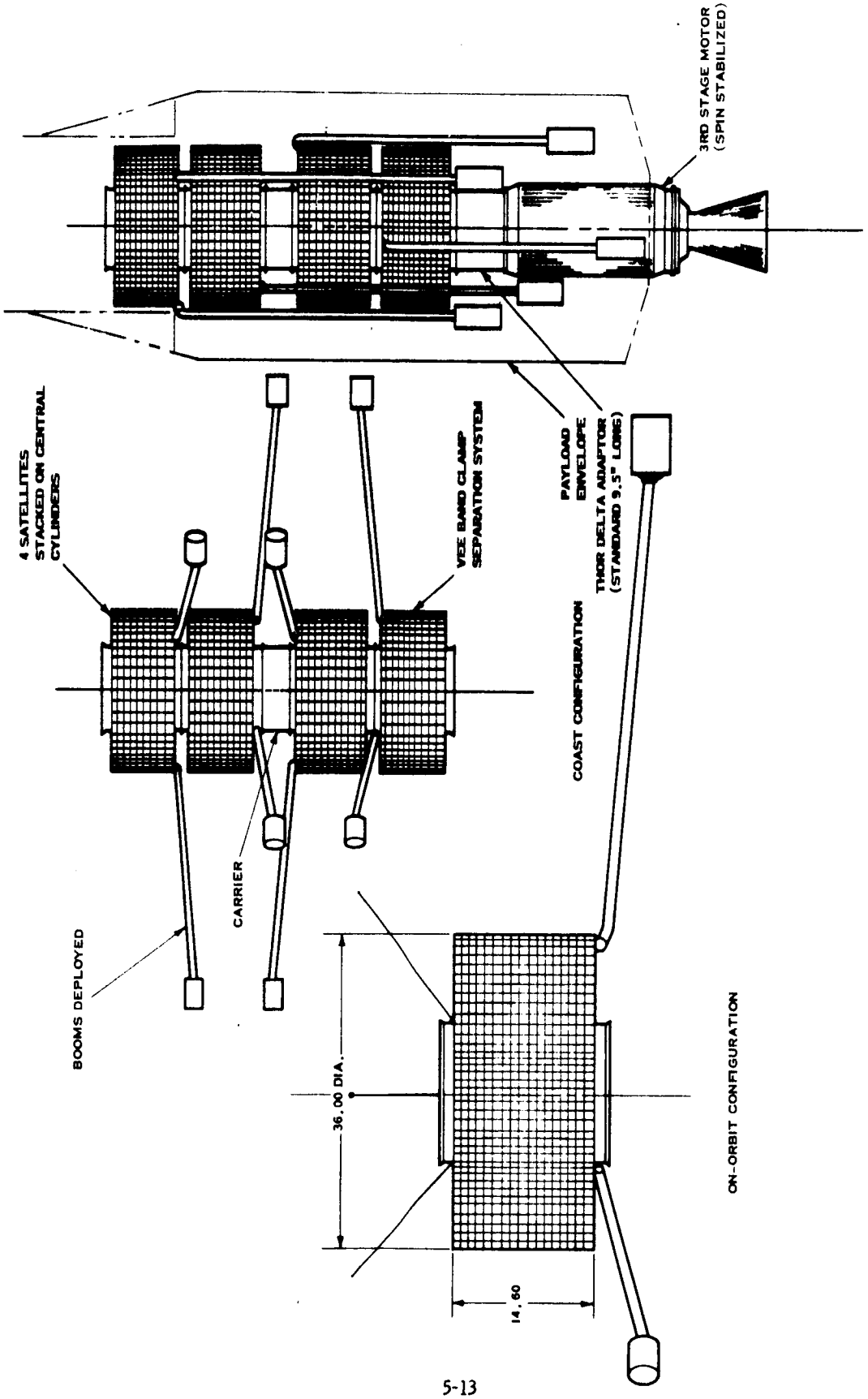

Figure 5.1-5 Concept No. 1, Stacked Payload

three booms of each satellite are folded along the body-mounted solar arrays while in the launch attitude. The center of gravity of each of the satellites is situated approximately mid-way along each central cylinder.

This configuration, as far as the individual satellite is concerned, had promise of being the most simple of the stacked configurations examined. However, the assembled payload has such a high L/D ratio that stability could not be achieved even by deploying the booms. Had it been possible to increase the length of the booms to more than ten feet, a stable condition would have been attainable. Since this was not desirable, this concept was dropped from further consideration. Figure 5.1-5 shows an outline of this first concept.

Concept No. 2. The arrangement described above gradually evolved into the remaining two stacked configurations described here.

In an effort to reduce the L/D ratio of the payload and hence improve the stability characteristics, a payload of four paddle satellites was examined. The satellites in this payload consist of a small cylindrical module placed at the center to which three rectangular paddles are attached. The paddles are arranged in radial fashion on the module and are placed 120 degrees apart. Both sides of the paddles are covered with solar cells. All satellite equipment and scientific experiments are accommodated inside the central module. The distance from the spin axis to the outermost edge of each paddle is approximately equal to the radius of the cylindrical satellites of Concept No. 1. However, the central module is considerably shorter than the central cylinder of Concept No. 1. The length of the rectangular paddle is approximately twice that of the central module. When stacked on top of each other, the paddles of one satellite are stowed side by side with those of the adjacent satellite, as shown in Figure 5.1-6. The booms were hinged about the ends of the solar paddles and folded down in the launch attitude. A cylindrical carrier structure similar to Concept No. 1 is placed between the upper and lower satellite pairs.

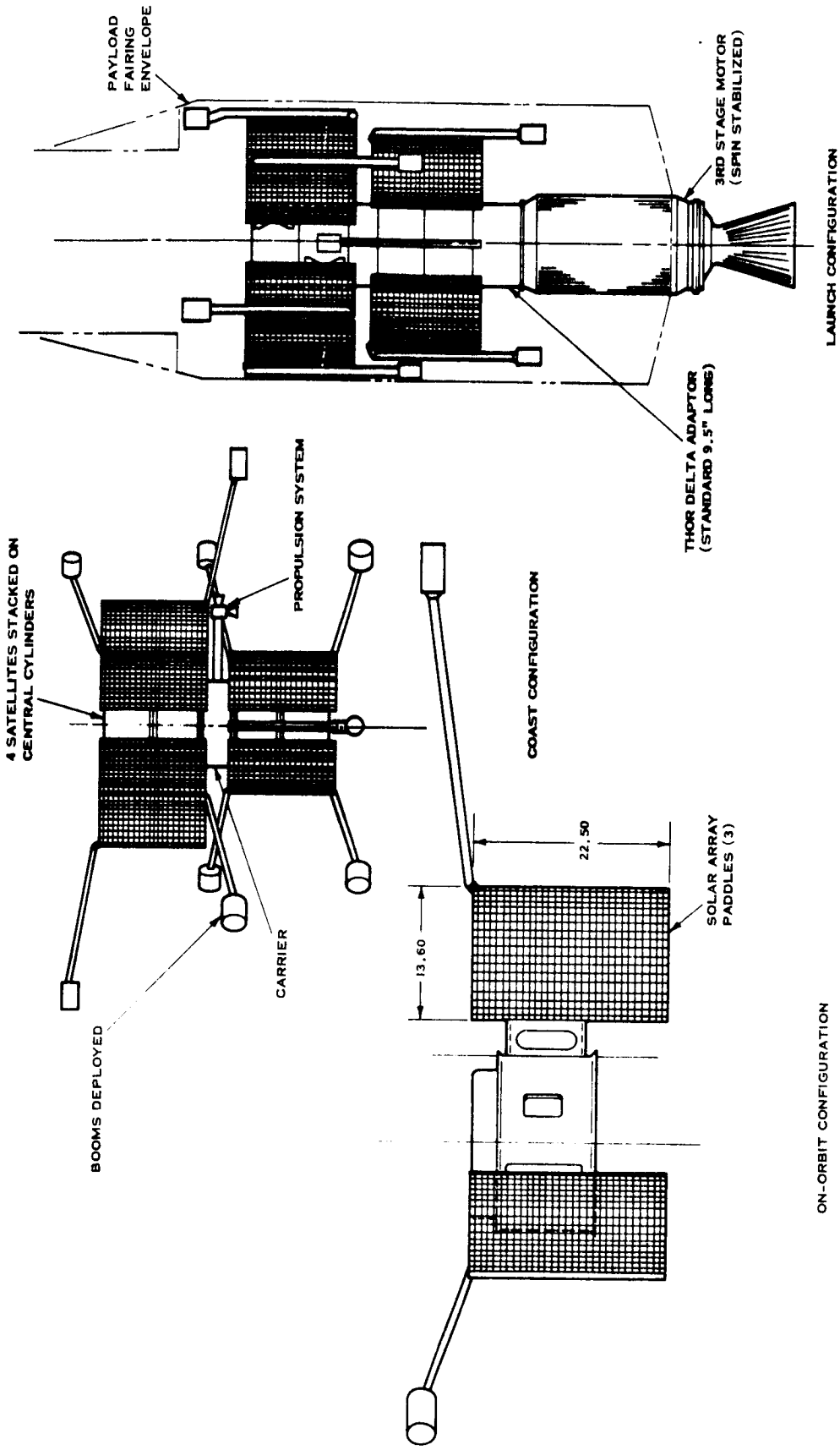

Figure 5.1-6 Concept No. 2 - Three Paddle Stacked Payload

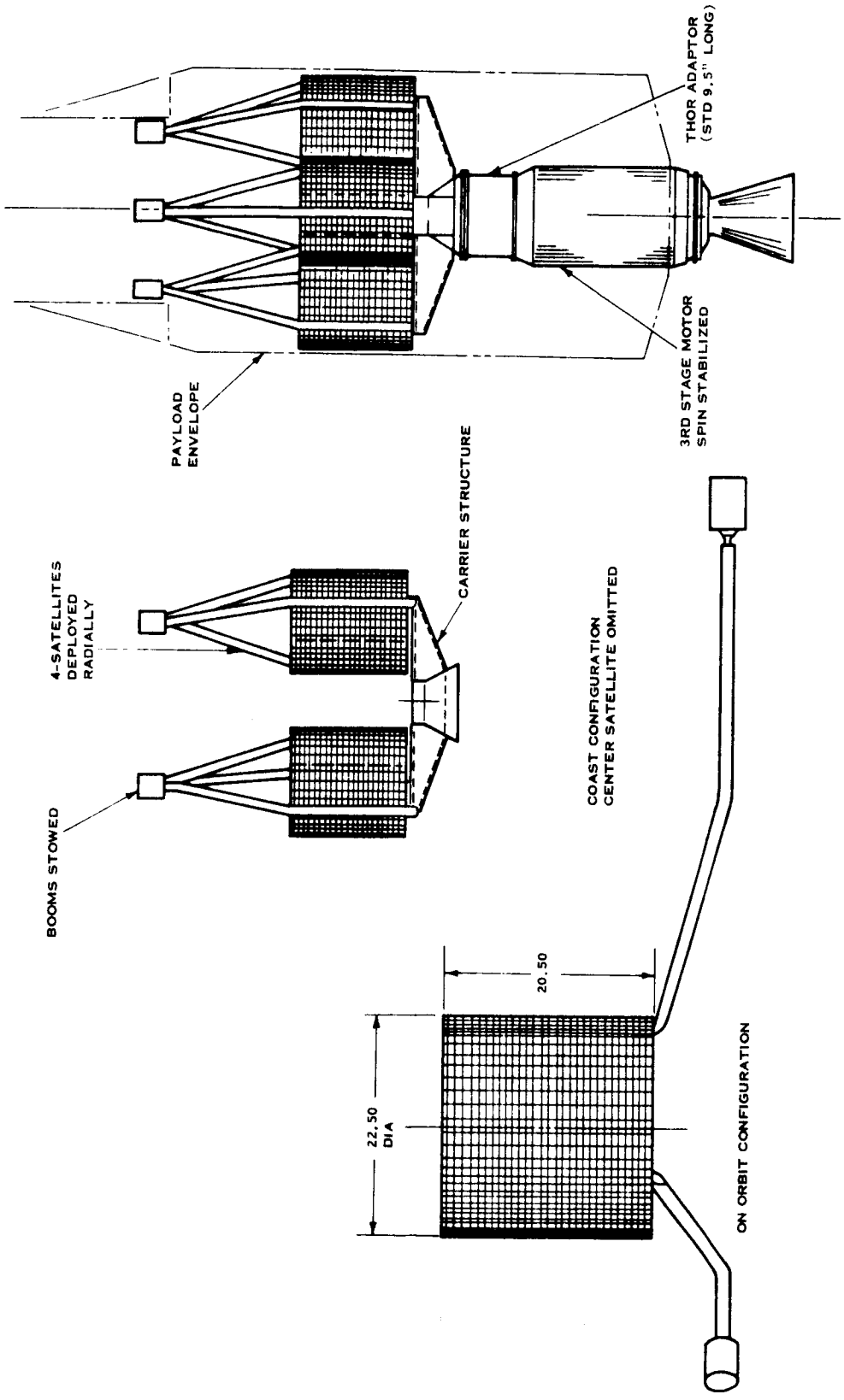

Figure 5.1-7 Concept No. 4 - Radial Payload

The assembled payload is then attached to the third stage motor by the Standard Delta Adaptor. This payload is considerably shorter than that of Concept No. 1 and, as a result, is stable when the booms are deployed. However, the configuration has some disadvantages that caused it to be eliminated. The disadvantges are as follows:

a. The central equipment module is small and must accommodate all the satellite equipment, including the solid rocket motors for achieving the necessary velocity. It is considered too small and does not allow for future growth.

b. Clearances between satellites during deployment are critical since the solar paddles must pass over the central module of the adjacent satellite.

The latter disadvantage could be tolerated and possibly compensated for by careful design, but the available volume was considered of sufficient importance to eliminate this concept from further consideration.

Table 5.1-1 compares the moment of inertia of the payloads and satellites in the "booms stowed" and "booms deployed" conditions for Concepts No. 1, 2 and 3. Concept No. 3 is the final version of the stacked configurations and has been examined in more detail. This concept is described in Section 5.1.4 of this report.

5.1.3.2 Radial Concepts.

Concept No. 4. This first iteration of the radial deployment concept consists of four small diameter satellites supported on a carrier structure. This, in turn, is attached to the third stage motor by the Standard Thor Delta adaptor. The carrier structure extends outward from the adaptor attachment in the form of a cross and supports each satellite at a distance of approximately 16.5 inches from the vehicle spin axis. Hence, each satellite is supported on a beam, which is cantilevered from the central support. The individual satellites are of conventional construction with a central cylinder. The central cylinder is attached to the cantilever beam

TABLE 5.1-1

MASS PROPERTIES OF STACKED CONCEPTS

		Booms Stowed			Booms Deployed		
Concept	Config.	I_{spin}	I_{trans}	Inertia Ratio	I_{spin}	I_{trans}	Inertia Ratio
No. 1	4 Sat				34.00	46.34	.73
	2 Sat				17.00	12.84	1.32
	1 Sat				8.49	4.80	1.76
No. 2	4 Sat	8.75	21.67	.41	31.50	28.08	1.12
	2 Sat	4.36	7.13	.61	15.70	10.31	1.52
	1 Sat	2.18	2.64	.83	7.88	4.23	1.86
No. 3	4 Sat	15.19	28.02	.54	35.80	34.78	1.03
	2 Sat	7.58	8.18	.93	17.91	11.56	1.55
	1 Sat	3.79	3.23	1.17	8.96	4.93	2.0

All inertias are in slugs/ft^2.

A stable condition requires that the inertia ratio, $\frac{I_{spin}}{I_{trans}}$, be greater than 1.0

structure by means of a V-band clamp. Since a spin rate of approximately 140 rpm is required to achieve the necessary deployment velocity, bending stresses are experienced in the carrier beam due to centrifugal forces at the satellite. In addition, bending in the carrier occurs as a result of payload accelerations along the spin axis at first, second, and third stage motor burn. Third stage motor accelerations also add to the beam bending stresses. These effects are the critical design conditions for the supporting carrier structure and result in high bending moments, causing an excessively heavy structure. This fact alone was the principal reason for dropping this scheme and proceeding with the next and final iteration, Concept No. 5, which is described in detail in Section 5.1-5 of this report. Figure 5.1-7 shows an outline of Concept No. 4. No stability problem exists with either of the radial concepts.

5.1.4 Stacked Payload

Concept No. 3 of the stacked payloads evolved from Concepts Nos. 1 and 2. It was an attempt to achieve a stable configuration without employing the excessively long booms used in Concept No. 1, and at the same time to obtain sufficient volume to accommodate scientific equipment with room for growth. From the earlier investigation it was obvious that to achieve these conditions means would have to be devised to concentrate the main bulk of the satellites (the equipment and scientific experiments) as close to the payload center of gravity as possible. Figure 5.1.8 shows an assembly drawing of this payload in which these objectives have been achieved. The satellites are cylindrical in shape, as in Concept No. 1 and are constructed around a central cylinder. However, the carrier structure is not placed in line with the central cylinders as in Concept Nos. 1 and 2. Instead, the inner satellites are joined directly together at their central cylinders by means of a V-band clamp. Each satellite has its equipment mounted on horizontal honeycomb panels such that the equipment is placed above the top edge of the cylindrical solar array so that when the inner pair of satellites is attached together their solar array panels are separated by approximately 17.0 inches. By this means all equipment that requires a field of view such as attitude sensors, plasma probes, antennas, etc., can do so without penetrating the solar array panels. Also, the 17.0-inch space between the inner pair of satellites is used to accommodate the carrier structure. The outer satellites a re joined to the inner pair by means of their

central cylinders such that their equipment sections are stowed within the "skirt" of the adjacent satellite formed by its solar array panels.

The resulting configuration provides a payload that has all of the equipment sections of each satellite placed as close together as possible. One V-band clamp attachment has been eliminated, since the inner satellites are joined directly together rather than through a carrier structure. The carrier structure is supported by the structures of the inner pair of satellites such that no pins, clamps or other means requiring a release mechanism are used at its attachment. When folded all booms (twelve) are locked to the carrier structure so that all may be released simultaneously by a carrier-mounted release system. The carrier structure also supports the payload attitude and orbit control propulsion system. A standard Thor Delta adapter is used with this concept.

The following sections describe the salient features of the design of the individual satellites and the carrier, and a weight tabulation.

Satellite. Figure 5.1-9 shows an assembly drawing of the satellite. All satellites in the payload are identical with various exceptions.

The satellite consists of a central cylinder around which the remainder of the structure is constructed. An equipment platform in the form of an annular ring is attached at its inner diameter at the central cylinder and is supported at its outer diameter by a truss structure. The truss structure consists of six groups of radial members equally spaced around the satellite which also provide support for the six sections of the solar array panels. Three of the truss groups also provide structural support for the three booms whose hinges are situated below the lower edge of the solar array. The equipment panels provide the means of resisting torsional loads on the structure due to spin up accelerations or decelerations at boom deployment. The equipment panel is divided into six segments, three of which are utilized for the support of satellite equipment. The three equipment modules thus formed are provided with covers for thermal protection. A tape recorder is mounted within the central cylinder, as is the small solid rocket motor.

The three equipment modules contain the science experiments together with the remaining satellite electronic equipment. The S-band antenna utilized with this satellite consists of thirty-six, two-inch square, cavity-backed elements arranged around the circumference immediately above the solar array panels.

At the joint between each solar array panel (equally spaced around the circumference) longitudinal structural members are placed, to which the array panels are attached. These members form part of the internal supporting truss structure. In addition, one end of these members is specially prepared to allow a connection to be made with the carrier structure. This connection is one in which shear and compression forces can be transmitted across the joint but which separates under tension loads (separation of the two inner satellites from the carrier). The joint concept shown in Figure 5.1-8 is a pair of mating serrated fittings capable of being separated without hangup.

At one end of the central cylinder a single coil spring provides the small separation velocity. Since there are only three separation systems and three V-band clamps, certain minor differences exist between satellites. That is, the first two satellites to be separated retain a V-band clamp while the springs are held by the remaining two satellites in the payload. Similarly, when the second pair of satellites separate the V-band clamp remains with one of them while the springs go with the other.

Three booms are equally spaced around the satellite and are hinged about the three support points on the truss structure. Deployment of the booms occurs while the satellite is still part of the payload assembly. Centrifugal forces extend the booms after release from the carrier and they are depressed approximately 15 degrees below the horizontal when fully deployed so as to avoid solar array shadowing at extreme sun angles. The booms are depressed to their final position by means of springs and positively locked. Damping during deployment is provided for each boom by a viscous fluid dashpot. Since the booms are deployed at the time that the satellites are separated from the payload, they must be designed to withstand the separation accelerations including the solid rocket motor thrust. However, it can be shown that these conditions are not critical.

Assuming a spin rate of 60 rpm, a boom tip mass W_F = 2 lb, and a boom mass W_B = 1 lb., moment about hinge H due to spin

$$M_S = \left[15.7 \times \frac{W_T}{386} \times \left(\frac{2\pi}{60}\right)^2 \times 60 \times 69.95\right] + \left[\frac{7.85}{386} \times \left(\frac{2\pi}{60}\right)^2 \; 60 \times 46.35\right] = 262 \text{ in.-lbs.}$$

Moment about hinge H due to separation acceleration (a)

$$M_A = -\left[(2 \times 47.2) + (1 \times 23.6)\right] a$$
$$= -118\, a \text{ in.-lb.}$$

It can be seen from the above calculations that the separation accelerations induce small bending moments in the boom compared to those induced by the spin rate; in fact, accelerations of more than 2g are required to balance the moments due to spin. The spin induced moments are of opposite sense to those induced by separation acceleration.

Carrier. Figure 5.1-8 also shows the carrier structure, which is placed between the inner pair of satellites. The primary function of the carrier is to support the components of the payload attitude and orbit control system, to provide locks for the folded booms, and to support the communications subsystem including antenna. The structure consists of an upper and lower ring separated by a tubular truss. At the intersections of the truss members and the rings, contact between the carrier and the longitudinal members in the satellite is made. Some adjustment is required at these points to compensate for manufacturing tolerances and to allow a slight preload to be applied after mating the central cylinders of the two satellites.

Components of the attitude and orbit control subsystem are mounted to honeycomb equipment platforms which are attached to the carrier-truss members. This equipment includes:

a. Axial thrust chambers and nozzle for erection normal to orbit plane
b. Radial thrust chambers and nozzle for in plane maneuvers after separation of first two satellites

c. Attitude control logic
d. VHF TLM transmitter and command receiver
e. Digital TLM unit and timer
f. Propulsion and attitude control system fuel tanks
g. Four VHF whip antennas.

Power for operation of this equipment is made available from the power subsystem of one of the inner satellites, necessitating an electrical interface between the carrier and the satellite. The four whip antennas are stowed in the launch configuration by wrapping around the circumference of the carrier and are held in place and released by the boom lock/release system. The boom locks are released simultaneously by means of a pyrotechnic device linking all twelve locks together.

Table 5.1-2 shows a preliminary weight breakdown of the stacked satellite and the payload in the two- and four-satellite configurations. The two-satellite payload for the forty earth radii mission employs the two inner satellites only.

TABLE 5.1-2 WEIGHT BREAKDOWN - STACKED (LESS SCIENCE)

Item	Satellite	Payloads	
		Four Satellites	Two Satellites
Structure	11.50	---	---
Solar Array	7.23	---	---
Electronics	25.00	---	---
Booms	5.58	---	---
Carrier	---	6.60	6.60
Attitude Control	---	12.50	12.50
Propulsion	1.0	---	---
Separation System	4.0	---	---
Adapter	---	17.70	17.70
Total Satellite Weight	54.31	217.24	108.62
Total Payload Weight	---	254.04	145.42

5.1.5 Radial Payload

In an effort to eliminate the most significant undesirable feature of Concept No. 4, that is, the high bending moments induced in the supporting structure, the final version of the radial payload was evolved. Figure 5.1-10 shows a drawing of this payload in its four-satellite configurations.

In this arrangement, the four satellites are attached to a central structure at the center (spin axis) of the payload so that the centrifugal forces induced by the spin rate are resisted in tension by the attachment of the satellite to the central structure. The central structure (release module) attaches the satellite together in such a way as to make the satellite cluster an integral unit up until the time of satellite deployment. The cluster unit is then supported on an adapter structure, which provides the means of resisting longitudinal and transverse loads. The standard Delta adapter is not used with this configuration but instead is replaced by a special light-weight truss structure, which is permanently attached to the forward flange of the third stage motor. The tubular truss adapter provides a more structurally efficient means of supporting the satellite cluster without high bending moments. The adapter has four support hardpoints on which the four satellites are supported and at which four matched springs are used to provide a small velocity at payload separation. Means are provided at each of the hardpoints to resist shear forces due to lateral acceleration of the vehicle. Centrifugal forces due to spin-up are not transmitted to the adapter structure but are entirely handled by the central release module.

Two methods are feasible of resisting the longitudinal accelerations of the launch vehicle caused by first, second, and third stage engine shutdown, which tend to lift the payload off the four supporting hardpoints, as follows:

a. Individual connections at the four hardpoints which would be released at payload separation by four individual squib actuated release systems. Alternatively, the four release systems (pin pullers) could be linked together by means of a pyrotechnic mild detonating fuse which would be activated by a centrally located actuator.

b. A single connection (tie bar) between the central release module and the truss adapter which would be preloaded in tension to prevent the payload from lifting off the hard-points during periods of forward acceleration. This method would cause bending moments that peak to a maximum at the center of the release module and would have to be resisted by the module to satellite connections. Separation of the payload from the adapter would be accomplished with a single squib actuated bolt cutter at the central tie bar.

The latter scheme requires only one event (the squib activated bolt cutter) to separate the payload but induces the highest structural loads while the former requires four events (four pin pullers) to separate the payload. Either system is feasible, however, since the pyrotechnic fuse from the actuator to the pin pullers can be made equal in length and relatively short in scheme (a). The speed of burning of MDF is of the order of 23000 ft/sec.; therefore, it is judged that the time differential between the four releases would be negligible.

Also, since the most significant forward accelerations occur at third stage motor shutdown (approximately 18g), the amount of preload in the tie bar is not unreasonable. The preload would be approximately the mass of the burned out third state motor x 18.

$$50.6 \text{ lbs} \times 18 = 910 \text{ lbs.}$$

The single tie bar concept is recommended. The tie bar also provides a convenient mounting for the VHF antenna which is required for the command system. The whip antenna would be deployed upon separation by the bolt cutter to provide communication during the coast to apogee.

The following sections describe the salient feature of the proposed design, including the individual satellite, the release module and a weight tabulation.

Release Module. The central structure, which ties the four satellites together prior to satellite deployment at apogee, is essentially a housing for the satellite release mechanism. In addition, it supports the equipment required to command the satellite release including a battery, command receiver, timer and VHF antenna.

Figure 5.1-10 shows the release module and indicates the means of satellite release. Each satellite is connected to the module by four pads capable of transmitting shear and compression load across the interface. Tension loads (due to centrifugal forces) are resisted by a connection that is aligned with the satellite center of gravity and preloaded to prevent separation of the shear pads under the action of the centrifugal forces. Each of the four release mechnisms consists of two hooks which engage two attachment pins on each satellite. The two hooks are pivoted about a single point, which is attached to a tension cable. Four tension cables from each satellite release mechanism are passed through a squib actuated cable cutter, which is capable of severing all four cables at one time. Each of the cables also has an individual adjustment with which the system can be preloaded in tension.

The amount of preload necessary to offset the centrifugal forces is quite nominal and may be calculated as follows (assuming a spin rate of 142 rpm and a satellite weight of 70 pounds each).

$$\text{Preload} = m\omega^2 r$$

$$= \frac{70}{32.2}\left(\frac{2\pi 142}{60}\right)^2 \cdot \frac{16.5}{12}$$

$$= \underline{662 \text{ lbs.}}$$

After severing of the four cables, each satellite moves out radially from the module, pulling the pair of hooks up against two pins fixed in the module structure which force the hooks apart, releasing the satellite. Thus, the centrifugal forces are used to unlock the satellite release system.

Satellite. Figure 5.1-11 shows a drawing of the proposed radially deployed satellite. It consists of a cylindrical equipment module in which the satellite electronic equipment and scientific experiments are mounted and two sections of cylindrical solar arrays. The module is made up of two circular honeycomb equipment platforms situated at each end of a sheet metal cylinder. The two solar array cylinders are mounted at each end of the module so that a "belly band"

is formed around the center of the satellite. All sensors, experiments, etc., requiring a field of view are mounted within the equipment module so that no penetration of the solar array panels occurs. Attachment of the satellite to the release module is also effected in the area of the "belly band". On the center line of each satellite, a mast projects upward, which supports at its top a bi-conical S-band antenna. The mast is primarily provided to support the antenna and to separate it sufficiently from the satellite. However, it also provides a convenient structure that helps to support the extreme ends of the three booms when folded in the launch and ascent configuration.

The three booms are of the single hinge type, pivoted about three points located at the extreme lower edge of solar array cylinders and supported by an internal truss structure. Deployment of the booms is effected by centrifugal forces due to the initial spin rate. Viscous fluid dashpots are provided to damp the motion of the booms during deployment. The booms are depressed below the horizontal by means of springs at the hinge points and locked in their final position. In the stowed position they are locked together at the central mast. A single locking device can then provide the release after separation of the satellites from the payload at apogee.

Table 5.1-3 shows the mass properties data of the radially deployed payloads and satellites. It can be seen that the spin axis mass moment of inertia of the satellite undergoes a large change as the booms deploy, resulting in a loss in spin rate from the initial rate of 142 rps to 20.8 rpm when fully deployed. Since the final spin rate required is 50 - 70 rpm, spin-up after boom deployment is required. However, since at the low spin rate the least amount of energy is required to erect the satellite normal to the ecliptic, this is done prior to spin-up.

The attitude control/spin-up system is mounted at the end of one of the three booms together with a nutation damper. This system can also provide, with the expenditure of a little extra fuel, the thrust required for an out-of-plane maneuver of one or all of the satellites prior to erection normal to the ecliptic, if required.

Table 5.1-4 shows a weight breakdown of the four- and two-satellite payloads and the individual satellites.

In the event of a forty earth radii mission with two satellites, ballast weight would have to be provided to replace the two satellites omitted from the payload in order to retain an inherently stable condition. Two of these weights could be placed at approximately 30 inches from the spin axis and would be approximately 36 pounds in weight each. They would be rigidly attached to the central release module and not be separated at satellite deployment.

TABLE 5.1-3 MASS PROPERTIES - RADIAL PAYLOAD

Configuration	Booms Stowed			Booms Deployed		
Configuration	I_{Spin}	I_{Trans}	Inertia Ratio	I_{Spin}	I_{Trans}	Inertia Ratio
Payload	18.1	15.30	1.17	---	---	---
Satellite only	.72	1.92	.37	4.91	3.07	1.59

TABLE 5.1-4 WEIGHT BREAKDOWN- RADIAL (LESS SCIENCE)

Item	Satellite	Payloads	
		Four Satellites	Two Satellites
Structure	8.75	---	---
Solar Array	7.23	---	---
Electronics	25.00	---	---
Booms	6.15	---	---
Carrier	---	5.0	5.0
Attitude Control	2.70	---	---
Adaptor	---	12.20	12.20
Ballast	---	---	72.00
Total Satellite Weight	49.83	199.32	99.66
Total Payload Weight		216.32	188.86

5.1.6 Thermal Considerations

The spacecraft temperature control system uses passive techniques for both configurations. Temperature control is not required during ascent, if the launch vehicle shields the spacecraft.

5.1.6.1 Requirements. Thermal design requirements are listed in Table 5.1-5. The solar flux is 442 Btu/hr-ft^2. The seasonal variation is neglected.)

TABLE 5.1-5
THERMAL DESIGN REQUIREMENTS

Mission Phases	Satellite Configuration	
	Radial	Stacked
Coast Phase		
Total Duration (Hours)	24	24-72
Eclipse Duration (Minutes)	None	25 max.
β Excursion* (Angular Degrees)	±26	±15°
Power Dissipation (Watts)	0	0
Orbital Phase		
Period (Hours)	48	48
β Excursion* (Angular Degrees)	±5	±15
Power Dissipation (Watts)	20	21
Eclipse Duration, (Typ. Max.)	1 hour	1 hour

* β is defined in Figure 5.1-12.

Allowable equipment operating temperature range is 0°F to 120°F. (Exceptions are the battery and ammonia system, which have limits of 40°F to 100°F.

5. 1. 6. 2 Satellite Thermal Characteristics. The satellites are spin-stabilized cylinders, and the spin rate is sufficiently high to assure constant temperatures during a spin cycle.

From the standpoint of thermal design the basic satellite configuration can be divided into four categories.

a. Equipment Modules
b. Solar Cell Panels and Satellite Structure
c. Boom-Mounted Units
d. Carrier Structure

Equipment Modules. In each configuration, the equipment modules should be thermally isolated from the solar cell panels. Temperature of the equipment modules is controlled by adjusting the exterior surface properties of the equipment modules.

Figure 5. 1-12a and b show the radial and stacked configurations.

a. Radial Configuration. The equipment module for the radial configuration is a cylindrical section with equipment mounted to aluminum honeycomb panels, which form the ends of the cylinder. The honeycomb panels are thermally conductive to obtain a substantially isothermal equipment panel. The units are placed for nearly uniform heat dissipation on the panel. To reduce heat losses during eclipses, the equipment panels are thermally insulated from the structure and the solar panels by low thermal conductivity washers.

   Because of the small excursion in the solar vector (±5 degrees), the equipment module is (for all practical purposes) uniformly illuminated with solar energy. The exterior of the equipment panels and the cylinder section of the equipment module are finished with alumatone paint (α_s = .20 and ϵ = .24). This maintains the equipment near its upper temperature level during sunlight operation and avoids excessive heat losses during eclipse.

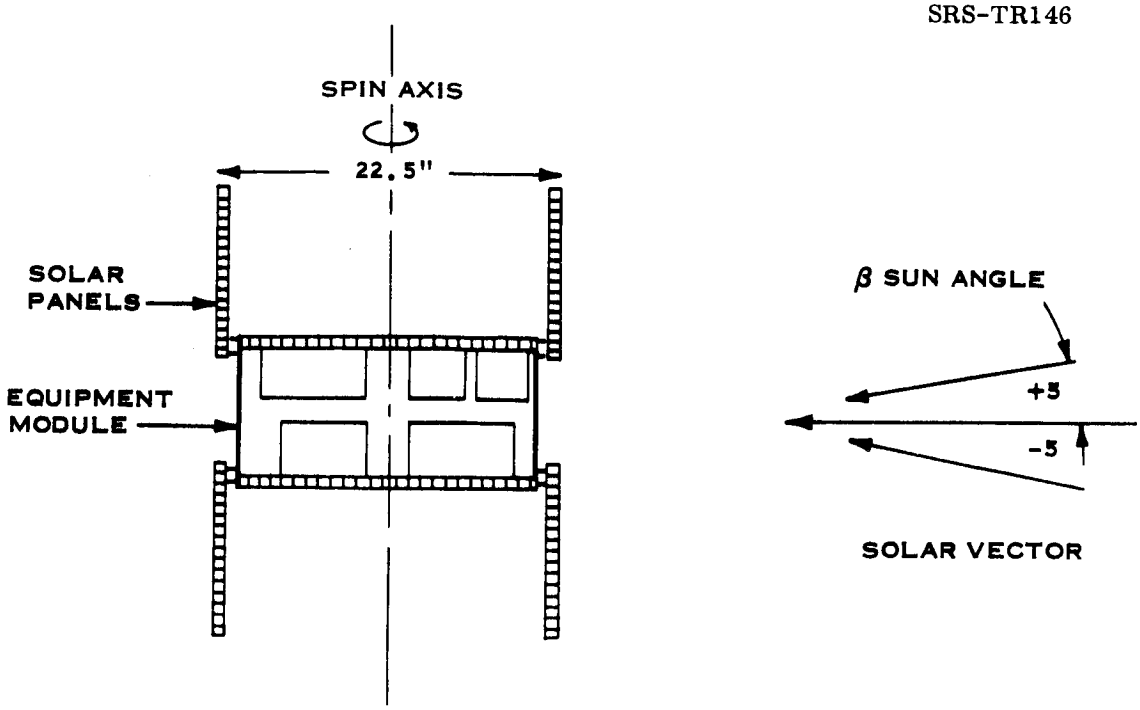

Figure 5.1-12a Radial Configuration (No Scale)

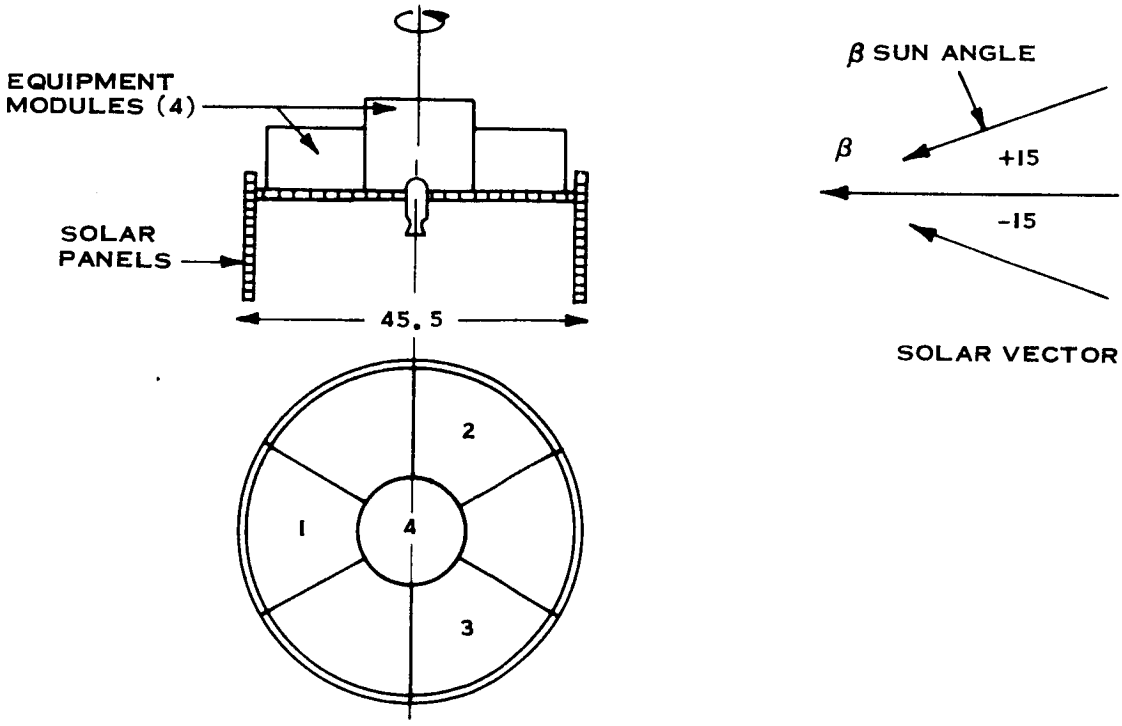

Figure 5.1-12b Stacked Configuration (No Scale)

b. Stacked Configuration. The equipment for the stacked configuration is distributed between four equipment modules, numbered 1-4 for identification purposes. (See Figure 5.1-12b) The equipment allocation, weight, and average power dissipation for each of the four modules are listed in Table 5.1-6.

TABLE 5.1-6

EQUIPMENT ALLOCATION FOR STACKED CONFIGURATION

Component	Weight (lbs)	Average Power (watts)
Equipment Module No. 1		
Transponder	5.0	10.0
Power Control Unit	2.5	1.5
DC/DC Converter	2.5	0.5
TOTALS	10.0	12.0
Equipment Module No. 2		
ARC Magnetometer	5.0	3.5
Program Timer	2.0	0.5
Battery	3.5	0
TOTALS	10.5	4.0
Equipment Module No. 3		
Plasma Probe	6.5	3.5
TLM Generator Comm.	3.5	1.5
TOTALS	10.0	5.0
Equipment Module No. 4		
Tape Recorder	5.0	0.2
Solid Propellant Motor	0	0
TOTALS	5.0	0.2

The equipment modules are thermally isolated from the solar cell panels by the same mounting techniques discussed for the radial configuration. The equipment for each module is located on aluminum honeycomb, and aluminum cover are coupled to the mounting base to insure adequate thermal paths and to provide an isothermal enclosure for the equipment.

The temperature level of equipment can be maintained by selection of surface coatings for exterior surfaces and adjustment of heat transfer paths from the equipment panels to individual components.

The variation in sun angle, ±15 degrees causes larger excursions in predicted orbit temperatures of components for the stacked configuration than those for the radial configuration.

Because of low power dissipation in module No. 4, the tape recorder experiences the maximum excursion in temperature during its orbital life. Insulation could be applied to surfaces of module No. 4 to decrease the predicted temperature excursions.

Solar Cell Panels and Satellite Structure. The equipment modules for both satellite configurations are isolated from the solar cell panels and the spacecraft structure to reduce temperature excursions of the equipment during eclipse.

The surface properties of the solar cells (solar absorptivity = 0.76, emissivity = 0.83) provide a satisfactory steady state temperature of the solar cells and satellite structure during sunlight operation. Allowing the back surface of the solar cell panels to radiate to space reduces the operational temperature of the solar cells and increases their available electrical power output.

The solid propellant kick motor for the stacked configuration only operates for less than one second and dissipates a negligible amount of thermal energy; this energy has been neglected for these preliminary analyses. Its empty case is also a negligible thermal mass.

Boom-Mounted Units. Satisfactory temperature control of the booms and the boom-mounted units can be obtained for each of the two satellite configurations by adjusting their exterior surface properties. Steady-state equilibrium temperatures can be adjusted over a wide range. For example, for the ammonia control system, a pattern of 50 percent alumatone paint and 50 percent colorless MIL-C-5541 on the sides of the case and 100 percent alumatone paint on the ends of the case will maintain a satisfactory case temperature.

Carrier Structure. The carrier consists of a structure that supports the satellites during the coast phase and contains communication equipment which is operational during the coast phase. For the two configurations, the temperature level of the equipment located on the carrier can be controlled by selection of the proper exterior surface properties on the exterior covers of the equipment.

In the stacked satellite configuration, for which the coast phase is a maximum of 72 hours, the equipment on the carrier structure must endure an eclipse period. To insure that the communication equipment does not get too cold during eclipse the exterior surface coating of this equipment is finished with a high α_s IE ratio. This insures a high initial temperature prior to eclipse.

5.1.6.3 Temperature Predictions

Equipment Module. Temperature predictions are based on preliminary thermal analyses, assuming that the equipment modules and equipment are represented by a single isothermal node.

a. Radial Configuration. When the solar vector is normal to the spin axis, the average orbital temperature of an equipment module finished with a alumatone paint is 65°F. The ±5 degree sun angle variation has no significant effect on predicted temperatures because the change in projected area is less than one percent.

   Without internal power dissipation, the predicted minimum temperature of the equipment module, assuming a single isothermal node, is 15° F

for a one-hour eclipse and 40°F for a half-hour eclipse. To maintain the temperature of all the equipment at or above 40°F (the minimum required temperature of the battery) for the one hour eclipse, a standby power dissipation of approximately 20 watts would be required.

The temperatures predicted by the single node equipment model are representative of a type of average for the external radiating surfaces and the equipment. The temperatures of the equipment dissipating power can be controlled to higher levels depending on the degree of isolation from the radiating surfaces. A more detailed analysis, similar to that performed in Reference 1, would show that by isolating the batteries from the power-dissipating equipment, the temperature of the batteries would be maintained at or above +40°F during eclipse without any standby power, while the temperature of the remaining equipment would decrease to approximately +10°F.

During the coast phase, the average temperature of the radial-configuration satellites would be approximately 50°F for the solar vector normal to spin axis. For an excursion of ±26 degrees in the sun angle, the back surfaces of the solar panels would be exposed to solar energy, but the ends of an equipment module are shadowed and its temperature would decrease to approximately 35°F.

b. Stacked Configuration. The predicted temperature of the stacked configuration is dependent on the sun angle, β. The assumed paint patterns and predicted temperatures are listed in Table 5.1-7. Each of the four equipment modules for the stacked configuration is assumed to be represented by a single isothermal node receiving and reradiating solar energy to space and insulated from other components of the satellite.

Each single-node equipment module can be passively maintained within its respective temperature limits with the exception of the batteries located in equipment module No. 2. During a one-hour eclipse period, the batteries reach a minimum temperature of roughly 17°F; to maintain

TABLE 5.1-7

ORBITAL TEMPERATURE PREDICTIONS FOR
STACKED-CONFIGURATION SATELLITES, °F

Equipment Module No. (Fig. 1b)	Surface Finish Requirements			Sun Angle, β			Eclipse*	
	Sides	Top	Bottom	-15	0	+15	One Hour	1/2 Hour
1	50% ALT 50% MIL	ALT	MIL	50	75	82	20	35
2	30% ALT 70% MIL	70% ALT 30% MIL	MIL	42	46	80	17**	30***
3	30% ALT 70% MIL	70% ALT 30% MIL	MIL	44	48	85	25	32
4	MIL	ALT	MIL	44	53	84	5	27

ALT -- Alumatone Aluminum $\alpha = 0.2$, $\epsilon = 0.24$, $\alpha/\epsilon = 0.83$

MIL -- MIL-C-5541 (Colorless) $\alpha = 0.35$, $\epsilon = 0.10$, $\alpha/\epsilon = 3.5$

* Based on $T_{initial} = T\ (\rho = -15°)$

** Power Required to Maintain Temperature at 40°F = 4.5 watts

*** Power Required to Maintain Temperature at 40°F = 2.5 watts

the temperature at 40°F or above requires 4.5 watts of heater power. For a half-hour eclipse, the minimum temperature is 30°F and 2.5 watts of power are required. Again, a more detailed analysis would probably show that the battery temperature during eclipse could be maintained at or above 40°F by isolating the batteries from the external surfaces of the equipment modules.

During the coast phase of flight, the average temperature of the stacked-configuration satellites would be 70°F. During the eclipse, the satellite temperatures would cool to 20°F for a one-hour eclipse and 35°F for a half-hour eclipse.

Solar Cell Panels and Satellite Structure. The solar cell panels for the radial configuration have steady state orbital temperatures of approximately 30°F. The low temperature is attributed to the fact that the backsides of the panels are free to radiate to deep space. The back surface of the solar cell panels should be painted with Skyspare white paint ($\alpha_s = 0.22$, $\epsilon = .91$). The white paint and the small angular excursion in the sun angle (±5 degrees) causes a negligible change in the predicted temperatures.

For the stacked configuration, the excursion in the sun angle is ±15 degrees. With white paint on the back surface of the solar panels, the predicted temperature ranges from +25°F to 55°F. The higher temperature is attributed to the fact that when the sun angle is -15 degrees from normal, over 40 percent of the back surface is illuminated with solar energy.

Boom-Mounted Units. Satisfactory temperature control can be maintained for the boom-mounted components during orbit by proper selection of radiative properties of exterior surfaces. The surface properties of the boom sensors can be selected so that their case temperature is +60°F, and the case temperature of the ammonia system is 70°F. The minimum temperature of these units during maximum eclipse is +15°F.

Carrier-Structure. The carrier structure equipment temperature, like the satellite, can be controlled over a wide range of temperatures dependent on the prescribed surface properties and power dissipation.

Assuming an open structure of aluminum struts with an anodized finish, the temperature during the coast phase is 40°F. During the 25-minute maximum eclipse of the coast phase, the structure temperature for the stacked configuration would cool to +15°F.

The equipment mounted on the carrier structure can be thermally controlled by isolating the equipment from the structure and controlling the surface properties of the equipment covers. For example, the VHF equipment could be controlled to 90°F during coast and to +10°F during eclipse by finishing the cover with 5 percent MIL C-5541 and 50 percent alumatone paint for the stacked configuration.

5.2 ATTITUDE CONTROL STUDIES

The principal aim of the attitude control studies was to define control schemes that met system requirements, and to select the best scheme for each of the conceptual configurations investigated. The requirements and constraints on the control system were as follows:

- Spin-stabilization at 50-70 rpm
- Spin axis orientation preferably normal to the ecliptic
- Relatively coarse pointing (3 to 5 degrees).

These general constraints were used to determine whether the control system should be placed on the carrier or on the individual satellites, and whether it should be self-contained or ground-commanded. The operational constraints implied by these alternates were also studied, as were nutation damper requirements, propulsion system parameters, optimum sensor geometry, attitude and pulse synchronizing references, sequences of events, and logic schemes for accomplishing the required sequences.

The configuration studies narrowed down the design concepts to two: the radial configuration and the stacked configuration. The radial configuration has an attitude control system on each satellite and is oriented with the spin axis normal to the ecliptic plane. The stacked configuration has the attitude control on the carrier and is oriented with the spin axis normal to the orbit plane. After both ground-commanded and automatic systems were investigated, the ground-commanded system was found preferable in both configurations. Error budgets appear to confirm that the separation velocities can be kept within 5 degrees of the normal to the orbital velocity vector, as required by the mission analysis. A nutation damper is recommended on the carrier of both configurations, as well as a boom-mounted nutation damper on the individual satellites of the radial configuration.

The attitude control systems for the stacked and radial configurations (ground-commanded) are equally complex; thus, no clear advantage of one over the other

exists in that regard. However, the lower spin axis drift rates of the radial configuration combined with its capability for attitude updating, make it the recommended approach.

One of the first tasks was to determine whether the satellite attitude needed updating after the initial orientation. This was answered by determining the expected precession rates of the spin axes of the various configurations, and comparing the resulting offsets at the end of life with mission accuracy requirements.

5.2.1 Spin Axis Precession Analysis

Since the attitude is spin-stabilized, torque causes the spin axis to precess. The principal sources of disturbance torque are solar pressure, magnetic fields, gravity gradient effects, air drag effects, and outgassing. Very little can be predicted about outgassing, but the other disturbance torques have been assessed in a preliminary manner in the following sections.

5.2.1.1 Solar Torque. Solar torque is obviously different for the stacked and the radial configurations. The first approach was to estimate the total cross-sectional area and assume a certain distance from the center-of-pressure to the center-of-gravity. The absorptance of the solar array was taken as 0.7, and for other areas, 0.3.

With the sun in the spin plane, the cross-sectional areas of the different parts of the stacked configuration satellite are roughly as follows:

Solar array	$= 3.5\ ft^2$	$\alpha = 0.7$
Equipment modules	$= 1\ ft^2$	$\alpha = 0.3$
Equipment on end of booms	$= 0.4\ ft^2$	$\alpha = 0.3$
Booms	$= 0.6\ ft^2$	$\alpha = 0.5$

With the booms canted 15 degrees from the bottom of the solar array, the center-of-pressure is about 7.5 inches below the plane of the top of the solar array. For a solar constant of 10^{-7} lbs/ft^2, the total pressure is about 7.8×10^{-7} lbs. If the c.g. is located within 1 inch of the c.p., the solar torque is about 6.5×10^{-8} ft-lb. However, in this configuration, the c.g. is likely to be only an inch or two below the top of the solar array, which gives a moment arm of $\sim$ 6 inches, or a torque of $\sim 3.9 \times 10^{-7}$ ft-lb. This torque corresponds to $\sim$ 1 degree precession per month, resulting in a precession cone with about a 2 degree half-angle. The long term precession is in the form of a cone because of the motion of the satellite about the sun.

For the radial configuration, the solar array is split into two parts with a band between. The areas and reflectivities are:

Solar array	= 3.2 ft^2	$\alpha = 0.7$
Mid band	= 0.93 ft^2	$\alpha = 0.3$
Equipment on end of booms	= 0.4 ft^2	$\alpha = 0.3$
Booms	= 0.6 ft^2	$\alpha = 0.5$

Summing the moments caused by these areas and reflectivities locates the c.p. 7.85 inches from the end of the satelite where the booms are hinged. The pressure exerted is $\sim 7.5 \times 10^{-7}$ lb. A one-inch c.p. - c.g. distance causes a torque of 6.25×10^{-8} ft-lb., corresponding to $\sim$ 0.3 degree precession per month. If, as is likely, the c.g. is located in the plane of the edge of the belly-band nearest the boom hinges, then the solar torque increases to $\sim 1.5 \times 10^{-7}$ ft-lb, corresponding to $\sim$ 0.71 degree per month precession. This again demonstrates that control of the c.g. location by design may be necessary to keep drift rates acceptably low.

5.2.1.2 Magnetic Torque. The magnetic torque on the satellite is given by:

$$\overline{T} = \overline{M}_S \times \overline{B}_E$$

where:

$\overline{T}$ = torque on the satellite

$\overline{M}_S$ = magnetic moment on the satellite

$\overline{B}_E$ = magnetic field of the environment.

The magnetic moment on the satellite was estimated by assuming a dipole at the satellite c.g., aligned with the spin axis. Its strength was assumed to be such that it generated all of the permissible 0.50 gamma at the magnetometer head. The magnetometer head is located at ~190 cm from the c.g., giving a magnetic moment of:

$$M_S = Hr^3 = 34.4 \text{ oersted-cm}^3.$$

The magnetic field of the environment is hard to evaluate because of the eccentricity of the orbit and the resulting wide range of altitudes. At apogee, the satellite is outside the magnetosphere and essentially in the interplanetary magnetic field. Below about 10 earth radii, the magnetic field of the earth prevails. To estimate the magnetic torques it was assumed that the principal effect occurs between a true anomaly of 270 degrees and 90 degrees (i.e., near perigee), which assumes that the effects above 2 earth radii are of second order.

Since the time required to go from 270 degrees to 90 degrees true anomaly is less than an hour, the rotation of the earth during the pass was ignored. The earth's magnetic field was assumed to be a dipole at the earth's center, tilted 11.5 degrees with respect to the north geographic pole, in the plane of 70 degrees West longitude. Averaging the torque that was produced during the low part of the pass over the whole orbit gave a magnetic torque of less than:

$$T_m \leq 2 \times 10^{-9} \text{ ft-lb.}$$

5.2.1.3 Gravity-Gradient Torques. Torques due to gravity-gradient exist only if the spin-axis is not maintained normal to the orbit plane. As will be pointed out in Paragraph 5.2.2, the stacked configuration has its spin-axis normal to the orbit plane; thus the gravity-gradient actually tends to maintain the spin-axis normal to the orbit plane. The radial configuration, however, has its spin-axis normal to the ecliptic; thus, the gravity-gradient produces a disturbing torque.

In general, the gravity-gradient torque can be expressed by:

$$T_g = \frac{3\mu}{2R^3} (I_s - I_\perp) \sin 2\gamma$$

where:

μ = gravitational constant = 1.406×10^{16}
R = radius of satellite from center of earth
I_s = spin moment of inertia
$I_\perp$ = transverse moment of inertia
γ = angle between spin-axis and local horizontal

For the radial configuration, $I_s = 4.9$ slug-ft^2 and $I_\perp = 3.1$ slug-ft^2. The angle γ is a function of the inclination of the orbit with respect to the ecliptic, the true anomaly, and the line of intersection of the orbit plane and ecliptic plane. The line of intersection between the two planes is assumed to be within 10 degrees of the line of apsides; it can therefore be neglected. The angle γ can then be expressed as

$$\gamma = \gamma_o \left| \sin \eta \right|$$

where:

γ_o = angle between ecliptic and orbit planes
η = true anomaly of satellite

If the maximum inclination between the orbit plane and ecliptic is assumed to be 5 degrees, then the gravity-gradient torque can be expressed as:

$$T_g = \frac{6.63 \times 10^{15} |\sin \eta|}{R^3}$$

The time average of the function $\frac{|\sin \eta|}{R^3}$ is $\sim 10^{-24}$, giving an average gravity-gradient torque of:

$$T_g = 6.6 \times 10^{-9} \text{ ft-lb.}$$

5.2.1.4 Air Drag Torque. Air drag torque was evaluated by calculating the velocity change for each pass, relating this ΔV to a linear impulse, and applying the linear impulse at a center of pressure that is not coincident with the center of gravity. Extrapolation of data contained in Reference 1 indicates that the rate of change in perigee at 100 n. mi. perigee altitude is about 5×10^{-8} km/sec (16.4×10^{-5} ft/sec) for the reference orbit. The change in perigee velocity with respect to perigee distance is:

$$\frac{\partial V_p}{\partial r_p} = -1/2 \, r_p^{-3/2} \sqrt{\mu(1 + r)}$$

where:

V_p = perigee velocity

r_p = perigee radius

r = eccentricity = 0.897

μ = 1.4×10^{16} ft^3/sec^2

Reference 1: Space Flight Handbooks, Volume 1, Orbital Flight Handbook, Sect. V, "Satellite Lifetimes," by G. E. Townsend, Jr.

For small changes at a perigee radius of 2.18×10^{7} ft

$$\Delta V_p = 8.2 \times 10^{-4} \Delta r_p$$

Multiplying the rate of change of perigee by the orbital period gives a change in perigee radius on the order of 30 feet for each pass. Thus, for a satellite with a mass of 2, the impulse imparted by air drag is about 5×10^{-2} lb-seconds on each pass. If the impulse is delivered on a 1-inch moment arm for the radial case and a 6-inch moment arm for the stacked case (the same order of magnitude as solar pressure moment arm), then the angular impulse per pass is 0.42×10^{-2} ft-lb-second and 2.5×10^{-2} ft-lb-second respectively, giving an average torque over the orbit of

$$T_{AD} = 2.4 \times 10^{-8} \text{ ft-lb (radial)}$$
$$T_{AD} = 14.4 \times 10^{-8} \text{ ft-lb (stacked)}$$

5.2.1.5 Summary of Torque Effects. Table 5.2-1 summarizes the torques acting on the stacked and radial configurations and gives the resulting precession rates for the combined RSS torque. The solar torque used for the stacked configuration corresponds to a 6-inch moment arm, whereas the radial solar torque number corresponds to a 1-inch moment arm. This was done because the equipment location in the stacked configuration is much less flexible than in the radial configuration. There is thus a much better possibility of adjusting the c.g. location on the radial configuration to correspond to the c.p. location.

Table 5.2-1 shows that even if the solar torque is not balanced, the precession rates are low enough so that attitude updating is not required during the satellite lifetime. This means that a separate control system is not needed for each satellite to counter the long term torque effects.

TABLE 5. 2-1

TORQUE EFFECTS

Configuration / Torque	Stacked	Radial
Solar	39.0×10^{-8}	6.3×10^{-8}
Magnetic	0.2×10^{-8}	0.2×10^{-8}
Gravity-Gradient	---	0.66×10^{-8}
Air Drag	14.4×10^{-8}	2.4×10^{-8}
RSS TOTAL	41.6×10^{-8}	6.8×10^{-8}
Precession Rate*	1.09 deg/mo.	0.33 deg/mo
*Spin Speed = 60 rpm		

5. 2. 2 Operational Schemes for Initial Orientation

The major trade-off study performed involved an examination of the self-contained and ground-commanded orientation schemes. To determine the optimum control scheme, it was necessary to define potential problem areas by first defining for each scheme its operational constraints, logic requirements, optimum sensor geometry, and optimum pulse synchronizing reference.

For the stacked configuration, the ground rule was to orient the carrier spin axis normal to the orbit plane, while the four satellites are still attached to the carrier. This allowed the satellites to be ejected with a ΔV orthogonal to the orbit velocity vector near apogee. It was decided that the orbit plane would be close enough to the ecliptic plane to obviate spin axis reorientation after ejection, thus eliminating the need for a control system on each satellite in addition to the one already on the carrier.

For the radial configuration, the ground rule was to provide for initial orientation after release of the satellites from the carrier. This permitted the tangential velocity of spin at the moment of release to be utilized in obtaining the required separation ΔV. Since no in-track ΔV is wanted, the spin axis must be pointed as closely as possible to the velocity vector at the moment of release. Also, since initial orientation occurs after release, four separate control systems are provided -- one for each satellite. To avoid using a fifth control system to control the spin axis orientation of the combination, release occurs when the spin axis is collinear with the orbit velocity vector, i.e., at apogee. Since each satellite has its own control system, an additional ground rule is to orient the spin axis normal to the ecliptic rather than to the orbit plane.

5.2.2.1 Self-Contained Systems. The desirability of the self-contained systems lies in the fact that, for the initial erection maneuver, no telemetry interface is required between the satellite and the ground. In the stacked configuration, this eliminates the need for separate telemetry equipment on the carrier. In the radial configuration, eliminating the telemetry interface is of no advantage, since the initial orientation occurs after release from the carrier.

5.2.2.1.1 Stacked Configuration

Operational Constraints. The operational constraints are to some extent determined by the attitude reference chosen and how it is utilized. There are two basic ways of orienting the spin axis normal to the orbit plane. The simplest is to use a horizon scanning system that utilizes only the earth as an attitude reference. A more complex way is to use both the sun and earth as an attitude reference when they are in quadrature.

The second method, that of using both the earth and the sun as attitude references, is too complicated for an automatic system. Local roll information can be obtained from the horizon sensor system; the other axis, local yaw, is sensed by a sun angle indicator. Sensing the angle is not difficult, but the angle the spin axis makes with respect to the sun in order to be normal to the orbit plane, is not constant, being a function of the day, and time of day of launch. The desired angle with respect

to the sun must, therefore, be set into the control system a few minutes before launch time. This can be done, but the lack of significant advantages over the system that uses only earth sensors, plus the added weight of the sun angle indicator, excludes this approach from further consideration.

The first method, using earth sensors only, is simpler because no sun angle indicator is required, nor must the earth and sun be detected when in quadrature. This method takes advantage of the fact that the roll and yaw angles of a spinning satellite interchange every quarter of an orbit. Thus, a local yaw angle at perigee becomes a local roll angle at 90 degrees true anomaly. It can be seen then, that nulling local roll at some point in the orbit leaves only a local yaw error, which can be removed 90 degrees later as local roll.

A sketch of the orbit shows only two pair of points separated by 90 degrees true anomaly that have equal altitude. These pairs are at 135/225 degrees and 315/45 degrees. If initial orientation is desired before first apogee, it is obviously impossible to make the two roll nulling maneuvers at the same altitude. Horizon sensor geometry must therefore be arranged for satisfactory performance over a wide range of altitudes. There are arguments against using the equal altitude points, other than desiring to complete initial orientation before first apogee. If the pair near perigee is used (315/45 degrees true anomaly), there is not enough time for completion of the required maneuvers unless very high torque levels are used, with consequent reductions in resolution. Use of the pair near apogee (135/225 degrees) unduly complicates the sensing and logic requirements, since the residual roll error after the initial erection maneuver could easily be large enough to cause the horizon sensors to miss the earth. This would require use of the sun for pulse synchronizing and possibly a sun angle indicator. Also, since the events will be timer initiated, the necessity of waiting until second apogee means the period dispersions will cause a larger position uncertainty than if separation is initiated near first apogee.

These considerations show the desirability of initially orienting the satellite before first apogee. Since the earth subtends such a small angle near apogee, and since the maximum dynamic range capability in terms of roll offset is directly proportional

to the angle subtended by the earth, it is desirable to complete all maneuvers at as low an altitude as possible. From sensor considerations, it is desirable to complete the final roll nulling maneuver before 135 to 140 degrees true anomaly, where the earth subtends an angle of 18 to 20 degrees. This means that the initial orientation and roll nulling must be completed no later than 50 degrees true anomaly (~9. 5 minutes from injection). These considerations are the primary factors governing the choice of the representative sequence of events shown in Table 5. 2-2.

TABLE 5. 2-2

SEQUENCE OF EVENTS

True Anomaly (Deg.)	Time From Injection	Event Description
0	0	Injection
5	0. 75 min	Start Initial Spin Axis Erection (Local Yaw)
35	6. 0 min	Terminate Local Yaw Maneuver
		Initiate Local Roll Nulling
50	9. 5 min	Terminate Local Roll Nulling
138	2. 25 hrs	Initiate Local Roll Nulling
140	2. 50 hrs	Terminate Local Roll Nulling

For the initial part of the maneuver, at low altitude, the yaw and roll motions require about 115 degrees of spin axis maneuver, as explained later. To accomplish this rotation in the time allotted requires an average precession rate of 0.22 degree/second, which implies relatively high torque levels for this configuration. Figure 5.2-1 shows the attitude resolution versus torque level for a torque pulse angle of 90 degrees of rotation. At 50 rpm, 0.26 degree/pulse is required, while at 70 rpm, 0.19 degree/pulse is required. Thus, an average torque at 25 percent duty cycle of 5 ft-lbs should be adequate, giving a little margin. Decreasing the duty cycle, of course, increases the required torque level.

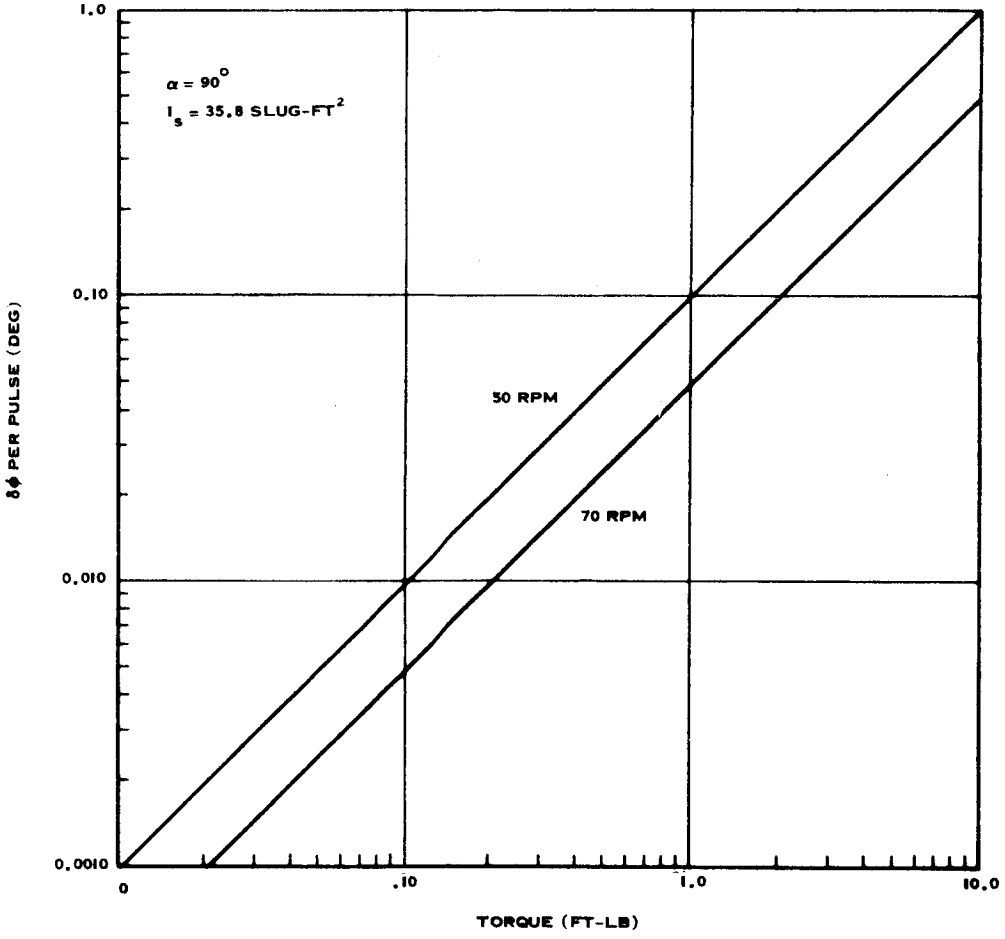

Figure 5.2-1 Stacked Configuration, Attitude Resolution vs. Torque Level

Logic Requirements. Since the instantaneous measurement of true anomaly from the spacecraft is difficult, if not impossible, the true anomaly must be deduced from the time from injection and the reference orbit. A timer would be necessary to initiate and terminate the various events at the appropriate time.

In addition to the timer, synchronizing signals must be generated during each spin cycle to provide a local yaw or local roll motion of the spin axis. The first maneuver required is a local yaw of the spin axis. This maneuver requires the torque pulses to be symmetrical about the center of the earth pulses, i.e., the center of the torque pulse should coincide with the center of the earth pulse. The two subsequent roll maneuvers require the center of the thrust pulse to be ±90 degrees out of phase with the center of the earth pulse. The sign of the phase shift is a function of the sign of the roll angle.

There are several ways to synchronize the torque pulses, including schemes that compute the spin speed and delay the torque pulses the appropriate number of degrees of spin. For simplicity of implementation, the study was directed towards geometrical arrangements of the sensors on board to provide the required synchronization. To detect a roll error of a spinning satellite, two IR horizon scanners are commonly attached to the spacecraft in such a way that the spin of the satellite causes the two fields-of-view to scan narrow cones, above and below the spin plane.

One synchronizing scheme considered uses the two roll detection scanners for synchronizing the thruster for the positive and negative roll corrections; the initial yaw maneuver is synchronized by a third scanner. Figure 5.2-2 shows the relative locations of the thrusters and the horizon sensor fields-of view. Horizon scanners

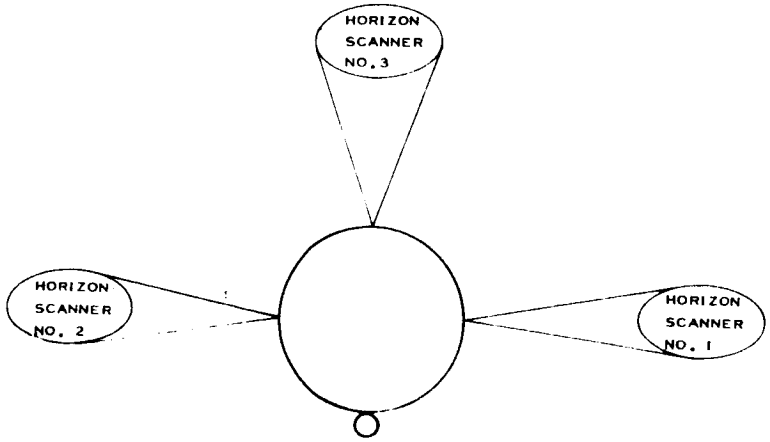

Figure 5.2-2 Sensor/Thruster Geometry

No. 1 and No. 2 sense the roll and serve as pulse synchronizers by turning on the thruster during the time they scan the earth if a roll correction is needed. Horizon scanner No. 3 is used only during the initial yaw maneuver, and it also turns on the thruster during the time it scans the earth. It is apparent that during the lower parts of the orbit, the pulse width is going to be rather large, typically varying from ~150 to 120 degrees for the initial yaw utilizing horizon scanner No. 3.

Another scheme eliminates the third horizon scanner and also gives a shorter, more efficient torque pulse during the initial yaw. In this scheme, logic is provided that turns the thruster on when horizon scanner No. 1 leaves the earth and turns it off when horizon scanner No. 2 intersects the earth. This provides synchronization for the initial yaw maneuver with pulse widths varying from 35 to 50 degrees. The roll correction synchronization is identical to the previous scheme. The main disadvantage of this approach is that the pulse widths are almost too narrow, which requires a significant increase in the thrust level required to deliver the necessary impulse in the allotted time.

Of the two methods, the latter is preferred since it does not require the third sensor, and also because the yaw maneuver is more efficient.

In addition to the above logic requirements, there is also a problem in selecting the time to stop pulsing the satellite. A simple roll deadband system is inadequate for two reasons. First, a simple deadband system causes attitude instability* in the presence of inadequate nutation damping. Second, the large nutation angle that may exist causes the deadband to be crossed several pulses before the center of the nutation angle is near the desired attitude. Figure 5.2-3 shows the maximum nutation angle that can be expected during pulsing, as a function of torque level. For a 5 ft-lb torque level, the angle is ~5 degrees.

---

* "Final Report, Spin Replenishment and Spin Axis Attitude Control System", Philco-Ford, Aeronutronic Division, Publication No. U-2939, 14 December 1964, p. 1-33.

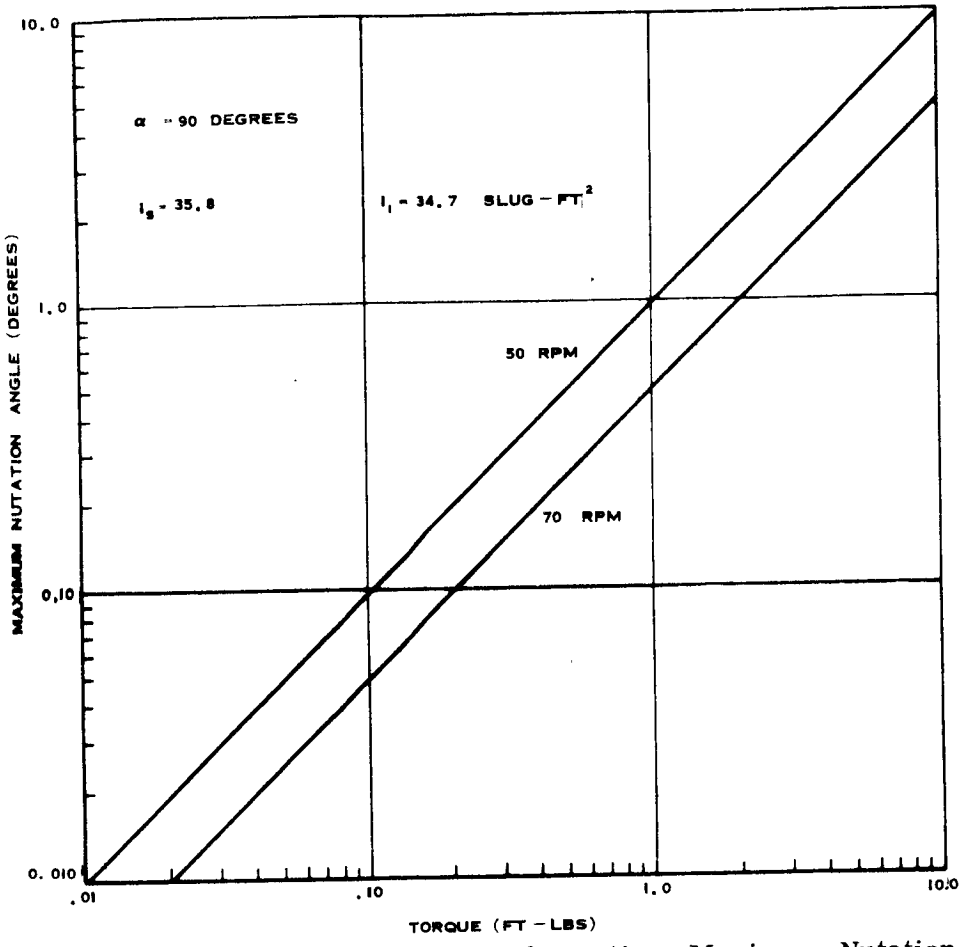

Figure 5.2-3 Stacked Configuration, Maximum Nutation Angle as a Function of Torque Level

Figure 5.2-4 shows typical spin axis motion when subjected to a series of torque pulses. For the stacked configuration the inertia ratio is 1.03, which means that a minimum nutation angle is reached every 33 pulses rather than the 16 shown. Due to the wide range of nutation angles possible, the average roll position (center of the nutation angle) may not cross the deadband until several cycles after the first crossing. At an average resolution of 1/4 degree per pulse, the first deadband crossing may occur anywhere from 4 to 20 pulses before the average roll angle comes within the deadband, making a counter impractical. Since it is the average roll angle we wish to control, this points up the need for extensive filtering of the roll angle information to eliminate the variations at nutation frequency. Therefore, the deadband must be set with some consideration given to the lag inherent in the filter. The presence of the filter means that only the average roll angle is fed to the deadband circuit, and the instability mentioned previously does not exist.

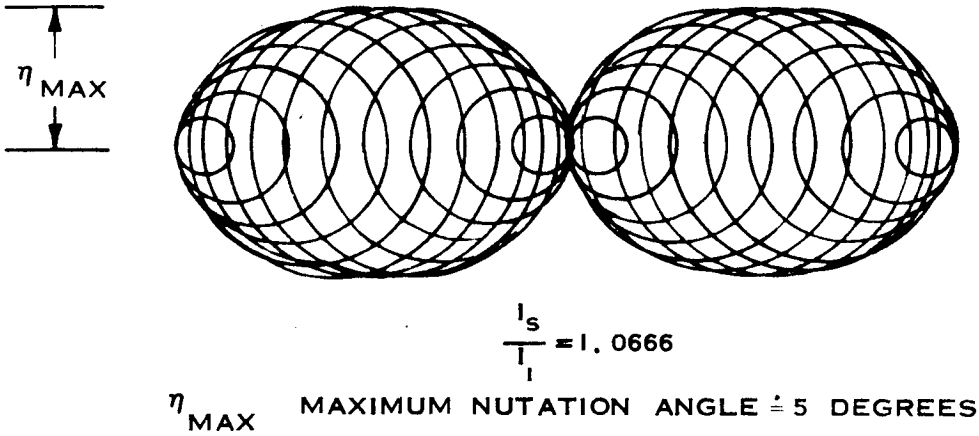

Figure 5.2-4 Representative Spin Axis Motion During Maneuvers

Since the filtering is not complete, i.e., some variation remains, there must be some logic to ensure stability even though a variation of the roll angle still exists. A counter can be used to bring the average roll angle to within the deadband by more than the expected variation. The number of pulses required is a function of the resolution of the control system and the amount of variation remaining on the roll signal after filtering.

Sensor Requirements and Selection. As pointed out previously, the self-contained stacked configuration requires two IR sensor heads looking in opposite directions, as in figure 5.2-5. To provide roll information, the fields of view of the sensors should be canted as shown. The optimum angle from the spin plane is a function of the satellite altitude and the desired dynamic range of the sensor.

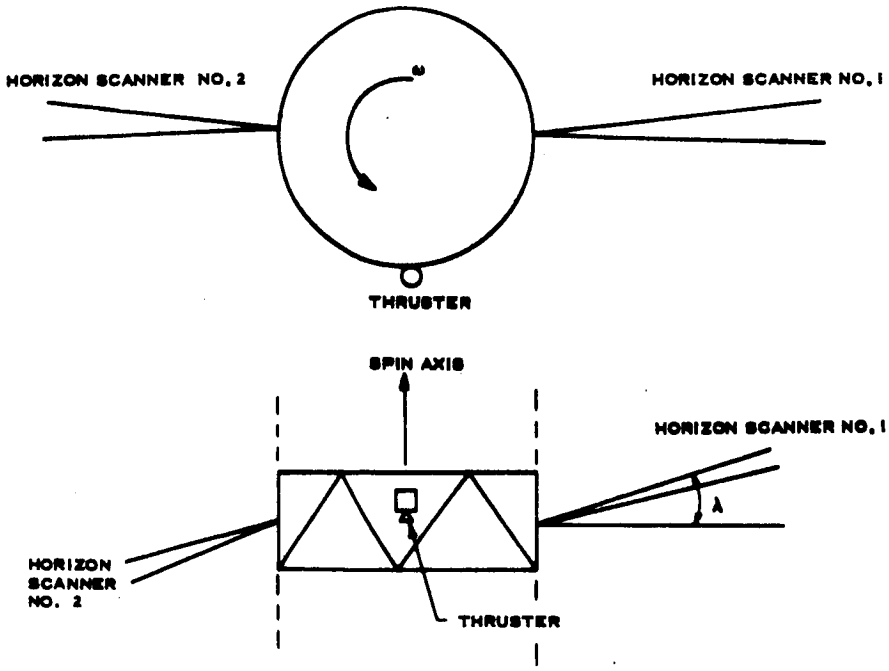

Figure 5.2-5 Sensor/Valve Configuration for Stacked, Self-Contained Configuration

A linear approximation of the transfer function of the horizon sensor is:

$$\phi = k \Delta \theta$$

where: ϕ = roll ange indicated

k = constant of proportionality

$\Delta\theta$ = difference in earth pulse widths of the two blippers

The constant k is defined as:

$$k = \frac{\sqrt{\cos^2 \lambda - \cos^2 \lambda_o}}{4 \sin \lambda}$$

where: λ = angle between center of sensor field-of-view and spin plane

$2\lambda_o$ = angle subtended by earth

To include both maneuvers, the sensor must be usable at altitudes of 150 to 20,000 nm. Accuracy is of importance primarily during the two roll nulling maneuvers at 4200 nm and 20,000 nm from the center of the earth. Parametric studies have determined the optimum offset angle as a function of geometric gain, signal-to-noise ratio, pulse rise time, and linearity of the actual transfer function. Results of these studies indicate that, for the initial roll nulling maneuver, the optimum offset angle, λ, should be about 30 to 35 degrees. The optimum offset angle at the time of the second roll nulling is about 5 degrees. Choosing a compromise of 8 degrees gives a linear range at 20,000 nm of 2 degrees and a synchronizing reference for ±18 degrees of roll. The low altitude performance is compromised somewhat because of the smaller than optimum offset angle. At 8 degrees, the low altitude gain is 1.45 and the high altitude gain is 0.20. This wide range of geometric gains (k) requires gain switching between the first and second roll nulling maneuvers for accuracy reasons. This is discussed further in the error analysis section.

Logic Definition and Description. Figure 5.2–5 shows the relative orientations of the sensor fields of view and the thruster. Positive and negative roll are defined in the conventional aircraft sense, i.e., positive roll is "right wing down". Figure 5.2-6 shows the logic diagram necessary to accomplish the objectives listed in previous sections.

System operation is as follows. Because of the satellite spin, the fields of view of the IR sensors are scanned across the disc of the earth, generating a pulse train. The pulse trains from the two sensors are subtracted and run through a low pass filter to obtain the average pulse width difference, which is a measure of the local roll angle. The output of the low pass filter is fed into deadband circuitry. The deadband circuitry energizes a counter brake if the attitude is outside the deadband. The counter has an output until the preselected number of pulses has been counted to get the average attitude well within the deadband. This output is used to ensure continued pulsing after the deadband circuitry output is zero. The momentary timer function that energizes the relay connecting the deadband circuitry to the counter brake is provided to restart the roll nulling logic for the second roll nulling maneuver. The timer also resets the pulse counter.

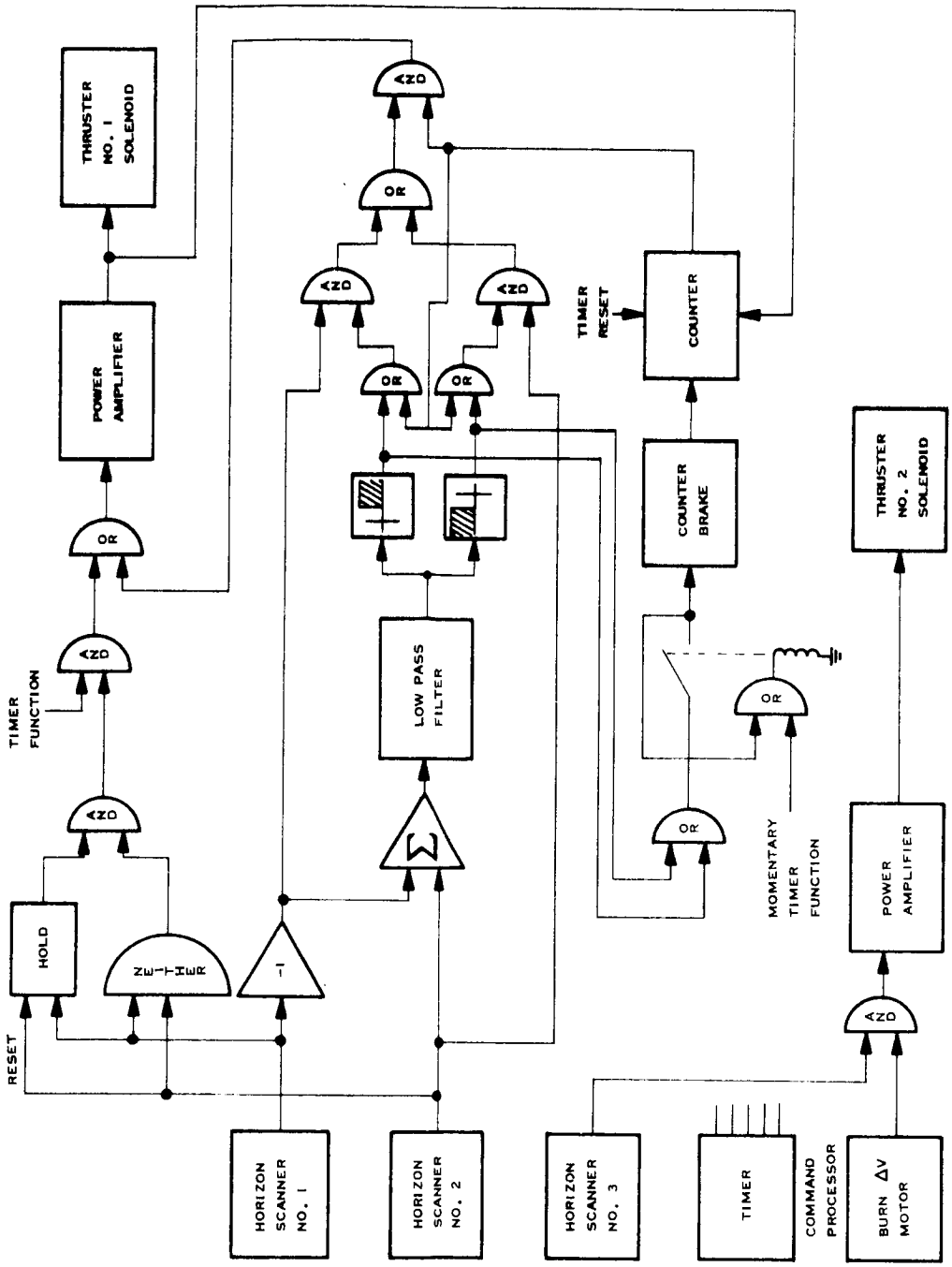

Figure 5.2-6 Logic Diagram, Stacked Configuration

The initial yaw maneuver is performed as long as the timer provides a voltage to the indicated "and" gate in the upper left of Figure 5.2-6. The "hold" circuit holds a voltage from the time horizon scanner No. 1 leaves the earth until reset to zero by the intersection of the earth's horizon by horizon scanner No. 2. The "neither" circuit generates an output when neither horizon scanner sees the earth, and when "anded" with the "hold" circuit output it provides the desired pulse sync for the initial yaw maneuver.

A power amplifier is used to drive the thrust valve from the final "or" gate.

5.2.2.1.2 Radial Configuration. In the radial configuration, a control system is placed on each individual satellite. For this reason, it was decided to orient its spin axis normal to the ecliptic, rather than normal to the orbit. For spin axis erection normal to the orbit plane, the system is similar to the one described in Paragraph 5.2.2.1.1, except that the thrust levels and required impulse are different. The timer functions occur at different times because of the different starting point (apogee).

An automatic system capable of erecting the spin axis normal to the ecliptic is much more complex. Sun angle information is easily enough obtained, but for control of the other axis another source must be found. A star could be used, but difficulty is immediately encountered in automatically processing star scanner data on the satellite. If the earth is used, then horizon scanners must be used. Prior knowledge of the orbit parameters would allow selecting two spots in the orbit where a pure roll angle would be the required information/maneuver. However, the required angle changes as a result of injection dispersions, as well as the point in the orbit where the horizon scanner reads out the angle between the orbit plane and the ecliptic.

As a result of the above difficulties, it was not considered desirable to proceed with detailed definition of an automatic control system for this configuration.

5.2.2.2 Ground-Commanded Systems. Ground-commanded systems offer the distinct advantage of greater flexibility in the event of unforeseen circumstances. The main disadvantage, of course, is the greater requirement for a ground station interface. More command and readout capability is also required.

5.2.2.2.1 Radial Configuration.

Operational Constraints. The operational constraints for the radial configuration are derived from the requirement to orient the spin-axis normal to the ecliptic plane, plus the fact that the satellite is to be ground-commanded.

During the lower portion of the orbit (<90 degrees true anomaly), the speed of the satellite is so high that a ground station is not in view long enough to complete a long maneuver. It was therefore decided to perform attitude maneuvers only when the satellite is more than ±90 degrees true anomaly.

A sun angle sensor is required to orient the spin-axis normal to the sun. The other axis of information is supplied by earth sensors. Sun sensors, looking out from the satellite at 90 degree angles with respect to each other, can be used to provide constant pulse widths for the thruster. This is done by using one sensor to turn the thruster on, the next one to turn it off; thus, a 90 degree width is always obtained.

If the spin-axis is not initially normal to the sun line, using the sun as a pulse reference causes the spin-axis to describe a cone when being maneuvered about the sun line. The half-angle of the cone is the initial angle between the sun and the spin axis. Therefore, to assure a planar maneuver for the initial erection, it is necessary to first normalize the spin-axis with respect to the sun. This maneuver is also desirable as the first step in orienting the attitude normal to the ecliptic, since the spin-axis must always be normal to the sun line if it is to be normal to the ecliptic.

After normalizing the spin-axis to the sun line, it is necessary to rotate about the sun line for approximately 90 degrees. The exact amount depends on the orientation of the orbit plane with respect to the ecliptic. If the angle between planes is small, then 90 degrees would be rotated. If the angle is, say, 20 degrees then only 70 degrees need be rotated.

After the satellite is oriented approximately normal to the ecliptic, additional readings must be taken from the earth sensors to determine whether further rotation about the sun line is needed.

With the above considerations in mind, the sequence of events given in Table 5.2-3 was derived.

TABLE 5.2-3

RADIAL CONFIGURATION SEQUENCE OF EVENTS

True Anomaly (Deg.)	Event Description
180	Release of 4 satellites from carrier
185	Normalize spin-axis to sun
195	Rotate ~90 degrees about sun line
240	Spin-up
260	Read out angles from earth sensors
120	Read out angles from earth sensors
150	Read out angles from earth sensors
250	Rotate about sun line if necessary

It should be emphasized that the true anomaly of the above events is not critical. One of the sensor read-outs should occur as near as possible to the time when the earth and sun are in quadrature, another when the roll angle is in the same plane as the maximum angle between the orbit and ecliptic planes.

Logic Requirements. The logic requirements for this configuration are almost entirely for pulse synchronizing, since all attitude data are sent to the ground for processing.

As shown previously, all attitude maneuvers are either toward or away from the sun, or about the sun line, making use of the sun as pulse synchronizer the logical choice. There are two ways of using the sun: have a clock count down the required number of milliseconds from a sun pulse before firing the thruster, or have four sun sensors in quadrature to turn the thruster on and off.

The disadvantage of the clocked method is its greater complexity. The command format must be able to handle a quantitative command that contains the number of milliseconds to delay from the sun pulse. A register for storage of this number is necessary, as well as a clock and separate register for counting it down.

The alternate method (using the four sun sensors to turn the thruster on and off) has been chosen because of its greater simplicity in electronics and command format. Also, it is not necessary to generate spin rate information, as is required in the clocked configuration.

Sensor Requirements and Selection. Since the satellite is not oriented nor its attitude controlled until it is released from the carrier, accuracy requirements are not as severe as for the stacked configuration. The capability for subsequent attitude adjustments relaxes accuracy requirements to 3 to 4 degrees. This means that albedo sensors could be used, which are lighter, simpler, and cheaper.

The geometrical arrangement of the albedo sensors should be such that the angle between the orbit plane and the ecliptic can be measured when the spin axis is normal to the ecliptic. With an angle of ~25 degrees between planes and a λ = 10 degrees, the earth sensors may not see the earth unless the subtended angle of the earth is at least 30 degrees. This corresponds to a true anomaly of ±125 degrees. Using a λ = 8 degrees would restrict the angle even further to ±119 degrees true anomaly. A λ = 10 degrees will be chosen to give the longer time for the sensor information to be observed on the ground.

In addition to the albedo sensors, a sun angle indicator must be provided for measuring the angle the spin-axis makes with the sun. The Philco-Ford sun angle indicator can also be used to provide a sun pulse, so that only three other sun sensors are needed to activate the thrusters.

Figure 5.2-7 shows a typical sensor layout. The orientation about the circumference of the albedo sensors is not critical. The sun angle indicator can be placed at any one of the four S/S locations.

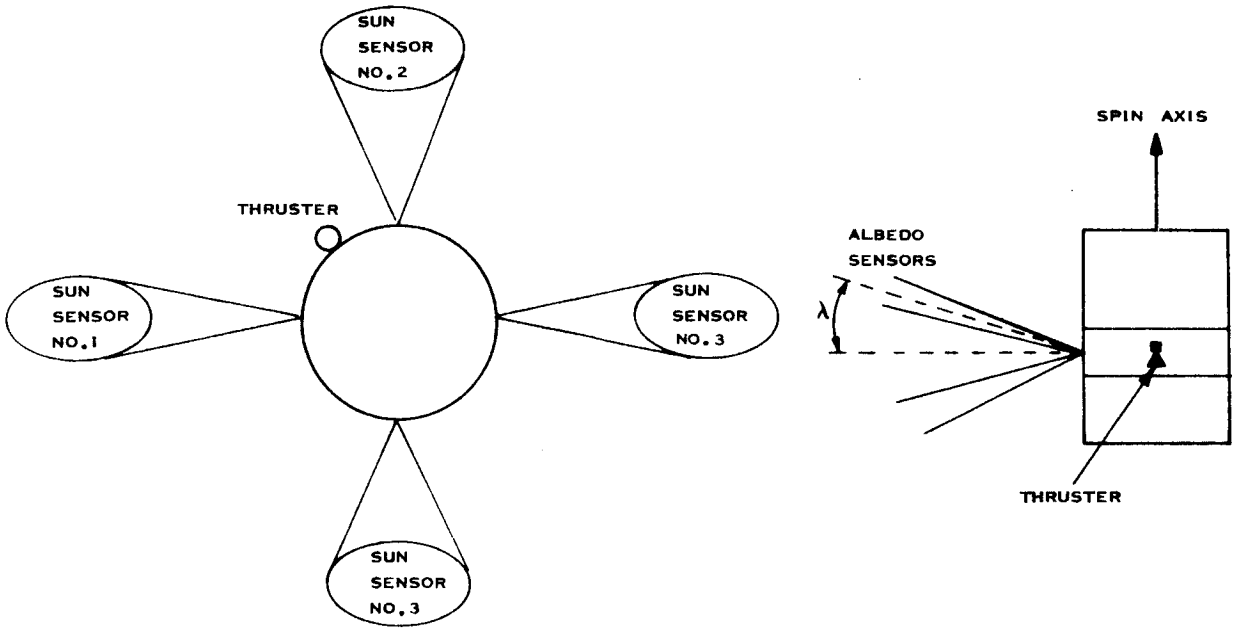

Figure 5.2-7 Sun Sensor Layout for Radial Configuration

Logic Definition and Description. As mentioned previously, a 90 degree torque pulse width is obtained independently of spin speed by using one sun sensor to turn on the thruster, and the next to turn it off. Rotation of the spin axis towards the sun line requires the thruster to be turned on by sun sensor No. 2 and turned off by sun sensor No. 3. Rotation of the spin-axis away from the sun line requires turn-on by sun sensor No. 4 and turn-off by sun sensor No. 1. For rotation clockwise about the sun line, thrusting should be turned on by sun sensor No. 1 and turned off by sun sensor No. 2. Counterclockwise rotation about the sun line requires thrust turn-on by sun sensor No. 3 and turn-off by sun sensor No. 4.

Figure 5.2-8 shows the logic necessary to turn on the thruster at the required times. The system is turned on and off in real time by ground command. A command is sent to enable the control system after the command is sent indicating the type of motion desired. Suppose it is desired to move the spin-axis clockwise about the sun line. The command processor applies a signal to the top two "and" gates in Figure 5.2-8. When sun sensor No. 1 sees the sun, it applies a signal to the other input to the "and" gate, which then sets the flip-flop so that the thruster is turned on. After 90 degrees of spin, sun sensor No. 2 views the sun, causing the "and" gate second from the top to generate a signal and reset the flip-flop through the other "or" circuit.

To provide a backup shutoff of the thruster, the flip-flop circuit can be a monostable circuit, which would normally return to its stable state in a little more than 90 degrees of rotation. The reset signal would then merely return the monostable to its stable state a little before it would do so automatically. While a failure of a sun sensor or "and" gate would not be catastrophic, it would consume extra fuel and the motion would not be quite as desired, as some impulse would be applied about an orthogonal axis.

An alternate, which requires a quantitative command is a counter, which would then apply a signal to the "and" gate driving the power amplifier until the appropriate number of pulses had been fired. The counter command would be sent before commanding the desired maneuver and pulsing would occur until the desired number of pulses had been fired. The previous scheme requires no counter nor quantitative command, making it the favored scheme. The torque level can be made low enough so that real-time commanding presents no resolution problem.

5.2.2.2.2 Stacked Configuration

Operational Constraints. The operational constraints for the stacked configuration are derived from the requirement to orient the spin-axis normal to the orbit plane, plus the constraint of being ground commanded.

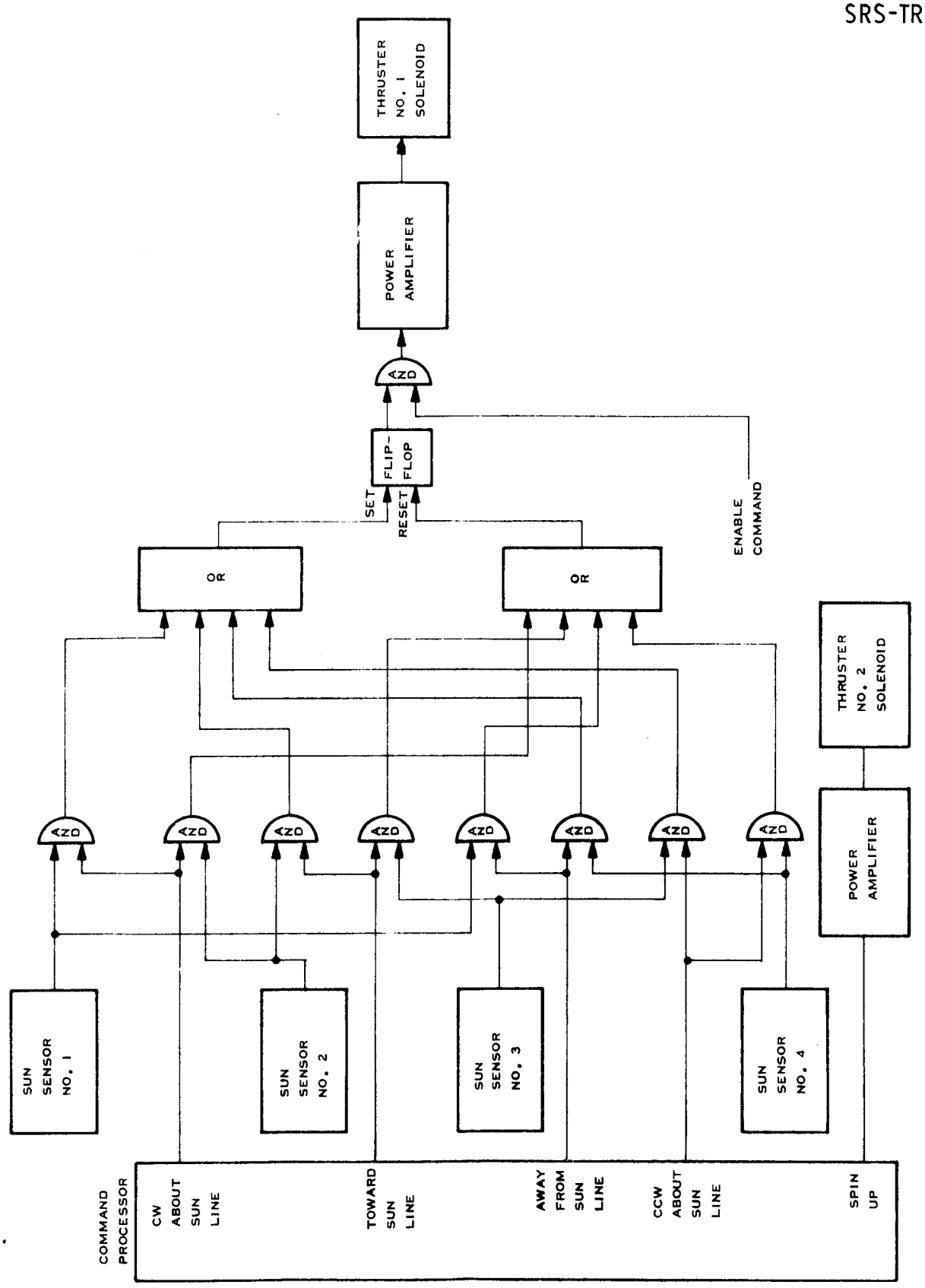

Figure 5.2-8 Radial Configuration Logic Diagram

As with the radial configuration, being ground-commanded implies that attitude maneuvers must be performed on the high side of ± 90 degrees true anomaly. At this time the earth sensors do not scan the earth and cannot supply the required synchronization pulses for the initial erection maneuver. Therefore, these maneuvers are performed with respect to the sun, i.e., towards or away from the sun or about the sun line.

Subsequent roll nulling maneuvers are made using the earth sensors as a pulse synchronization reference. This eliminates the need for spin rate information, a quantitative command containing the number of milliseconds to wait from the sun pulse, a register to store the wait, and a second register and clock for counting down to the firing time each cycle.

The fact that initial erection cannot be accomplished before first apogee presents an additional constraint. This is the result of the requirement to make two roll nulling maneuvers separated by 90 degrees true anomaly. Since the first roll nulling maneuver cannot be made until sometime after 90 degrees true anomaly, the second one cannot be made until after first apogee (180 degrees true anomaly).

Since the sun can be as far as 26 degrees from the line of apsides, a motion about the sun line, without first normalizing the spin-axis to the sun, is a cone with a 64 degree half-angle. Therefore, the first maneuver must normalize the spin-axis with respect to the sun line. After this, the spin-axis is rotated 90 degrees open loop about the sun line to get it approximately normal to the orbit plane. The roll angle is then nulled at 225 degrees true anomaly and again at 135 degrees true anomaly. Since the spin-axis should be normal to the orbit plane by this time, the control system may be shut off. Table 5. 2-4 shows a representative sequence of events for the stacked configuration.

Logic Requirements. The logic circuitry (with sensors) must do the following: provide torque pulse synchronization for maneuvers of the spin-axis towards or away from the sun; provide torque pulse synchronization for spin-axis precession clockwise or counterclockwise about the sun line; and provide torque pulse synchronization for positive or negative local roll maneuvers.

TABLE 5.2-4

SEQUENCE OF EVENT, STACKED CONFIGURATION

True Anomaly (Degree)	Event Description
0	Injection
90	Normalize spin axis to sun line
110	Perform 90 degree maneuver about sun line
132	Start nulling local roll
135	Stop nulling local roll
222	Start nulling local roll
225	Stop nulling local roll
132	Start nulling local roll (if necessary)
135	Stop nulling local roll
176	Eject First pair of satellites
	Burn ΔV motor
178	Eject second pair of satellites

These requirements can be met by using a clock and counting down from a sun pulse as before. However, since it is desired to use only tonal type commands without any quantitative command requirement, sensor arrangements are preferred for synchronization.

The sensing and command scheme used for the radial configuration provides all the required logic except the earth roll nulling synchronization. Figure 5.2-9 shows the sensor layout required to provide the above logic and sensing functions.

Sensor Requirements and Selection. Because of accuracy requirements for the roll nulling maneuvers IR horizon scanners are required in place of albedo sensors. Two scanners, 180 degrees apart, look out from the spin-axis. Since all roll nulling maneuvers are supposed to take place at ± 135 degrees true anomaly, the sensor geometry can be optimized for this altitude (5.7 earth radii from earth center). At this altitude, the earth subtends an angle of about 20 degrees. The optimum offset angle, λ, is determined by accuracy and dynamic range requirements.

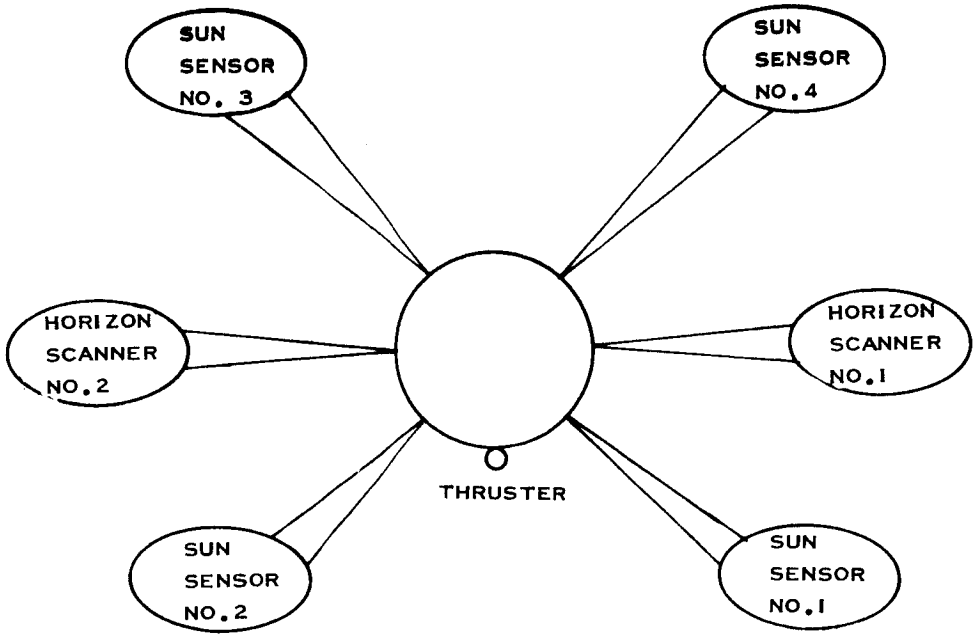

Figure 5.2-9 Ground Commanded Stacked Configuration Sensor Arrangement

Small offset angles of 1 or 2 degrees provide less sensitivity to bolometer noise, but the larger offset angles provide greater dynamic range. For this altitude it appears that an offset angle of ~5 degrees would give a good compromise between accuracy and dynamic range. One sensor will start missing the earth at about a 5 degree roll error, but a synchronizing signal will be available for roll angles as large as 15 degrees.

In addition to the two IR horizon sensors, a sun angle sensor is needed for the initial normalizing to the sun. It is also used to generate one of the sun pulses. Three additional timing sun sensors are required to complete the synchronizing sensor scheme.

Logic Definition and Description. The 90 degree torque pulse width is obtained independently of spin speed by using two successive timing sun sensors to turn the thruster on and off. Rotation of the spin axis toward the sun requires turn-on of the thruster by sun sensor No. 2 (Figure 5.2-8) and turn-off sun sensor No. 3. Rotation away from the sun requires turn-on by sun-sensor No. 4 and turn-off by sun sensor No. 1. Clockwise precession of the spin axis about the sun line requires thruster turn-on by sun sensor No. 1 and turn-off by sun sensor No. 2. Counter-clockwise precession requires turn-on by sun sensor No. 3 and turn-off by sun sensor No. 4. A positive local roll maneuver requires thrusting to occur while horizon scanner No. 2 views the earth. A negative local roll maneuver requires thrusting while horizon scanner No. 1 is viewing the earth. While doing local roll maneuvers the pulse width is less than 90 degrees; thus, the resolution of the system is better during the final touch-up of spin-axis orientation than during the initial portions of erection.

Figure 5.2-10 shows the logic block diagram for the stacked configuration. The system operates as follows. The command processor decodes tonal commands and applies a signal to the appropriate wire until a new command is received to remove the signal. These signals represent the type of motion desired, and for motions with respect to the sun the logic works exactly the same as for the radial case. If a positive roll maneuver is desired, then the power amplifier will have an input whenever horizon scanner No. 2 is scanning across the disc of the earth. The

thrust level will be chosen so that real-time shut-off by the pulse train presents no resolution problems. The alternative, of course, is a pulse counter, with its attendant requirement for a quantitative command.

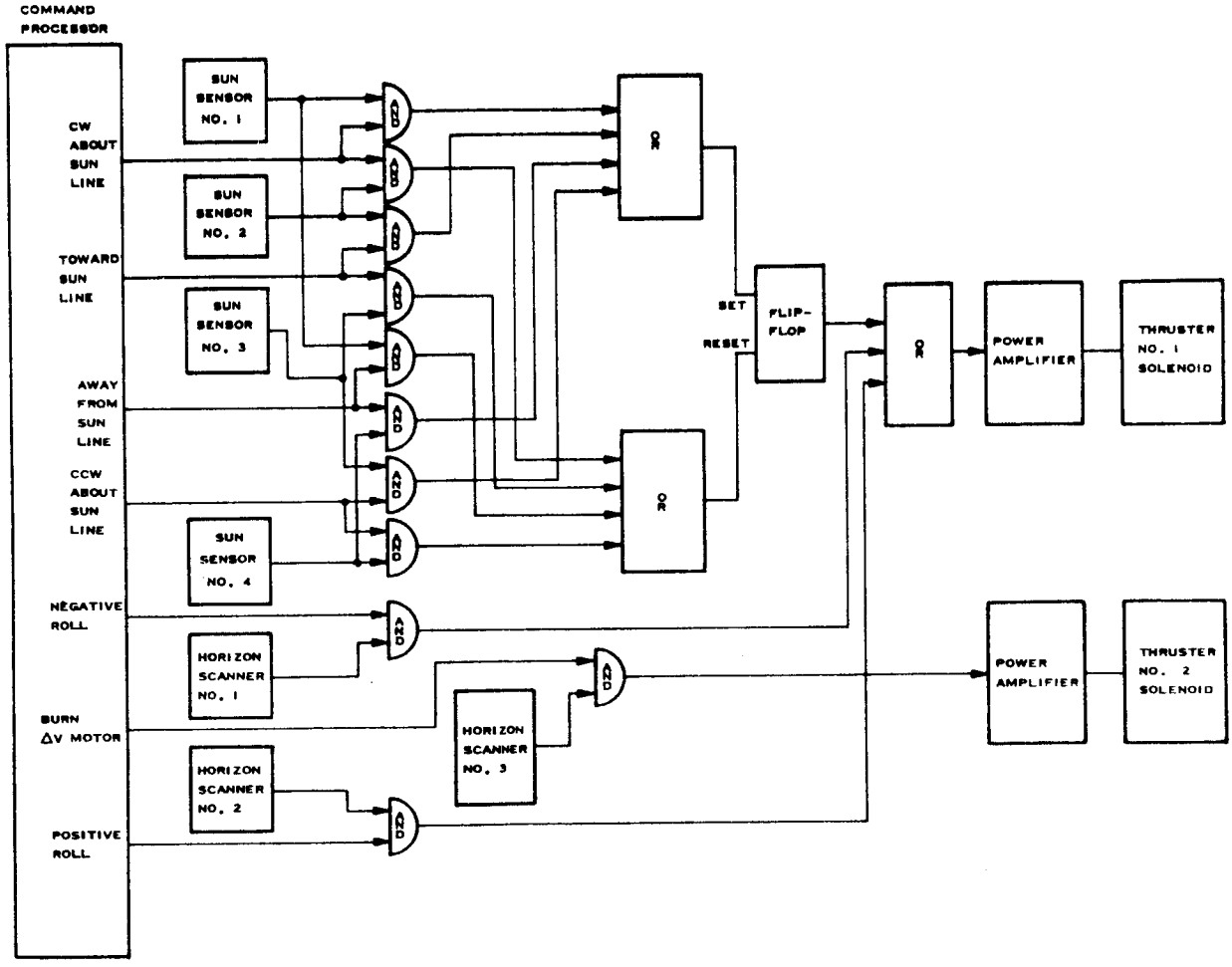

Figure 5.2-10 Stacked Configuration Ground Commanded Logic Diagram

5.2.3 Subsystem Requirements

5.2.3.1 Initial Orientation Accuracy. Because of the difference in initial deployment schemes, the accuracy requirements for the initial orientation of the radial and stacked configurations are not the same. The overall accuracy requirement for attitude orientation is rather coarse, 3 to 5 degrees. Since, in the radial configuration, release of the satellites occurs before initial orientation, the initial orientation accuracy desired is 3 to 5 degrees. Capability of subsequent attitude corrections to compensate for drift due to distrubance torques also eases the initial orientation accuracy requirements.

The initial orientation accuracy requirements for the stacked configuration are a little more stringent. At the time of ejection of the final pair of satellites, a spin axis orientation within 2 to 3 degrees of the orbit normal is desirable to keep the ΔV imparted along the orbital velocity vector at a low value. A 5-degree error at the time of ejection leads to marginal satellite positions at the end of one year. The higher drift rates due to distrubance torques also make it desirable to have the error small at ejection. The lack of correction after first ejection and orbit adjustment means that errors induced by these events still exist at second ejection. Therefore, it appears that the initial orientation should be made to at least 1 to 2 degrees to the orbit normal. A more complete error analysis appears in Paragraph 5.2.4. This accuracy requirement is valid for both the automatic and ground-commanded versions of the stacked configuration.

5.2.3.2 Ground Station Requirements. The ground station requirements for the radial configuration will be treated first. To command the release of the satellites from the carrier, a ground station should be available when the total payload is at apogee. This occurs between 21 and 28.5 hours from injection, depending on injection parameters. After satellite release, each satellite may require from 15 to 20 minutes of real-time commanded attitude maneuvers. This accomplishes the initial erection, after which attitude data need be taken at only one or two points in the orbit. Subsequent real-time commanding of attitude maneuvers takes less than

5 minutes for final orientation, with possibly 5 minutes additional every three months until the fuel is exhausted. The timing of these subsequent maneuvers is not critical, although there may be a 1 or 2-hour tolerance as to when attitude measurements should be made.

For the stacked configuration, two sets of ground station requirements must be enumerated. For the self-contained system, the only ground station requirements are derived from the ejection sequence. At 176 degrees true anomaly (±0.25 degrees), a command must be sent to eject one pair of satellites and initiate the ΔV maneuver. The ΔV maneuver may take as long as 15 minutes, at which time it is terminated by a real-time command. At 178 degrees (±2 degrees) true anomaly, the second pair is ejected by real-time command. This sequence yields an array that is planar for all practical purposes. When a non-planar array is desired, the sequence of events is slightly different, as indicated in the section on mission analysis. First ejection occurs by real-time command at 170 degrees true anomaly; second ejection occur at 190 degrees true anomaly. The in-plane ΔV is performed individually by the satellites, so that each needs a command for the out-of-plane and in-plane maneuvers.

For the ground-commanded stacked configuration, a ground station is required at ±135 degrees true anomaly (±10 degrees) for two roll nulling maneuvers of less than 10 minutes each. In addition, the initial maneuvering requires one-half hour of real-time commanding between a true anomaly of 90 and 125 degrees. There are also the ejection requirements mentioned previously for the self-contained system. Figure 5.2-11 summarizes ground station coverage requirements.

5.2.3.3 Command and Telemetry Requirements. The command and telemetry requirements are summarized in Table 5.2-5. For the sake of simplicity in the command system, no quantitative commands have been used. To do this, it has been necessary to require the capability of turning off a command in real-time at the end of a predetermined number of revolutions. Also, counter read-out is necessary to know how many pulses were applied during a particular maneuver.

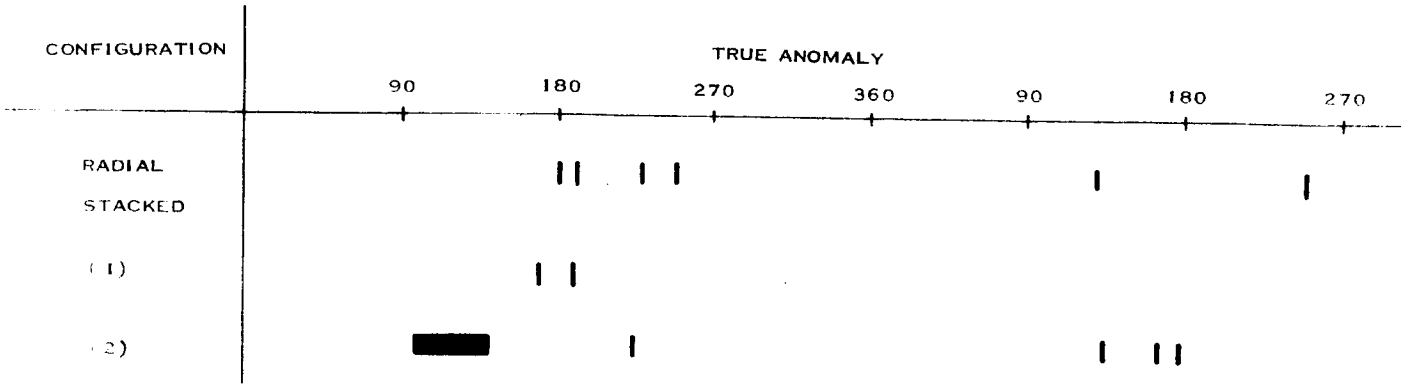

Figure 5.2-11 Summary of Ground Stations Coverage Requirements

TABLE 5.2-5

SUMMARY OF COMMAND AND TELEMETRY REQUIREMENTS

Configuration	Command	Telemetry
Radial	1. Rotate towards Sun-Line 2. Rotate away from Sun-Line 3. Rotate clockwise about Sun-Line 4. Rotate CCW about Sun-Line 5. Spin-up 6. Turn Heater "ON" 7. Turn Heater "OFF"	1. Sun Angle: 8 Bits 2. Roll Angle: 5 Bits 3. Spin Counter: 5 Bits
Stacked 1. Automatic	1. Eject first pair 2. Burn ΔV 3. Eject second	1. Pressure Transducer; 5 bits 2. Pulse Counter; 10 Bits
2. Ground Commanded	1. Rotate towards Sun-Line 2. Rotate away from Sun-Line 3. Rotate CW about Sun-Line 4. Rotate CCW about Sun-Line 5. Rotate in + Roll Direction 6. Rotate in - Roll Direction 7. Eject first pair of satellites 8. Perform ΔV Maneuver 9. Eject second pair	1. Pressure Transducer; 5 bits 2. Sun Angle: 8 Bits 3. Roll Angle: 5 Bits 4. Pulse Counter; 11 Bits

In the stacked configuration, a pressure transducer must be read out to know how many pulses a maneuver should require. In the ground-commanded system, sun angle and roll angle information must be telemetered to the ground. Ejection and orbit adjust commands must be provided, in addition to maneuver commands required by the ground-commanded system.

In the radial configuration, sun angle and roll angle information must be telemetered, along with spin rate information to provide spin-up requirement information. The command requirements include the four maneuver requirements, spin-up, and (since an ammonia system is used) a command to turn a fuel heater on and off.

5.2.3.4 Nutation Damper Requirements.

Stacked Configuration. The requirement for nutation dampers is derived from a consideration of the events that must take place and how a nutation of the spin axis would affect these events. For the ejection maneuvers, little or no nutation is desired,so that the orientation at separation can be more precisely controlled. Zero nutation also minimizes the possibility of the booms colliding with the carrier and two remaining satellites after ejection of the first pair.

The carrier with four satellites is expected to separate from the last stage of the booster with as much as a 2-degree nutation angle. During the first roll nulling maneuver, the wide pulse width and high torque level may leave as much as 8 to 10 degrees of nutation, in addition to that due to injection, depending on where in the pulse train the torquing is stopped. With such high nutation angles occurring before ejection, a nutation damper is needed on the stacked configuration.

One of the simplest, lightest nutation dampers (and one that has undergone extensive analysis and testing at Philco-Ford) is the ball-in-tube damper (Figure 5.2-12). This damper, consisting of a tungsten carbide ball, nitrogen gas, and an aluminum tube weighing a total of approximately 0.2 to 0.4 pound, can provide a nutation damping time constant on the order of a few minutes. The damping is provided by the viscosity of the nitrogen gas at one atmosphere contained within the tube.

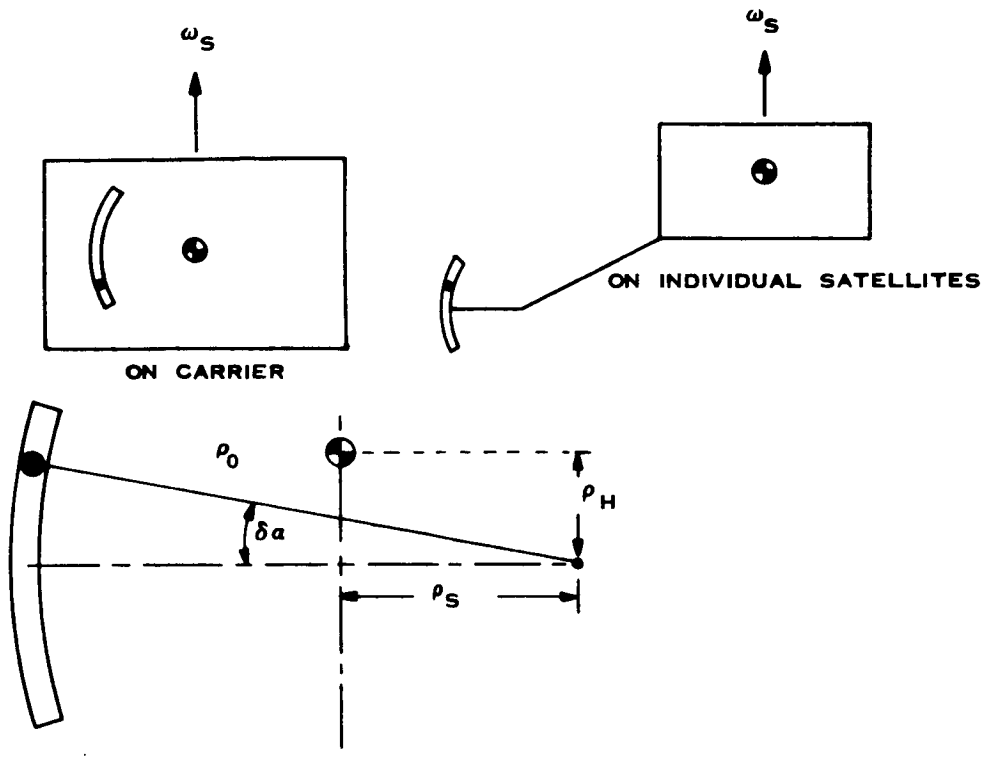

Figure 5.2-12 Nutation Damper Location and Geometry

This damper was developed for an NRL satellite[2] and could be used for the present application without major redesign. Only the tube length and radius of curvature would be varied.

The equations of motion of the stacked configuration were written for a nutation damper on-board, and an expression for the damping time constant was derived. Since nutation induced at ejection of individual satellites is negligible, a nutation damper on each satellite is not necessary. The fact that the inertia ratio is so close to unity makes it difficult to get small time constants, and the size of the

[2] "Nutation Dampers for the NRL Solar Radiation Satellite - Final Report," by R. R. Auelmann, Philco-Ford, Aeronutronic Division, Pub. No. U-3022, 20 February 1965.

satellite adds to the problem. It was found during the course of a parametric study of the problem, that by lengthening the NRL damper by 7 inches, a 2-hour time constant could be obtained for the payload before ejection of the first pair, and a 5.7-minute time constant between the two ejections. A time constant of one-half hour could be obtained by increasing the tube radius of curvature to 12 feet, but the penalty paid is a residual nutation during the time between ejections of 0.59 degree, which was felt to be prohibitive. Table 5.2-6 shows the damper parameters that give the 2-hour time constant with a 0.2 degree residual nutation.

Radial Configuration. On the radial configuration, the initial nutation from the last booster stage is the same as for the stacked configuration (2 degrees). This nutation should be removed before satellite separation at apogee. In addition, since each satellite has its own control system, it is desirable to place a nutation damper on each satellite to damp out the induced nutation angle in a reasonable time. The nutation induced by action of the attitude control system is small, and structural

TABLE 5.2-6

DAMPER DESIGN PARAMETERS FOR STACKED CONFIGURATION

Parameter	Carrier Assembly and Four Satellites
Tube radius of curvature, ρ_o	6.0 ft.
Distance from spin-axis, $\Delta\rho$	1.75 ft.
Tube length, ℓ	15.1 in.
Tube inside diameter, d_t	0.694 in.
Ball diameter, d_b	0.687 in.
Ball weight	0.0925 lb
Tube weight	0.158 lb
Friction coefficient, b	0.00891 lb/ft./sec
Maximum nutation, η_{max}	5.0 deg
Residual nutation, $\eta_{res.}$	0.2 deg
Tube alignment error, $\delta\alpha_{error}$	1.0 deg
Damping time constant, τ	2 hrs (4 satellites) 5.7 min (2 satellites)
Nitrogen gas at one atmosphere	

damping would remove it if given enough time. However, the amount of structural damping available is rather unpredictable, so a damper has been included on each satellite to ensure an adequate time constant.

The dampers on the individual satellites are mounted on the satellite booms to increase their effectiveness. Prior to satellite release from the carrier, the booms are stowed in such a way that they do not provide damping, making it necessary to add a fifth nutation damper (one each for the satellites and one for the carrier).

The same criteria were used in the selection of nutation damper parameters as for the stacked configuration, i.e., minimal change to the NRL camper. Table 5.2-7 shows damper parameters that meet the requirements. The damper on the carrier assembly is the same as the NRL damper, except that it is 8.9 inches longer. The dampers on the individual satellites are also identical to the NRL damper, except that they are 2.25 inches longer.

5.2.3.5 Impulse Requirements

Radial Configuration. The impulse requirements are based on the sequence of events given in Table 5.2-3. The magnitude of the maneuvers depends on the angle between the orbit plane and the ecliptic, and also on the angle between the sun line and the line of apsides. The first maneuver is to normalize the spin axis to the sun line; thus, if the sun line is along the line of apsides, no maneuver is required. The worst case occurs when the sun is at its maximum angle of ±26 degrees from the line of apsides. This position requires a 26-degree maneuver.

After normalizing with respect to the sun, the satellite must be rolled about the sun line to bring the spin axis normal to the ecliptic. If the angle between the orbit plane and the ecliptic is 20 degrees, then it would only be necessary to roll 70 degrees about the sun line to get the spin axis normal to the ecliptic. The worst case would occur if the orbit plane were in the ecliptic plane, which would require a 90 degree roll about the sun line. With a subsequent roll correction of 4 degrees, the total maneuver requirement before spin up is 120 degrees maximum.

TABLE 5.2-7

DAMPER DESIGN PARAMETERS FOR RADIAL CONFIGURATION

Parameter	Carrier Assembly	Satellite Before Spin-Up	Satellite After Spin-Up
Tube radius of curvature, ρ_o	6.0 ft	6.0 ft	6.0 ft
Distance from spin-axis, $\Delta\rho$	7 in	6.0 ft	6.0 ft
Tube length, ℓ	16.9 in	10.25 in	10.25 in
Tube inside diameter, d_i	0.694 in	0.694 in	0.694 in
Ball diameter, d_b	0.687 in	0.687 in	0.687 in
Ball weight	0.0925 lb	0.0925 lb	0.0925 lb
Tube weight	0.176 lb	0.107 lb	0.107 lb
Friction coefficient, b	0.00891 lb/$\frac{ft}{sec}$	0.00891 lb/$\frac{ft}{sec}$	0.00891 lb/$\frac{ft}{sec}$
Maximum mutation, η_{max}	5.0 deg	5.0 deg	1.27 deg
Residual mutation, $\eta_{res.}$	0.175 deg	0.324 deg	0.0697 deg
Tube alignment error, $\delta\alpha$ error	1.0 deg	1.0 deg	1.0 deg
Damping time constant, τ	8.07 min	2.33 min	1.03 min
Nitrogen gas at one atmosphere.			

For a large number of pulses, the average angle precessed by the spin axis per pulse is given by:

$$\theta_p = \frac{2T}{I_s \omega_s^2} \quad \sin \alpha/2 \quad \text{radian/pulse}$$

where:

T = torque (ft-lb)

I_s = spin moment of inertia (slug-ft^2)

ω_s = spin rate (radians/second)

α = firing angle of control thruster ($\pi/2$ radians)

The impulse per pulse is the torque times time, which, for a 90-degree pulse width, is:

$$T \cdot t = \frac{T\pi}{2\omega_s}$$

and the total angular impulse required can be expressed by:

$$\Delta H = \frac{\theta_T}{\theta_p} \times (\text{impulse/pulse}) = \frac{\theta_T \theta_F I_s \omega_s}{2 \times 57.3^2 \sin \theta_F/2} \quad \text{ft-lb-sec.}$$

where

θ_T = total angle precessed during maneuver (deg)

θ_F = $\pi/2$ = firing angle of thruster.

For the first part of the maneuvers, θ_T = 120 degrees and ω_s = 2.095 rad/sec (before spin-up). The total angular impulse is then:

$$\Delta H = 24 \text{ ft-lb-seconds}$$

After spin-up, it is assumed that ~ 15 degrees of attitude maneuver is required, giving, by the same process, ω_s = 7.33 rad/sec

$$\Delta H = 10.5 \text{ ft-lb-seconds.}$$

Putting the thruster on a 6-foot moment arm makes the above angular impulse requirements of 34.5 ft-lb-seconds a linear impulse requirement of 5.75 lb-seconds for attitude maneuvers.

The spin speed during the initial maneuvering is about 20 rpm. The spin-up maneuver increases the speed to about 60 rpm. With the thruster on a 6-foot moment arm, the impulse required for this is:

$$\Delta H = \frac{I\Delta\omega}{6} = 3.5 \text{ lb-seconds}$$

In addition to the above requirements, two of the satellites require a ΔV along the velocity vector of about 3 ft./second. This gives an additional linear impulse requirement of 7 lb-seconds, for a non-planar array.

With a 15 per cent margin, the total required impulse capability is about 18.7 lb-seconds.

Stacked Configuration. The impulse requirements for the stacked configuration must be calculated separately for the self-contained and ground-commanded systems. The impulse requirements are based on the maneuvers listed in Tables 5.2-2 and 5.2-4, and the logic schemes chosen in Paragraph 5.2.2. The self-contained system will be treated first.

The exact amount of impulse required for the initial yaw maneuver is difficult to determine analytically for the logic used. First of all, the pulse width varies as the angle subtended by the earth changes. The initial pulse width is ~ 30 degrees wide; the final pulse width is ~ 55 degrees wide. The pulse efficiency is therefore changing. Furthermore, the combined effects of the rapidly changing true anomaly and the spin axis motion cause the spin axis precession to be in a cone rather than in a plane. A more detailed investigation of the motion shows that the cone does not pass through the orbit normal. Depending on the logic used, the minimum angle between the precession cone and the orbit normal varies from 15 to 30 degrees. One case investigated used a constant impulse per pulse, which is similar to this case, since the pulse width is increasing at the same time that the thrust level is decreasing because of the drop in fuel tank pressure. The spin axis came no closer than 30 degrees to the orbit normal, which occurred after precessing the spin axis 75 degrees. The 30 degrees was then removed as a roll error. The angular impulse required for a maneuver, θ_T, with a firing angle, θ_F, and spin rate, ω_s, is given by:

$$\Delta H = \frac{\theta_T \theta_F I_s \omega_s}{2 \times 57.3^2 \sin \theta_F/2} = .040 \frac{\theta_T \theta_F}{\sin \theta_F/2}$$

For this case, I_s = 35.8 slug-ft^2; ω_s = 7.33 rad/sec, maximum. The initial maneuver is 75 degrees at a maximum pulse width of θ_F = 50 degrees, giving an angular impulse of:

$$\Delta H_1 = 356 \text{ ft-lb-seconds}$$

The subsequent nulling of the 30-degree roll error is done with an average pulse width of ~ 115 degrees = θ_F, giving an additional angular impulse of:

$$\Delta H_2 = 164 \text{ ft-lb-seconds.}$$

It is further assumed that an additional 15 degrees of roll nulling is required at 135 degrees true anomaly, where $\theta \doteq 15$ degrees, giving the third angular impulse requirement of:

$$\Delta H_3 = 69 \text{ ft-lb-seconds}$$

Since the thruster is on a moment arm of ~ 2 feet, the total linear impulse requirement for attitude maneuvers is ~295 lb-seconds.

The ΔV required for the orbit adjust maneuver is given as 30 feet per second. At the time of the maneuver, two satellites have been ejected, leaving a total mass of around 5.5 slugs. This gives a linear impulse requirement of 165 lb-seconds. As a result of the satellite spin, the thruster is not always directed in the direction of the desired ΔV. The geometric efficiency of the thruster follows the relationship:

$$\eta_G = \frac{\sin \theta_{F/2}}{\theta_{F/2}}$$

The firing angle chosen is < 90 degrees. (See Paragraph 5.2.3.6.) Therefore, the geometric efficiency becomes:

$$\eta_G \geq 90 \text{ percent}$$

Thus, to obtain 165 lb-seconds of impulse along the desired direction, it is necessary to use 184 lb-seconds. Allowing a 10 percent margin on total required impulse gives a total for the self-contained stacked configuration of:

$$I_T = 527 \text{ lb-seconds}$$

For the sequence of events leading to the three dimensional array, each of the satellites contains the equipment for the ΔV maneuvers. Each satellite is required to perform an in-plane maneuver of 16.4 ft/second, which requires an impulse of 39 lb-seconds on each satellite at a geometric efficiency of 90 percent. For this case, the total impulse required on the carrier is:

$$I_{TC} = 325 \text{ lb-seconds}$$

and the total impulse required on the satellites for the in-plane maneuvers is

I_{TS} = 156 lb-seconds (all 4 satellites)

For the ground-commanded system, the use of the sun as a pulse synchronizer fixes the pulse width at 90 degrees, making the calculation of the required impulse easier. From Table 5.2-4 the first maneuver is seen to be normalizing with respect to the sun, which requires at a maximum a 26 degree maneuver. There is a subsequent 90 degree maneuver to arrive at approximately normal to the orbit plane.

If the sun is above or below the orbit plane by 24 degrees, this angle must also be maneuvered through. The total maneuver with a 90 degree width is a maximum of 140 degrees. The angular impulse required is then:

ΔH_1 = 713 ft-lb-seconds

Further allowance must be made for subsequent roll nulling at ± 135 degrees true anomaly. Allowing for a 15-degree maneuver at a pulse width of θ_F = 15 degrees gives an additional impulse requirement of:

ΔH_2 = 69 ft-lb-seconds

With the thruster on a 2-foot moment arm, the linear impulse required is:

I_1 = 391 lb-seconds

The ΔV impulse requirements are identical to the self-contained case. Again allowing a 10 percent margin, the total impulse requirement for the ground-commanded system is:

I_T = 632 lb-seconds (for planar array)
I_{TC} = 430 lb-seconds (carrier)
I_{TS} = 156 lb-seconds (four satellites)
} for non-planar array

5.2.3.6 Separation Requirements and Analysis. The difference in the separation sequences for the radial and stacked configurations leads to different logic requirements. In the radial configuration, satellite release is planned as a single event, performed at apogee. The spin is used to provide each satellite with a ΔV that is perpendicular to the orbit velocity vector. To avoid imparting velocity along the flight path direction, the spin axis should be as close as possible to the flight path. The flight path angle dispersion at injection is 1.08 degrees (3σ) in pitch and yaw, so that the total angle between the spin axis and velocity vector has a dispersion of 1.52 degrees.

For the stacked configuration, the first pair of satellites should be ejected normal to the orbit plane at a true anomaly of $\sim$ 176 degrees $\pm$ 2 degrees. After the first pair of satellites are ejected, a ΔV must be applied to the remaining pair in the plane of the orbit and orthogonal to the orbital velocity vector. Finally, the remaining two satellites are ejected normal to the orbit plane at 178 degrees $\pm$ 2 degrees true anomaly. For the non-planar array, the first pair is ejected out-of-plane at 170 degrees true anomaly and then given a relative velocity in-plane, but normal to the flight path. The second pair is ejected out-of-plane at 190 degrees true anomaly and also given a relative velocity in-plane. The two ejections are ground-commanded to obtain the desired accuracy on the true anomaly.

To avoid reorienting the two satellites plus carrier for the ΔV between ejections, a radial thruster is operated in a pulsed mode. The pulses must be synchronized with the spin rate to ensure orthogonality between the imparted ΔV and the orbital velocity vector. Either the earth or the sun may be used as a pulse synchronizer. Use of the sun adds a slight amount of complexity to the system as a result of the changing earth-sun geometry. As the launch time varies, the angle between the sun line and the line of apsides varies. Thus, at 176 degrees true anomaly, a line perpendicular to the orbital velocity vector makes a varying angle with respect to the sun line, depending upon the time of day of launch. If the sun is used for synchronization, this changing angle represents a changing phase between a sun pulse and the desired position of the ΔV thrust pulse. To be able to change the phase between a sun pulse and a torque pulse requires a quantitative command format to read-in a delay in milliseconds, a register to store the delay, and another register

that is counted down by a clock and reloaded every spin cycle from the first register. If the true anomaly of the ΔV is unimportant, or if the position of the sun with respect to the line of apsides varies less than $\pm$ 26 degrees, then it is possible to use the sun as synchronizer without this added complexity.

Using the earth as a pulse synchronizer makes the geometry independent of launch time. For any launch time, the flight path angle at 176 degrees true anomaly does not vary; hence, the orientation of the required ΔV vector with respect to the earth is also constant. The injection parameters have a dispersion that has some effect on the geometry at 176 degrees true anomaly. These effects can be compensated by performing the ΔV maneuver at a true anomaly slightly different than 176 degrees. For the expected injection dispersions, the variations in true anomaly at a given flight path angle are typically 2/3 degrees. For a typical trajectory, the flight path angle is $\sim$ 34 degrees at 176 degrees true anomaly, and the angle changes at roughly 8 degrees per hour. To keep the ΔV within 2 degrees of the normal to the velocity vector, the maneuver must be accomplished within a relatively short time. A maneuver completion time of 15 minutes assures orthogonality to within 2 degrees; however, if thrust level and duty cycle cannot be arranged to give this short a time for completion, then the maneuver may be started prior to the ideal time and completed after the ideal time. In this way, the in-track ΔV tends to partially cancel, giving a net ΔV that is within 2 degrees of being orthogonal to the orbital velocity vector.

Looking down at the orbit plane at 176 degrees true anomaly, we can see the geometric relationsihp between the earth center and the required ΔV orientation. Figure 5.2-13 shows the essential geometric relations. At 176 degrees true anomaly, the earth nominally subtends an angle of $\sim$ 5.8 degrees. Utilizing a horizon scanner with a 1 degree x 1 degree field of view gives only a pulse width of $\sim$ 6.8 degrees, which is too short to accomplish the ΔV maneuver in the time desired. Therefore, a horizon sensor with a fan-shaped field of view could be used. The large dimension is chosen to provide a wide enough pulse to accomplish the required ΔV at the expected thrust levels in the small time allotted. From the propulsion system section, the thrust at this time is such as to require a pulse width of $\sim$ 36 degrees to complete the maneuver in 15 minutes. This corresponds to a sensor field-of-view of 1.0 degrees x 30 degrees.

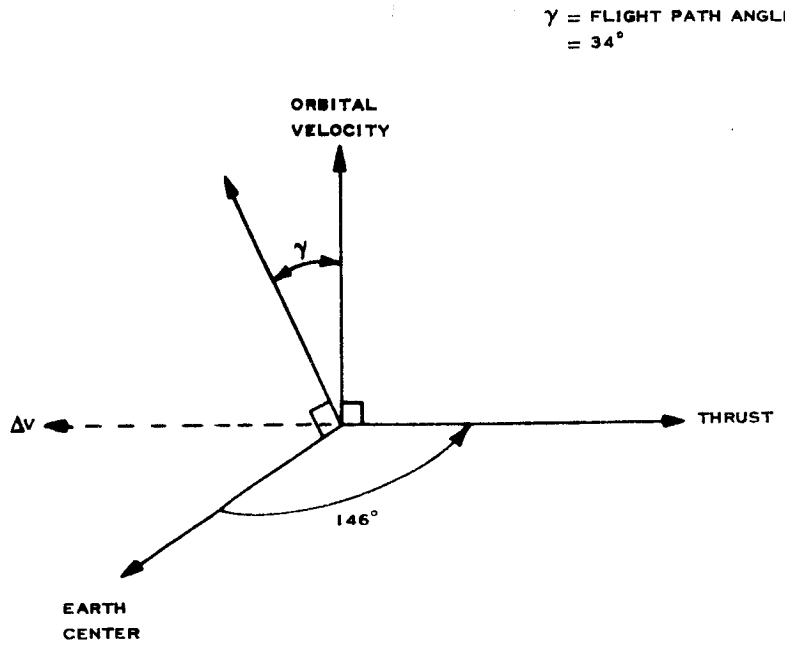

Figure 5.2-13 Geometric Relations

For the three-dimensional array, the angles in Figure 5.2-13 must be changed to correspond to those existing at 170 degrees for the first pair, and those existing at 190 degrees for the second pair. A sun sensor gives suitable sync pulses for this case.

5.2.3.7 Power and Weight Summaries. Tables 5.2-8 through 5.2-10 contain the power and weight summaries for the three control system options.

TABLE 5.2-8

POWER AND WEIGHT SUMMARY FOR RADIAL CONFIGURATION

Component	Qty.	Weight (lb.)	Power (Watts)	Remarks
Nutation Damper	4	1.2	---	
Torquer System (with fuel)*	4	5.32	2 15	Solenoid power, 25% duty cycle during maneuvers. Heater power, 26 VDC during maneuvers.
Electronics	4	1.0	0.30	
Albedo Sensors	8	0.161	---	
Sun Angle Sensor (+ electronics)	4	3.60	0.25	26 vdc
Timing Sun Sensors	12	0.241	---	
Total		11.522		
Per Satellite		2.88	17.55 16	Max Average during maneuvers

*To obtain a non-planar array, two of the satellites require an additional 0.1 lb of fuel

TABLE 5.2-9

POWER AND WEIGHT SUMMARY FOR STACKED CONFIGURATION
SELF-CONTAINED

Component	Qty.	Weight (lbs.)	Power (watts)	Remarks
Nutation Damper	1	0.30	---	
Torquer System (with fuel)	1	7.93	2.0	26 vdc required only during maneuvers at < 25% duty cycle.
IR Horizon Sensors	3	2.25	.78	1 head may be turned off until start of ejection sequence
Timer	1	1.00	1.5	
Electronics	1	0.35	.6	4 vdc
Totals		11.83*	4.88	Peak
			3.38	Average during maneuvers

*Two pounds must be added to each satellite to obtain a non-planar array. Torquer system weight would then be 1 pound less than shown.

TABLE 5.2-10

POWER AND WEIGHT SUMMARY FOR STACKED CONFIGURATION
GROUND COMMANDED

Component	Qty.	Weight (lbs.)	Power (Watts)	Remarks
Nutation Damper	1	0.3	---	
Torquer & ΔV System (with fuel)	1	7.93	2.0	26 vdc 25% duty cycle during maneuvers
IR Horizon Sensors	3	2.25	0.5	1 head may be turned off until ejection sequence
Electronics	1	0.25	0.3	4 vdc
Timing Sun Sensor	3	0.0603	---	
Digital Sun Angle Sensor	1	0.90	0.25	26 vdc
Totals		11.69*	3.05	Peak
			1.55	Average during maneuvers

*Two pounds must be added to each satellite to obtain a non-planar array. Torquer system weight would then be 1 pound less than shown.

5.2.4 Error Budgets

5.2.4.1 Radial Configuration. The sources of error in the radial configuration are sensor errors, control system resolution, thruster misalignment, principal axis shift, and long term drift. Only the accuracy of the initial orientation is considered here, the long term drifts having been treated in Paragraph 5.2.1.

Sensor errors can be broken down into two components: the error about the sun line, and the error towards the sun line. The angle towards or away from the sun line is measured by a sun angle sensor. The angle about the sun line is measured with the albedo sensors. The digital sun angle sensor has an accuracy of ±0.575 degree. The albedo sensor has an accuracy of better than 2 degrees, including noise, albedo variation, and cloud effects. The rss sensor uncertainty is then 2.06 degrees.

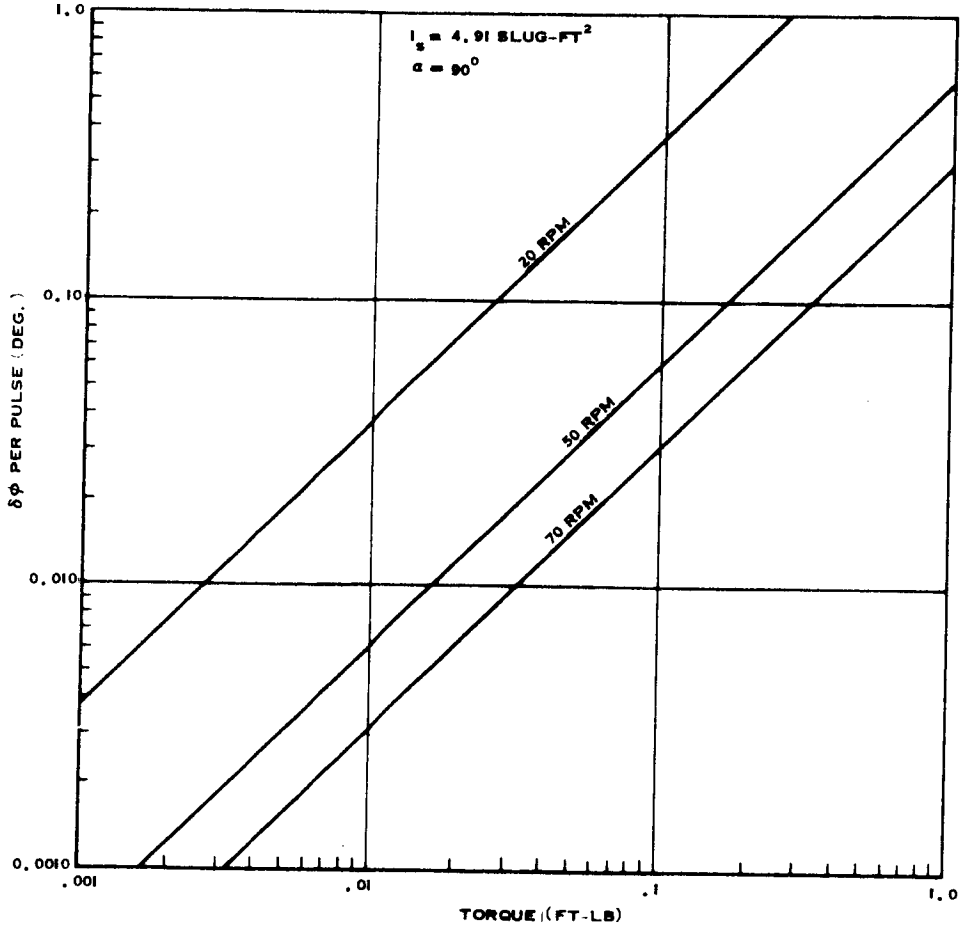

Figure 5.2-14 Control System Resolution for Radial Configuration

Control system resolution is another potential source of error. Figure 5.2-14 shows the average angle precessed per torque pulse as a function of torque magnitude. In Paragraph 5.2.5, a torque level of 0.06 ft-lb is chosen, giving a resolution of 0.04 degree per pulse (at 50 rpm). This represents an error similar to a digital encoding error, and half of it should be added vectorially with the other errors.

Thruster misalignment also contributes an error by applying part of the desired inpulse about the wrong axis. For misalignments of 1 to 2 degrees, the impulse applied about the wrong axis is from two to four per cent of the total impulse expended. For small maneuvers of 1 or 2 pulses, the effects are negligible, but for the longer maneuvers during initial erection of 20 to 30 degrees, the effect is enough to require correction about the other axis. Therefore, with subsequent corrections possible (as is the case with the radial configuration), this effect can be regarded as an inefficiency in fuel usage.

The placing of the control system fuel on the boom and subsequent depletion of that fuel causes the principal axes of the satellite to shift. The shift is on the order of 1 to 1.5 degrees. Since most of the fuel is used in the first two or three orbits, the sensors may be aligned to the principal axes after fuel depletion. The flat cone scanned by the sensors before fuel depletion has a negligible effect on system operation.

To summarize, the major error source is sensor inaccuracy. The total rss error from this source is expected to be ~ 2.1 degrees.

5.2.4.2 Stacked Configuration, Ground-Commanded. For the stacked configuration, each of the two pairs of satellites has slightly different errors induced by the various ejection events.

The initial spin axis alignment is accomplished by use of a horizon sensing system that nulls the roll error at ±135 degrees true anomaly. If an IR earth sensor is used, the expected error due to sensor inaccuracy is ~ 0.5 degree, including

sensor misalignment and detector noise. To the sensor inaccuracy must be added half of the torque pulse resolution. The torque level at this time is about 6.4 ft-lbs, and the duty cycle about 4 per cent, giving a resolution of 0.1 degree. Taking the rrs total of the errors in both of the two orthogonal axes gives a total initial misalignment error of 0.71 degree.

The ejection sequence consists of a spring ejection of the first pair, with a solid rocket motor ignited in each satellite after ejection to provide each with a 15 ft/sec velocity with respect to the carrier and remaining pair. The carrier and remaining pair are then given a velocity of 30 ft/sec in the orbit plane, but normal to the orbital velocity vector. The second pair is then ejected with springs, and a solid rocket motor gives each an additional 15 ft/sec normal to the reference orbit.

The following assumptions are made in computing the disturbance to attitude caused by the spring ejection and solid motor burn:

a. The direction of thrust of the spring is known to one-half degree.
b. The spring force is applied 3 inches from the satellite center-of-gravity.
c. The satellite c.g. location has a 3σ dispersion of 0.01 inch.
d. The satellite is spinning at 60 rpm at kick-off.
e. The solid motor provides 14 ft/sec and the spring, 1 ft-second.
f. The motor thrust can be aligned to within one-half degree.
g. The motor thrust is applied at 3 inches from the satellite c.g.

Based on the above assumptions, the rss error of the first pair of satellites due to ejection is only 0.1 degree. The error reflected back to the carrier with the two remaining satellites is $\sim$0.04 degree.

The ΔV burn between ejections causes an attitude offset to the last pair only. It was assumed that the thruster was located 2 feet from the c.g. and aligned to

one-half degree, as before. The c.g. was assumed to be known to within 0.01 inch and the valve was assumed positioned to within 0.05 inch. These assumptions, coupled with the precession angle formulas given in Paragraph 5.2.3, give the total angular offset (rss) of ~ 2.9 degrees induced by the ΔV maneuver on the last two satellites.

If a three dimensional array is required, then the preceding numbers must be modified. Each satellite would have a ΔV maneuver half that performed for the other case. However, since the moments of inertia are also half of those before, the effect on the attitude of each satellite is the same as it was on the combination.

5.2.4.3 Stacked Configuration, Automatic. The error analysis for the ejection sequence is identical with the previous case. The different logic used during the initial erection sequence causes a slight change in that part of the error budget because of the presence of the deadband, counter, etc. Since the horizon sensor system must be used over a wide range of altitudes, the geometric gain varies significantly. To keep the system reasonably accurate, the system gain must be switched by a timer function so that the correct gain is being used at each roll nulling altitude. By changing the gain between the roll nulling maneuvers, the indicated roll angle available to the roll logic is accurate to ~ 0.5 degree, as before (including sensor noise and alignment errors).

The presence of the ripple remaining on the imperfectly filtered sensor signals can probably be made less than 0.2 degree. To this number must be added the torque pulse resolution, which is different for the two roll nulling maneuvers because of the different pulse widths and thrust levels. At the low altitude roll nulling, where the pulse is wide (~ 110 degrees) and thrust level high, the resolution is 0.76 degree per pulse. At the higher altitude, where the pulse width is about 15 degrees, the resolution drops to 0.12 degree per pulse. The initial orientation error is made up of two parts, with a 1-degree error for the orientation about the first axis and a 0.3-degree error for the second axis. The vectorial sum of these gives a total initial orientation error of 1.05 degrees. Table 5.2-11 summarizes the error budgets for the two stacked configurations.

TABLE 5.2-11

ERROR BUDGETS (DEG) FOR STACKED CONFIGURATIONS

Error Source	Self-Contained		Ground-Command	
	1st Pair	2nd Pair	1st Pair	2nd Pair
Initial Orientation	1.05	1.05	0.71	0.71
Ejection of 1st Pair	0.1	0.04	0.10	0.04
Burn ΔV	--	2.9	--	2.9
Ejection of 2nd Pair	--	0.1	--	0.1
rss Totals	1.05	3.08	0.716	3.0
Worst Case Totals	1.15	4.09	0.81	3.75

5.2.5 Reaction Control System Selection

5.2.5.1 Radial Configuration. The impulse requirement of the radial configuration is 10.6 lb-seconds (20 lb-seconds for the three-dimensional array). Since there is no need to execute the required maneuvers rapidly, a low thrust system is acceptable. The low impulse requirement means that fuel weight will be small regardless of the propellant used. Since thrust level is not critical, the use of an ammonia vapor system becomes practical. The weights of an ammonia vapor system and a nitrogen system are compared in Table 5.2-12. Because of its reduced tankage weight, the ammonia vapor system has a distinct weight advantage over either of the nitrogen systems. For this reason, an ammonia vapor system has been chosen for the radial configuration.

One of the disadvantages of an ammonia vapor reaction control system is that, to maintain a steady thrust, a heater must be provided to vaporize additional liquid ammonia as the vapor is drawn off for maneuvers. The power required by the heater depends on the fuel flow rate and the latent heat of vaporization of the fuel. The fuel flow rate is a function of the thrust level and the specific impulse:

$$\dot{W} = \frac{\text{Thrust}}{\text{Specific Impulse}}$$

The specific impulse (I_{sp}) is assumed to be 90 lb-sec/lb. The thrust is not specified, but would depend on the desired resolution of the control system. Figure 5.2-13 shows the control system resolution as a function of torque level for the spin rates expected. For a resolution of 0.2 degree per pulse at a spin rate of 20 rpm, the required torque is 0.06 ft-lb., which, on a 6-foot moment arm, gives a thrust level of 0.01 pound. The flow rate would be 0.00011 lb/sec. for a continuous thrust of 0.01 lb and 0.00003 lb/second average at a 25 percent duty cycle. At a latent heat of vaporization of 508 BTU/lb., the thermal power input requirement is:

$$P = \dot{W} \cdot 508 \doteq 1.5 \times 10^{-2} \text{ BTU/sec}$$

$$P = 16 \text{ watts}$$

TABLE 5.2-12

REACTION CONTROL SYSTEM WEIGHT COMPARISON (LBS)

Component	NH_3	N_2	N_2 (Capillary)
Fuel	0.12	0.24	0.24
Fuel Tank	0.10	0.50	0.50
Regulator	--	0.80	--
Valve & Nozzle	0.35	0.40	0.40
Fill Fitting	0.20	0.20	0.20
Lines & Fittings	0.20	0.30	0.30
Pressure Transducer	0.16	0.16	0.16
Heater	0.20	--	--
Totals	1.33	2.60	1.80

This thermal power is required for constant thrust operation and is composed of thermal energy from the sun and the thermal energy from the heater.

5.2.5.2 Stacked Configuration. The impulse requirements for the automatic and ground-commanded systems are nearly the same. Therefore, only one system selection and design is necessary for tank size, fittings, etc. A smaller axial thruster could be utilized for attitude control on the ground-commanded scheme, since time constraints on the initial erection are not as severe as in the automatic case. For sizing the tanks and selecting the fuel, the impulse requirement is taken as 630 lb-seconds. For an impulse requirement of this magnitude, the weight of fuel and tankage for a nitrogen system is prohibitive. A mono-propellant, such as hydrogen peroxide or hydrazine, is more suitable because of its higher specific impulse and lower storage pressure, making the tanks lighter.

For hydrogen peroxide, the I_{sp} is 110 to 120 seconds, and for hydrazine the I_{sp} is 190 to 210 seconds. Thus, a significant savings in fuel weight can be achieved with hydrazine. Since the systems are essentially identical in other respects, the hydrazine system has been chosen for further definition.

The thrust of a hydrazine system is a function of the pressure in the supply tank. As the fuel is consumed, the volume occupied by the pressurizing gas increases. Without a separate gas supply and pressure regulator for the pressurizing gas, the tank pressure decreases as the volume increases, allowing the fuel flow rate to decrease. This causes the thrust level to decrease as the fuel is used up. In sizing the fuel tanks, it is necessary to take this into account so that the required impulse can be delivered in the required time. The most critical maneuvers are the initial yaw maneuver for the automatic scheme, and the ΔV burn.

The initial yaw maneuver requires an impulse of 178 lb-seconds to be delivered in ~44 seconds of firing time. The impulse is:

$$I = \int_{o}^{65} F dt \quad \text{lb-seconds}$$

where:

I = delivered impulse
F = thrust of valve (lb)

or alternatively:

$$I = I_{sp} \int_{o}^{t} \dot{M}_F dt$$

where:

I_{sp} = specific impulse
$\dot{M}_F$ = fuel flow rate (lb/second)

For a hydrazine system that has been built and tested, the relationship between fuel flow rate and tank and combustion chamber pressure was shown to be:

$$\dot{M} = k(P_T - P_C)^{\frac{1}{1.8}}$$

where:

k = constant of proportionality

P_T = fuel tank pressure

P_C = combustion chamber pressure

Assuming that the pressurizing gas obeys the ideal gas law, that the combustion chamber pressure is a constant percentage of the tank pressure, and that the thrust is proportional to the fuel flow rate, it can be shown that.

$$t_F = \frac{7.25\left[(V_i + .138\, I)^{1.555} - V_i^{1.555}\right]}{I_{sp}\, k(1-K)^{.555}\, (P_{Ti}V_i)^{.555}}$$

where:

V_i = initial volume of pressurizing gas

P_{Ti} = initial pressure of pressurizing gas

t_F = total firing time to expend impulse I

$k(1-K)^{.555}$ = constants of proportionality

The constant of proportionality is evaluated by letting the thrust be 2.5 pounds at a tank pressure of 200 lbs/in^2, giving:

$$k(1-K)^{.555} = \frac{\dot{M}}{P_T^{.555}} = 0.66 \times 10^{-3}$$

If the initial volume of pressurizing gas is 100 in^3 and an impulse of 260 lb-seconds must be delivered in t_F = 104 seconds, then the initial tank pressure is:

$$P_{Ti} = 500 \text{ lbs/in}^2$$

If the nominal thrust at 200 psi is increased to 5.0 lbs, the initial pressure can be reduced to ~150 psi.

The other critical maneuver is the ΔV of 30 ft/second at 176 degrees true anomaly. The impulse required is 184 lb-seconds. For the ground-commanded system, the impulse used in maneuvers up to the ΔV maneuver is ~390 lb-seconds, or about 2 lb of fuel (~58 in^3). The initial pressure for the maneuver is 316 psi, and the volume of pressurizing gas is 158 in^3. Using the previously developed formula, the total firing time, t_F, required to deliver this impulse is:

$$t_F \doteq 95 \text{ seconds}$$

The firing time for the automatic system is slightly less since less impulse is used prior to the maneuver. This gives a higher fuel pressure and thrust. A firing time of 95 seconds over a 15-minute period represents about a 10 percent duty cycle.

To fire the thruster in the correct direction at a 10 percent duty cycle requires a horizon sensor with a 1 degree × 30 degree field of view. The center of the field of view would be about 146 degrees from the thrust axis, as shown in Figure 5.2-12.

To summarize, hydrazine appears the most feasible fuel for the stacked configuration. A blowdown pressurizing system can be used if the volume of pressurizing gas is initially 100 in^3, pressurized at 500 psi. Table 5.2-13 gives a weight breakdown of the hydrazine reaction control system.

TABLE 5.2-13

HYDRAZINE REACTION CONTROL SYSTEM
WEIGHT BUDGET

Item	Weight (lbs)
Tankage	1.200
Relief Valve	0.194
Relief Valve Vent Tube	0.010
Pressure Transducer	0.229
N_2H_4 Fill and Drain	0.097
N_2 Fill and Vent	0.100
Radial and Axial Motor	1.300
Manifolding and Tees and Lines	0.900
Bracketry	0.250
System Pressurant Weight	0.150
Propellant Charge Weight	3.500
TOTAL	7.930

5.3 ELECTRIC POWER CONCEPTS

This discussion considers the electric power requirements and associated design concepts for the two basic payload arrangements: the radial and stacked configurations. The carrier modules and the satellite power subsystem are covered for each configuration. The magnetic fields due to paddle wheel and cylindrical solar arrays are also discussed.

5.3.1 Configurations and Sequences

Figures 5.3-1 and 5.3-2 give the significant details of the electrical system for each configuration. Figure 5.3-1 shows the electrical system for the stacked configuration. The carrier module contains a command receiver, telemetry transmitter, command processor, attitude control electronics, attitude sensors, and reaction control equipment. Squibs are provided for boom deployment (all booms are restrained at the carrier module) and satellite separation. Power for the carrier module is obtained from the satellite adjacent to the carrier and nearest the booster. The entire payload is spun-up by the third stage and remains electrically inert until separation from the third stage interface activates the carrier equipment. The sequence of operation from this point on is illustraed by the power profile given in Figure 5.3-3. Detailed power requirements for the carrier are summarized in Table 5.3-1.

After separation from the third stage, the carrier initiates boom deployment as soon as possible by timer operation so as to obtain a stable configuration. The payload begins to orient the spin axis approximately normal to the orbit plane. Orientation is accomplished by the carrier module equipment with control by ground command. Since the orientation cannot be accomplished within 24 hours or by the first apogee, this mode continues until the second apogee, 72 hours from launch.

At the second apogee, the carrier module is commanded to ignite the appropriate pyrotechnics, separating the two outboard satellites. After separation, a separation switch in each satellite activates the satellite equipment and a timer ignites

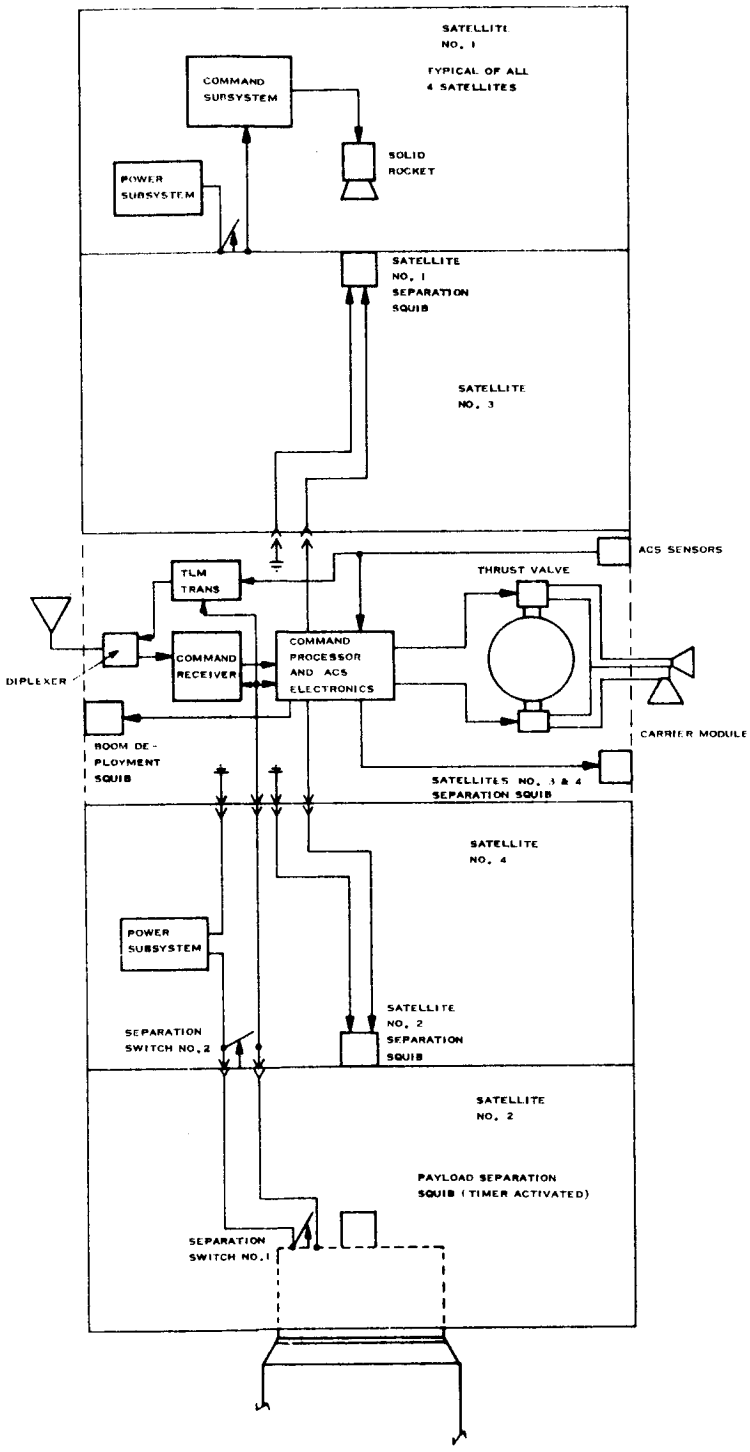

Figure 5.3-1 Stacked Cylinder Configuration Payload Separation, Deployment, and Control Electrical Diagram

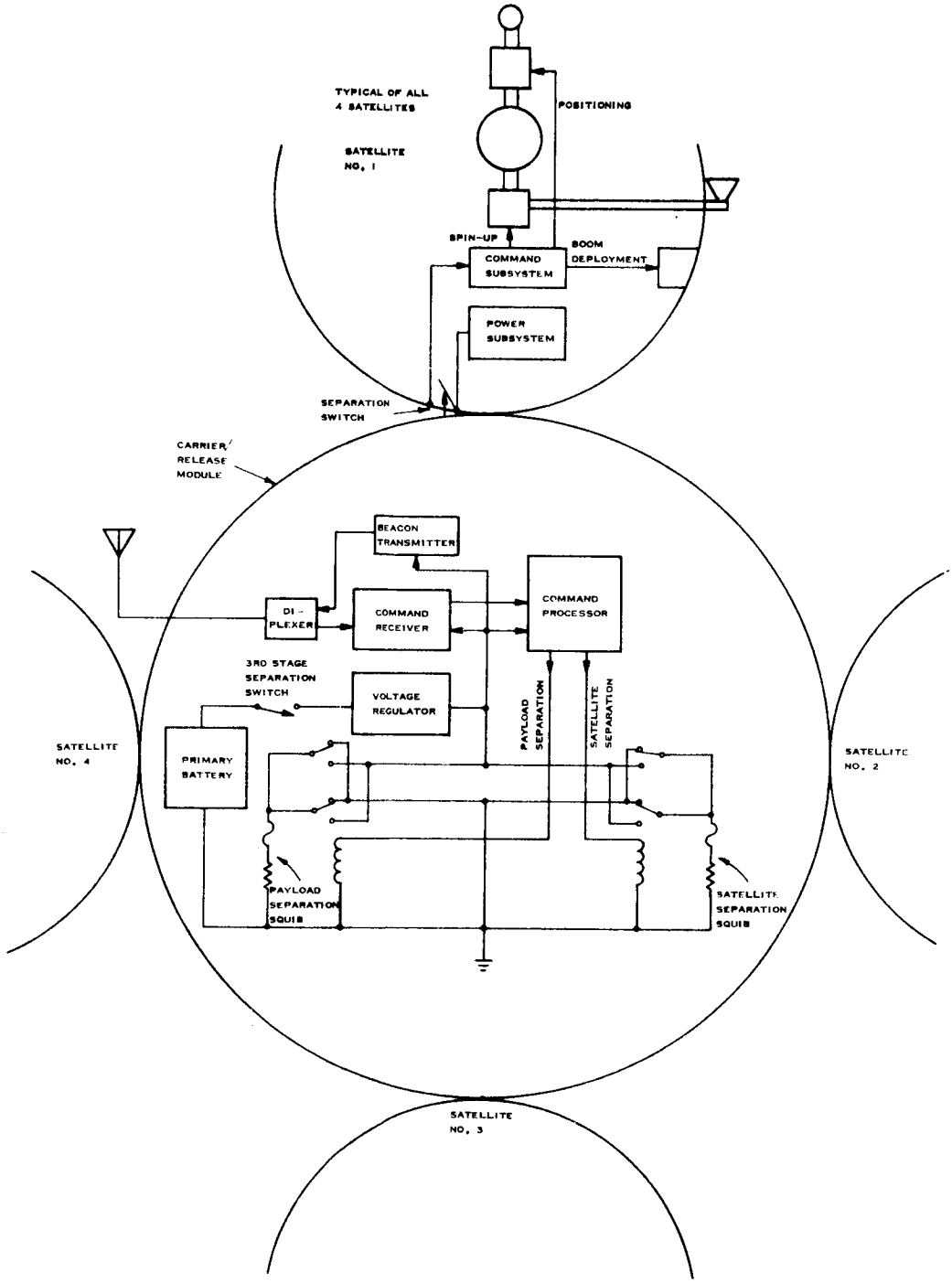

Figure 5.3-2 Radial Configuration, Payload Deployment - Separation and Control Electrical Diagram

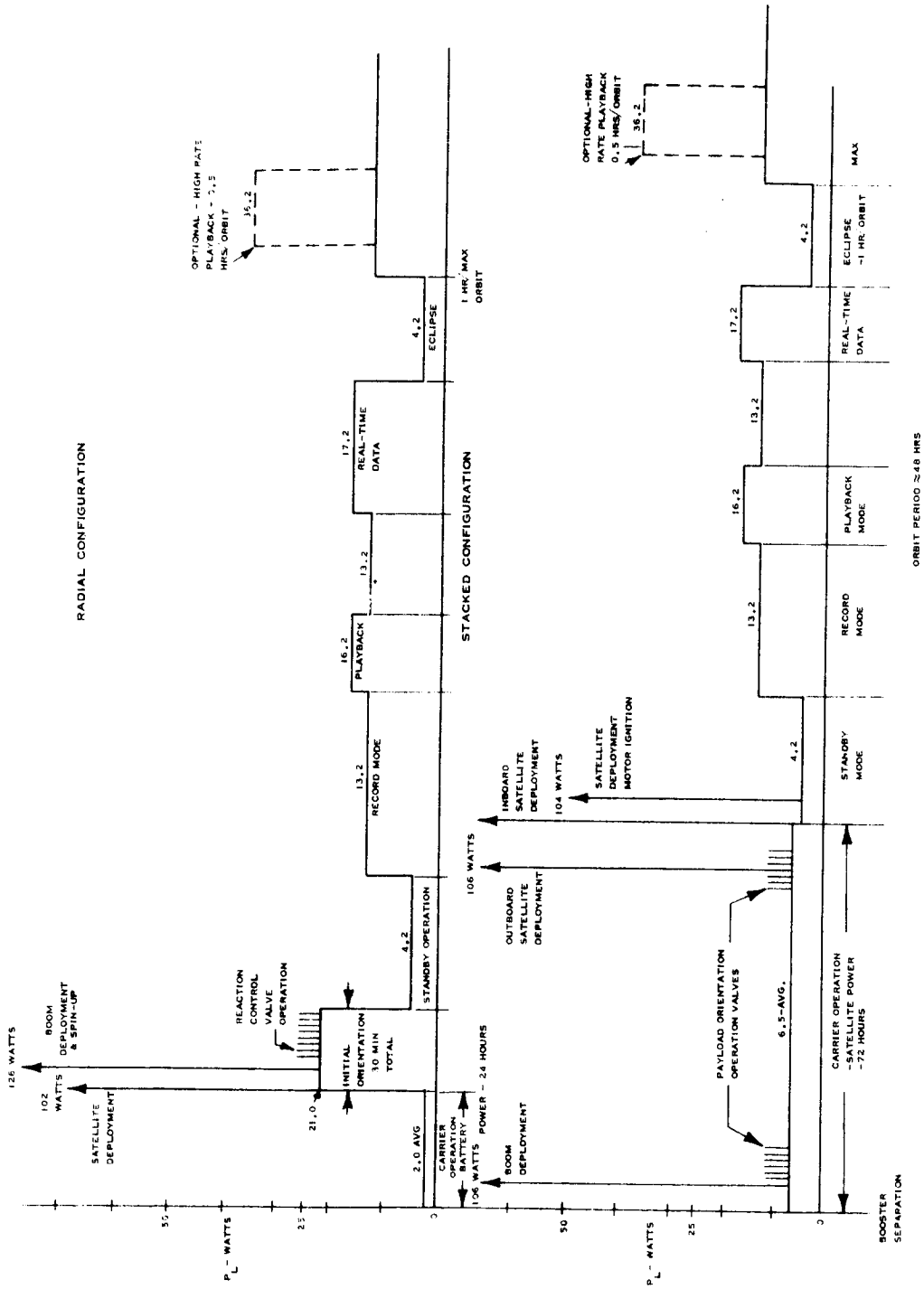

Figure 5.3-3 Typical Load Power Profiles

TABLE 5.3-1

CARRIER POWER REQUIREMENTS SUMMARY

Radial Configuration	
Equipment	**Watts**
Release Module	
Command Receiver	1.0
Beacon Transmitter	0.5
Timer	0.5
Total Average Load	2.0
Regulation & Dist. Losses	1.0
Total Battery Power Rqmts.	3.0 (avg. - 24 hours)
Pyrotechnics	5 amps for < 1 sec.
Stacked Configuration	
Carrier	
VHF Command Receiver	1.0
TLM Transmitter	1.5
TLM (Digital)	0.5
Timer	0.5
ACS Electronics	3.0/9.0 (avg./peak)
Total average power supplied by an inboard satellite	6.5 (for 72 hours)

Pyrotechnics 2 - 1 for each outboard sat.
1 for both inboard sat.
1 boom deployment

Each pyrotechnic to require 5 amps for < 1 sec.

Power values are assumed to be at 28 volts dc.

the small solid motor, which gives each satellite the necessary velocity increment normal to the orbit plane. In the inboard satellite supplying power to the carrier, a second separation switch operates to continue power availability to the carrier. The reaction control equipment on the carrier is then commanded to provide a velocity increment to position the inboard pair of satellites.

Each satellite in turn is activated at separation and initiates the operation of the solid rocket thruster to provide the necessary velocity increment for final satellite deployment.

A satellite power subsystem provides power to the carrier, rather than a separate primary battery on the carrier or a separate solar cell battery power supply on the carrier. This reduces the weight of the carrier. Only one satellite is used since the solar array - battery capacity is adequate if suitable sun angle is maintained. Such an arrangement also simplifies the interface.

Figure 5.3-2 illustrates the electrical system for the radial configuration. The power profile for both the carrier/release module and the satellites is illustrated in Figure 5.3-3; Table 5.3-1 summarizes the release module power requirements. Power for the release module is supplied by a silver-zinc primary battery. There is no electrical interface between the carrier and the individual satellites.

The release module equipment is activated by separation from the booster third stage. Separation from the third stage is timer activated. The equipment on the carrier includes a command receiver and processor, a beacon transmitter, and a satellite separation or deployment mechanism. The payload separation mechanism separates the truss and structure that mates the release module and satellites to the third stage adapter.

The satellites remain electrically inert until released by the release module or ground command. Separation of the satellites from the carrier at the first apogee activates the satellites. A timer in each satellite operates pyrotechnics, which deploy the booms for stability. Each satellite is then oriented normal to the ecliptic and spun-up to the desired orbital rate by command controlled operation of the on-board reaction control equipment.

The primary battery and related voltage regulator used in the release module must provide an average load power of 2 watts and peak currents of up to 5 amperes for one second to a 1-ohm load for squib operation. Using a basic energy density of 60 watt hours per pound for manually activated silver-zinc primary batteries and a maximum depth of discharge of 50 percent in 24 hours requires a battery weight of approximately 2.4 lbs. The voltage regulator would weigh approximately 0.5 lb.

5.3.2 Satellite Power Subsystem Details

5.3.2.1 Requirements. The satellite power subsystem must provide electric power in adequate quantity and quality for all operating modes of the vehicle. The present satellite load and system power requirements are summarized in Table 5.3-2 and illustrated in Figure 5.3-3. The critical mode in the power subsystem design is the real-time data transmission mode, which may be used for an extended period with a net load power requirement of 17.2 watts average at 28 volts dc and a primary power source requirement (solar array) of 21.5 watts. The radial payload configuration satellites have an on-board attitude control subsystem, which requires power during initial on-orbit operations; the stacked configuration satellites do not. Either configuration may be required to support a high rate playback mode at increased transmitter power as an option. This would be required for a maximum of 30 minutes per orbit. During eclipse operation (assumed a maxium of 1 hour), the loads are maintained in the standby mode.

5.3.2.2 Subsystem Functions and Elements. To provide the required power, the power subsystem utilizes the following functional elements as indicated in the block diagram of Figure 5.3-4.

a. The primary energy source is an array of silicon solar cells mounted on the surface of the spacecraft and suitably connected and covered.

b. The secondary energy source, is a rechargeable, sealed silver-cadmium or silver-zinc battery, which supplies peak and eclipse loads.

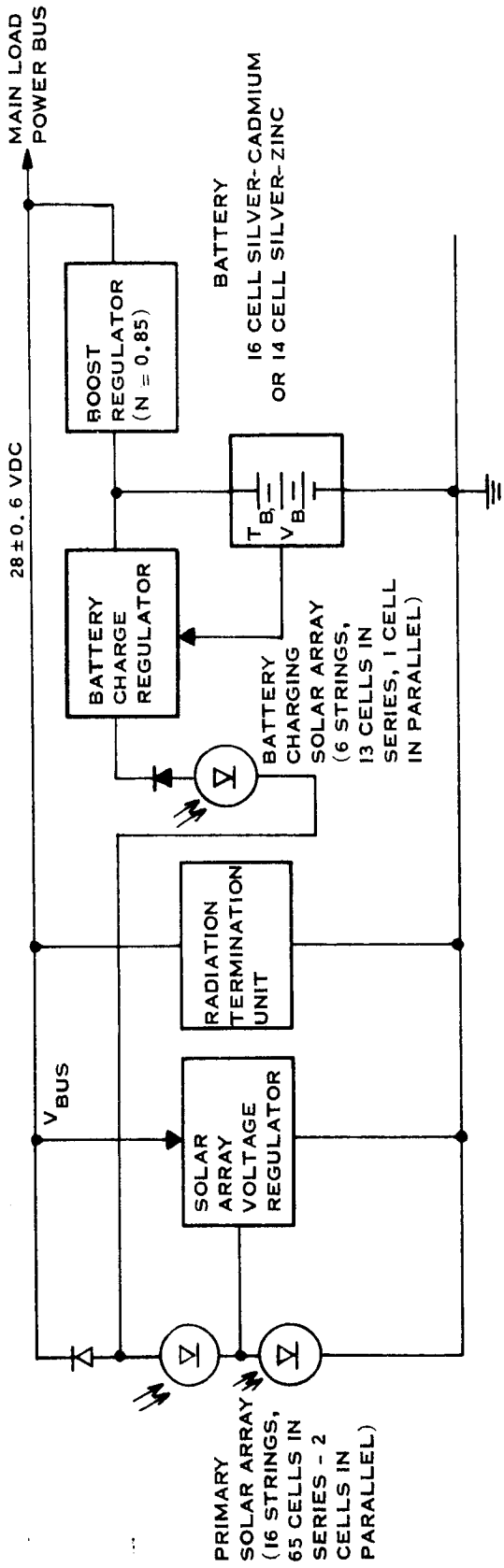

Figure 5.3-4 Power Subsystem Block Diagram
(Radial and Stacked Configurations)

TABLE 5.3-2

SATELLITE POWER REQUIREMENTS SUMMARY*

Equipment Item	Mode					
	Initial** On-Orbit Operation (30 min)	Standby	Record	Playback	Real-Time	Playback High Bit Rate (30 min/or bit)
Attitude and Orbit Control	15.75/21.75		-	-	-	-
Telemetry	1.0/1.0	1.0/1.0	2.0/2.0	1.0/1.0	2.0/2.0	1.0/1.0
Receiver	1.0/1.0	1.0/1.0	1.0/1.0	1.0/1.0	1.0/1.0	1.0/1.0
Programmer	0.5/0.5	0.5/0.5	0.5/0.5	0.5/0.5	0.5/0.5	0.5/0.5
Power Control	1.2/1.2	1.2/1.2	1.2/1.2	1.2/1.2	1.2/1.2	1.2/1.2
RTU	0.5/0.5	0.5/0.5	0.5/0.5	0.5/0.5	0.5/0.5	0.5/0.5
Recorder	-	-	1.0/6.0	2.0/6.0	-	2.0/6.0
Transmitter	-	-	-	10.0/10.0	5.0/5.0	30.0/30.0
Experiments	-	-	7.0/7.0	-	7.0/7.0	-
Pyrotechnics	0/100	-	-	-	-	-
Total Load Power	20/126	4.2/4.2	13.2/18.2	16.2/20/2	17.2/17.2	36.2/40.2
Battery Charging	-	3.6	3.6	3.6	3.6	-
System Losses (Diodes, $I^2 R$ etc.	1.0	0.2	0.6	0.7	0.7	2.0
Total Satellite Average Power Requirement	21.0	8.0	17.4	20.5	21.5	38.2

*All power values assumed to be at 28 volts dc.

**Applies to radial configuration only, averaged over a period of 30 minutes.

c. The output of the solar array and battery is regulated at a common point to provide conditioned power to spacecraft loads.

d. A battery charger and necessary sensing and logic circuitry provide for control of the elements of the power subsystem.

5.3.2.3 Subsystem Description. Both payload satellite configurations utilize an identical power subsystem as illustrated in Figure 5.3-4. The only difference is in the solar array. The stacked configuration has a solar array consisting of one cylinder, 45.5 inches in diameter and 11 inches in height. The solar array for the radial configuration is made up in two cylinders, each 22.5 inches in diameter and 11 inches in height. In each case, a main solar array provides the energy requirements of the spacecraft during sunlight operation. A secondary solar array is connected to the main array and is used to provide the increment of power required for controlling recharge of the battery. The output of the main solar array is regulated by a shunt regulator, which shunts a portion of the solar array output. A boost regulator connects the battery to a common load bus, which is regulated to 28 ± 0.6 volts dc by the combined operation of the solar array regulator and boost regulator. The subsystem elements are described in greater detail in the following paragraphs.

Solar Array. The solar array utilizes the surface of the cylindrical spacecraft body to mount 2,158, 2 x 1 cm, 7-14 ohm-cm, N-on-P silicon solar cells. Characteristics of the cells are indicated in Figure 5.3-5. Each cell is provided with a 0.006-inch quartz cover slide utilizing an anti-reflection coating and a blue filter. The solar cell panels are wired as indicated in Figure 5.3-6, with the 2-cm dimension of the cell located vertically. The main solar array is made up of 32 strings of solar cells, each string consisting of 65 cells in series and 2 cells in parallel at the cell level. The battery charging portion of the solar array consists of 6 strings of cells, 13 connected in series, one in parallel. This portion of the solar array limits the maximum current to the battery to 0.1 ampere and provides up to 6 volts for the voltage drop across the proportional series regulator, which serves as the charge regulator. Figure 5.3-7 gives the degraded solar array I-V curves.

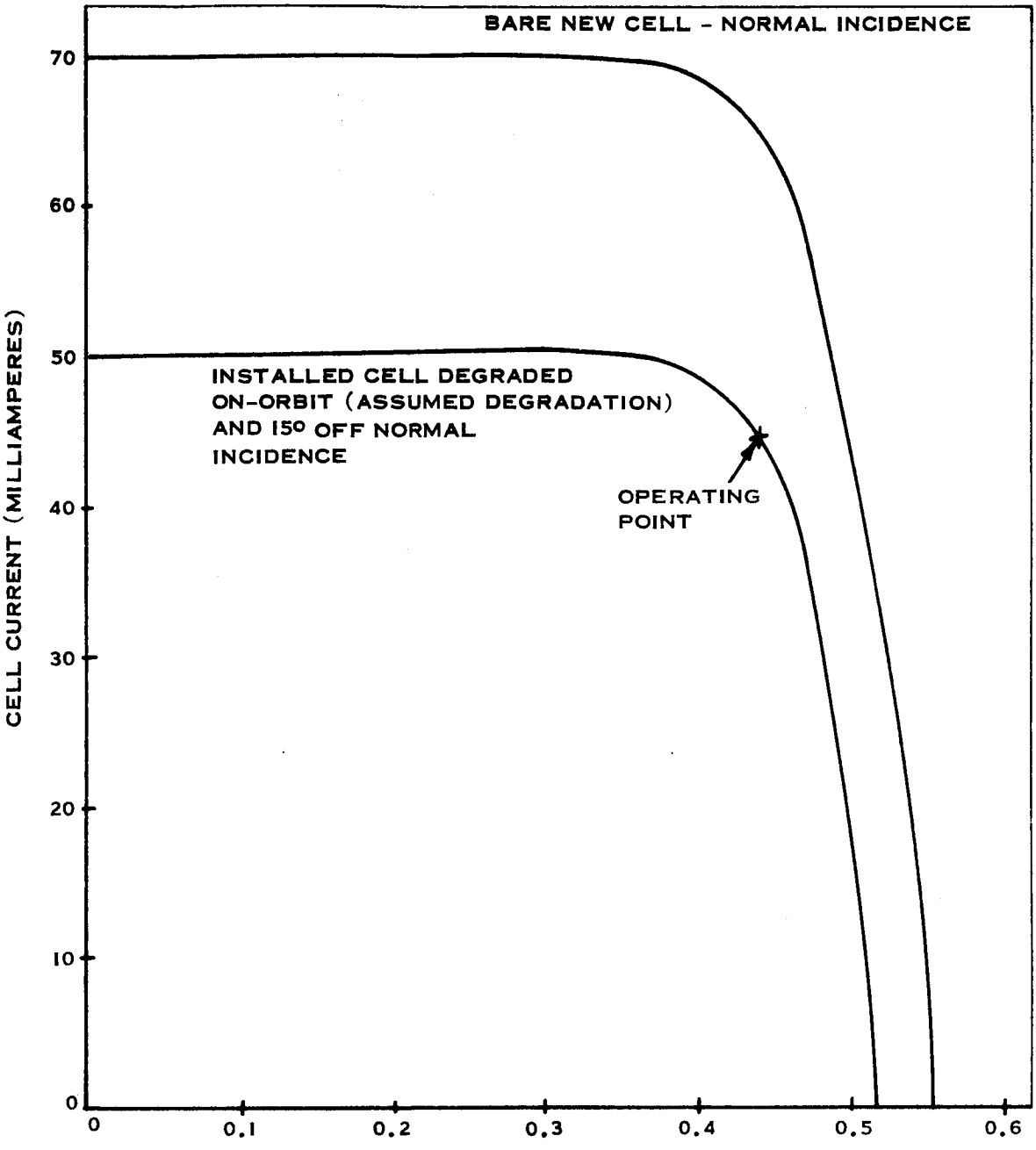

Figure 5.3-5 Cell I-V Characteristics for 2 x 1 Solar Cell, Silicon N/P, 7-14 ohm cm, 140 mw/cm^2, 75°F

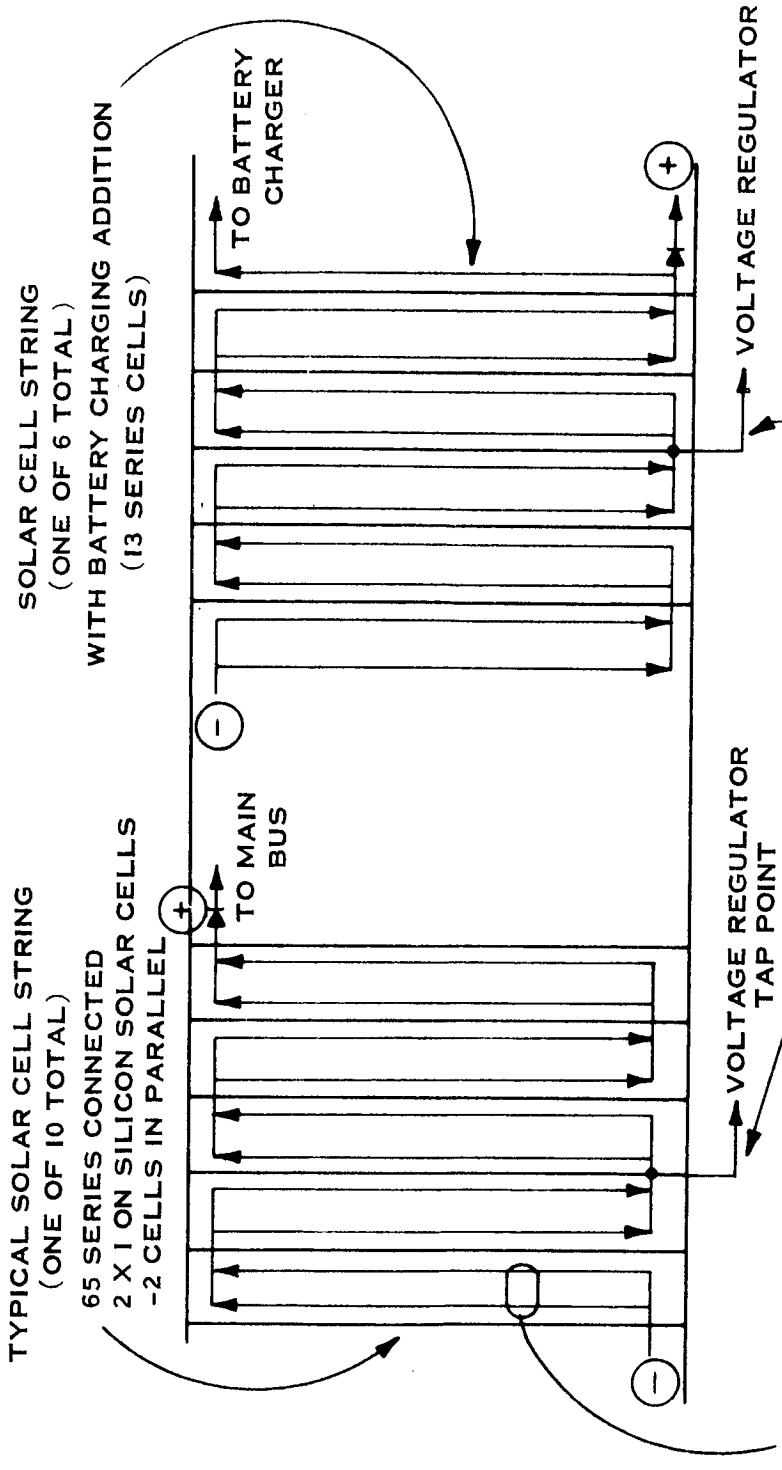

Figure 5.3-6 Typical Solar Array Wiring Diagram

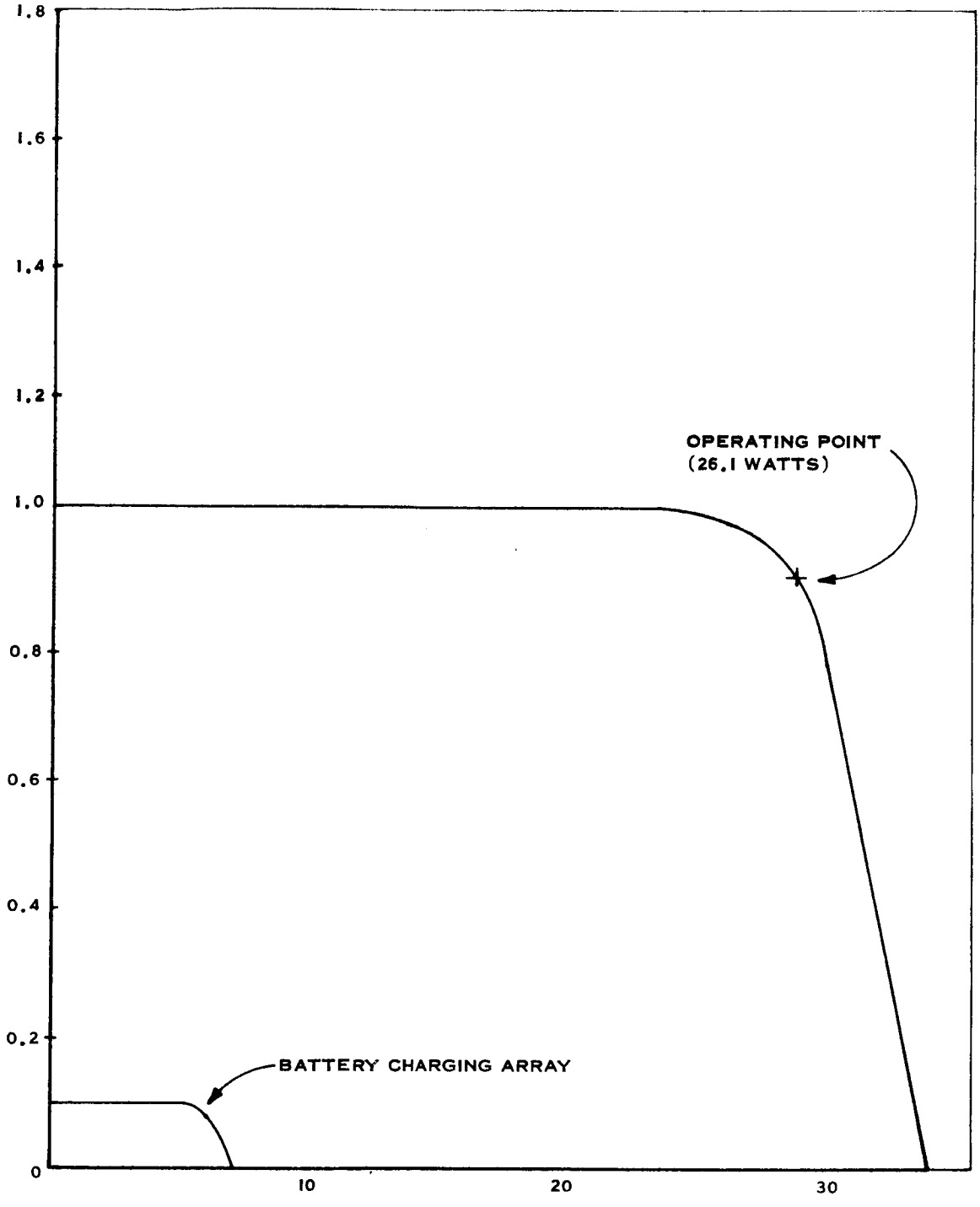

Figure 5.3-7 Solar Array I-V Curves, Degraded Condition
(75^0 F, 15 degrees off normal incidence)

The following calculations are used to evaluate the load power available from the degraded solar array.

a. Main Solar Array - 26.1 watts at 28.6 volts or 0.914 amperes

b. Allow 0.6 volt drop for diodes, resulting in 0.914 x 28 = 25.6 watts at bus voltage.

c. Subtract 0.1 ampere for battery charging, resulting in 0.814 x 28 = 22.8 watts available for load power requirements at 28 volts.

Since the system power requirement for the real-time data transmission mode is 17.9 watts (which does not include battery charging), there is a resulting power margin of 5.1 watts, which allows for the normal growth in power requirements as well as a margin.

The arbitrarily assumed solar cell degradation is a conservative value for one year on orbit; the solar array design described is well within reasonable limits and design practices. The primary solar array characteristics are summarized in Table 5.3-3.

Battery. Only silver-cadmium or silver-zinc secondary batteries meet both the life cycle and low residual magnetic field requirements associated with this application. In six months, approximately 90 eclipses (maximum) could be experienced. While the silver-cadmium cells exhibit greater cycle life capabilities, the silver-zinc cell can withstand several hundred cycles of operation and exhibits better voltage regulation characteristics, as well as a lower weight. Nickel-cadmium batteries can not be considered because of their highly magnetic characteristics. Both silver-zinc and silver-cadmium cells must be used in low rate of charge applications, since charge control is difficult at high rates. This application, with a 48-hour orbit and minimal eclipse power requirement, lends itself to the use of these batteries.

TABLE 5.3-3

POWER SUBSYSTEM WEIGHT AND PERFORMANCE SUMMARY
(RADIAL AND STACKED SATELLITE CONFIGURATIONS)

Solar Array

- 2,158 Silicon solar cells - 2 x 1 cm, N/P, 7-14 ohm cm
- 2,080 Main solar array cells (65 in series 32 in parallel)
- Battery charging additions 78 cells (13 in series, 6 in parallel)
- Weight (including substrate) 7.23 lbs (0.67 lbs/ft^2)
- Load Power Available (x 1 year) 22.8 watts at 28 volts and 75°F and 15° off normal orientation.

Battery

- Silver Cadmium Option
  - 16 cell - 1 ampere-hour battery
  - Charge voltage (max) - 25.6V
  - Discharge voltage (min) - 16.0V
  - Maximum charge current - 0.1 amp
  - Depth of Discharge (max on-orbit) - 25 percent (eclipse)
  - Weight - 1.2 lbs
  - Dimensions - 4 x 3 x 2.5 inches
  - Allowable temperature range - 40 to 100°F
- Silver Zinc Option
  - 14 cell - 1 ampere-hour battery
  - Charge Voltage (max) - 27.3V
  - Discharge Voltage (min) - 18.2V
  - Maximum Charge current - 0.1 amp
  - Depth of Discharge (max on-orbit) - 25 percent (eclipse)
  - Weight - 1.2 lbs
  - Dimensions - 4 x 3 x 2.5 inches
  - Allowable temperature range - 40 to 100°F

Roost Regulator/Battery Charger (same for both configurations)

- Type - Series regulator for battery charging, boost DC/DC converter for output voltage regulation
- Boost regulator efficiency - 85 percent full load
- Output Regulation - 27.7 ± 0.3 vdc
- Weight - 2 lbs
- Dimensions - 2.5 x 3 x 4 inches

Solar Array voltage regulator and load controls

- Type - Proportional - partial shunt
- Efficiency - 98 percent full load
- Output Regulation 28.4 ± 0.2 vdc
- Dimensions - 2.5 x 5.5 x 6.0 inches

RTU (Radiation Termination Unit)

- Weight - 0.5 lbs.
- Dimensions - 2 x 2 x 2.5 inches

The battery depth of discharge during a one-hour eclipse is approximately 25 percent maximum for either type of battery with the sizing used. For the optional mode of operation at high rate transmission and playback, the maximum depth of discharge is approximately 38 percent. Since recharge can take place over a minimum period of 46.5 hours, a very low rate can be used. The charge control technique limits battery voltage as a function of battery temperature. The battery charging section of the solar array limits maximum battery charge current to 0.1 ampere or a rate of C/10. This available current can be further limited by the charge regulating circuit.

The weight, volume, and other major characteristics of the battery options are summarized in Table 5.3-3.

Electronic Equipment. The electronic equipment associated with the power subsystem consists mainly of the solar array voltage regulator, battery charger, radiation termination unit, and boost regulator as indicated in Figure 5.3-4. Load sharing and control logic are required, as well as telemetry and control sensors. All the electronic equipment except the radiation termination unit would be packaged in two units, whose characteristics are summarized in Table 5.3-3.

The solar array voltage regulator would be almost identical to one developed and flown successfully on Philco-Ford Initial Defense Communication System Program. Since the regulator is a shunt type, it exhibits a full load efficiency approaching 100 percent. The regulator does dissipate relatively large amounts of power during periods of light load. This light load dissipation is the primary reason for operating the regulator from the tap point of the solar array, since the light load dissipation is reduced. The maximum regulator dissipation at light load would be approximately 10 watts.

The battery charger would be a simple transistor regulator, which would operate with inputs of sensed values of battery current, voltage, and temperature to limit battery charge current and voltage as a function of temperature. While the regulator itself is simple, the control level circuitry is sophisticated. Provisions would be made to control the operation of the battery charger from the ground.

The boost regulator would be a high efficienty (85 percent) regulator typical of those developed on similar programs. It consists basically of a dc/dc converter circuit connected as a boost type auto transformer. The regulator would include a linear, non-saturating power amplifier, a saturating drive oscillator, a voltage reference circuit, and an output rectifier and filter. On-off control, such as interlock with the solar array regulator, can be accomplished at the drive oscillator level with little power required.

The radiation termination unit is a timer and switch that disables the power subsystem at the end of a pre-selected period. This would be identical to a unit developed for the Initial Defense Communications System Program.

5.3.3 Magnetic Field Analysis

During the contract, Philco-Ford studied the magnetic fields generated by the solar arrays of spin-stabilized spacecraft. The results of this study, while over-simplified and applicable only in a general sense, are useful nonetheless in comparing the paddle wheel and cylindrical configurations. The study reveals that the magnetic fields at a boom sensor point vary in time as a result of the solar array currents.

5.3.3.1 Spacecraft Configurations. The two configurations considered are illustrated in Figures 5.3-8 and 5.3-9. Figure 5.3-8 illustrates a paddle wheel configuration considered on this study. There are three paddle type solar array panels, each covered on both sides by solar cells. Experiment sensors are mounted on booms on the ends of each panel. Figure 5.3-9 is a cylindrical satellite with body-mounted solar cells. The projected areas of the cylinder are 1.5 times that of each of the panels of the configuration in Figure 5.3-8 and the experiment booms are shown mounted in the same position relative to the body of the spacecraft. The factor of 1.5 equates the minimum projected area of solar cells for the two configurations. Important dimensions are given for each configuration.

5.3.3.2 Summary and Conclusions. The analysis, based on numerous assumptions, but apparently sound overall relationships, indicates that, for both the paddle wheel satellite configuration and the cylindrical spacecraft, there is a time varying magnetic field at the boom tip sensor location due to the solar array currents. In the paddle wheel configuration, the variation results in a variation in the paddle currents as the solar array rotates. In the cylindrical configuration, it is caused by the movement of the boom through a field that remains fixed in space. No absolute magnitudes can be determined from this analysis. However, it is apparent that a significant time-varying field (with magnitudes perhaps as great a 0.3 gamma) could exist at the boom tip sensor location if care is not exercised in minimizing and cancelling the contributions from the solar array panels. The field components tangential to the spin cylinder and radial to the spin axis appear to be the most significant.

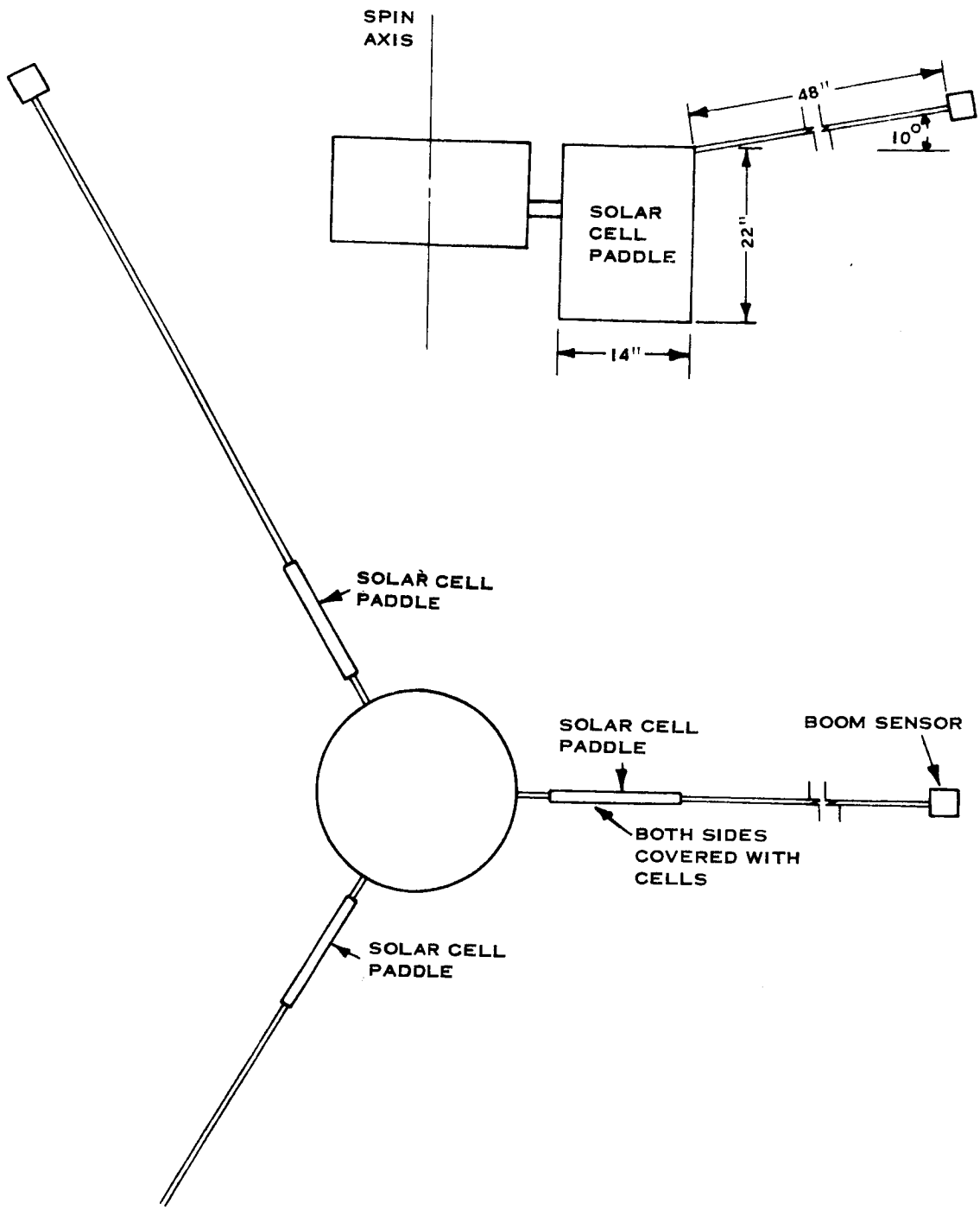

Figure 5.3-8 Paddle Wheel Configuration

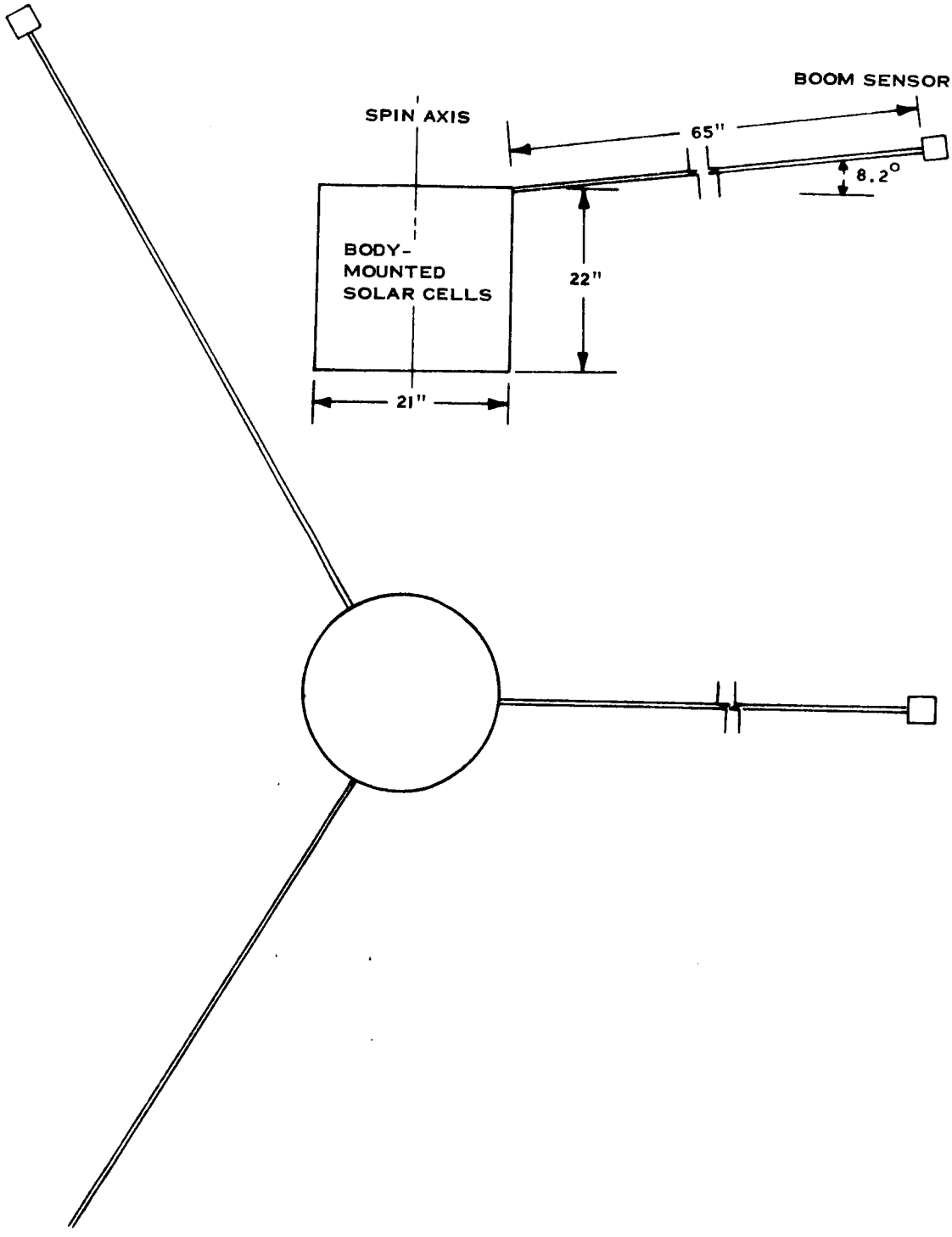

Figure 5.3-9 Cylindrical Configuration

5.3.3.3 Analysis

Paddle Wheel Satellite. For the purposes of this analysis, it is assumed that each solar paddle can be replaced by a circular coil in the plane of the paddle whose diameter fits within the approximate outline of the panel. This coil represents the uncompensated current loops in the solar paddle and is assumed to represent the contributions from both sides of the paddle. The actual current depends upon which side is illuminated. A circular coil is assumed for reasons of simplicity in performing the analysis and it is realized that it is not a rigorous assumption. The results should be indicative of time variations and the relative importance of various factors. However, it is assumed that all three paddles can be represented by identical coils carrying currents with identical maximum values. Actual field values will certainly depend on specific wiring techniques and will exhibit variations from paddle to paddle.

For this analysis, a coil 1 foot in diameter, with its center at the paddle center, is assumed to replace each paddle. The geometry of each coil remains fixed with respect to the end of the booms. As the spacecraft spins, the currents in each coil vary with time, resulting in a time-varying field at the end of the booms with contributions from each coil. It is further assumed that the paddles are wired so that current flow in the coil is always in the same relative direction. The above discussion is clarified in Figure 5.3-10, which is a sketch of the assumed model.

The magnetic field contribution at any point relative to an ideal circular coil or loop can be determined in terms of cylindrical coordinates and assumed current. The following equations for the radial and axial magnetic field components were obtained from "Static and Dynamic Electricity" by Smythe.

$$B_{(\rho)}(\text{radial component}) = \frac{\mu I}{2\pi} \frac{Z}{\rho\left[(a+\rho)^2 + Z^2\right]^{1/2}} \left[-K + \frac{a^2 + \rho^2 + Z^2}{(a-\rho)^2 + Z^2} E\right]$$

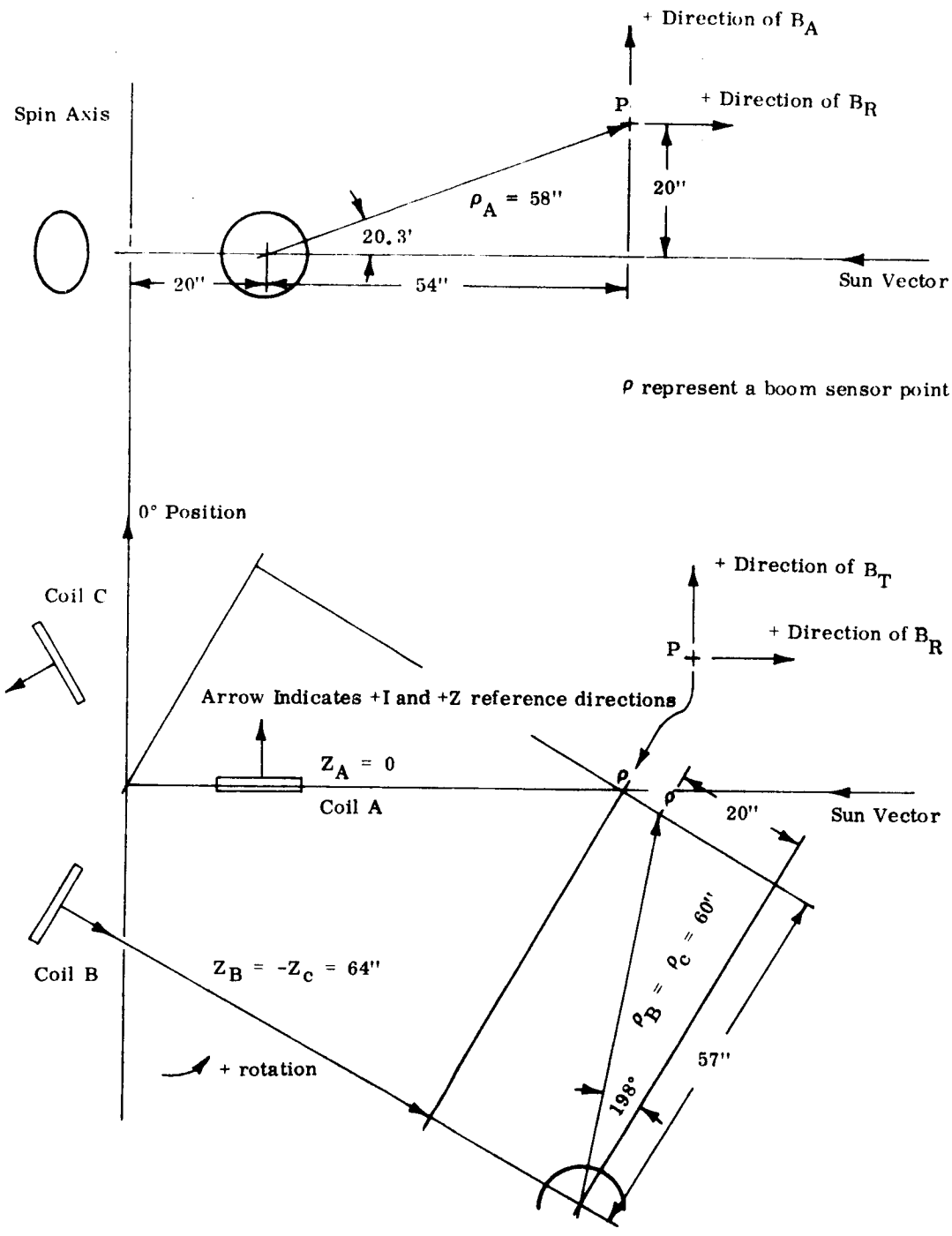

Figure 5.3-10 Model for Paddle Wheel Configuration

$$B_{(Z)} \text{ (axial component)} = \frac{\mu I}{2\pi} \frac{1}{\left[(a+\rho)^2 + Z^2\right] 1/2} \left[K + \frac{a^2 - \rho^2 - Z^2}{(a-\rho)^2 + Z^2} E \right]$$

where K and E are functions of k

$$\text{and } k^2 = \frac{4a\rho}{\left[(a+\rho)^2 + Z^2\right]}$$

and
- I = coil current
- a = coil radius
- ρ = radius to point from coil axis
- Z = distance from point to plane of coil

$B_{(\rho)}$ is the flux density contribution in the radial direction from the coil axis, and $B_{(Z)}$ is the flux density contribution in a direction normal to the coil plane. K and E can be obtained from tables of complete elliptic functions. When the above dimensions are in meters and $u = 4\pi \times 10^{-7}$, the units of flux density are webers per square meter. Multiplication by 10^9 converts these units to the unit of gammas.

Applying the dimensions of Figure 5.3-10 to the above equations gives the following relationships for the contributions of the three coils, A, B, and C, to the magnetic field of P:

$$B_{A(\rho)} = B_{(\rho)} \text{ Coil A} = 0$$

$$B_{A(z)} = B_{(z)} \text{ Coil A} = -2.51\ I_A \text{ gamma}$$

$$B_{B(\rho)} = B_{(\rho)} \text{ Coil B} = 1.01\ I_B \text{ gamma}$$

$$B_{B(z)} = B_{(z)} \text{ Coil B} = 0.36\ I_B \text{ gamma}$$

$$B_{C(\rho)} = B_{(\rho)} \text{ Coil C} = -1.01\ I_C \text{ gamma}$$

$$B_{C(z)} = B_{(z)} \text{ Coil C} = 0.36\ I_C \text{ gamma}$$

To be useful, the above field components must be related to spacecraft coordinates and summed. The coordinates chosen are:

a. Tangential or perpendicular to the plane formed by the boom and spacecraft spin axis (B_T).

b. Radial or perpendicular to the spin axis (B_R).

c. Axial or in a direction parallel to the spin axis (B_A).

The assumed positive directions for those components are shown in Figure 5.3-10. Combining the contributions from the three coils in the chosen coordinates gives the following relationships:

$$B_{T(\text{tangential})} = B_{A(Z)} - \left(B_{B(Z)} + B_{C(Z)}\right)\sin 30° + \left(B_{B(\rho)} - B_{C(\rho)}\right) \cos 19.3° \cos 30°$$

$$B_{R(\text{radial})} = \left(B_{B(Z)} - B_{C(Z)}\right) \cos 30° + \left(B_{B(\rho)} + B_{C(\rho)}\right) \cos 19.3° \sin 30°$$

$$B_{A(\text{axial})} = \left(B_{B(\rho)} + B_{C(\rho)}\right)\sin 19.3°$$

Combining the above relationships with the expression for the various coil contributions in terms of coil currents yields:

$$B_T = -2.51\ I_A + 0.645\ (I_B + I_C) \text{ gamma}$$

$$B_R = +0.788\ (I_B - I_C) \quad \text{gamma}$$

$$B_A = +0.334\ (I_B - I_C) \quad \text{gamma}$$

The next step is to determine the relationship of the paddle and therefore the coil currents as a function of time. Assuming the spin axis is normal to the sun, the configuration shown in Figure 5.3-8 can be used to evaluate paddle current at each

position of the spacecraft for one complete revolution. The result of this evaluation is given in Figure 5.3-11, which is a simplified plot of paddle currents for one complete revolution in terms of maximum paddle current. The wave form is one of a rectified sine wave for each paddle, with a gap which corresponds to the portion of a revolution when both sides of a paddle are shadowed by the body of the spacecraft or another paddle. The three currents are 120 degrees out of phase. This time variation would also apply to the coil currents of the simplified model. These functions could be represented by a Fourier series but, for purposes of this study, a graphical approach is taken.

Figure 5.3-12 plots the three field components at a boom sensor point in terms of maximum coil current. The relative currents have been combined and plotted as a function of spacecraft rotation and time. As would be suspected, the tangential component (B_T) has the greatest relative magnitude since it is primarily due to the current in coil A or paddle A, the paddle on which the particular boom is mounted. The contributions of the other coil or paddle currents are smaller at this point. The axial field component (B_R) appears least important.

While it is not possible to obtain absolute magnitude information from this study, the following further exercise was undertaken with the model developed. On the Initial Defense Communication Satellite Program, solar panel magnetic fields were measured and found to be 2 to 30 gamma at 1 foot, worst axis. If each paddle of the paddle wheel configuration is assumed to generate 30 gamma at 1 foot measured on the assumed coil axis, a maximum coil current can be determined for the model, since, on the axis of the coil:

$$B_{(Z)} = \frac{1/2\,\mu\, a^2\, I_{coil}}{(a^2 + Z^2)^{3/2}}$$

$$\therefore\ I_{coil} = \frac{B_{(Z)}\,(a^2 + z^2)^{3/2}}{1/2\,\mu\, a^2}$$

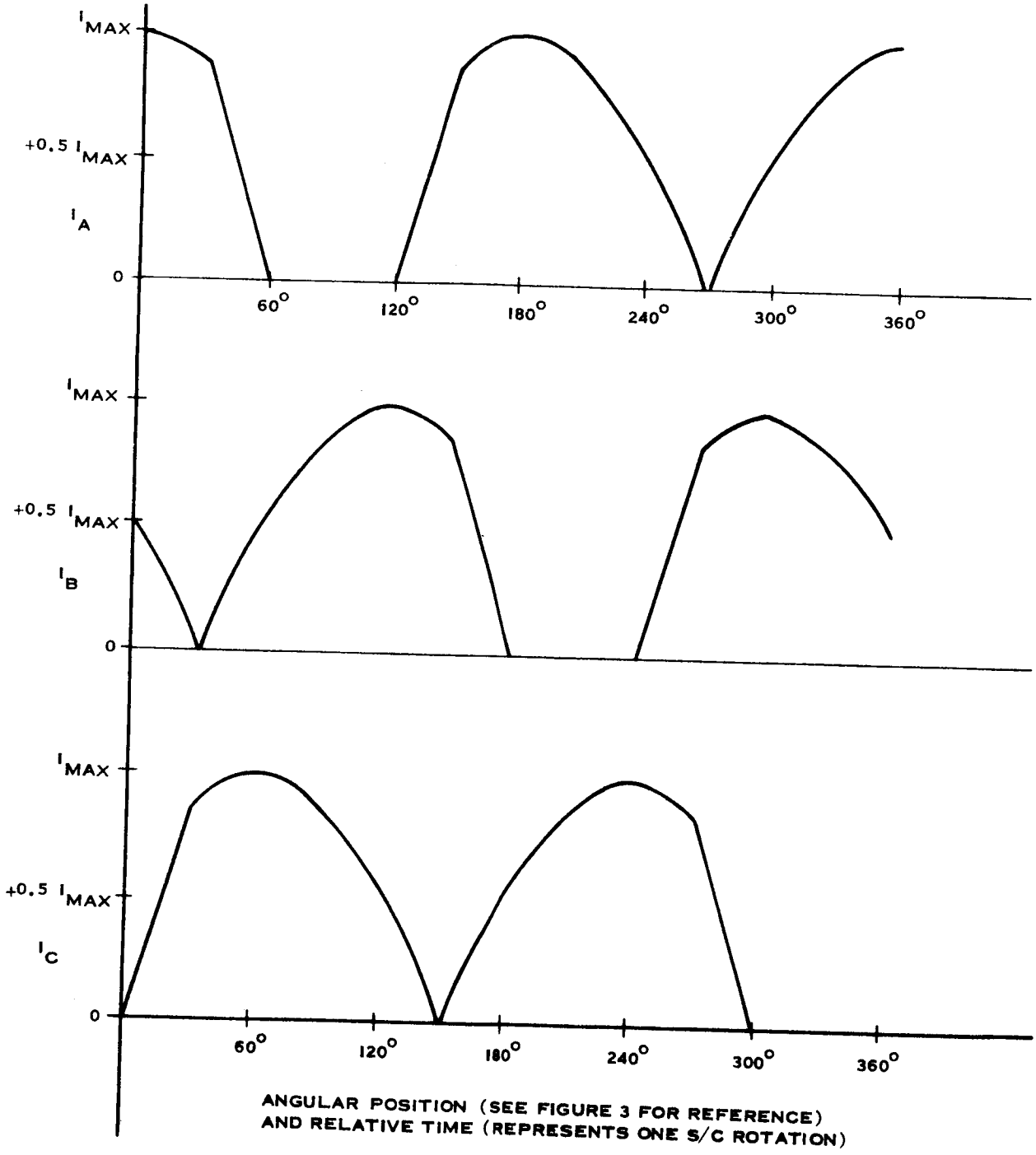

Figure 5.3-11 Simplified Plot of Normalized Solar Paddle Currents

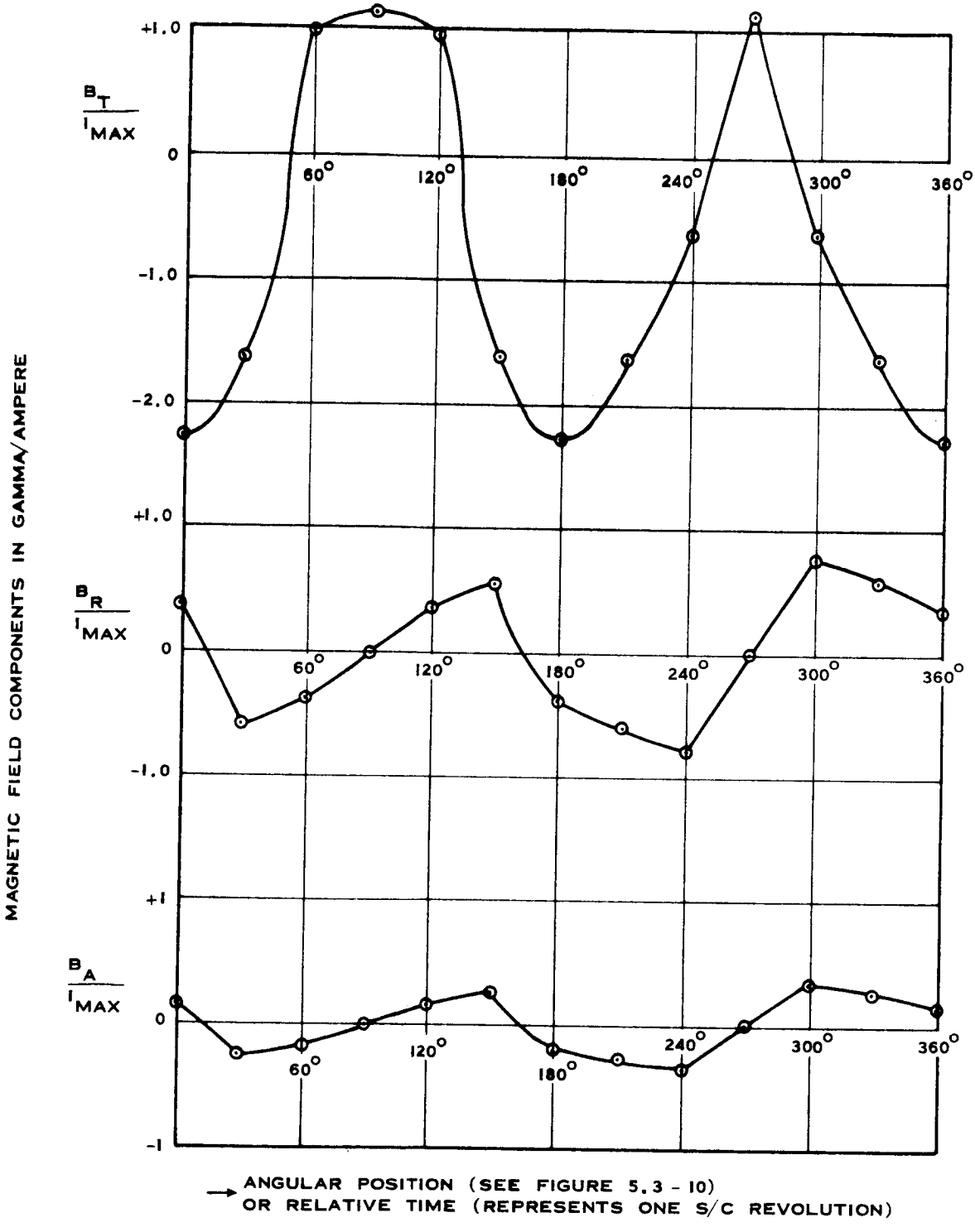

Figure 5.3-12 Magnetic Field Component at Boom Sensor as a Function of Angular Position & Currect (Paddle Wheel Configuration)

For the assumed dimensions and a $B_{(Z)} = 30$ gamma;

$$I_{coil\ (maximum)} = 0.085 \text{ amperes.}$$

Relating this maximum coil current back to the plots of Figure 5.3-12, a magnetic field varying from -0.2 gamma to + 0.1 gamma in the tangential direction is obtained as the spacecraft rotates. The field components have a fundamental frequency of twice the frequency of rotation. Based on the same type of assumption, the peak magnetic field contribution could be as low as 0.013 gamma for an assumed 2 gamma level at 1 foot on the coil axis.

Cylindrical Satellite. The cylindrical configuration appears more difficult to represent than the paddle wheel. The cylindrical solar array does bear a similarity to the rotor of a dc machine however. As the spacecraft spins, only the half of the cylinder that is illuminated has strings that carry current. The distribution of current due to solar cell strings remains nearly constant in space, as one string is occluded, another is illuminated, etc. This current distribution will have an uncompensated or net magnetic field contribution, which also tends to remain stationary in space as the satellite rotates, just as the net magnetic field produced by the currents in the rotor of a dc machine remains fixed in space as the rotor spins past the pole pieces. In this case, the pole pieces are analogous to the sun. This assumption is particularly good if it is assumed all sections of the solar array surface are identical. This means that it should be possible to represent at least some portion of the magnetic field contribution of a cylindrical solar array by a stationary or fixed coil carrying an unknown constant current as indicated in Figure 5.3-13. The diameter of the cylindrical vehicle is assumed to be 1.5 times the width of the paddles on the paddle wheel satellite; thus, the required relative dimensions are roughly compatible from a projected area standpoint. The coil representing the uncompensated, fixed, solar array field is assumed to be 2 feet in diameter to roughly fit the projected area and is assumed to be located at the center of the cylinder so as to simplify the calculations. The booms are assumed to be located in a position identical to the paddle wheel configuration.

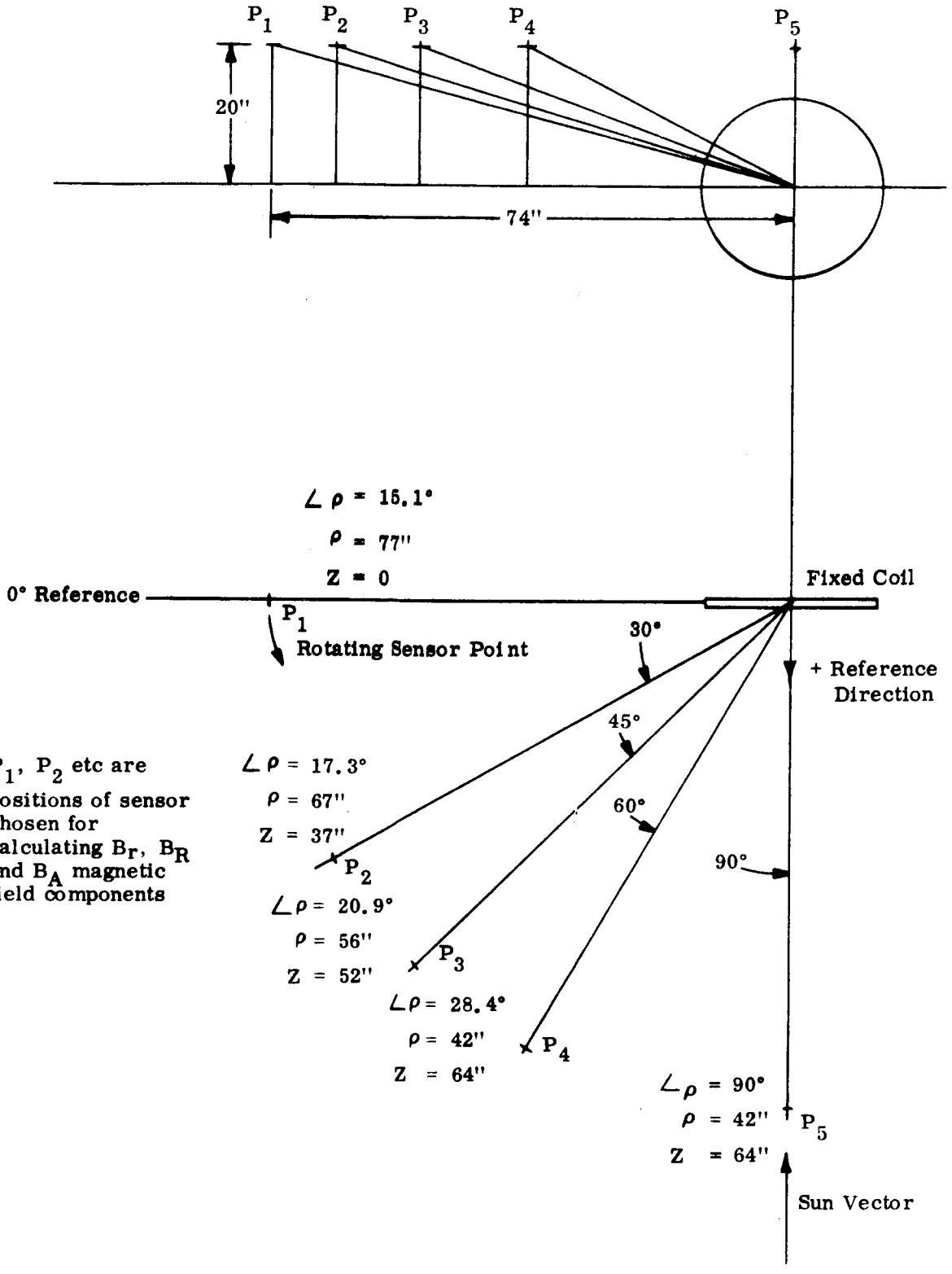

Figure 5.3-13 Model for Cylindrical Configuration

The equation for the magnetic field due to a current loop is used again for this analysis. Five positions are used to obtain the field contributions at a boom tip as the boom rotates through the fixed field of the coil. The radial and axial field components (relative to the fixed coil) at the boom tip for the five positions shown in Figure 5.3-12 are:

Position	$B_{(\rho)}$ (gamma)	$B_{(Z)}$ (gamma)
1	0	-4.11 I
2	+5.25 I	-1.24 I
3	+4.94 I	+2.72 I
4	+5.51 I	+4.34 I
5	+2.8 I	+6.93 I

These components can be combined into tangential, radial, and axial components relative to the spacecraft at each indicated position as follows:

Position 1

$$B_T = B_{(Z)}$$

$$B_R = 0$$

$$B_A = 0$$

Position 2

$$B_T = B_{(Z)} \cos 30° - B_{(\rho)} \cos 60° \cos 17.3°$$

$$B_R = B_{(Z)} \sin 30° + B_{(\rho)} \cos 30° \cos 17.3°$$

$$B_A = B_{(\rho)} \sin 17.3°$$

Position 3

$$B_T = B_{(Z)} \cos 45° - B_{(\rho)} \cos 45° \cos 20.9°$$

$$B_R = B_{(Z)} \sin 45° + B_{(\rho)} \cos 45° \cos 20.9°$$

$$B_A = B_{(\rho)} \sin 20.9°$$

Position 4

$$B_T = B_{(Z)} \cos 60° - B_{(\rho)} \cos 30° \cos 28.4°$$

$$B_R = B_{(Z)} \cos 30° + B_{(\rho)} \cos 60° \cos 28.4°$$

$$B_A = B_{(\rho)} \sin 28.4°$$

Position 5

$$B_T = 0$$

$$B_R = B_{(Z)}$$

$$B_A = B_{(\rho)}$$

The above relationships can be combined with the previously determined expressions for radial and axial components (relative to the fixed coil) and expressed in terms of coil current to obtain the net field as a function of position and time. The resulting field components are plotted as a function of time or spacecraft position as shown in Figure 5.3-14. For this model, the tangential and radial components assume the greatest relative importance with a magnitude around two times greater than the axial component. Note, that while the current delivered by the solar array is nearly constant, the sensor or the boom can experience a time-varying magnetic field as the spacecraft rotates, just as in the case of the paddle wheel configuration. In this case the fundamental frequency is the frequency of rotation.

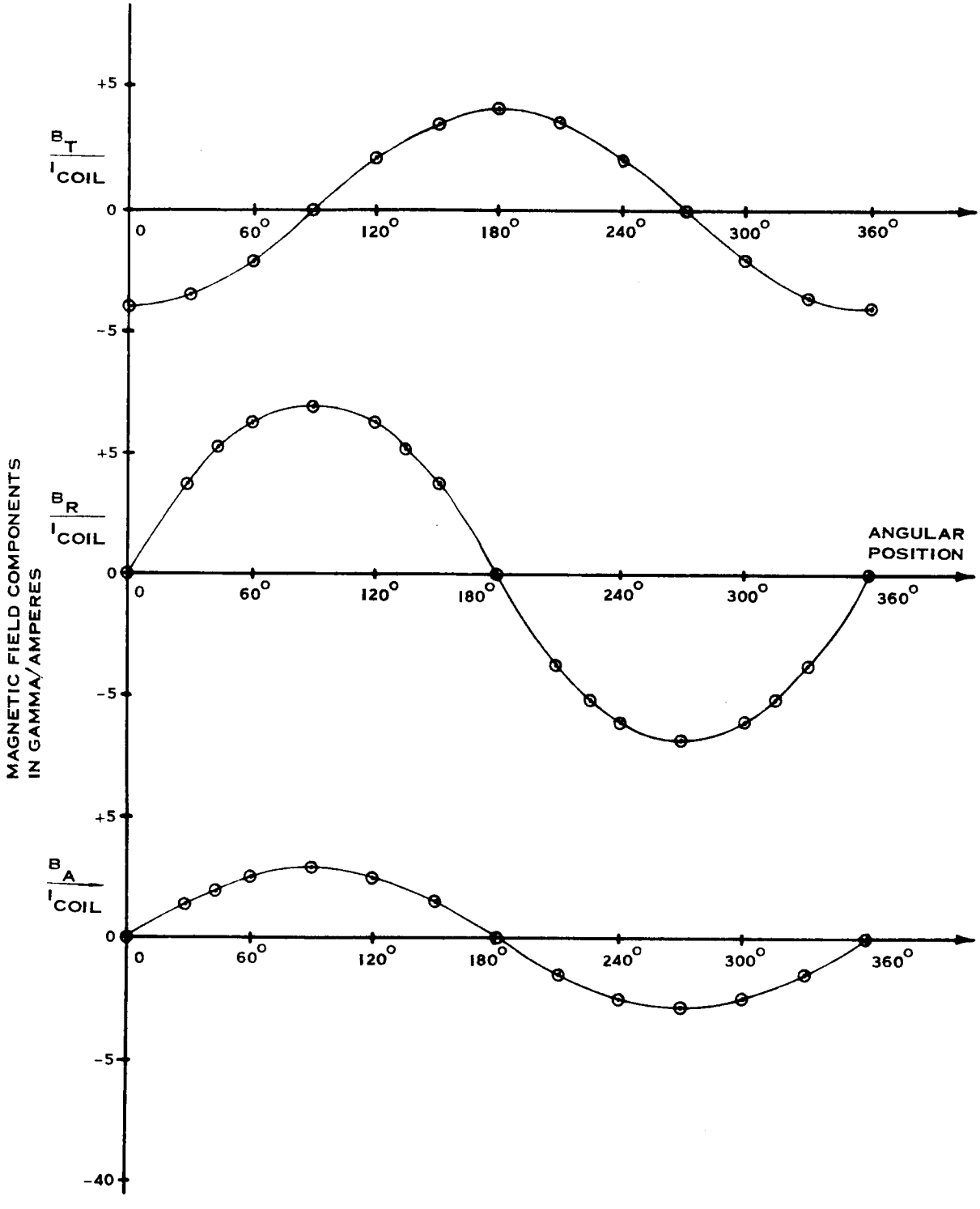

Figure 5.3-14 Magnetic Field Components at Boom Sensor as a Function of Angular Position and Current (Cylindrical Configuration)

To finish the exercise, again the Initial Defense Communications Program data on magnetic fields due to solar panels is used with rather broad assumtpions to obtain an absolute value for the field evaluation. As before, it must be understood that only empirical data can be used to accurately determine the field strengths. However, it was again assumed that the coil produced a worst case uncompensated field of 30 gamma at 1 foot along the axis. For the 2 foot diameter assumed, this would be related to a coil current of 0.041 amperes. Using this coil current and the plots of Figure 5.3-14, a tangential component variation of +0.16 to -0.16 gamma is predicted and a radial component variation of +0.3 to -0.3 gamma is predicted. The axial component ranges between 0.12 and -0.12 gamma.

SECTION 6

TELECOMMUNICATIONS

6.1 COMMUNICATION SYSTEM REQUIREMENTS AND CONSTRAINTS

Aside from the requirement to transmit all of the scientific data that is collected by instrumentation aboard a set of four satellites in a highly elliptical orbit, there are few constraints placed upon the telecommunication subsystem by the science subsystem. It is pertinent that the data collected by the four satellites achieve the primary objective of a multiple satellite system -- namely, the simultaneous collection of data at several points in a particular space region. Of importance also is accurate time-tagging of the data collected by the multiple satellites. From the communications point of view, the primary constraint is to assure that all of the time-correlated data acquired in the regions of interest be reliably transmitted to ground stations at intervals whose position and length will be optimum from a standpoint of quantity and quality, and not interfere with the collection of data.

Fully real-time transmission of science data is not a primary requirement, and might, in fact, be a detriment if it were to be effected, since much data might be lost due to inavailability of ground stations for its reception and subsequent reduction. However, in concert with other objectives, the real-time transmission of scientific data on an "as required" basis is desirable, and will be considered in this study.

The principal objective of the telecommunications portion of the multiple satellite program study is to perform a parametric analysis of alternate methods to accomplish the scientific mission. To that end, this portion of the study concerns itself with data acquisition, tracking, and command. The following discussion assumes that the mission is accomplished by four satellites, of either the "radial" or "stacked" configuration. The orbit is assumed to be highly elliptical, with apogee at twenty earth radii.

6.1.1 Mission Requirements

Data Transmission Requirements. The primary requirement of the data transmission subsystem is to transmit all data efficiently, whether in real-time, or from storage. This implies that all data collected in one orbit period should be transmitted in one orbit and that the transmission should not interfere with data collection. This requirement is reflected primarily in the fact that the power needed to conduct experiments restricts the power available for data transmission. An assumed requirement on the communications subsystem is that the quantity and quality of data transmitted be maximized within the constraints imposed by other factors in the system design. One criterion for communication system design which derives from this latter requirement is maximization of the experimental data rate.

In addition to transmission of science and status data from individual satellites, attitude control data and command verification data must be transmitted from the satellite carrier module in real time.

A data transmission requirement that applies both to the satellites and to the carrier module is that the modulation, carrier frequencies, power levels, and data rates be compatible with the capabilities of the STADAN network.

Command Requirements. Individual satellites must be capable of receiving coded command signals from the ground to reset clocks, activate gates for the transponding of ranging signals, and a variety of other tasks. From the communication viewpoint, the primary requirements are that there exist adequate system margins to guarantee reliable reception of legitimate command signals and that the satellite receiver be compatible with the requirements of the STADAN network.

In addition to commanding the individual satellites, it is a requirement that the carrier module be commanded to effect attitude correction, boom deployment, and separation of the satellites from the carrier.

Tracking Requirements. One of the essential tracking requirements is that tracking measurements be sufficient in number and quality to define the orbit quickly and to an accuracy that permits execution of the maneuvers necessary for separation of the satellites from their carrier vehicle. A second requirement of particular importance in this multiple-satellite configuration is that the position of each satellite in space and with respect to each other be established with a high degree of accuracy in order to correlate the scientific data of each satellite with the position of the satellite at the time of data collection.

6.1.2 Constraints

Design constraints are of two types, extrinsic and intrinsic. The intrinsic constraints are those imposed by natural phenomena such as propagation losses, refraction effects, and noise environment. The extrinsic constraints are those imposed upon the system by considerations of such factors as ground station support time, the type of orbit, the maximum size weight and power allocated to the communication subsystem, and the characteristics of the ground station support.

Data Transmission Constraints. The primary constraints that apply to data transmission are:

a. Limited amount of time available because of ground station scheduling.

b. Limited data rate possible because of range at which transmission begins and power availability.

c. Limited flexibility in changing data rates because of added complexity and consequent system unreliability.

d. Limited interval available for data transmission because of satellite antenna coverage at lower altitudes.

Although the above factors are listed separately, they are interdependent, and will be treated as trade-offs in the material which follows.

Satellite Antenna Coverage Constraints. Aside from the fact that the physical configuration of the satellite antenna places restrictions on the coverage possible, the relationship between maximum realizable gain and broadest possible beamwidth results presumably in an optimum beamwidth. Due to the fact, however, that the spin-axis is tilted with respect to the orbit normal, this beamwidth places limits on where in the orbit earth coverage is adequate for data transmission. To minimize the effects of this constraint, the design recommends a beam-shaping approach, which appears feasible for the types of spacecraft antenna recommended.

Satellite Attitude and Separation Constraints. Because of orbital dynamics, the separation of the satellites tend to disperse as they approach the earth. In particular, in the region of the orbit below ten earth radii, which is the primary region for data transmission, the satellite separation exceeds the beamwidth of the ground-based antenna. Thus, simultaneous reception from two or more satellites is precluded, and, sequential access to the satellites is required. Since only one ground-based antenna for either S-Band or VHF is available at each site, the total amount of data that can be read out per orbit is restricted.

An additional constraint is placed on the design of the carrier module communications capability by the attitude of the carrier and by the particular carrier configuration under consideration.

For the "stacked" configuration, an essential requirement is to command separation near apogee. To achieve uniform azimuthal coverage in a plane normal to the spin-axis is desirable; however, this carrier module must also be accessible during the early stages of the coast phase in order to effect erection of the spin-axis normal to the orbital plane. This implies a constraint of not having deep nulls along the spin axis in the direction pointing towards earth.

In the "radial" configuration of the carrier module, the antenna beamwidth must be sufficiently broad to provide access by a ground-based antenna continuously throughout the "coast" phase. In particular, a uniform azimuthal pattern is mandatory to avoid signal degradation at the time of satellite separation.

6.1.3 Ground Network Capabilities and Constraints.

As stated earlier, one of the fundemental requirements of the proposed system design is that it be compatible with the configuration and capabilities of the STADAN network for the period 1970-72. Since the STADAN network is currently undergoing many changes, no planning document is available. The existing STADAN is a hybrid collection of a large variety of subsystems whose capabilities have been gleaned from the following documents:

a. NASA-GSFC Report X-530-66-33, "Space Tracking and Data Acquisition Network Facilities Report" (STADAN), December 1965.

b. NASA-GSFC Report X-560-63-2, "Aerospace Data Systems Standards," January 1963, Revised May 2, 1966.

c. NASA-GSFC Specification S-531-P-17, "Goddard Range & Range Rate System Specifications," Exhibit A, May 1966.

Since the first two of these documents apply generally to current configurations and requirements, and since the period of interest is 1970-72, these two documents have been used primarily for guidance. The Goddard Range and Range Rate (GRARR) specification, however, is a detailed specification of an integrated tracking telemetry and command ground support system for both S-Band and VHF, which is to be installed at major STADAN sites in the time period of interest. Also, the recommendation has been made by members of the advanced Development Division of the Tracking and Data System Directorate of NASA/GSFC that our design be based on the functional characteristics outlined in the GRARR specification.

The basic ground support system capabilities assumed to be available for this program will exist at the following sites:

- Rosman, North Carolina
- Tananarive, Republic of Malagasay

- Carnarvon, Australia
- Fairbanks, Alaska
- Santiago, Chile

The systems will operate in the following frequency allocations:

S-Band

Primary

a. Down-link: 2253 MHz
b. Up-link: 1800 MHz

Secondary

a. Down-link: 2243 MHz
b. Up-link: 1792 MHz

VHF

a. Down-link: 135-139 MHz
b. Up-link: 145-160 MHz

6.1.3.1 Receiving Capabilities. The characteristics of the Goddard Range and Range Rate Receiving system are treated in detail in Reference 1. Certain of these characteristics have been selected and are repeated here since they are directly pertinent to the discussion which follows.

Figure 6.1-1 is a block diagram of the multi-functional receiver assumed as part of the baseline ground support system. The receiver subsystem consists of the subunits:

a. VHF Preamp-Converter
b. S-Band Paramp Converter
c. Multicouplers
d. Multi-functional Receiver

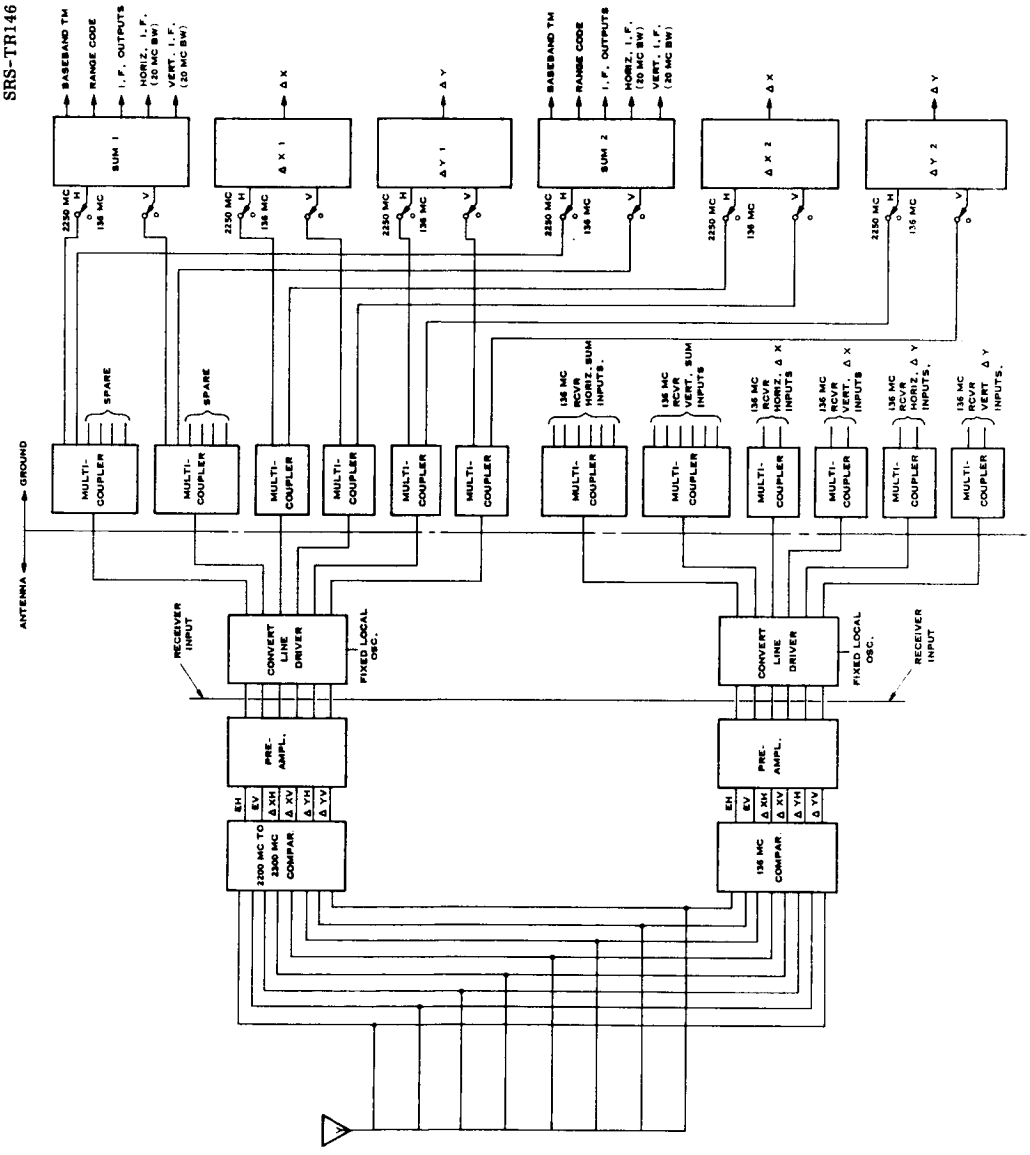

Figure 6.1-1 Multifunctional Receiver

6-7/6-8

e. Subcarrier Receiver (both VHF and S-Band)

f. Doppler Extractor and Digital Rate Aid Unit

6.1.3.2 Transmitter Capabilities. The ground transmitters projected to be available for the 1970-72 period are those specified in Reference 1 with the exception that 5 kilowatts of output power is assumed rather than the 1 kw or 10 kw noted in the above reference.

VHF Transmitter. The output bandwidth of the VHF transmitter is 2 MHz to the 3 db points over a tunable range of 145 to 160 MHz.

S-Band Transmitter. The output bandwidth of the S-Band transmitter is 10 MHz to the 3 db points over a tunable frequency range of 1750 to 1850 MHz.

6.1.3.3 Antenna Capabilities. The best available description of the ground support antenna capabilities projected for the 1970-72 period appear in Reference 1. The following capabilities have been selected from that source and are noted separately below since they are pertinent to the trade-off considerations which follow.

VHF Antenna. The VHF antenna is a 28-foot array of cavity-backed slots arranged in four quadrants for phase-monopulse tracking. It is capable of the simultaneous functions of transmitting, data reception and monopulse tracking. The antenna has an X-Y mount and is capable of being pointed at any point from 0 degrees above the horizon (except for keyholes) during tracking operations. The VHF antenna is a "leader" for the S-Band antenna or any other antenna at the site. When operating as a receiving array, the VHF antenna is a simultaneous lobing type, phase monopulse array with the following outputs:

a. Two sum channels

b. Two X-error channels

c. Two Y-error channels

TABLE 6.1-1

ANTENNA CHARCTERISTICS

	GRARR VHF Antenna	GRARR S-Band Antenna
Frequency		
a. Receive	137 ± 3 MHz	2200-2300 MHz
b. Transmit	148 ± 2 MHz (154 MHz Future)	1750-1850 MHz (1) 2090-2120 MHz (2)
Gain		
a. Receive	20 db (min.)	42.0 db
b. Transmit	20 db (min.)	41.5 db (1) 42.5 db (2)
Polarization	(Polarization tracking)	
a. Receive	Linear: Horizontal & vertical. Circular: Right & left hand. (simultaneous)	Linear: Horizontal & vertical. Circular: Right & left hand. (simultaneous)
b. Transmit	Linear: Horizontal & vertical. Circular: Right & left hand. (simultaneous)	Linear: Horizontal & vertical. Circular: Right & left hand. (simultaneous)
Coverage:	From 0° above horizontal	From 0° above horizontal.

(1) Goddard Range & Range Rate Transmit frequencies
(2) Apollo Unified S-Band Transmit Frequencies

TABLE 6.1-1

ANTENNA CHARACTERISTICS (Continued)

	GRARR VHF Antenna	GRARR S-Band Antenna
Beamwidth:	X = 18° nominal Y = 15° nominal (a function of polarization)	1.5°
Pointing Accuracy	1.0°	0.1°
Velocity	5°/Sec (Max.)	5°/Sec (Max.)
Accel.	5°-10°/Sec (Max.)	5°-10°/Sec (Max.)
Xmit. Power Capab.	15 kw, continuous	15 kw, continuous 20 kw, peak
Avail. Sites	Rosman, N. C. Fairbanks, Alaska Santiago, Chile Tananarive, Malagasy Carnarvon, Australia	Rosman, N. C. Fairbanks, Alaska Santiago, Chile Tananarive, Malagasy Carnarvon, Australia

S-Band Antenna. The S-Band antenna is a 30-foot diameter paraboloid reflector. The feed system is a cassegrain feed system and consists of a composite feed capable of transmitting and receiving in the 2 GHz band. The composite feed-horn accomplishes the following functions:

a. Transmits in the 1750-1850 MHz band.

b. Receives in the 2200-2300 MHz band.

c. Provides monopulse two-dimensional sum and difference information.

The antenna has an X-Y mount and is capable of being pointed at any point in the sky from 0 degrees (except for keyholes) during the tracking and transmitting operations. It is capable of the simultaneous functions of transmitting, tracking, and data reception. Table 6.1-1 summarizes the capabilities of both the VHF and S-Band antennas assumed available at STADAN in the 1970-72 period.

6.1.4 Other System Constraints

In addition to the constraints due primarily to equipment characteristics, there exist limitations primarily on the transmission of data due to:

a. Availability of ground stations during the period of data readout.

b. Ability to track only one satellite at a time due to ground antenna beamwidth.

c. Limited time for emptying satellite recorder contents during data transmission interval.

These and other considerations will be developed in the material which follows.

6.1.5 Tracking Considerations

The objective of the tracking system is to determine the location and motion of the carrier module and of the satellites, to rapidly define the orbits of the carrier module and each of the satellites, and to periodically update orbit parameters for time correlation of position information with scientific data. Updated tracking data is also required for programming of ground antennas prior to satellite pass. Within the STADAN network there are at least five available methods of tracking which might be used for this program. The characteristics of these methods are listed in Table 6.1-2, and are discussed in the following section.

The following tracking methods will be considered:

a. Minitrack
b. One- Way Doppler
c. Angle Tracking
d. VHF Goddard Range & Range Rate
e. S-band Range and Range Rate

Minitrack. Minitrack, which is one of the earliest tracking networks, was designed primarily for tracking satellites in low circular orbits. It operates on the principle of the radio interferometer which measures the angle between the observer's reference plane and the line from a reference point in this plane to the satellite. This measurement is based on the difference in arrival time of the wavefront from a distant point source at each of a pair of multiple pairs of antennas. These ground antennas are fixed, slot-type antennas precisely positioned geographically, and are linearly polarized.

The antennas are of two types: 1) a long baseline ("fine") type for highly accurate angle measurements, and 2) short baseline type for ambiguity resolution. The "ambiguity" antenna merely defines the particular wavelength received by the "fine" antenna. This system requires the use of only a simple beacon on the spacecraft to act as the point source, and therefore is very attractive as a possible tracking technique.

TABLE 6.1-2
TRACKING METHODS

Characteristics	Minitrack	One-Way Doppler (VHF)	VHF Angle Tracking	VHF-GR&RR	S-Band GR&RR
Ground Transmitter	None	None	None	5 kw	5 kw
Acquisition	Fixed	Manual (Satan)	Pre-Program	Pre-Program	Slaved to VHF
Tracking	Fixed	Automatic (Satan)	Automatic (Monopulse)	Automatic (Monopulse)	Automatic (Monopulse)
Operational Range	Limited due to 6.4 db ambiguity antenna gain	High elev. due to refraction effects	10^6 km at 1 watt	250,000 km	1,200,000 km
Accuracy	20 arc seconds	Depends on S/C oscillator stability (typical R=30 $\frac{met}{sec}$)	1.0 degrees	R = 50 meters R = 1 met/sec 0 = 1.0 degree	15 meters 0.1 meters/sec 0 = 1.5 arc minutes
Availability	Doubtful in 1971-72	Requires additional ground equipment	Scheduled for 1970-71	Scheduled for 1970-71	Scheduled for 1970-71
Satellite Equipment	Beacon	Stable Beacon	1 Watt Beacon	Cooperative Transponder	Cooperative Transponder
Simultaneous Ground Fixes	Unlimited	Unlimited	Unlimited	1	3
STADAN Compatibility	Yes	No	Yes	Yes	Yes
Integrated Command Capability	No	No	No	Yes	Yes
Polarization Divers.	No	Yes (Satan)	Yes	Yes	Yes
Polarization Tracking	No	No	Yes	Yes	Yes

The "fine" antenna array has a fan beam of 10.75 degrees in one direction and 76 degrees in the orthogonal direction. The ambiguity antennas have fan shaped beams of 78 degrees in one direction and 108 degrees in the orthogonal direction. The very low gain (6.4 db) of these ambiguity antennas is a limiting factor in their application to this design. Assuming the ability of the ground station to resolve a 136 MHz signal waveform to within 1 millimeter, by use of heterodyning and precision timing techniques, and assuming baseline lengths of 46 wavelength as listed in the STADAN facility report, establishes an angular resolution of 48 microradians. At 20 earth radii this corresponds to distances across the line of sight of approximately 6 kilometers. This accuracy is close to the maximum attainable, and ignores the degrading effects of ionospheric refraction. In addition, the accuracy of an angle measuring system suffers in highly elliptical orbits because of the great distances the spacecraft can move with little change in angle.

One-Way Doppler. One-way doppler is attractive as a tracking technique, because it too requires only a frequency-stable, low-power beacon on board the spacecraft. Theoretically, with perfect instrumentation and no atmosphere, the orbit of a satellite produces a unique time dependence of the doppler shift, and thus one should be able to determine the orbit from a single satellite pass, except for secular variations in the orbit. The accuracy of one-way doppler measurements is affected by two fundamental sources of error: oscillator instability and ionospheric refraction effects. Typical (one sigma) range rate accuracies at S-band measured over a 60-second sampling interval are 30 meters per second for short-term oscillator stabilities of 10^{-7}.

Errors due to ionospheric refraction effects contribute directly to range inaccuracies, and the refraction of radio waves by the ionosphere is an extremely complex subject. These refraction effects can be understood qualitatively by noting that the maximum slope of the doppler curve (Figure 6.1-2) is a rough measure of the slant range, and that refraction has a direct effect upon this slope. The effect of refraction is to decrease the slope and thus indicate an increased range due to ionospheric refraction. These ionospheric refraction effects are inversely proportional to transmitter frequency, and so, use of this technique at higher frequencies is to be preferred. The table below shows the deviations from the

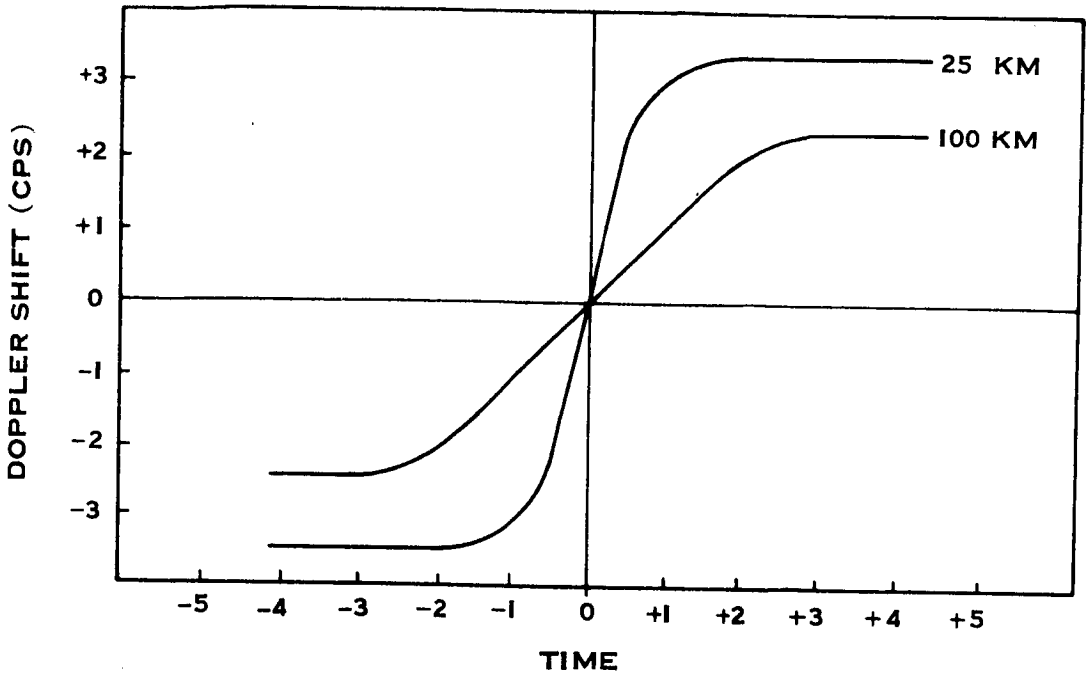

Figure 6.1-2 Refraction Effects on Doppler Shift

geometrical Doppler Shift for different transmitter frequencies assuming a high elevation, horizontal trajectory, straight-line propagation, and ± 5 km/sec satellite velocity component.[2]

Frequency (MHz)	Deviations due to Ionosphere (Hz)
100	± 2
400	± 0.5
1000	± 0.2
2000	± 0.1

A more practical constraint upon the use of one-way doppler measurements for orbit determination is the fact that since one-way doppler tracking is not presently employed in the STADAN network, instrumentation for its use in orbit determination is not presently available and would have to be provided at proposed ground sites.

Angle-Tracking. As is true for the interferometer and the one-way doppler tracking techniques, angle-tracking requires only a simple beacon on-board the spacecraft, and thus appears worthy of consideration in this study. An important difference between angle-tracking and the two-techniques considered thus far is that there will exist an angle-tracking capability as part of the STADAN facility in 1970-71. Angle-tracking as a distinct tracking mode is inherent in the Goddard Range and Range Rate System at either VHF or S-band. Figure 6.1-3 is a simplified functional block diagram of the GRARR S-band angle-tracking system.

In Figure 6.1-3, only the X-axis portion of the servo system has been shown, since the Y-axis is identical.

The S-band antenna is a 30-foot parabolic reflector mounted on an X-Y pedestal. A Cassegrain feed provides for amplitude comparison, simultaneous lobing, angle tracking. The received feed uses a 12-horn concentric ring, grouped into four quadrants to provide a sum and two error signals. The sum channel receiver phase-locks to the received carrier and generates an AGC voltage in the AGC detector. Two error channel receivers provide for the demodulation of two error signals. In the autotrack mode, the outputs of the two error receivers are connected to the servo amplifiers, providing for automatic angle-tracking of the received signal. A 16-bit angle encoder and line amplifiers are mounted on the antenna. The gated storage registers and code converters, which are in the instrumentation building, provide angle readouts in a binary coded decimal parallel form.

The VHF angle-tracking system is essentially the same as the S-band system except for the antenna and RF circuitry. The antenna is an array of crossed dipoles which generate a sum and two difference patterns, providing simultaneous lobing, angle-tracking. The tracking signals are amplified and converted to a 60 MHz I-F after which point the circuitry is the same as shown in Figure 6.1-3. The angle-tracking errors are of two major types: tracking errors and pointing errors. The tracking errors consist of servo errors, which cause the RF axis to shift from the line of sight, and boresight errors, which cause the optical axis and the RF axis to differ. The pointing errors determine the accuracy to which the true optical axis can be measured. The pointing errors are initial alignment errors,

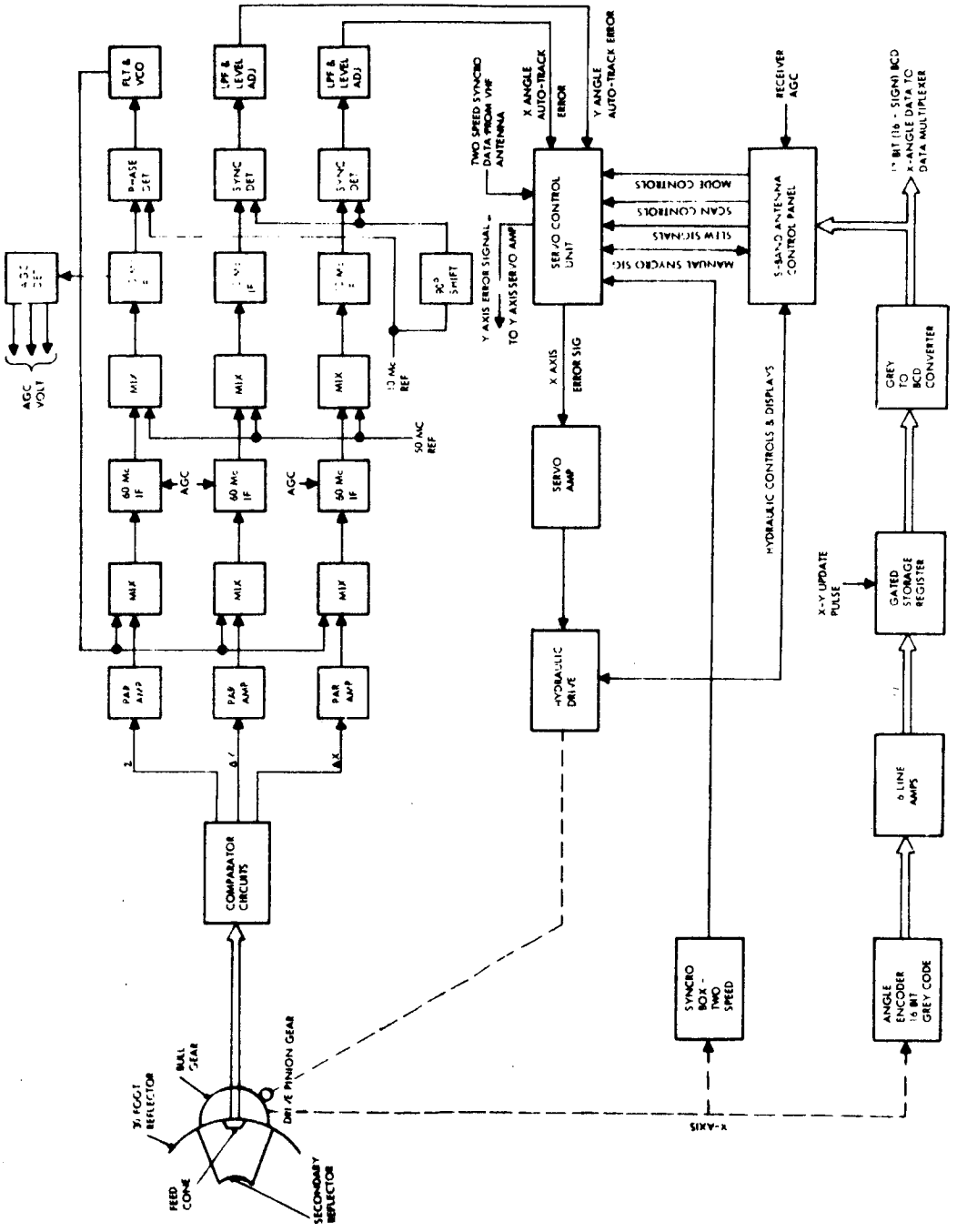

Figure 6.1-3 S-band Angle Tracking System, Simplified Functional Block Diagram

angle encoder errors, and mount alignment errors. Table 6.1-3 summarizes the errors and their sources for the S-band and VHF autotrack modes.

The values in Table 6.1-3 were taken from a design evaluation report[3] of the GRARR System, and may be considered typical of future system performance for comparative evaluation purposes. The different polarization errors for the two frequencies are due to the increased beamwidth of VHF over S-band, since this error is interpreted as 3 percent of the sum pattern beamwidth. The difference in collimation errors is due primarily to ionospheric refraction effects, and as noted earlier is approximately one order of magnitude worse for VHF than for S-band. The rms sum of the errors for the two systems evaluated here is, however, about five times less than the errors specified for those systems to be installed by 1970-71. We may, therefore, consider any design based on the specifications as conservative.

TABLE 6.1-3

ANGLE-TRACK ERROR BUDGET FOR VHF AND S-BAND

Error Sources	Typical Values (Sec) S-Band	Typical Values (Sec) VHF
Servo Loop Errors	54	54
Polarization	70	540
Mechanical and Electrical Feed Errors	47	51
Refraction	20	20
Multipath	32	3.34
Receiver Errors	68	46
Collimation Errors	39	360
RMS Sum	130	734

Goddard Range and Range Rate System. There exists a large amount of literature on the principles and performance of the Goddard Range and Range Rate System, and so its development and implementation will not be treated here in great detail. The obvious advantage of this sidetone rangine technique is the improved accuracy and flexibility of the system for orbit determination and satellite tracking. Table 6.1-2 contains a brief summary of the characteristics of both the VHF and S-band Goddard Range and Range Rate Systems. Figure 6.1-4 is a simplified block diagram of the GRARR system. Despite its operational advantages, the GRARR system suffers the disadvantage that in place of the simple beacon required of the systems considered earlier the GRARR system requires a cooperative transponder in the satellite. Spacecraft limitation on size, weight and power place severe restrictions on the degree of sophistication allowable for providing the tracking function. Fortunately, the GRARR system does not require the elaboration required of coherent turn-around ranging systems wherein the range data is demodulated to baseband and remodulated on the down-link carrier. In this system, range tones phase-modulate the up-link carrier to the satellite and are translated into a low I-F frequency in the satellite, and the entire up-link spectrum modulates the down-link carrier. In addition, the transponder can either time-share or frequency-share the up-and-down link for command and telemetry, providing an integrated tracking telemetry and command system. The size, weight and power penalty associated with the transponder is thus reduced, since a command receiver and telemetry transmitter would be required in any event.

Range measurements are made using basic sidetone ranging techniques and a hybrid combination of sidetones coupled with unambiguous coding techniques. In one mode, of system operation the S-band portion of the system is used to determine range, range-rate and angle data with the VHF system guiding the S-band antenna in the initial acquisition of the spacecraft. In another mode of operation, the VHF antenna sector scans until the VHF transponder carrier frequency is acquired by the VHF ground receiver. The VHF antenna then goes into the autotrack mode and range tones are applied to the up-link carrier. The VHF ground receiver then extracts range, range rate, and angle data.

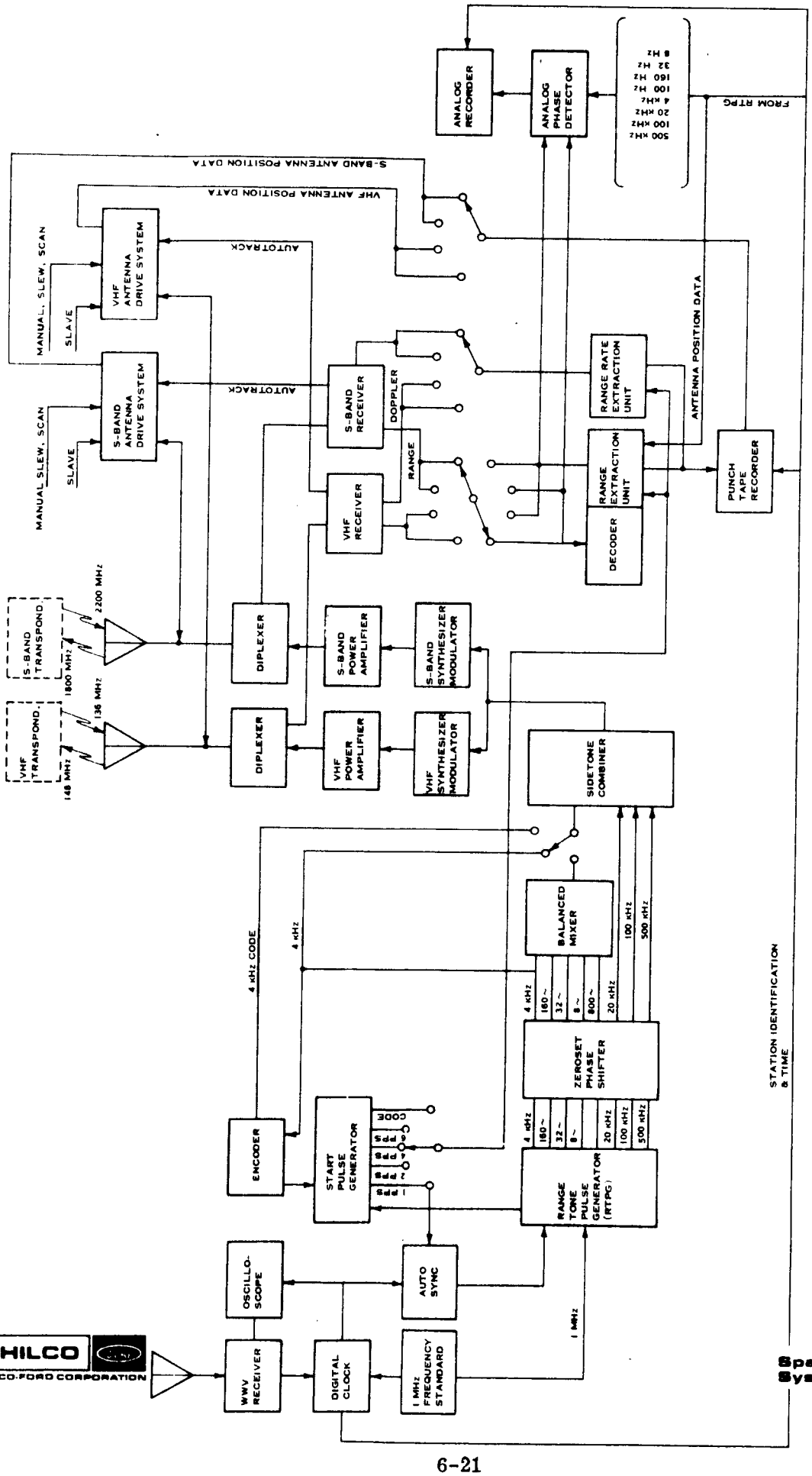

Figure 6.1-4 GRARR System Block Diagram

PHILCO
PHILCO-FORD CORPORATION

Space & Re-entry Systems Division

The fundamental differences between the S-band and the VHF system are:

a. The S -band system provides more accurate range, range rate and angle data.

b. The S-band system can be used to make simultaneous measurements from three ground stations, thus potentially giving a complete orbit solution from one observation interval.

The primary reason for the increased accuracy of the S-band system is that the rms range error is a function of the highest range tone frequency and of the S/N ratio as follows:

$$\sigma_R = \frac{0.056C}{f_R \sqrt{S/N}}$$

where σ_R = rms range error

C = velocity of signal propagation

f_R = highest range tone frequency

S/N = Signal to noise ratio in the tone isolation PLL

Figure 6.1-5 is a plot of the above equation for three range tone frequencies. Obviously, then, the higher the range tone frequency, the greater the range accuracy. The S-band system is designed to accommodate a major range tone of 500 kHz, while the VHF system, being bandwidth limited, can accommodate a highest range tone of only 20 kHz.

An outstanding feature of this system is that range rate measurements are made with all of the advantages of two-way doppler, but without the need for a coherent transponder. The reasons for this are basically that the doppler shifted signal received on the ground consists of a carrier whose frequency is $60(f_o + f_{od})$.

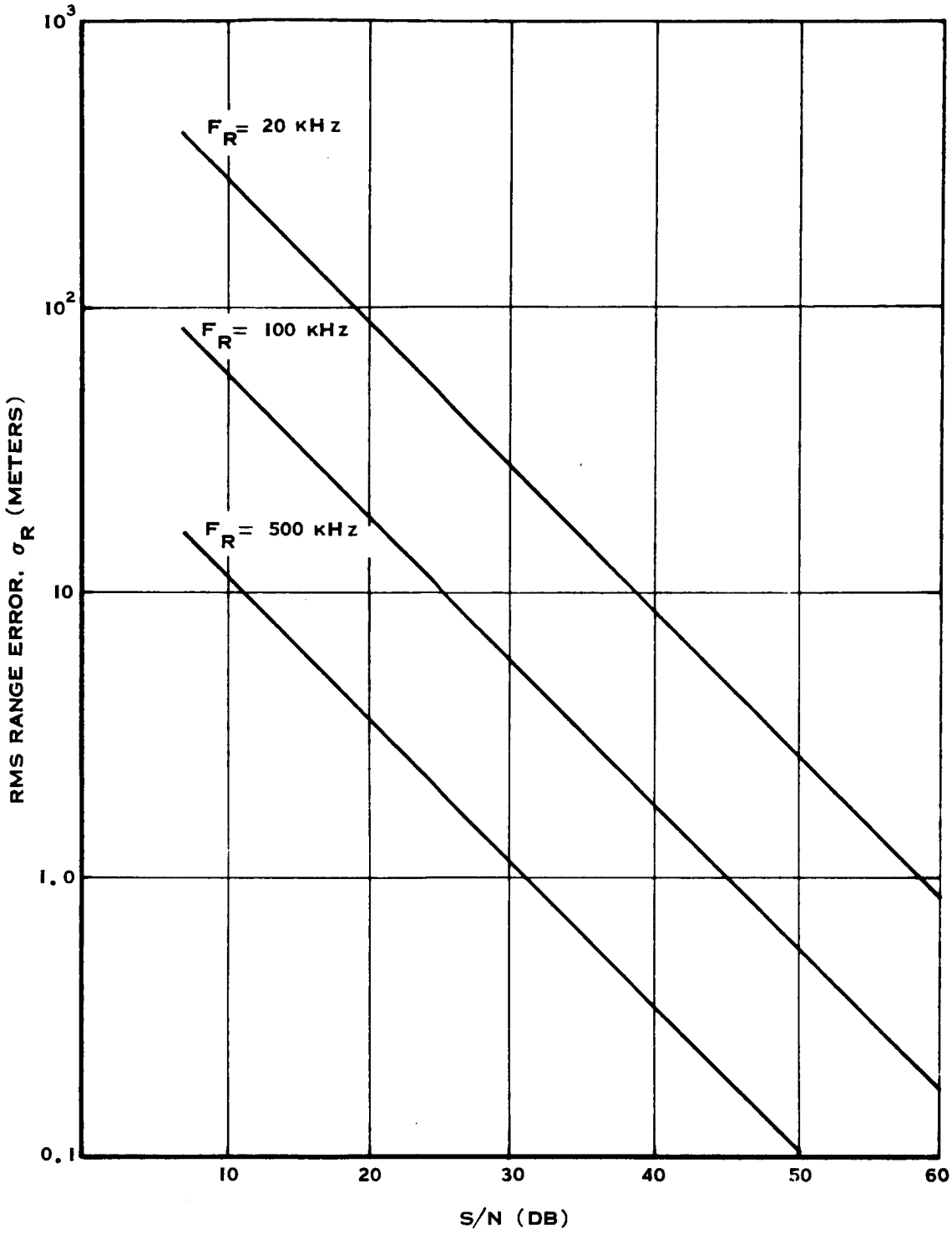

Figure 6.1-5 Range Error vs S/N in Range Tone Filter Bandwidth for Various Range Tune Frequencies

where f_o = transponder oscillator frequency

f_{od} = doppler shift on transponder oscillator frequency

and a subcarrier whose frequency is

$$80 (f_o t + f_{od}) - (f_{up} + 2f_{upd})$$

where f_{up} = up-link frequency

f_{upd} = doppler shift on up-link frequency

These two frequencies, along with a known transmitter frequency, $f_{up}/80$ are combined in a doppler extractor to give a suitably biased coherent two-way doppler shift signal of 500 kHz + $2f_{upd}$, thus yielding the necessary information for range rate determination. This process tends to cancel out the effects of oscillator instability in the transponder oscillator, provided that the instabilities are tracked by both carrier and sub-carrier phase-locked loops.

Preferred Tracking Alternatives. Based on the capabilities and limitations of the various tracking alternatives considered, use of the S-band GRARR system on each satellite is indicated. Based on the capabilities of the angle-tracking technique and on the constraints imposed by antenna and reliability considerations, use of the VHF angle-tracking system is indicated for the carrier module.

6.2 OPERATIONAL CONSIDERATIONS

6.2.1 Orbit Characteristics

The orbit of the multiple satellites is highly elliptical, with an apogee of 20 earth radii. For communication purposes the orbit may be visualized as shown in Figure 6.2-1. A unique feature of highly eccentric orbits is that during the

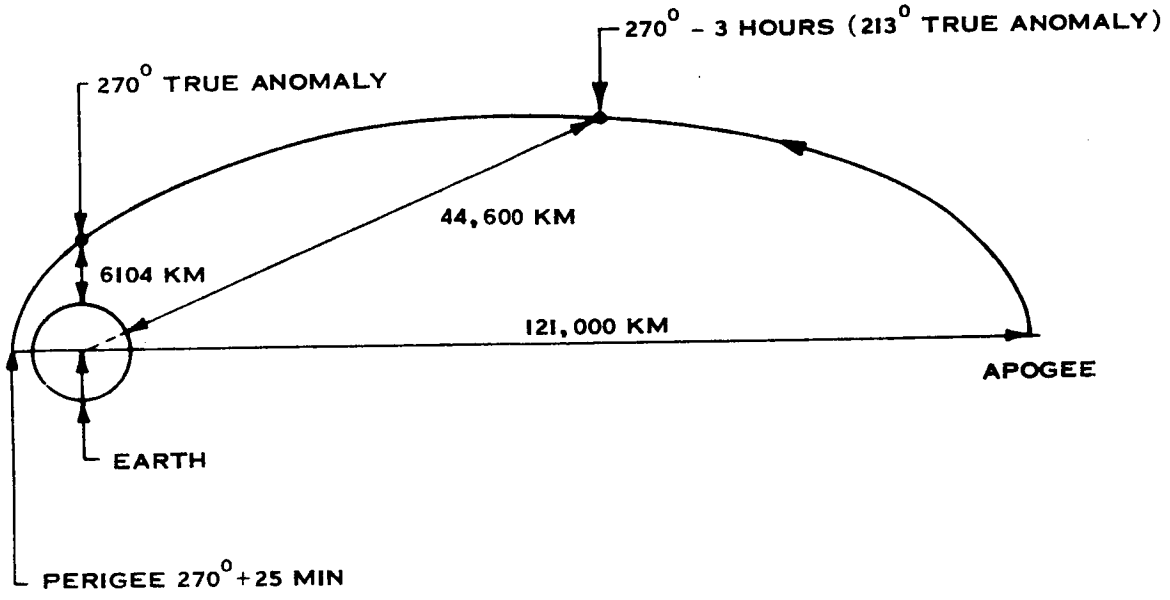

Figure 6.2-1 Distances to surface of Earth

interval of science data collection (beyond 10 R_e), the spacecraft moves very slowly; while near perigee the spacecraft velocity is so high that the time available for data transmission is very short. This circumstance is a fortunate one for collection of data, but an unfortunate one for data transmission.

If, for reasons of satellite antenna coverage, which will be developed later, it is assumed that transmission will occur between 10 R_e and 270 degrees true anomaly on the inbound leg and between 90 degrees true anomaly and 10 R_e on

the outbound leg, the maximum time available for transmission on either leg is as shown in Figure 6.2-2. Inspection of this curve indicates several interesting points. Since the slope of the curve decreases rapidly as we approach 270 degrees true anomaly, we rapidly run out of available time; so, one should prefer to begin data transmission as soon as possible after 10 R_e has been reached. Although transmission at ranges beyond 10 R_e is assumed unavailable, it is apparent from Figure 6.2-2 that the time parameter is much less constraining in this region.

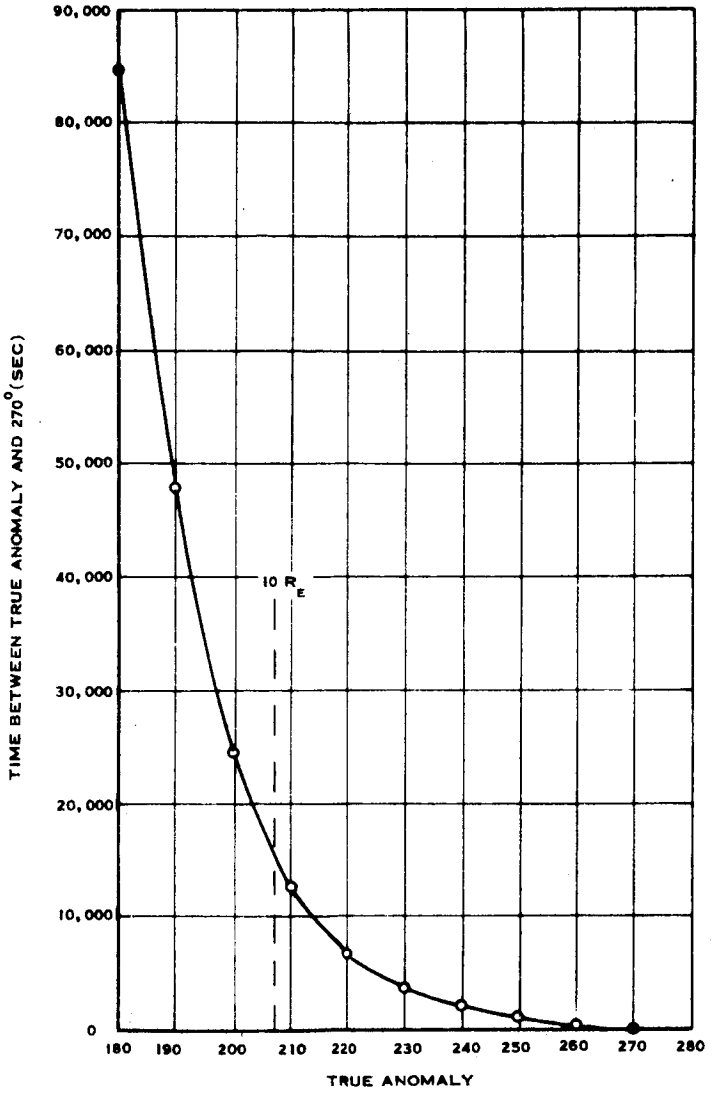

Figure 6.2-2 Transmission Time Available vs True Anomaly

Another consideration of importance in planning for the optimum point in the orbit at which to begin transmission is the data rate. Figure 6.2-3 is a plot of maximum possible data rate as a function of true anomaly based on the assumption of a two-watt, S-Band satellite transmitter, and on the assumption, as before, that transmission occurs on the inbound leg of the orbit. As expected, the allowable

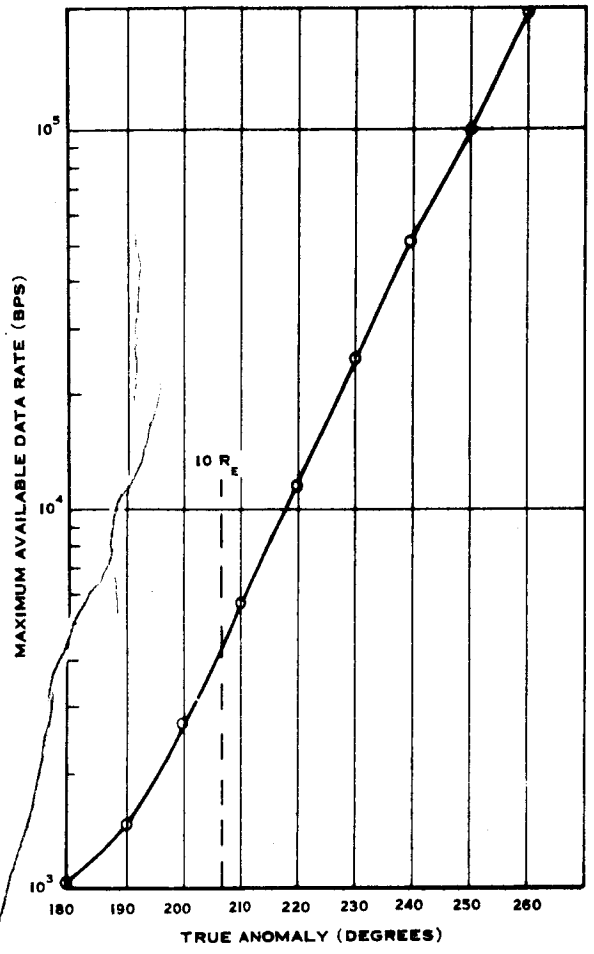

Figure 6.2-3 Maximum Available Data Rate vs True Anomaly for 2-Watt, S-band Satellite Transmitter

data rate under fixed power conditions increases as the spacecraft approaches the earth. The indicated preference, based on this consideration, then appears to be to transmit closer to earth, thus taking advantage of the increased allowable data rate. This is in contrast to the preference based on "time" considerations.

A third, and more meaningful, criterion on which to base the system design is the total amount of data read out. This is simply the product of the available time and the available data rate. Figure 6.2-4 is a plot of total data read out as a function of position in orbit based on the assumptions stated earlier. From this plot it is apparent that there is an optimum position in the orbit to begin data transmission.

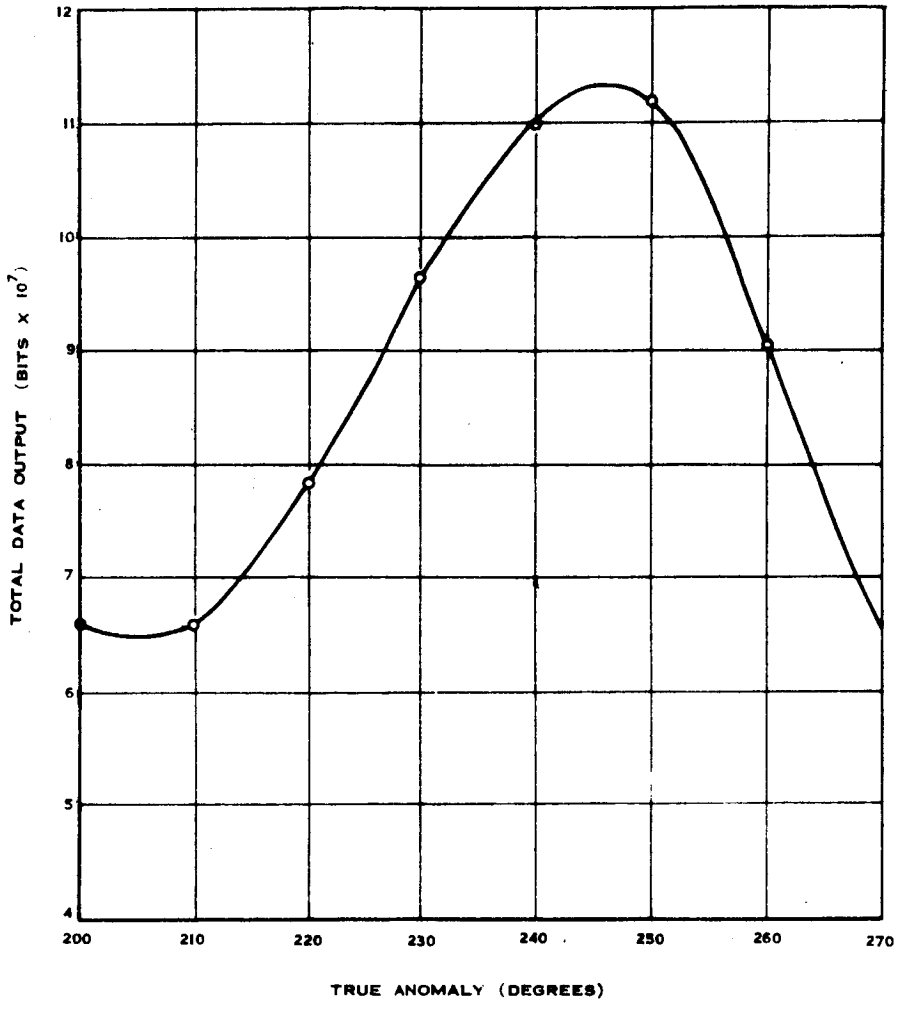

Figure 6.2-4 Total Data Readout vs Position in Orbit

The results of this curve must be interpreted with some caution. From Figure 6.2-4 it appears that it is possible to transmit a maximum of 11.4×10^7 bits of data. Practical tape recorder capacities are well below this limit; thus, the full capability of the transmission system, based on this criterion can not be realized. In addition, it must be borne in mind that although the four satellites are widely separated in space in this orbital region, the time separation between satellites is essentially constant throughout the orbit. Table 6.2-1 below indicates the separation in time between the first and last satellites for various passes.

TABLE 6.2-1

TIME SEPARATION ALONG ORBIT PATH
BETWEEN FIRST AND LAST SATELLITES

Orbit Pass Number	Time Separation (Sec)
0	240
10	440
30	840
60	1640
90	2040

For example, if based on Figure 6.2-4, one would initiate transmission at 245 degrees true anomaly (optimum point) and transmission would continue at the maximum allowable data rate of 70,000 bits per sec.; and, assuming a recorder capacity of approximately 4×10^7 bits, the remaining satellites would have passed the point in the orbit which would permit total recorded data read out.

Simultaneous Vs. Sequential Readout.

Alternatively, if all four satellites could transmit simultaneously, this criterion could be used effectively to define transmission scheduling and data transfer rates. A first consideration is the capability of the ground support network. As noted

above, simultaneous reception of two spacecraft on separate frequencies can be accommodated by the ground receiver. Thus, assuming the existence of only one S-Band antenna, and assuming that at least two spacecraft are within the beam of this antenna, simultaneous reception of, at most, two satellites is possible.

To establish the feasibility of tracking two or more satellites simultaneously, an investigation of intercepted arc lenght along the orbit and satellite separation as a function of position in orbit was initiated. Figure 6.2-5 shows the arc length

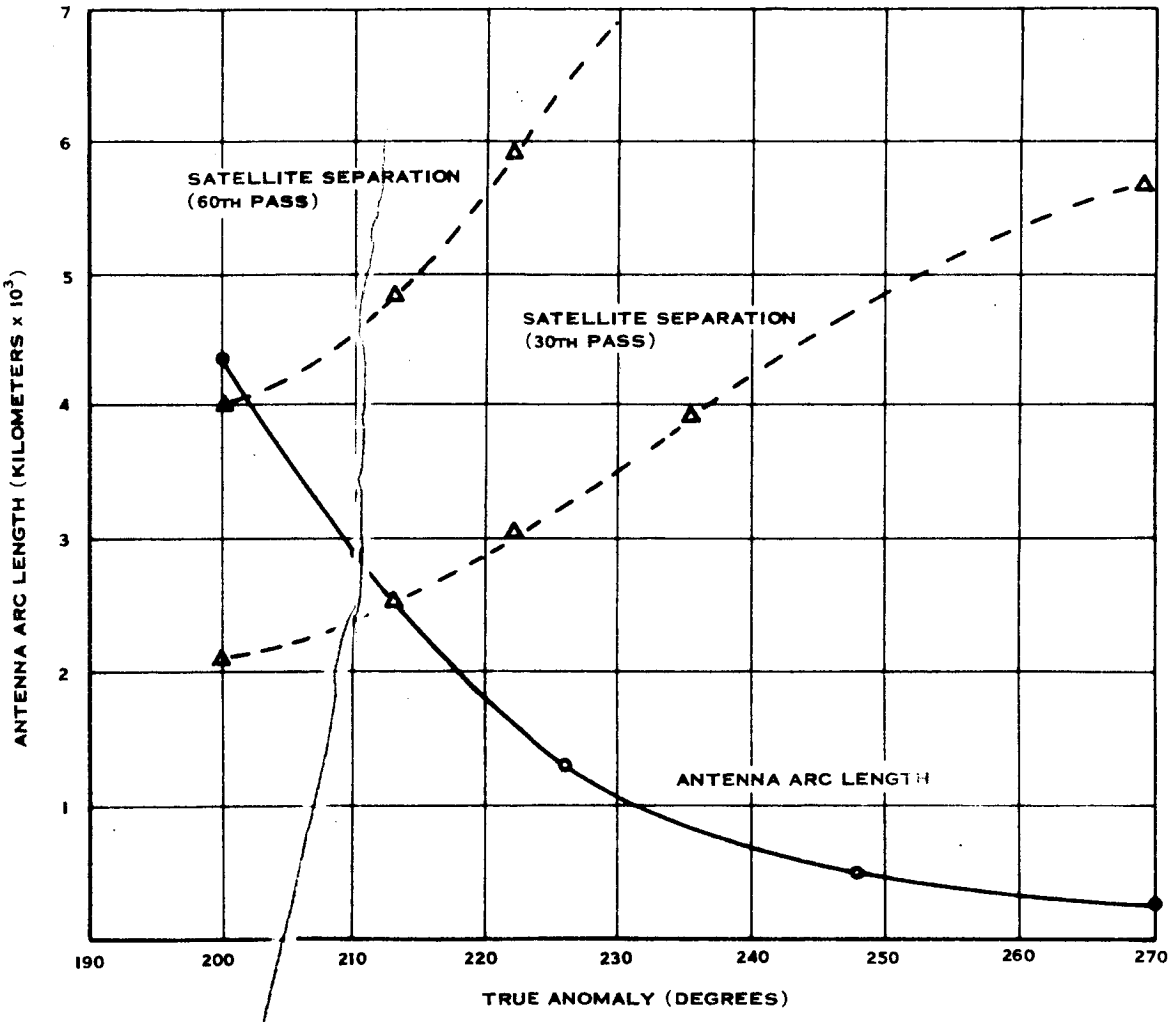

Figure 6.2-5 Interception of Satellite Pairs by 30-Foot Parabolic Antenna

intercepted by the antenna beam of the S-Band 30-foot parabolic antenna as a function of true anomaly. The values for this curve were computed on the basis of a simplified model (Figure 6.2-6), which assumed that the minimum antenna elevation angle was 5 degrees above the horizon, and that antenna beamwidth was 1.5 degrees. The arc length was computed for elevation angles of 5, 30, 60 and 90 degrees. Since in the region of interest the arc length changes only slightly (± 5 percent) as a function of elevation angle, a mean value of arc length for the several elevation angles was plotted in Figure 6.2-5 as a function of true anomaly.

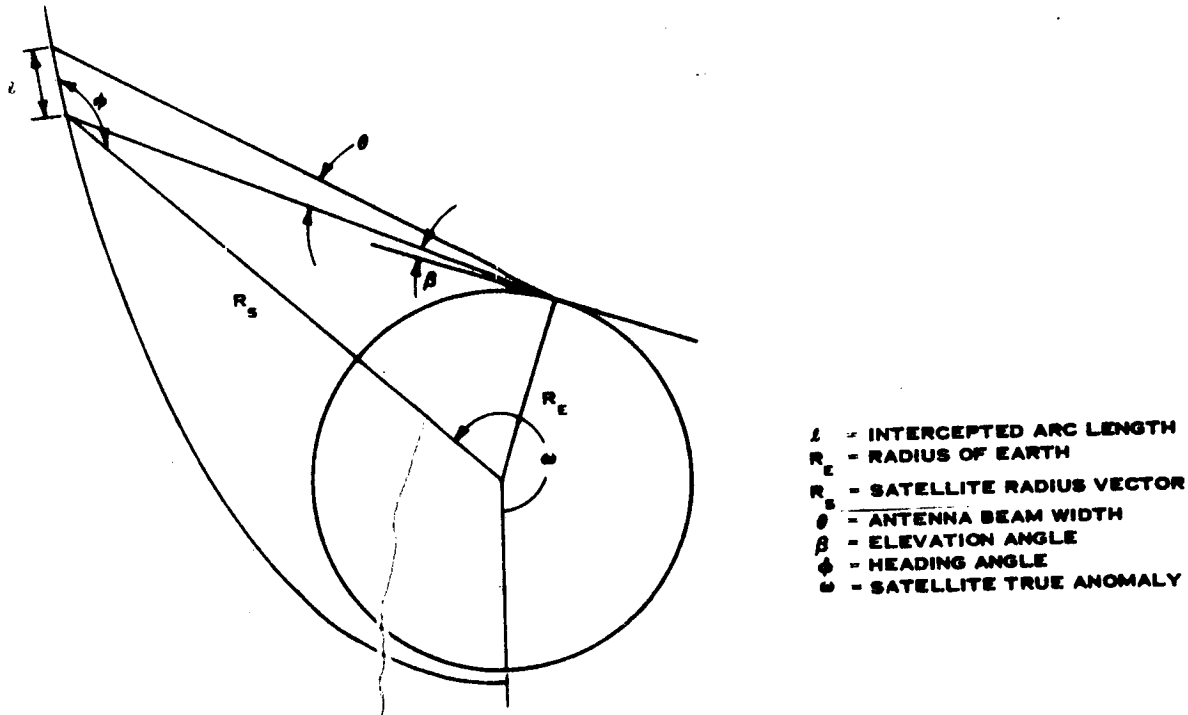

Figure 6.2-4 Model of Ground Antenna Coverage

Knowing the arc length is equivalent to knowing the permissible separation of satellites for simultaneous antenna access, and so the separation of satellite pairs was plotted as a function of true anomaly for the 30th and 60th passes. It is clear from Figure 6.2-5 that for values of true anomaly greater than those where the satellite separation exceeds the antenna arc length, access to a pair of satellites is not possible. Since for even the 30th pass (2 months in orbit) the separation exceeds the antenna beamwidth for values of true anomaly greater than about 213 degrees, simultaneous communication with satellite pairs is

impossible with a single antenna. Further, the situation deteriorates with time as can be seen from the separation curve for the 60th pass. The data from which these separation curves as plotted includes the effects of a composite 5-degree error. The conclusion to be drawn from these curves is that since each ground station has but one S-Band antenna, the satellites must be accessed sequentially.

6.2.2 Scheduling of Ground Equipment

Since it has been established that sequential transmission from each satellite is required, the scheduling of transmissions in some optimum manner is required. This scheduling on a sequential basis assumes the following factors.

a. Single station contact of three hours per day for all four satellites is available.

b. Pre-pass programming and postpass calibration are included in the ground support time.

Based on these assumptions, one-half hour per satellite of transmission time is assumed, therefore, as a baseline. This allows 15 minutes per satellite for station preparation. With few exceptions, this constraint is reflected in the development which follows.

6.2.3 Modulation

The type of modulation to be used for transmission of serial PCM data from the satellite to ground has a significant influence upon the final value of the RF parameters of the telemetry system and consequently upon the final design of the telecommunication subsystem. The choice of modulation is based upon a minimum number of significant criteria.

a. The system must be efficient. In terms of the type of modulation, this means that some measure of modulation efficiency must be optimized.

b. The satellite subsystem must be compatible with existing ground facilities. In terms of the modulation technique to be employed by the satellite telecommunication subsystem, this means that the type of modulation employed must be compatible with the ability of STADAN ground stations to satisfactorily demodulate the received signals.

For purpose of comparing modulation types, we shall assume that the TCM subsystem transmits a serial stream of binary PCM data, thus ruling out consideration of M-ary systems, where the data waveform has more than two levels. We shall also assume, for purposes of comparison, that all systems transmit information at the same rate. The performance of all systems will be given as a function of the signal energy per bit per one-sided noise spectral density, $\frac{E/n}{N_o}$. This parameter is related to the more familiar average signal-to-noise ratio (S/N) by the relationship

$$\frac{E/n}{N_o} = \frac{S}{N} \text{ (TW)}$$

Where, n = 1 (binary coding)
T = Bit length in seconds
W = Receiver bandwidth (equivalent noise bandwidth in H_z)

We shall further assume the performance of systems in the presence of gaussian noise into the receiver, usually a justifiable assumption for most radio links.

Carrier vs. Subcarrier. One of the first considerations concerning the type of modulation is whether the PCM data from the telemetry subsystem should modulate the carrier directly, or whether the data should modulate one or more subcarriers which in turn modulate the carrier.

Relative to the criterion of efficiency, a comparison of subcarrier and non-subcarrier systems is given in Table 6.2-2. Based on the assumptions listed earlier, we can compare the efficiency of the two system types in terms of the required E/N_o for some fixed P_e and for an optimized ρ, correlation coefficient between two possible transmitted waveforms. In Table 6.2-2, $P_e = 10^{-5}$, but the results for other error

TABLE 6.2-2

CARRIER VS SUBCARRIER SIGNAL ENERGY REQUIREMENTS

Type of Modulation	Type of Detection	Required E/N_o (db) for $P_e = 10^{-5}$	
		Non-Sub Carrier	Subcarrier*
PCM/PM	Matched Filter	9.6	11.1
PCM/PM	Phase Comparison	10.3	12.0
PCM/PM	Discriminator	11.2	12.9
PCM/FM	Matched Filter	11.8	13.5
PCM/FM	Discriminator	12.5	14.2
PCM/FM	Envelope Detect	13.3	15.0
PCM/AM	Matched Filter	12.6	17.3
PCM/AM	Envelope Detect	12.9	17.6

*Note: All subcarriers are either PM or FM.

rates show the same trend; namely, that for all of the types of modulation shown, and for all the types of detection shown, there is a significantly higher required E/N_o for subcarrier systems than for systems where the carrier is modulated directly. Further, the validity of this conclusion is even more graphically displayed in Figures 6.2-7 and Figure 6.2-8, where P_e is plotted as a function of required E/N_o for subcarrier and non-subcarrier systems.

With regard to the second criterion, compatibility of STADAN networks to demodulate direct carrier modulated signals, Figure 6.2-9 is a much simplified system block diagram illustrating the use of the primary Goddard Range and Range Rate receiving system supplemented by a phase-lock demodulator such as the ELECTRAC 215C, but modified to accept a 10 MHz I-F input signal. The PCM data handling equipment shown could be similar to the Magnavox PCM/DHE which is presently available at

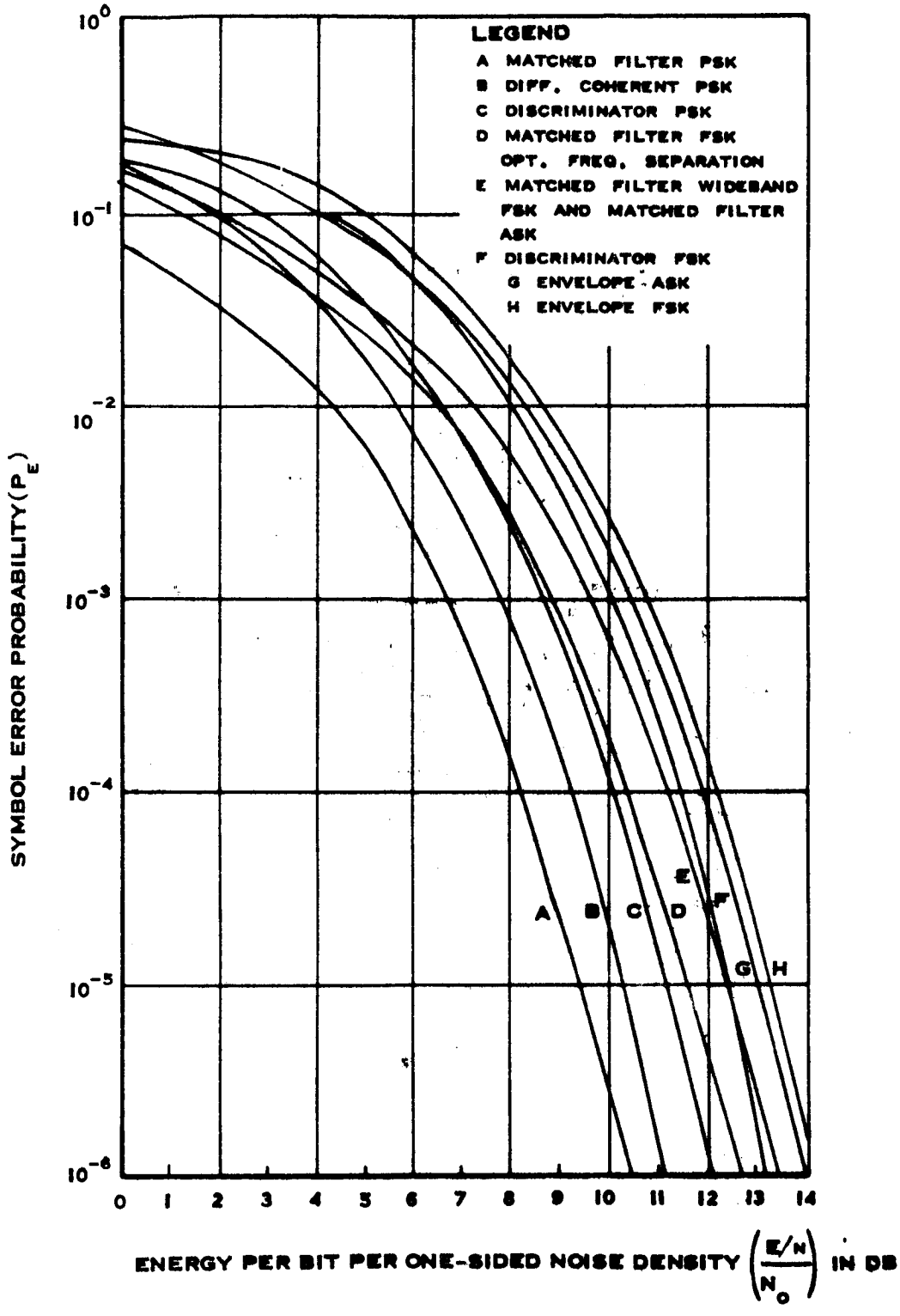

Figure 6.2-7 P_e for Non-Subcarrier Binary Systems

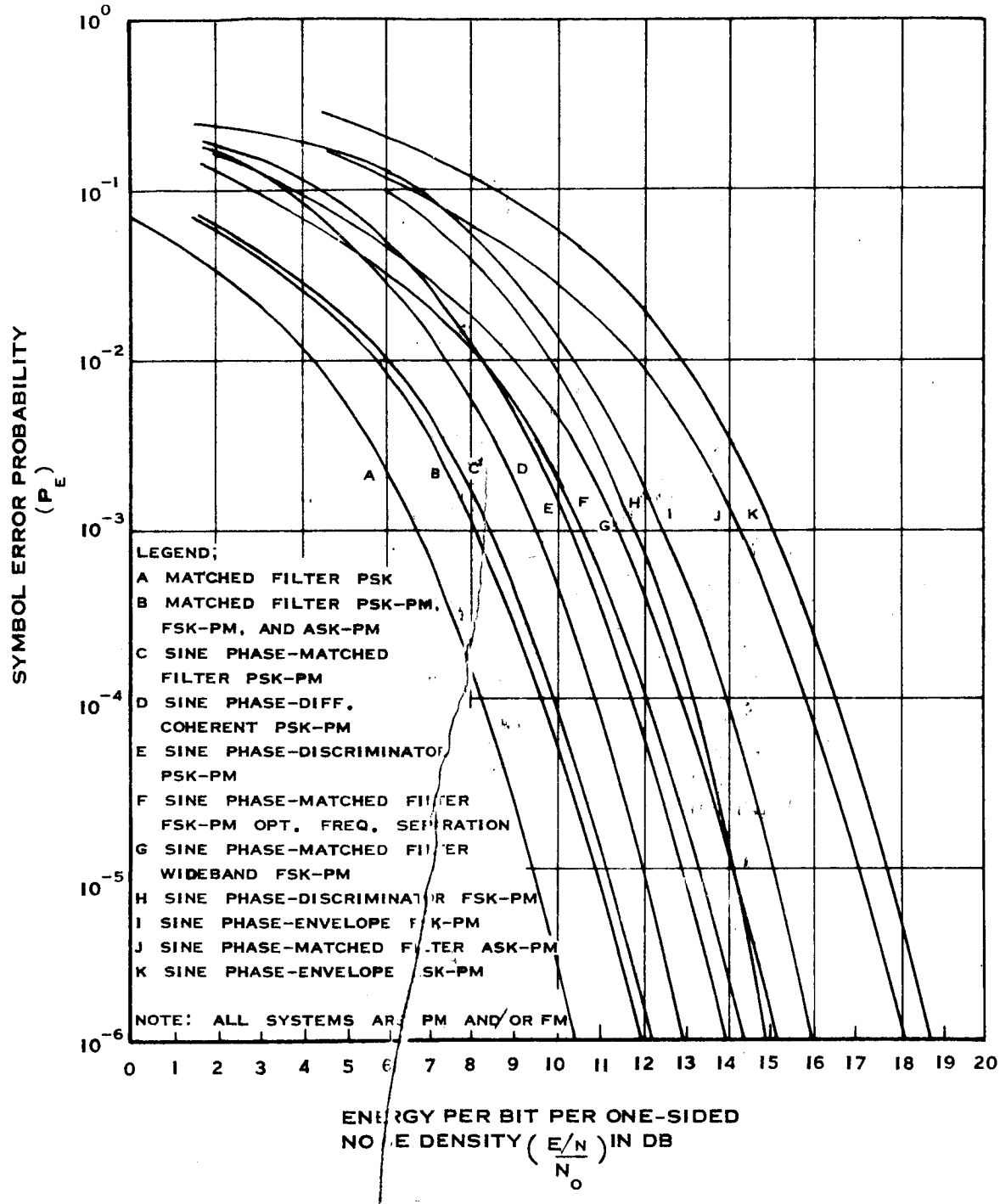

Figure 6.2-8 P_e for Subcarrier Binary Systems

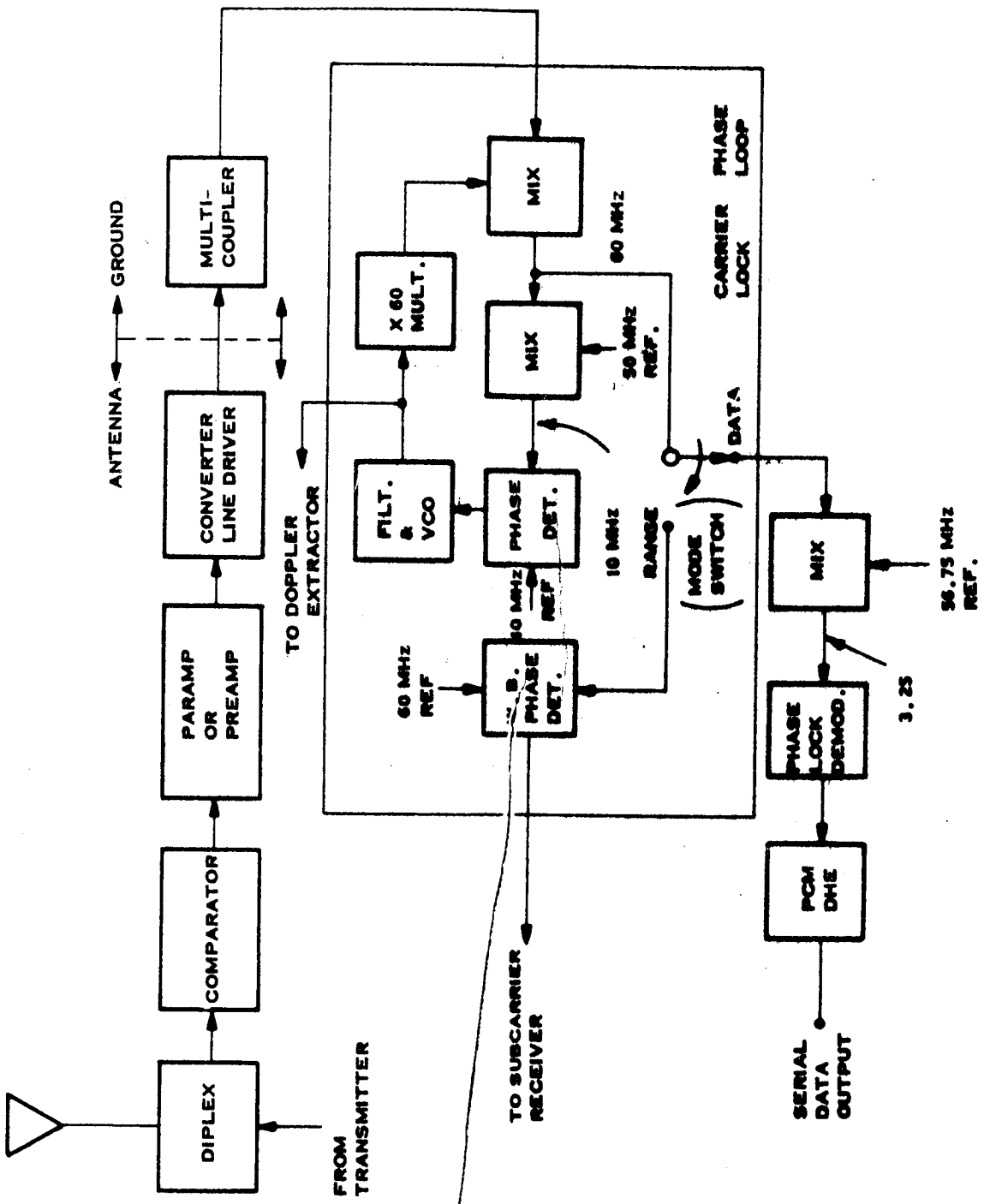

Figure 6.2-9 S-Band Range Rate System in Primary Receiving Mode

three of the five planned GRARR sites. PCM/DHE capabilities are planned for installation at all STADAN sites by 1969.

There is, however, one caution which must be observed when advocating PSK, bi-phase modulation of the carrier, and that is to avoid complete carrier suppression by an appropriate choice of modulation index at the telemetry-transmitter. Part III of "Aerospace DATA SYSTEMS STANDARDS," prepared by NASA/GSFC and dated November 4, 1965 states, that STADAN network stations are not currently equipped for PSK (± 90 degrees) bi-phase demodulation, and to avoid carrier suppression, at least 10 percent of the total transmitted power shall be left in the carrier. This will be accomplished by shifting the phase of the carrier a nominal ± 70 degrees, which permits coherent detection, and which permits transmission of ample carrier power for faithful lock-on and tracking of the carrier by the ground receiver.

In the two-stage process of modulating subcarriers, which when added together modulate the carrier, one is generally interested in providing a relatively small number of channels where the ability to separate the channels is of significance. For small satellites, frequency division multiplexing does not provide the user with equipment which easily allows for efficient changes in channel bandwidth. Greater flexibility and simpler equipment results when time division multiplexing is used. For these reasons then, the choice for this system was one wherein the carrier is directly phase modulated, and where the channel bandwidth varies as a function of the data rate.

Type of Modulation. In space communication systems, primary emphasis is placed on frequency or phase modulation methods, because of the inherent efficiency of these methods when proper design approaches are used. From the standpoint of efficiency, reference is again made to Table 6.2-2. It is apparent that, under the assumptions of optimum choice of modulation indices, PCM/PM is superior to PCM/FM.

Comparison of relative system performance with an absolute standard is not easily done using only bit probabilty of error as a criterion. However, Hancock[4] uses Shanmon's formula for channel capacity

$$C_c = W_c \log_2 \left(1 + \frac{S_{in}}{N_{in}}\right)$$

$$= W_c \log_2 \left(1 + \frac{S_{in}}{2 W_c}\right)$$

or $$\frac{C_c}{W_c} = \log_2 \left[1 + \frac{\beta}{2} \left(\frac{C_c}{W_c}\right)\right]$$

where $$\beta = \frac{S_{in}}{\epsilon C_c} = \frac{E_{min}}{\epsilon}$$

E_{min} = minimum received signal energy required per bit of information

S_{in} = required input signal power

C_c = channel capacity (bits/sec)

W_c = channel information bandwidth

ϵ = noise power spectral density (assumed Gaussian)

to derive an often used measure of system efficiency in terms of the minimum received signal energy per bit of information. A plot of β as a function of P_e is shown in Figure 6.2-10. From this curve we see that in the region of most interest (low P_e) phase-modulated systems are superior to frequency modulated systems for binary transmissions.

Modulation Index. As we stated earlier, direct bi-phase modulation (± 90 degrees) of the carrier is not feasible, since the attendent carrier power reduction prevents coherent detection of the signal unless carrier reconstruction is effected at the ground sites. To avoid this difficulty and to avoid the complexity and inefficiency of data modulation of a subcarrier, the modulation index is chosen so that there will remain sufficient carrier power to effect coherent detection on the ground.

The signal-to-noise output in terms of peak modulation index for a coherent demodulator operating in white Gaussian noise is given by:[5]

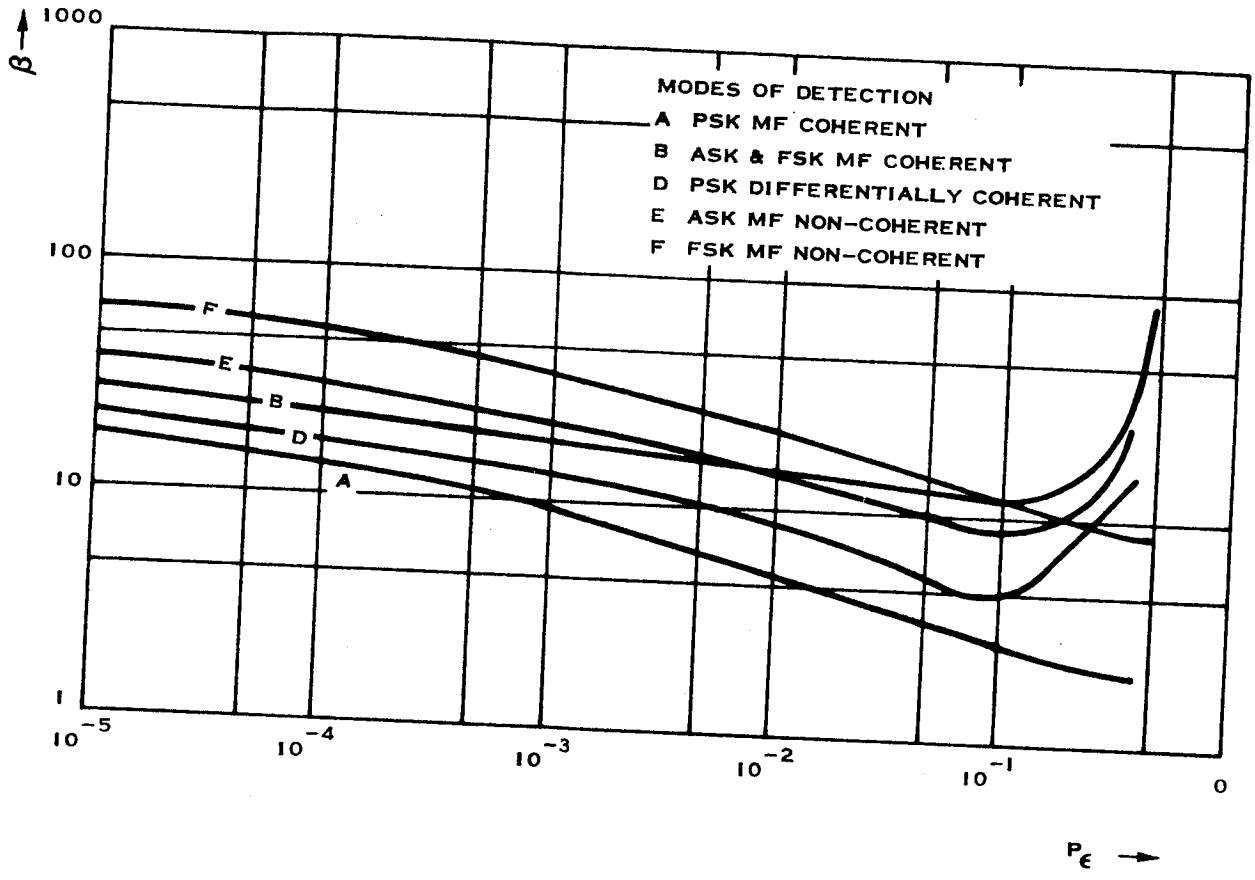

Figure 6.2-10 Comparison of Binary Systems on a β Factor Basis

(1)

$$\frac{S}{N} = \frac{S_r T_b}{N_o} \left\{1 - \cos \left[2 \phi m (t)\right]\right\}$$

where

$S_r = \frac{E^2}{2}$ (average received signal power)

T_b = Bit time in (seconds)

N_o = Noise power spectral density

ϕ = Peak modulation index (radians)

$m(t)$ = Modulation function (0-1)

It can be seen from the above equation that the optimal value for ϕ is $\pm$(90 degrees). If a modulation index of $\pm$ (70 degrees) is used, the system suffers a degradation of 0.54 db, which is insignificant when compared to the use of subcarrier phase reversal where, for an optimized carrier modulation index, the best performance is at least 1 db worse than for direct carrier phase modulation. Figure 6.2-11 shows the additional carrier power required relative to carrier phase reversal for two types of subcarrier demodulation.

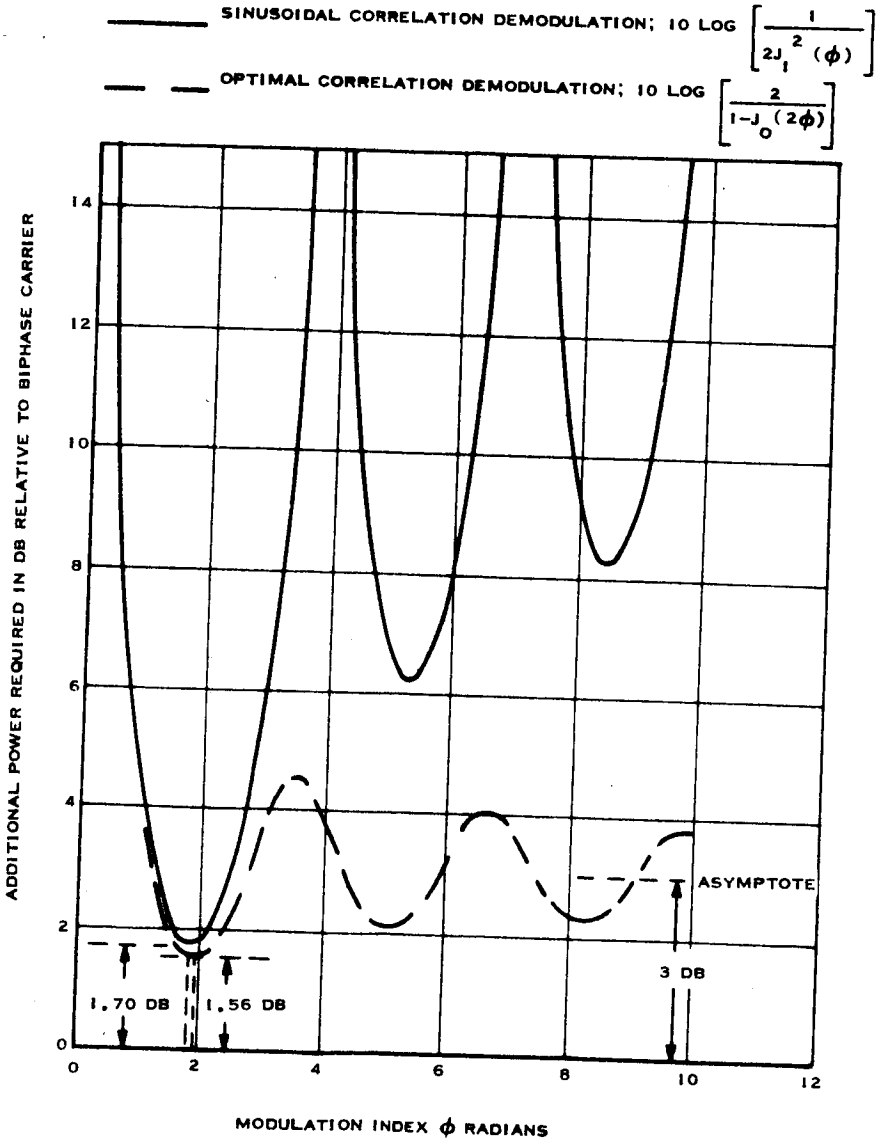

Figure 6.2-11 Comparison of Subcarrier Binary Phase Modulation for $m(t) = \sin\omega t$ and Carrier Binary Phase Modulation

Viterbi[6] has shown that the performance of a coherent demodulation process is strongly influenced by the form of the modulating spectrum as well as by the modulation index. The output SNR depends upon the SNR in the modulating spectrum, and is shown graphically in Figure 6.2-12 as a function of α for various n:

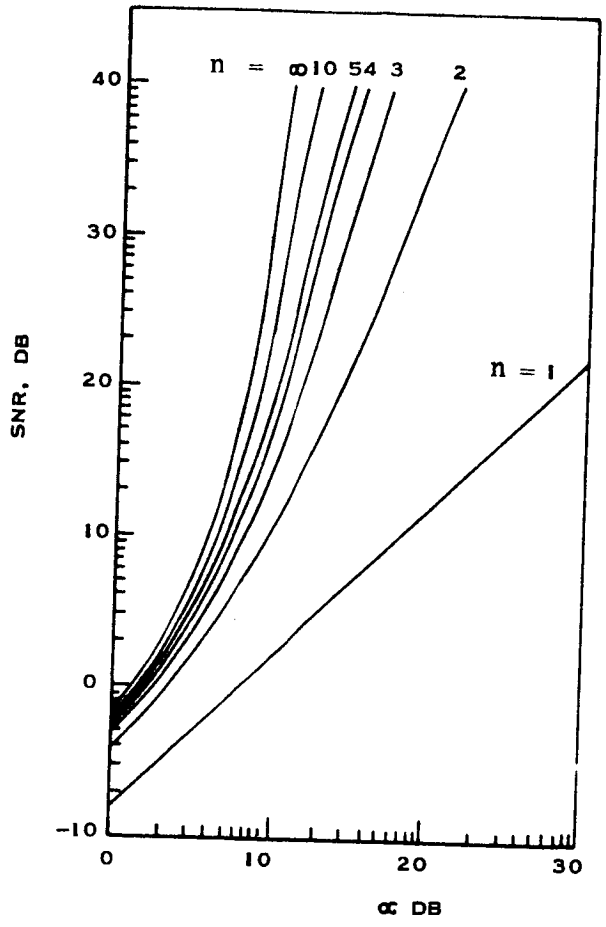

Figure 6.2-12 SNR for Optimized Phase-Modulation Receiver

where

$$\alpha = \frac{\sigma^2}{e\sigma^2} \quad \frac{A^2}{N_o B}$$

σ^2 = phase error in Phase Locked Loop.

$\left[\frac{A^2}{N_o B}\right]$ = channel SNR in the modulation bandwidth.

2n = order of the polynomial representing the modulation process.

For a given value of SNR in the modulation bandwidth, $\left[\frac{A^2}{N_o B}\right]$, equation (2) relates the modulation index Km (radians/volt) to the parameter α, defined above.

(2) $$\frac{Km^2}{\sigma 2} = \frac{\left(\frac{\alpha}{\pi} \sin \pi/2n + 1\right) - 1}{\alpha \left(\frac{\sin \pi/2n}{\pi/2n}\right)}$$

For large n, the above relationship is approximately:

$$\frac{Km^2}{\sigma 2} \approx \frac{e^{\alpha} - 1}{\alpha}$$

Thus, the larger the data rate, and consequently the modulation bandwidth B, the greater should be the modulation index. At short transmission ranges where the output SNR increases, and where larger data rates can be accommodated, modulation index should be increased accordingly for an optimized transmission link design.

6.2.4 Data Transmission

It was established in Section 6.2 that due to the orbital dynamics of the satellites and to scheduling constraints, a baseline of one-half hour per satellite of transmission time would be assumed. In addition, NASA/GSFC has recommend that S-band be preferred for telecommunications support. As shown in the link analysis studies, operation at S-Band has an advantage in link capacity over VHF. Figure 6.2-13 shows the data rate as a function of range for S-band and VHF links.

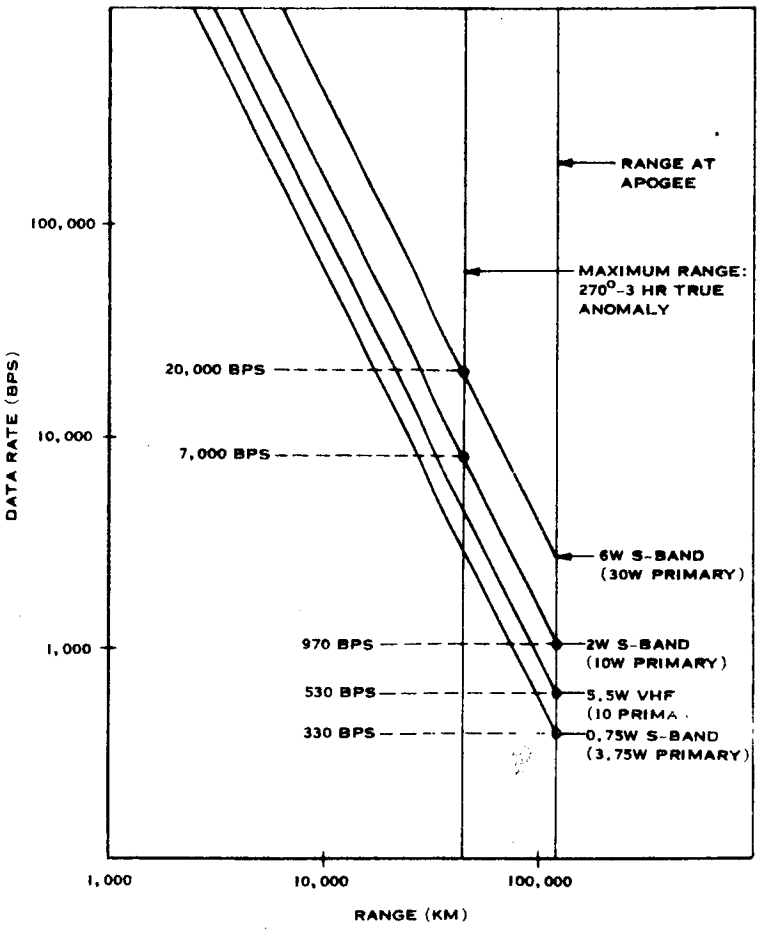

Figure 6.2-13 Data Rate vs Range for Various Transmitter Powers at S-band and VHF

If we allocate 30 minutes per satellite of transmission time plus an additional hour for set-up, reacquisition, and postpass calibration, then a total of three hours operational time is required from the STADAN network for all four satellites during each orbit. Thus the network can usually be scheduled as a single three-hour

operation without interruption from a single station. We choose a minimum satellite altitude of 6100 kilometers which corresponds on the inbound leg to 270 degrees true anomaly. A smaller altitude is undesirable due to increasingly large tracking rates and reduced station coverage. The maximum range of 44,600 kilometers is equal to 213 degrees true anomaly. This maximum range corresponds to a three hour transit time on the inbound leg from 213 to 270 degrees true anomaly.

Figure 6.2-14 shows earth coverage for the five GRARR stations at Carnarvon, Fairbanks, Rosman, Santiago and Tananarive. The superimposed sub-satellite trace for the orbiting satellites illustrates that nearly complete coverage is offered for the orbit segment of interest. The trace shown is for the initial pass, and the trace will translate across the map with succeeding passes. The segment of interest is that part of the trace shown dotted. The two dotted segments the 3-hour transmission intervals on the inbound and outbond legs of the orbit.

Referring to Figure 6.2-13, we note that at 44,600 km the maximum data rate for a two watt S-band transmitter is 7000 bits per second. If 7000 bits per second is transmitted for 30 minutes, a total of approximately 1.3×10^7 bits per satellite is received at the ground station. Based on an experiment schedule of ten hours per orbit (two hours at apogee and four hours before and four hours after apogee), this corresponds to an experiment data rate of 360 bits per second. Figure 6.2-15 is a plot of data rate as a function of primary power, and illustrates the situation discussed above for a primary power input of ten watts and an assumed transmitter efficiency of 20 per cent.

Figure 6.2-15 also illustrates the trade-off of primary power inout vs. experiment data rate for two values of transmitter efficiency. Increased experiment data rate can be achieved by adjustment of several system parameters, but the ultimate constraint is the capacity of the tape recorder. Projected estimates of a six-pound tape recorder available by 1970 indicate a capacity of 4×10^7 bits, which corresponds to an experiment data rate of approximately 1100 bits per second. One way to achieve this maximum science data rate is to increase the primary power input. Figure 6.2-15 indicates a primary power input for a 20 per cent efficient transmitter of 32 watts. At higher power outputs, present state-of-the-art solid-state, S-band

operation without interruption from a single station. We choose a minimum satellite altitude of 6100 kilometers which corresponds on the inbound leg to 270 degrees true anomaly. A smaller altitude is undesirable due to increasingly large tracking rates and reduced station coverage. The maximum range of 44,600 kilometers is equal to 213 degrees true anomaly. This maximum range corresponds to a three hour transit time on the inbound leg from 213 to 270 degrees true anomaly.

Figure 6.2-14 shows earth coverage for the five GRARR stations at Carnarvon, Fairbanks, Rosman, Santiago and Tananarive. The superimposed sub-satellite trace for the orbiting satellites illustrates that nearly complete coverage is offered for the orbit segment of interest. The trace shown is for the initial pass, and the trace will translate across the map with succeeding passes. The segment of interest is that part of the trace shown dotted. The two dotted segments the 3-hour transmission intervals on the inbound and outbond legs of the orbit.

Referring to Figure 6.2-13, we note that at 44,600 km the maximum data rate for a two watt S-band transmitter is 7000 bits per second. If 7000 bits per second is transmitted for 30 minutes, a total of approximately 1.3×10^7 bits per satellite is received at the ground station. Based on an experiment schedule of ten hours per orbit (two hours at apogee and four hours before and four hours after apogee), this corresponds to an experiment data rate of 360 bits per second. Figure 6.2-15 is a plot of data rate as a function of primary power, and illustrates the situation discussed above for a primary power input of ten watts and an assumed transmitter efficiency of 20 per cent.

Figure 6.2-15 also illustrates the trade-off of primary power inout vs. experiment data rate for two values of transmitter efficiency. Increased experiment data rate can be achieved by adjustment of several system parameters, but the ultimate constraint is the capacity of the tape recorder. Projected estimates of a six-pound tape recorder available by 1970 indicate a capacity of 4×10^7 bits, which corresponds to an experiment data rate of approximately 1100 bits per second. One way to achieve this maximum science data rate is to increase the primary power input. Figure 6.2-15 indicates a primary power input for a 20 per cent efficient transmitter of 32 watts. At higher power outputs, present state-of-the-art solid-state, S-band

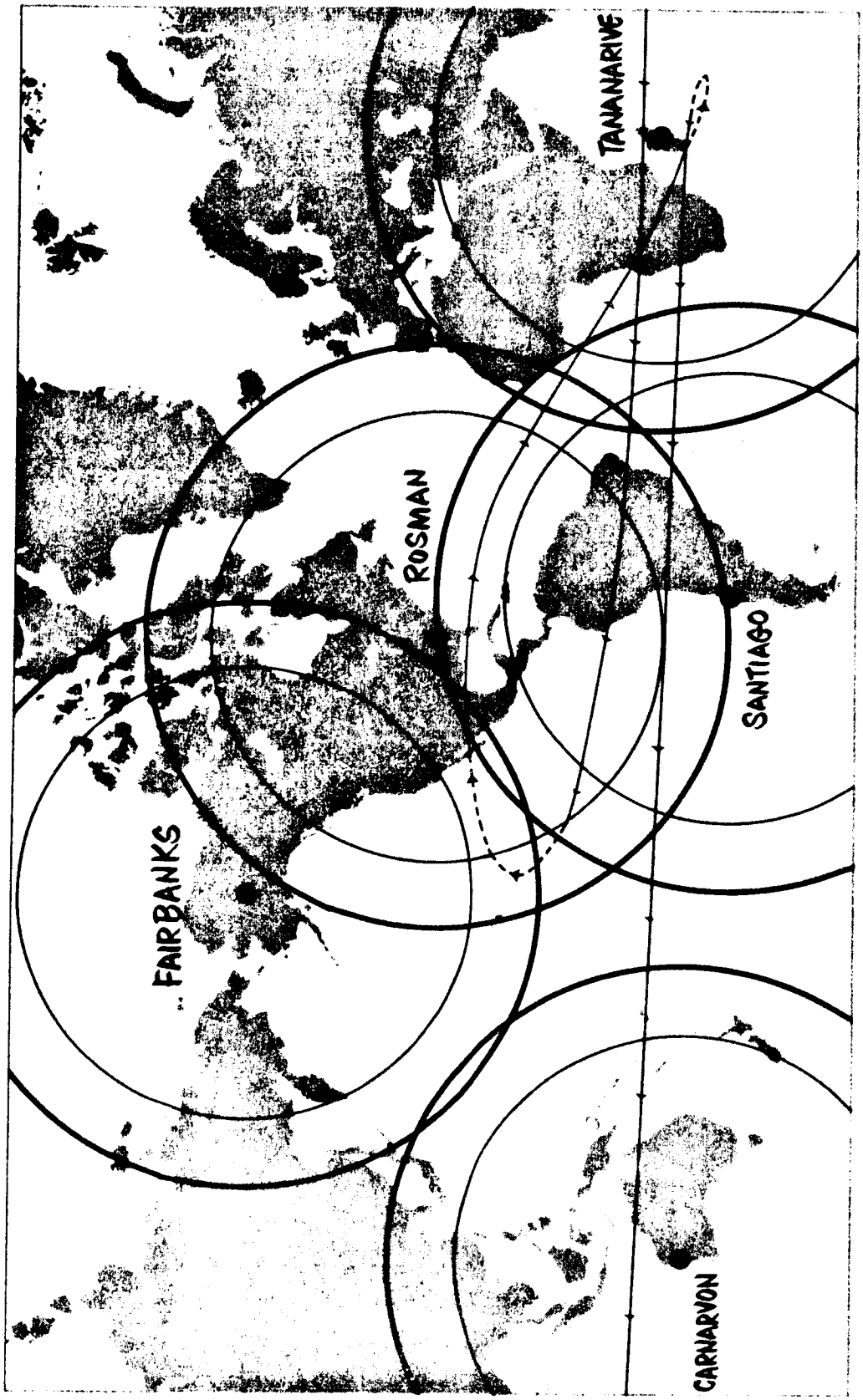

Figure 6.2-14 Earth Coverage and Ground Track for STADAN Network and Ames Multi-Satellite

transmitters have reduced efficiency. For a 15 per cent efficient transmitter, the primary power input would be 42 watts.

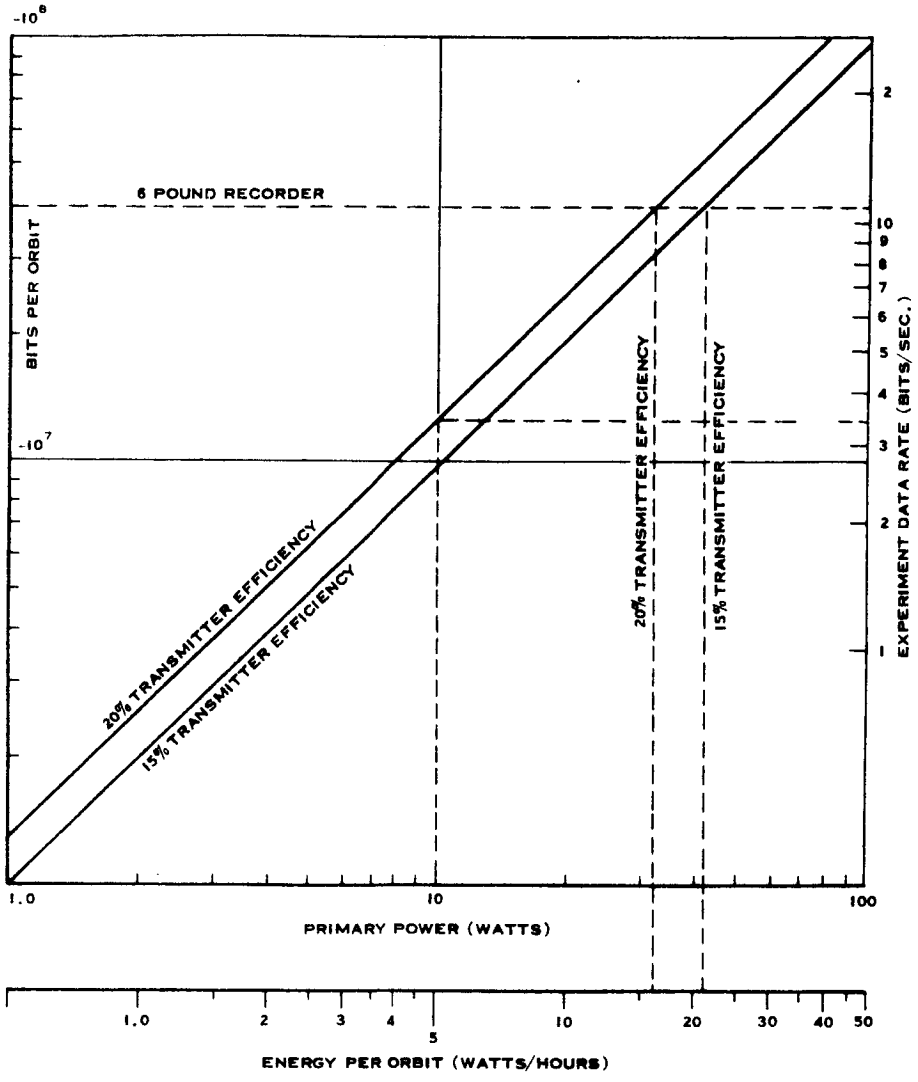

Figure 6.2-15 S-band Telemetry Link Performance

Table 6.2-3 illustrates the S-band telemetry link performance for the alternatives discussed above. Note should be taken of the fact that the data rate can be increased by using the battery for the additional power.

Telemetry Alternatives. As shown above it is feasible to increase the system data rate by using reserve battery power for short intervals. The various alternative methods considered are discussed below.

TABLE 6.2-3

TELEMETRY LINK PERFORMANCE

Telemetry Data Rate 44,600 KM	7,000 bps	20,000 bps
Total Bits per orbit (per satellite)	1.3×10^7 bits	3.6×10^7 bits
Experiment Data Rate (10 hrs. per orbit)	360 bps	1000 bps
Additional Energy requirement	None	10 watt-hrs.

The first technique considered was to begin transmission earlier in the orbit. This method is suggested by the fact that at greater ranges the satellite velocity is less, thus allowing more time for data transmission, and possibly acquiring a pair of satellites in the antenna, since, farther out in the orbit, the satellites are closer to each other. The disadvantage of this alternative is that if transmission is initiated beyond ten earth radii, science data collection is interferred with. In addition, as the range increases, the allowable data rate decreases for constant power output so that the net gain is reduced. More significantly, the limitation on ground station support time precludes further consideration of this alternative.

The second alternative is to increase transmitter power output while maintaining the ground support time limitation. This alternative has been discussed, and is a feasible approach. The resulting increased data rates may impose transmitter design problems resulting in increased equipment costs, but this does not appear to be of major significance for data rates of approximately 20,000 bits per second at S-band.

The third alternative is to change the data rate in each satellite as the satellite approaches perigee from ten earth radii. This could be effected upon command from the ground, or by a pre-programmed timer in the satellite. If it is assumed that the data rate would be changed three times during the orbit for each satellite, the flexibility of twelve discrete data rates would be required in each satellite, since the satellites alternate position with succeeding orbits. That is, the satellite which is first on pass 1 might be second on pass 10 and fourth on pass 30. This imposes an unnecessarily complex requirement on tape recorder flexibility. In addition, it would be necessary to reverse the data record at the switching time in order to assure continuous data flow while switching from one data rate to another. In spite of its increased data discharge capability, this method appears to have overiding disadvantages, but it does suggest the fourth alternative.

The fourth alternative is to include in each satellite the ability to read data out at four different data rates. Since the satellites are accessed sequentially, each satellite transmits data at a different rate in a single pass dependimg upon its range when acquired, but any one satellite maintains the same rate for each pass. The first satellite to reach maximum range of 10 R_e (57,500 Km) transmits at its maximum allowable rate until it has completely discharged the contents of its recorder (assumed as 4.32×10^7 bits). At the end of this transmission the second satellite is acquired and initiates transmission at its maximum allowable rate for the reduced range (29,500 km), and transmits until it has discharged the contents of its recorder. This process is continued for the third and fourth satellite, taking advantage of increased data rate capability due to decreased range.

The fifth alternative is to utilize the entire three-hour interval on the inbound leg to read data out of the first two satellites and the succeeding three-hour interval on the outbound leg to read data out of the two remaining satellites. This alternative assumes the same data transmission rate from all satellites, and is suggested by the need for additional time to completely discharge the contents of the recorder. Although this technique imposes no equipment complexity penalties, it must be discarded because of the constraint of a total of three hours of ground station support time for all four satellites. This technique does, however, suggest the sixth alternative.

The sixth alternative for increasing the total amount of science data transmitted is to playback data from the first two spacecraft within 1-1/2 hours from 270 degrees true anomaly on the inbound leg and from the remaining two spacecraft within 1-1/2 hours from 90 degrees true anomaly on the outbound leg. Since transmission is initiated at a lower altitude (14,000 km), the data rate can be increased while maintaining constant transmitter power output. This alternative would permit complete discharge of tape recorder contents without imposing additional power drain penalties, but would require that at least two ground stations provide support for reception of data collected in one orbit pass.

With the exception of the second alternative (increased transmitter power), the techniques noted for increasing data playback involve, primarily, operational considerations. The relative merits of the several alternatives depend more upon their practicability from a ground-support viewpoint, and so recommended adoption of any specific alternative must be withheld pending consideration by those concerned.

6.2.5 Real-Time Telemetry Options

Real-time transmission of perishable data is vital to the success of the multiple satellite mission. Although the bulk of scientific data will be identified by time and space coordinates which accompany the data record, there may arise a requirement for a "quick-look" at either scientific or status data. Discussions thus far considered data transmission on a store-and-forward basis only. This section considers the real-time transmission of data for two modes of operation:

a. Real-time telemetry
b. Real-time telemetry with GRARR tracking

The capabilities for real-time data transmission in both instances are based upon worst-case tolerances and the analyses are made for transmission at apogee.

Real Time Telemetry. Table 6.2-4 is a comparative summary of performance for the primary data playback mode and the real-time mode. During the real-time mode the majority of the primary power is used for operating and controlling the

scientific instrumentation. The tape recorder power consumption is assumed negligible since the recorder is on standby. The primary power available for data transmission is thus 5.00 watts. An overall transmitter efficiency of 15 percent has been assumed, resulting in an RF power output of 0.75 watt. Transmission is assumed to be at S-band, using direct carrier PCM/PM (± 70 degrees) modulation and a bit error probability, $P_e = 10^{-4}$. Referring to Figure 6.2-13, the data rate at apogee is 330 bits per second.

TABLE 6.2-4

REAL TIME TELEMETRY OPTION

Item \ Mode	Primary Data Playback	Backup Real Time Data Readout
Experiment	1.0 watts	7.0 watts
Tape Recorder	2.0 watts	0.0 watts
Misc. (Receiver, Telm., Power Control, etc.)	4.0 watts	5.2 watts
Transmitter*	10.0 watts	5.0 watts
Primary Power avail.	17.2 watts	17.2 watts
RF Power out (S-Band)	2.0 watts	0.75 watts
Max. Range	44,600 K.M.	121,000 K.M.
Bit Rate	7,000 Bits/sec.	330 Bits/sec

*Transmitter power switching by either:

(1) Bias control of parallel output transistors.
(2) Change DC collector voltage from 40 volts to 28 volts.

Since transmission in two modes of primary power input requires an additional degree of flexibility in transmitter design, the practicability of accomplishing this was investigated. There are several methods for switching the same transmitter between the 5 and 10 watt dc modes:

a. Parallel output transistors can be used with one unit biased or switched off. An advantage of this method is that a measure of redundancy can be obtained by switching both transistors.

b. The dc voltage can be changed to either 40 volts or 28 volts, corresponding to the input power level of 5 or 10 watts.

It is anticipated that any dual mode configuration would result in a lower efficiency for one of the modes. In this example an efficiency reduction from the primary to the lower power mode of 5 percent was assumed. This is possible in excess of what might be realized.

Real-Time Telemetry with GRARR Tracking. In the real-time telemetry option considered above, it was assumed that data would directly modulate the carrier frequency. The Goddard Range and Range Rate system provides the facility for simultaneous side tone ranging and telemetry transmission, but in this mode telemetry data is treated like range-tone data; i. e., it is placed on a sub-carrier for transmission on the down-link. The GRARR sub-carrier receiver on the ground demodulates the telemetry signal to baseband for data extraction by external equipment. The objective of this analysis was to determine the amount of useable sideband power in the telemetry channel, and thus establish the channel data rate. As distinct from the case considered earlier, two subcarriers exist here: one phase modulated with range tones, and the other phase modulated with telemetry data. Table 6. 2-5 presents the link analysis for simultaneous telemetry and side tone ranging.

Table 6. 2-6 summarizes the results of this analysis. Based on these results one may conclude that real-time telemetry near apogee is feasible with or without tracking, but at much reduced data rates.

TABLE 6.2-5

PROJECT: AMES MULTIPLE SATELLITE DATE:

CHANNEL: GRARR S-Band, Down-Link, f_c = 2253 MH$_z$

MODE: Simultaneous Telemetry & Side-Tone Ranging

NO.	PARAMETER	VALUE	TOLERANCE		SOURCE
1	Total Transmitter Power 0.75 watts	28.75 dbm	+1.0	-1.0db	Specified
2	Transmitting Circuit Loss	-1.0 db	+0.0	-1.0db	Estimated
3	Transmitting Antenna Gain	+2.0 db	+3.0	-1.0db	Estimated
4	Transmitting Antenna Pointing Loss	Included in (3)			
5	Space Loss (2253 mc, 121,000 km)	-201.16 db			Calculated
6	Polarization Loss	-0.5 db	+0.3	-0.5db	REF #1
7	Receiving Antenna Gain	+42.0 db	+1.0	-0.5db	REF #1
8	Receiving Antenna Pointing Loss	-0.1 db	+0.1	-0.1db	Calculated
9	Receiving Circuit Loss	-0.5 db	+0.1	-0.4db	REF #1
10	Net Circuit Loss	-159.26 db	+4.5	-3.5db	Σ (2 ·9)
11	Total Received Power	-130.51 dbm	+5.5	-4.5db	1 + 10
12	Receiver Noise Spectral Density (N/B) (T System = ^oK)	-175.2 dbm/Hz	+1.4	-0.0db	Calculated
13	Carrier Modulation Loss	-5.82 db	+0.5	-0.5	REF #2
14	Received Carrier Power	-136.33 db	+6.0	-5.0db	11 - 13
15	Carrier APC Noise BW ($2B_{LO}$ = 20 Hz)	13.0 db	+0.5	-0.5db	REF #1
	CARRIER PERFORMANCE - TRACKING (One-Way)				
16	Threshold SNR in $2B_{LO}$				
17	Threshold Carrier Power				
18	Performance Margin				
	CARRIER PERFORMANCE - TRACKING (Two-Way)				
19	Threshold SNR in $2B_{LO}$				
20	Threshold Carrier Power				
21	Performance Margin				
	CARRIER PERFORMANCE -				
22	Threshold SNR in $2B_{LO}$				
23	Threshold Carrier Power				
24	Performance Margin				
	DATA CHANNEL				
25	Modulation Loss	-9.94	-	-	Calculated
26	Received Data Subcarrier Power	-140.45 dbm	+5.5	-4.5db	11 - 25
27	Bit Rate (1/T)	19.15 db			
28	Required ST/N/B	9.2 db	+0.5	-0.5db	Calculated
29	Threshold Subcarrier Power	-146.85	+1.9	-0.9db	12 + 27 + 28
30	Performance Margin	+6.4		-6.4db	26 - 29
	SYNC CHANNEL				
31	Modulation Loss				
32	Received Sync Subcarrier Power				
33	Sync APC Noise BW($2B_{LO}$ =)				
34	Threshold SNR in $2B_{LO}$				
35	Threshold Subcarrier Power				
36	Performance Margin				

COMMENTS:

REF #1: Goddard Range & Range Rate System Specification, Exhibit "A", NASA/GSFC S-531-P-17, May 1966

REF #2: The Goddard Range and Range Rate Tracking System Concept, Design and Performance by G.C. Kronmiller & E.J. Baghdady, Space Science Reviews, Vol. 5, Mar. 1966, pp. 265-307.

TABLE 6.2-6

REAL-TIME TELEMETRY OPTIONS

Parameter	Real-Time Telemetry	Real-Time Telemetry & Tracking
Frequency (MHz)	2253	2253
Range (Km)	121,000	121,000
Spectral Noise Density (dbm/Hz)	-175.2	-175.2
Modulation	PCM/PM	PCM/PM/PM
Carrier Modulation Indix (radians)	1.22	1.5
Subcarrier Modul. Index (radians)	———	0.75
Required ST/No (db)	9.2	9.2
Received Data Channel Power (dbm)	-133.95	-140.45
Data Rate (bits/sec)	330	82

6.3 LINK ANALYSIS AND DESIGN

6.3.1 Parametric Analysis

The selection of the proper RF parameters for optimum performance of a telecommunications system requires analysis of the three functions of telemetry, tracking, and command. This section includes the supporting background information upon which many of the operational trade-offs were based.

Telemetry Link. The principal criterion of a data transmission system performance is the maximum data rate available within certain fixed physical constraints. As was established earlier, the most efficient modulation technique for PCM telemetry is direct phase modulation of the carrier by the serial stream of PCM data.

S-band Telemetry. Table 6.3-1 contains a tabulation of gains and losses based on a spacecraft power of two watts operating at a frequency of 2253 MHz, and a distance of 121,000 kilometers, corresponding to the nominal slant range at apogee. The spacecraft antenna was assumed to be either a biconical horn or cylindrical array having a forward gain of 2 db. The ground receiving system was assumed to be that specified for the Goddard Range and Range Rate System, and presumes use of a 30-foot parabolic reflector and a specified receiver noise figure of 2.0 db.

Certain items in Table 6.3-1 should be noted. The equivalent noise temperature of the receiver includes the effect of transmission line loss as well as sky temperature and receiver noise figure as follows:

$$N_o = KT_e$$

$$\text{where } T_e = \frac{1}{L} T_a + \left(\frac{L-1}{L}\right) T_L + (F-1) T_o$$

L = Line Loss = 0.5 db = 1.1

T_A = Sky Temperature = 15 K $\left(^{+75^o}_{-0}\right)$

F = Receiver Noise Figure = 2.0 db = 1.6

T_L = Transmission line temperature = 290^oK

TABLE 6.3-1

PROJECT: Arc Multiple Satellite DATE:

CHANNEL: Spacecraft-to-Earth, $P_e = 10^{-4}$, Modulation: PCM/PM

MODE: S-Band Telemetry from Apogee

NO.	PARAMETER	VALUE	TOLERANCE		SOURCE
1	Total Transmitter Power (2 watts)	33.0 dbm	+1.0	-1.0 db	Specified
2	Transmitting Circuit Loss	-1.0 db	+0.0	-1.0 db	Estimated
3	Transmitting Antenna Gain	+2.0 db	+3.0	-1.0 db	Estimated
4	Transmitting Antenna Pointing Loss	Included in (3)			
5	Space Loss (2253 mc, 121,000km)	-201.16 db	-	-	Calculated
6	Polarization Loss	- 0.5 db	+0.3	-0.5	Estimated
7	Receiving Antenna Gain	+42.0 db	+1.0	-0.5	Ref. #1
8	Receiving Antenna Pointing Loss	-0.1 db	+0.1	-0.1	Calculated
9	Receiving Circuit Loss	-0.5 db	+0.1	-0.4	Ref. #1
10	Net Circuit Loss	-159.26 db	+4.5	-3.5	(2 ( )
11	Total Received Power	-126.26 dbm	+5.5	-4.5	1 + 10
12	Receiver Noise Spectral Density (N/B) (T System = 214 +68 °K)	-175.2 dbm/Hz	+1.4	-0.0	Calculated
13	Carrier Modulation Loss -0	-3.6 db	+0.5	-0.5	Calculated
14	Received Carrier Power $\Delta\phi$ = 70°	-129.86 dbm	+6.0	-5.0	11 + 13
15	Carrier APC Noise BW ($2B_{LO}$ = 60 Hz)	17.8 db/Hz	+0.5	-0.5	Ref. #1
	CARRIER PERFORMANCE - TRACKING (One-Way)				
16	Threshold SNR in $2B_{LO}$				
17	Threshold Carrier Power				
18	Performance Margin				
	CARRIER PERFORMANCE - TRACKING (Two-Way)				
19	Threshold SNR in $2B_{LO}$				
20	Threshold Carrier Power				
21	Performance Margin				
	CARRIER PERFORMANCE -				
22	Threshold SNR in $2B_{LO}$	9.0 db	-	-	Estimated
23	Threshold Carrier Power	-148.4 dbm	+1.9	-0.5	12 + 15 + 22
24	Performance Margin	+18.5 db	+5.5	-6.9	14 - 23
	DATA CHANNEL				
25	Modulation Loss $\Delta\phi$ = 70°	- 3.0 db	+0.5	-0.5	Calculated
26	Received Data Subcarrier Power	-129.2 dbm	+6.0	-5.0	11 - 25
27	Bit Rate (1/T)	+29.8 db-bps	-	-	Derived
28	Required ST/N/B	+9.2 db	+0.5	-0.5	Calculated
29	Threshold Subcarrier Power	-136.1 dbm	+1.9	-0.5	12 + 27 + 28
30	Performance Margin	6.9 db		-6.9	
	SYNC CHANNEL				
31	Modulation Loss				
32	Received Sync Subcarrier Power				
33	Sync APC Noise BW($2B_{LO}$ =)				
34	Threshold SNR in $2B_{LO}$				
35	Threshold Subcarrier Power				
36	Performance Margin				

COMMENTS:

$$T_o = \text{Ground Temperature} = 290^oK$$

Computing T_e:

$$T_e = \frac{15}{1.1} + \frac{(1.1-1)\ 290}{1.1} + (1.6-1)\ 290$$

$$T_e = 214^oK \begin{pmatrix} +68 \\ -0 \end{pmatrix}$$

The polarization loss (0.5 ±0.1 db) was calculated on the basis of a 3 db axial ratio for a circularly polarized satellite antenna and for a maximum ground antenna axial ratio of 2.5 db circularly polarized in the same sense. The receiving antenna pointing loss is based on a specified minimum pointing accuracy of 0.1 degrees. The values for receiving antenna gain and receiving circuit loss are those specified for the GRARR, S-band ground system. The two-sided carrier bandwidth was chosen as 60 Hz, since this represents a reasonable compromise between tracking rate capabilities of the ground receiver, and signal spectral components for the low data rates anticipated at this distance. For the modulation index chosen (1.22 rad) about 45 percent of the power remains in the carrier, and about 50 percent is usable sideband power. Only about 5 percent of the power is thus wasted in unusable sidebands. This was considered the maximum index which would be consistent on the one hand with the requirement for maintaining sufficient carrier power to assure carrier tracking, and on the other hand keep wasted sideband power at a minimum.

The carrier tracking loop has a "worst case" performance margin of almost 12 db which is quite adequate. The maximum available bit rate at this range (973 bps) was calculated on the basis of a "worst case" performance margin of zero db. The nominal margin is 6.9 db, but negative tolerances reduce this to zero for the "worst case" condition.

VHF Telemetry. Table 6.3-2 is a tabulation of the VHF telemetry link budget similar to the S-band telemetry link, except for choice of operating frequency, antenna configurations, transmitter efficiencies and system losses and gains at this frequency. The primary purpose of this analysis was, as stated earlier, to permit evaluation of performance of VHF versus S-band.

TABLE 6.3-2

PROJECT: Arc Multiple Satellite DATE:

CHANNEL: Spacecraft-to-Earth, $P_e = 10^{-4}$, Modulation: PCM/PM

MODE: VHF Telemetry From Apogee

NO.	PARAMETER	VALUE	TOLERANCE		SOURCE
1	Total Transmitter Power (5.5 watts)	+37.4 dbm	+1.0	-1.0db	Specified
2	Transmitting Circuit Loss	- 1.0 db	0.0	-1.0	Estimated
3	Transmitting Antenna Gain	- 1.5 db	+1.5	-1.5	Estimated
4	Transmitting Antenna Pointing Loss	Include in (3)			
5	Space Loss (136 mc, 121,000 km)	-176.8 db	---	---	Calculated
6	Polarization Loss	- 1.5 db	- 1.5	+1.5	Estimated
7	Receiving Antenna Gain	+22.2 db	+1.0	-0.5	STADAN SPEC.
8	Receiving Antenna Pointing Loss	Included in (7)	---	---	
9	Receiving Circuit Loss	" " "	---	---	STADAN SPEC
10	Net Circuit Loss	-158.6 db	+4.0	-4.5	Σ (2 → g)
11	Total Received Power	-121.2 db	+5.0	-5.5	1 + 10
12	Receiver Noise Spectral Density (N/B) (T System = $913\ ^{+680}_{-135}$ °K)	-169.0dbm/Hz	+2.4	-0.5	Calculated
13	Carrier Modulation Loss $\Delta\phi = \pm 70^{o}$	- 3.6 db	+0.5	-0.5	Calculated
14	Received Carrier Power	-124.8 dbm	+5.5	-6.0	11 - 13
15	Carrier APC Noise BW ($2B_{LO}$ = 60 Hz)	17.8 db-Hz	+0.5	-0.5	Ref. #1
	CARRIER PERFORMANCE - TRACKING (One-Way)				
16	Threshold SNR in $2B_{LO}$				
17	Threshold Carrier Power				
18	Performance Margin				
	CARRIER PERFORMANCE - TRACKING (Two-Way)				
19	Threshold SNR in $2B_{LO}$				
20	Threshold Carrier Power				
21	Performance Margin				
	CARRIER PERFORMANCE -				
22	Threshold SNR in $2B_{LO}$	9.0 db	---	---	STADAN SPEC.
23	Threshold Carrier Power	-142.2dbm	+2.9	-1.0	22 + 12 + 15
24	Performance Margin	+17.4 db	+6.5	-8.9	14 - 23
	DATA CHANNEL				
25	Modulation Loss $\Delta\phi = \pm 70^{o}$	- 3.0 db	+0.5	0.5	Calculated
26	Received Data Subcarrier Power	-124.2 dbm	+5.5	-6.0	11 - 25
27	Bit Rate (1/T) (470 bps)	+26.7db-bps	---	---	
28	Required ST/N/B ($P_e = 10^{-4}$)	+ 9.2 db	+0.5	-0.5	Calculated
29	Threshold Subcarrier Power	-133.1 dbm	+2.9	-1.0	12 + 27 + 28
30	Performance Margin	8.9 db	+6.5	-8.9	26 - 29
	SYNC CHANNEL				
31	Modulation Loss				
32	Received Sync Subcarrier Power				
33	Sync APC Noise BW($2B_{LO}$ =)				
34	Threshold SNR in $2B_{LO}$				
35	Threshold Subcarrier Power				
36	Performance Margin				

COMMENTS:

The results of this analysis clearly indicate the improvement to be realized in using S-band.

The maximum available bit rate under "worst-case" conditions is 470 bits per second compared with 973 bits at S-band for the same primary power input. This represents in excess of 3 db improvement of S-band over VHF. The primary contributions to degraded performance at VHF can be noted in certain items of Table 6.3-2. Despite the much higher transmitter efficiency and reduced space loss at VHF, the antenna gains and reduced noise temperatures at S-band more than offset these factors.

The satellite antenna assumed for this analysis was a turnstile type, radiating circular polarized energy off the spin axis, and linearly polarized energy in the orbit plane. The ground receiving antenna was assumed to be the SATAN antenna whose gain is slightly greater than that of the GRARR crossed dipole array. The receiver noise figure was assumed to be 3.5 db, as specified in the STADAN Facility Report. The required ST/N_0 was calculated as 8.3 db theoretical, plus 0.9 db allowance for equipment degradation. The polarization loss for the "worst case" is 3.0 db, since the ground antennas may be tracking circular polarization, and the satellite is so oriented as to radiate linear polarization.

For the VHF link the modulation index is the same as for S-band, since the same criteria of usable sideband power and carrier power apply. However, the carrier performance margin at VHF, though adequate (8.5 db, "worst case"), is not as great as for S-band. The assumptions pertinent to the data channel at VHF are the same as for S-band -- namely, a derived data rate based on a "worst case" performance margin of zero db.

6.3.2 Command Link Analysis

Analysis of the command link is fairly straightforward if it is assumed that by 1970 installation of a proposed Programmable Command Generator will have been effected. Recent information[8] from NASA/GSFC indicates that the Command Subcommittee of the Data Systems Requirements Committee is in the process of revising the present standard to take advantage of an advanced flexible command system to be implemented into the STADAN network beginning in 1968. For this analysis it will be assumed that the command system will employ PCM/FSK/PM modulation, and that it will be integrated with the (unified) GRARR system. The Aerospace Data System Standards specify amplitude modulation of the RF carrier for both the Tone Digital Command and the PCM Instruction Command; however, use of the integrated GRARR system requires that all carriers be phase-modulated, and that the modulation index be variable from 0 to 1.5 radians peak. The PCM command data are translated to an intermediate band by FSK modulation of a subcarrier in the 7.0 to 11.0 kHz band. A sinusoidal bit synchronization signal is 50 percent amplitude-modulated onto the data subcarrier at the data bit rate, thus providing unambiguous bit synchronization.

The input signal to the command subcarrier demodulator in the spacecraft can be expressed as:

$$E(t) = \frac{E_i}{2}\left[1 + U(t)\right]\left[1 + m\cos(\omega t + \theta)\right]\cos(\omega_1 t + \phi_1)$$
$$+ \frac{E_i}{2}\left[1 + V(t)\right]\left[1 + m\cos(\omega t + \theta)\right]\cos(\omega_2 t + \phi_2)$$
$$+ N(t)$$

where

E_i = received subcarrier amplitude

$\frac{E_i^2}{2} = S_i = 2 J_1^2(\beta) S_c$ = received subcarrier power

β = subcarrier deviation on carrier

S_c = received carrier power

m = modulation index of AM sync sine wave

N(t) = White Gaussian noise

ω_s = Sync sinewave frequency

$\omega_1 \& \omega_2$ = FSK subcarrier frequencies

$\phi_1 \& \phi_2$ = phase of FSK subcarriers

The one sided spectral density of the command data signal is given by:

$$G(f) = \frac{2}{H} \left[\frac{\sin \pi f/H}{\pi f/H} \right]^2$$

where H = keying frequency

The sync sinewave consists of a discrete subcarrier component and two discrete-frequency subcarrier sideband components which are separated from the subcarrier by an amount equal to the keying frequency. The spectral density of the received signal is as shown in Figure 6.3-1, where rather than sharp transitions between bipolar levels, some form of shaped transitions are assumed in order to reduce spectral tails.

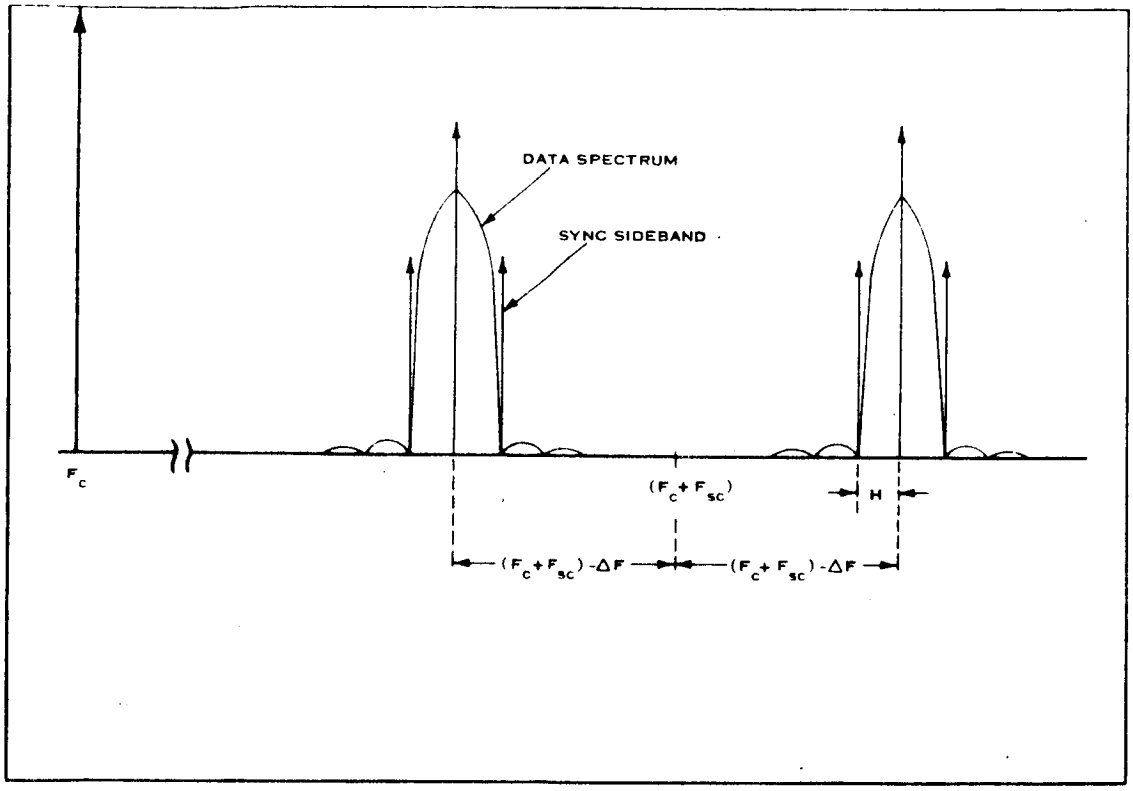

Figure 6.3-1 Spectral Density of FSK Command Signal

The FSK detection in the spacecraft is non-coherent, and employs the two filter technique with sampling of the filter envelopes. For a probability of bit error, $P_e = 10^{-4}$, the predetection ST/N/B is 12.9 db. To this has been added 0.3 db to account for the sync power which is modulated into the sidebands.

In the tabulation of the command channels at both VHF and S-Band (Tables 6.3-3 and Table 6.3-4), the bit rate is assumed to be 128 bps. Command standards require that the two tones be separated by at least twice this amount; practically, separation is many times greater and filter bandwidths only wide enough to pass the energy spectrum defined by the bit rate.

With the above considerations in mind, it is interesting to note the results of the analysis. Inspection of both Tables 6.3-3 and 6.3-4 show that the performance margins are quite adequate. For the VHF carrier, the worst-case margin is 32.7 db and for S-band, 37.7 db. The data channel margin, worst-case, is 25.2 db for VHF, and 33.0 db for S-band. These comfortable margins are due largely to the

TABLE 6.3-3

PROJECT: ARC MULTIPLE SATELLITE DATE:

CHANNEL: Earth-to-Satellite, PCM/FSK/PM, $P_e = 10^{-4}$, R_B = 128 bps

MODE: VHF Command Link, Grnd. Ant = 20 db, P_o = 5 kw

NO.	PARAMETER	VALUE	TOLERANCE		SOURCE
1	Total Transmitter Power (5 kw)	67.0 dbm	+1.0	-1.0db	Specified
2	Transmitting Circuit Loss	-1.5 db	+0.5	-0.0db	Specified
3	Transmitting Antenna Gain	20.0 db	+0.2	-0.5	Calculated
4	Transmitting Antenna Pointing Loss	-0.2 db	+0.2	-0.5	Calculated
5	Space Loss (148 mc, 121,000 km)	-177.5 db	---	---	Calculated
6	Polarization Loss	-1.5 db	+1.5	-1.5	Estimated
7	Receiving Antenna Gain	-1.5 db	+1.5	-1.5	Estimated
8	Receiving Antenna Pointing Loss	-0.2 db	+0.2	-0.5	Estimated
9	Receiving Circuit Loss	-1.3 db	+0.0	-0.8	Estimated
10	Net Circuit Loss	-163.7 db	+5.9	-4.8	$\Sigma(2 \rightarrow g)$
11	Total Received Power	-96.7 dbm	+6.9	-5.8	1 + 10
12	Receiver Noise Spectral Density (N/B) (T System = 1560±250 °K)	-166.7 dbm/Hz	+0.8	-0.8	Calculated
13	Carrier Modulation Loss $\Delta\phi = \pm 70^\circ$	-3.6 db	+0.5	-0.5	Calculated
14	Received Carrier Power	-100.3 dbm	+7.4	-6.3	11 - 13
15	Carrier APC Noise BW ($2B_{LO}$ • 100 Hz)	20.db - Hz	+1.0	-1.0	Assumed
	CARRIER PERFORMANCE - TRACKING (One-Way)				
16	Threshold SNR in $2B_{LO}$				
17	Threshold Carrier Power				
18	Performance Margin				
	CARRIER PERFORMANCE - TRACKING (Two-Way)				
19	Threshold SNR in $2B_{LO}$				
20	Threshold Carrier Power				
21	Performance Margin				
	CARRIER PERFORMANCE -				
22	Threshold SNR in $2B_{LO}$	9 db	---	---	Estimated
23	Threshold Carrier Power	-137.7 dbm	+1.8	-1.8	12 + 15 + 22
24	Performance Margin	41.0 db	+9.2	-8.3	14 - 23
	DATA CHANNEL				
25	Modulation Loss $\Delta\phi = +70^\circ$	- 3.0 db	+0.5	-0.5	Calculated
26	Received Data Subcarrier Power	-99.7 dbm	+7.4	-6.3	11 - 25
27	Bit Rate (1/T) 128 bps	21.1 db-Hz	---	---	Calculated
28	Required ST/N/B	13.2 db	+0.5	-0.5	Calculated
29	Threshold Subcarrier Power	-133.5 dbm	1.3	-1.3	12 + 27 + 28
30	Performance Margin	+32.8 db	+8.7	-7.6	26 - 29
	SYNC CHANNEL				
31	Modulation Loss				
32	Received Sync Subcarrier Power				
33	Sync APC Noise BW($2B_{LO}$ •)				
34	Threshold SNR in $2B_{LO}$				
35	Threshold Subcarrier Power				
36	Performance Margin				

COMMENTS:

TABLE 6.3-4

PROJECT: ARC MULTI-SATELLITE DATE: 12/21/66

CHANNEL: Ground to Satellite PCM/FSK/PM; $P_e = 10^{-4}$; R_B = 128 b/s;

MODE: S-band (1800 MHz) Command Link, Ground Antenna = 41.5 db, Po = 5 kw

NO.	PARAMETER	VALUE	TOLERANCE		SOURCE
1	Total Transmitter Power (5 kw)	67.0 dbm	+1.0	-1.0 db	Reference #1
2	Transmitting Circuit Loss	-1.5 db	+0.5	-0 db	Reference #1
3	Transmitting Antenna Gain	41.5 db	+0.5	-0.5 db	Reference #1
4	Transmitting Antenna Pointing Loss	-0.1 db	+0	-0 db	Calculated
5	Space Loss (1800 mc, 121,000 km)	-199.2 db	-	-	Calculated
6	Polarization Loss	-0.5 db	+0.1	0.1 db	Calculated
7	Receiving Antenna Gain	+2.0 db	+3.0	-1.0 db	Estimated
8	Receiving Antenna Pointing Loss	0 db	+0.0	-2.0 db	Estimated
9	Receiving Circuit Loss	-1.0 db	+0	-1 db	Estimated
10	Net Circuit Loss	-158.8 db	+4.1	-4.6 db	Σ (2-9)
11	Total Received Power	-91.8 dbm	+5.1	-5.6 db	Σ (1-10)
12	Receiver Noise Spectral Density (N/B) (T System = 700, +280, -360°K)	-170.1 dbm/Hz	+1.4	-3.2 db	Calculated
13	Carrier Modulation Loss $\Delta\phi$ = 70°	-3.6 db	+0.5	-0.5 db	Calculated
14	Received Carrier Power	-95.4 dbm	+5.6	-6.1 db	11-13
15	Carrier APC Noise BW ($2B_{LO}$ = 100 Hz)	20 db-Hz	+0.5	-0.5 db	
	CARRIER PERFORMANCE - TRACKING (One-Way)				
16	Threshold SNR in $2B_{LO}$				
17	Threshold Carrier Power				
18	Performance Margin				
	CARRIER PERFORMANCE - TRACKING (Two-Way)				
19	Threshold SNR in $2B_{LO}$				
20	Threshold Carrier Power				
21	Performance Margin				
	CARRIER PERFORMANCE -				
22	Threshold SNR in $2B_{LO}$	9 db	-	-	Estimated
23	Threshold Carrier Power	-141.1 dbm	+1.9	-3.7 db	12 + 15 + 22
24	Performance Margin	+45.7 db	+6.4	-8.0 db	14 - 23
	DATA CHANNEL				
25	Modulation Loss ϕ = 70°	-3 db	+0.5	-0.5 db	Calculated
26	Received Data Subcarrier Power	-94.8 dbm	+5.6	-6.1 db	11 + 25
27	Bit Rate (1/T) = 128 bps	21.1 db-Hz	-	-	Calculated
28	Required ST/N/B $P_e = 10^{-4}$	13.2 db	+0.5	-0.5 db	Calculated
29	Threshold Subcarrier Power	-135.8 db	+1.9	-3.7 db	12 + 27 + 28
30	Performance Margin	+41.0 db	+6.2	-8.0 db	26 - 29
	SYNC CHANNEL				
31	Modulation Loss				
32	Received Sync Subcarrier Power				
33	Sync APC Noise BW($2B_{LO}$ =)				
34	Threshold SNR in $2B_{LO}$				
35	Threshold Subcarrier Power				
36	Performance Margin				

COMMENTS:

Reference #1: Goddard Range & Range Rate System Specification, Exhibit "A", S-531-P-17, May 1966.

5-kilowatt transmitter power assumed. Unintentional activation of the command system by spurious signals in the command frequency band is not an uncommon experience, and such activation can seriously affect mission accomplishment. These margins are particularly attractive, therefore, since they accrue with no penalty to the primary criterion of scientific data collection and transmission.

There are few parametric trade-offs involved in the RF portion of the command subsystem. For example, increasing the modulation index to accommodate higher command data rates results, of course, in more power in the data channel and less in the carrier. However, command data rates for the 1970-71 period are not expected to exceed 2000 bits per second, and the requirement for higher data rates does not exist for this mission. The selection of either VHF or S-band is not clearly indicated on the basis of a link analysis. Such a choice depends on exterior considerations such as spacecraft antenna, spectrum occupancy, range tone transponding and ground support facility.

The assumptions underlying certain estimates in Tables 6.3-3 and 6.3-4 are noteworthy. Item 12, the receiver noise temperature, was based on a transmission line temperature range of 0° - 120°F and a receiver noise figure of 6 db. This noise figure represents a cost item, and, in view of system margin, might be relaxed to 8 db. Carrier APC noise bandwidth was assumed as 100 Hz. This was based on previous transponder designs and represents a compromise between false-carrier lock and large acquisition time for phase-coherent carrier detection. This item also represents a possible cost trade-off, since a discriminator, rather than a carrier phase-lock-loop might be employed in view of the signal-to-noise margins. This, however, must be considered in terms of spectrum occupancy and the probability of spurious commands entering the receiver. The remaining estimates are based on the same considerations which apply to the telemetry link.

6.3.3 Tracking Link Analysis

It was established in Section 6.1.5 that the S-band Goddard Range and Range Rate system was preferred for satellite tracking and that angle-tracking was preferred for the carrier module. The following analysis considers first the up-link and

down-link budgets for the S-band GRARR systems, then a comparative link analysis for VHF vs. S-band GRARR down-links, and finally a link analysis of the VHF beacon for angle tracking.

Table 6.3-5 is a tabulation of items pertinent to the up-link performance of the S-band GRARR system. The basic system gains and losses (Items 1-12) are the same as for the command link. The modulation index (ϕ = 1.06 radians) is that specified in a performance analysis by Kronmiller and Baghdady.[7] Item 15, Carrier APC bandwidth, assumes use of a carrier tracking loop in the satellite. As in the discussion concerning performance of the command link, the requirement for a narrow band carrier tracking loop must be justified on the basis of other system considerations, since the carrier performance margin of 39 db in the worst case is more than adequate.

Item 27 assumes an IF bandwidth wide enough to pass the highest frequency range tone, 500 kHz. Since the range tones are not detected, but are translated to an IF frequency, a signal-to-noise ratio of 10 db in this bandwidth was postulated. The effect of these assumptions is to add the up-link noise to the down-link noise. This reduces the carrier power available for the ranging, because it modulates the carrier along with the range tones. This effect will be considered in the down-link analysis. The up-link performance margin for the worst case is noted to be 2.6 db.

Table 6.3-6, a tabulation of the down-link tracking budget, assumes a 2.0 watt transmitter power in the satellite, where only 1.8 watts (or 90 percent of 2 watts) is available signal power. The remaining 0.2 watt is up-link noise power which, after space attenuation, is added to the noise power at the ground receiver.

TABLE 6.3-5

PROJECT: ARC MULTIPLE SATELLITE DATE:

CHANNEL: GRARR UP-LINK; S-Band,

MODE: TRACKING

NO.	PARAMETER	VALUE	TOLERANCE		SOURCE
1	Total Transmitter Power 5 kw	67.0 dbm	+1.0	-1.0db	REF #1
2	Transmitting Circuit Loss	-1.5 db	+0.5	-0 db	REF #1
3	Transmitting Antenna Gain	+41.5 db	+0.5	-0.5 db	REF #1
4	Transmitting Antenna Pointing Loss	-0.1 db	+0	-0 db	Calculated
5	Space Loss (1800 mc, 121,000 km)	-199.2 db	---	---	Calculated
6	Polarization Loss	-0.5 db	+0.1	-0.1	Calculated
7	Receiving Antenna Gain	+2.0 db	+3.0	-1.0	Estimated
8	Receiving Antenna Pointing Loss	0 db	+0	-2.0db	Estimated
9	Receiving Circuit Loss	-1.0 db	+0	-1.0db	Estimated
10	Net Circuit Loss	-158.8 db	+4.1	-4.6db	Σ (2 → 9)
11	Total Received Power	-91.8 db	+5.1	-5.6 db	1 + 10
12	Receiver Noise Spectral Density (N/B) (T System = 700^{+280}_{-360} ^{o}K)	-170.1 dbm/Hz	+1.4	-3.2db	Calculated
13	Carrier Modulation Loss $\Sigma\phi$ =1.06rad	-2.7 db	+0.1	-0.1db	Calculated
14	Received Carrier Power	-94.5 dbm	+5.2	-5.7db	11 - 13
15	Carrier APC Noise BW ($2B_{LO}$ = 100Hz)	20 db-Hz	+0.5	-0.5db	
	CARRIER PERFORMANCE - TRACKING (One-Way)				
16	Threshold SNR in $2B_{LO}$				
17	Threshold Carrier Power				
18	Performance Margin				
	CARRIER PERFORMANCE - TRACKING (Two-Way)				
19	Threshold SNR in $2B_{LO}$				
20	Threshold Carrier Power				
21	Performance Margin				
	CARRIER PERFORMANCE -				
22	Threshold SNR in $2B_{LO}$	+9 db	---	---	Estimated
23	Threshold Carrier Power	-141.1 db	+1.9	-3.7	22+12+15
24	Performance Margin	+46.6 db	+8.9	-7.6	14-23
	DATA CHANNEL				
25	Modulation Loss $\pm\phi$ = 1.06	-3.8 db	+0.5	-0.5db	Calculated
26	Received Data Subcarrier Power	-95.6 db	+5.6	-6.1db	11-25
27	Bandwidth 1 MHz	60 db-Hz	+0.5	-0.5	Assumed
28	Required ST/N/B	10 db	+0.5	-0.5	Assumed
29	Threshold Subcarrier Power	-100.1 db	+2.4	-4.2	12+27+28
30	Performance Margin	4.5 db	+3.2	-1.9	26 - 29
	SYNC CHANNEL				
31	Modulation Loss				
32	Received Sync Subcarrier Power				
33	Sync APC Noise BW($2B_{LO}$ =)				
34	Threshold SNR in $2B_{LO}$				
35	Threshold Subcarrier Power				
36	Performance Margin				

COMMENTS:

REF #1: GRARR System Specification, Exhibit "A", NASA/GSFC, S-531-P-17, May 1966.

TABLE 6.3-6

PROJECT: ARC MULTI-SATELLITE DATE:

CHANNEL: SPACECRAFT TO EARTH; S-BAND 2253 MHz, TRANSPONDING

MODE: GRARR System Down-Link

NO.	PARAMETER	VALUE	TOLERANCE		SOURCE
1	Total Transmitter Power (1.8watts)*	32.65 dbm	+1.0	-1.0db	Specified
2	Transmitting Circuit Loss	-1.0 db	+0.0	-1.0db	Estimated
3	Transmitting Antenna Gain	+2.0 db	+3.0	-1.0db	Estimated
4	Transmitting Antenna Pointing Loss	Included in #3			
5	Space Loss (2253 mc, 121,000 km)	-201.16 db	---	---	Calculated
6	Polarization Loss	-0.5 db	+0.3	-0.5	Calculated
7	Receiving Antenna Gain (30' dish)	+42.0 db	+1.0	-0.5	Specified
8	Receiving Antenna Pointing Loss	-0.1 db	+0.1	-0.1	Estimated
9	Receiving Circuit Loss	-0.5 db	+0.1	-0.4	Estimated
10	Net Circuit Loss	-159.26 db	+4.5	-3.5	Σ (2 - 9)
11	Total Received Power	-126.61 dbm	+5.5	-4.5	Σ (1 - 9)
12	Receiver Noise Spectral Density (N/B) (T System = 220^{+80}_{0} °K)	-175.2dbm/Hz	+1.4	-0.0	Calculated
13	Carrier Modulation Loss $\Delta\phi = 70^{o} = 1.22$	-3.6 db	+0.5	-0.5	Calculated
14	Received Carrier Power	-129.21 dbm	+5.5	-5.0	11 - 13
15	Carrier APC Noise BW ($2B_{LO}$ • 60 Hz)	17.8db-Hz	+0.5	-0.5	
	CARRIER PERFORMANCE - TRACKING (One-Way)				
16	Threshold SNR in $2B_{LO}$				
17	Threshold Carrier Power				
18	Performance Margin				
	CARRIER PERFORMANCE - TRACKING (Two-Way)				
19	Threshold SNR in $2B_{LO}$				
20	Threshold Carrier Power				
21	Performance Margin				
	CARRIER PERFORMANCE -				
22	Threshold SNR in $2B_{LO}$	16	---	---	Specified
23	Threshold Carrier Power	-141.4 dbm	+1.9	-0.5	12+15+22
24	Performance Margin	12.2 db	+7.4	-5.5	14 - 23
	DATA CHANNEL				
25	Modulation Loss $\Delta\phi = 70^{o} = 1.22$	-3.0 db	+0.5	-0.5	Calculated
26	Received Data Subcarrier Power	-129.61 dbm	+6.0	-5.0	11 - 25
27	Bandwidth (60Hz)	+17.8 db-Hz	---	---	---
28	Required ST/N/B	+11.0 db	---	---	REF #7
29	Threshold Subcarrier Power	-146.4 dbm	+1.9	-0.5	28+27+12
30	Performance Margin	+16.8 db	+7.9	-5.5	26 - 29
	SYNC CHANNEL				
31	Modulation Loss				
32	Received Sync Subcarrier Power				
33	Sync APC Noise BW($2B_{LO}$ •)				
34	Threshold SNR in $2B_{LO}$				
35	Threshold Subcarrier Power				
36	Performance Margin				

COMMENTS * Total Signal Power for 10 db S/N = (0.9)(2.0)=1.8 watts

** Transmitted Noise from S/C = 3/4°K. This is accounted for in the tolerances.

REF #7 "The Goddard Range and Range Rate Tracking System Concept, Design and Performance," by Kronmiller and Raghdady, p. 10-C19.

Items 1 through 15 (Table 6.3-6) are the same as those for the telemetry link. The 0.2 watt of noise power in the 1 MHz bandwidth represents a noise contribution at the satellite of -37 dbm/Hz. When attenuated by the net circuit loss of -159.26 db, this represents a noise spectral density at the ground receiver of -196.26 dbm/Hz. This is more than 20 db below the noise spectral density due to system noise, and can thus be neglected in computing system performance.

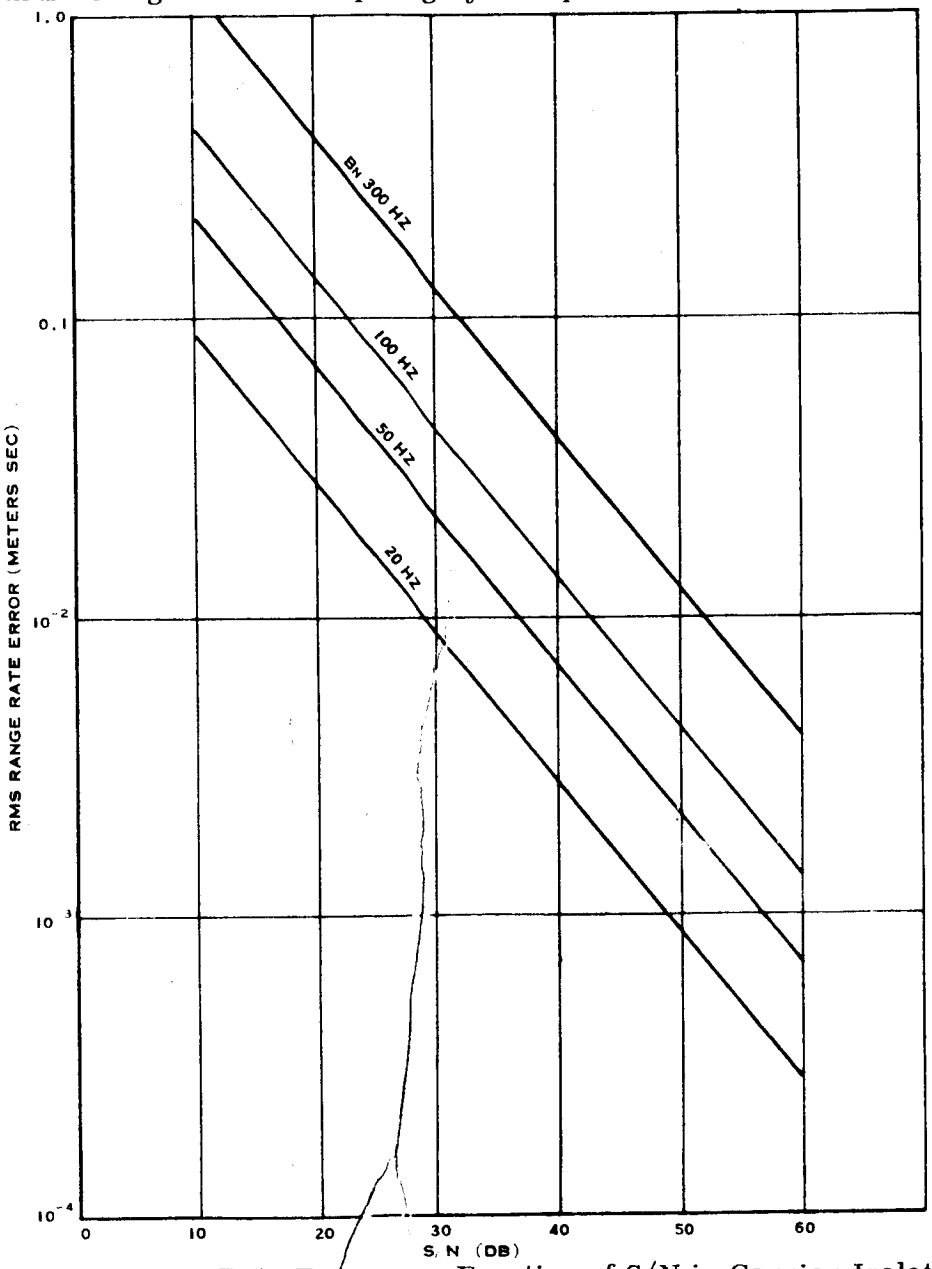

Figure 6.3-2 "Range Rate Error as a Function of S/N in Carrier Isolation Bandwidths for Various Values of Bandwidth and for S-band GRARR S-band Design Parameters"

Item 22, the threshold S/N in the carrier isolation bandwidth, is related to system range rate error as shown in Figure 6.3-2, and for a $2B_{Lo}$ of 60 Hz is 16 db. Under these conditions we note that the worst-case carrier margin is 6.7 db.

Item 28 (Table 6.3-6), the required ST/N/B, is related to the range error, and is plotted in Figure 6.1-5. For a specified range error of 10 meters, the required S/N is 11 db. Item 30, the worst-case range channel performance margin, is greater than 10 db, which summarizes the total transponding link analysis.

TABLE 6.3-7

TRACKING LINK DESIGN

Assume: P_{in} = 10 watts	VHF		S-band	
$\Delta\phi$ carrier = rad. $\Delta\phi$ 20 kHz tone = 0.7 rad. $\Delta\phi$ 500 kHz tone = 1.06 rad. 1 channel oper. @ S-band	carrier	20 kHz tone	carrier	500 kHz tone
Total XMTR	37.4 dbm (5.5 watts)		33.0 dbm (2.0 watts)	
Spacecraft power out	35.07 dbm	22.08 dbm	27.18 dbm	26.07 dbm
Space loss (121,000 km)	-176.2 db	-176.2 db	-201.16 db	-201.16 db
Satellite Antenna gain	-1.5 db	-1.5 db	+2.0 db	+2.0 db
Ground Antenna gain	+22.2 db	+22.2 db	+41.5 db	+41.5 db
Misellaneous losses	-2.5 db	-2.5 db	-2.1 db	-2.1 db
Received signal power	-122.93 dbm	-135.92 dbm	-134.58 dbm	-135.69 dbm
Receiver noise density	-169 dbm/Hz	-169 dbm/Hz	-175.2 dbm/Hz	-175.2 dbm/Hz
Receiver bandwidth	20 Hz	0.1 Hz	20 Hz	0.1 Hz
Received S/N ratio	+33.07 db	+43.08 db	+27.62 db	+49.51 db
rmz range error (meter)	5.5 meters		0.1 meters	

Since the use of either S-band or VHF Goddard Range and Range Rate Tracking was one of the options available for evaluation, a comparative analysis was made of the down-links of both systems. Table 6.3-7 presents the results of this analysis. It was assumed that the primary input power was ten watts in both cases. The constraints are that the VHF systems highest major side-tone was 20 kHz, and that only one-channel of the three available at S-band was employed. The modulation indices assumed were those specified as optimum for both systems. The results of this analysis clearly indicate the advantage of S-band over VHF.

VHF Beacon. To provide angle tracking at VHF requires only sufficient signal to noise power ratio in the ground receiver. For "sum" channel noise ratios of 10 db, the rms angle tracking error due to thermal noise in the receiver can be expressed as[9]:

$$\sigma_\theta = \frac{1}{K} \quad S/N \quad ^{-1/2} \qquad \text{(Milliradians)}$$

where $K = 0.077 \quad mr^{-1}$

A S/N = 10 db results in an rms angle error of 0.75 degrees, which is within the accuracy specified in Table 6.1-2. Table 6.3-8 is a tabulation of losses and gains for a 1 watt VHF beacon Spacecraft-to-Earth link operating in the tracking loop, Item 18, performance margin indicates a worst-case margin of 1.5 db. Thus, tracking within the specified accuracy is feasible. In addition, a very low telemetry data rate, such as might be required for the radial configuration could be accommodated. Higher telemetry rates could be accommodated at shorter ranges, or with reduced tracking accuracy. These options have not been evaluated here, but a trade-off of these two alternatives versus increased beacon power would provide guidance in a final choice of design parameters.

TABLE 6.3-8

PROJECT: ARC MULTIPLE SATELLITE DATE:

CHANNEL: VHF BEACON, P_o = 1 watt, (136.0 MHz)

MODE: ANGLE TRACKING

NO.	PARAMETER	VALUE	TOLERANCE		SOURCE
1	Total Transmitter Power 1 watt	30 dbm	+1.0	-1.0db	Specified
2	Transmitting Circuit Loss	-1.0 db	0.0	-1.0 db	"
3	Transmitting Antenna Gain	-1.5 db	+1.5	-1.5db	"
4	Transmitting Antenna Pointing Loss	Included in 3			"
5	Space Loss (136 mc, 121,000 km)	-176.8 db	---	---	Calculated
6	Polarization Loss	- 1.5 db	+1.5	-1.5db	Estimated
7	Receiving Antenna Gain	20.0 db	+1.0	-0.5db	Specified
8	Receiving Antenna Pointing Loss	Included in #7			Specified
9	Receiving Circuit Loss	" " "			Specified
10	Net Circuit Loss	-160.8 db	+4.0	-4.5	Σ (2 → 9)
11	Total Received Power	-130.8 dbm	+5.0	-5.5	1 + 10
12	Receiver Noise Spectral Density (N/B) (T System = 913 $+^{680}_{135}$ °K)	-169.0 dbm/Hz	+2.4	-0.5	Calculated
13	Carrier Modulation Loss	-0-			(Beacon)
14	Received Carrier Power	-130.8 dbm	+5.0	-5.5	11 - 13
15	Carrier APC Noise BW ($2B_{LO}$ = 60 Hz)	17.8 db-Hz	+0.5	-0.5	Specified

CARRIER PERFORMANCE - TRACKING (One-Way)

16	Threshold SNR in $2B_{LO}$	+10 db	+0.5	-0.5db	Calculated
17	Threshold Carrier Power	-141.2 dbm	+3.4	-1.5	12+15+16
18	Performance Margin	10.4 db	+6.5	-8.9	14 - 17

CARRIER PERFORMANCE - TRACKING (Two-Way)

19	Threshold SNR in $2B_{LO}$				
20	Threshold Carrier Power				
21	Performance Margin				

CARRIER PERFORMANCE -

22	Threshold SNR in $2B_{LO}$				
23	Threshold Carrier Power				
24	Performance Margin				

DATA CHANNEL

25	Modulation Loss				
26	Received Data Subcarrier Power				
27	Bit Rate (1/T)				
28	Required ST/N/B				
29	Threshold Subcarrier Power				
30	Performance Margin				

SYNC CHANNEL

31	Modulation Loss				
32	Received Sync Subcarrier Power				
33	Sync APC Noise BW($2B_{LO}$ =)				
34	Threshold SNR in $2B_{LO}$				
35	Threshold Subcarrier Power				
36	Performance Margin				

COMMENTS:

6.4 SPACECRAFT ANTENNA CONSIDERATIONS

The spacecraft antenna considerations fall into two groups: carrier module antena and satellite antenna. Within each of these groups, consideration is given to the two proposed configurations: radial and stacked.

6.4.1 Carrier-Module Antenna

In the configurations considered, a group of four satellites is clustered together after having been spin-stabilized and boosted to final orbit velocity. After the booster is jettisoned, the cluster is left in a "coast" condition. At the appropriate time, commands are transmitted which cause satellite separation, placing the satellites in their proper orbits. A command antenna is therefore required for the carrier module, or cluster. This antenna is also to be used with a beacon transmitter for tracking and telemetry.

Figure 6.4-1 shows the orientation of the radial configuration at various positions in the orbit. The arrows indicate the direction of the forward end of the cluster. Figure 6.4-2 illustrates the fact that for the stacked configuration, the carrier module spin-axis will be erected normal to the orbit plane, thus imposing different antenna pattern requirements. Figure 6.4-3 is a close-up view of the radial configuration, and Figure 6.4-4 is a close-up view of the stacked configuration. The following paragraphs discuss antenna concepts for the two carrier module configurations.

Stacked Cylinder Configuration. The command antenna for this configuration is to have pattern coverage near 90 degrees to the spin axis with coverage continuing through the region toward the rear, or toward the position of the third stage motor. Coverage is to be omni-directional about the spin axis. S-band or VHF may be used for this command function. At the time of use of this system, the booms will have been deployed, but the effect of boom excitation is probably negligible.

- S-band circular array of one satellite. One suggestion for the telemetry antenna for this configuration was a cylindrical array

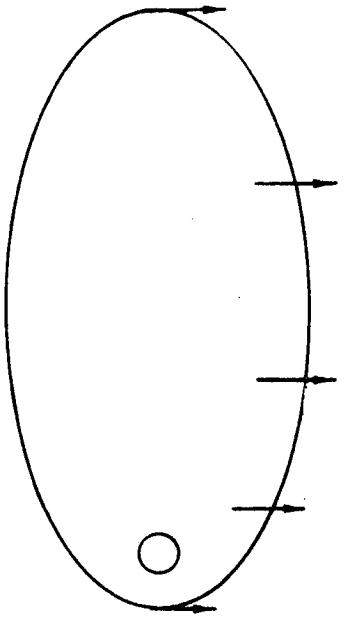

Figure 6.4-1 Orientation, Radial Configuration

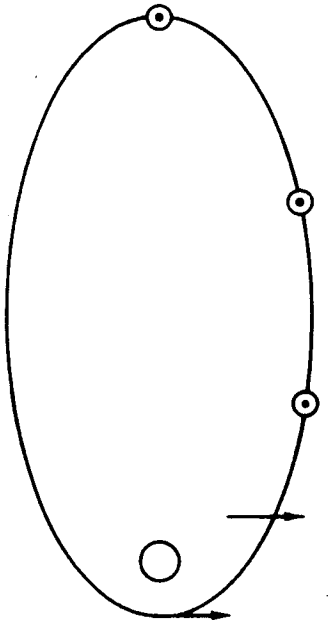

Figure 6.4-2 Orientation, Stacked Configuration

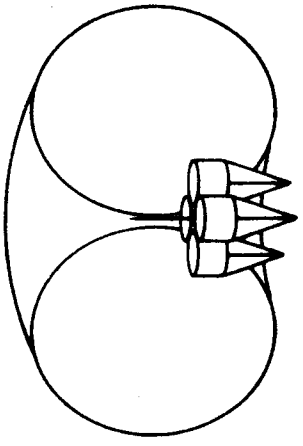

Figure 6.4-3 Radial Configuration

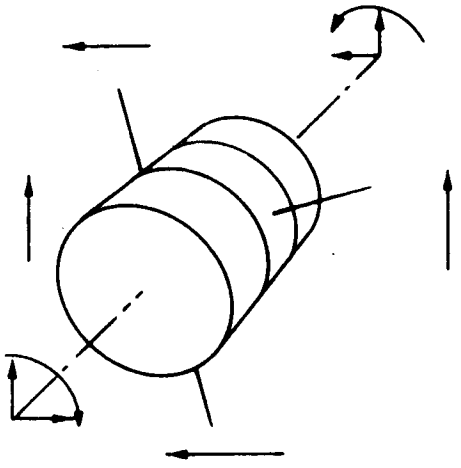

Figure 6.4-4 Stacked Configuration

about the satellite. This antenna on one of the two central units might be used for the command system. The pattern while looking through the carrier truss is undetermined but it may be suitably uniform in azimuth. A drawback will be that the lobe (gain) will fall off rapidly toward the rear direction.

- An S-Band "bent stub" array on the aft satellite. A cylindrical array of vertical stubs on the cylinder face will generate an omni-directional azimuth pattern if near enough to the edge. If the stubs are all bent inward and fed in a phase progression of 2π radians around the circle, circular polarized energy will be available in the aft direction. A second array would be required on the inner satellite pair. This approach would probably require a large number of elements placed within inches of the edge of the face to achieve reasonable broadside directivity and seems unnecessarily complex.

- A VHF "bent stub" array. This array could consist of just four elements placed at corners of a square of about $\lambda/3$ on a side. The wavelength is long enough compared to vehicle size (42.5" dia.) for a good azimuth pattern. Phase progression feeding will fill in the aft null. Again, a second array is required for the inner satellite pair.

- A single VHF stub placed in the center face of the forward satellite. At this long wavelength, the azimuth coverage will be good. However, the deep null in the aft direction may not permit use of the single stub antenna.

- A turnstile array at VHF (136 MHz) about the mid-section. This antenna will develop circular polarization off the tail and linear in the 90 degree equatorial plane. Since the elements will be over a half wavelength apart, some pattern ripple will occur in this 90 degree azimuth plane. However, an important advantage for the antenna is that only one is required with no complexity of separating coaxial cables during the vehicle separation.

Radial Configuration. The command antenna for this configuration is to have pattern coverage in the azimuth about spin axis. The expected requirement will be in directions near 90 degrees from the spin axis with no requirement at angles near the spin axis except as required by the transponder. Booms will not be deployed when this command antenna is required.

Suggested telemetry antennas for this configuration included a belt cylindrical array about each satellite or an S-band unit that nests up within the booms prior to their deployment. Neither of these approaches offers much promise as a command antenna prior to vehicle separation. An S-band approach does not appear reasonable for this configuration (nor the other configuration for that matter) because of gross vehicle size. An S-band unit would probably need to be held about five or more feet away to reduce the effect of the vehicle on pattern coverage. The following VHF antenna alternatives, therefore, were considered.

- A four element VHF array, one element on each satellite aft face. This group would not use bent stubs since aft coverage is not required. These radiators would now be near enough to the edge of these aft faces so that reasonable omni-directional azimuth coverage is provided.

- A single VHF stub centrally located on the aft faces and erected after third stage separation. At a low enough frequency (136 MHz) this unit would give reasonable dipole type coverage; the totla of four satellite faces is only about one half wavelength in diameter. The antenna does, however, have a deep polarization null off the aft axis. Its major advantage is that upon the separation of the four vehicles, no coaxial lines need be broken or separated.

Based on these considerations, the preferred antenna design alternative for the radial configuration is a VHF quarter-wave whip, spring mounted to the carrier mechanism and erected after separation of the booster. For the stacked configuration the preferred alternative is a VHF turnstile (crossed dipoles) which will provide spherical coverage -- an important consideration because of carrier reorientation prior to satellite separation.

6.4.2 TT&C of Carrier Module by Satellite Telecommunication Subsystem.

For the radial configuration, serious consideration was given the alternative of using the S-band antenna and associated transponder on-board one of the satellites in the cluster. This alternative was discarded on the basis of the following considerations.

Assuming the use of a bi-conical horn, and assuming that the satellite booms are folded during the "coast" phase, the boom structure, which is fabricated of conducting material will cause pattern distortion in the equatorial plane of the module as illustrated in Figure 6.4-5, where point "A" represents the spin-axis of one of the four radially mounted satellites. Nulls exceeding 10 db might be expected for a window of 0 to 270 degrees.

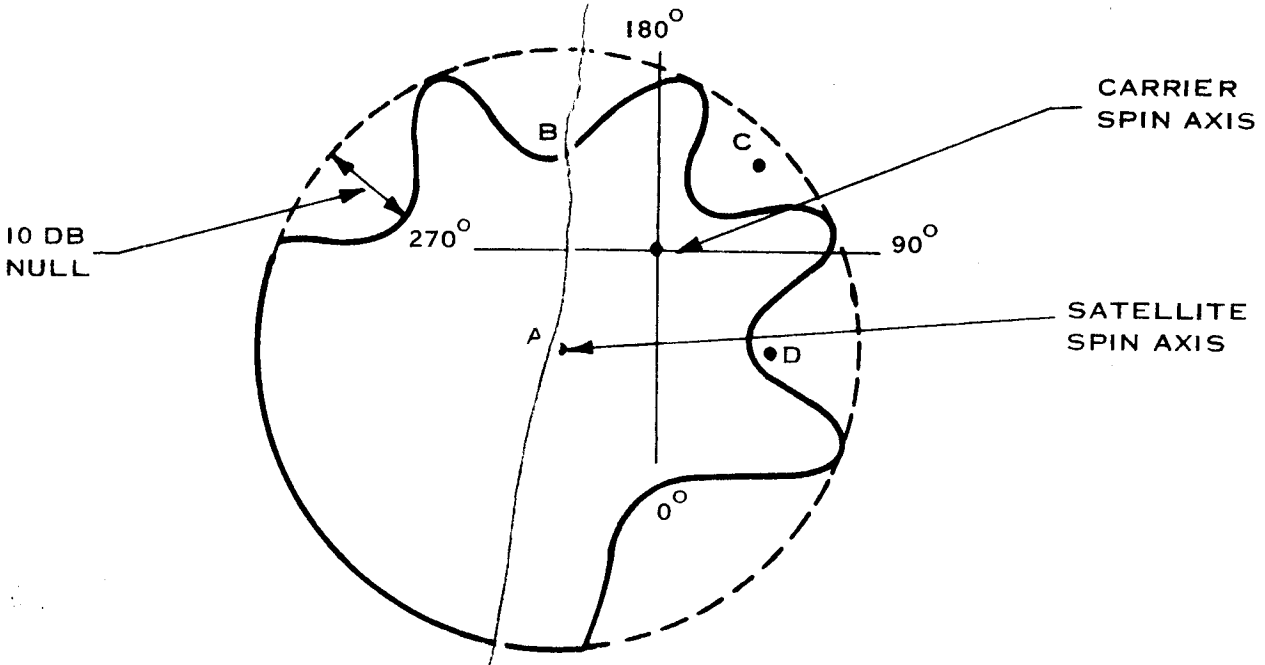

Figure 6.4-5 Antenna Pattern Distortion on Radial Cluster

For this situation, and for a dispenser spin rate of 120 rpm, or 2 cps, full signal strength exists for 125 milliseconds, with the balance of one revolution of the dispenser experiencing nulls. Since the radiated signal is assumed to be the transponded down-link S-band range and range rate signal, a requirement of at least 10 db margin exists in the tracking down-link I-F system lock is to be maintained. This is not the case as can be verified by inspection of the down-link budget analysis (Table 6.2-5).

Alternatively, if 125 milliseconds is adequate for the GRARR system to acquire lock and perform a measurement, this technique might work effectively. The time to acquire and perform range and range rate measurements is the time to perform the following operations:

a. Ground receiver phase-lock loop acquires
b. Sub-carrier phase-lock loop acquires
c. Apply ranging tones to signal transmitted from the ground
d. Propagate range tones to satellite receiver and back to ground
e. Pull in and lock range loops
f. Lock-in of Hybrid Acquisition system
g. Multiplication and integration of received and reference codes.

Assuming a carrier loop acquisition bandwidth of 200 Hz, a threshold signal level of -142 dbm (10^5 km range, 1 watt transponder), and a parallel mode of operation wherein all ranging tones acquire concurrently, the following tabulation indicates the time required for acquisition. This time is exclusive of the smoothing time necessary for realization of stated range and range rate system accuracies.

a.	Turn on transponder & RF returns to ground receiver	0.64 sec.
b.	Carrier loop locks	6.7 sec.
c.	Subcarrier loop locks	6.7 sec.
d.	Range tones transmitted and received	0.64 sec.
e.	Tone loop lock time	negligible
f.	Digital tone extractor locks	0.13 sec.
g.	Hybrid acquisition begins	0.38 sec.
h.	Code designate time	negligible

Total Acquisition Time is 16.31 + (4.0) N seconds where N - number of correlations of received and reference code sequences. Clearly, the system acquisition and data measurement time far exceeds the time available in a fraction of the dispenser rotation cycle.

Additional considerations for use of satellite S-band transponder in "cruise" phase. The initial concept envisioned use of a single satellite GR&RR subsystem; however, antenna pattern distortion and unbalanced power drain among the four satellites generated the idea of possibly activating all four satellites. In this mode, if all four satellite transmitters radiate on the same frequency, the tracking of individual satellites following separation is precluded, and would be impractical, if not, in fact, contrary to the principles and practices of ground station support. Alternatively, the transmission of signals on separate frequencies makes the acquisition problem due to antenna pattern distortion similar to the problem when only a single satellite of the four is energized. For these reasons, use for carrier module telemetry tracking and command was abandoned in favor of an independent TT&C receiver-transmitter-antenna mounted on the carrier frame.

6.4.3 Satellite Antenna

An S-band antenna ($\lambda \approx$ 5-1/2 inches) is required which will develop a uniform toroidal (azimuth) pattern about the spin axis of the vehicle. Nulls are allowed on or near the spin axis, and beam narrowing may be permitted if significant antenna gain is required. This azimuth radiation pattern should remain fairly constant for any given cone angle measured from the spin axis. This is because any amplitude variationof the pattern will appear as an amplitude modulation of the received signal at the vehicle spin rate. The following paragraphs present design alternatives for statellite antennas.

Stacked Configuration. One vehicle configuration for consideration is a flat cylinder, 43 inches in diameter and 12 inches high (stacked configuration). Three booms are to be erected in space, located 120 degrees apart around the cylinder. Such a design is not conducive to the development of good azimuth coverage at a short wavelength.

- Boom-Mounted Dipole. The usual method to obtain such coverage would be from a dipole, or biconical type of radiator with axis on the spin axis. However, the vehicle may interfere with this pattern since it is large, about 8 wavelengths in diameter. Such an antenna would need to be mounted some distance away to avoid this problem. An erecting boom might be used to accomplish this. An experimental pattern study would be needed to determine the best arrangement for this.

- Cylindrical Array. A cylindrical array will also generate an omnidirec- azimuth pattern. Ideally, a continuous "in phase" radiating source around the cylinder is required. This may be simulated by closely spaced discrete sources. As fewer sources are used, becoming farther apart, the azimuth pattern develops larger relative lobes until finally deep nulls are registered. A maximum spacing of about 3/4 wavelength might be used for maintaining a good uniform pattern. Again, this depends upon system tolerance of signal amplitude variation as the vehicle spins.

  The 43-inch diameter indicates that 33 radiating elements are required at a spacing of about 0.744 wavelengths. These elements could be a variety of things as follows:

  a. The planar spiral, cavity backed. A planar spiral (printed) about 0.7 wavelength diameter and backed by a cavity about 2 inches deep. This will develop circular polarization.

  b. Dipoles mounted either longitudinally or circumferentially about the cylinder. These half wave dipoles should be placed about 1/4 wavelength from the cylinder surface. Linear polarization.

  c. Crossed dipoles mounted as above and in phase quadrature will develop circular polarization.

Radial Configuration. Another (and more desirable from the antenna standpoint), configuration has been suggested. This cylindrical design is 21 inches in diameter and 26 inches long with a recessed belt area around the central region which may be ideal for mounting a cylindrical array. The array could consist of 16 radiators mounted within the belt region. The longitudinal dimension of the radiators may be extended to achieve a narrower elevation beam and additional gain. The elements would be the same as those discussed above. Also for this configuration the use of a dipole (biconical) on the spin axis becomes more attractive. The smaller diameter will tolerate a closer spacing of antenna to vehicle body.

Based on considerations of satellite dimensions, pattern coverage, and mechanical constraints, the preferred alternatives for an S-band satellite are the biconical-horn for the radial configuration, (Figure 6.4-6) and the cylindrical array for the stacked configuration (Figure 6.4-7).

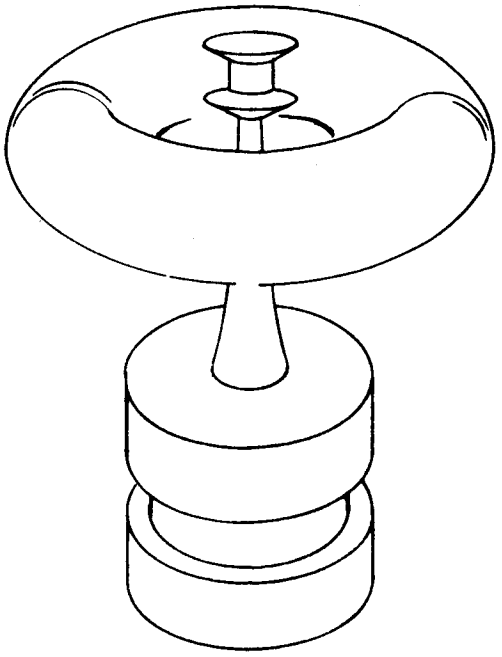

Figure 6.4-6 Bi-conical Horn Satellite Antenna

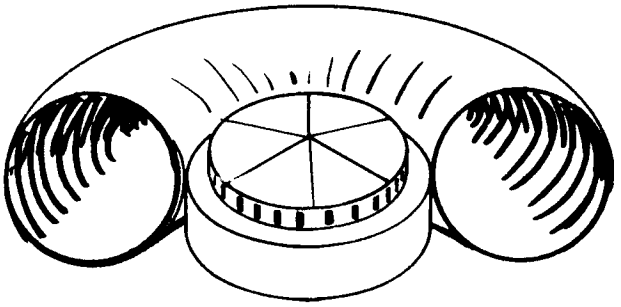

Figure 6.4-7 Cylindrical Spiral Array Satellite Antenna

6.4.4 Antenna Beam Shaping

In the development of satellite antenna trade-offs, a problem of providing adequate earth coverage at low altitudes while maintaining maximum antenna gain presents itself. The problem arises because the satellite spin axis is normal to the ecliptic and not normal to the orbital plane. This phenomenon is discussed at greater length in Section 7.4. Figure 6.4-8 illustrates the situation.

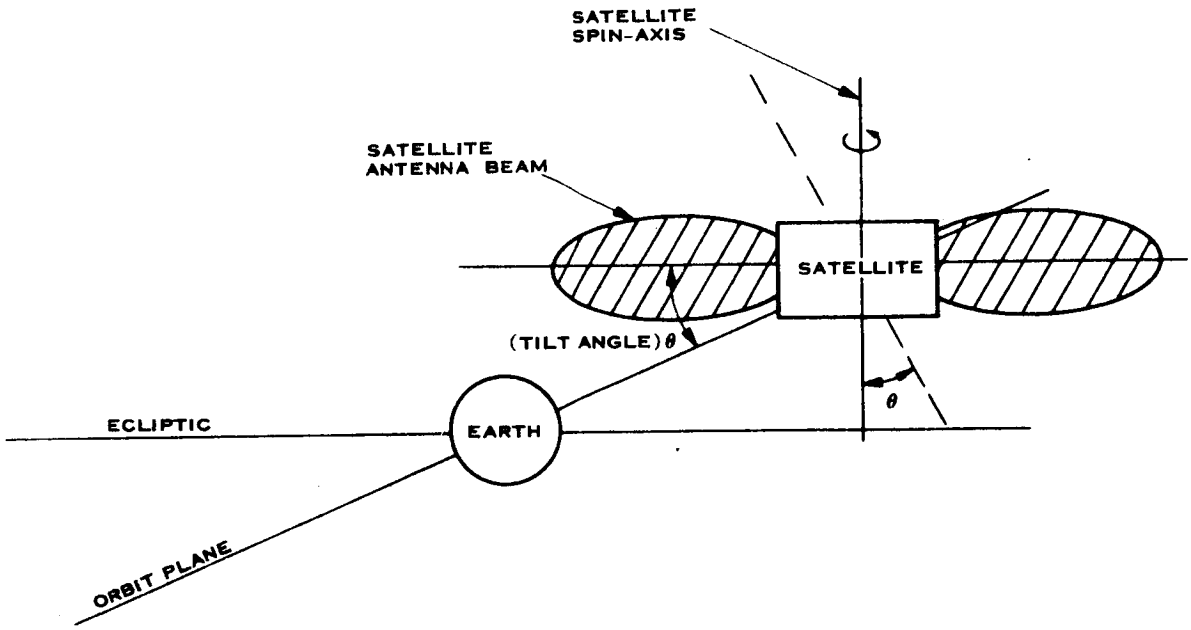

Figure 6.4-8 Satellite to Orientation Relative to Orbit Plane

It is fortuitous that the effect of the "tilt" is greater at smaller slant ranges, because this allows us to postulate a hypothetical antenna pattern which will meet both the earth coverage and gain requirements. Table 6.4-1 tabulates the "tilt" angle, the slant range and the required gain versus true anomaly in orbit. Since

the tilt angle is the same as the beam angle in the elevation plane, and since the required gain can be defined in terms of this angle, an antenna pattern can be derived.

The antenna pattern shown dotted in Figure 6.4-9 represents relative power levels required as a function of the angle measured from the spin-axis normal. Therefore, the dotted pattern represents the required relative antenna gain based on considering the tilt of the spin axis relative to the orbit normal (which is the view angle from the satellite antenna to earth) and the slant range, both as a function of the satellite position (true anomaly) in orbit. The solid line represents a possible antenna pattern which, in fact, can be approximated by a simple dipole.

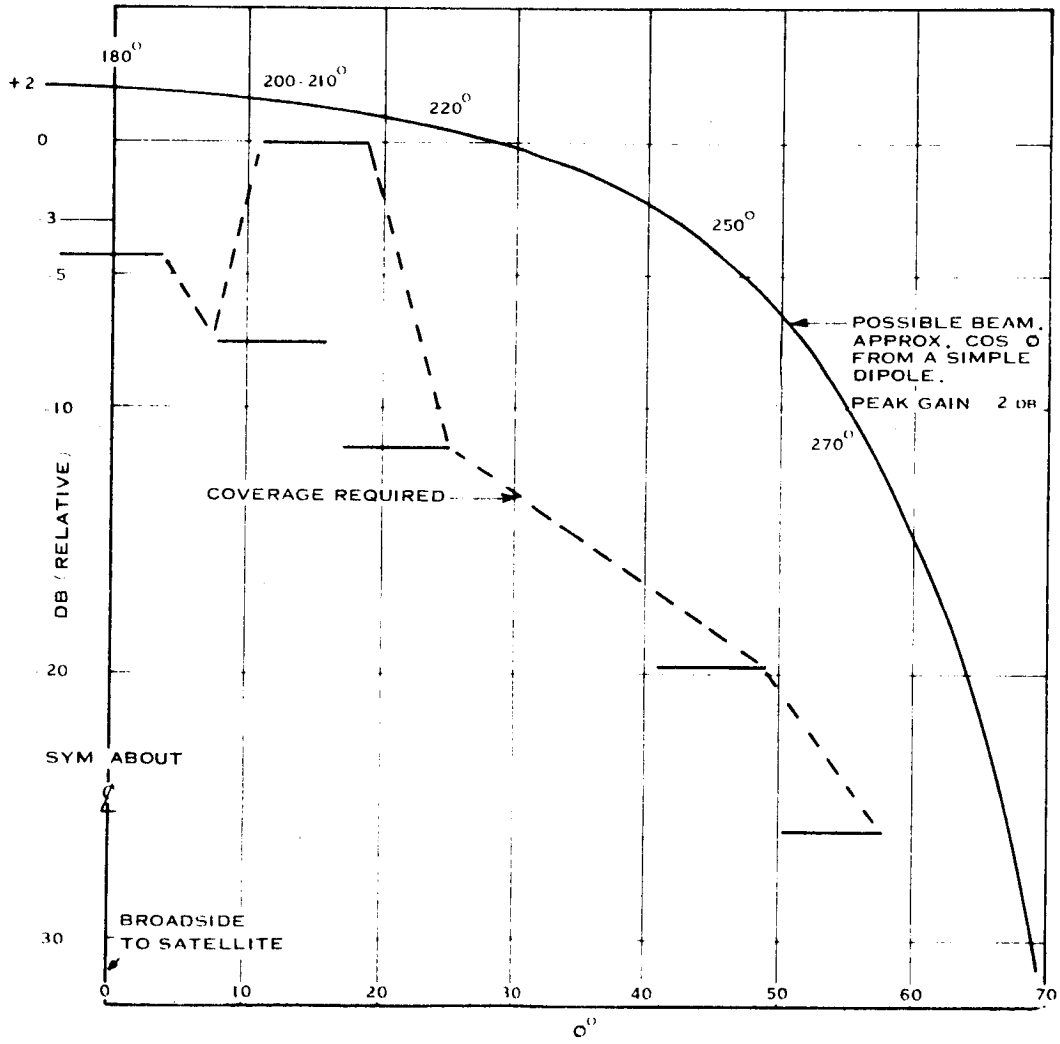

Figure 6.4-9 Elevation Plane Antenna Pattern

TABLE 6.4-1

"TILT" ANGLE, SLANT RANGE, AND GAIN FOR ORBIT ANOMALIES

True Anomaly	Off-Axis Angle (degrees)	Slant Range (KM)	Required Antenna Gain (db)
180	15° ± 4°	12,181	0
200	0 ± 4°	75,412	4.16
210	12° ± 4°	51,491	7.44
220	21° ± 4°	39,505	11.6
225	25° ± 4°	27,687	12.8
250	45° ± 4°	12,986	19.8
270	59° ± 4°	6,104	25.9

Note that the first null must exceed a 60-degree half-angle to obtain full coverage. The solid curve is chosen to have its first null at 70 degrees, and this approximates the half-power beamwidth; i.e., 70 degrees. This pattern is not that of a simple dipole which has a half-power beamwidth of 78 degrees, but is instead a beam somewhat narrower. It should be noted that the peak gain can be greater than that from a dipole, and, depending upon the actual design, may exceed 2db which was assumed as an antenna gain figure in the link budgets for S-band. For instance, a bi-conical antenna nearly a wavelength long might be used to obtain this particular beamwidth.

6.5 TELEMETRY SUBSYSTEM FUNCTIONAL DESCRIPTION

6.5.1 General

The telemetry subsystems of the satellites monitor and encode data from the scientific experiments, attitude control sensors, and engineering status activities. These data are processed for storage by means of a high performance tape recorder for subsequent playback. The data may also be transmitted to the STADAN ground stations in real-time depending on the mission phase.

In addition, the parameters associated with the multiple satellite holding structure, attitude control, and dispensing mechanism, may be monitored and transmitted to the ground by a parallel channel in real-time.

6.5.2 Mission Requirements

6.5.2.1 Primary Satellite Telemetry Requirements. The primary satellite telemetry requirements are:

a. Accept data from on-board scientific experiments, encode and relay this data to the ground stations.

b. Operate with two scientific instruments: a magnetic field measuring device and a particle / energy detector. The bandwidths of these instruments will be less than or equal to 1 Hz.

c. PCM telemetry data format for accuracy and compatibility with future data processing and data link trends.

d. PCM word length of 7 bits for system resolution and accuracy capabilities.

e. Error rate of 1 in 10^4 for PCM data, 1 in 10^3 worst case.

f. On-board time reference base for experiment data acquisition time correlation.

g. Operate with existing STADAN ground station and data processing equipment.

h. Provide for status and diagnostic telemetry, specific points to be defined.

6.5.2.2 Secondary Requirements. In addition to the specific requirements stated in the previous paragraph, the following additional recommendations are made:

a. Operational: The satellite orbit and power place limitations on the TLM data transmission rates and hence on the data measurements and the sampling rates. To meet the mission requirements, several telemetry modes are proposed. These are described in Section 4.

b. Configuration: To meet the system requirements, the following configuration centerlines have been established:

- Incorporation of a tape memory to permit recording of essential data at apogee and playback to the ground stations at perigee.

- Maximum use of high reliability parts and space proven techniques to meet the projected one-year lifetime. (This is in preference to a partially or fully redundant system which would increase the space and power required and the manufacturing cost.)

- Maximum use of the Space & Re-entry Systems Divisions existing field-effect transistor (FET) and integrated circuit (IC) components and technology to minimize the development costs on the subsystem.

c. A separate real-time channel to accommodate the limited TLM requirements for the multiple satellite holding, altitude control, and dispensing mechanism.

6.5.3 Required Subsystem Functions

6.5.3.1 Mission Telemetry Profiles. Figures 6.5.1 and 6.5.2 illustrate the mission profile as it relates to telemetry operations. The figures are subdivided into two main categories - vehicle and satellite activities and telemetry (TLM) activities. During each phase of the mission, the scope and degree of interest in TLM measurements shifts. This is indicated in the figures by the profiles of the TLM parameters from the various TLM sources.

a. During launch, ascent, and up to payload separation, TLM will not be required.

b. Following payload separation, attitude data will be transmitted in real-time from the carrier module for the stacked configuration.

c. As the STADAN stations acquire, the initial setup and verification of the satellite orientations and orbits will take place. During this period, engineering data (which includes attitude data) will be transmitted in real-time from either the central module and/or the satellites depending on the particular configuration and phase.

d. Following the proper orientation of the spin-axes of the satellites and the orbital determinations, the mission will enter the phase during which the scientific data will be of most interest. During this portion of the missions, the TLM subsystem will be required to operate in five distinct modes as indicated in Section 6.5.4.

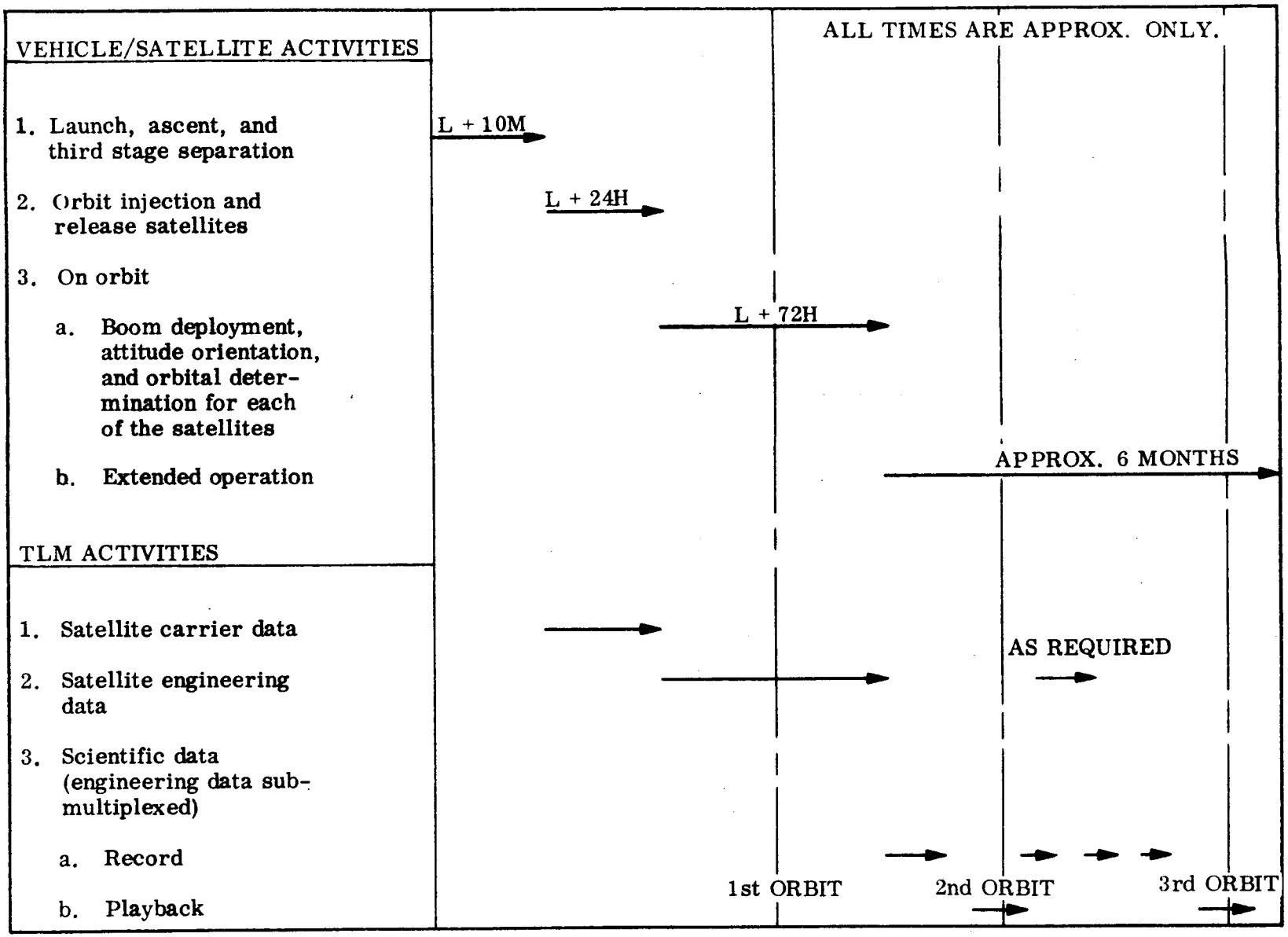

Figure 6.5-1 Mission TLM Profile (Radial Configuration)

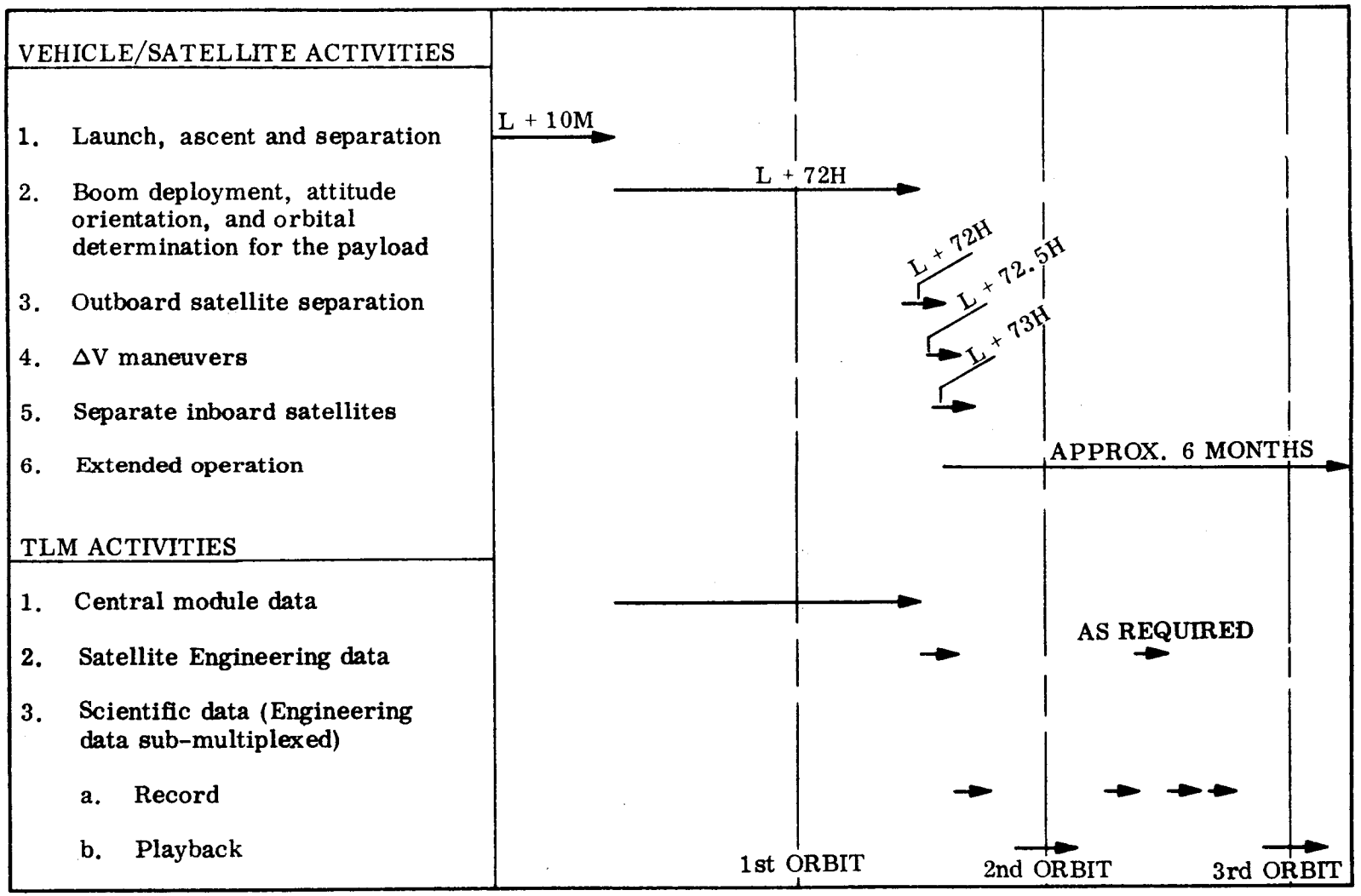

Figure 6.5-2 Mission TLM Profile (Stacked Configuration)

TABLE 6.5-1

DATA PARAMETERS

Subsystem	No. of Input Data Parameters	
	Analog	Discrete
Experiments		
Magnetometer	3	
Particle Detector	2	2
Attitude Control[1]		
Pressure		1
Spin Rate[2]		1
Sun Angle		1
Roll Angle		1
Command Decoder		8
Power	16	
TLM		
Encoder/MPLX	3	4
Tape Recorder	3	6
Time Data		2
RF		
Receiver	2	1
Transmitter	3	2
Total	30	29

[1] The Attitude Control subsystem parameters are monitored on the Central Module for the stacked configuration or on each of the satellites for the radial configuration.

[2] Not required to be monitored for the stacked configuration.

6.5.4 Telemetry Modes

The requirements and various operating conditions described in the preceding paragraphs can be summarized in terms of modes as follows:

Mode 1 - Standby, no telemetry equipment in operation.

Mode 2 - Engineering data transmitted in real-time at the low bit rate of approximately 112 bits per second. These data will be transmitted from the carrier module for the stacked configuration.

Modes 3a and 3b - Science and Engineering data transmitted in real time at the medium bit rate of 1120 bits per second. These data will be transmitted from the satellites; Mode 3a emphasizes science data and Mode 3b emphasizes engineering data.

Mode 4 - Science and engineering data recorded at the medium rate of approximately 1120 bits per second. The science data will constitute approximately 95 percent of the data recorded. The record time is a function on the recorder capacity and will range from a minimum of 3.0 hours for a recorder capacity of 1.25×10^7 bits to 10 hours for a recorder capacity of 4.0×10^7 bits. At the conclusion of Mode 4, the telemetry subsystem will normally reset to Mode 1.

Mode 5 - Playback of the magnetic tape memory at a high rate. The cycle time for this mode will be a function of the tape recorder capacity, and the playback rate. The playback rate depends on variables such as the available power and the ground station availability. Figure 6.5-3 illustrates the relation between recorder capacity, playback rate, and playback time.

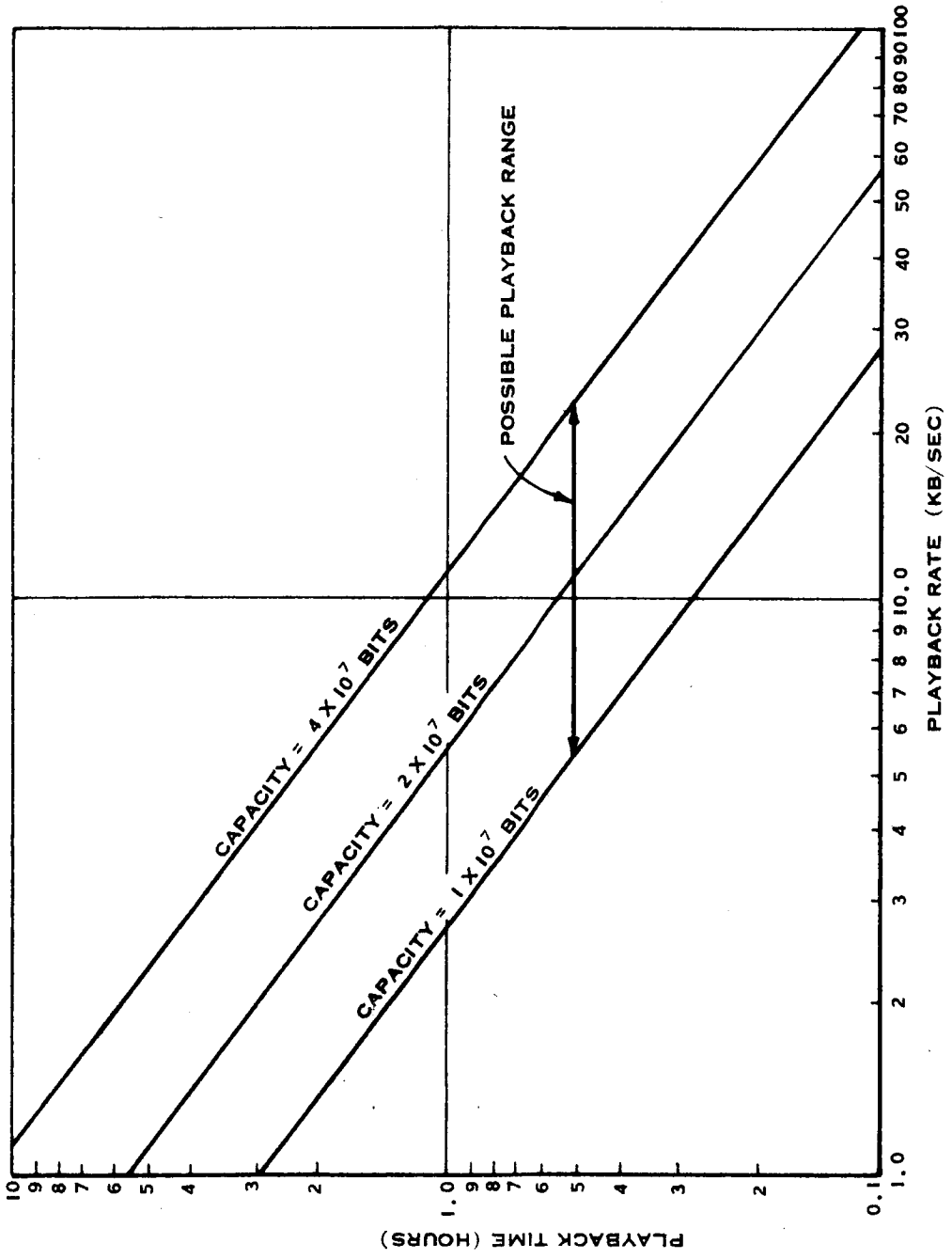

Figure 6.5-3 Playback Time as a Function of Playback Rate for various Tape Memory Capacities

6.5.5 Performance and Operational Parameters

6.5.5.1 Telemetry Data Format. The proposed data frame format for real-time telemetry in Mode 3a and delayed telemetry in Modes 4 and 5 is illustrated in Figure 6.5-4. Some of the more pertinent parameters of the format are as follows:

Main Frame Length. 1024 bits including 144 data words and 16 bits of frame sync.

Subframe Length. 56 bits which includes 8 data words.

Subcommutated Frame Length. 72 words

Word Size. 7 Bits

Bit Rate. 1120 bits per second in Modes 3 and 4. 5.5 Kb/sec to 21 kb/sec in Mode 5 depending on tape memory capacity and transmitter power available.

Data Cycle. The basic sample rate is based on the subframe rate of approximately twenty per second, which provides a basic sampling rate for each of the experiment parameters of 20 samples per second. Using a 40 db/decade input filter, this results in an aliasing error of less than 1/2 percent up to a data frequency of 1 Hz and less than 1.5 percent up to 10 Hz. The question of errors is discussed more fully in Section 5.2. The remaining engineering data are subcommutated into word (channel) number 8 of the subframe. This provides an effective low sampling rate of 20/72 = 1 sample per 3.6 seconds. Some parameters may be assigned multiple subcom words so that the effective rate may be higher than 1 sample per 3.6 seconds.

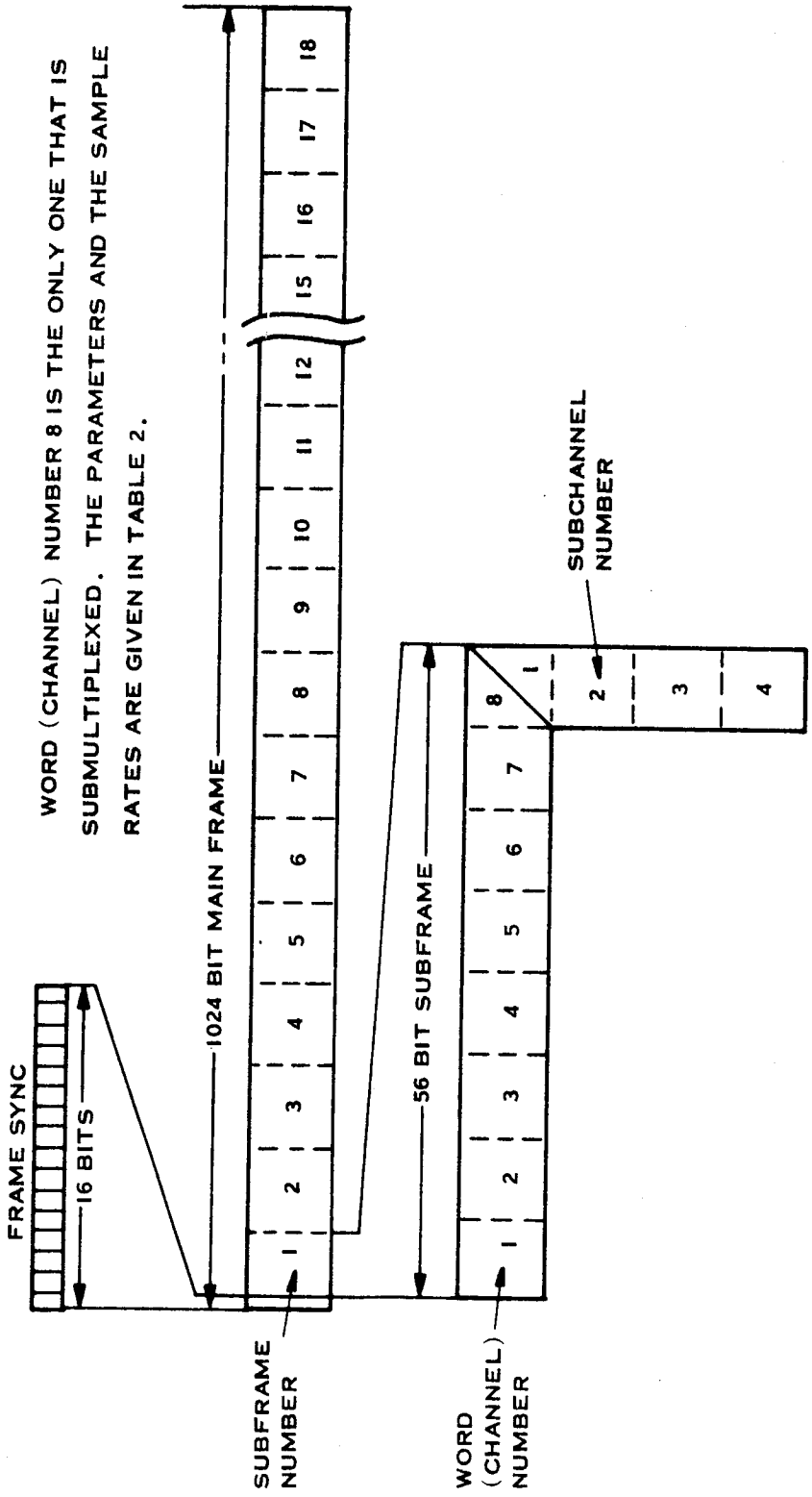

Figure 6.5-4 Proposed Data Frame Format For Modes 3a, 4 and 5.

Sync. Synchronization of the main frame is accomplished by recognition of the 16-bit frame sunc. word at the beginning of each data frame. Synchronization of the subcommutated frame in word 8 is accomplished by recognition of the complement of the 16 bit main frame sync. word.

Mode Recognition. A partial recognition of the particular mode may be accomplished by noting the frequency of the data subcarrier. For a particular subcarrier frequency, the remainder of the recognition may be performed by identifying one of the subcommutated words in channel 8.

The proposed data frame format for real time telemetry in Modes 2 and 3b is illustrated in Figure 6.5-5. The main parameters of this frame are the same as those for the data frame utilized in Modes 3a, 4 and 5, except the bit rate in Mode 2 is approximately 112 bits per second. The main difference lies in the assignment of the data to be monitored to the available word slots or channels. For Modes 3a, 4 and 5, the scientific experiment data was assigned to almost all the available word slots with the engineering data being submultiplexed into one of the available word slots. For Mode 2 and 3b, on the other hand, engineering data samples are commutated into the available word slots and the subcommutation feature is not used at all.

Mode recognition is accomplished by complementing of the main frame sync word and recognition of mode designation words in the data frame.

6.5.5.2 Telemetry Errors. The performance of the telemetry subsystem in terms of accuracy can be allocated to the following factors:

a. Pre-multiplex filtering

b. Aliasing or frequency-spectrum foldover errors

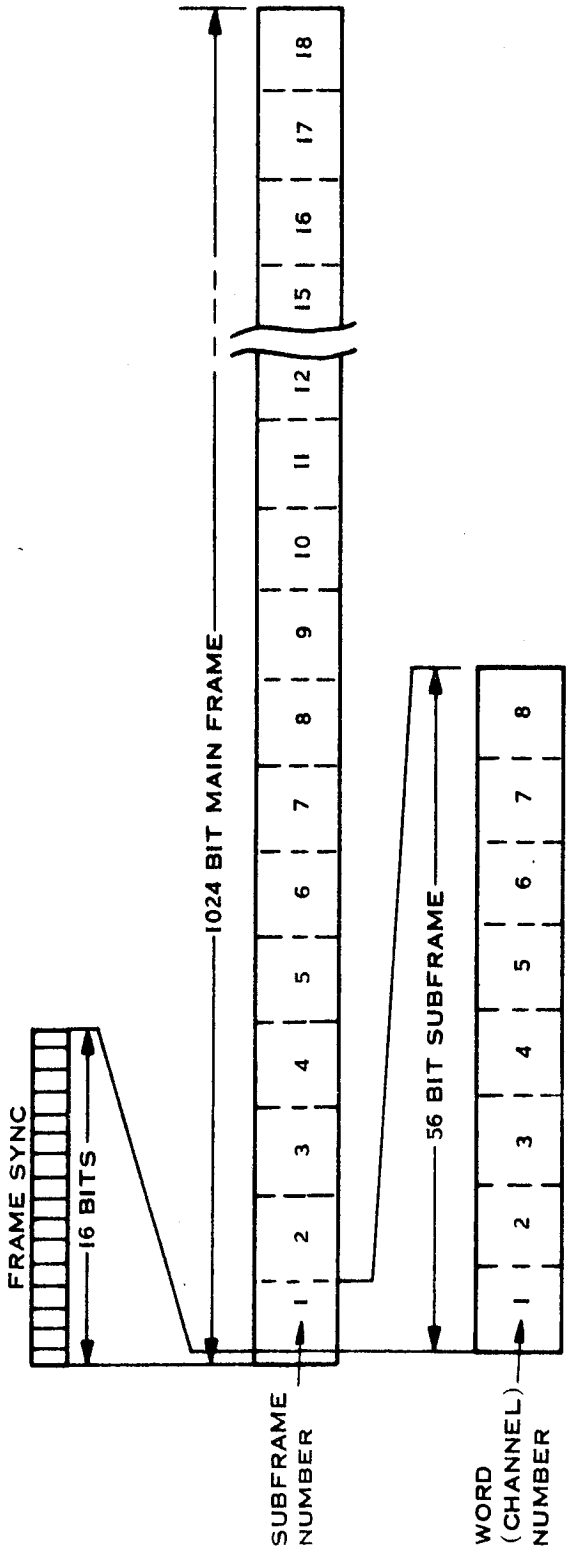

Figure 6.5-5 Proposed Data Frame Format For Real Time TLM Modes 2 and 3b

c. Multiplex errors

d. Quantizing errors

e. PCM link errors

f. Tape-memory playback errors

It is assumed that the decoding by the ground stations is essentially error-free compared to the encoding process. Utilizing a 7 bit PCM system introduces a peak quantizing error of ±0.375 percent. The multiplex errors can be held to ≤ ±0.1 percent. The PCM link errors are equivalent to an average error of ≤ ±0.05 percent. Similarly the errors involved in playback of the tape memory can be averaged out to ≤ ±0.05 percent.

The main errors aside from the quantizing error are errors introduced because of the pre-multiplex filtering to restrict the bandwidth of the data signal input to the telemetry encoder and errors introduced because of frequency spectrum foldover errors (aliasing errors) which arise from a limited sampling rate as compared to the highest data frequency.

For the case under consideration, the frequency response of the basic magnetometer (using Pioneer and the LSM programs as guidelines) is of the order of 50 Hz. The power spectral distribution, undoubtedly extends up to 100 Hz or 200 Hz before the power components are down 40 db or so.

Bandwidths of this magnitude would require two or three orders of magnitude increased recording capacity and telemetry link capacity for the data collection periods contemplated (i.e., of the order of ten hours). Therefore, it seems reasonable to restrict the bandwidth. The effective output bandwidth of the Pioneer magnetometer is 0.3 Hz and the LSM magnetometer 0.5 Hz. Therefore, data bandwidths of this order of magnitude have been deemed reasonable

for this application. However, there is one additional factor which cannot be overlooked and this is the contribution of the satellite spin to the frequency spectrum of the magnetometer output. The maximum spin rate of the satellite is estimated to be 90 rpm or 1.5 revolutions per second. Thus, the basic magnetometer data will be modulated by or will modulate the 1.5 cps satellite spin component.

There are two choices with respect to obtaining the desired magnetometer data. One would be to process the data on board to remove the spin component. The other alternative would be to transmit the entire spectrum to the ground and to process the data on the ground.

It turns out in this particular case that the spin rate component is located in the spectrum such that it can be conveniently sampled and transmitted within the existing telemetry link requirements. The alternate technique of on-board data processing require sophisticated and complex equipment. Thus the solution that has been chosen is to send the entire data spectrum, including the spin rate components, down the link and reduce the data on the ground. Nevertheless, a pre-multiplex filter is required between the experiments and the telemetry system with a "cutoff" frequency of 1.5 Hz, and an attenuation beyond the cutoff frequency of 40 db/decade.

With these parameters and a sampling rate of 20 samples/sec, the resulting error due to spectrum foldover can be interpolated from the curves in Figure 6.5-6. For Fs/Fc = 13, the aliasing error is seen to be approximately 0.5 percent for all frequencies below 1 Hz. Even in the range from 1 Hz to 10 Hz, the peak error does not exceed 1.5 percent. Error curves for Fs/Fc = 8.0 and Fs/Fc = 3.0 are also illustrated to show that to achieve a 1 percent system, an Fs/Fc of at least 10 is required. This area is amenable to trade-offs, however, and if a higher percentage of error can be accepted, the bandwidth can be increased or the sample rate decreased.

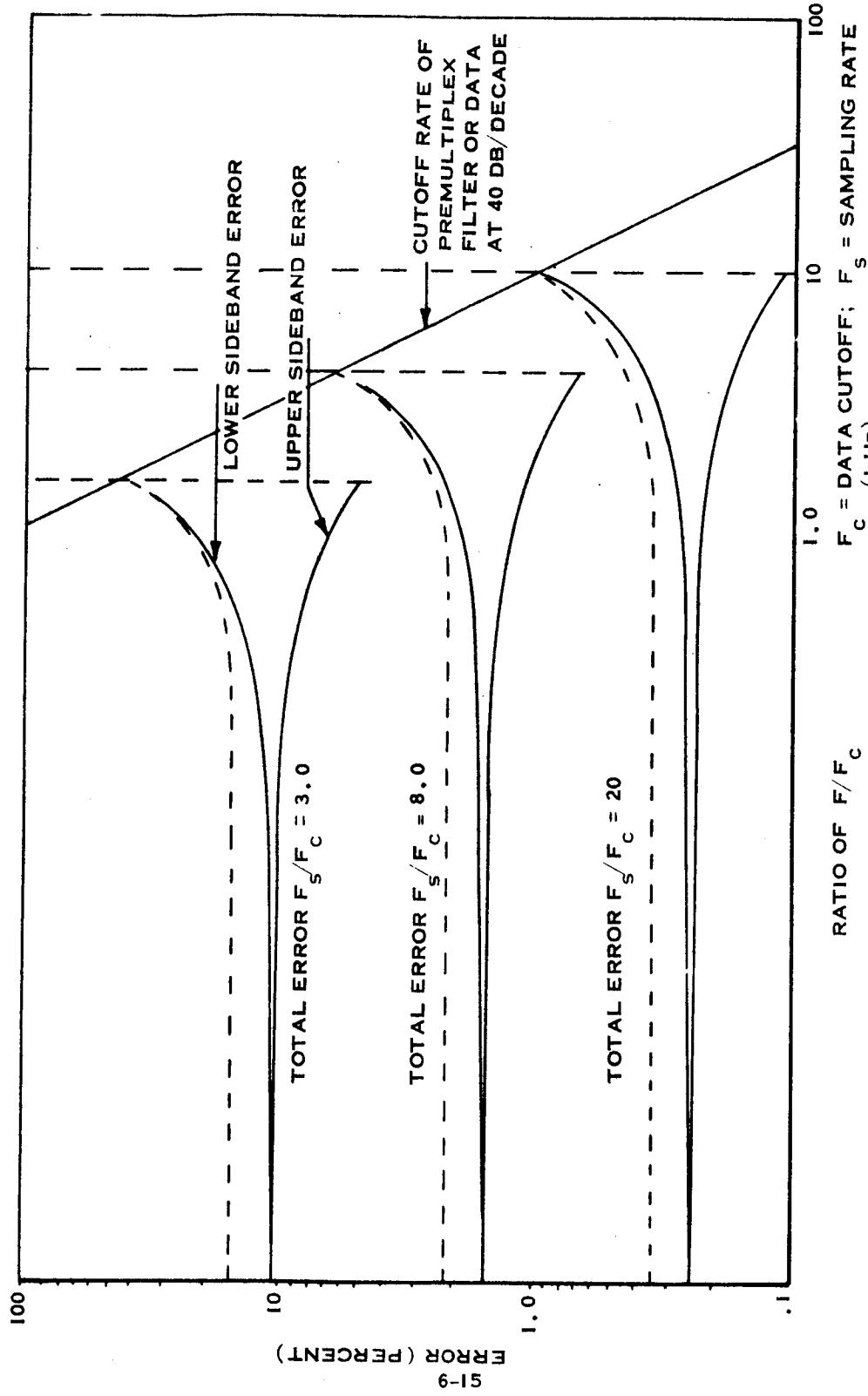

Figure 6.5-6 Aliasing Error as a Function of Sampling Rate

6-15

In addition to the aliasing error, the error introduced by the pre-multiplexing filter must be considered. This error may be divided into two parts: that part due to the steady state response of the filter and the part due to changes in the filter characteristic as a result of environmental and component changes. Presumably, the first portion of the error can be corrected to a degree by calibration. The second portion of the error must be taken into account. The variable portion of the error can be held to ±0.1 db or ±1.16 percent over the environmental range.

Summing the errors, the total maximum error turns out to be approximately ±2.095 percent. The average error should be less.

6.5.5.3 Sample Rate Summary. Table 6.5-2 summarizes the sample rates for the various parameters to be monitored. The variation of sample rates for the different modes is shown.

TABLE 6.5-2

SAMPLING RATES (SAMPLES PER SECOND)

Equipment	Mode 2 Note 1		Mode 3		Mode 4	
	Analog 7-Bit	Discrete	Analog 7-Bit	Discrete	Analog 7-Bit	Discrete
Experiments						
Magnetometer			20		20	
Particle Detector			20	20	20	20
Attitude Control[1]						
Pressure	2					
Spin Rate[2]	2					
Sun Angle	2					
Roll Angle	2			1.112		1.112
Command Decoder				.278		.278
Power			.278		.278	
Telemetry						
Encoder/MPLX			.278	.278	.278	.278
Tape Recorder			.278	.278	.278	.278
Time Data				1.112		1.112
RF						
Receiver			.278	.278	.278	.278
Transmitter			.278	.278	.278	.278

Note 1 - The A/C parameters are monitored on the Central Module for the radial configuration or on each of the satellites for the stacked configuration.

Note 2 - Not required to be monitored for the stacked configuration.

6.5.6 Subsystem Elements

The proposed telemetry subsystems for the satellite and the central module are illustrated in the functional block diagrams, Figures 6.5-7 and 6.5-8.

The subsystems include the following functions:

a. Science Data Multiplexing
b. Engineering Data Multiplexing
c. Attitude Data Encoding
d. Clock, Pulse Rate Division (PRD's) and Accumulation
e. Sequence and Control Logic
f. A/D Conversion
g. PCM Format Logic
h. Magnetic Tape Memory
i. Data Selection
j. TLM DC-DC Conversion

It should be emphasized that these are functions, not separate equipment modules. The description in the following sections envisions an integrated hardware approach.

6.5.7 Subsystem Implementation

Possible means of implementing the telemetry subsystem functions shown in block diagram form in Figures 6.5-7 and 6.5-8 are described in the following paragraphs.

6.5.7.1 Input Multiplexing. The prime and submultiplexers will accept the analog data from the experiments and the various housekeeping sensors in the form of conditioned inputs in the range of 0 to +5.12 v. The input signals will be filtered to restrict the bandwidth to the required range. The appropriate input parameter will then be selected and the data transmitted to the analog-to-digital converter. The data signal to the analog-to-digital converter will be a time-multiplexed, analog pulse train 0 to 5.12 volts in amplitude.

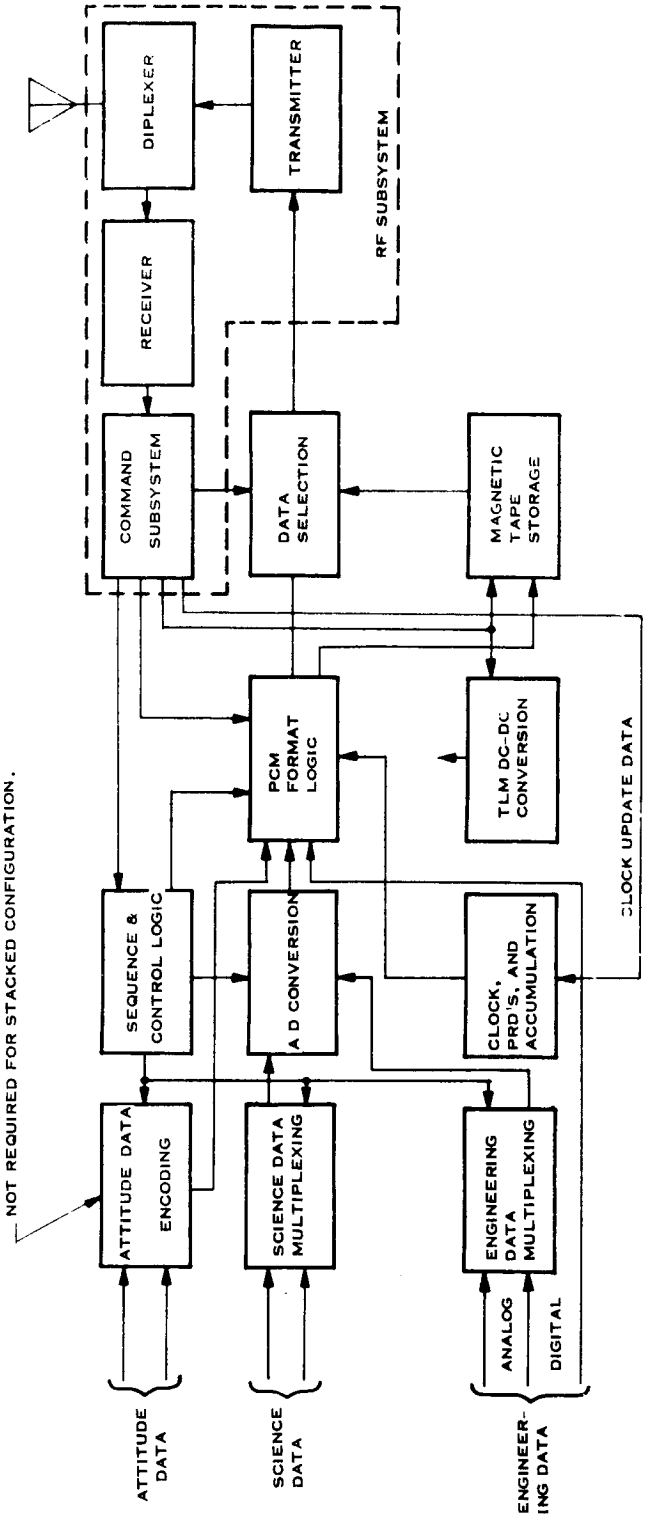

Figure 6.5-7 Satellite Telemetry Subsystem Functional Block Diagram

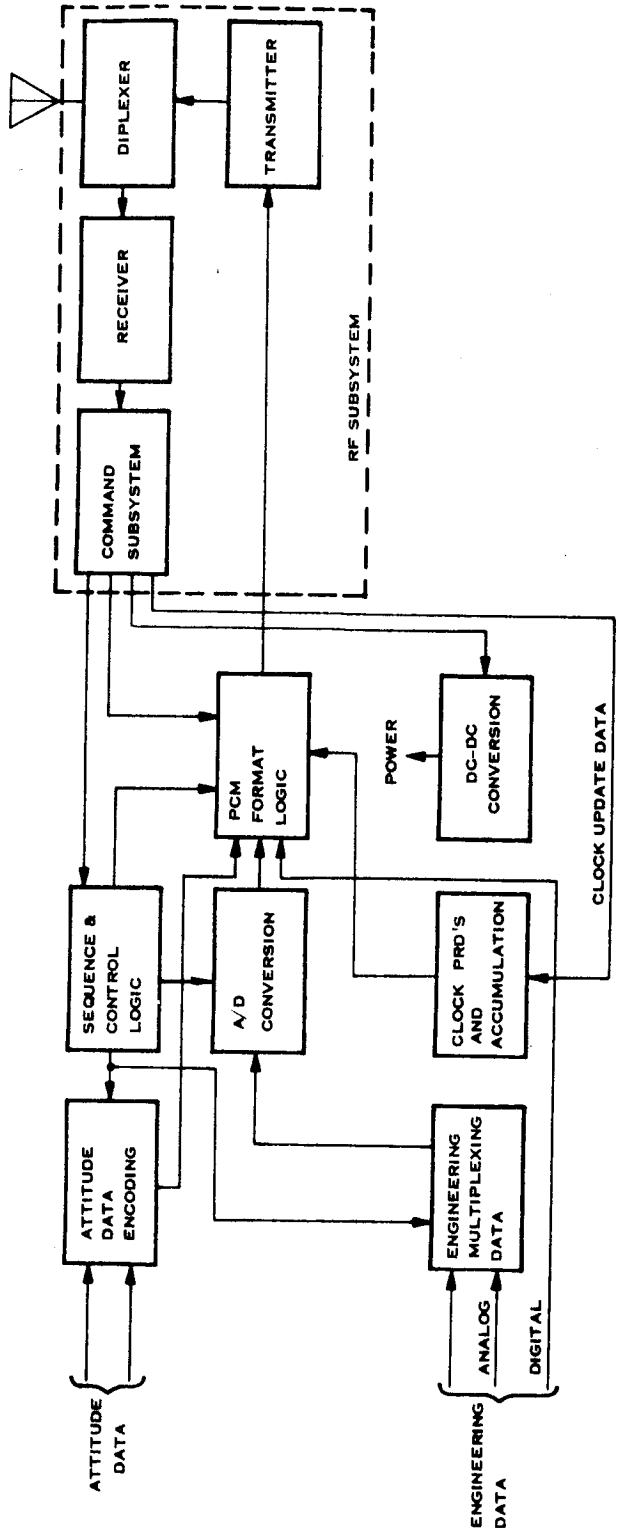

Figure 6.5-8 Stacked Configuration Carrier Module Telemetry Subsystem Functional Block Diagram

The control of each of the input multiplexers will be exercised by the sequence and control logic which receives control signals from the Command Subsystem as to the mode of operation desired. The sequence and control logic will also provide control signals to the A/D converter and to the PCM format logic.

The input multiplexers will be composed of field-effect-transistor (FET) input switches, integrated circuit driver circuits, amplifiers, and control logic lements, and hybrid filters.

Figure 6. 5-9 is a typical schematic of an analog FET input switch.

6. 5. 7. 2 Attitude Data Encoding. To encode the attitude control data for transmission over the TLM link, special logic circuits will be utilized. A block diagram of a typical attitude control data encoder is shown in Figure 6. 5-10. These circuits perform a serial A/D conversion by pulse counting techniques.

To encode the inputs from the horizon sensors, a level sensor converts the analog inputs to digital pulses. The length of the pulses is proportional to the time that the horizon sensor outputs exceed a given level which is proportional to the "time duration" of the output of the horizon sensors. The leading edges of the outputs from the level sensors reset and start the mod 7 counters and the trailing edges stop the counters. The outputs of the counters are read through the read gates into the PCM bit stream.

A similar process is utilized to encode the spin rate. In this case, however, the sun sensor pulse starts the counter at the beginning af a revolution, the counter counts for one revolution, and the sun pulse then stops the count at the end of the revolution. The count is proportional to the period of revolution or inversely proportional to the spin rate. This count is then through the read gate into the PCM bit stream on the revolution following the revolution on which the period was measured. Upon data readout the counter is reset.

The sun angle data is used to correlate the sun reference position during data acquisition and is read directly from the sun angle sensor into the data bit stream in two 7-bit words.

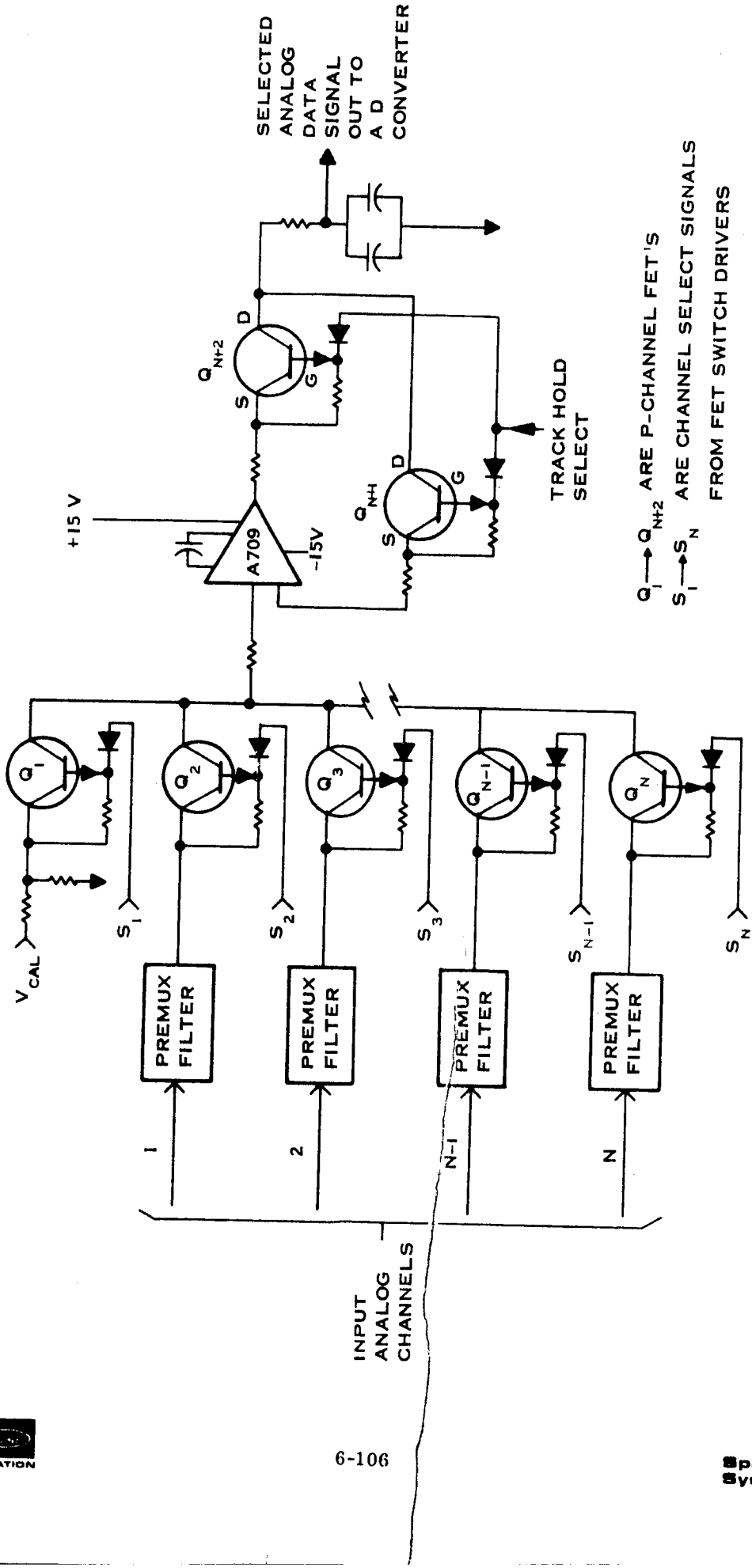

Figure 6.5-9 Schematic of Analog Switches and Sample and Hold

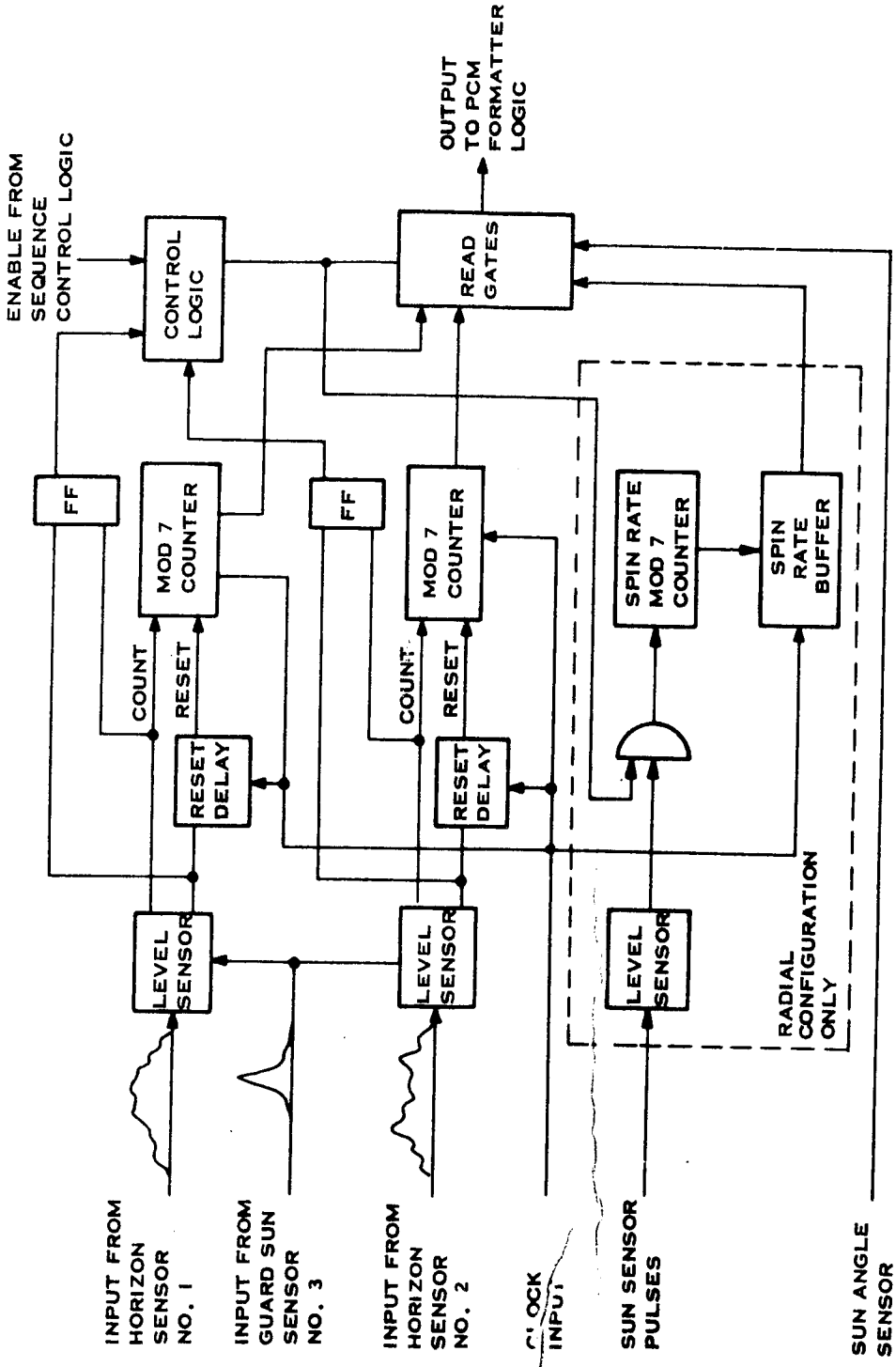

Figure 6.5-10 Attitude Data Encoder

The size of the counters, 7 bits, plus the clock rates are designed to give 7-bit precision to the measurements of the horizon sensor pulses and the spin rate and 8 bit precision to the sun angle data.

6.5.7.3 Analog/Digital Conversion. The A/D converter is a seven bit encoder that operates on a 0 to +5.12 volt range of the input signal. It will receive as an input, a time-multiplexed analog data signal from the input multiplexers and control signals from the sequence and control logic and provide encoded data to the PCM format logic. A block diagram of a proposed analog-to-digital converter is shown in Figure 6.5-11.

The A/D converter will be of a straightforward design utilizing a serial approximation technique. The incoming signal to be digitized is continuously compared to an internal signal generated in a binary "ladder" resistance network. The ladder network produces an output signal which has a binary relationship to discrete input signals. The output of the comparison amplifier gates pulses from a timing register to increase or decrease the state of a ladder memory which drives the resistance ladder through appropriate drivers. This process continues until the internally generated voltage and the external input voltage balance each other. The value of the internal voltage is "read out" by monitoring the state of the ladder memory through output gates. The overall process is controlled by means of the control and sequence logic.

The converter will be implemented largely by means of integrated circuits. The reference supply and the binary ladder will be hybrid units, i.e., partly I.C. and partly discrete components.

6.5.7.4 Sequence and Control Logic and PCM Format Logic. The commands transmitted from the ground will be translated into detailed timing and logic controls by the Sequence and Control Logic and the PCM Format Logic.

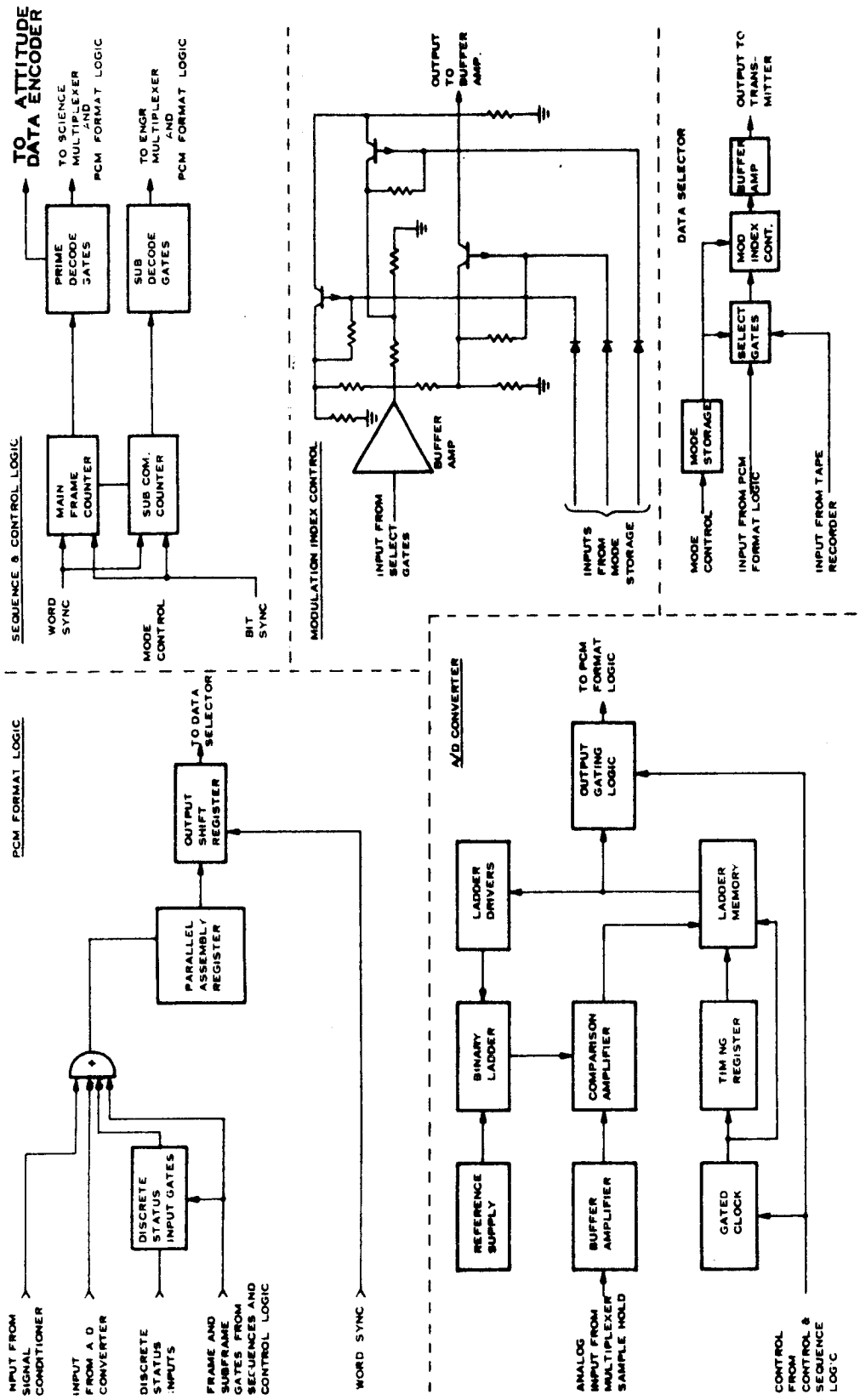

Figure 6.5-11 TLM Elements

Figure 6.5-11 is a block diagram of a typical Sequence and Control Logic and PCM Format Logic. The implementation of these two units will be entirely by means of integrated circuit logic elements.

6.5.7.5 Data Selector. The data selector will accept data either from the PCM format logic or the magnetic tape memory and transmit the selected data to the transmitter for transmission to the ground.

A secondary function of the data selector will be to control the modulation index of the signal to the transmitter. This will be primarily a function of the mode therefore, the output of the mode storage is utilized to switch the outputs of resistive dividers which set the amplitude of the signal to the transmitters. A typical arrangement of the data selector and mode control is shown in Figure 6.5-11.

6.5.7.6 Clock, Pulse Rate Divider, and Accumulator. In order to accomplish the processing of the TLM data, a variety of pulse rates will be required. In addition, it is desired to have time data to provide a reference for data correlation. This is accomplished by means of the logic shown in Figure 6.5-12.

The operation of these timing circuits is relatively straightforward, consisting of a precision crystal clock driving integrated circuit pulse rate dividers. The outputs of the PRD's feed the TLM logic circuits through buffer amplifiers and the data accumulator. The time data accumulator also incorporates provisions for resetting the state to zero from the command subsystem. The clock can accumulate up to 16000 minutes with a resolution of 1 minute. The accumulator is reset and synchronizes with ground time up to a maximum of every 4 orbits.

6.5.7.7 Magnetic Tape Storage. Tape storage specifications which have been tentatively decided upon to meet the requirements of this application are as follows:

The maximum capacity of the unit will be 3.9×10^7 bits. The data recorded at 1120 bits/second for 10 hours. The playback will be at a rate of 7 to 21 kilobits/second, depending on the available transmitter power. The data is input to the memory is in the final format, (i.e., Serial NRZ-PCM) and is read out in the same

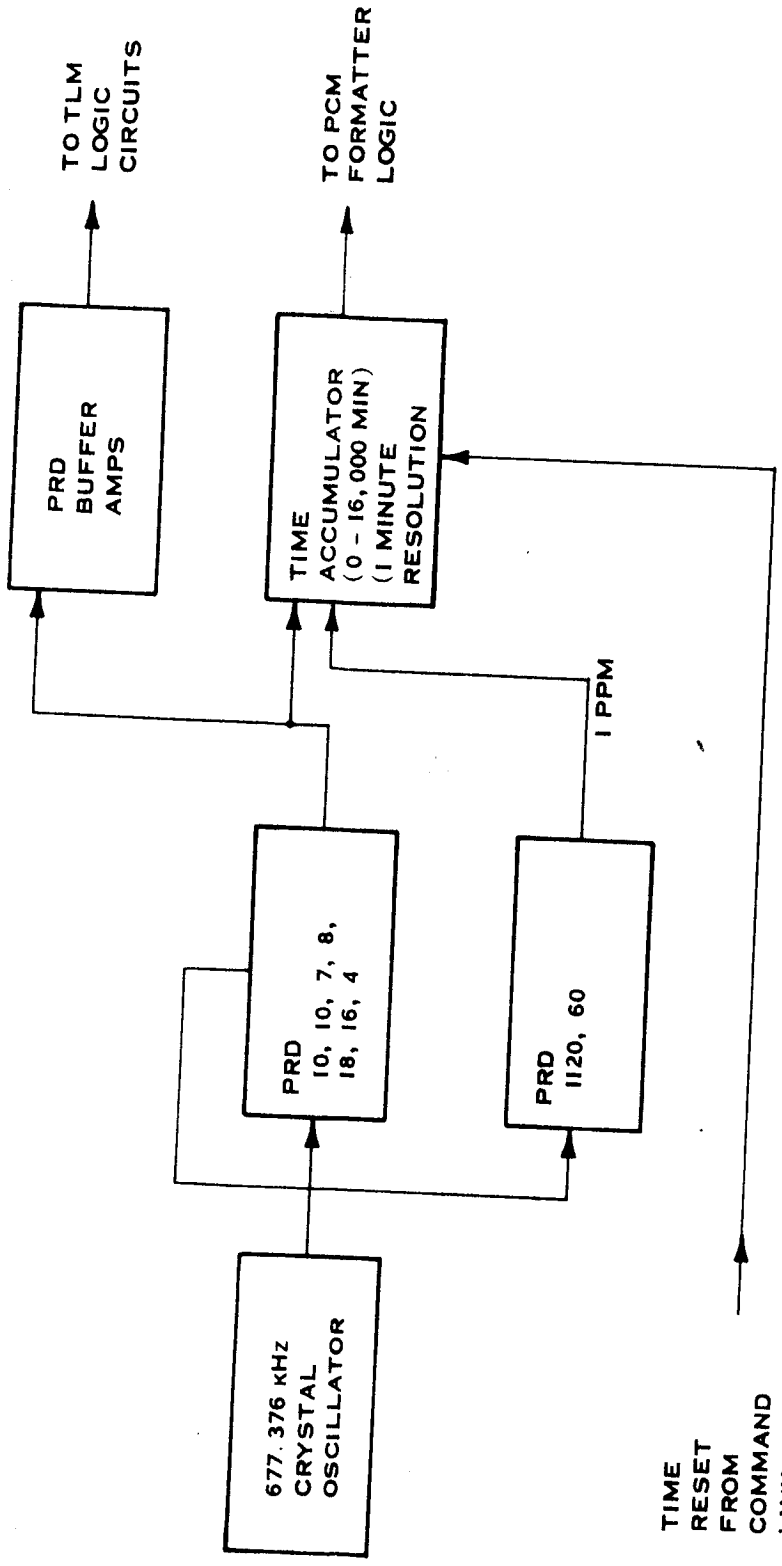

Figure 6.5-12 TLM Clock, PRD, and Accumulator Logic

form, serial NRZ-PCM. The recorder will incorporate the necessary electronics to perform internal formatting and clocking for both the record and playback functions.

Some additional pertinent specifications are shown in Table 6.5-3.

A thorough investigation of presently available units was conducted to select the tape memory most suitable for this application. The following basic types were covered:

a. Endless loop
b. Coaxial reel-to-reel
c. Coplanar reel-to-reel

The endless loop type was deemed to be the best choice for this application.

6.5.7.8 DC-DC Conversion. The power required by the TLM subsystem can be supplied by a high efficiency converter. Where precision voltages are required, each output can be individually regulated. Low precision voltages (±2%) can be supplied by a single converter whose output voltages are independent of input variation and sufficiently low in source impedance to maintain the required regulation.

The regulators consist of power switching transistors, transformers, integrating inductors, filter capacitors, and a feedback control loop. The monitored voltage is compared with a reference voltage then amplified to control the duty cycle of the power switching transistors. An overall efficiency of 90% can be achieved with the limited range of the input voltage.

A block diagram of a converter to furnish several low precision voltages is shown in Figure 6.5-13.

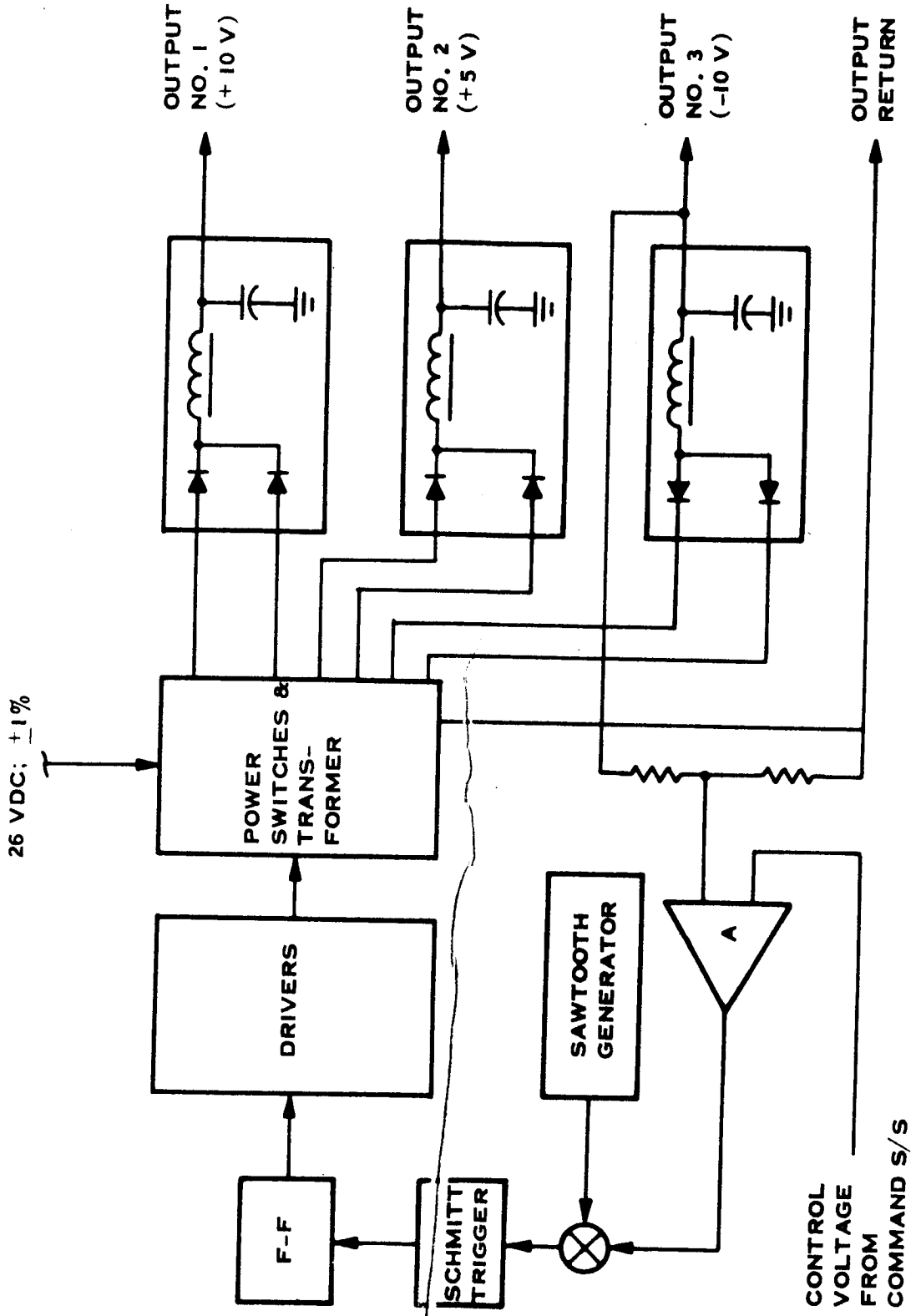

Figure 6.5-13 DC-DC Converter, Block Diagram

TABLE 6.5-3

MAGNETIC TAPE MEMORY SPECIFICATIONS

Capacity	4.0×10^7 bits
Input Record Rates	1100 bits per second
Output Playback Rate	7 → 21 kb/sec possible
Tape Speeds:	
Record	0.1 ips
Playback	1.5 ips
Number of Tracks	8
Bit Packing Density	1500 bits/inch
Weight	6 lb
Volume	150 in^3
Power:	
Record	1 watt
Playback	2 watts
Bit Error Rate	<1 in 10^6 for 100 tape passes
Wow and Flutter	5% max.

6. 5. 8 Interfaces

6. 5. 8. 1 Mechanical. The elctronics will be packaged in RFI-tight enclosures. For the different classes of circuits, different physical forms are appropriate. Analog circuits will utilize a combination of discrete components and integrated circuits, potted and surrounded by the enclosing frame structure. Construction will be of a welded cordwood form.

Digital circuits will be multilayer flat pack assemblies, welded and potted, and supported by the enclosing frame. The interconnections will be (welded) printed circuits. The power assemblies will be potted.

6. 5. 8. 2 Magnetic Considerations. The nature of the scientific calculations makes it imperative that each satellite component be as magnetically "clean" as possible.

Philco-SRS has accumulated a great deal of experience in constructing magnetically clean electronic assemblies for the Lunar Surface Magnetometer program for NASA.

The only possible problem source is the magnetic tape memory. The present state-of-the-art appears to be in a rudimentary state as regards the magnetic signature of available tape recorders.

Philco-SRS can insure that the magnetic characteristics of the chosen recorder will be below the critical level.

6.6 COMMAND SUBSYSTEM FUNCTIONAL DESCRIPTION

6.6.1 General

The command subsystem receives commands in STADAN compatible instruction format, detects and decodes the commands, and delivers the decoded commands to the various subsystems. The commands to the various subsystems are utilized to control the operation of the satellite carrier and/or the operation of the individual satellites.

The functions included in the command subsystem include the baseband-to-digital signal conversion, the decoding and storage of commands, and the power control driving and switching of the decoded commands.

In addition, sequencing and programming functions have been included to schedule the initial setup and turn-on of the subsystem.

6.6.2 Mission Requirements

6.6.2.1 Primary Requirements. Primary requirements are:

a. In order to facilitate operations, compatibility with existing equipment in STADAN ground stations is required.

b. Ability to command the satellite carrier and/or the individual satellites during the various mission phases of the flight.

c. Six month lifetime.

6.6.2.2 Secondary Requirements. To meet the overall mission requirements, the following additional constraints are proposed:

a. The command subsystem for the individual satellites shall be based on the PCM Instruction Command System capability of the STADAN stations.

The command subsystem for the satellite carrier shall be PCM Instruction or Tone Digital depending on the quantity and precision of commands eventually required.

b. The capacity to accomodate either discrete or quantative commands shall be incorporated.

c. Incorporation of preprogrammed command instructions and sequence for the early mission phases of the flight.

d. Updatable stored quantitative command capability shall be included for the satellites. This would be utilized primarily to control the operation of the tape recorder.

e. Maximum use of space proven devices, components, and technology utilized by Philco-Ford SRSD on previous space programs.

6.6.3 Required Subsystem Functions

6.6.3.1 Mission Command Profile. Figures 6.6-1 and 6.6-2 show the mission profile as it relates to command activities. The figures are subdivided into two main categories - satellite activities and command subsystem functions. During each phase of the mission, the scope and degree of interest in the command functions shifts. This shift of interest is indicated in the figures by the profiles of the command functions.

a. During launch, ascent, spin-up and separation of the third stage, commanding will not be required.

b. Following separation of the third stage, the command subsystem on the satellite carrier will be activated by a preprogrammed command.

c. Commanding of the satellite carrier will then be accomplished. For the radial configuration thus will involve only release of the satellites.

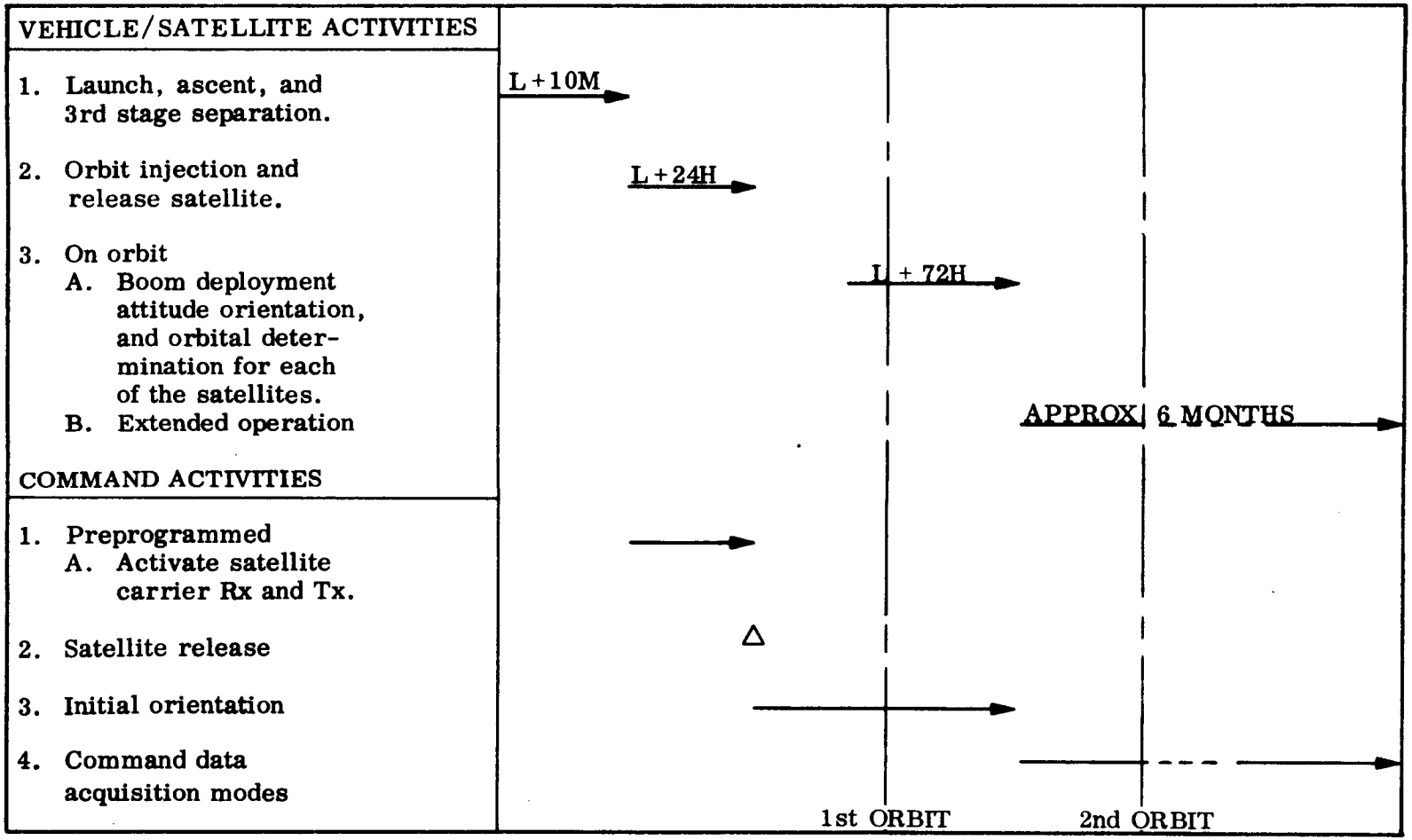

Figure 6.6-1 Mission Command Profile (Radial Configuration)

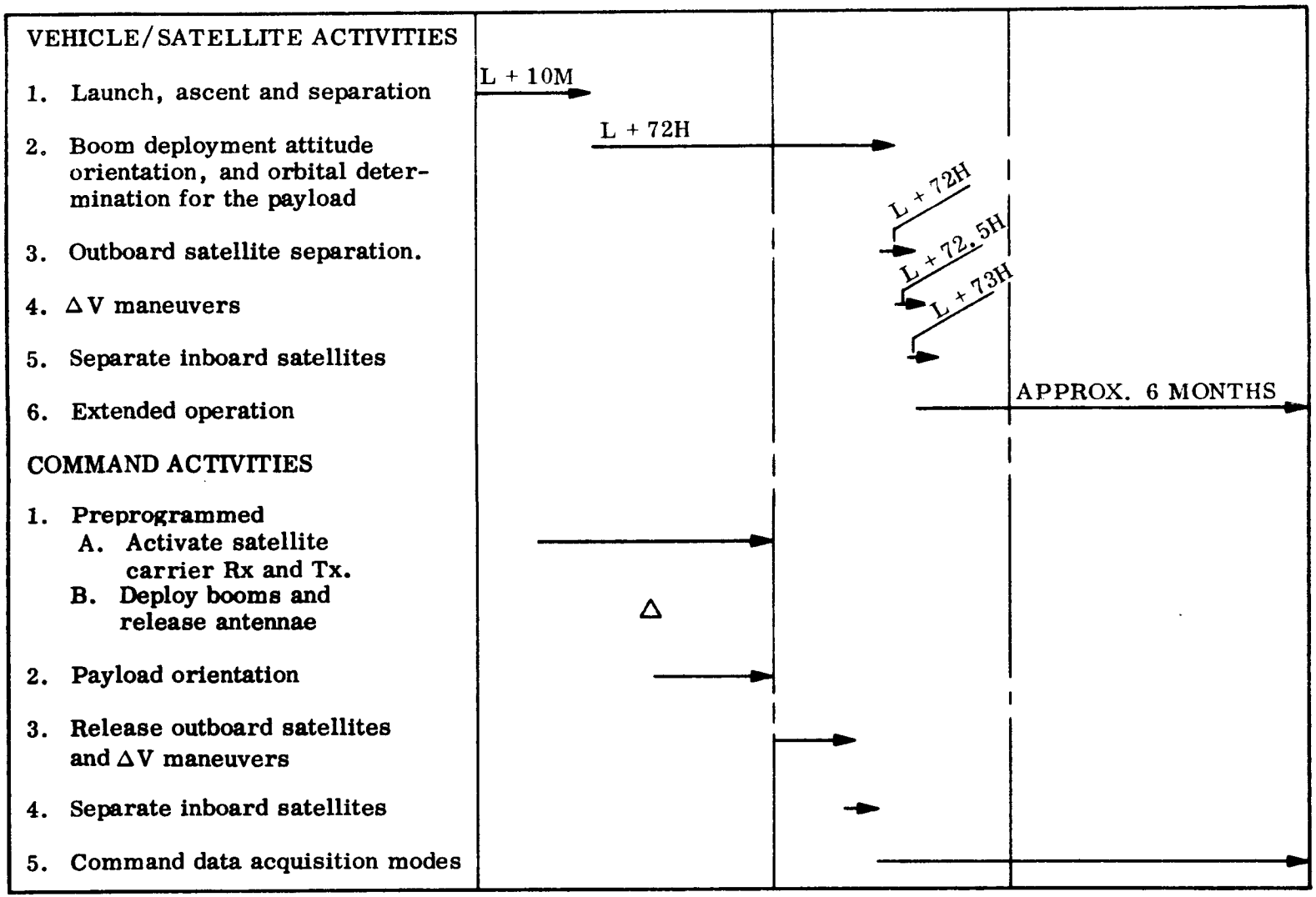

Figure 6.6-2 Mission Command Profile (Stacked Configuration)

For the stacked configurations initial setup and orientation will be accomplished for the carrier and satellites and then the satellites will be released upon command.

d. Following separation from the carrier, additional commanding will be accomplished. For the radial configuration this includes boom deployment and orientation. For the stacked configuration, no additional orientation commanding is required.

e. After the setup and orientation of the satellites, the mission enters the period during which scientific data from the experiments will be of prime interest. During this period, the command system of the individual satellites will operate in three distinct fashions. First, commands will be processed in real time from the STADAN ground stations to control the satellite operations such as the readout of the tape recorder near perigee. Second, commands will be stored and acted upon following a specificed time delay. This pertains primarily to the turn-on of the tape recorder following a command and a delay period. Clock resolution is 1 minute. Third, for the radial configuration the command subsystem will be involved in the control loop of the attitude control subsystem to maintain the desired orientation of the spin-axis of the satellite. These last three functions will alternate, as required, until the satellite end-of-life.

6.6.3.2 Command Summary List. Table 6.6-1 and 6.6-2 are a summary of the commands to be supplied to the various satellite subsystems are for the PCM Instruction Command function and the Tone Digital Command function.

6.6.4 Performance and Operational Parameters

6.6.4.1 PCM Instruction Command Word Format. The proposed command word signal modulation and format for the PCM Instruction Command function are illustrated in Figure 6.6-3. Some of the pertinent parameters of this signal are as follows:

TABLE 6.6-1
PCM INSTRUCTION COMMAND SUMMARY LIST

Command Number	Command Function	Description							Subsystem Supplied
		Pre-Programmed	High Level	Low Level	Real Time	Stored	Discrete	Quantitative	
--	Deploy Booms	X	X				X		Structure
--	Turn-on TLM Comm/RF	X	X				X		TLM/Comm/RF
1, 2	A/C Maneuver #1-ON/OFF Rotate towards sun-line			X	X		X		Attitude Control
3, 4	A/C Maneuver #2-ON/OFF Rotate away from sun-line.			X	X		X		Attitude Control
5, 6	A/C Maneuver #3-ON/OFF Rotate clockwise about sun-line.			X	X		X		Attitude Control
7, 8	A/C Maneuver #4-ON/OFF Rotate CCW about sun-line			X	X		X		Attitude Control
9, 10	A/C Maneuver #5-ON/OFF (Spin-up)			X	X		X		Attitude Control
11, 12	Heater ON/OFF		X	X			X		Attitude Control
13, 14	Mode 2 ON/OFF		X		X		X		TLM-RF
15, 16	Modes 3a and b ON/OFF		X		X		X		TLM-RF
17, 18	Mode 4 ON/OFF		X		X		X		TLM-RF
19, 20	Mode 5 ON/OFF		X		X		X		TLM-RF
21, 22	Battery Charger ON/OFF		X		X		X		Power
23, 24	Under Voltage Inhibit ON/OFF		X		X		X		Power
25, 26	Boost Regulator ON/OFF		X		X		X		Power
27,	Kick Motor Ignition		X		X		X		Propulsion
28	Boom Deployment Backup		X		X		X		Structure
29	Recorder Delay Update			X		X		X	Command
30	Time Clock Reset			X	X		X		TLM
31	Reset Commands 25			X	X		X		Command

Note: Commands 1, 2, 3, 4, 5, 6, 7, 8, 9, 10 performed by the tone digital command system on the satellite carrier for the stacked configuration.

TABLE 6.6-2
TONE DIGITAL COMMAND SUMMARY LIST

Command Number	Command Function	Description							Subsystem Supplied
		Pre-Programmed	High Level	Low Level	Real Time	Stored	Discrete	Quantitative	
--	Deploy Booms	X	X						Structure
--	Tur-on TLM/Comm/RF	X	X				X		TLM/Comm/RF
1, 2	A/C Maneuver #1-ON/OFF (Rotate towards sun-line)			X	X		X		Attitude Control
3, 4	A/C Maneuver #2-ON/OFF (Rotate away from sun-line			X	X		X		Attitude Control
5, 6	A/C Maneuver #3-Rotate CW about sun-line			X	X		X		Attitude Control
7, 8	A/C Maneuver #4-Rotate CCW about sun-line			X	X		X		Attitude Control
9, 10 9, 10	A/C Maneuver #5 Rotate in & Roll Direction			X	X		X		Attitude Control
11, 12	A/C Maneuver #6 Rotate in roll direction			X	X		X		Attitude Control
13	Eject first pair of satellites		X		X		X		Structures
14, 15	ΔV Arm and Execute		X		X		X		Propulsion
16	Eject second pair of satellites		X		X		X		Structure
17, 18	Reset 10 and XX			X	X		X		Command

Note - Commands 1 through 8 not required for stacked on-board A/C system.

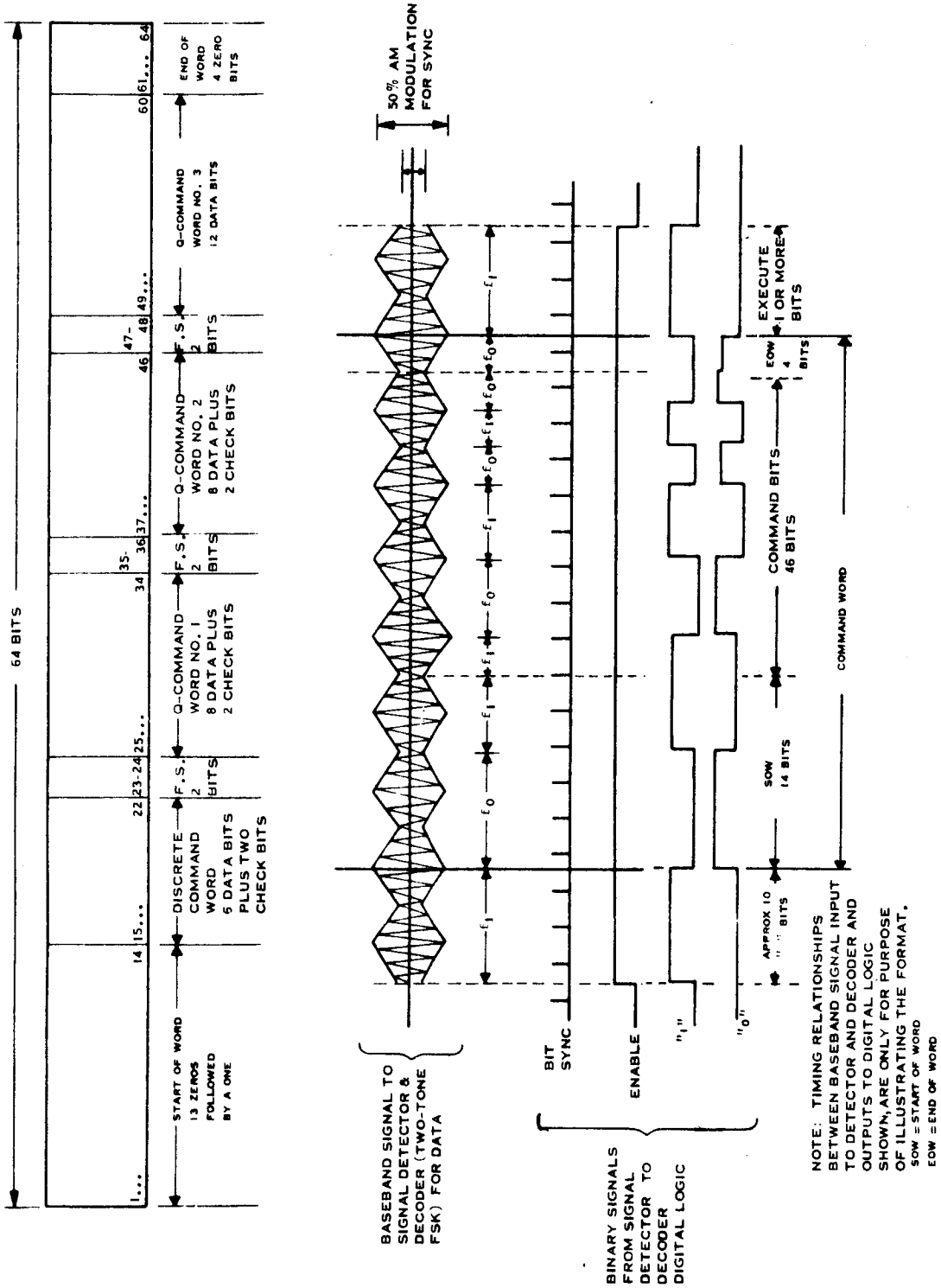

Figure 6.6-3 PCM Instruction Command Word Signal and Format

Baseband Modulation:

Data: FSK in the 7.0 to 11.0 KHz band
Sync: 50% AM of the data subcarrier at the bit rate of 128 bps.

Digital Command:

Bit Format: PCM, NRZ-C
Bit Rate: 128 bits/second
Command Word Length: 64 bits, including 40 bits of data and 24 bits of sync.
Command Word Period: 1/2 second
Command Word Rep. Rate: Approximately 1 per second.

The command word sync information is contained in 24 bits distributed throughout the word in the following fashion. A "start-of-word" consisting of 14 bits prefaces the discrete and quantitative command data. In addition to the 14 bits of start-of-word, an additional 6 bits are spaced throughout the word to reduce the probability of unintentional spoofing.

At the conclusion of the command word, 4 bits are utilized as an "end-of-word." The start-of-word and the end-of-word are part of the standard STADAN format. The additional "sync" bits are added as part of the command structure for the UCLA satellite.

In addition to the "sync" information, 4 data words are included in the command word. These may be summarized as follows:

Discrete Command Word: 1 each - 6 data plus 2 check bits
Type 1 Quantitative Command Words: 2 each - 8 data plus 2 check bits
Type 2 Quantitative Command Word: 1 each - 12 data bits

6.6.4.2 PCM Instruction Command Capability Summary. The command word format outlined in the preceding section is capable of the following:

Discrete Commands: 64

Type 1 Quantitative Commands: 2 words with a resolution of 1 part in 256

Type 2 Quantitative Command: 1 word with a resolution of 1 part in 4096.

Utilizing the check bit structure outlined to detect errors, the command error rate can reasonably be expected to exceed 1 part in 10^6.

6.6.4.3 Tone Digital Command Message Signal and Word Format. The proposed command message signal and word format for the Tone Digital Command function are illustrated in Figure 6.6-4. Some of the pertinent parameters of this signal are as follows:

Baseband Modulation:

Data: PDM (100% AM) of one of the eight GSFC standard tones in the band from 7.0 KHz to 11.024 KHz.

Sync: Transitions of the leading edge of the data pulses.

Digital Command:

Bit Format: PCM-NRZ

Bit Rate: 1/72 of the tone frequency

Command Word Length: 10 bits, including 8 bits of data, 1 blank, and 1 word sync pulse

Command Frame: 5 command words, including 1 vehicle address word plus a repeat, and 1 execute word plus two repeats and a blank period.

Command Frame Period: Approximately 1/2 second.

Command Word Rep Rate: Approximately 1 per second.

6.6.4.4 Tone Digital Command Capability Summary. The command word format outlined in the preceding section is capable of accommodating approximately 70 discrete commands.

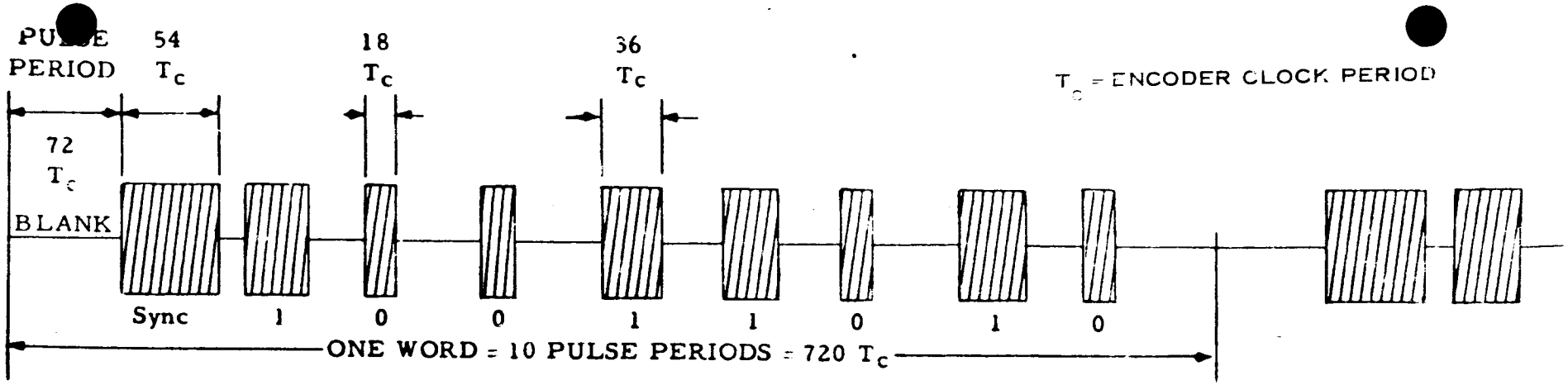

COMMAND WORD STRUCTURE

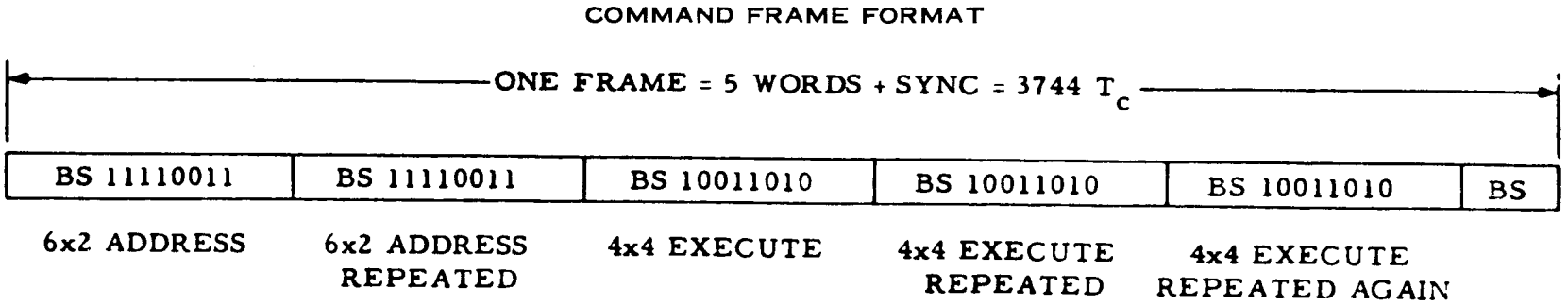

COMMAND FRAME FORMAT

Figure 6.6-4 Tone Digital Command Subsystem Word and Frame Format

6.6.5 Subsystem Elements

6.6.5.1 PCM Instruction Command Subsystem. A functional block diagram of the PCM Instruction Command Subsystem for the satellites is shown in Figure 6.6-5.

The interface with the R-F and TLM subsystems is indicated in summary form. The functions of the command subsystem proper are as follows:

1. Signal Detection
2. Input Gating Logic
3. Valid Command Logic
4. 64 Bit Buffering
5. Discrete Command Decoding Logic
6. Power Control Driving and Switching
7. Quantitative Command Storage
8. Preprogrammed Command Logic
9. Command DC-DC Conversion.

The serial FSK signal from the command receiver is demodulated into digital data, bit sync, and an enable signal by the signal detector. Following the input gating logic (which prevents inadvertant overlapping of commands) the data is stored in the 64 bit buffer. The contents of the buffer are examined by the valid command logic to insure that a correct command is indeed in the register and then the command data is operated on in two ways. Discrete commands are decoded completely in parallel by the discrete command decode logic, and the outputs of this logic control the satellite modes of operation via the power control drivers and switches. Quantitative command data is transferred to quantitative command registers where it is held for as long as required. The quantitative command data may be utilized in the attitude control subsystem, or to delay the tape memory operation.

Provisions are also incorporated to decode outputs from the clock to provide the initial preprogrammed commands. The command subsystem also includes provisions for monitoring critical points for return to the ground station via the TLM link. Lastly the command subsystem incorporates DC-DC conversion for supplying power to the subsystem elements.

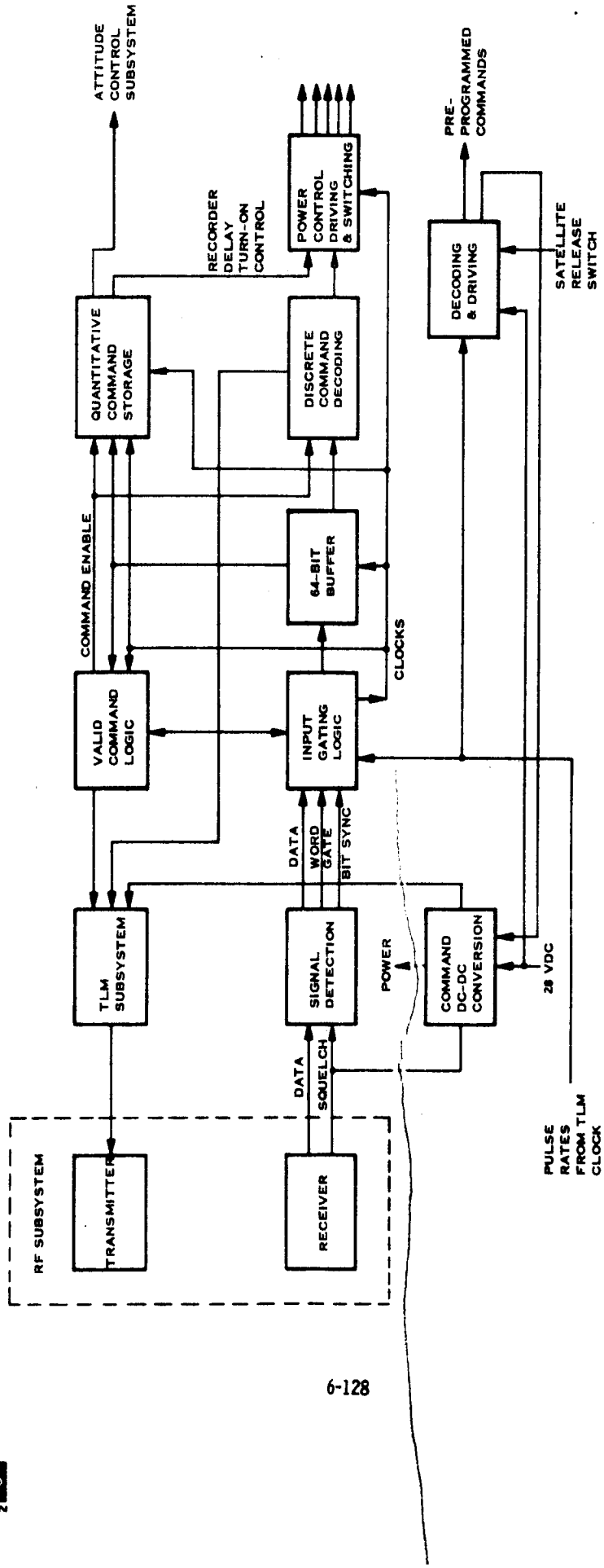

Figure 6.6-5 PCM Instruction Command Subsystem, Functional Block Diagram

6.6.5.2 Tone Digital Command Subsystem. A functional block diagram of the Tone Digital Command Subsystem for the satellite carrier is shown in Figure 6.6-6.

The interface with the R-F and TLM subsystems is indicated in summary form. The elements of the command subsystem proper are as follows:

1. Signal Detection
2. Input Gating Logic
3. Valid Command Logic
4. 10 Bit Buffer
5. Discrete Command Decoding Logic
6. Power Control Driveing and Switching
7. Preprogrammed Command Logic
8. Command DC-DC Conversion

The serial PDM signal from the command receiver is demodulated into digital data, bit sync, and an enable signal by the signal detector. Following the input gating logic (which prevents inadvertant overlapping of commands) the data is stored in the 10 bit buffer. The contents of the buffer are examined by the valid command logic to insure that 5 correct command words indeed passed thru the register and then the command data is operated on. The discrete commands are decoded completely in parallel, by the discrete command decode logic, and the outputs of this logic control the satellite carrier operations via the power control driving and switching.

6.6.6 Command Subsystem Description.

A possible implementation of the command subsystem (shown in block diagram form in Figures 6.6-5 and 6.6-6) are described in the following paragraphs.

6.6.7 PCM Instruction Command Signal Detection and Decoding

6.6.7.1 Signal Detection. A review of Section 6.3-2 on the command link shows that there is adequate S/N margin under worst case link conditions to insure reliable commanding.

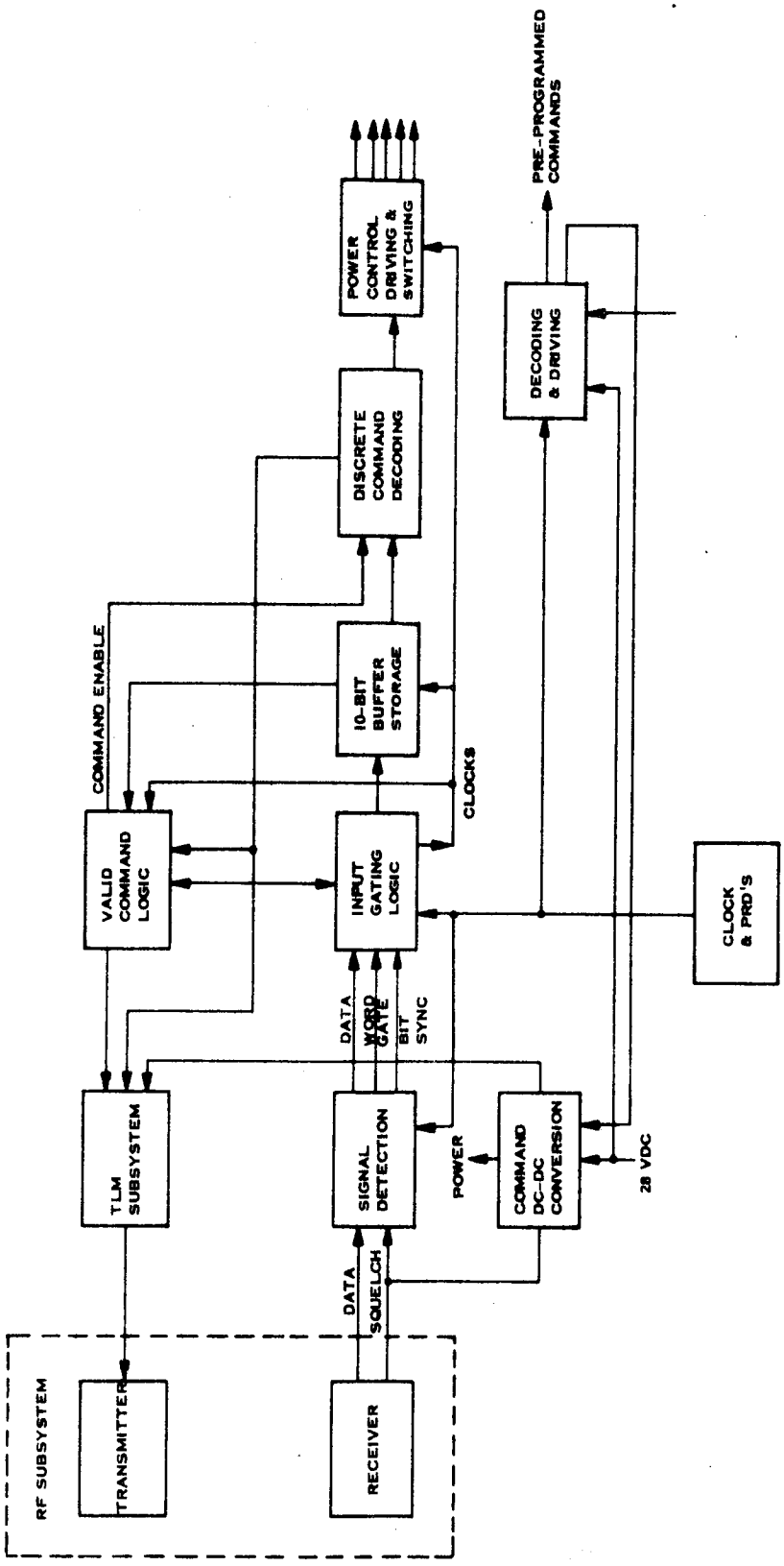

Figure 6.6-6 Tone Digital Command Subsystem, Functional Block Diagram

As a consequence, simple and reliable methods for demodulating the FSK baseband signal may be utilized.

The recommended approach for this particular application is a two-filter envelope detector. This technique is slightly less efficient than limiter-discriminator detection or a near optimum matched-filter phase-coherent system. On the other hand, the two-filer envelope detector is easier to implement than either of the alternate techniques. As a consequence, satisfactory performance is achieved with a minimum of detection circuitry and a maximum of reliability.

Figure 6.6-7 is a representative block diagram for the FSK signal detection function.

One disadvantage of the two-tone approach is the lack of a separate word sync. In this case word sync must be established by pattern recognition on the digital data. This method is less resistant to spoofing, (i.e., recognizing a valid command pattern in a group of data bits caused by noise) then, a three-tone FSK technique, where the additional tone is utilized to establish word sync.

This unit will consist largely of integrated circuits to minimize component count, volume and weight. This includes the tone filters which will be active element designs based upon Philco-Ford units utilized in other space programs.

6.6.7.2 Decoding Input Gating Logic. To control the input to the command word storage register, input gating logic will be required. This logic limits inputs to the command word storage register to data which occurs within the limits of the enable gate generated by the signal detector and decoder. This operation minimizes the probability of unintentional spoofing of the unit due to a possibly valid code occuring within an otherwise random stream of data. In addition, once a valid command is recognized, this logic will prevent further entry until the received command has been properly executed. A logic diagram for a typical input gating logic is shown in Figure 6.6-8.

6.6.7.3 Decoding Command Word 64 Bit Buffer Storage. A detailed analysis of the 64 bit command shows that in order to prevent unintentional spoofing additional

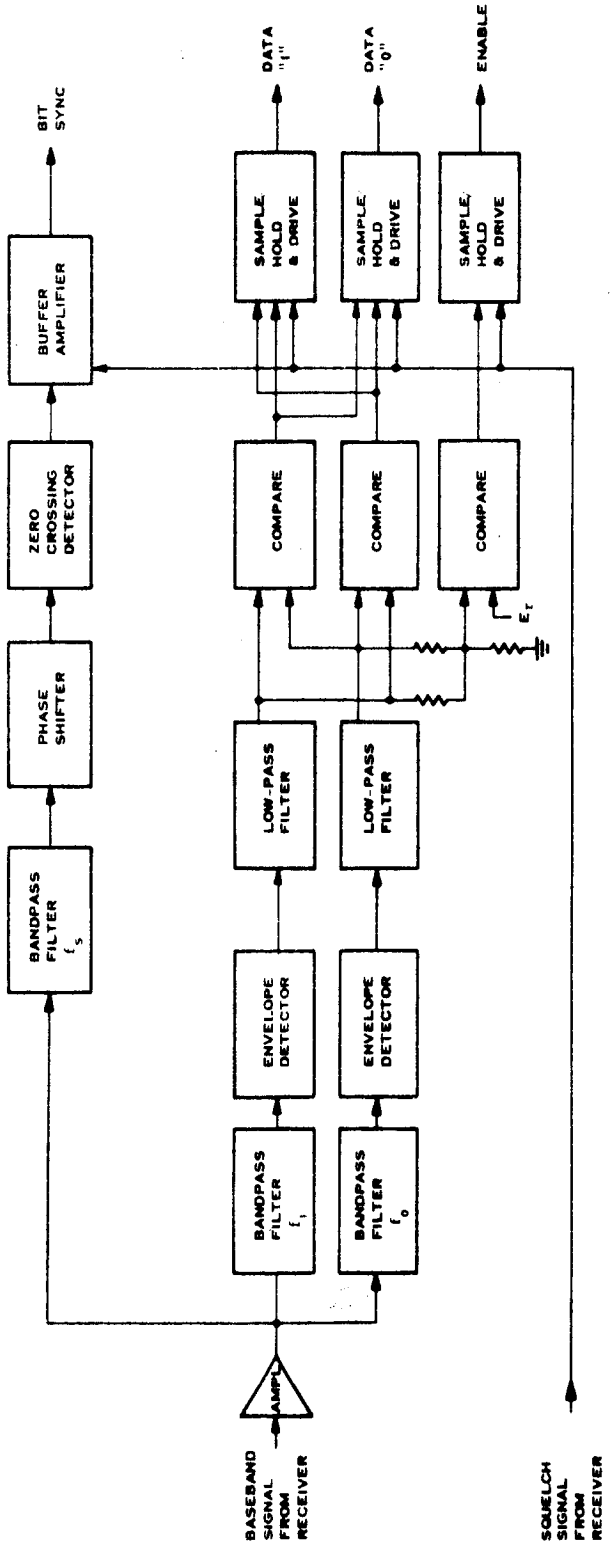

Figure 6.6-7 Signal Detector and Decoder (Two-Tone FSK) Utilized for PCM Command System

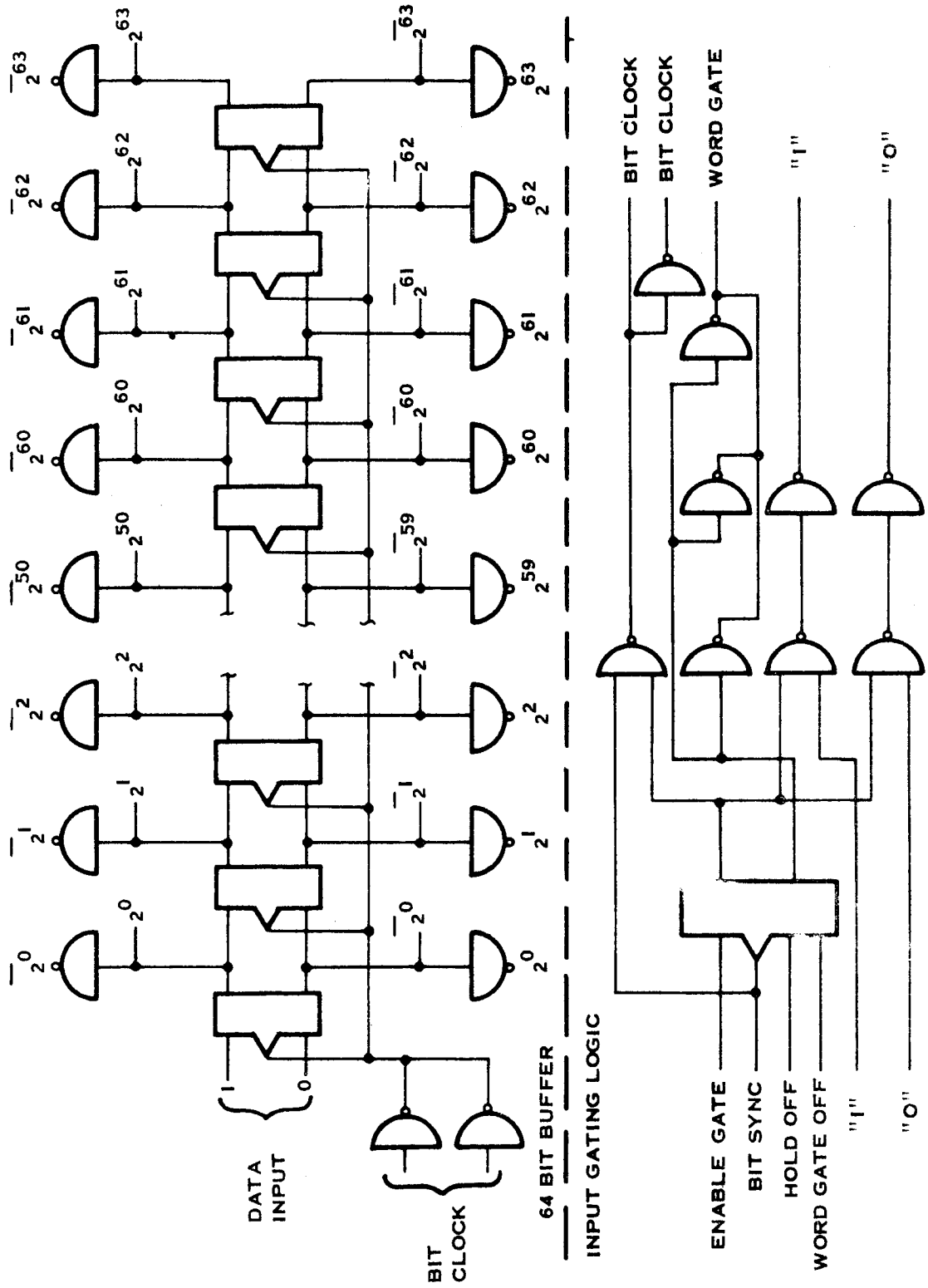

Figure 6.6-8 Typical Buffer Storage Elements and Buffers for Command Subsystem

bits are required over and above those provided in the standard STADAN format. These may conveniently be included in the format because the data does not require the full format. In processing the data, the entire check bit structure must be analyzed prior to executing the command. This function may be done either in a serial or parallel fashion. Serial processing requires a separate bit counter and decoding structure. Performing this operation in parallel does not require a separate counter but does require a 64 bit storage register. With the advent of integrated circuits, this storage does not present too formidable a problem. Therefore, the method suggested to implement the initial entry of the command word is a 64 bit storage shift register. This register and associated buffers drive the related decoding gates to perform the decoding of commands.

A typical serial input, parallel read-out, shift register is shown in Figure 6.6-8.

6.6.7.4 Discrete Command Decode. A portion of the command word stored in the command word storage register will be decoded to produce discrete commands. Six bits of the available data have been allocated for this function. This provides the capability of decoding up to 64 discrete commands. This is adequate to handle the anticipated command load. Making provisions for 64 commands in the command word does not impose a penalty on the hardware as only the necessary decoding gates for the required commands are actually included in the hardware.

The data inputs to the decode gates are from the command word storage register and the enable input from the valid command word logic.

The decoding is a straightforward parallel decode by means of NAND logic gates whose outputs go to the driver circuits.

A pulse forming one-shot is included to stretch the input data to the time interval required to execute the command. In most cases this will be a few milliseconds.

6.6.7.5 Valid Command Logic. This portion of the logic decodes those portions of the command word designated as vehicle address, sync bits, and additional bits inserted to prevent unintentional spoofing. Upon recognition of a valid command

word, the input is gated off. The logic is held in this condition until the particular command is executed at which time the input is unlocked and additional data may be entered into the command word register.

The structure of this control logic is not typified by any particular arrangement but will be unique for the satellite.

6.6.7.6 Quantitative Command Register. To handle quantitative command information, the data in the command word shift register is parallel loaded into the quantitative command data register. A block diagram of this logic is shown in Figure 6.6-9.

The operation is straightforward. When a quantitative word is in the register, the fact is recognized by the presence of the appropriate discrete command and bits. This is "anded" with the input from the valid command logic to gate the information from the 64 bit buffer into the appropriate quantitative data register.

The data for the recorder delay operations is jam-transferred via the transfer gates to 12-bit registers. These registers also double as counters which operate on the data in the following fashion.

The data set into the recorder delay registers, is the desired delay from the command to the turn-on and the turn-off of mode 4. Upon activation of this circuit by setting the recorder delay flip-flop, the register acting in its count mode begins to decrement. When a count of zero is reached, the recorder is set in mode 4 operation and the delay circuits reset. At this time a second register begins to decrement. When it reaches a count of zero the recorder is shut off. The registers have a 12-bit capacity. The input clock is at a rate of one pulse per minute. This results in a resolution of one minute for a period of 68 hours which is adequate to meet the anticipated recorder turn-on and turn-off delay requirements. The counter is interlocked to prevent inadvertent entry of new data until the current operation has been completed. A reset feature has also been incorporated to clear the register in the case of inadvertent "lock-up".

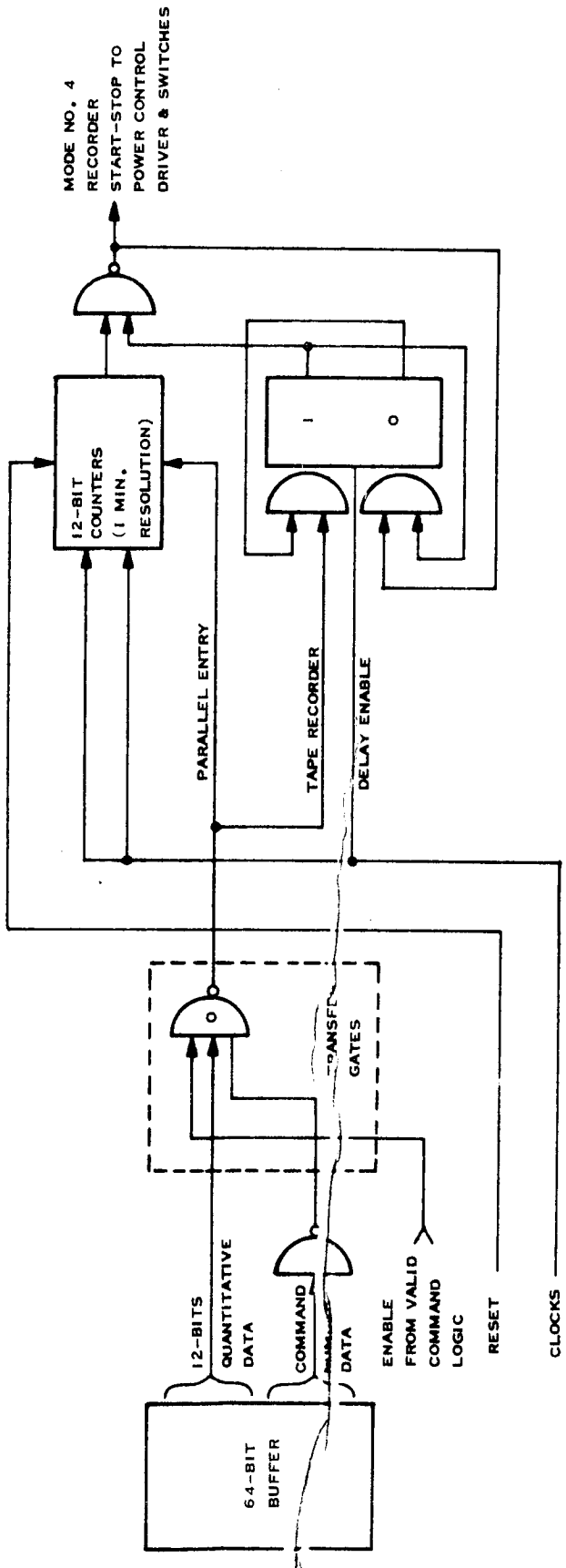

Figure 6.6-9 Quantitative Command Data Register

6.6.7.7 Discrete Power Control Driver and Switch Circuits. The outputs of the command word decode gates are at a low level, i.e., ≤ 5 vdc and ≤ 1 ma. In order to provide the power and voltage transformations required to drive the peripheral devices, such as the tape recorder, it is necessary to buffer the output of the logic circuits. This is accomplished by the discrete power control and driver circuits.

6.6.7.8 Preprogrammed Commands. The implementation of the preprogrammed command logic will include only the decode gates and drivers in the command subsystem. The decode gates and drivers will be driven by the oscillator and pulse rate dividers in the TLM subsystem. These items are shared with the time clock provided to reference the TLM data. Power will be applied to the logic chain by means of a separation switch which controls a power switch. Power will be taken directly from the 26-volt bus for this function, since the DC-DC converter will not be in operation at this time. Once power is applied, the oscillator starts to drive the divider chain. When the correct count has been reached, the decode gates and drivers will initiate the particular event. The events called for are as follows:

- Deployment of the booms
- Turn on of the command, TLM, and RF subsystem power converters.

6.6.8 Tone Digital Command Detector

6.6.8.1 Signal Detection. A review of Section 6.3.2 on the command link shows that there is adequate S/N margin under worst case link conditions to insure reliable commanding. As a consequence, simple and reliable methods for demodulating the PDM baseband signal may be utilized.

The recommended approach for this particular application is a digital detector. With the advent of integrated circuits such a technique can be implemented in a small size with low power consumption and excellent reliability. In addition the cost per function of integrated circuits is rapidly decreasing so that the future cost of such a unit should be more than competitive with a discrete component analog unit. Figure 6.6-10 is a representative block diagram for the tone digital PDM signal detection function.

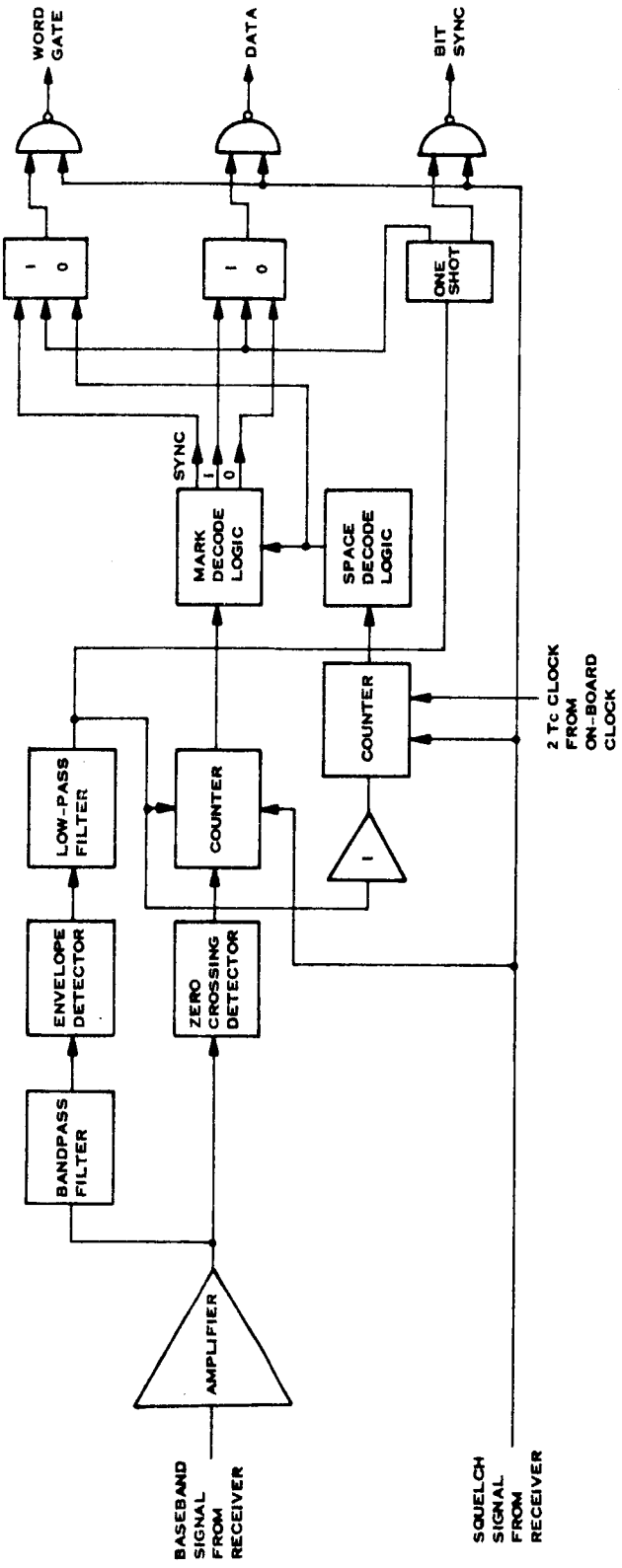

Figure 6.6-10 PDM Signal Detection Functional Block Diagram as Utilized for the Tone Digital Command System

The detected signal from the receiver is (after buffering) processed in 2 ways. First the signal is filtered, 2nd detected, and then filtered again. This provides an envelope from which the bit sync is retrieved by triggering a fixed duration one-shot on the leading edge of the envelope. The envelope also serves as a control signal for the digital counters which measure the width of the "marks" and "spaces".

Second the analog input signal is processed by a zero crossing detector and then the number of zero crossings after each envelope leading edge is counted.

Likewise a counter operating on an internal clock at twice the encoder frequency, 2 Tc. counts the number of clock pulses in each "space" following an envelope trailing edge. The outputs of the two counters are fed to a decoding network where the counts are decoded into a sync pulse, a "one" pulse and a "zero" pulse. The pulse outputs of the decode logics are routed to flip-flops and stored to provide an NRZ format to the remainder of the logic.

The entire signal detection function is gated by the squelch signal from the receiver to prevent processing erroneous data in the absence of a valid received signal. This unit will consist largely of integrated circuits to minimize component count, volume and weight. This includes the tone filters which will be active element designs based upon Philco-Ford units in other space programs.

6. 6. 8. 2 Input Gating Logic. To control the input to the commend word storage register, input gating logic is required. This logic limits inputs to the command word storage register to data which occurs within the limits of the enable gate generated by the signal detector and decoder. This operation minimizes the probability of unintentional spoofing of the unit due to a possibly valid code occuring within an otherwise random stream of data. In addition, once a valid command is recognized, this logic prevents further entry until the received command has been properly executed. A logic diagram for a typical input gating logic was shown in Figure 6. 6-8.

6. 6. 8. 3 Command Word 10 Bit Buffer. In processing the data, the entire check bit structure must be analyzed prior to processing the command word and may be

done either in a serial or parallel fashion. Serial processing requires a separate bit counter and decoding structure. Performing this operation in parallel does not require a separate counter but does require a 10 bit storage register. With the advent of integrated circuits, this storage does not present too formidable a problem. Therefore, the method chosen to implement the initial entry of each command word is a 10 bit storage shift register. This register and associated buffers drive the related decoding gates to perform the decoding of commands.

A typical and serial input, parallel read-out, shift register was shown in Figure 6.6-8.

6.6.8.4 Valid Command Logic. This portion of the logic keeps track of those portions of the command frame designated as vehicle address, and execute. Upon recognition of a valid address and execute the input is gated off. The logic is held in this condition until the particular command is executed at which time the input is unlocked and additional data may be entered into the command word register.

The structure of this control logic is not typified by any particular arrangement but is unique for the satellite.

The logic will consist almost exclusively of integrated circuit logic elements.

6.6.8.5 Discrete Command Decode. The execute portion of the command frame stored in the command word storage register is decoded to produce discrete commands. The decode is based on a 4 out of 8 code. This provides the capability of decoding up to 70 discrete commands. This is adequate to handle the anticipated command load. Making provisions for 70 commands in the command word does not impose a penalty on the hardware as only the necessary decoding gates for the required commands are actually included in the hardware.

The data inputs to the decode gates are from the command word storage register and the enable input from the valid command word logic.

The decoding is a straightforward parallel decode by means of NAND logic gates whose outputs go to the driver circuits.

A pulse forming one-shot is included to stretch the input data to the time interval required to execute the command. In most cases this will be a few milliseconds.

6.6.8.6 Discrete Power Control Driver and Switch Circuits. The outputs of the command word decode gates are at a low level, i.e., ≤ 5 vds and ≤ 1ma. In order to provide the power and voltage transformations required to drive the peripheral devices, such as the tape recorder, it is necessary to buffer the output of the logic circuits. This buffering is provided by the discrete power control driver and switch circuits. These circuits also provide relay storage when required.

6.6.8.7 Preprogrammed Commands. The implementation of the preprogrammed command logic will include only the decode gates and drivers in the command subsystem. The decode gates and drivers will be driven by an oscillator and pulse rate dividers. Power will be applied to the logic chain by means of a separation switch which controls a power switch. Power will be taken directly from the 26-volt bus for this function, since the DC-DC converter will not be in operation at this time. Once power is applied, the oscillator starts to drive the divider chain. When the correct count has been reached, the decode gates and drivers will initiate the particular event. The events called for are as follows:

- Deployment of the booms
- Turn on of the command, TLM, and RF subsystem power converters.

6.6.8.8 Clock and Pulse Rate Dividers. In order to accomplish the operation of the tone digital command system on the carrier module, several pulse rates are required. The necessary pulse rates are provided by a precision crystal oscillator and associated pulse rate dividers. These circuits may be realized mostly by integrated circuit logic and hence are small, reliable, and low power.

6.6.9 DC-DC Converter

The power required by the command subsystems will be supplied by high efficiency converters. Where precision voltages are required, each output will be individually regulated. Low precisions voltages (±1%) will be supplied by a single converter whose output voltages are independent of input variabion and sufficiently low in source impedance to maintain the required regulation.

The regulators will consist of power switching transistors, transformers, integrating inductors, filter capacitors, and a feedback control loop. The monitored voltage is compared with a reference voltage then amplified to control the duty cycle of the power switching transistors. An overall efficiency of 90% can be achieved with the limited range of the input voltage.

These units will be implemented by means of high density welded cordwood packaging techniques.

A block diagram of a converter to furnish several low precision voltages is shown in Figure 6.6-11.

6.6.10 Mechanical Interfaces

The electronics will be packaged in RFI tight enclosures. For the different classes of circuits, different physical forms are appropriate. Analog circuits will utilize a combination of discrete components and integrated circuits, potted and surrounded by the enclosing frame structure. Construction is of a welded cordwood form.

Digital circuits will be multilayer flat pack assemblies, welded and potted, and supported by the enclosing frame. The interconnections will be (welded) printed circuits. The power assemblies will be potted.

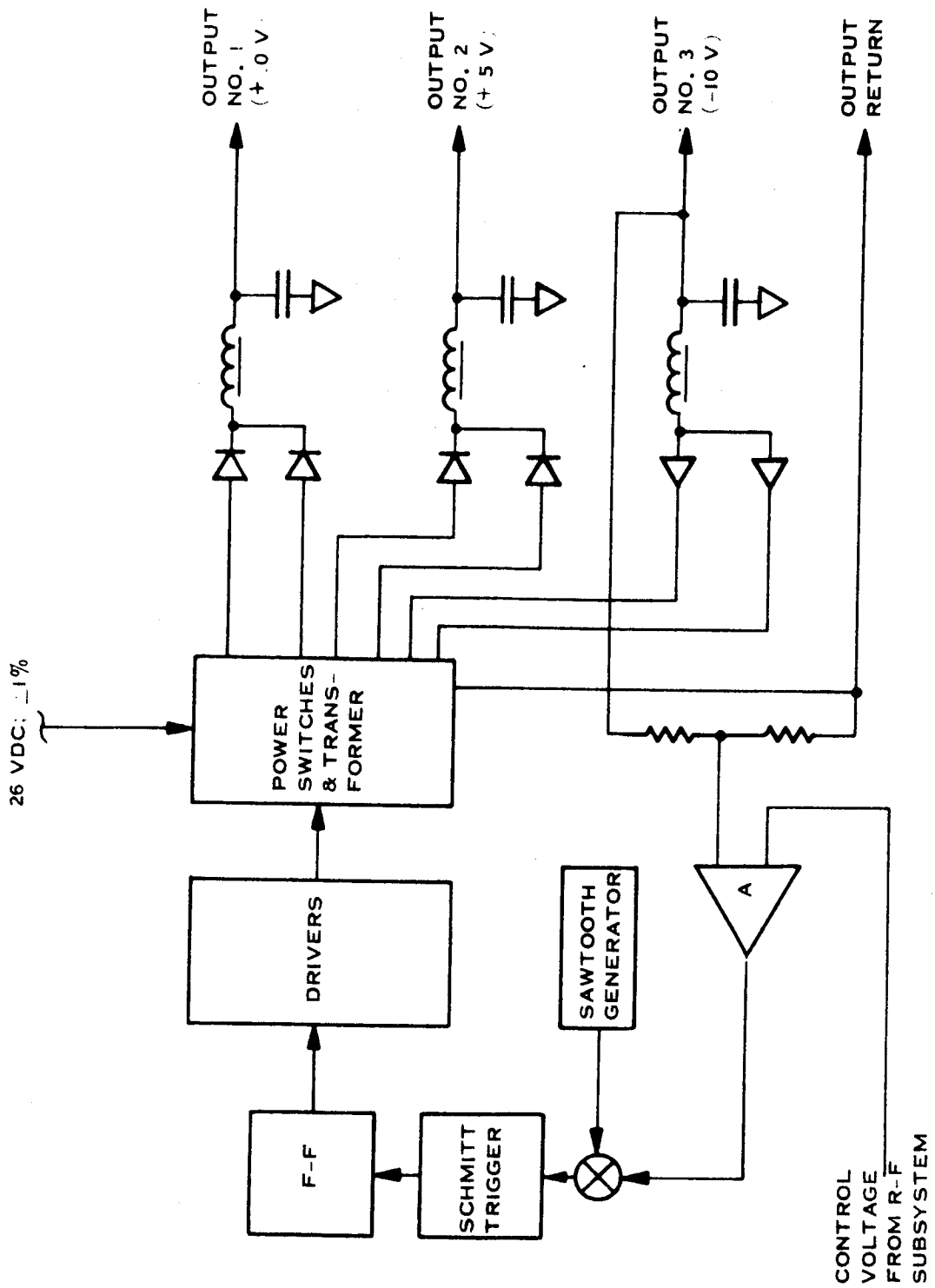

Figure 6.6-11 DC-DC Converter, Block Diagram

6.7 SECTION 6 BIBLIOGRAPHY

The following references pertain to notes through the preceding paragraphs of Section 6:

1. Goddard Range and Range Rate System Specification, Exhibit "A," S-531-P-17, May 1966.

2. P. R. Arendt, "Natural Tolerance Limits of Doppler Measurements of Outer Space Radio Signal." U. S. ASRDL Tech Report 2253, Feb. 1962.

3. "Design Evaluation Report for Goddard Range and Range Rate System (GRR-2)." General Electric Co., Military Communications Department, Contract No. NAS 5-9731, November 1964.

4. "On Comparing the Modulation Systems," by John C. Hancock, NEC Proc., Vol. 18, 1962, p. 48.

5. "A Note on Product Demodulation of Binary PCM/PM Signals," J. A. Develet, Jr. Space Tech Lab., 8949-0002-NU-000, 12 Feb. 1961.

6. "Optimum Coherent Phase and Frequency Demodulation of a Class of Modulating Spectra," by A. J. Viterbi and C. R. Cahn, IEEE Trans. on Space Electronics and Telemetry, September 1964.

7. "The Goddard Range and Range Rate Tracking System Concept, Design and Performance" by G. C. Kronmiller and E. J. Baghdady, Space Science Reviews, Vol. 5, Mar. 1966.

8. Personal Correspondence from E. E. Melendy, Head Command and Control Section, Advanced Development Division, NASA/GSFC, 27 Oct. 1966.

9. "Maximum Angular Accuracy of Tracking a Radio Star by Lobe Comparison," IRE Trans. on Antennas and Propagation, January 1960.

SECTION 7

SYSTEM ANALYSIS

7.1 LAUNCH VEHICLE SELECTION

One of the program requirements states that the launch vehicle is to be one of the Thor-Delta family of vehicles. Selection of a particular vehicle combination from this family will be made on the basis of payload capability, comparative injection accuracy, vehicle availability, and costs.

7.1.1 Payload Capability

Table 7-1 lists four launch vehicle combinations of the Thor-Delta family that are appropriate for this mission. For each vehicle the table shows the estimated total useful payload weight that can be injected into a nominal earth orbit of 150 nautical mile perigee height and 20 earth radii apogee, using an eastward launch and direct injection from the Eastern Test Range. The estimated total payload weight requirements are:

- Radial configuration, 266 lb.
- Stacked configuration, 302 lb.

The table also shows corresponding payload margins for each launch vehicle. Some of these excess capabilities should be considered as design margin. (In this early stage of design development, approximately 10 percent would be a prudent value.) The remainder of the margin represents growth potential, i.e., capacity for increasing the experimental instrument load and attendant additional support equipment (mainly increased solar array weight).

The table shows that the DSV3E (FW4) vehicle provides an excess capability of 2-1/2 lb. for the stacked configuration and 11 lb. for the radial configuration, per satellite. In the early program phase, this margin is not adequate for the stacked configuration.

TABLE 7-1

LAUNCH VEHICLE SELECTION

Payload Capability
DSV-3E: 312 lb. DSV-3J: 435 lb. DSV-3E/B II: 255 lb. DSV-3L/B II: 400 lb.
Design Margin & Growth Potential, Per Satellite
Radial (with DSV-3E): 11 lb. Radial (with DSV-3J): 42 lb. Stacked (with DSV-3E): 2-1/2 lb. Stacked (with DSV-3J): 33 lb.
* Based on Estimated Total Payload Weights, Including 12 lbs. of Experiments per Satellite, Of: Radial 266 lb. Stacked 302 lb.

The design margin is probably barely adequate for the radial configuration, but there is no growth potential. In contrast, the DSV3J vehicle can boost additional experiment packages of 26 and 35 lb. (These weights are in addition to 10 percent design margins.)

The table lists Burner II configurations primarily to demonstrate that the standard DSV3E Thor-Delta is inadequate if Burner II is used as a third stage. Obviously, the use of Burner II is not advantageous purely from a payload standpoint, but must be evaluated on the basis of flexibility of maneuvers and of comparative overall program costs. To obtain adequate payload capability, a Burner II upper stage must be used in combination with the projected DSV3L booster (or, alternatively, an Atlas booster).

Another consideration affecting payload capability is the relationship to orbit parameters. It is conceivable, for example, that an acceptable lowering of apogee would result in a substantial increase in payload capability, and thus affect the vehicle selection. To evaluate these possibilities, the parametric relationships between payload weight, perigee height, and apogee distance were developed for the DSV3E (FW4) vehicle as a representative case, and are shown in Figure 7-1. It is seen that there is a large variation in payload weight with perigee height. However, as has been explained in Section 4, the nominal perigee height is chosen as the minimum required to assure that subsequent perigee decay due to lunar and solar gravitation will not result in an unacceptable level of aerodynamic drag; therefore, there is no freedom to decrease this initial perigee height. The other parameter that might be manipulated is apogee distance. Figure 7-1 shows, however, that the variation of payload weight capability with apogee distance is very small. (This, of course, is a reflection of the fact that in highly eccentric orbits, apogee distance is extremely sensitive to orbit energy.) In the region of 20 Re apogee, the slope is about one-half lb. payload per earth radius of apogee change. This effect is so weak as to warrant its exclusion as a consideration. Thus it is seen that reasonable changes in orbit parameters, from the reference orbit, have a negligible effect on payload capability and therefore do not enter into launch vehicle selection.

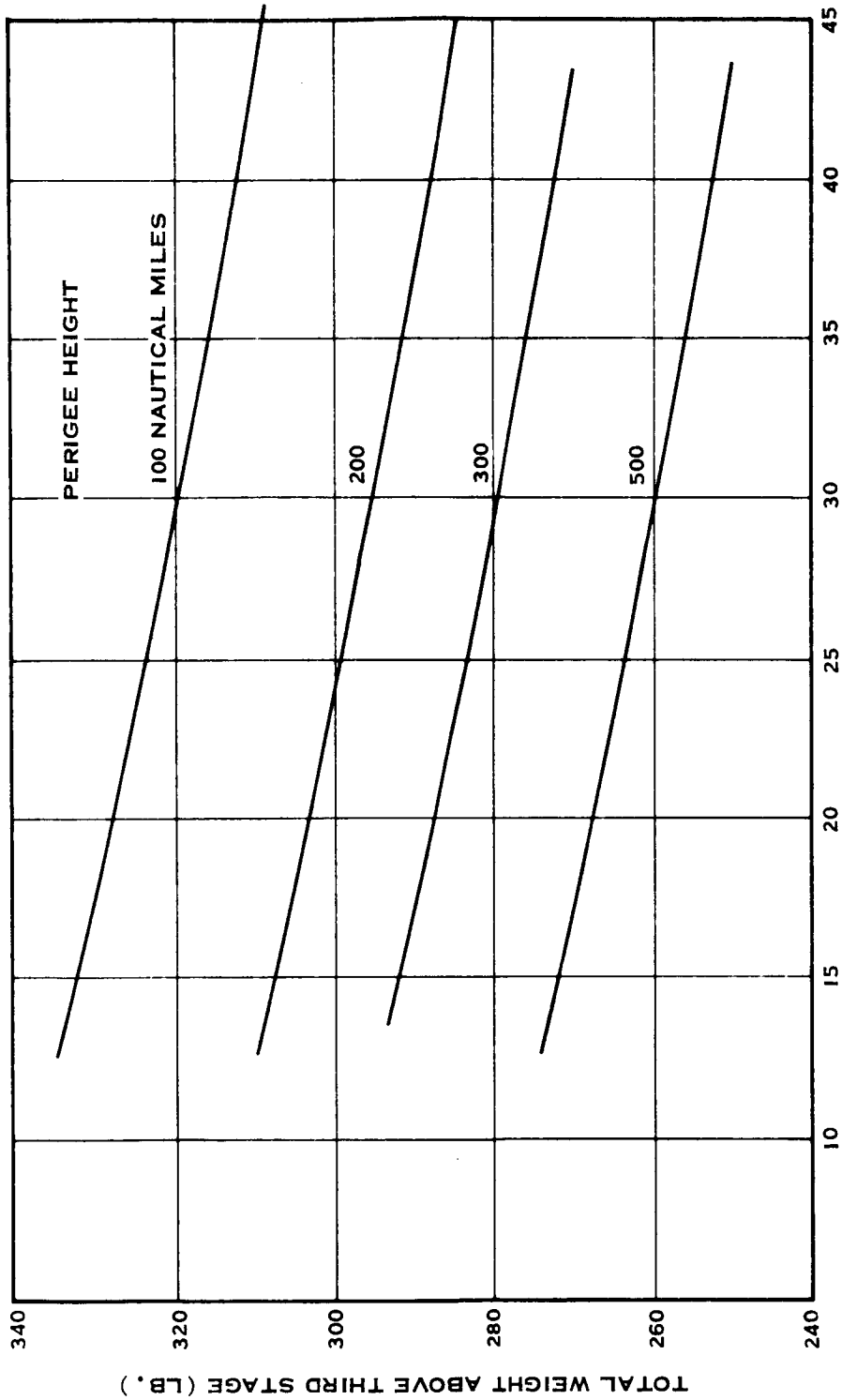

Figure 7-1 Payload Variation with Orbit Parameters DSV 3E Launch E From AMR

7.1.2 Injection Errors

The injection accuracies of the DSV3E (FW4) and DSV3J will be essentially the same. Analysis of the injection accuracy performance of the DSV3E (FW4) as applied to the Pioneer mission, which has an ascent profile that is representative of the type of interest, gives the following standard deviations (one sigma):

- Burnout velocity ± 32 ft/sec
- Flight path angle (pitch & yaw) ± 0.36 deg
- Radius vector ± 11 nautical miles
- Longitude ± 0.10 deg
- Latitude ± 0.07 deg

The DSV3J, which has not yet been flown, will realize a slightly better proportional accuracy, due to the more modern design of the TE364-3 third stage motor. However, because of the somewhat larger absolute value of velocity increment, the resulting dispersion will be approximately the same.

7.1.3 Program Status & Vehicle Availability

DSV3E (FW4). The DSV3E is the most recent standard member of Douglas' Thor-Delta family; it consists of the standard DSV-2C Thrust-Augmented-Thor booster and the Improved Delta second stage. The FW4 third stage motor has now supplanted the X-258 as the standard kick stage on this booster, for NASA and Comsat applications. This vehicle combination has been flight-proven in the Intelsat II program, and is currently available.

DSV3J. This is the same Thrust Augmented Improved Delta, but with a TE364-3 third stage motor. This spherical motor is an adaption of Thiokol' s Surveyor main retro rocket. The launch vehicle combination will be used first in the NASA Radio Astronomy Explorer program, with the initial launch scheduled for third quarter, 1967. The vehicle will also be used for communications satellite launches in the next three years and will be a standard NASA launch vehicle in 1970.

DSV3E/BII. The Burner II is Boeing's Model 946 upper stage vehicle, which incorporates the TE364-2 motor. The stage currently is in production, for use on the Thor booster in a classified USAF program. The first launch, which was conducted with an operational payload last September, was successful. The Burner II structure is adaptable to mating directly to the Delta. It would be used in place of the third-stage kick motor.

DSV3L/BII. The DSV3L is the "Thorad", with the Improved Delta second stage. The first-stage propellant tanks are lengthened, and the strap-on solid propellant motors are slightly uprated. This vehicle, at present, is not funded for development or scheduled for a particular program. Douglas planning is to make it available by 1969, possibly for use on the Aerocomsat program.

7.1.4 Comparative Costs

The cost increment between the DSV3E (FW4) and the DSV3J will be due almost entirely to the difference in motor price, about $15,000 each, and the increased cost of a new and larger spin table, which will amount to approximately $20,000 per vehicle. Thus the total increase in recurring cost per vehicle will be less than $50,000, out of an approximate total per vehicle of $3.5 million. Presumably the development costs, which are not major, will have been amortized by 1970.

The total recurring cost of the Burner II stage projected for the 1970's will be approximately $500,000.

Based on the foregoing considerations, the DSV3J vehicle is the preferred configuration of the combinations with a simple spin-stabilized third stage. It offers a substantial increase in capability, for a very modest cost differential. It will definitely be available in the time period of interest. It would seem to be a wise decision, from a scientific experiment standpoint, to incorporate the satellite growth potential inherent in the use of this vehicle.

An alternative is the use of the Burner II upper stage. A principal task of the design study phase for this program would be a comprehensive cost estimate for

the development and production of a satellite carrier including attitude control and reaction control subsystems. This must then be compared with the combined costs of a simpler satellite and a Burner II stage, to see which will give the lower total program costs. This, together with a detailed comparative analysis of maneuver capabilities, will form the basis for deciding between the two alternatives.

7.2 ASCENT AND COAST PHASE

7.2.1 Radial Configuration

Sequence of Events. The sequence of operations, from launch through the beginning of orbit operations, is shown in Table 7-2. The coast phase, though not a discrete event, is included to indicate that certain equipments must be operating during that period.

Command and Control Requirements. There are two discrete events which must be initiated while the satellites are in the ascent configuration: separation of the payload from the expended final-stage rocket case, and the simultaneous separation of the four satellites from the central module. The first event must be accomplished very soon after third-stage burnout, since the moments of inertia of the payload-final stage combination are such that the spin stability is poor. The elapsed time between injection (final stage burnout) and acquisition by the first ground station (Johannesburg) is about 20 minutes. This is an undesirable length of time to be spent in the dynamically unstable condition; therefore, it is highly desirable to preprogram this event. The satellite separation will occur about 24 hours later, near the first apogee, when the spin vector is again along the orbital velocity vector. To ascertain whether this event also can be preprogrammed, it is necessary to determine the period dispersion resulting from launch vehicle injection errors. The 3-sigma dispersion in injection velocity, which was quoted by Douglas for this type of Delta ascent, is ± 96 ft/sec. This would result in a period dispersion of approximately +8.7, -6.6 hours, which would mean a change from the nominal time to reach first apogee of about +4.4 or -3.3 hours. In order to maintain the desired Δ V directions, it is necessary to execute the separation within about a quarter degree of true anomaly at apogee (see Section 4), which corresponds to a

TABLE 7-2

SEQUENCE OF EVENTS, RADIAL CONFIGURATION

1. Launch & Ascent, Through Delta Burnout
2. Third Stage Spin-up & Separation (Activate Payload Separation Timer)
3. 3rd Stage Burn
4. Payload Separation (Activate Command Receiver)
5. Coast to Apogee (24 Hours)*
6. Simultaneously Release 4 Satellites (By Command)

For Each Satellite:

7. Sense Separation & Activate Satellite Command Receivers
8. Release, Deploy, & Lock 3 Single-Hinge Booms
9. Erect Spin Axis Approx Normal to Ecliptic
10. Make Attitude Measurements
11. Make Spin Axis Roll Correction
12. Spin-up to Desired Orbital Rate
13. Make Attitude Measurements
14. Make 2nd Spin Axis Roll Correction

*Central Module VHF Beacon ON for Tracking & Command

time "window" of about a half hour. Clearly, tracking must be accomplished to establish the actual apogee before the separation event can be scheduled, i.e., preprogramming is not possible. It would be desirable, however, to have a timer backup for this event so that, in case of failure of the VHF command receiver, the satellites can still be separated and operable, albeit not in the desired array. Following satellite separation, the orbital S-band command link will be used to control the reaction control system for the necessary maneuvers.

Communications & Tracking Requirements. As established above, orbit determination must be accomplished by tracking during the first half-orbit. As analyzed in Section 6, angle tracking only will be sufficient to obtain the desired accuracy. Therefore, a simple beacon will be required on the payload. Except for command verification, there is no telemetry that is essential during ascent. Following satellite separation, the orbital S-band telemetry will be used to transmit satellite attitude data.

Antenna Considerations. Consideration has been given to use of the S-band antenna and electronics on one of the satellites for accomplishing the coast functions. This possibility depends primarily upon the suitability of the antenna pattern in the ascent configuration. Unfortunately, the satellite antennas are facing in the general direction away from the earth during the ascent. This fact, together with the effects of the booms folded around the antenna mast and of the clustered satellites themselves, results in deep nulls in the pattern in the direction of the earth. Only one satellite down-link could be operating, since more than one radiating antenna in the cluster would result in intolerable interferometer effects. As the one radiating antenna rotated about the payload center line at a spin rate of about 2 cps, it would pass through nulls, corresponding to blockage by the other three satellites, which would certainly be below the link margin. Therefore the ground receiver would have to reacquire the signal about every half-second, which is not feasible. It is evident that the satellite orbital antenna cannot be depended upon during ascent, and therefore a separate transponder and antenna for ascent is indicated. Since a VHF antenna will give a more nearly omnidirectional pattern for command reception, and a VHF system will be compatible with the STADAN network, a VHF beacon will be used. This will be installed in the central module, precluding any electrical

interfaces with the satellites. A simple whip antenna, along the spin axis out the "back" of the cluster, will give an effective pattern and will be relatively easy to implement.

Power Requirements. The input power requirement of this ascent VHF beacon, timer, and command receiver will be approximately 2 watts. Therefore, a small primary battery, weighting about 2 lbs., will be adequate. This will also be installed in the central module.

Interface Requirements. With a separate small beacon and battery package located in the central module, there will be no electrical interface at all between the central module and the satellites.

7.2.2 Stacked Configuration

Sequence of Events. The sequence of ascent operations is shown in Table 7-3.

Command & Control Requirements. In this configuration, the satellite deployment maneuvers must be controlled by ground command of the carrier. These maneuvers are the separation of the first satellite pair, the execution of a specified number of pulses of the V thruster, and the separation of the second satellite pair. There are two approaches to the attitude control of this configuration: automatic and ground controlled. In the ground-controlled case, which is the preferred approach, commands are required to pulse the spin axis precession thrustor, for the initial erection and for the two subsequent local roll corrections. An on-board timer also will be required for the proper sequencing of these events.

Communications & Tracking Requirements. As with the radial configuration, it is necessary to determine the orbit parameters by angle tracking before the separation maneuvers can be properly sequenced. In addition to the tracking requirement, the open-loop attitude control system requires that a certain amount of attitude senaor data be telemetered to the ground, for computation of the appropriate attitude correction commands. Therefore, a VHF transmitter for telemetry and tracking as well as a command receiver will be incorporated in the carrier.

TABLE 7-3

SEQUENCE OF EVENTS, STACKED CONFIGURATION

1. Launch & Ascent, Through Delta Burnout
2. Third Stage Spin-up & Separation (Activate Payload Separation Timer)
3. 3rd Stage Burn
4. Payload Separation (Activate VHF Command Receiver in Carrier)
5. Release, Deploy, & Lock 12 Single-Hinge Booms and Release 4 VHF Whip Antennae on Carrier
6. Erect Payload Spin Axis Approx Normal to Orbit Plane
7. Coast (72 Hours)*
8. Make Attitude Measurements
9. Make Spin Axis Roll Correction
10. Make Attitude Measurements
11. Make 2nd Spin Axis Roll Correction
12. Separate Two Outboard Satellites (Near 2nd Apogee)
13. Make In-Plane Δ V Maneuver (Pulsed Thrustor Operation, Synched to Earth Sensor)
14. Separate Two In-Board Satellites

For Each Satellite:

15. Sense Separation & Activate Command Receivers
16. Fire Solid Rockets for Out-of-Plane Δ V

*Carrier VHF Transponder ON for Tracking & Command

Antenna Considerations. Use of the satellites' orbital strip-array S-band antennas during ascent is impossible, because they are nested within the solar array skirt or the carrier framework. A VHF turnstile antenna with four radial whips will be used on the carrier.

Power Requirements. Use of a ground-commanded attitude control mode will mean a coast period of about 72 hours, to second apogee. The power requirement of the transponder will be about double what it was in the radial case, or 2 watts, in order to provide for the attitude sensor telemetry. The average power requirement of the attitude control subsystem itself is 3 watts, (the total power requirement during coast is about 6.5 watts, corresponding to a battery on the order of 20 lbs.) which is quite expensive in terms of payload weight. Therefore it would be desirable to obtain solar power from one or more satellites during ascent.

Interface Requirements. An electrical interface is required between the carrier and each of the inboard satellites, to transmit the signal to fire the pyrotechnic devices for the separation of the outboard satellites. It is also necessary to transmit the payload separation signal initiated by a microswitch in the satellite adjacent to the booster) to the carrier, for activation of the ascent command receiver. Finally, the power transfer interface is required between the carrier and an adjacent satellite.

7.3 ORBITAL OPERATIONS

7.3.1 Experiment Scheduling

The region of scientific interest lies roughly between 10 and 14 R_e from the earth; therefore, the instruments will be turned on and data recorded over this interval, on both the inbound and outbound legs of the orbit. The elapsed time spent in this region is about 3.8 hours on each leg. Including a couple of hours of collecting reference solar plasma data in the region of apogee, a nominal experiment time of 10 hours per orbit has been chosen.

7.3.2 Playback Scheduling

As has been developed in Section 6, it will be necessary to read out data from each of the four satellites sequentially. This, together with ground network constraints, results in a playback time of approximately 30 minutes per orbit, for each satellite.

7.3.3 Operating Modes

There are four operational modes, as follows:

a. Record mode, in which the instruments are making their measurements and the scientific data are being recorded (there is no transmission during this period)

b. Readout mode, in which the scientific data is recovered from the recorder and transmitted via the data link to the ground station, together with engineering status information

c. Standby mode, in which no data is handled

d. Real time mode, which is only a backup mode in case of recorder failure, in which data is taken directly from the instruments and from engineering status sensors and transmitted simultaneously to the ground station, using the transmitter in a reduced bit rate, reduced power mode.

A listing of the equipments that are operating during these various modes, and their respective power requirements, is given in Table 5.3-2. In addition to the orbital modes, there is a specialized mode during the first orbit of the radially deployed satellites, when the electrically heated ammonia reaction control system is being used. This heater consumes about 15 watts, so that no recording or transmitting of scientific data can be done while the attitude orientations are being accomplished.

During eclipse, the satellite is maintained in the standby operating mode, powered by a small secondary battery. As shown in Paragraph 5.3, the existence of this battery also makes possible the optional operating mode of high rate data playback and transmission (6 watts RF output). It should be noted that standby operation of the satellite is desirable in order to keep the on-board sequencer running, as well as to avoid sizable calibration shifts in experiment elements. As indicated in the thermal analysis section, standby power is not required purely for temperature control, for eclipse periods of up to an hour. A definitive occulation time analysis has not been done for varying launch data, but it can be stated that eclipse periods in excess of one hour will not occur for at least 4 months following launch. Beyond this, and depending upon the actual ecliptic inclination of the orbit, modest additional increments of standby power might be required for temperature control.

7.4 SPIN AXIS ORIENTATION

One of the system requirement questions which must be answered is: What should be the inertial orientation of the satellite spin axis? The two orientations of special interest are normal to the ecliptic plane, and normal to the orbit plane. From the experimenter's point of view, alignment normal to the ecliptic is

preferable. It remains to determine whether this is possible and reasonable from the point of view of spacecraft requirements.

In the case of the stacked configuration, in which the orientation is established by the carrier, the choice is constrained by the separation requirement that all velocity increments be normal to the orbital velocity vector. Any deviation from this will result in period differentials and therefore in secular drift rates. Since implementation of the out-of-plane velocity increment, either by springs or by solid rockets, requires that the separation velocity be along the spin axis, the spin axis must be normal to the orbital velocity vector. This condition cannot be satisfied by an ecliptic alignment. Making the spin axis normal to the orbit plane does, of course, satisfy this necessary condition, and also simplifies the mechanization of the attitude control sensors and logic. Therefore, the orientation of the spin axis is dictated in this configuration by the separation method.

In the radial configuration, in which the individual satellite spin axes are oriented after separation, there is no constraint on the orientation due to the separation method. The principal effect on spacecraft requirements of aligning the spin axis normal to the ecliptic plane is the resulting increase in antenna beamwidth requirement. The essence of this analysis is shown in Figure 7-2. The plot shows the variation with true anomaly of the angle subtended by the earth's disc, and the angle between the spin plane of the satellite and the earth-satellite line. The sum of these, together with an allowance for attitude error, is the total angle required to provide full earth coverage; this composite also is shown on the plot. The spin plane tilt shown is based on a reference orbit which has an inclination to the ecliptic of 26 degrees. The most interesting point on this plot is in the region of 90 to 100 degrees true anomaly, below which satellite communications will not be scheduled, due to operational considerations (i.e., station availability and ground antenna tracking rate limitations). This region then represents the maximum requirement on beamwidth.

From the plot, the total beamwidth required is about 110 degrees. This happens to be just about the maximum toroidal beam which is feasible with the antenna configurations which are proposed. It should be noted that the ecliptic inclination

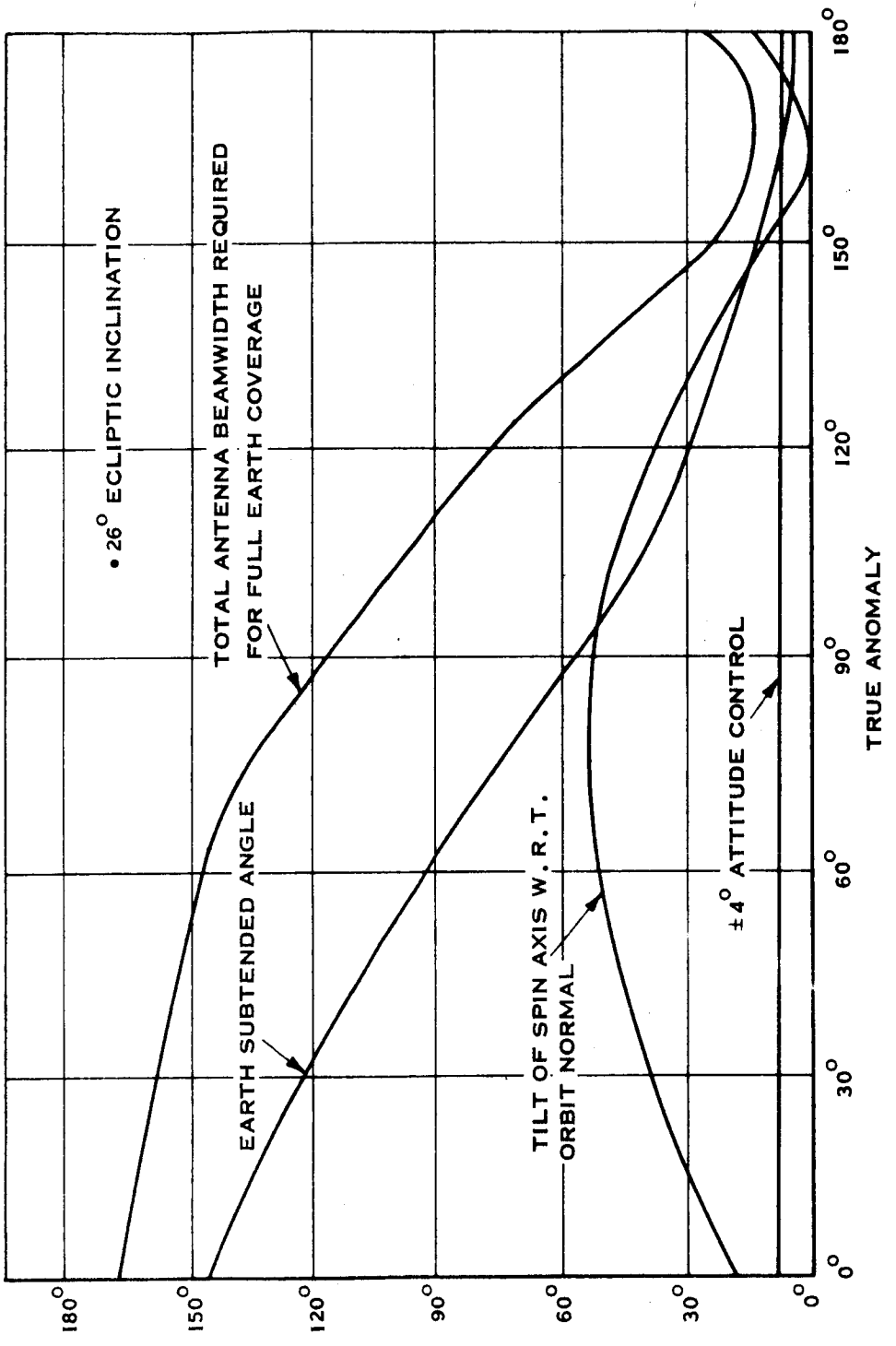

Figure 7-2 Antenna Beamwidth Requirement, Radial Configuration

of 26 degrees represents a very conservative case. The actual selection of an optimized launch date will result in ecliptic inclinations on the order of 5 to 10 degrees, and this will decrease the beamwidth requirement correspondingly. Another factor which makes this a conservative analysis is a degree of flexibility in scheduling the playback times. For example, should the actual antenna design result in a beamwidth of 90 degrees, the plot shows that full earth coverage would be available down to a true anomaly of about 110 degrees. Shifting the end of the playback zone from 90 to 110 degrees true anomaly means a rescheduling of less 20 minutes. Because the satellite is moving much more slowly at the beginning of the 2-hour playback period than at the end, the increase in range at the beginning of playback is only slight (about 3000 km) and there still is no interference between the playback region and the measurement and record region. It is therefore concluded that for the radial configuration, the experimentally desirable alignment of the spin axis to the ecliptic does not result in any unreasonable spacecraft or system requirements, and therefore this alignment is recommended.

7.5 CONFIGURATION COMPARISON

In Table 7-4 is given a summary of the comparison of salient features of the two principal configuration alternatives. The chief points of comparison, and some explanatory remarks concerning the entries in the table, are as follows:

7.5.1 Design

Weight. Based on our preliminary design studies, estimates of total payload weight have been made, as follows: radial configuration, 266 lbs; stacked configuration, 302 lbs. These estimates included an assumed experiment load of 12 lbs. per satellite. Although these figures would be refined by further design studies, the comparison is valid and shows a substantial advantage for the radial concept. This is due to a combination of individual satellite design features, as well as the ability to use a relatively lightweight trusswork adapter for the radial configuration, rather than the standard Delta adapter. Also, the carrier module required for the stacked case is a considerable additional weight.

TABLE 7-4

CONFIGURATION COMPARISON SUMMARY

	RADIAL	STACKED
• DESIGN		
Weight	266 lb.	302 lb.
Power Available, Maximum	30 Watts	25 Watts
P/L Separation Complexity	Bolt Cutter	STD Delta Separation V-Band Clamp
Satellite Separation Complexity	Single Event	3 Separation Events + ΔV Maneuver + Solid Rockets
Boom Complexity	Single Event for Satellite; Satellites Independent	Single Event For Payload
Spin-Up Requirement	Each Satellite	None
Attitude Control Requirements	4 Separate Systems NH_3 RCS Sun Sensors Albedo Earth Sensor	Single System N_2H_2 RCS Sun Sensors IR Earth Sensors
Orbital Antenna	Biconical S-Band	Strip-Array S-Band
Ascent Antenna	VHF Whip	VHF Turnstile
Ascent Equipment	VHF Beacon & Command RCVR	VHF Telemetry Transmitter & Command RCVR
Ascent Power	Battery; No Interfaces	Solar Power From Satellites
• RELIABILITY		
Probability of Survival, 4 Satellites for 3 Months	.59	.56
Risk Factor	Satellites Deployed Independently	2nd Pair Deployment Dependent on 1st
• OPERATIONS		
Ascent	24 hours Angle Track & Command	72 Hours Angle Track, Receive TLM & Command
Orbital	GRRR Track Receive TLM & Command	GRRR Track, Receive TLM & Command
• EXPERIMENT SUITABILITY		
Spin Axis Alignment	Normal to Ecliptic	Normal to Orbit Plane
Array Configuration	No Essential Difference, if Translational Capability is Added to One Radial Satellite	
Expected Drift Rates		
Adaptability for Orbital Maneuvers	Can Make ΔV Maneuvers for 3D Array	No Orbital ΔV Capability

Power. An estimate has been made for each configuration of the inherent growth potential in power availability. These were based on the maximum possible extension of the longitudinal dimensions of the solar arrays, constrained only by the shroud envelope (the diameters already are maximized). The results were that the maximum power available from the radial configuration satellite would be about 30 watts, and from the stacked about 25 watts (these figures are for conditioned load power at the end of six months). This additional power for the radial case would be a decided advantage particularly if it were desired to use the more capable DSV-3J launch vehicle and incorporate added experiments.

Payload Separation Complexity. The radial configuration payload is separated from the third stage adapter using a pyrotechnic bolt cutter and a set of matched springs. The stacked configuration uses the standard Delta separation device consisting of compressed springs and a pyrotechnically-actuated V-band clamp. There is very little difference in complexity between the two systems.

Satellite Separation Complexity. The deployment of the four radial satellites is accomplished by a single event, the firing of a pyrotechnic cable cutter. A redundant pyro device could easily be added for reliability. By contrast, the stacked configuration requires three separate pyrotechnic events, the in plane ΔV maneuver, and the firing of the solid rocket on each of the four satellites, for the out-of-plane velocity increment. The pyro events are V-band clamp separations to release the satellites: one for each of the two outboard satellites (these two are fired simultaneously), and a common one for separation of the two inboard satellites. The in plane ΔV maneuver involves the pulsed operation of the radial thruster of the hydrazine reaction control system in the carrier.

The comparative simplicity of the radial configuration in this regard is the most persuasive single feature in its favor.

Adaptability for Orbital Maneuvers. The on-board reaction control system of the radial configuration satellite could be used, with the addition of a small amount of propellant, for making ΔV maneuvers in order to obtain a particular three-dimensional orbital array. The stacked configuration satellite has no such potential; should the capability for orbital maneuvers be desired, the requisite hardware would have to be added.

Boom Deployment Complexity. The boom design in the two cases is essentially the same: a rigid, single-hinged boom which is released by a pyrotechnically-actuated latch and deployed by a spring-and-damper mechanism. In the radial case, a separate event on each satellite releases the three booms on that satellite whereas in the stacked case a single event on the payload releases all twelve booms. The radial case has a disadvantage in that it requires four events rather than one, but, since the satellites deploy their booms independently, a failure would result in losing one satellite only, instead of the entire group.

Attitude Control Requirements. The most obvious difference between the two concepts is that the radial requires four attitude control systems, one on each satellite, compared to only one on the carrier of the stacked configuration. Again the situation is that a failure is more likely with four separate systems than with one, but the results of a failure are less disastrous. This presumes that three operable satellites are to be preferred over none at all.

Beyond this overall comparison, the attitude control sybsystem elements are different. They each have the same type of moving parts, solenoid-operated propellant valves, and the radial case requires an ammonia heater, whereas the hydrazine thrusters require a catalyst chamber ammonia heater, whereas the hydrazine thrusters require a catalyst chamber and propellant injector assembly. The same type of sun sensor is required for each case. The radial case can use an albedo-type of horizon sensor, while the more stringent accuracy requirements of the stacked configuration dictate the use of infrared-type horizon sensors, which are more complex and costlier.

Spin-Up Requirements. In the radial case, each satellite must have the capability to spin up to the desired orbital rate, following deployment of the booms. In the stacked configuration, the inertia ratios are such that the proper spin rate can be obtained directly from the launch vehicle, and no spin-up capability is required on the satellites. This is an advantage of simplicity in favor of the stacked configuration.

Antenna Configurations. The orbital antenna which is most suitable for the radial configuration is an S-band biconical horn on top of a central mast. For the stacked configuration, a strip array of planar spiral elements with associated resonant cavities appears to be the best choice. The former configuration is considerably simpler both in design and in operation.

For ascent operations, the respective VHF antennas are a whip, for the radial configuration, and a turnstile, for the stacked. These are both very simple, and offer about the same level of performance.

Ascent Communications and Control Equipment. The release module of the radial configuration requires a VHF beacon, and a command receiver with an associated sequence timer. The carrier of the stacked configuration also needs these, and has the additional requirement for a digital telemetry unit and telemetry transmitter.

Ascent Power Supply. The radial configuration can be operated during ascent by a small primary battery, whereas the power requirement and coast phase duration of the stacked configuration are such that the additional complexity of an umbilical electrical interface between the carrier and the solar array-supplied power subsystem of an adjacent satellite is required for power transfer.

7.5.2 Reliability

Based on a single-string failure rate analysis, the radial configuration has a slight advantage in probability of deployment and survival of four satellites for three months, 0.59 to 0.56. Failure modes and effects analyses and the indicated

low-level redundancies would easily bring either of these to the desired 0.70 value. There are reliability features, however, which are not readily reflected in a mathematical failure rate model. One of these is the risk factor involved in the stacked configuration in that the first pair of satellites must be separated before the second pair can be separated, whereas in the radial case the separations of the four satellites are independent. Also, the existence on the radial satellites of an attitude control system gives a certain functional flexibility, i.e., reorientations could be made in response to unexpected occurrences. Mainly because of these qualitative evaluations, the radial configuration appears to offer a reliability advantage.

7.5.3 Operations

Ascent Coverage. The support required of the ground network during ascent is, in the radial case, of 24 hours duration, and consists of angle tracking for essentially the entire period, computation of the apogee angle, and the command control near apogee. Subsequent to separation, command control of attitude maneuvers is required for short periods during the first orbit. In the stacked case, the ascent phase during which the satellites remain together lasts for 72 hours. The requirement for angle tracking and orbit determination is the same. The stacked payload imposes the additional requirement for reception of telemetry (principally attitude data), computation of required orientation commands, and transmission of the attitude control and deployment maneuver commands. But all of this, with the exception of the ΔV maneuver, must be done also for each of the radial satellites following separation, so that there is very little to choose between the two configurations in this regard.

Orbital Coverage. There is no difference between the two configurations in the network support required for tracking, data reception and management, and command control operations.

7.5.4 Experiment Suitability

Spin Plane. The radial configuration has the capability to align the spin plane with the ecliptic, which is desirable from the experimenter's point of view, whereas the separation method of the stacked configuration requires that the spin axis be normal to the orbit plane, which results in a fixed bias of the spin plane with respect to the ecliptic on the order of 5 to 10 degrees, depending on launch date.

Array Configuration. There is no fundamental difference in the satellite arrays which are obtainable using the two concepts. In the case of an array which is initially planar, the radial concept might be considered to have a disadvantage in that it must be separated at apogee, and thus the relationship of the sun to the satellite array is fixed by the launch date, whereas in the stacked case there is freedom to trade off this sun angle relationship against a varying true anomaly of separation. The radial concept has a slight advantage, however, should it be desired to establish the array initially in a three-dimensional configuration, because it takes a lesser number of maneuvers to accomplish this.

Drift Rates. The arrays which are established by both concepts are subject to asymmetric elongations which increase over the life of the mission, due to the secular drifts of the individual satellites with respect to each other. These drifts are associated with period differentials, which, in turn, are caused by a combination of deployment errors and subsequent differential drag perturbations. Error analyses of the two concepts have shown that the magnitude of expected velocity direction errors is about the same in either case. Therefore, there is no reason to prefer one concept over the other for reasons of lower expected drift rate.

In summary, of the two alternative concepts which were studied, the radial concept offers a configuration which is lighter, simpler, more adaptable to growth versions, and has at least equivalent experiment value, and therefore this is the preferred concept.

SECTION 8

RELIABILITY ANALYSIS

8.1 INTRODUCTION

The major reliability gains in a system are made in the initial concept selection. The concept selected basically constraint system reliability improvement except in the areas of basic reliability improvements of parts and materials used. It is assumed that the system will be implemented with the most reliable parts and materials available and the quality variance of the parts and materials will be controlled by a 100 percent screening and burn-in type program on the 250 to 500 hour level. In respect to maximizing the inherent design reliability, the preferred system concept is the one that best provides:

- High resistance to complete mission failure due to single part/material failures.
- Functional simplicity and independency of operation
- Functional flexibility
- Potential growth capability
- High worth of possible failure modes in achieving partial mission objectives.

The radial and stacked system concepts were evaluated in respect to the above criteria and the results are discussed in the following paragraphs.

8.2 SYSTEM RELIABILITY ANALYSIS SUMMARY

For the scientific data acquisition mission for this system, the preferred concept that offers the highest potential of meeting the required level of reliability is the radial payload system. The specified requirement for the four-satellite array to be designed to achieve at least a 0.70 probability of success for system installation and three months orbital operation can best be realized in the radial type concept. Conservative assessment of the design indicates total functional success. The probability that all four satellites will successfully survive three months without any redundancy or special failure hazard reduction features is in the region of 0.56. This is only a factor of 1.7 below the specified requirement of 0.70. Based on past experience, this level of improvement is usually realized in the detail design mechanization by nominal reliability improvement efforts.

8.3 SYSTEM CONCEPT TRADES

The results of alternate system concept trades are dependent on the mission objectives and design criteria used to evaluate the concepts. The evaluation criteria are stated in the following paragraphs.

8.3.1 Mission Objectives

The overall mission objective is to establish four scientific instrument "platforms" in an array to acquire time and geometrically coherent data on the physical parameters of interest.

The significance of this objective is that a space-time coherent scientific data acquisition mission of this type requires a system concept that recognizes in its design calibration, establishment and maintenance of the system geometrical parameters within the scientific accuracy required.

8.3.2 Overall Mission Success Criteria

Total mission success in respect to the objectives is dependent on the following specific success criterion:

a. Placement of Science Instruments. Successful placement and orientation of instruments in the regions of scientific interest specified.

b. Science Data Acquisition. Successful acquisition, processing and transmission of science measurement data.

c. Experiment Control. Successful control of science instrument measurements, orientation, processing, and transmission.

d. Calibration Data Acquisition. Successful acquisition, processing and transmission of data on placement, orientation, instrument parameters, data processing parameters and transmission parameters for calibration and error analysis of science measurement data.

e. Engineering Data Acquisition. Successful acquisition of general satellite performance parameters to verify/analyze the satellite's performance effect on valid science and calibration data acquisition, processing and transmission.

8.3.3 Inherent Reliability Criteria

The alternate concepts were evaluated in respect to the following specific criteria to provide the engineering confidence in relative achievement of mission objectives to the success criteria.

a. Reliability of scientific data acquisition

b. Functional flexibility

c. Failure mode effect in terms of partial scientific data acquisition

d. Potential growth capability for reliability improvement/failure hazard reduction in the implementation phase

e. Functional independency and simplicity of operation to achieve total and/or partial mission objectives

A brief expansion on each criterion is necessary to assure understanding of the trades discussion.

Reliable Data Acquisition. Reliable data acquisition is dependent upon:

a. Design adequacy of the system array to sense and acquire the data.

b. Real time verification of acquired data validity.

c. Prelaunch calibration of sensors and instrument platform.

d. Real time monitoring of performance to assure calibration data for correction of systematic errors induced by degradation/aging of the sensor equipment and platform.

e. Identification of systematic and non-systematic scientific data error sensors.

Functional Flexibility. By definition, scientific measurements to determine uppredictable characteristics of a transient nature imply a flexibility in measurement control. In this sense, reliability of scientific data acquisition is dependent to some degree on the capability to maneuver the instrument platform's orientation in respect to the space coordinates and to the satellite array coordinates. The degree of flexibility required can not be clearly delineated until the initial reference point is established with data reduction and correlation of the data obtained in the early orbit.

The mission success criterion for system trades can be viewed as the probability of acquiring useful scientific data as a function of unplanned events such as failures and unexpected data perturbations requiring analysis by instrument platform reorientation.

Failure Mode Effect on Scientific Data Acquisition. The consideration of the effects of failure modes on scientific data acquisition per missionis a significant trade factor. In the reliability evaluation of two alternate system concepts to achieve the same mission, the relative worth of failure mode effects are given weight in the trade-off. The basis of this criterion is that: given a single catastrophic part/material failure in the design, the effect of the failure should not result in a complete mission failure. Although it is practically impossible to meet this criterion without considerable part, circuit and equipment level redundancy, two system concepts can be evaluated for their inherent resistance to complete catastrophic failure.

Potential Growth Capability. As the detail characteristics of a system design become visible in the development and compatibility test phase, unacceptable hazard areas become evident. A system that has intrinsic capability for flexibility, relocation of equipment, and minor reconfiguration is more reliable in the sense that risk areas can be obviated by corrective action design without major perturbation in the system design, cost and schedule.

Functional Independency and Simpliicity. The more complexity, interfaces, and functional interdependency a system has, the more unreliable it tends to be when compared with a competing system design to achieve the same mission objectives.

8.4 RADIAL VERSUS STACKED CONCEPT TRADES

Shown in Figure 8-1 is a delineation of the functional/event flow of the Radial and Stacked with point of departure identified. With this diagram as an aid, the major significant factors in reliability tradeoffs are discussed.

8.4.1 Placement of Scientific Instruments.

The variance between the alternate concepts is greatest for accomplishment of this success criteria. The major differences are:

a. Carrier Configuration. The stacked carrier has the disadvantage of potential structural design requirements variance as a function of satellite position in the configuration. Since the stress loading of the 3rd stage burn is a significant stress region this can be a constraint in assuring an adequate strength to loading margin within weight and volume allocation in respect to standardizing satellite designs. The radial carrier concept lends itself to standardized design due to its symmetrical interface with the carrier orthogonal to the thrust vector.

b. Extended Coast Time. The requirement of the stacked concept for a 72 hour coast phase versus 24 hour period for the radial is a significant factor in battery reliability and maintaining thermal control without compromising optimum orbital operation thermal design.

c. Delta Velocity Increment. The radial concept takes advantage of the 3rd stage stability RPM energy to inpart a delta velocity to each satellite as a function of timed release. The stacked requires a satellite solid fuel rocket combined with a carrier delta velocity function to achieve the array dispersion matrix.

d. Conditional Functions/Events. Placement of satellites in the stacked payload are conditionally dependent on successful functioning of the carrier attitude control system. Separation of the satellites are serially dependent, i.e., hang-up of a satellite will either affect an inboard satellite or introduce sufficient instability in the system to preclude recovery by the carrier attitude control system.

8.4.2 Science Data Acquisition

Relative achievement for the alternative concepts based on this criterion favors the radial due to its flexibility. Since the satellites have independent attitude control capability and the measurements are vector as well as amplitude type, the likelihood of achieving valid data even with satellite failures in the array or partial failures in the satellites is improved by reorientation capability.

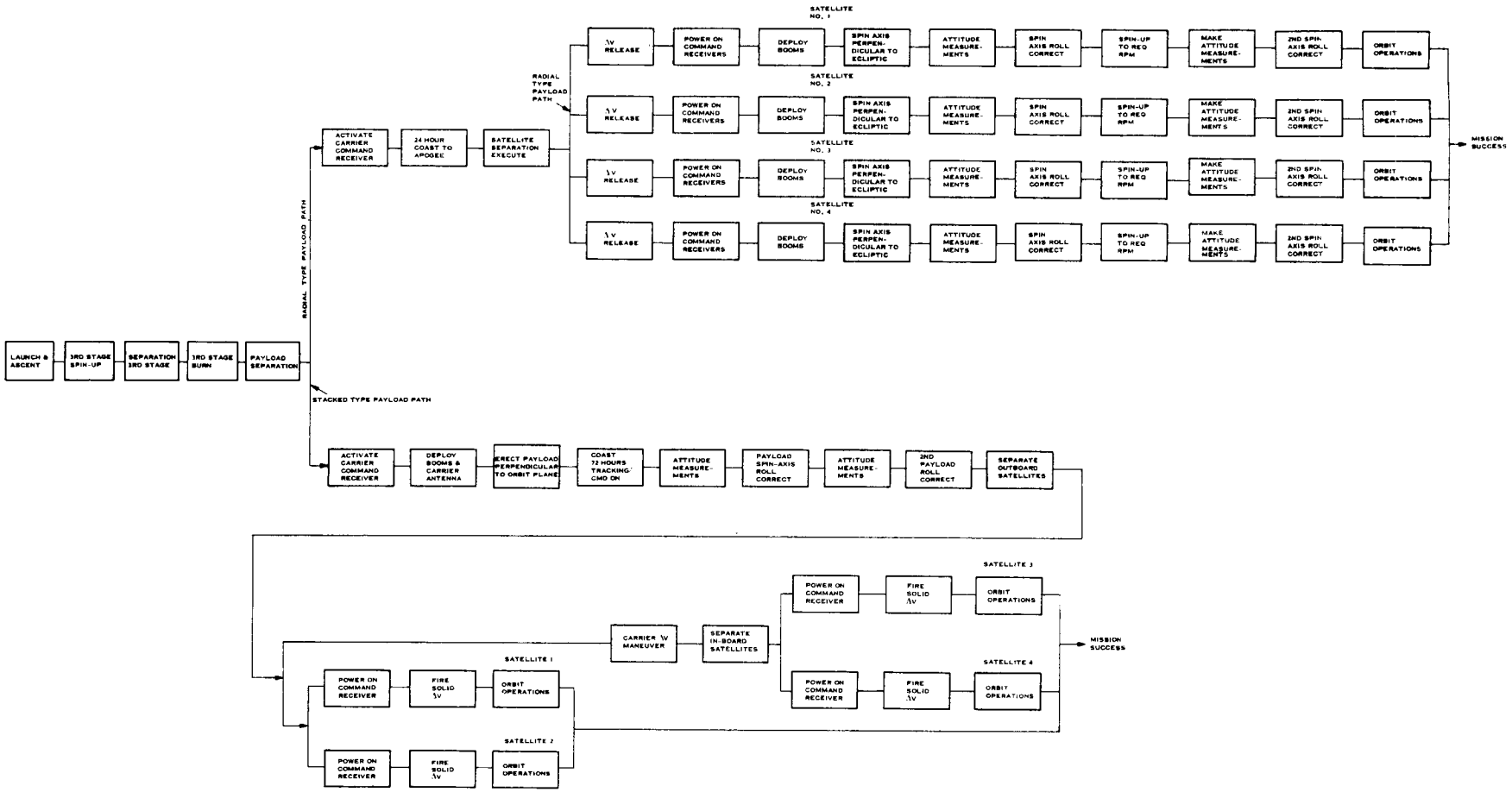

Figure 8-1 Mission Success Path Comparison, Radial vs Stacked Payload

8-7/8-8

8.4.3 Experimental Control

This probably is the most important criterion for evaluating relative degree of inherent reliability achievement. The degree of control of the satellites as instrument platforms in context of unplanned events such as failures or unexpected data perturbations can make the difference in a successful mission. The radial concept, due to its satellites having independent attitude control, provides significant flexibility and failure recovery capability. Besides the obvious advantage of the experimenter being able to change orientation in array or satellite either prior to launch or post launch, the significant gain is that each satellite can drop to a non-coherent Pioneer type mission, e.g., failure of the booster to achieve planned trajectory would not abort mission since the radial concept can separate four Pioneer class experiments and adjust each satellite to obtain the most useful data for its type of orbit.

8.4.4 Calibration Data Acquisition

The radial provides the maneuvering capability to re-orient instruments to test data in orthogonal planes or to verify a sensor's performance by change of sensor orientation to the measured field.

8.4.5 Engineering Data Acquisition

No significant differences were noted in the alternate concepts for inherent capability to this success criterion.

8.5 QUANTITATIVE ASSESSMENT

The following paragraphs discuss the quantitative assessment of the alternate concepts based on a systems part count type assessment and the variance in mission profiles. The results of the assessment were:

1. The radially mounted configuration is preferred for reliability reasons. Table 8-1 provides a comparative listing of the characteristics of the

two configurations considered. The radial design shows significant advantages over the stacked configuration.

2. The significant requirement is the 0.70 probability of survival (P_s) for the set of four satellites during the first three months in orbit.

3. The reliability requirements are feasible if selected redundancies are allowed.

4. The implementation of both a Failure Modes and Effects Analysis are assumed to allow upgrading the reliability expected.

8.5.1 Quantitative Requirement

The reliability requirement for the four satellite array was specified as total functional success for installation and operation for three months with a probability of success of 0.70. This is an effective requirement of 0.92 for each satellite for three months or a equivalent failure rate of 4.1%/1000 hours.

Preliminary estimates give the following for an individual satellite:

*Probability of Survival - 1 satellite - 3 months = 0.75336
Probability of Survival - 4 satellites - 3 months = 0.32211 for
$\Sigma \lambda$ = 12930 Bits (1 Bit = 1 failure/10^8 hours)

The reliability improvement required can be measured by

$$\frac{\lambda \text{eff}}{\lambda \text{req'd}} = \frac{12930}{4128} = 3.1$$

Subsequently, more detailed analysis should show that achievement of the required reliability is feasible. Analyses not possible at the present design level typically show feasible reduction of λ eff up to 0.56 from improved system and equipment-failure definition alone.

TABLE 8-1

RELIABILITY CHARACTERISTICS COMPARISON - SUMMARY

RADIAL		STACKED	
Advantages	Disadvantages	Advantages	Disadvantages
Shorter time to satellite separation.			Longer time to satellite separation.
Failure of one attitude system still permits stabilization of remaining 3.	Four attitude control systems. Added possibility of failure.	One attitude control systems. Less probability of failure.	Failure of attitude control affects are satellites.
All satellites separated simultaneously.			Satellite separated pairwise. Second separation dependent on first being successful.
		Failure of one ΔV motor will still permit remaining satellites to be properly deployed.	Requires ΔV motor in each satellite. Adds to probability of failure.
Release sequence relatively simple.			Release sequence relatively complex.
Higher numerical reliability estimate.			Lower reliability numerical estimate.

Then we have

$$\frac{\lambda \text{ eff}}{\lambda \text{ req'd}} = \frac{7241}{4128} = 1.7$$

8.5.2 Single Satellite Assessment

The on-orbit reliability factors are relatively independent of the launch configuration used. The launch reliability (through separation of the satellites) is different for the two configurations resulting in a slightly higher reliability for the radial configuration. Although the attitude control function is found in all four satellites, the added failure fractions are more than offset by the 48 hour longer period to effect separation of the stacked configuration.

8.5.2.1 Orbit Phase. Table 8-2 summarizes the failure fraction contribution of the various subsystems for the orbital phase. Both configurations are assumed the same during the orbit phase - after complete separation. The table includes the basic failure rate; a failure rate adjusted for expected influence of the failure modes and effects analysis and end life degradation analysis ($\lambda' = 0.56\ \lambda$); appropriate mission phase environment-time factors (KT) and values of λ KT and λ' (adj.) KT. The reliability values - probability of survival - are given for one satellite. Values for four satellites will be found in Table 8-3.

8.5.2.2 Launch Phase. Table 8-4 provides launch phase data for the two alternate configurations. The configurations here are not the same. The stacked configuration has the attitude control function contained in the central cylinder. The radial system requires four attitude control systems. The stacked system requires 48 hours longer to complete separation than the radial configuration, thus delaying the initiation of the orbit phase. The failure rate adjustment factors described in 8.5.2.1 are not applicable during launch and are omitted from the table.

8.5.3 Quantitative Reliability Assessment Summary

Table 8-3 summarizes Tables 8-1 and 8-2 and presents a composite of the reliability estimates. The probability for 4, 3, 2, 1, and 0 satellites surviving the three-month required period are also given. Numerically, the indication is that the radial configuration is to be preferred for reliability reasons.

TABLE 8-2

RELIABILITY ESTIMATES - ORBIT PHASE

Satellite Subsystem	λ (Bits)*	λ' = 0.56	T = 3 Months			T = 1 Year		
			KT	λ'Σ KT	λΣ KT	KT	λ'Σ KT	λΣ KT
Structural	46	26	20	0.000005	0.00001	80	0.00002	0.00004
Power	907	512	2225	0.01139	0.02018	8900	0.04557	0.08072
Communication	2054	1150	2225	0.02559	0.04570	8900	0.10235	0.18281
Data Process & Storage	6041	3383	1690	0.05717	0.10209	6760	0.22869	0.40837
Command and Control	2920	1635	2000	0.03270	0.05840	8000	0.13080	0.23360
TOTAL				0.12686	0.22638		0.50743	0.90554

* Bits = failures/10^8 hours

λ' is the anticipated analytical value for failure rate subsequent to completion of a Failure Modes and Effects Analysis and an End-Life Degradation Analysis.

TABLE 8-3

COMPOSITE - RELIABILITY
LAUNCH THROUGH ORBIT OPERATIONS

	Radial		Stacked	
Satellites Surviving Launch				
0 satellite				
1 satellite				
2 satellite	0.00006		0.00047	
3 satellite	0.01040		0.03462	
4 satellite	0.98956		0.96491	
Expected No. Surviving Launch	3.99		3.96	
Orbit (3 months)				
No. of Satellites Surviving				
0	0.00169	0.00020	0.00169	0.00020
1	0.02654	0.00599	0.02654	0.00597
2	0.15666	0.06618	0.15666	0.06618
3	0.41092	0.32590	0.41092	0.32590
4	0.40418	0.60175	0.40418	0.60175
Expected No. Surviving 3 months Orbit	3.19	3.52	3.19	3.52
Launch Through Orbit 3 months				
Satellites Surviving				
0	0.00175	0.00021	0.00194	0.00026
1	0.02718	0.00156	0.02918	0.00716
2	0.15867	0.06791	0.16483	0.07384
3	0.41175	0.32877	0.41405	0.33811
4	0.40064	0.59687	0.39002	0.58063
Expected Surviving Launch Through 3 months	3.18	3.52	3.16	3.49

TABLE 8-4

RELIABILITY ESTIMATES - LAUNCH PHASE

	(Bits)*	Radial Design		Stacked Design	
		KT***	KT	KT	KT
Structural	56	95	0.000044	143	0.00007
Separation	163	15	0.000024	63	0.00010
Orbit Insertion	200	15	0.000030	63	0.00013
Stabilization/Orientation	1774	15	0.000266	63	0.00112
Power	907	15	0.000136	63	0.00056
Communication	2054	15	0.000308	63	0.00129
Data Processing & Storage	6041	15	0.000906	63	0.00381
Command and Control	2920	15	0.000438	63	0.00184
TOTAL KT			0.00215		0.00893
P_S**(KT)			0.99738		0.99111
4 SATELLITES KT			0.00861		0.03512
P_S**(KT)			0.99143		0.96549

* Bits = Failures/10^8 Hours

** P_S(KT) = Probability of Survival for Time Required

T = 0.2 Hrs. (Radial)
0.2 Hrs. + 48 Coast (Stacked)

K = Failure Rate Acceleration Factor - For Launch:
Mechanical Items K = 800
Electronic Items K = 80
For Coast K = 1

GLOSSARY

Apogee, the point of greatest excursion of an Earth satellite.

Conic section, the locus in a plane of all points having a constant ratio ϵ (eccentricity) between the distance r from a fixed point F (focus) and the distance d from a fixed line (directrix).

Eccentricity, see conic section.

Path angle, ϕ the acute angle between the velocity vector and the normal to the radius vector.

Perigee, the point of closest approach of an Earth satellite.

Period, γ, the time required for a body to complete one complete revolution.

Phase shift, Δt, the time between two satellites closest approach to a given point.

Rotation angle, ρ, the angle between the initial orbit plane and the orbit plane of the satellite after an out-of-plane maneuver.

Semi-major axis, a, the radius of the smallest circle which will circumscribe an ellipse.

Semi-minor axis, b, the radius of the greatest circle which may be inscribed in an ellipse.

Semi-latus rectum, p, the radius at 90 degrees true anomaly.

True anomaly, θ, the angle to the radius vector measured from the radius at perigee.

APPENDIX I

BURNER II FOR MULTI-SATELLITE MISSION

A cursory examination has been made of the applicability of the Burner II upper stage to the multi-satellite mission. The conclusion is that this is a feasible application, and should be further evaluated as an alternative approach.

1. BASIC MISSION CONCEPT

The basic concept that is recommended for the Burner II application to the Satellite mission is as follows:

a. Boost (DSV-3L or SLV-3A with Burner II)

b. Burner II main propulsion burn

c. Burner II vernier for precise perigee velocity control

d. Burner II and satellites coast to apogee (approximately 24 hrs.)

   (1) Burner II velocity meter and telemetry turned off during coast.

e. Pre-programmed event turns command receiver and T/M on prior to initiation of satellite deployment.

f. Command event initiates satellite deployment sequence.

g. Pre-programmed deployment sequence is a series of 14 events as described in Section 3.

2. FOUR SATELLITE ARRANGEMENT ON BURNER II

The configuration shown in Figure I-1 is representative of the concept recommended for use with the Burner II deployment scheme described herein. The available solar panel area shown is about 75 percent more than the minimum required. The greater area is shown to indicate the growth potential within the available envelope of the Nimbus shroud with the Burner II. The folded booms shown will deploy to a radius of 63 inches from satellite center. Seventy-five inch radius booms are stowable in the same manner but are not shown for the sake of concept clarity. A minimum solar cell area stack of four satellites could be 32 inches shorter than the one shown. The satellite will be deployed sequentially starting with No. 1. The separation concept involves V-band clamps with a small spring to impart 1 ft./sec. separation velocity. A small solid rocket provides the spin up torque after separation.

3. SATELLITE DEPLOYMENT CONCEPT

The satellite deployment scheme described here involves a tandem stack of four satellites mounted on Burner II as shown in Figure I-2. The method of deployment described results in the satellites acquiring a 5 meter/sec. separation velocity relative to a center point within the deployed array. The deployment of the satellites is accomplished by providing the required velocity vector with the Burner II H_2O_2 thrusters and then by attitude maneuvering to properly orient the satellite spin axis prior to each satellite separation. The concept assumes that satellite separation is accomplished by V-band joints and springs with spin up accomplished by satellite mounted spin rockets.

A chronological description of the deployment concept shown in Figure I-2 is as follows:

Starting Condition	=	Longitudinal axis along flight path velocity vector, payloads forward.
Event No. 1	=	90 degree yaw, to point vehicle in direction to align satellite spin axis perpendicular to orbit plane.
Event No. 2	=	Separate No. 1 satellite and ignite spin rockets on No. 1.

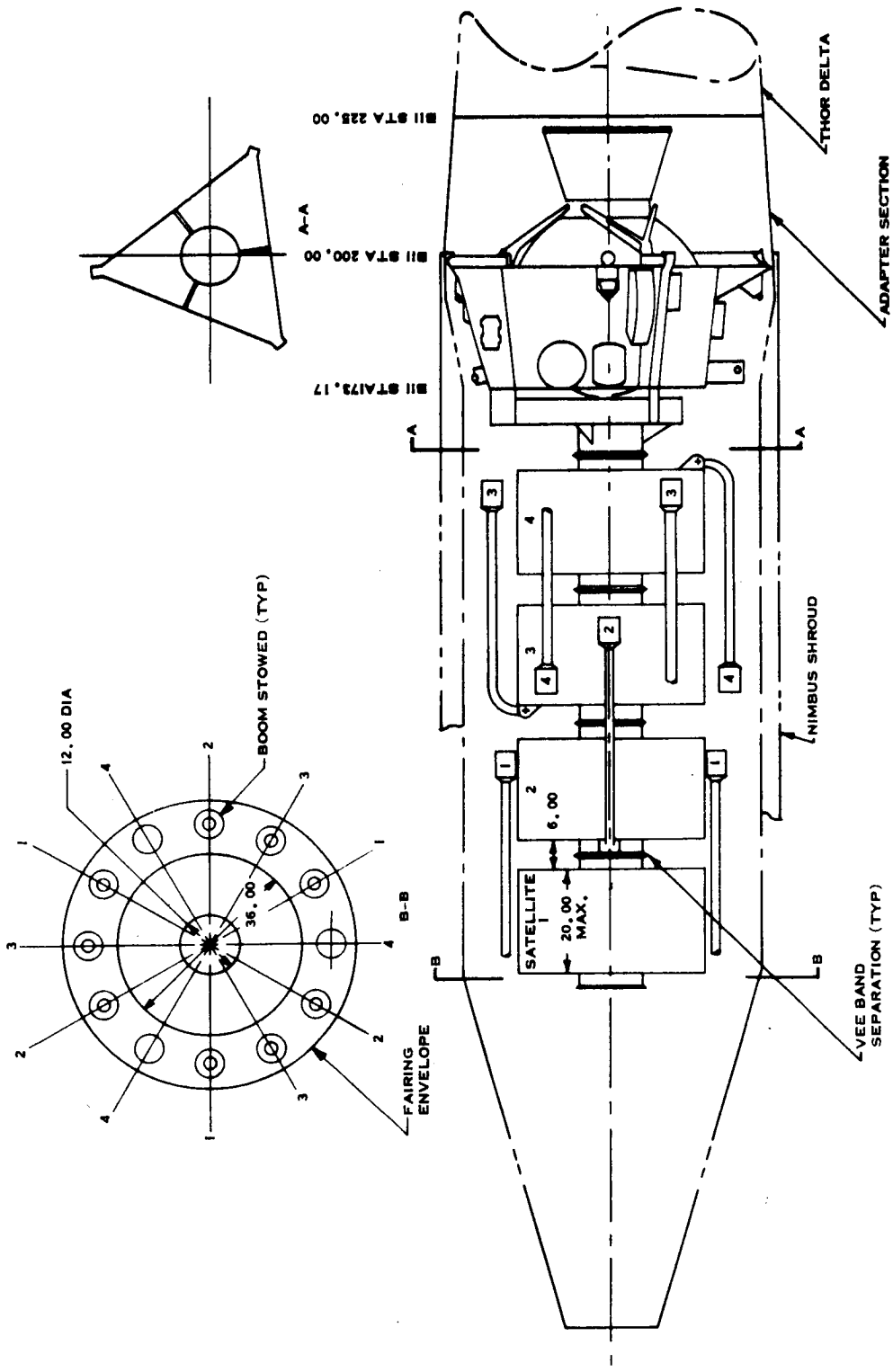

Figure I-1 Burner II/Multi-Satellite

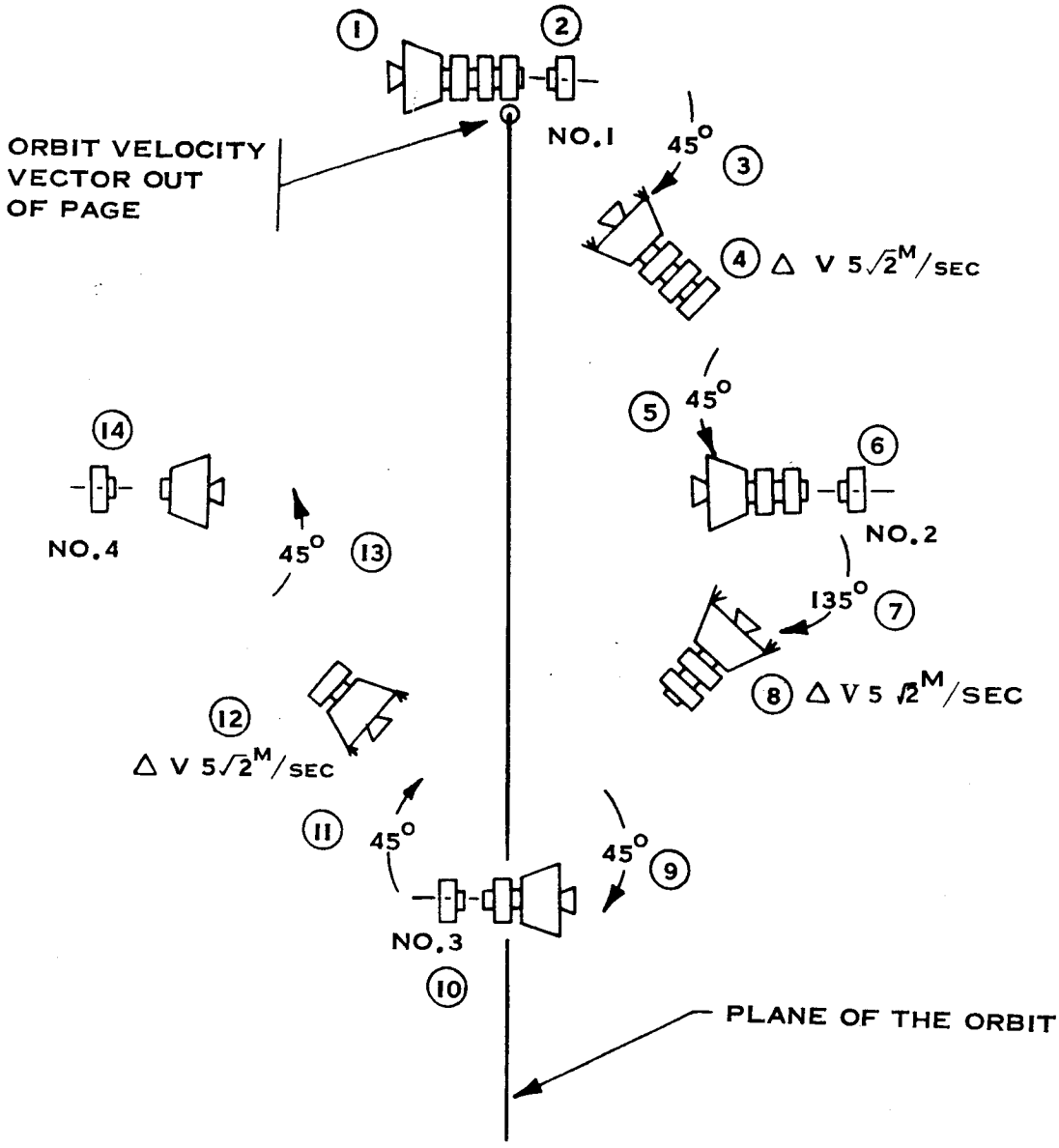

Figure I-2 Burner II/Multi-Satellite Deployment Concept

Event No. 3 = 45 degree roll down, to point vehicle for proper velocity vector for No. 2 satellite.

Event No. 4 = $\Delta V\ 5\sqrt{2}$ m/sec, H_2O_2 thrusters.

Event No. 5 = 45 degree roll up, to align satellite spin axis perpendicular to orbit plane.

Event No. 6 = Separate No. 2 satellite and ignite spin rockets on No. 2.

Event No. 7 = 135 degree roll down, to point vehicle for proper velocity vector for No. 3 satellite.

Event No. 8 = $\Delta V\ 5\sqrt{2}$ m/sec, H_2O_2 thrusters.

Event No. 9 = 45 degree roll down, to align satellite spin axis one to orbit plane.

Event No. 10 = Separate No. 3 satellite and ignite spin rockets on No. 3.

Event No. 11 = 45 degree roll down, to point vehicle for proper velocity vector for No. 4 satellite.

Event No. 12 = $\Delta V\ 5\sqrt{2}$ m/sec, H_2O_2 thrusters.

Event No. 13 = 45 degree roll up to align satellite spin axis one to orbit plane.

Event No. 14 = Separate No. 4 satellite and ignite spin rockets on No. 4.

Some of the events in the above sequence require start-stop action so the start of one action and the terminating of the preceeding one can be combined to reduce the total number of events to be programmed on the Burner II intervalometer. Programmed attitude changes on Burner II are made by initiating a rate, holding it for the proper time interval, and then terminating the attitude change rate.

The deployment concept described refers to orienting the satellite spin axis perpendicular to the orbit plane. This is done for simplification in describing the concept while being aware that it is desirable to have the spin axis approximately perpendicular to the ecliptic plane. The attitude position angles of 45 degrees immediately prior to the satellite separation events can be adjusted, based on launch date to compensate for ecliptic inclination of the orbit plane.

Accuracy of Spin Separation. A single small spring can be used to separate payloads with 1 ft/sec ΔV. (Spring constant 26 lbs/in. one inch stroke). The 1 ft/sec will enable simultaneous sequencing of events as indicated above. Preload will be 26 lbs. which, with 0.1-inch c.g. offset on the sping and a 2 second delay to free spin-up will give only 0.5 degree pointing error, including the effect of the Burner II N_2 attitude system limit cycle rates.

Spin-up by a small solid rocket requires tight tolerances on installation design and rocket motor selection. Assumptions pertinent to the accuracy quoted here are that the spin rocket is mounted so that less than 1 percent of the torque produced is in a cross axis and the products of inertia are such that the principle axis is within 1 degree of the desired spin axis. Other assumptions were: $I_s/I_x = 1.5$ before booms are deployed, 1.8 after boom deployment. Spin-up to 140 rpm (booms folded) to give 60 rpm (booms deployed) requires a solid motor of approximately 0.9 lb. Calculated errors for the above assumptions with the previously described deployment concept are:

Pointing = 3.3 degrees
Wobble = 2.2 degrees.

4. BURNER II MODIFICATIONS

Reaction Control System. The reaction control system requires three changes due to the Payload c.g. height above Burner II, the amount of H_2O_2 required to complete the deployment maneuvers, and the coast time of 24 hours to apogee.

a. Install 40 lb. thrust motors in place of the current 22 lb. thrust motors. (The larger motors use the same valve as the current ones and are available from the current motor supplier).

b. Install two 18 lb. capacity H_2O_2 tanks in place of the current two 9 lb. H_2O_2 tanks (18 lb. H_2O_2 tanks are presently used in the Scout program as are 9 lb. tanks so they are available from the current supplier).

c. Install a low pressure regulator and valve in the N_2 system to provide 50 psia N_2 to the N_2 thrusters during the coast phase. The regulated pressure currently is 420 psia. The new regulator would be pre-programmed to be in the system only during the long coast. The current N_2 tanks have adequate N_2 capacity for the 24 hours coast with the addition of the low pressure regulator.

Electrical Power and Distribution System. The recommended Burner II configuration for the multi-satellite mission would make use of available satellite power during the coast to apogee. Power for the velocity meter and the T/M system would be shut off after Burner II vernier burn at perigee. The T/M would be turned back on at apogee for the satellite deployment data. The net increase in Burner II battery weight is 3 pounds using this operational concept. Solar panel illumination during coast is planned on the basis of rolling at six rev/hr. for gyro drift cancellation.

Command Link System. A command link system and a tracking beacon will be added, so that tracking can be used during the first half orbit to determine the actual orbit, and to command initiation of the satellite deployment sequence at the appropriate true anomaly.

Weight Effect of Burner II Modifications. The weight additions to the basic Burner II for the modifications discussed are:

319 lbs	=	Basic Burner with weight saving items presently planned incorporated.	
37 lbs	=	Payload support increase to accommodate for four 80 lb. satellites.	
		Battery addition	
		H_2O_2 Tank capacity increase	
		Low Pressure Regulator and Valve addition	
		H_2O_2 motor thrust increase	
		Tracking beacon and command receiver	
		Misc. for power switching, wires and timer concept	
Total 356 lbs	=	Burn out weight of Burner II for multi-satellite mission	

5. PERFORMANCE

The payload capability for the DSV-3L/Burner II and the SLV-3A/Burner II to 70,000 n. mi. apogee is shown in Figure I-3. The data is plotted to show the performance effect of perigee variation. The Burner II version in the performance curve is as modified for the multi-satellite mission. Performance shown is for launching due east at ETR.

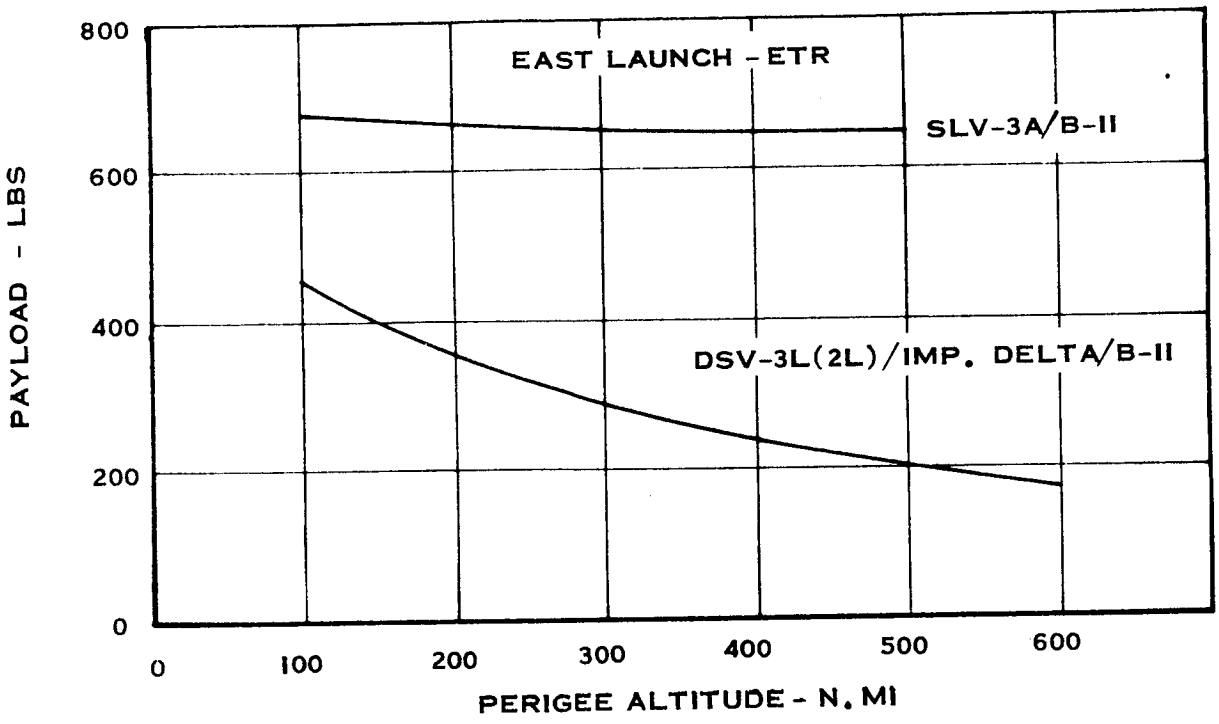

Figure I-3 Elliptical Orbit Capability, Apogee Altitude = 70,000 N. Miles

6. SUBJECTS FOR CONTINUED STUDY

It is recommended that the following items be included in subsequent phases of the multi-satellite studies:

a. DSV-3L/Burner II and SLV-3A/Burner II Error Analysis. This is needed to accurately determine the range angle tolerances on apogee. Determination of time to apogee predictability is vital to the concept

of pre-programming the start of the satellite deployment sequence, which is a possible alternative method.

b. Trade Studies for Integrated Power and Electronic Systems. Studies are required to establish the optimum power tie between the satellites and Burner II. Questions of telemetry requirements, tracking beacon, and command link need further study.

c. Burner II/Satellite Interface Study. Structural and functional interfaces need to be defined once the concept is established.